Multiscale Modelling of Perfusion and Mechanics in Poroelastic Biological Tissues

by

Laura Mary Miller

A thesis submitted to the
College of Science and Engineering
at the University of Glasgow
for the degree of
Doctor of Philosophy

August 2022

Abstract

The Theory of Poroelasticity is embraced to model the effective mechanical behaviour of a porous elastic structure with fluid percolating in the pores. Key examples of the linear theory include hard hierarchical tissues, such as the bones, the interstitial matrix in healthy and tumorous biological tissues, the human eye, artificial constructs and biomaterials, as well as rocks and soil. Nonlinear poroelasticity has been applied to modelling tumour growth and in imaging to locate tumours in an incompressible medium, to the lungs and to consider the perfused myocardium. Poroelasticity has also been applied to studying the artery walls.

The current modelling approaches assume simplistic microstructures for the materials which are in general unrealistic for the desired applications. This thesis will extend the current literature by proposing exciting, novel computationally feasible macroscale models that account for realistic microstructures and can help capture the true behaviour of materials. To fulfil this modelling goal we use the asymptotic homogenization technique.

To provide a complete overview of the area we begin with a re-derivation of standard Biot's poroelasticity via the asymptotic homogenization technique. In the following chapters we build upon this to create appropriate models for complex, realistic biological scenarios.

We begin our development by deriving the quasi-static governing equations for the macroscale behaviour of a linear elastic porous composite comprising a matrix interacting with inclusions and/or fibres, and an incompressible Newtonian fluid flowing in the pores. This is a novel model that can account for interactions between a variety of phases at the porescale which is much more realistic of biological tissues than the previously assumed matrix homogeneity. We then further extend this theory to assume that both the matrix and fibres/inclusions are hyperelastic, thus providing one of the first few works to use asymptotic homogenization in the context of nonlinear elasticity and making the theory

more applicable to the heart and arteries.

We continue the development by considering an approach over three microstructural scales. We derive the balance equations for a double poroelastic material which comprises a matrix with embedded subphases. Both the matrix and subphases can be described by Biot's anisotropic, heterogeneous, compressible poroelasticity. This gives us a macroscale model that can account for the difference in a full set of poroelastic parameters and encodes structural details on three scales.

We complete our analysis by investigating our novel poroelastic composite model numerically. We perform a study to investigate the role that the microstructure of a poroelastic material has on the resulting elastic parameters. We are considering how important an effect that multiple elastic and fluid phases at the same scale have on the estimation of the material's elastic parameters when compared with a standard poroelastic approach. This work justifies the work of this thesis. That is, the introduction of novel models with detailed microstructures should be used instead of the previously known Biot's poroelasticity for materials with non-homogeneous microstructures. The final part of this thesis applies the novel poroelastic composite model to investigate how physiologically observed microstructural changes induced by myocardial infarction impact the elastic parameters of the heart.

Acknowledgements

First of all I would like to thank EPSRC for funding my PhD studies and making all the work in this thesis possible. To the University of Glasgow, I have been a student here since 2013 and it has been the most wonderful place to study and grow in and such a positive environment to work. It has been the best 9 years (with a few more to come)!

I would like to thank my supervisors Dr Raimondo Penta and Professor Nick Hill. It has been a priviledge to work with and learn from you. Raimondo this thesis would not have been possible without all of your guidance, patience and effort in teaching me. I am also very grateful to both of you for all the help in applying for Post doctoral positions.

I would also like to acknowledge Professor Ray Ogden and Professor Xiaoyu Luo who supervised my level 4 and 5 undergraduate projects and inspired my love for continuum mechanics and nonlinear elasticity theory. It was a privilege to have the opportunity to work with you both. These projects are the reason I applied for a PhD and I am grateful to both of you for sharing your expertise and passion on the subject.

I also wish to thank my fellow PhD students in room 231 (both past and present) who always made it a pleasure to come into the office. I wish you all the best of luck with your own studies.

My final thanks go to my family for encouraging and supporting me during the last four years. To my parents, John and Hilda, my brothers, Craig and Scott, and of course my four-legged friend, Jasper, I could not have completed this journey without you.

The last words of these acknowledgments should rightly go to my grandmother, Mary, who sadly passed away shortly before I began this PhD journey. I wish you could have been here to see me submit this thesis and become a doctor. This doctoral thesis is dedicated to you and your memory which will forever live on.

Declaration & Publications

I Declare that all work in this thesis was carried out by myself unless otherwise explicitly stated and has not been submitted for any other degree at the University of Glasgow or any other institution.

The following publications are based on this thesis:

1. **L. Miller** and R. Penta, Effective Balance Equations for Poroelastic Composites, *Continuum Mechanics and Thermodynamics*, 32, pp. 1533-1557 (2020).

2. **L. Miller** and R. Penta, Double poroelasticity derived from the microstructure, *Acta Mechanica*, (2021).

3. **L. Miller** and R. Penta, Homogenized balance equations for nonlinear poroelastic composites, *Applied Sciences*, 11 (14), (2021).

4. **L. Miller** and R. Penta, Micromechanical analysis of the effective stiffness of poroelastic composites, *European Journal of Mechanics A Solids*, Submitted.

5. **L. Miller** and R. Penta, Investigating the effects of microstructural changes induced by myocardial infarction on the elastic parameters of the heart, *Biomechanics and Modelling in Mechanobiology*, submitted.

List of Symbols

Ω	Full domain through all chapters
Ω_{s}	Solid part of the domain through all chapters
Ω_{f}	Fluid part of the domain through all chapters
d	Porescale length through all chapters
L	Macroscale length in Ch. 2, 3, 4/ local scale length Ch. 5
ϵ	Scale separation parameter through all chapters
$\mathbb{C}$	Elasticity tensor in Ch. 2
$\mathbf{u}$	Elastic displacement through all chapters
ξ	Symetric Gradient operator through all chapters
T_{s}	Solid stress tensor in Ch. 2
T_{f}	fluid stress tensor in Ch. 2, 3, 4
p	Fluid pressure through all chapters
$\mathbf{v}$	Fluid velocity through all chapters
μ	Fluid viscosity through all chapters
$\mathbf{I}$	Identity tensor through all chapters
∇	Gradient operator through all chapters
Γ	Fluid solid interface in Ch. 2
$\dot{\mathbf{u}}$	Solid velocity through all chapters
C_p	Characteristic Pressure gradient through all chapters
$\mathbf{x}$	Macroscale variable Ch. 2, 3, 5
$\mathbf{y}$	Microscale variable Ch. 2, 3, 5
φ	A typical field through all chapters
$\mathbf{w}$	Relative fluid- solid velocity through all chapters
$\mathbf{\Pi}$	Auxiliary vector solving fluid problem through all chapters
W	Auxiliary tensor solving fluid problem through all chapters

ϕ	Porosity through all chapters
$\langle\rangle$	Integral average through all chapters
A	Auxiliary 3rd rank tensor solving elastic problem Ch. 2
$\mathbf{a}$	Auxiliary vector solving elastic problem Ch. 2
$\mathbb{M}$	Forth rank tensor, gradient of A Ch. 2
Q	Second rank tensor, gradient of $\mathbf{a}$ Ch. 2
$\mathbf{T}_{\text{Eff}}$	Effective stress tensor for standard poroelastic material Ch. 2
M	Biot's modulus for standard poroelastic material Ch. 2
$\boldsymbol{\alpha}$	Biot's tensor of coefficients for standard poroelastic material Ch. 2
Ω_{II}	Matrix domain Ch. 3
Ω_{I}	Collection of elastic subphases/ The subphase in the periodic cell Ch. 3
Ω_α	Individual elastic subphases Ch. 3
T_{II}	Solid elastic stress in the matrix Ch. 3
T_α	Solid elastic stress in the α-th subphase Ch. 3
$\mathbf{u}_{\text{II}}$	Elastic displacement in the matrix Ch. 3
$\mathbf{u}_\alpha$	elastic displacement in the α-th subphase Ch. 3
$\mathbb{C}_{\text{II}}$	Elasticity tensor for the matrix Ch. 3
$\mathbb{C}_\alpha$	Elasticity tensor for the α-th subphase Ch. 3
Γ_{II}	Interface between the matrix and fluid Ch. 3
Γ_α	Interface between the α-th subphase and fluid Ch. 3
$\Gamma_{\alpha\text{II}}$	Interface between the α-th subphase and matrix Ch. 3
$\dot{\mathbf{u}}_{\text{II}}$	Solid velocity in the matrix Ch. 3
$\dot{\mathbf{u}}_\alpha$	Solid velocity in the α-th subphase Ch. 3
$\mathbf{n}_{\text{II}}$	Normal to the interface between the matrix and fluid Ch. 3
$\mathbf{n}_\alpha$	Normal to the interface between the α-th subphase and fluid Ch. 3
$\mathbf{n}_{\alpha\text{II}}$	Normal to the interface between the α-th subphase and matrix Ch. 3
T_{I}	Solid elastic stress in the single periodic cell subphase Ch. 3
$\mathbf{u}_{\text{I}}$	Elastic displacement in the single periodic cell subphase Ch. 3
$\mathbb{C}_{\text{I}}$	Elasticity tensor for the single periodic cell subphase Ch. 3
Γ_{I}	Interface between the single periodic cell subphase and fluid Ch. 3
Γ_{III}	Interface between the single periodic cell subphase and matrix Ch. 3
$\dot{\mathbf{u}}_{\text{I}}$	Solid velocity in the single periodic cell subphase Ch. 3
$\mathbf{n}_{\text{I}}$	Normal to the interface between the single subphase and fluid Ch. 3

$\mathbf{n}_{\text{II}}$	Normal to the interface between the α-th subphase and matrix Ch. 3
A_{I}	Auxiliary 3rd rank tensor solving elastic problem in Ch. 3
A_{II}	Auxiliary 3rd rank tensor solving elastic problem in Ch. 3, 6
$\mathbf{a}_{\text{I}}$	Auxiliary vector solving elastic problem in Ch. 3
$\mathbf{a}_{\text{II}}$	Auxiliary vector solving elastic problem in Ch. 3, 6
$\mathbb{M}_{\text{I}}$	Fourth rank tensor, gradient of A_{I} Ch. 3, 6
$\mathbb{M}_{\text{II}}$	Fourth rank tensor, gradient of A_{I} Ch. 3, 6
Q_{I}	Second rank tensor, gradient of $\mathbf{a}_{\text{I}}$ Ch. 3
Q_{II}	Second rank tensor, gradient of $\mathbf{a}_{\text{II}}$ Ch. 3, 6
$\hat{\mathsf{T}}_{\text{Eff}}$	Effective stress tensor for poroelastic composites Ch. 3
$\hat{M}$	Biot's modulus for poroelastic composite material Ch. 3
$\hat{\boldsymbol{\alpha}}$	Biot's tensor of coefficients for poroelastic composite material Ch. 3
$\widehat{\mathbb{C}}$	Effective elasticity tensor for poroelastic composite Ch. 3
$\boldsymbol{\gamma}$	Negative of Biot's tensor of coefficients Ch. 3
β	Denominator of Biot's Modulus for poroelastic composites Ch. 3
$\mathscr{B}_0$	Reference body Ch. 4
$\mathscr{B}_t$	Current/deformed body Ch. 4
$\mathbf{X}$	Position vector in the reference body Ch. 4
$\mathbf{x}$	Position vector in the current/deformed body Ch. 4
Ω^0_{II}	Matrix domain in reference configuration Ch. 4
Ω^0_{I}	Collection of Elastic subphases/ specific subphase in reference periodic cell Ch. 4
Ω^0_α	Individual α-th elastic subphase in the reference configuration Ch. 4
Ω^t_{II}	Matrix domain in current configuration Ch. 4
Ω^t_{I}	Collection of Elastic subphases/ specific subphase in current periodic cell Ch. 4
Ω^t_α	Individual elastic subphase in the current configuration Ch. 4
$\mathbf{F}$	Deformation gradient Ch. 4
χ	Deformation function Ch. 4
$\mathbf{P}_\alpha$	First Piola stress in the α-th subphase Ch. 4
$\mathbf{P}_{\text{II}}$	First Piola stress in the matrix Ch. 4
ψ_α	Strain energy function for the α-th subphase Ch. 4
ψ_{II}	Strain energy function for the matrix Ch. 4
$\mathbf{F}_\alpha$	The α-th subphase deformation gradient Ch. 4
$\mathbf{F}_{\text{II}}$	Matrix deformation gradient Ch. 4

$\mathbf{F}_{\mathrm{f}}$	Fluid deformation gradient Ch. 4
Γ^0_{II}	Interface between the matrix and fluid Ch. 4
Γ^0_{α}	Interface between the α-th subphase and fluid Ch. 4
$\Gamma^0_{\alpha\mathrm{II}}$	Interface between the α-th subphase and matrix Ch. 4
$\mathbf{n}^0_{\mathrm{II}}$	Normal to the interface between the fluid and matrix Ch. 4
$\mathbf{n}^0_{\alpha}$	Normal to the interface between the α-th subphase and fluid Ch. 4
$\mathbf{n}^0_{\alpha\mathrm{II}}$	Normal to the interface between the α-th subphase and matrix Ch. 4
J	Jacobian Ch. 4
G	Piola transformation Ch. 4
G_{α}	Piola transformation in the subphases Ch. 4
G_{II}	Piola transformation in the matrix Ch. 4
G_{f}	Piola transformation in the fluid Ch. 4
ζ	A general scalar field Ch. 4
$\mathbf{z}$	A general vector field Ch. 4
Z	A general tensor field Ch. 4
$\mathbf{V}$	Fluid velocity in the reference configuration Ch. 4
$\frac{\partial \mathbf{u}_{\alpha}}{\partial t}$	Solid velocity of the α-th subphase Ch. 4
$\frac{\partial \mathbf{u}_{\mathrm{II}}}{\partial t}$	Solid velocity of the matrix Ch. 4
$\bar{\mathbf{Y}}$	Microscale variable in the reference configuration Ch. 4
$\bar{\mathbf{X}}$	Macroscale variable in the reference configuration Ch. 4
Γ^0_{I}	Interface between the single periodic cell subphase and fluid Ch. 4
Γ^0_{III}	Interface between the single periodic cell subphase and matrix Ch. 4
$\mathbf{n}^0_{\mathrm{I}}$	Normal to the interface between the periodic cell subphase and fluid Ch. 4
$\mathbf{n}^0_{\mathrm{III}}$	Normal to the interface between the periodic cell subphase and matrix Ch. 4
$\mathbf{P}_{\mathrm{I}}$	First Piola stress in the periodic cell subphase Ch. 4
ψ_{I}	Strain energy function for the periodic cell subphase Ch. 4
$\mathbf{F}_{\mathrm{I}}$	Periodic cell suphase deformation gradient Ch. 4
$\frac{\partial \mathbf{u}_{\mathrm{I}}}{\partial t}$	Solid velocity of the subphase in the periodic cell Ch. 4
G_{I}	Piola transformation in the periodic cell subphase Ch. 4
$\hat{W}$	Second rank auxiliary tensor solving fluid problem Ch. 4
$\hat{\mathbf{\Pi}}$	Auxiliary vector solving fluid problem Ch. 4
$\bar{\mathsf{T}}_{\mathrm{Eff}}$	Effective stress tensor for nonlinear poroelastic composite Ch. 4
$\mathbf{E}_{\mathrm{I}}$	Green-Lagrangian strain tensor in the periodic cell subphase Ch. 4

$\mathbf{E}_{\text{II}}$	Green-Lagrangian strain tensor in the matrix Ch. 4
$\mathbf{S}_{\text{I}}$	Second piola stress in the periodic cell subphase Ch. 4
$\mathbf{S}_{\text{I}}$	Second Piola stress in the matrix Ch. 4
$\mathbf{H}_{\text{I}}$	The non identity part of $\mathbf{F}_{\text{I}}^{(0)}$ Ch. 4
$\mathbf{H}_{\text{II}}$	The non identity part of $\mathbf{F}_{\text{II}}^{(0)}$ Ch. 4
$\hat{A}_{\text{I}}$	Auxiliary 3rd rank tensor solving elastic problem in Ch. 4
$\hat{A}_{\text{II}}$	Auxiliary 3rd rank tensor solving elastic problem in Ch. 4
$\hat{\mathbf{a}}_{\text{I}}$	Auxiliary vector solving elastic problem Ch. 4
$\hat{\mathbf{a}}_{\text{II}}$	Auxiliary vector solving elastic problem Ch. 4
$\hat{\mathbb{M}}_{\text{I}}$	Fourth rank tensor, gradient of $\hat{A}_{\text{I}}$ Ch. 4
$\hat{\mathbb{M}}_{\text{II}}$	Forth rank tensor, gradient of $\hat{A}_{\text{I}}$ Ch. 4
$\hat{Q}_{\text{I}}$	Second rank tensor, gradient of $\hat{\mathbf{a}}_{\text{I}}$ Ch. 4
$\hat{Q}_{\text{II}}$	Second rank tensor, gradient of $\hat{\mathbf{a}}_{\text{II}}$ Ch. 4
$\bar{M}$	Biot's modulus for nonlinear poroelastic composite Ch. 4
$\bar{\boldsymbol{\alpha}}$	Biot's tensor of coefficients for nonlinear poroelastic composite Ch. 4
$\widetilde{\mathbb{C}}$	Effective elasticity tensor for nonlinear poroelastic composite Ch. 4
Ω_{M}	Poroelastic matrix domain Ch. 5
Ω_{Sub}	Union of poroelastic subphases/ single poroelastic subphase periodic cell Ch. 5
Ω_{η}	The individual η-th poroelastic subphase Ch. 5
$\boldsymbol{\sigma}_{\text{M}}$	The effective stress tensor in the matrix Ch. 5
$\boldsymbol{\sigma}_{\eta}$	The effective stress tensor in the η-th subphase Ch. 5
$\mathbb{C}_{\text{M}}$	Effective elasticity tensor in the matrix Ch. 5
$\mathbb{C}_{\eta}$	Effective elasticity tensor in the η-th subphase Ch. 5
$\mathbf{u}_{\text{M}}$	Elastic displacement in the matrix Ch. 5
$\mathbf{u}_{\eta}$	Elastic displacement in the η-th subphase Ch. 5
$\boldsymbol{\alpha}_{\text{M}}$	Biot's tensor of coefficients in the matrix Ch. 5
$\boldsymbol{\alpha}_{\eta}$	Biot's tensor of coefficients in the η-th subphase Ch. 5
ϑ_{M}	Pressure in the matrix Ch. 5
ϑ_{η}	Pressure in the η-th subphase Ch. 5
$\mathbf{w}_{\text{M}}$	Relative fluid-solid velocity in the matrix Ch. 5
$\mathbf{w}_{\eta}$	Relative fluid-solid velocity in the η-th subphase Ch. 5
K_{M}	Hydraulic conductivity in the matrix Ch. 5
K_{η}	Hydraulic conductivity in the η-th subphase Ch. 5

$\mathcal{M}_{\mathrm{M}}$ Biot's modulus in the matrix Ch. 5

$\mathcal{M}_{\eta}$ Biot's modulus in the η-th subphase Ch. 5

$\dot{\mathbf{u}}_{\mathrm{M}}$ Solid velocity in the matrix Ch. 5

$\dot{\mathbf{u}}_{\eta}$ Solid velocity in the η-th subphase Ch. 5

Υ_{η} The interface between the matrix and the η-th subphase Ch. 5

$\mathbf{n}_{\eta}$ The normal to the interface between the matrix and the η-th subphase Ch. 5

D Global scale length Ch. 5

$\boldsymbol{\sigma}_{\mathrm{S}}$ The effective stress tensor in the periodic cell subphase Ch. 5

$\mathbb{C}_{\mathrm{S}}$ Effective elasticity tensor in the periodic cell subphase Ch. 5

$\mathbf{u}_{\mathrm{S}}$ Elastic displacement in the periodic cell subphase Ch. 5

$\boldsymbol{\alpha}_{\mathrm{S}}$ Biot's tensor of coefficients in the periodic cell subphase Ch. 5

ϑ_{S} Pressure in the periodic cell subphase Ch. 5

$\mathbf{w}_{\mathrm{S}}$ Relative fluid-solid velocity in the periodic cell subphase Ch. 5

K_{S} Hydraulic conductivity in the periodic cell subphase Ch. 5

$\mathcal{M}_{\mathrm{S}}$ Biot's modulus in the periodic cell subphase Ch. 5

$\dot{\mathbf{u}}_{\mathrm{S}}$ Solid velocity in the periodic cell subphase Ch. 5

Υ The interface between the matrix and the periodic cell subphase Ch. 5

$\mathbf{n}_{\Upsilon}$ The normal to the interface *Upsilon* Ch. 5

B_{M} Auxiliary 3rd rank tensor solving elastic problem Ch. 5

B_{S} Auxiliary 3rd rank tensor solving elastic problem Ch. 5

$\mathbf{b}_{\mathrm{M}}$ Auxiliary vector solving the elastic problem Ch. 5

$\mathbf{b}_{\mathrm{S}}$ Auxiliary vector solving the elastic problem Ch. 5

$\mathbb{L}_{\mathrm{M}}$ Fourth rank tensor, gradient of B_{M} Ch. 5

$\mathbb{L}_{\mathrm{S}}$ Fourth rank tensor, gradient of B_{S} Ch. 5

$\boldsymbol{\tau}_{\mathrm{M}}$ Second rank tensor, gradient of $\mathbf{b}_{\mathrm{M}}$ Ch. 5

$\boldsymbol{\tau}_{\mathrm{S}}$ Second rank tensor, gradient of $\mathbf{b}_{\mathrm{S}}$ Ch. 5

$\boldsymbol{\sigma}_{\mathrm{eff}}$ The effective stress tensor for a double poroelastic material Ch. 5

$\bar{\mathbb{C}}$ Effective drained elasticity tensor for double poroelastic material Ch. 5

$\hat{\boldsymbol{\vartheta}}_{\mathrm{M}}$ Auxiliary vector solving the anisotropic poisson type problem Ch. 5

$\hat{\boldsymbol{\vartheta}}_{\mathrm{S}}$ Auxiliary vector solving the anisotropic poisson type problem Ch. 5

R_{M} Second rank tensor, gradient of $\hat{\boldsymbol{\vartheta}}_{\mathrm{M}}$ Ch. 5

R_{S} Second rank tensor, gradient of $\hat{\boldsymbol{\vartheta}}_{\mathrm{S}}$ Ch. 5

$\mathbf{w}_{\mathrm{eff}}$ Effective relative fluid-solid velocity Ch. 5

W	Hydraulic conductivity tensor for a double poroelastic material Ch. 5
$\bar{\mathcal{M}}$	The Biot's modulus for a double poroelastic material Ch. 5
$\widetilde{\boldsymbol{\alpha}}$	Biot's tensor of coeffiecients for a double poroelastic material Ch. 5
$\bar{\boldsymbol{\gamma}}$	Coefficient that is the negative of $\widetilde{\boldsymbol{\alpha}}$ Ch. 5
$\boldsymbol{\sigma}'_{\text{eff}}$	Effective stress tensor for double poroelastic material subphase has no fluid Ch. 5
$\bar{\mathbb{C}}'$	Effective drained elasticity tensor when subphase no fluid Ch. 5
$\bar{\boldsymbol{\gamma}}'$	Coefficient that is the negative of $\widetilde{\boldsymbol{\alpha}}'$ Ch. 5
$\mathbf{w}'_{\text{eff}}$	Effective relative fluid-solid velocity when subphase has no fluid Ch. 5
W'	Hydraulic conductivity tensor when subphase has no fluid Ch. 5
$\bar{\mathcal{M}}'$	The Biot's modulus double poroelastic material limit subphase has no fluid Ch. 5
$\widetilde{\boldsymbol{\alpha}}'$	Biot's tensor of coeffiecients when subphase has no fluid Ch. 5
$\mathsf{T}_{\text{Eff}}^{\text{LMRP}}$	Effective stress tensor for LMRP model (Laura Miller and Raimondo Penta Poroelastic composite model) Ch. 6
$\boldsymbol{\alpha}^{\text{LMRP}}$	Biot's tensor of coefficients LMRP (Laura Miller and Raimondo Penta Poroelastic composite model) Ch. 6
M^{LMRP}	Biot's modulus for LMRP (Laura Miller and Raimondo Penta Poroelastic composite model) Ch. 6
$\boldsymbol{\gamma}^{\text{LMRP}}$	Poroelastic coefficient in LMRP (Laura Miller and Raimondo Penta Poroelastic composite model) Ch. 6
$\widetilde{\mathbb{C}}^{\text{LMRP}}$	The effective elasticity tensor for LMRP model (Laura Miller and Raimondo Penta Poroelastic composite model) Ch. 6
Ω_{PM}	The porous matrix domain Ch. 6
Γ_{PM}	Interface between porous matrix and elastic subphase Ch. 6
$\mathsf{T}_{\text{Eff}}^{\text{SP}}$	Effective stress tensor for Standard Poroelastic Ch. 6
$\mathbb{C}_{\text{I}}^{\text{SP}}$	The elasticity tensor for the subphase in the Standard Poroelastic model Ch. 6
$\mathbb{M}_{\text{I}}^{\text{SP}}$	Fourth rank tensor, solves cell problem for porous matrix and inclusion Ch. 6
$\mathbb{C}_{\text{PM}}$	The effective elasticity tensor for the porous matrix Ch. 6
$\mathbb{M}_{\text{II}}^{\text{SP}}$	Fourth rank tensor, solves cell problem for porous matrix and inclusion Ch. 6
$\boldsymbol{\gamma}^{\text{SP}}$	poroelastic coefficient of SP model Ch. 6
Q_{I}^{SP}	Second rank tensor, solves cell problem for porous matrix and inclusion Ch. 6
$Q_{\text{II}}^{\text{SP}}$	Second rank tensor, solves cell problem for porous matrix and inclusion Ch. 6
$\widetilde{\mathbb{C}}^{\text{SP}}$	Effective elasticity tensor for the SP approach Ch. 6
$\hat{\mathbf{u}}^{(0)}$	Elastic displacement Standard Poroelastic model Ch. 6

$\hat{p}^{(0)}$	Pressure Standard Poroelastic model Ch. 6
M^{SP}	Biot's modulus Standard Poroelastic model Ch. 6
$\boldsymbol{\alpha}^{\mathrm{SP}}$	Biot's tensor of coefficients Standard Poroelastic model Ch. 6
$\mathcal{M}_{\mathrm{PM}}$	Biot's modulus porous matrix Ch. 6
λ^{I}	First Lamé parameter in the inclusion Ch. 6
λ^{II}	First Lamé parameter in the matrix Ch. 6
μ^{I}	Second Lamé parameter in the inclusion Ch. 6
μ^{I}	Second Lamé parameter in the matrix Ch. 6
$f_i^{\Gamma_{\mathrm{III}}}$	Forces on 3D interface Γ_{III} Ch. 6
$f_i^{\Gamma_{\mathrm{II}}}$	The forces on 3D interface Γ_{II} Ch. 6
D_{I}	The 2D counterpart of Ω_{I} Ch. 6
D_{II}	The 2D counterpart of Ω_{II} Ch. 6
$\partial D_{\mathrm{I}} \cap \partial D_{\mathrm{II}}$	2D Interface between the matrix inclusion LMRP Ch. 6
∂D_{f}	2D Interface between the fluid-matrix LMRP Ch. 6.
$f_{\mathrm{anti}}^{\partial D_{\mathrm{I}} \cap \partial D_{\mathrm{II}}}$	Force in the 2D antiplane problem Ch. 6
$f_{\mathrm{anti}}^{\partial D_{\mathrm{f}}}$	Force in the 2D antiplane problem Ch. 6
$\mathbf{f}^{\partial D_{\mathrm{I}} \cap \partial D_{\mathrm{II}}}$	Force in the 2D inplane problem Ch. 6
$\mathbf{f}^{\partial D_{\mathrm{f}}}$	Force in the 2D inplane problem Ch. 6
$\mathbb{C}_{\mathrm{Mat}}$	Elasticity tensor for the matrix part of the porous matrix Ch. 6
$\mathbb{M}_{\mathrm{Mat}}$	Fourth rank tensor, solves elastic problem for porous matrix Ch. 6
B	Third rank tensor solving drained porous matrix cell problem Ch. 6
Γ_{M}	Interface between the matrix and fluid in the porous matrix Ch. 6
F_{I}	Third rank tensor solving the 3D cell problem Ch. 6
F_{II}	Third rank tensor solving the 3D cell problem Ch. 6
$f_i^{\Gamma_{\mathrm{PM}}}$	Forces on interface between porous matrix and elastic inclusion Ch. 6
$\lambda^{\mathrm{I}^{\mathrm{SP}}}$	First Lamé parameter in the inclusion SP model Ch. 6
$\mu^{\mathrm{I}^{\mathrm{SP}}}$	Second Lamé parameter in the inclusion SP model Ch. 6
Ω_{Mat}	Matrix portion of Ω_{PM} Ch. 6
D_{M}	This is the corresponding 2D slice of Ω_{Mat} Ch. 6
λ_{M}	First Lamé parameter of the matrix Ch. 6
μ_{M}	Second Lamé parameter of the matrix Ch. 6
$\partial D_{\mathrm{f}} \cap \partial D_{\mathrm{M}}$	The 2D projection of interface Γ_{M} Ch. 6
$f_{\mathrm{anti}}^{\partial D_{\mathrm{f}} \cap \partial D_{\mathrm{M}}}$	The 2D antiplane force used for the matrix fluid interface SP Ch. 6
$\mathbf{f}^{\partial D_{\mathrm{f}} \cap \partial D_{\mathrm{M}}}$	The 2D inplane force used for the matrix fluid interface SP

D_{PM}	The 2D slice of Ω_{PM} Ch. 6
$\partial D_{\mathrm{I}} \cap \partial D_{\mathrm{PM}}$	2D projection of interface between inclusion and porous matrix Ch. 6
$f_{\mathrm{anti}}^{\partial D_{\mathrm{I}} \cap \partial D_{\mathrm{PM}}}$	2D antiplane force used on porous matrix inclusion interface SP Ch. 6
$\mathbf{f}^{\partial D_{\mathrm{I}} \cap \partial D_{\mathrm{PM}}}$	2D inplane force used for porous matrix inclusion interface SP Ch. 6
E_1^{LMRP}	Transverse Youngs modulus LMRP Ch. 6
E_1^{SP}	Transverse Youngs modulus SP Ch. 6
E_3^{LMRP}	Axial Youngs modulus LMRP Ch. 6
E_3^{SP}	Axial Youngs modulus SP Ch. 6
C_{44}^{LMRP}	Shear for LMRP model Ch. 6
C_{66}^{LMRP}	Shear for LMRP model Ch. 6
C_{44}^{SP}	Shear for SP model Ch. 6
C_{66}^{SP}	Shear for SP model Ch. 6
$\mathbb{C}_{\mathrm{Myo}}$	Elasticity tensor myocyte Ch. 7
$\mathbb{C}_{\mathrm{IM}}$	Elasticity tensor interstitial matrix Ch. 7
A^{Myo}	Third rank auxiliary tensor solving cell problem Ch. 7
A^{IM}	Third rank auxiliary tensor solving cell problem Ch. 7
$\mathbf{a}^{\mathrm{Myo}}$	Auxiliary vector solving cell problem Ch. 7
$\mathbf{a}^{\mathrm{IM}}$	Auxiliary vector solving cell problem Ch. 7
$\mathbb{M}_{\mathrm{Myo}}$	Fourth rank tensor, gradient of A^{Myo} Ch. 7
$\mathbb{M}_{\mathrm{IM}}$	Fourth rank tensor, gradient of A^{IM} Ch. 7
Q_{Myo}	Second rank tensor, gradient of $\mathbf{a}^{\mathrm{Myo}}$ Ch. 7
Q_{IM}	Second rank tensor, gradient of $\mathbf{a}^{\mathrm{IM}}$ Ch. 7
E_{myo}	Input Youngs modulus myocyte Ch. 7
E_{matrix}	Input Youngs modulus matrix Ch. 7
ν_{myo}	Input Poisson ratio myocyte Ch. 7
ν_{matrix}	Input Poisson ratio matrix Ch. 7
E_1	Transverse Youngs modulus Ch. 7
E_3	Axial Youngs modulus Ch. 7
C_{44}	Shear Ch. 7
C_{66}	Shear Ch. 7
E_{disc}	Input Youngs modulus intercalated disc Ch. 7
ν_{myo}	Input Poisson ratio intercalated disc Ch. 7

List of Figures

List of Tables

Contents

Chapter 1

Introduction

The Theory of Poroelasticity [12–15] is a widely known modelling framework which is usually embraced to model the effective mechanical behaviour of a fluid-filled porous elastic structure. There exists a large variety of physical systems where porescale interactions between a deformable solid and a fluid phase take place, thus motivating a poroelastic modelling approach. Key examples include hard hierarchical tissues, such as the bone [30, 117], the interstitial matrix in healthy and tumorous biological tissues (see, e.g., [16, 40]), the human eye [20, 55], artificial constructs and biomaterials ([21, 57]), as well as rocks and soil [60, 115].

Due to the desire to apply poroelasticity to biological tissues, the theory was adapted to nonlinearities in [8, 11, 77, 122]. The poroelastic modelling framework is applicable to a wide variety of physical scenarios, in particular to biological tissues, where the deformations are in general nonlinear. For example, a poroelastic approach has been taken to model organs such as lungs (see, e.g., [9]) and to consider the perfused myocardium [22,66]. The theory has also been applied to studying the artery walls (see, e.g., [5, 121]). Another application is to modelling tumour growth [41] and in imaging to locate tumours in an incompressible medium [6]. It is also of interest in porous thermoelasticity (see [46]). For a general overview of the micromechanics of porous media, we refer the reader to [37], where an overview of upscaling techniques, the linear theory of porous media and also the extension of the analysis to the nonlinear homogenization of a large range of scenarios including strength homogenization, non saturated microporomechanics, microporoplasticity and microporofracture and microporodamage theory were discussed.

The types of materials that can be classified as poroelastic media generally exhibit an intrinsically multiscale structure. That is, the average pore radius and also the distance

between the pores (*the porescale*), is generally much smaller than the average size of the entire medium (*the macroscale*) which is effectively behaving as a poroelastic material.

Models of materials at one scale, either the macroscale or microscale, are unsatisfactory. Generally a macroscale model is too simplistic and even though they are cheap computationally they cannot describe the material well enough to gain any insight into the behaviour. A thorough understanding of the effective macroscale properties of the material requires relating them to the properties and interactions of the porescale constituents. However, computationally it would be potentially impossible to resolve all the porescale details and interactions. For this reason multiscale models are developed to reduce the computational cost whilst still retaining important microstructural information.

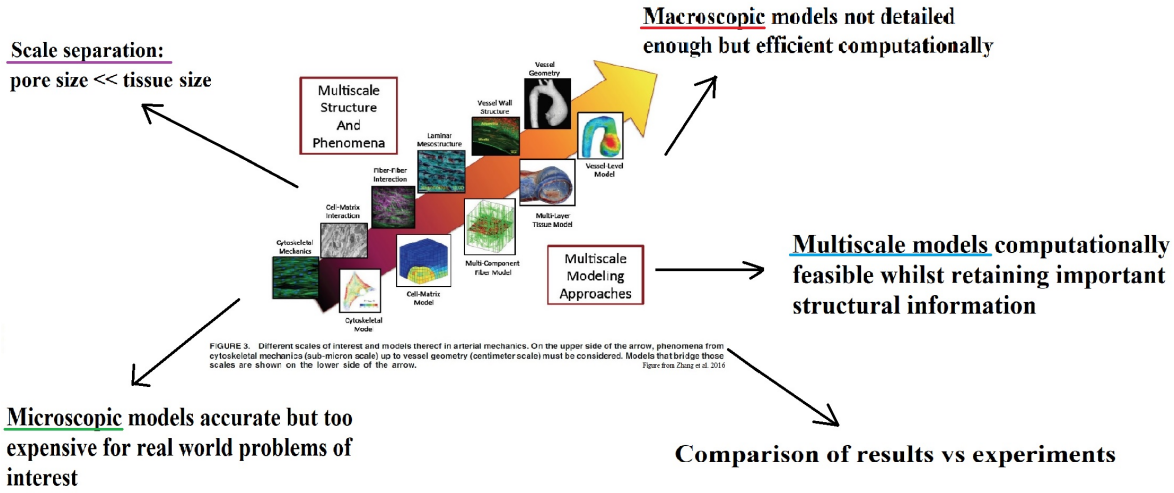

Figure 1.1: Image taken from [124] showing the different physical phenonmena occurring at different microstructural levels in the arteries and the modelling approaches to bridge the scales. The figure has been edited to add additional summary points relating to multiscale modelling.

For the reasons discussed previously, a variety of *homogenization techniques* have been developed. The coupled fluid–structure balance equations that describe the material on the porescale can be used in an upscaling process to obtain the macroscale governing equations of a poroelastic material. The upscaling process can be carried out by a variety of *homogenization* techniques. These homogenization techniques include effective medium theory, mixture theory, volume averaging and asymptotic homogenization. These techniques were discussed and described in [33, 51] where they provide a comparison between the alternative approaches for both fluid and solid mechanics, respectively.

The techniques effective medium theory and mixture theory represent micromechanical approximations which can provide an estimate of the macroscale coefficients for specific

geometries of the pores (such as ellipsoidal, penny-shaped or spherical), or for diluted pores (see, e.g. [25]), as well as closed form analytic formulas relating drained and undrained poroelastic coefficients, as those reported for example in [10, 65, 115]. Volume averaging approaches are suitable for deriving the functional form of the macroscale equations, and are based on relationships between the porescale and macroscale energy of the system, see also [51]. However, with volume averaging approaches the macroscale coefficients are usually not related to the underlying microstructure, and physical arguments and/or experimental data are to be supplemented in order to determine them. This is indeed a key difference between this technique and the asymptotic homogenization technique that allows for precise prescription of the macroscale coefficients.

The asymptotic homogenization technique ([4], [48], [68], [90]) exploits the sharp length scale separation which exists in the system to decouple spatial variations that occur on different scales. The relevant fields (e.g. velocities, displacements, and pressures) are expressed in terms of power series of the ratio between representative microscopic and macroscopic length scales. The resulting governing equations describe the behaviour of the system in terms of the leading (zero-th) order fields in a homogenized macroscale domain where the microstructure is smoothed out. This technique is in general characterized by a higher algebraic complexity compared to average fields approaches, however, it provides a precise prescription for computing the coefficients of the model. These are based on the solution of microstructural differential problems where the constitutive behaviour and geometrical arrangement of the individual phases is clearly specified.

In the asymptotic homogenization literature, the majority of the applications are focussed on linearised balance equations. This is due to the fact that in the linearised case, it is possible to fully decouple the porescale and the macroscale (under some simplifying assumptions). This decoupling then leads to a large reduction in the computational complexity of the system. In the literature, the homogenization of systems involving nonlinear mechanics is generally carried out by other homogenization techniques, such as average field techniques (see, e.g., [95, 96] and the references therein). These other techniques do not provide a precise description of the model coefficients in the way that the asymptotic homogenization technique can and, instead, provide bounds for the model coefficients.

The asymptotic homogenization technique has been applied to poroelastic materials by [19], [115] and [62]. The theory has since been extended to model a vast range of scenarios including growth of poroelastic materials [87], vascularised poroelastic materials [91].

Recently there has also been a development of the theory for nonlinear poroelastic materials. In [17], the effective poroelastic model of Biot was extended to a nonlinear Biot model that includes porescale deformation. In [28], a system of effective equations that describe the flow, elastic deformation and transport in an active medium was derived. The authors considered the spatial homogenization of a coupled transport and fluid–structure interaction model. In [102], the asymptotic homogenization technique was applied to the equations that describe the dynamics of a heterogeneous material with an evolving microstructure to obtain a set of effective equations. The heterogeneous body is assumed to be composed of two hyperelastic materials, and the evolution of the microstructure is through plastic-like distortions. The theory has also been investigated with various additional scales such as poroelastic materials with elastic inclusion [105] and [24].

Current poroelastic models focus on a microstructure where the deformable solid is homogeneous, this however is not in general representative of the biological tissue to which these theories are applied. In this thesis we aim to tackle this issue by extending the theory of poroelasticity to incorporate detailed microstructures that are more representative of the biological scenarios that we wish to study. We begin with a re-derivation of the model of standard Biot's poroelasticity in [92]. We then begin to extended the theory by incorporating a variety of different solid phases with the percolating fluid in a novel theoretical model for poroelastic composites [69]. This was then extended to the situation where the solid composite structure exhibits nonlinear elastic behaviour in our novel theoretical model for poroelastic composites [71]. Then by considering a hierarchical structure of the material we have proposed the novel model for double poroelastic materials [70], where the microstructure is composed of a variety of poroelastic materials with different properties. These models are applicable to a wide variety of biological scenarios, including bones, tendons, heart and lungs, with the added benefit that they all possess more microstructural detail than standard poroelasticity. We show the benefit of using a model with a more detailed microstructure than the standard poroelastic approach in [73]. We then can use the more detailed microstructural models to focus on the application to modelling the elastic parameters of the heart (both healthy and infarcted).

The models developed through this thesis have a wide range of applications. The linear elastic models can be straight away applied to hard hierarchical materials such as bones and tendons as these materials have small deformations. We can also take a piecewise linear approach to use the linear models for soft biological tissues such as the heart and

lungs. Or of course the nonlinear models are indeed a good fit for applications such as the heart, lungs and other soft biological tissues.

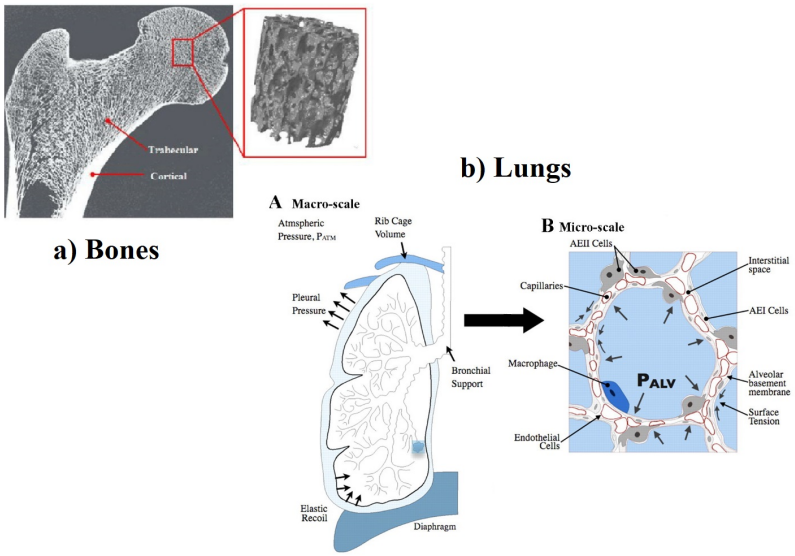

Figure 1.2: Image created from pictures found in [47], [104], showing the different potential biological applications, with their microstructure, for the models developed in this thesis.

The bones can be modelled by a poroelastic approach. In Fig. 1.2 we can see that the bones have a matrix made of collegen and mineral with water interplaying through the pores [30, 117].

In particular, the lungs have previously been approached in a biphasic (tissue and air) manner [9]. However, the lung microstructure is more complex, and there exist collagen and elastin fibres embedded in the matrix and in the fluid, so it could therefore be beneficial to use a more detailed microstructural approach to modelling, such as a nonlinear poroelastic composite. Another key example in the modelling of arteries. the work [121] considers the interaction between pulsatile blood flow and the arterial wall mechanics. The blood flow was modelled as an incompressible viscous fluid, confined by Biot's equations of poroelasticity for the artery wall. Since artery wall microstructure is not homogeneous, it would be appropriate to consider as a poroelastic composite or a double poroelastic material.

The heart muscle has three layers, the middle of which is the myocardium that has a structure where there are cardiac myocytes (muscle cells) embedded in a collagen matrix, which is produced by the cardiac fibroblasts, with an interconnected fluid (blood) flow through permeating vasculature. These structures are visible on a microscale length which

is much smaller than the size of the heart muscle. The myocardial microstructure is complex geometrically and is strongly impacted by a variety of diseases, in particular myocardial infarction (heart attack). In the case of myocardial infarction blood flow is reduced to an area of myocardium tissue, this results in the death of the cardiac myocytes and in their place, we find collagen rich scar tissue produced by the fibroblasts to retain the structural integrity of the myocardium [39], [54]. The size and amount of scar tissue affects the heart's functionality post recovery [38]. As a result of the loss of cardiac myocytes, the remaining myocytes in the area surrounding the infarct increase in volume to attempt to retain homeostasis in the heart [59]. The growth and remodelling of the surviving myocytes corresponds to the infarct size [79], [78], [3].

There have been a variety of approaches taken to model the heart summarised in the review articles [84], [80], [108]. The most prominent of these include constitutive non-linear elastic approaches using Holzapfel-Ogden Law [50]. The work [50] describes the myocardium as a non-homogeneous, anisotropic, nonlinear elastic and incompressible material and then proposes a general theoretical framework that uses invariants associated with the three orthogonal directions that can be identified within the material. This method proposes a strain energy function for the materials with parameters that are informed from biological measurements. This work has paved the way for a variety of extensions in an attempt to understand the phenomena of the heart behaviour such as in [45] and [116], and different methods of numerical implementation such as [94]. A viscoelastic approach to understanding the myocardium has also been taken by [43] and [76]. Within these works there is the aim to address the viscoelastic phenonmena observed experimentally by modifying the constitutive laws previously used for the myocardium. There has also been a poroelastic approach taken by [66], [29] and [23]. This approach aims to incorporate the porescale fluid flow into the overall behaviour of the myocardium and to consider the perfused muscle. Our novel model in this thesis aims to investigate how the microstructural changes induced by myocardial infarction affect the elastic parameters of the heart.

In Chapter 2 we provide a re-derivation of the governing equations of poroelasticity. This chapter can be thought of as the starting point from which the following chapters develop theoretically and numerically. In Chapter 3 we extend the theory by deriving a novel model for poroelastic composites. This model extends standard poroelasticity by describing the interactions of multiple solid and elastic phases at the porescale and therefore is

more biologically realistic. We then extend this work in Chapter 4 by extending to nonlinear poroelastic composites which is among the first nonlinear asymptotic homogenization works and can be useful in modelling the heart and lungs. In Chapter 5 we propose a novel model for a multiscale structure that upscales the governing equations of poroelasticity to obtain a theoretical model for double poroelastic materials, where the new model can account for the difference in a complete set of poroelastic parameters. In Chapter 6 we investigate numerically the benefit of using a model with a more detailed microstructure compared with standard poroelasticity when considering the elastic parameters. In Chapter 7 we investigate the elastic parameters of the heart (healthy and infarcted) using our novel model for poroelastic composites. Finally in Chapter 8 we provide some concluding remarks.

Chapter 2

Introduction to the theory of poroelasticity

In this chapter we focus on the derivation of the equations of poroelasticity for a porous, elastic material characterized by a Newtonian incompressible fluid flowing, at low Reynolds number, in the pores (which is often the case for biological tissues), and we embrace the asymptotic homogenization technique to derive the macroscale system of partial differential equations (PDEs). In Sec. 2.1 we introduce the fluid-structure interaction problem for our stucture, which we then non-dimensionalise in Sec. 2.2. We then apply the asymptotic homogenization technique in Sec. 2.3 to upscale the fluid-structure interaction problem to obtain the system of governing macroscale PDEs which we present in Sec. 2.4. Overall this chapter aims to provide an introductory example of applying the asymptotic homogenization technique that will be applied to a variety of scenarios in the chapters that follow and also to introduce the macroscale model of poroelastic materials that the novel models derived in the following chapters build upon and advance.

2.1 The fluid-structure interaction formulation

We begin by considering a set $\Omega \in \mathbb{R}^3$ where Ω is the union of a porous solid compartment Ω_s and a fluid compartment Ω_f satisfying $\bar{\Omega} = \bar{\Omega}_\mathrm{s} \cup \bar{\Omega}_\mathrm{f}$, where the $\bar{\ }$ denotes that the boundaries are included in each domain. We assume a structure where the typical length scale of the pores, denoted by d, is small compared to the size of the domain, which we

denote L. This means that we have the ratio

$$\frac{d}{L} = \epsilon \ll 1. \tag{2.1}$$

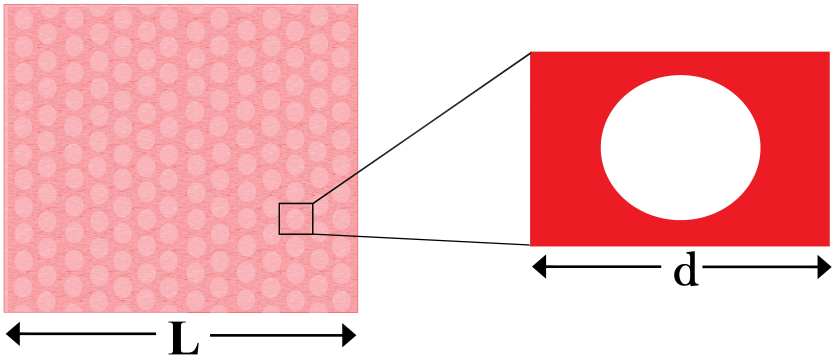

Figure 2.1: A 2D sketch representing the domain Ω, where the domain has length L and it is shown that the pores have length d.

We make the assumption that the porous solid compartment is an anisotropic linear elastic solid, the mechanics of which can be described by

$$\nabla \cdot \mathbf{T}_\mathrm{s} = 0 \quad \text{in} \quad \Omega_\mathrm{s}, \tag{2.2}$$

where we have that $\mathbf{T}_\mathrm{s}$ is the solid stress tensor. We then can define the solid Cauchy stress tensor by

$$\mathbf{T}_\mathrm{s} = \mathbb{C}\nabla\mathbf{u}, \tag{2.3}$$

where $\mathbf{u}$ is the elastic displacement in the porous solid and $\mathbb{C}$ is the fourth rank elasticity tensor with components C_{ijkl}. We note that $\mathbb{C}$ is equipped with major and minor symmetries namely,

$$C_{ijkl} = C_{ijlk}, \tag{2.4}$$

$$C_{ijkl} = C_{klij}, \tag{2.5}$$

and therefore also left minor symmetries follow by combining (2.4-2.5). In particular, by applying right minor symmetries we can equivalently rewrite the constitutive equation (2.3)

$$\mathsf{T}_\mathrm{s} = \mathbb{C}\xi(\mathbf{u}), \tag{2.6}$$

where

$$\xi(\bullet) = \frac{\nabla(\bullet) + (\nabla(\bullet))^T}{2} \tag{2.7}$$

In the fluid compartment we begin with Navier Stokes equation

$$\rho \frac{D\mathbf{v}}{Dt} = \nabla \cdot \mathbf{T}_\mathrm{f} + \mathbf{b} \tag{2.8}$$

where $\frac{D}{Dt}$ is the material time derivative. Since we are considering a quasi-static regime, neglecting inertia and with no body forces this reduces to

$$\nabla \cdot \mathbf{T}_\mathrm{f} = 0 \quad \text{in} \quad \Omega_\mathrm{f}, \tag{2.9}$$

where $\mathbf{T}_\mathrm{f}$ is the fluid stress tensor which is defined by

$$\mathbf{T}_\mathrm{f} = -p\mathbf{I} + 2\mu\xi(\mathbf{v}) \quad \text{with} \quad \xi(\mathbf{v}) = \frac{\nabla\mathbf{v} + (\nabla\mathbf{v})^\mathrm{T}}{2} \tag{2.10}$$

and $\mathbf{v}$, p, μ are the fluid velocity, pressure and viscosity, respectively. The incompressibility constraint reads

$$\nabla \cdot \mathbf{v} = 0 \quad \text{in} \quad \Omega_\mathrm{f}. \tag{2.11}$$

We note here that computing the divergence of $\mathbf{T}_\mathrm{f}$ in (2.10) using (2.11) gives

$$\mu\nabla^2\mathbf{v} = \nabla p, \tag{2.12}$$

which represents, together with constraint (2.11), the Stokes' problem for an incompressible Newtonian fluid. We now need to setup an appropriate fluid-structure interaction problem between the fluid and solid phases. We therefore require interface conditions across the interface between Ω_s and Ω_f. We define the boundary between the phases as $\Gamma := \partial\Omega_\mathrm{s} \cap \partial\Omega_\mathrm{f}$ and assume continuity of velocities and tractions across the interface, namely

$$\dot{\mathbf{u}} = \mathbf{v} \qquad \text{on} \quad \Gamma \tag{2.13}$$

$$\mathbf{T}_\mathrm{f}\mathbf{n} = \mathbf{T}_\mathrm{s}\mathbf{n} \qquad \text{on} \quad \Gamma, \tag{2.14}$$

where $\dot{\mathbf{u}}$ is the solid velocity.

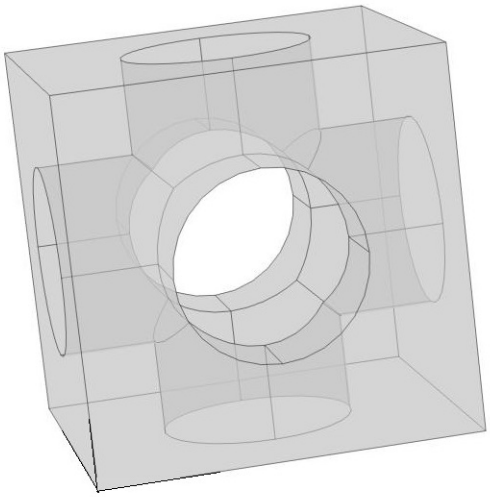

Figure 2.2: A 3D sketch representing a single periodic cell in our structure. We have the fluid, which is three interconnected cylinders and the solid elastic phase.

We can sketch a 2D schematic of this structure as follows.

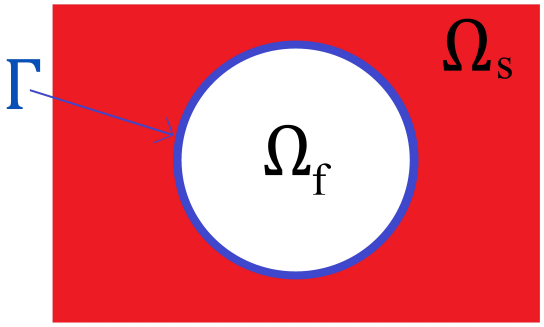

Figure 2.3: A 2D sketch representing a single periodic cell in our structure. We have the fluid, which is a cross-section of three interconnected cylinders, shown in white and the solid elastic phase shown in red and their interface Γ is highlighted in blue.

2.2 Non-dimensionalization of the FSI problem

It is important to formulate the model in non-dimensional form in order to understand the proper asymptotic behaviour of the model with respect to the scale separation parameter ϵ. We rescale using

$$\begin{gathered}\mathbf{x} = L\mathbf{x}', \quad \nabla = \frac{1}{L}\nabla', \quad \mathbb{C} = C_p L\mathbb{C}', \quad \mathbf{u} = L\mathbf{u}', \quad \mathbf{v} = \frac{C_p d^2}{\mu}\mathbf{v}', \\ \mathbf{T}_\mathrm{s} = C_p L\mathbf{T}'_\mathrm{s}, \quad \mathbf{T}_\mathrm{f} = C_p L\mathbf{T}'_\mathrm{f}, \quad p = C_p L p'\end{gathered} \tag{2.15}$$

where C_p is the characteristic pressure gradient. Then using (2.15) and dropping the primes for simplicity of notation, equations (2.2), (2.3), (2.10)−(2.14) become

$$\nabla \cdot (\mathbb{C}\xi(\mathbf{u})) = 0 \qquad \text{in} \quad \Omega_{\mathrm{s}} \tag{2.16}$$

$$\nabla \cdot \mathbf{T}_{\mathrm{f}} = 0 \qquad \text{in} \quad \Omega_{\mathrm{f}} \tag{2.17}$$

$$-p\mathbf{I} + \epsilon^2(\nabla\mathbf{v} + (\nabla\mathbf{v})^{\mathrm{T}}) = \mathbf{T}_{\mathrm{f}} \qquad \text{in} \quad \Omega_{\mathrm{f}} \tag{2.18}$$

$$\dot{\mathbf{u}} = \mathbf{v} \qquad \text{on} \quad \Gamma \tag{2.19}$$

$$\epsilon^2\nabla^2\mathbf{v} = \nabla p \qquad \text{in} \quad \Omega_{\mathrm{f}} \tag{2.20}$$

$$\mathbf{T}_{\mathrm{f}}\mathbf{n} = \mathbf{T}_{\mathrm{s}}\mathbf{n} \qquad \text{on} \quad \Gamma \tag{2.21}$$

$$\mathbf{T}_{\mathrm{s}} = \mathbb{C}\xi(\mathbf{u}) \qquad \text{in} \quad \Omega_{\mathrm{s}} \tag{2.22}$$

$$\nabla \cdot \mathbf{v} = 0 \qquad \text{in} \quad \Omega_{\mathrm{f}} \tag{2.23}$$

$$\nabla \cdot \mathbf{T}_{\mathrm{s}} = 0 \qquad \text{in} \quad \Omega_{\mathrm{s}}. \tag{2.24}$$

2.3 The Asymptotic Homogenization Technique

Within this section we will use a two-scale asymptotic expansion to derive a macroscale model for the equations (2.16) − (2.24). Since $\epsilon \ll 1$, we can enforce a sharp length scale separation between the microscale d and the macroscale L with

$$\mathbf{y} = \frac{\mathbf{x}}{\epsilon}. \tag{2.25}$$

We will now be assuming that $\mathbf{x}$ and $\mathbf{y}$ are independent variables which represent the macroscale and the microscale respectively. We also have that the elasticity tensor $\mathbb{C} = \mathbb{C}(\mathbf{x}, \mathbf{y})$ (i.e. is a function of both variables) and the gradient operator becomes

$$\nabla \to \nabla_{\mathbf{x}} + \frac{1}{\epsilon}\nabla_{\mathbf{y}}. \tag{2.26}$$

We now can perform the multiple scales expansion in power series of ϵ for every field φ. In particular, we assume that the latter, which collectively denotes each field and material property appearing in (2.16)−(2.24), is given by

$$\varphi^{\epsilon}(\mathbf{x}, \mathbf{y}, t) = \sum_{l=0}^{\infty} \varphi^{(l)}(\mathbf{x}, \mathbf{y}, t)\epsilon^l. \tag{2.27}$$

We also assume regularity of the microstructure, so that we have $\varphi^{(l)}$ and $\mathbb{C}$ are $\mathbf{y}$-periodic. Applying the asymptotic homogenization technique the equations (2.16) – (2.24) then become

$$\nabla_{\mathbf{y}} \cdot (\mathbb{C}\xi_{\mathbf{y}}(\mathbf{u}^\epsilon)) + \epsilon\nabla_{\mathbf{y}} \cdot (\mathbb{C}\xi_{\mathbf{x}}(\mathbf{u}^\epsilon)) + \epsilon\nabla_{\mathbf{x}} \cdot (\mathbb{C}\xi_{\mathbf{y}}(\mathbf{u}^\epsilon)) + \epsilon^2\nabla_{\mathbf{x}} \cdot (\mathbb{C}\xi_{\mathbf{x}}(\mathbf{u}^\epsilon)) = 0 \tag{2.28}$$

$$\nabla_{\mathbf{y}} \cdot \mathbf{T}^\epsilon{}_{\mathrm{f}} + \epsilon\nabla_{\mathbf{x}} \cdot \mathbf{T}^\epsilon{}_{\mathrm{f}} = 0 \tag{2.29}$$

$$\mathbf{T}^\epsilon{}_{\mathrm{f}} = -p^\epsilon\mathbf{I} + \epsilon(\nabla_{\mathbf{y}}\mathbf{v}^\epsilon + (\nabla_{\mathbf{y}}\mathbf{v}^\epsilon)^{\mathrm{T}}) + \epsilon^2(\nabla_{\mathbf{x}}\mathbf{v}^\epsilon + (\nabla_{\mathbf{x}}\mathbf{v}^\epsilon)^{\mathrm{T}}) \tag{2.30}$$

$$\dot{\mathbf{u}}^\epsilon = \mathbf{v}^\epsilon \tag{2.31}$$

$$\epsilon^3\nabla_{\mathbf{x}}^2\mathbf{v}^\epsilon + \epsilon^2\nabla_{\mathbf{x}} \cdot (\nabla_{\mathbf{y}}\mathbf{v}^\epsilon) + \epsilon^2\nabla_{\mathbf{y}} \cdot (\nabla_{\mathbf{x}}\mathbf{v}^\epsilon) + \epsilon\nabla_{\mathbf{y}}^2\mathbf{v}^\epsilon = \nabla_{\mathbf{y}}p^\epsilon + \epsilon\nabla_{\mathbf{x}}p^\epsilon \tag{2.32}$$

$$\mathbf{T}^\epsilon_{\mathrm{f}}\mathbf{n} = \mathbf{T}^\epsilon_{\mathrm{s}}\mathbf{n} \tag{2.33}$$

$$\epsilon\mathbf{T}^\epsilon_{\mathrm{s}} = \mathbb{C}\xi_{\mathbf{y}}(\mathbf{u}^\epsilon) + \epsilon\mathbb{C}\xi_{\mathbf{x}}(\mathbf{u}^\epsilon) \tag{2.34}$$

$$\nabla_{\mathbf{y}} \cdot \mathbf{v}^\epsilon + \epsilon\nabla_{\mathbf{x}} \cdot \mathbf{v}^\epsilon = 0 \tag{2.35}$$

$$\nabla_{\mathbf{y}} \cdot \mathbf{T}^\epsilon_{\mathrm{s}} + \epsilon\nabla_{\mathbf{x}} \cdot \mathbf{T}^\epsilon_{\mathrm{s}} = 0. \tag{2.36}$$

Remark 1. *We make the assumption of regularity of the microstructure for the sake of convenience. In order to solve the problem, we need to restrict our analysis to a finite subset of the given microstructure. By assuming* $\mathbf{y}$*-periodicity, we are achieving the desired restriction, although the equations of poroelasticity can be derived by assuming local boundedness of the fields only, see [19]. In the case of assuming local boundedness of the fields we can only obtain the functional form of the macroscale model. This is since the prescriptions of the coefficients obtained this way are related to microscale problems which are, in principle, to be solved on the whole microstructure. Therefore, they cannot be used in practice unless further geometrical restrictions, such as periodicity of the microstructure, are imposed. This is the advantage of the asymptotic homogenization technique versus RVE tecniques as we obtain a precise prescription of the model coefficients.*

2.4 Macroscopic Model

We substitute power series of the type (2.27) into the relevant fields in (2.28)−(2.36). Then by equating the coefficients of ϵ^l for $l = 0, 1, ...$ this allows us to derive the macroscale model for the poroelastic material in terms of the relevant leading order fields. Whenever a component in the asymptotic expansion retains a dependence on the microscale, we can

take the integral average, which we define as

$$\langle \varphi \rangle_i = \frac{1}{|\Omega|} \int_{\Omega_i} \varphi(\mathbf{x}, \mathbf{y}, t) d\mathbf{y} \quad i = \mathrm{f}, \mathrm{s}, \tag{2.37}$$

where the integral average can be performed over one representative cell due to the assumption of $\mathbf{y}$-periodicity and $|\Omega|$ is the volume of the periodic cell, with solid and fluid portions still denoted by Ω_s and Ω_f, respectively.

Equating coefficients of ϵ^0 in (2.28) – (2.36) gives

$$\nabla_\mathbf{y} \cdot (\mathbb{C}\xi_\mathbf{y}(\mathbf{u}^{(0)})) = 0 \qquad \text{in} \quad \Omega_\mathrm{s} \tag{2.38}$$

$$\nabla_\mathbf{y} \cdot \mathbf{T}_\mathrm{f}^{(0)} = 0 \qquad \text{in} \quad \Omega_\mathrm{f} \tag{2.39}$$

$$\mathbf{T}_\mathrm{f}^{(0)} = -p^{(0)}\mathbf{I} \qquad \text{in} \quad \Omega_\mathrm{f} \tag{2.40}$$

$$\dot{\mathbf{u}}^{(0)} = \mathbf{v}^{(0)} \qquad \text{on} \quad \Gamma \tag{2.41}$$

$$\nabla_\mathbf{y} p^{(0)} = 0 \qquad \text{in} \quad \Omega_\mathrm{f} \tag{2.42}$$

$$\mathbf{T}_\mathrm{f}^{(0)}\mathbf{n} = \mathbf{T}_\mathrm{s}^{(0)}\mathbf{n} \qquad \text{on} \quad \Gamma \tag{2.43}$$

$$\mathbb{C}\xi_\mathbf{y}(\mathbf{u}^{(0)}) = 0 \qquad \text{in} \quad \Omega_\mathrm{s} \tag{2.44}$$

$$\nabla_\mathbf{y} \cdot \mathbf{v}^{(0)} = 0 \qquad \text{in} \quad \Omega_\mathrm{f} \tag{2.45}$$

$$\nabla_\mathbf{y} \cdot \mathbf{T}_\mathrm{s}{}^{(0)} = 0 \qquad \text{in} \quad \Omega_\mathrm{s}. \tag{2.46}$$

Similarly we now wish to equate the coefficients of ϵ^1 in equations (2.28) – (2.36) which gives

$$\nabla_\mathbf{y} \cdot (\mathbb{C}\xi_\mathbf{y}(\mathbf{u}^{(1)})) + \nabla_\mathbf{y} \cdot (\mathbb{C}\xi_\mathbf{x}(\mathbf{u}^{(0)})) + \nabla_\mathbf{x} \cdot (\mathbb{C}\xi_\mathbf{y}(\mathbf{u}^{(0)})) = 0 \qquad \text{in} \quad \Omega_\mathrm{s} \tag{2.47}$$

$$\nabla_\mathbf{y} \cdot \mathbf{T}_\mathrm{f}^{(1)} + \nabla_\mathbf{x} \cdot \mathbf{T}_\mathrm{f}^{(0)} = 0 \qquad \text{in} \quad \Omega_\mathrm{f} \tag{2.48}$$

$$\mathbf{T}_\mathrm{f}^{(1)} = -p^{(1)}\mathbf{I} + (\nabla_\mathbf{y}\mathbf{v}^{(0)} + (\nabla_\mathbf{y}\mathbf{v}^{(0)})^\mathrm{T}) \qquad \text{in} \quad \Omega_\mathrm{f} \tag{2.49}$$

$$\dot{\mathbf{u}}^{(1)} = \mathbf{v}^{(1)} \qquad \text{on} \quad \Gamma \tag{2.50}$$

$$\nabla_\mathbf{y}^2 \mathbf{v}^{(0)} = \nabla_\mathbf{y} p^{(1)} + \nabla_\mathbf{x} p^{(0)} \qquad \text{in} \quad \Omega_\mathrm{f} \tag{2.51}$$

$$\mathbf{T}_\mathrm{f}^{(1)}\mathbf{n} = \mathbf{T}_\mathrm{s}^{(1)}\mathbf{n} \qquad \text{on} \quad \Gamma \tag{2.52}$$

$$\mathbf{T}_\mathrm{s}^{(0)} = \mathbb{C}\xi_\mathbf{y}(\mathbf{u}^{(1)}) + \mathbb{C}\xi_\mathbf{x}(\mathbf{u}^{(0)}) \qquad \text{in} \quad \Omega_\mathrm{s} \tag{2.53}$$

$$\nabla_\mathbf{y} \cdot \mathbf{v}^{(1)} + \nabla_\mathbf{x} \cdot \mathbf{v}^{(0)} = 0 \qquad \text{in} \quad \Omega_\mathrm{f} \tag{2.54}$$

$$\nabla_\mathbf{y} \cdot \mathbf{T}_\mathrm{s}{}^{(1)} + \nabla_\mathbf{x} \cdot \mathbf{T}_\mathrm{s}{}^{(0)} = 0 \qquad \text{in} \quad \Omega_\mathrm{s} \tag{2.55}$$

From equations (2.39) and (2.40) we can see that $p^{(0)}$ does not depend on the microscale $\mathbf{y}$, so

$$p^{(0)} = p^{(0)}(\mathbf{x}, t). \tag{2.56}$$

We also have from equation (2.44) that $\mathbf{u}^{(0)}$ is a rigid body motion and therefore, by $\mathbf{y}$-periodicity

$$\mathbf{u}^{(0)} = \mathbf{u}^{(0)}(\mathbf{x}, t) \tag{2.57}$$

does not depend on the microscale $\mathbf{y}$.

2.4.1 Fluid Flow on the Macroscale

We now wish to investigate the leading order of the velocity which we denoted $\mathbf{v}^{(0)}$. We can define

$$\mathbf{w}(\mathbf{x}, \mathbf{y}, t) = \mathbf{v}^{(0)}(\mathbf{x}, \mathbf{y}, t) - \dot{\mathbf{u}}^{(0)}(\mathbf{x}, \mathbf{y}, t), \tag{2.58}$$

where $\mathbf{w}$ is the relative fluid-solid velocity. Using equations (2.40), (2.41), (2.48) and (2.49) we have a Stokes'-type periodic boundary value problem which is given by

$$\nabla_{\mathbf{y}}^2 \mathbf{w} - \nabla_{\mathbf{y}} p^{(1)} - \nabla_{\mathbf{x}} p^{(0)} = \mathbf{0} \qquad \text{in} \quad \Omega_{\mathrm{f}} \tag{2.59}$$

$$\nabla_{\mathbf{y}} \cdot \mathbf{w} = \mathbf{0} \qquad \text{in} \quad \Omega_{\mathrm{f}} \tag{2.60}$$

$$\mathbf{w} = \mathbf{0} \qquad \text{on} \quad \Gamma, \tag{2.61}$$

equipped with periodicity conditions on $\partial\Omega_{\mathrm{f}} \setminus \Gamma$. Exploiting linearity and using (2.56), we state the following ansatz

$$\mathbf{w} = -W \nabla_{\mathbf{x}} p^{(0)}, \tag{2.62}$$

$$p^{(1)} = -\boldsymbol{\Pi} \nabla_{\mathbf{x}} p^{(0)} + c(\mathbf{x}), \tag{2.63}$$

where $p^{(1)}$ is defined up to an arbitrary $\mathbf{y}$-constant function, $c(\mathbf{x})$. Equation (2.63) is the solution of the problem (2.59-2.61) provided that the auxiliary second rank tensor W and vector $\boldsymbol{\Pi}$ satisfy the following cell problem

$$\begin{cases} \nabla_{\mathbf{y}}^2 W^{\mathrm{T}} - \nabla_{\mathbf{y}} \boldsymbol{\Pi} + \mathbf{I} = \mathbf{0} & \text{in} \quad \Omega_{\mathrm{f}} \\ \nabla_{\mathbf{y}} \cdot W^{\mathrm{T}} = \mathbf{0} & \text{in} \quad \Omega_{\mathrm{f}} \\ W = \mathbf{0} & \text{on} \quad \Gamma, \end{cases} \tag{2.64}$$

where once again periodic conditions apply to the boundary $\partial\Omega_{\mathrm{f}}\backslash\Gamma$ and a further condition is to be imposed on $\mathbf{\Pi}$ for the solution to be unique (e.g. zero average on periodic cell). Taking the integral average of (2.62) over the fluid domain and keeping in mind the definition (2.58) we have

$$\langle \mathbf{w} \rangle_{\mathrm{f}} = -\langle W \rangle_{\mathrm{f}} \nabla_{\mathbf{x}} p^{(0)}, \tag{2.65}$$

i.e. the average relative leading order fluid velocity is described by Darcy's law.

2.4.2 Poroelasticity on the Macroscale

We now require the macroscale equations to close the system for the solid elastic displacement $\mathbf{u}^{(0)}$ and the fluid pressure $p^{(0)}$. Summing up the cell averages of equations (2.48) and (2.55) over Ω_{s} and Ω_{f}, respectively we have

$$\int_{\Omega_{\mathrm{s}}} \nabla_{\mathbf{y}} \cdot \mathbf{T}_{\mathrm{s}}^{(1)} \mathrm{d}\mathbf{y} + \int_{\Omega_{\mathrm{f}}} \nabla_{\mathbf{y}} \cdot \mathbf{T}_{\mathrm{f}}^{(1)} \mathrm{d}\mathbf{y} + \int_{\Omega_{\mathrm{s}}} \nabla_{\mathbf{x}} \cdot \mathbf{T}_{\mathrm{s}}^{(0)} \mathrm{d}\mathbf{y} + \int_{\Omega_{\mathrm{f}}} \nabla_{\mathbf{x}} \cdot \mathbf{T}_{\mathrm{f}}^{(0)} \mathrm{d}\mathbf{y} = 0. \tag{2.66}$$

Applying the divergence theorem with respect to $\mathbf{y}$ to the first two integrals and rearranging the last two terms we obtain

$$\begin{aligned} &\int_{\partial\Omega_{\mathrm{s}}/\Gamma} \mathbf{T}_{\mathrm{s}}^{(1)} \mathbf{n}_{\Omega_{\mathrm{s}}} \mathrm{dS} - \int_{\Gamma} \mathbf{T}_{\mathrm{s}}^{(1)} \mathbf{n} \mathrm{dS} + \int_{\partial\Omega_{\mathrm{f}}/\Gamma} \mathbf{T}_{\mathrm{f}}^{(1)} \mathbf{n}_{\Omega_{\mathrm{f}}} \mathrm{dS} \\ &+ \int_{\Gamma} \mathbf{T}_{\mathrm{f}}^{(1)} \mathbf{n} \mathrm{dS} + \nabla_{\mathbf{x}} \cdot \int_{\Omega_{\mathrm{s}}} \mathbf{T}_{\mathrm{s}}^{(0)} \mathrm{d}\mathbf{y} + \nabla_{\mathbf{x}} \cdot \int_{\Omega_{\mathrm{f}}} \mathbf{T}_{\mathrm{f}}^{(0)} \mathrm{d}\mathbf{y} = 0, \end{aligned} \tag{2.67}$$

where we recall that $\mathbf{n}$ is the unit outward normal to Γ with respect to the fluid region Ω_{f}, which is therefore pointing into the solid region, i.e. the corresponding unit outward normal to Γ with respect to the solid region Ω_{s} is given by $-\mathbf{n}$. The unit vectors $\mathbf{n}_{\Omega_{\mathrm{s}}}$ and $\mathbf{n}_{\Omega_{\mathrm{f}}}$ are the outward normals corresponding to $\partial\Omega_{\mathrm{s}}/\Gamma$ and $\partial\Omega_{\mathrm{f}}/\Gamma$, respectively.

Remark 2. *In equation* (2.67) *we have assumed that the microstructure is macroscopically uniform, i.e. the periodic cell portions* Ω_{s} *and* Ω_{f} *do not retain any parametric dependence on the macroscale variable* $\mathbf{x}$*. This assumption can in principle be relaxed by assuming that the medium is not macroscopically uniform. This way, only local periodicity is assumed, whereas the periodic representative cell is parametrically varying with respect to the macroscale coordinate, leading to macroscopically heterogeneous coefficients and additional terms in* (2.67) *due to proper application of the generalized Reynolds transport theorem. This approach [86, 87] requires the solution of a periodic cell problem (of the type solved in the present manuscript) for each point of the macroscale domain, thus leading to an*

increase in the computational cost, although alternative strategies to reduce it are rapidly emerging in the literature, see, e.g. [32].

Since the contributions over the external boundaries of Ω_s and Ω_f cancel out due to $\mathbf{y}$-periodicity (2.67) becomes

$$-\int_\Gamma \mathbf{T}_\mathrm{s}^{(1)}\mathbf{n}\mathrm{dS} + \int_\Gamma \mathbf{T}_\mathrm{f}^{(1)}\mathbf{n}\mathrm{dS} + \nabla_\mathbf{x}\cdot\int_{\Omega_\mathrm{s}} \mathbf{T}_\mathrm{s}^{(0)}\mathrm{d}\mathbf{y} + \nabla_\mathbf{x}\cdot\int_{\Omega_\mathrm{f}} \mathbf{T}_\mathrm{f}^{(0)}\mathrm{d}\mathbf{y} = 0. \tag{2.68}$$

Since equation (2.52) holds, the first two terms in (2.68) disappear and the final two terms become

$$\nabla_\mathbf{x}\cdot\langle\mathbf{T}_\mathrm{s}^{(0)}\rangle_\mathrm{s} - \phi\nabla_\mathbf{x}p^{(0)} = 0, \tag{2.69}$$

where $\phi := |\Omega_\mathrm{f}|/|\Omega|$ is the porosity of the material.

Exploiting (2.56) and (2.57) we can write equations (2.43), (2.46) and (2.53) as the following problem for $\mathbf{u}^{(1)}$

$$\nabla_\mathbf{y}\cdot(\mathbb{C}\xi_\mathbf{y}(\mathbf{u}^{(1)})) + \nabla_\mathbf{y}\cdot(\mathbb{C}\xi_\mathbf{x}(\mathbf{u}^{(0)})) = 0 \qquad \text{in} \quad \Omega_\mathrm{s} \tag{2.70}$$

$$(\mathbb{C}\xi_\mathbf{y}(\mathbf{u}^{(1)}) + \mathbb{C}\xi_\mathbf{x}(\mathbf{u}^{(0)}))\mathbf{n} = -p^{(0)}\mathbf{n} \qquad \text{on} \quad \Gamma, \tag{2.71}$$

with $\mathbf{y}$-periodicity in Ω_s. Due to local periodicity $\mathbf{u}^{(1)}$ is a bounded vector function of $\mathbf{y}$. The solution to the problem given by equations (2.70) and (2.71), exploiting linearity, is given as

$$\mathbf{u}^{(1)} = A\xi_\mathbf{x}(\mathbf{u}^{(0)}) + \mathbf{a}p^{(0)}, \tag{2.72}$$

where A is a tensor of order 3 and $\mathbf{a}$ is a vector. This is provided that the auxiliary quantities A and $\mathbf{a}$ solve the following cell problems. We have

$$\begin{cases} \nabla_\mathbf{y}\cdot(\mathbb{C}\xi_\mathbf{y}(A)) + \nabla_\mathbf{y}\cdot\mathbb{C} = 0 \quad \text{in} \quad \Omega_\mathrm{s} \\ \qquad (\mathbb{C}\xi_\mathbf{y}(A))\mathbf{n} + \mathbb{C}\mathbf{n} = 0 \quad \text{on} \quad \Gamma, \end{cases} \tag{2.73}$$

and

$$\begin{cases} \nabla_\mathbf{y}\cdot(\mathbb{C}\xi_\mathbf{y}(\mathbf{a})) = \mathbf{0} \quad \text{in} \quad \Omega_\mathrm{s} \\ (\mathbb{C}\xi_\mathbf{y}(\mathbf{a}) + \mathbf{I})\mathbf{n} = \mathbf{0} \quad \text{on} \quad \Gamma. \end{cases} \tag{2.74}$$

To ensure the uniqueness of the solution, we also require a further condition on A and $\mathbf{a}$,

for example:

$$\langle A\rangle_{\mathrm{s}} = 0 \quad \text{and} \quad \langle \mathbf{a}\rangle_{\mathrm{s}} = \mathbf{0}. \tag{2.75}$$

Since we have that $\mathbf{u}^{(1)}$ is related to $\mathbf{T}_{\mathrm{s}}^{(0)}$ in equation (2.53), then (2.72) shows that $\mathbf{T}_{\mathrm{s}}^{(0)}$ is a function of the gradient of $\mathbf{u}^{(0)}$ and $p^{(0)}$. Substituting $\mathbf{u}^{(1)}$ into equation (2.53) gives

$$\mathbf{T}_{\mathrm{s}}^{(0)} = \mathbb{C}\mathbb{M}\xi_{\mathbf{x}}(\mathbf{u}^{(0)}) + \mathbb{C}Qp^{(0)} + \mathbb{C}\xi_{\mathbf{x}}(\mathbf{u}^{(0)}), \tag{2.76}$$

where we have fourth rank tensor $\mathbb{M}$ and second rank tensor Q defined as

$$\mathbb{M} = \nabla_{\mathbf{y}} A \qquad \text{and} \qquad Q = \nabla_{\mathbf{y}}\mathbf{a}. \tag{2.77}$$

Then taking the integral average of (2.76) over the solid domain we obtain

$$\langle \mathbf{T}_{\mathrm{s}}^{(0)}\rangle_{\mathrm{s}} = \langle \mathbb{C}\mathbb{M} + \mathbb{C}\rangle_{\mathrm{s}}\xi_{\mathbf{x}}(\mathbf{u}^{(0)}) + \langle \mathbb{C}Q\rangle_{\mathrm{s}} p^{(0)}. \tag{2.78}$$

From (2.69) we have

$$\nabla_{\mathbf{x}} \cdot \mathbf{T}_{\mathrm{Eff}} = 0, \tag{2.79}$$

where we can define $\mathbf{T}_{\mathrm{Eff}}$ as

$$\begin{aligned} \mathbf{T}_{\mathrm{Eff}} &:= \langle \mathbf{T}_{\mathrm{s}}^{(0)}\rangle_{\mathrm{s}} - \phi p^{(0)}\mathbf{I} \\ &= \langle \mathbb{C}\mathbb{M} + \mathbb{C}\rangle_{\mathrm{s}} \nabla_{\mathbf{x}}\mathbf{u}^{(0)} + (\langle \mathbb{C}Q\rangle_{\mathrm{s}} - \phi\mathbf{I})p^{(0)}, \end{aligned} \tag{2.80}$$

as the effective stress. We can describe (2.79) and (2.80) as the average force balance equations for the poroelastic material.

We now return to the incompressibility constraint equation (2.54) and integrate. Applying the divergence theorem to the first integral, then using (2.50) and applying the divergence theorem again we obtain

$$0 = -\int_{\Omega_{\mathrm{s}}} \mathrm{Tr}(\nabla_{\mathbf{y}}\dot{\mathbf{u}}^{(1)})\mathrm{d}\mathbf{y} + \nabla_{\mathbf{x}} \cdot \langle \mathbf{v}^{(0)}\rangle_{\mathrm{f}}. \tag{2.81}$$

That is,

$$\nabla_{\mathbf{x}} \cdot \langle \mathbf{v}^{(0)}\rangle_{\mathrm{f}} = \langle \mathrm{Tr}(\nabla_{\mathbf{y}}\dot{\mathbf{u}}^{(1)})\rangle_{\mathrm{s}}. \tag{2.82}$$

Using (2.72) and (2.77) we have that

$$\nabla_{\mathbf{y}}\mathbf{u}^{(1)} = \mathbb{M}\nabla_{\mathbf{x}}\mathbf{u}^{(0)} + Qp^{(0)}, \tag{2.83}$$

and taking the time derivative we obtain

$$\nabla_{\mathbf{y}}\dot{\mathbf{u}}^{(1)} = \mathbb{M}\nabla_{\mathbf{x}}\dot{\mathbf{u}}^{(0)} + Q\dot{p}^{(0)}. \tag{2.84}$$

Therefore we can rewrite (2.82) by taking the integral average over the solid domain of the trace of (2.84). That is,

$$\nabla_{\mathbf{x}} \cdot \langle \mathbf{v}^{(0)} \rangle_{\mathrm{f}} = \langle \mathrm{Tr}\mathbb{M} \rangle_{\mathrm{s}} : \nabla_{\mathbf{x}}\dot{\mathbf{u}}^{(0)} + \langle \mathrm{Tr}Q \rangle_{\mathrm{s}}\dot{p}^{(0)}. \tag{2.85}$$

Returning to the expression for relative fluid-solid velocity, (2.58), restated here for convenience, we have that

$$\mathbf{w}(\mathbf{x}, \mathbf{y}, t) = \mathbf{v}^{(0)}(\mathbf{x}, \mathbf{y}, t) - \dot{\mathbf{u}}^{(0)}(\mathbf{x}, t). \tag{2.86}$$

Then taking the cell average over the fluid domain we obtain

$$\langle \mathbf{w} \rangle_{\mathrm{f}} = \langle \mathbf{v}^{(0)} \rangle_{\mathrm{f}} - \phi\dot{\mathbf{u}}^{(0)}, \tag{2.87}$$

where we can define the porosity as $\phi := |\Omega_{\mathrm{f}}|/|\Omega|$. Rearranging (2.87) gives

$$\langle \mathbf{v}^{(0)} \rangle_{\mathrm{f}} = \langle \mathbf{w} \rangle_{\mathrm{f}} + \phi\dot{\mathbf{u}}^{(0)}. \tag{2.88}$$

Then using (2.88), we can rewrite (2.85) as

$$\nabla_{\mathbf{x}} \cdot (\langle \mathbf{w} \rangle_{\mathrm{f}} + \phi\dot{\mathbf{u}}^{(0)}) = \langle \mathrm{Tr}\mathbb{M} \rangle_{\mathrm{s}} : \nabla_{\mathbf{x}}\dot{\mathbf{u}}^{(0)} + \langle \mathrm{Tr}Q \rangle_{\mathrm{s}}\dot{p}^{(0)}, \tag{2.89}$$

where we can expand the left hand side to obtain

$$\nabla_{\mathbf{x}} \cdot \langle \mathbf{w} \rangle_{\mathrm{f}} + \phi\nabla_{\mathbf{x}} \cdot \dot{\mathbf{u}}^{(0)} = \langle \mathrm{Tr}\mathbb{M} \rangle_{\mathrm{s}} : \nabla_{\mathbf{x}}\dot{\mathbf{u}}^{(0)} + \langle \mathrm{Tr}Q \rangle_{\mathrm{s}}\dot{p}^{(0)}. \tag{2.90}$$

We should note that we can write $\phi\nabla_{\mathbf{x}} \cdot \dot{\mathbf{u}}^{(0)}$ as $\phi\mathbf{I} : \nabla_{\mathbf{x}}\dot{\mathbf{u}}^{(0)}$ in equation (2.90) and we also note that $\phi = \text{Constant}$ due to the assumed geometric uniformity. We can now rearrange

(2.90) to determine an expression for $\dot{p}^{(0)}$. That is,

$$\dot{p}^{(0)} = \frac{1}{\langle \mathrm{Tr}Q\rangle_{\mathrm{s}}}\big(\nabla_{\mathbf{x}} \cdot \langle \mathbf{w}\rangle_{\mathrm{f}} + (\phi\mathbf{I} - \langle \mathrm{Tr}\mathbb{M}\rangle_{\mathrm{s}}) : \nabla_{\mathbf{x}}\dot{\mathbf{u}}^{(0)}\big), \tag{2.91}$$

where we can define

$$M := \frac{-1}{\langle \mathrm{Tr}Q\rangle_{\mathrm{s}}} \quad \text{and} \quad \boldsymbol{\alpha} := \phi\mathbf{I} - \langle \mathrm{Tr}\mathbb{M}\rangle_{\mathrm{s}}. \tag{2.92}$$

It is important to consider that in the case of isotropy that $\boldsymbol{\alpha}$ in (2.92) will reduce to $\boldsymbol{\alpha} = \alpha\mathbf{I}$. Continuing we can re-write (2.91) using (2.92) as

$$\dot{p}^{(0)} = -M(\nabla_{\mathbf{x}} \cdot \langle \mathbf{w}\rangle_{\mathrm{f}} + \boldsymbol{\alpha} : \nabla_{\mathbf{x}}\dot{\mathbf{u}}^{(0)}). \tag{2.93}$$

Then dividing through by M gives

$$\frac{\dot{p}^{(0)}}{M} = -\nabla_{\mathbf{x}} \cdot \langle \mathbf{w}\rangle_{\mathrm{f}} - \boldsymbol{\alpha} : \nabla_{\mathbf{x}}\dot{\mathbf{u}}^{(0)}, \tag{2.94}$$

and when $M \to +\infty$ and in the case of isotropy we have

$$\nabla_{\mathbf{x}} \cdot \langle \mathbf{w}\rangle_{\mathrm{f}} + \alpha \cdot \nabla_{\mathbf{x}}\dot{\mathbf{u}}^{(0)} = 0, \tag{2.95}$$

meaning we can deduce the α is the ratio of fluid to solid volume changes.

We have now derived all the equations required to be able to state our macroscale model. The equations in the macroscale model describe the effective poroelastic behaviour of the material relating to the pressure, the average fluid velocity and the elastic displacement. Therefore the macroscale model to be solved is given by

$$\begin{cases} \langle \mathbf{w}\rangle_{\mathrm{f}} = -\langle W\rangle_{\mathrm{f}}\nabla_{\mathbf{x}}p^{(0)}, \\ \nabla_{\mathbf{x}} \cdot \mathbf{T}_{\mathrm{Eff}} = 0, \\ \mathbf{T}_{\mathrm{Eff}} = \langle \mathbb{C}\mathbb{M} + \mathbb{C}\rangle_{\mathrm{s}}\nabla_{\mathbf{x}}\mathbf{u}^{(0)} + (\langle \mathbb{C}Q\rangle_{\mathrm{s}} - \phi\mathbf{I})p^{(0)}, \\ \dfrac{\dot{p}^{(0)}}{M} = -\nabla_{\mathbf{x}} \cdot \langle \mathbf{w}\rangle_{\mathrm{f}} - \boldsymbol{\alpha} : \nabla_{\mathbf{x}}\dot{\mathbf{u}}^{(0)}, \end{cases} \tag{2.96}$$

where we have that $p^{(0)}$ is the macroscale pressure, $\mathbf{u}^{(0)}$ is the macroscale solid displacement, $\dot{\mathbf{u}}^{(0)}$ is the solid velocity and $\mathbf{w}$ is the average fluid velocity. The first equation of the macroscale model represents Darcy's law for $\mathbf{w}$, where $\mathbf{w}$ is the relative fluid-solid velocity. The second of the macroscale PDEs is the stress balance equation for the poroelastic

material where the material has the constitutive law given by the third equation in our macroscale model. The final equation describes the conservation of mass for a poroelastic material. It also relates changes in the fluid pressure to changes in the fluid and solid volumes. We therefore have that the mechanical behaviour of the poroelastic material can be fully described by the effective elasticity tensor $\langle \mathbb{C}\mathbb{M} + \mathbb{C} \rangle_{\mathrm{s}}$, the hydraulic conductivity $\langle W \rangle_{\mathrm{f}}$, Biot's tensor of coefficients $\boldsymbol{\alpha}$ and Biot's modulus M. This macroscale model is that of Biot (up to a choice in notation) and is the starting point for the models developed in the following chapters of this thesis.

2.5 Scheme for Solving the Macroscale Model

We now aim to provide a clear step-by-step guide to how the macroscale model could be solved. The steps are generic to allow for this to be seen as a guide to the process with either numerical or analytical solutions computed within the steps. When we are considering a case where macroscopic uniformity applies then we can propose the following steps as a method for solving the macroscale model. The process is:

1. We begin by fixing the original material properties of the poroelastic material including fixing the elasticity tensor $\mathbb{C}$ and fixing the fluid viscosity μ.

2. Then, we must fix the microscale structure by defining the cell geometry of a unit cell in the material.

3. Then the cell problems can be solved. In this case we have that we can now solve the cell problems (2.64), (2.73) and (2.74). This can be done numerically or for specific geometries analytically.

4. In order to calculate the coefficients in the corresponding macroscale model we use the cell problem solutions that we obtained in step 3 with (2.77) and the integral average (2.37). Then we can substitute the obtained model coefficients into the macroscale equations.

5. The geometry of the macroscale must also be prescribed. The boundary conditions for the homogenized cell boundary, $\partial\Omega_H$, must be given, and the system is to be supplemented by appropriate initial conditions for $\mathbf{u}^{(0)}$ and $p^{(0)}$.

6. Finally the macroscale equations (2.96) for the material can be solved. This can again be numerically or analytically for specific geometries.

The latter algorithm has been recently enforced in [35] to investigate variations of the effective poroelastic parameters against porosity and compressibility of the solid matrix in the context of tumour modelling. The next natural step is the application of relevant multiscale models for diffusion of solutes [110], see, e.g. [64] for an example of application for a rigid, porous tumour mass. Extension of such approaches to deformable structures via poroelasticity, such as those studied in [91], will pave the way to gain a thorough understanding of the relative importance of the various factors which affect diffusion in porous media.

2.6 Concluding Remarks

We have performed a re-derivation of the governing equations of a poroelastic material. We begin by presenting the fluid-structure interaction problem (FSI) that characterises an elastic porous matrix with a low Reynolds number Newtonian incompressible fluid flowing in the pores. This structure is applicable to many real world scenarios including biological tissues, artificial constructs, soil and rocks. We then embrace the asymptotic homogenization technique to derive the macroscale system of partial differential equations (PDEs). The model encodes the properties of the microstructure in the coefficients of the model, i.e. the effective hydraulic conductivity tensor, elasticity tensor, Biot's modulus and Biot's tensor of coefficients, which are to be computed by solving appropriate periodic cell problems.

This model is derived by assuming periodicity of the microstructure and aims to provide an introductory example of applying the asymptotic homogenization technique that will be applied to a variety of scenarios in the chapters that follow. This chapter also introduces the macroscale model for standard Biot's poroelastic materials. The novel models derived in the following chapters aim to build upon and advance this model to increase the applicability to real world problems.

The model of standard poroelasticity has limitations and is open to a variety of extensions. The present formulation provides the effective governing equations in a quasi-static, linearised setting, and accounting for incompressibility of the fluid phase. It also makes the assumption that the elastic matrix is homogeneous. These assumptions make the

model not particularly accurate when it comes to real world applications of the theory. It is clear that for many applications, in particular biological ones that these assumptions cannot be realistic of the materials true properties. For this reason we are able to extend the theory without these assumptions. We can derive models with a more complicated microstructure, considering also nonlinear elastic materials. These novel models despite addressing a more complicated microstructure are computationally no more expensive than the standard Biot's poroelasticity.

In the next chapter we make the first steps towards creating more realistic poroelastic models. We derive the novel macroscale model for poroelastic composites. This work presents the governing equations for a poroelastic material that has an inhomogeneous matrix comprising a variety of different elastic subphases and inclusions. This type of structure is much more representative of biological tissues microstructure.

Chapter 3

Effective balance equations for poroelastic composites

In this work we aim to determine the effective behaviour of a material where the microstructure comprises both an elastic fluid-filled porous matrix, and a number of embedded elastic inclusions/fibres which can interplay with both the matrix and the fluid phase. Our chief motivation is the study of *poroelastic composites*, i.e. complex, multiscale physical systems where multiple adjacent elastic phases interacting with a fluid can be identified on the porescale. For example, this is the case in the biological tissues interstitial matrix, which can be considered a composite made of multiple constituents, such as cells and different type of collagen fibres [61], which are interacting with the fluid flowing in the interstitial space [40] on the porescale [106]. A similar scenario is encountered when dealing with hard hierarchical materials, such as bone and tendons, where water is interplaying with both collagen and mineral at the finest hierarchical levels of organization [117], as well as with the constituents of the osteonal structures [30].

In the present work we embrace the asymptotic homogenization technique to upscale the interaction between a number of linear elastic inclusions and/or fibres embedded in a porous matrix saturated with an incompressible Newtonian fluid. Both the elastic matrix and the various subphases are in general assumed to be interacting with the fluid flowing in the pores. We assume that the scale at which the various solid subphases are clearly resolved is comparable with the porescale and collectively denote it as *the microscale*, which is in turn assumed to be much smaller than the macroscale. The upscaling is then carried out by accounting for continuity of tractions and displacements across the interfaces

between solid phases, and continuity of tractions and velocities across at the fluid-solid interfaces. The resulting governing equations, which are presented in the quasi-static case, are of Biot's type and read as a generalization of both the standard formulation for linear elastic composites [89], and standard poroelasticity [19]. These two models are recovered when assuming that the matrix is not porous and that no elastic phase other than the matrix is present, respectively. The coefficients of the model encode the properties of the microstructure, and are to be computed by solving local differential problems which combine the properties of those arising in the context of multiscale composites [88,89] and poroelasticity [35].

The paper is organised as follows. In Sec. 3.1 we introduce the fluid-structure interaction problem which describes the interplay between the elastic matrix, subphases, and fluid percolating in the pores. In Sec 3.2 we perform a multiscale analysis of the system of partial differential equations illustrated in Section 3.1 and derive the new macroscale model which governs the homogenized mechanical behaviour of poroelastic composites. In section 3.3 we discuss the macroscale results and prove rigorous properties of the arising effective elasticity tensor, Biot's modulus, and Biot's tensor of coefficients. In section 3.4 we conclude our work by discussing the limitations of the model and further perspectives.

3.1 A multiphase fluid-structure interaction problem

We begin by considering a set $\Omega \in \mathbb{R}^3$, where Ω represents the union of a solid porous matrix Ω_{II}, a connected fluid compartment Ω_{f}, and a collection Ω_{I} of N disjoint subphases,which could represent either inclusions (fully embedded in the matrix) or fibres (running the length of the domain), Ω_α, such that

$$\Omega_{\text{I}} = \bigcup_{\alpha=1}^{N} \Omega_\alpha, \tag{3.1}$$

and $\bar{\Omega} = \bar{\Omega}_{\text{I}} \cup \bar{\Omega}_{\text{II}} \cup \bar{\Omega}_{\text{f}}$ and $\bar{\Omega}_{\text{s}} = \bar{\Omega}_{\text{I}} \cup \bar{\Omega}_{\text{II}}$, Where the notation $\bar{\ }$ denotes that the domain is including its own boundary. A sketch of a cross-section of the three dimensional domain Ω is shown in Figure 3.1.

The balance equations in the solid domains Ω_α and Ω_{II}, by neglecting volume forces and inertia then read, $\forall \alpha = 1...N$

$$\nabla \cdot \mathsf{T}_\alpha = 0 \quad \text{in} \quad \Omega_\alpha, \tag{3.2}$$

and

$$\nabla \cdot \mathsf{T}_{\text{II}} = 0 \quad \text{in} \quad \Omega_{\text{II}}. \tag{3.3}$$

The symbols T_α and T_{II} that appear in relationships (3.2-3.3) denote the solid stress tensors corresponding to each subphase Ω_α and the one corresponding to the matrix Ω_{II}, respectively. We then assume that both the matrix and each subphase are anisotropic linear elastic solids, so that the constitutive equations for T_α and T_{II} are given by

$$\mathsf{T}_\alpha = \mathbb{C}_\alpha \nabla \mathbf{u}_\alpha, \tag{3.4}$$

$$\mathsf{T}_{\text{II}} = \mathbb{C}_{\text{II}} \nabla \mathbf{u}_{\text{II}}, \tag{3.5}$$

where $\mathbf{u}_\alpha$ and $\mathbf{u}_{\text{II}}$ are the elastic displacement in each subphase and the matrix, respectively.

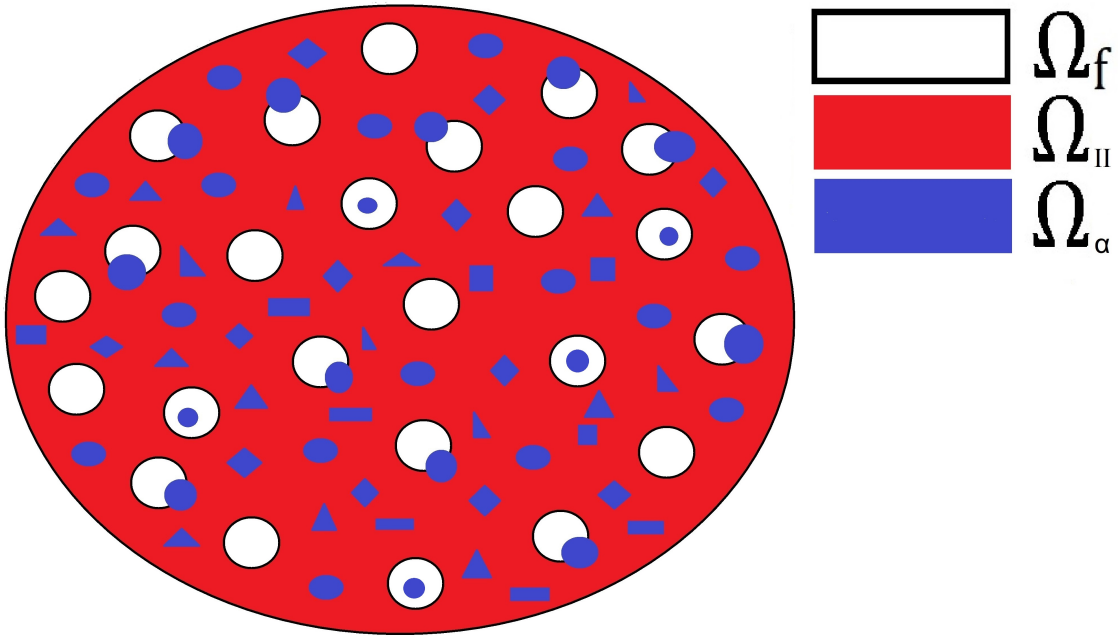

Figure 3.1: A 2D sketch representing a cross-section of the 3-dimensional domain Ω. The fluid phase flowing in the pores is represented in white, the porous elastic matrix is shown in red, and the subphases, which can be inclusions or fibres, are shown in blue. The inclusions and/or fibres can potentially be in contact with both the matrix and the fluid flowing in the pores or alternatively they can be fully embedded in the matrix or fully surrounded by the fluid, as illustrated throughout our schematic of the domain Ω.

In order to emphasise that the domain we are considering is 3D we have produced the following figure which is just an example of a subset of Ω.

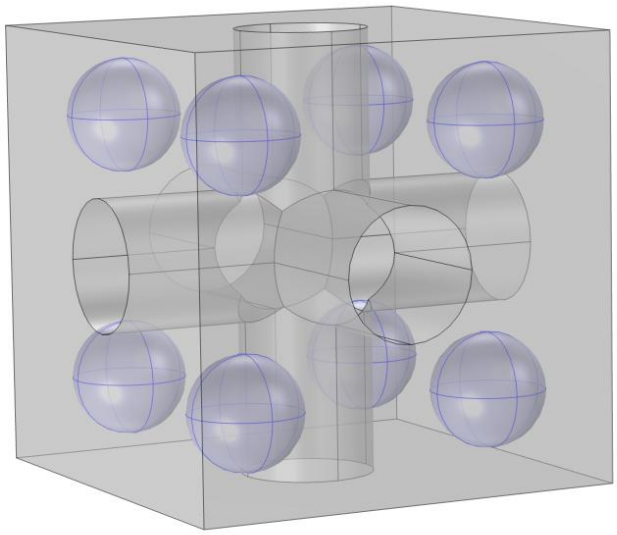

Figure 3.2: A 3D example of a section of the domain shown in Fig. 3.1 to show that the fluid flow is interconnected cylinders in 3 directions

The fourth rank tensors $\mathbb{C}_\alpha$ and $\mathbb{C}_{\text{II}}$ are the elasticity tensors in each subphase and the matrix, respectively, with corresponding components C^α_{ijkl} and C^{II}_{ijkl}, for $i,j,k,l = 1,2,3$. We note that each $\mathbb{C}_\alpha$ and $\mathbb{C}_{\text{II}}$ are equipped with right minor and major symmetries, namely

$$C^\alpha_{ijkl} = C^\alpha_{ijlk}; \quad C^{\text{II}}_{ijkl} = C^{\text{II}}_{ijlk}, \tag{3.6}$$

$$C^\alpha_{ijkl} = C^\alpha_{klij}; \quad C^{\text{II}}_{ijkl} = C^{\text{II}}_{klij}, \tag{3.7}$$

and therefore also left minor symmetries follow by combining (3.6-3.7). In particular, by applying right minor symmetries we can equivalently rewrite constitutive equations (3.4-3.5) as

$$\mathsf{T}_\alpha = \mathbb{C}_\alpha \xi(\mathbf{u}_\alpha), \tag{3.8}$$

$$\mathsf{T}_{\text{II}} = \mathbb{C}_{\text{II}} \xi(\mathbf{u}_{\text{II}}), \tag{3.9}$$

where

$$\xi(\bullet) = \frac{\nabla(\bullet) + (\nabla(\bullet))^T}{2} \tag{3.10}$$

is the symmetric part of the gradient operator.

The balance equation in the fluid compartment reads

$$\nabla \cdot \mathsf{T}_\mathsf{f} = 0 \quad \text{in} \quad \Omega_\mathrm{f}, \tag{3.11}$$

where T_f is the fluid stress tensor. We assume that the fluid compartment is an incompressible Newtonian fluid, so that the constitutive equation for T_f is given by

$$\mathsf{T}_\mathsf{f} = -p\mathsf{I} + 2\mu\xi(\mathbf{v}), \tag{3.12}$$

where $\mathbf{v}$ denotes fluid velocity, p the pressure and μ the viscosity, together with the incompressibility constraint

$$\nabla \cdot \mathbf{v} = 0 \quad \text{in} \quad \Omega_\mathrm{f}. \tag{3.13}$$

Substituting relationship (3.12) in (3.11) and using the the divergence-free condition (3.13) yields the Stokes' problem

$$\mu\nabla^2\mathbf{v} = \nabla p \quad \text{in} \quad \Omega_\mathrm{f}. \tag{3.14}$$

In order to close the fluid structure interaction problem in the whole domain Ω we also require interface conditions between the fluid and the solid phases. We first define the interface between the fluid phase and the α inclusion/fibre as $\Gamma_\alpha := \partial\Omega_\alpha \cap \partial\Omega_\mathrm{f}$ and the interface between the matrix and the fluid phase as $\Gamma_\mathrm{II} := \partial\Omega_\mathrm{II} \cap \partial\Omega_\mathrm{f}$. We then impose continuity of velocities and tractions across each Γ_α and Γ_II, namely

$$\dot{\mathbf{u}}_\alpha = \mathbf{v} \quad \text{on} \quad \Gamma_\alpha, \tag{3.15}$$

$$\mathsf{T}_\mathsf{f}\mathbf{n}_\alpha = \mathsf{T}_\alpha\mathbf{n}_\alpha \quad \text{on} \quad \Gamma_\alpha, \tag{3.16}$$

$$\dot{\mathbf{u}}_\mathrm{II} = \mathbf{v} \quad \text{on} \quad \Gamma_\mathrm{II}, \tag{3.17}$$

$$\mathsf{T}_\mathsf{f}\mathbf{n}_\mathrm{II} = \mathsf{T}_\mathrm{II}\mathbf{n}_\mathrm{II} \quad \text{on} \quad \Gamma_\mathrm{II}, \tag{3.18}$$

$\forall\alpha = 1...N$, where $\dot{\mathbf{u}}_\alpha$ and $\dot{\mathbf{u}}_\mathrm{II}$ are the solid velocities in each subphase Ω_α and the matrix Ω_II, respectively. The unit outward (i.e. pointing into the fluid domain Ω_f) vectors normal to the interfaces Γ_α and Γ_II are denoted by $\mathbf{n}_\alpha$ and $\mathbf{n}_\mathrm{II}$, respectively. Finally, we require continuity of tractions and displacements across the interface between each elastic subphase and the matrix. We define this boundary as $\Gamma_{\alpha\mathrm{II}} := \partial\Omega_\alpha \cap \partial\Omega_\mathrm{II}$, so that

$$\mathsf{T}_\alpha\mathbf{n}_{\alpha\mathrm{II}} = \mathsf{T}_\mathrm{II}\mathbf{n}_{\alpha\mathrm{II}} \quad \text{on} \quad \Gamma_{\alpha\mathrm{II}}. \tag{3.19}$$

$$\mathbf{u}_\alpha = \mathbf{u}_{\text{II}} \quad \text{on} \quad \Gamma_{\alpha\text{II}}, \tag{3.20}$$

$\forall \alpha = 1...N$, where $\mathbf{n}_{\alpha\text{II}}$ is the unit vector normal to the interface $\Gamma_{\alpha\text{II}}$ pointing into the fibre/inclusion Ω_α.

In the next section we perform a multiscale analysis by (a) non-dimensionalizing the partial differential equations (PDEs) described in this section and introducing two well-separated length scales, (b) applying the asymptotic homogenization technique to the resulting non-dimensional systems of PDEs, and (c) deriving the effective governing equations for the material as a whole.

3.2 Multiscale analysis

We now perform a multiscale analysis of the fluid-structure interaction problem introduced in the previous section, which is summarized below

$$\nabla \cdot \mathsf{T}_\alpha = 0 \quad \text{in} \quad \Omega_\alpha, \tag{3.21}$$

$$\nabla \cdot \mathsf{T}_{\text{II}} = 0 \quad \text{in} \quad \Omega_{\text{II}}, \tag{3.22}$$

$$\nabla \cdot \mathsf{T}_{\text{f}} = 0 \quad \text{in} \quad \Omega_{\text{f}}, \tag{3.23}$$

$$\nabla \cdot \mathbf{v} = 0 \quad \text{in} \quad \Omega_{\text{f}}, \tag{3.24}$$

$$\dot{\mathbf{u}}_\alpha = \mathbf{v} \quad \text{on} \quad \Gamma_\alpha, \tag{3.25}$$

$$\dot{\mathbf{u}}_{\text{II}} = \mathbf{v} \quad \text{on} \quad \Gamma_{\text{II}}, \tag{3.26}$$

$$\mathsf{T}_{\text{f}}\mathbf{n}_\alpha = \mathsf{T}_\alpha \mathbf{n}_\alpha \quad \text{on} \quad \Gamma_\alpha, \tag{3.27}$$

$$\mathsf{T}_{\text{f}}\mathbf{n}_{\text{II}} = \mathsf{T}_{\text{II}}\mathbf{n}_{\text{II}} \quad \text{on} \quad \Gamma_{\text{II}}, \tag{3.28}$$

$$\mathsf{T}_\alpha \mathbf{n}_{\alpha\text{II}} = \mathsf{T}_{\text{II}}\mathbf{n}_{\alpha\text{II}} \quad \text{on} \quad \Gamma_{\alpha\text{II}}, \tag{3.29}$$

$$\mathbf{u}_\alpha = \mathbf{u}_{\text{II}} \quad \text{on} \quad \Gamma_{\alpha\text{II}}, \tag{3.30}$$

where, by means of the constitutive relationships (3.8), (3.9), and (3.12), together with the incompressibility constraint (3.24), the balance equations (3.21), (3.22), and (3.23) can also be rewritten as

$$\nabla \cdot (\mathbb{C}_\alpha \xi(\mathbf{u}_\alpha)) = 0 \quad \text{in} \quad \Omega_\alpha \tag{3.31}$$

$$\nabla \cdot (\mathbb{C}_{\text{II}} \xi(\mathbf{u}_{\text{II}})) = 0 \quad \text{in} \quad \Omega_{\text{II}} \tag{3.32}$$

$$\mu\nabla^2\mathbf{v} = \nabla p \quad \text{in} \quad \Omega_{\mathrm{f}}, \tag{3.33}$$

$\forall\alpha = 1...N$. The problem (3.21-3.30) is then to be closed by prescribing suitable external boundary conditions on $\partial\Omega$. We assume that there exist two typical length scales in the system. In particular, we denote the average size of the whole domain Ω by L (*the macroscale*), while d refers to the porescale (*the microscale*), which in this work is assumed to be comparable with the distance between adjacent subphases interacting with the matrix and the fluid domain. In order to emphasize the difference between such scales, it is helpful to perform a non-dimensional analysis of the system of PDEs (3.21-3.30).

3.2.1 Non-dimensional form of the equations

We carry out the non-dimensional analysis by assuming that the system is characterized by a reference pressure gradient C_p, and that the characteristic (reference) fluid velocity is given by the typical parabolic profile proportional to that of a Newtonian fluid slowly flowing in a cylinder of radius d. This is the appropriate scaling that captures the scale separation between the microscale d and the macroscale L in a porous domain, as also discussed in [87]. Although different scaling choices for the fluid velocity are formally possible, these would not account for the appropriate effective behaviour of a fluid flowing through a porous solid matrix. An example of alternative choices which lead to an effective viscoelastic-type behavior are illustrated in [19]. The scalings that we use here are consistent throughout this work and are the same as those used in the previous chapter.

Therefore, in our case we have

$$\begin{gathered}\mathbf{x} = L\mathbf{x}', \quad \mathbb{C}_\alpha = C_p L\mathbb{C}'_\alpha, \quad \mathbb{C}_{\mathrm{II}} = C_p L\mathbb{C}'_{\mathrm{II}}, \\ \mathbf{u}_\alpha = L\mathbf{u}'_\alpha, \quad \mathbf{u}_{\mathrm{II}} = L\mathbf{u}'_{\mathrm{II}}, \quad \mathbf{v} = \frac{C_p d^2}{\mu}\mathbf{v}', \quad p = C_p L p'.\end{gathered} \tag{3.34}$$

From (3.34) we can deduce that time is scaled by

$$\frac{L}{V} = \frac{\mu L}{C_p d^2}, \tag{3.35}$$

where

$$V = \frac{C_p d^2}{\mu} \tag{3.36}$$

is the reference parabolic fluid profile which is embraced to upscale a fluid-structure in-

teraction problem to a poroelastic problem, as also explained in [87]. Equation (3.35) therefore represents the (macro) reference time scale for a fluid slowly flowing in the pores and is assumed to be analogous to the time scale for deformation of the elastic material, for the sake of consistency with continuity of velocities at the interface. We then exploit (3.34) and observe that

$$\nabla = \frac{1}{L}\nabla' \tag{3.37}$$

to obtain the non-dimensional form of the system of PDEs (3.21-3.30), namely

$$\nabla \cdot \mathsf{T}_\alpha = 0 \quad \text{in} \quad \Omega_\alpha \tag{3.38}$$

$$\nabla \cdot \mathsf{T}_{\text{II}} = 0 \quad \text{in} \quad \Omega_{\text{II}} \tag{3.39}$$

$$\nabla \cdot \mathsf{T}_{\text{f}} = 0 \quad \text{in} \quad \Omega_{\text{f}} \tag{3.40}$$

$$\nabla \cdot \mathbf{v} = 0 \quad \text{in} \quad \Omega_{\text{f}} \tag{3.41}$$

$$\dot{\mathbf{u}}_\alpha = \mathbf{v} \quad \text{on} \quad \Gamma_\alpha \tag{3.42}$$

$$\dot{\mathbf{u}}_{\text{II}} = \mathbf{v} \quad \text{on} \quad \Gamma_{\text{II}} \tag{3.43}$$

$$\mathsf{T}_{\text{f}}\mathbf{n}_\alpha = \mathsf{T}_\alpha \mathbf{n}_\alpha \quad \text{on} \quad \Gamma_\alpha \tag{3.44}$$

$$\mathsf{T}_{\text{f}}\mathbf{n}_{\text{II}} = \mathsf{T}_{\text{II}}\mathbf{n}_{\text{II}} \quad \text{on} \quad \Gamma_{\text{II}} \tag{3.45}$$

$$\mathsf{T}_\alpha \mathbf{n}_{\alpha\text{II}} = \mathsf{T}_{\text{II}}\mathbf{n}_{\alpha\text{II}} \quad \text{on} \quad \Gamma_{\alpha\text{II}} \tag{3.46}$$

$$\mathbf{u}_\alpha = \mathbf{u}_{\text{II}} \quad \text{on} \quad \Gamma_{\alpha\text{II}} \tag{3.47}$$

$\forall \alpha = 1...N$, where we have dropped the primes for the sake of simplicity of notation. The non-dimensionalized counterparts of constitutive relationships (3.8), (3.9), and (3.12) are given by

$$\mathsf{T}_{\text{f}} = -p\mathbf{I} + \epsilon^2(\nabla\mathbf{v} + (\nabla\mathbf{v})^{\text{T}}) \tag{3.48}$$

$$\mathsf{T}_\alpha = \mathbb{C}_\alpha \xi(\mathbf{u}_\alpha) \tag{3.49}$$

$$\mathsf{T}_{\text{II}} = \mathbb{C}_{\text{II}} \xi(\mathbf{u}_{\text{II}}), \tag{3.50}$$

so that the balance equations (3.38-3.40) rewrite

$$\epsilon^2 \nabla^2 \mathbf{v} = \nabla p \quad \text{in} \quad \Omega_{\text{f}} \tag{3.51}$$

$$\nabla \cdot (\mathbb{C}_\alpha \xi(\mathbf{u}_\alpha)) = 0 \quad \text{in} \quad \Omega_\alpha \tag{3.52}$$

$$\nabla \cdot (\mathbb{C}_{\text{II}} \xi(\mathbf{u}_{\text{II}})) = 0 \quad \text{in} \quad \Omega_{\text{II}}, \tag{3.53}$$

where

$$\epsilon = \frac{d}{L}. \tag{3.54}$$

In the next section we introduce the asymptotic homogenization technique which is used to upscale the non-dimensional system of PDEs (3.38-3.47) by formally assuming that the microscale and the macroscale are well separated.

3.2.2 The asymptotic homogenization technique

In this section we introduce the two-scale asymptotic homogenization technique which is used to derive a macroscale model for the equations (3.38−3.47). We first assume that the microscale (where the pores and individual inclusions/fibres are clearly resolved), denoted by d, is small compared to average size of the domain L, i.e.

$$\epsilon \ll 1. \tag{3.55}$$

We then introduce a local spatial variable to capture microscale variations of the field via setting

$$\mathbf{y} = \frac{\mathbf{x}}{\epsilon}. \tag{3.56}$$

The spatial variables $\mathbf{x}$ and $\mathbf{y}$ are to be considered formally independent and represent the macroscale and the microscale, respectively. The gradient operator then transforms as

$$\nabla \to \nabla_{\mathbf{x}} + \frac{1}{\epsilon}\nabla_{\mathbf{y}}. \tag{3.57}$$

We further assume that all the fields $\mathbf{u}_{\text{II}}, \mathbf{u}_\alpha, \mathbf{v}, p, \mathsf{T}_{\mathsf{f}}, \mathsf{T}_\alpha, \mathsf{T}_{\text{II}}$, as well as the elasticity tensors $\mathbb{C}_{\text{II}}$ and $\mathbb{C}_\alpha$, $\forall \alpha = 1...N$, are functions of both $\mathbf{x}$ and $\mathbf{y}$. We also assume that the fields $\mathbf{u}_{\text{II}}, \mathbf{u}_\alpha, \mathbf{v}, p, \mathsf{T}_{\mathsf{f}}, \mathsf{T}_\alpha, \mathsf{T}_{\text{II}}$ can be represented in terms of a series expansion in powers of ϵ, i.e.

$$\varphi^\epsilon(\mathbf{x}, \mathbf{y}, t) = \sum_{l=0}^{\infty} \varphi^{(l)}(\mathbf{x}, \mathbf{y}, t)\epsilon^l, \tag{3.58}$$

where φ collectively denotes each field involved in the present analysis.

Remark 3 (Microscale periodicity)**.** *We are now interested in obtaining a closed system of PDEs in terms of the leading (zero-th) order pressure, velocity, and displacement fields. This is done by applying relationships* (3.57) *and* (3.58) *to the system (3.38-3.47) and constitutive equations (3.48-3.50), and in turn to relationships (3.51-3.53). This way, by*

equating coefficients of the same power of ϵ, we can obtain various sets of differential conditions which can be combined to obtain a system of PDEs which holds on the macroscale $\mathbf{x} \in \Omega_H$. The domain Ω_H represents the homogenized domain where microscale heterogeneities are smoothed out. The coefficients of the model are then typically expressed averaging the solution of appropriate microscale local *problems. As each coefficient $\varphi^{(l)}$ that appears in* (3.58) *is required to be well-defined for arbitrary small values of ϵ, it is in principle necessary to assume that all the fields are* locally bounded, *i.e. finite with respect to the microscale variable $\mathbf{y}$ when $\epsilon \to 0$, see also [48, 90]. This is the least restrictive assumption that is to be embraced to successfully perform upscaling of a given system of PDEs when dealing with formal asymptotic homogenization. In [19] the authors derive Biot's equations of poroelasticity by assuming local boundedness of the fields. However, this approach is appropriate when the main goal is the functional form of the macroscale model only. This is since the prescriptions of the coefficients obtained this way are related to microscale problems which are, in principle, to be solved on the whole microstructure. Therefore, they cannot be used in practice unless further geometrical restrictions, such as periodicity of the microstructure, are imposed, as indeed suggested in [19]. We therefore assume that every $\varphi^{(l)}$, $\mathbb{C}_\alpha$, and $\mathbb{C}_{\text{II}}$ are $\mathbf{y}$-periodic. This latter technical assumption allows us to restrict the analysis of the microstructure to a single periodic cell, which could in any case contain several different subphases characterized by different geometry, arrangement and elastic properties, as shown in Figure 3.3.*

Remark 4 (Macroscopic uniformity)**.** *The microscale geometry can in principle vary with respect to the macroscale, however, this potential dependence is often (most of the time implicitly) neglected. Here, we assume that the medium is macroscopically uniform, i.e. the microscale geometry does not depend on the macroscale variable $\mathbf{x}$. In particular, this assumptions leads to the straightforward differentiation under the integral sign*

$$\int_\Omega \nabla_{\mathbf{x}} \cdot (\bullet)\, d\mathbf{y} = \nabla_{\mathbf{x}} \cdot \int_\Omega (\bullet)\, d\mathbf{y}. \tag{3.59}$$

Whenever $\Omega = \Omega(\mathbf{x})$, equation (3.59) *is not satisfied, and application of the generalized Reynolds' transport theorem may lead to additional macroscale contributions, see, e.g. [48, 87, 88].*

Finally, for the sake of clarity of presentation and without loss of generality with respect to the properties of the model, we can restrict our analysis by assuming that only one

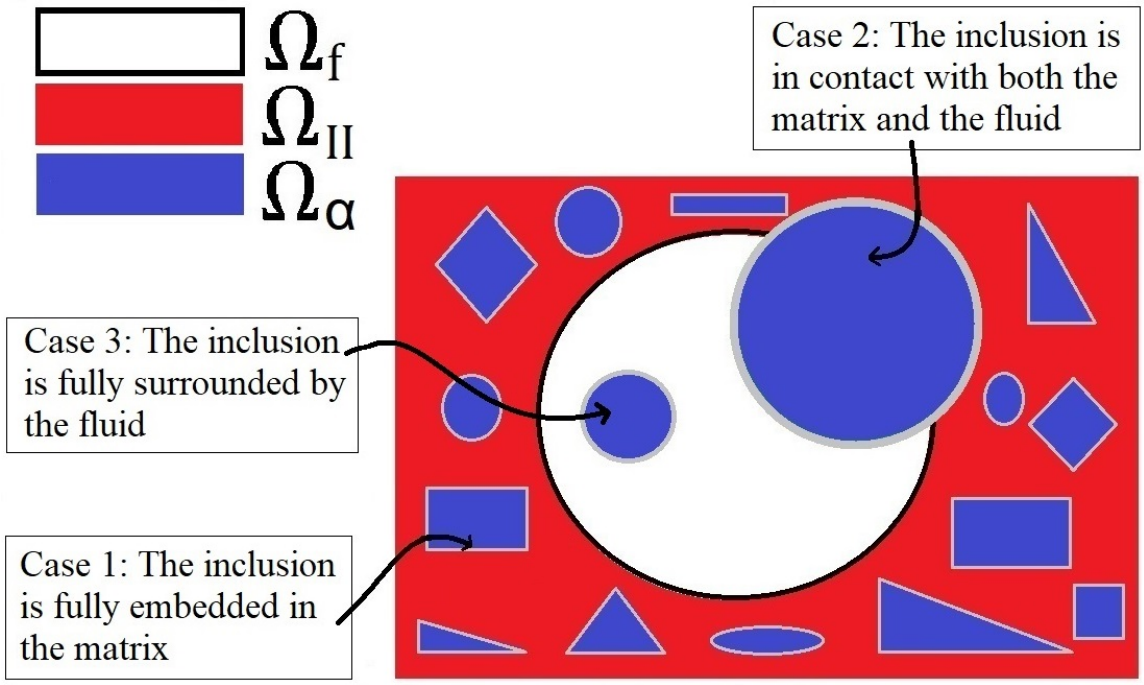

Figure 3.3: A 2D sketch representing a single periodic cell in our structure. This is a section of the domain Ω in Fig. 3.1 that has been zoomed in around one pore. We have the fluid represented in white, the porous matrix in red and the subphases in blue. The inclusions Ω_α for $\alpha = 1...N$, can be in contact with both the matrix and the fluid or be fully embedded in either the matrix or the fluid. Each of these cases is highlighted in the figure.

subphase is contained in each periodic cell, as shown in Figure 3.4. The model can be easily extended to a number of subphases within the periodic cell if necessary for a particular application, as done in the context of simple elastic composites in [88]. Therefore, the index α is no longer needed and we adjust the notation accordingly. We identify the domain Ω with its corresponding periodic cell, with fibre/inclusion, matrix, and fluid cell portions denoted by Ω_{I}, Ω_{II}, and Ω_{f}, respectively. The interfaces between the different phases are then denoted by $\Gamma_{\mathrm{I}} := \partial\Omega_{\mathrm{I}} \cap \partial\Omega_{\mathrm{f}}$, $\Gamma_{\mathrm{II}} := \partial\Omega_{\mathrm{II}} \cap \partial\Omega_{\mathrm{f}}$, and $\Gamma_{\mathrm{III}} := \partial\Omega_{\mathrm{I}} \cap \partial\Omega_{\mathrm{II}}$, with corresponding unit normal vectors $\mathbf{n}_{\mathrm{I}}$, $\mathbf{n}_{\mathrm{II}}$, and $\mathbf{n}_{\mathrm{III}}$, where Γ_{I} is the interface between the fluid and the inclusion, Γ_{II} is the interface between the fluid and the matrix and Γ_{III} is the interface between the matrix and the inclusion.

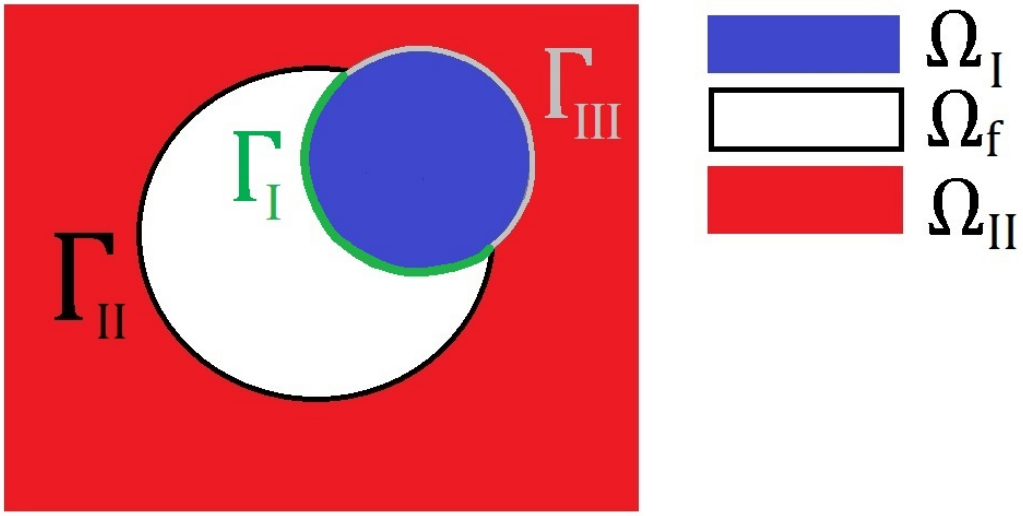

Figure 3.4: This is a 2D sketch representing the periodic cell that we focus on. In our case we focus on geometry case 2 from Fig. 3.3. We have one subphase fibre shown in blue that is in contact with the porous, solid, elastic matrix shown in red and the fluid flowing in the pores is shown in white. We also highlight the interfaces Γ_{I} which is shown in green between the inclusion and the fluid, Γ_{II} shown in black between the matrix and the fluid and Γ_{III} shown in grey between the inclusion and the matrix.

3.2.3 Derivation of the Macroscale Model

We apply the asymptotic homogenization assumptions (3.57) and (3.58) to equations (3.38-3.53) to obtain, accounting for periodicity, the following multiscale system of PDEs

$$\nabla_{\mathbf{y}} \cdot \mathsf{T}_{\text{I}}^{\epsilon} + \epsilon \nabla_{\mathbf{x}} \cdot \mathsf{T}_{\text{I}}^{\epsilon} = 0 \quad \text{in} \quad \Omega_{\text{I}} \tag{3.60}$$

$$\nabla_{\mathbf{y}} \cdot \mathsf{T}_{\text{II}}^{\epsilon} + \epsilon \nabla_{\mathbf{x}} \cdot \mathsf{T}_{\text{II}}^{\epsilon} = 0 \quad \text{in} \quad \Omega_{\text{II}} \tag{3.61}$$

$$\nabla_{\mathbf{y}} \cdot \mathsf{T}_{\text{f}}{}^{\epsilon} + \epsilon \nabla_{\mathbf{x}} \cdot \mathsf{T}_{\text{f}}{}^{\epsilon} = 0 \quad \text{in} \quad \Omega_{\text{f}} \tag{3.62}$$

$$\nabla_{\mathbf{y}} \cdot \mathbf{v}^{\epsilon} + \epsilon \nabla_{\mathbf{x}} \cdot \mathbf{v}^{\epsilon} = 0 \quad \text{in} \quad \Omega_{\text{f}} \tag{3.63}$$

$$\dot{\mathbf{u}}_{\text{I}}^{\epsilon} = \mathbf{v}^{\epsilon} \quad \text{on} \quad \Gamma_{\text{I}} \tag{3.64}$$

$$\dot{\mathbf{u}}_{\text{II}}^{\epsilon} = \mathbf{v}^{\epsilon} \quad \text{on} \quad \Gamma_{\text{II}} \tag{3.65}$$

$$\mathsf{T}_{\text{f}}{}^{\epsilon} \mathbf{n}_{\text{I}} = \mathsf{T}_{\text{I}}^{\epsilon} \mathbf{n}_{\text{I}} \quad \text{on} \quad \Gamma_{\text{I}} \tag{3.66}$$

$$\mathsf{T}_{\text{f}}{}^{\epsilon} \mathbf{n}_{\text{II}} = \mathsf{T}_{\text{II}}^{\epsilon} \mathbf{n}_{\text{II}} \quad \text{on} \quad \Gamma_{\text{II}} \tag{3.67}$$

$$\mathsf{T}_{\text{I}}^{\epsilon} \mathbf{n}_{\text{III}} = \mathsf{T}_{\text{II}}^{\epsilon} \mathbf{n}_{\text{III}} \quad \text{on} \quad \Gamma_{\text{III}} \tag{3.68}$$

$$\mathbf{u}_{\text{I}}^{\epsilon} = \mathbf{u}_{\text{II}}^{\epsilon} \quad \text{on} \quad \Gamma_{\text{III}}, \tag{3.69}$$

equipped with multiscale constitutive equations for the fluid and solid stress tensors $\mathsf{T_f}^\epsilon$, $\mathsf{T}_{\rm I}^\epsilon$, $\mathsf{T}_{\rm II}^\epsilon$, given by

$$\mathsf{T_f}^\epsilon = -p^\epsilon \mathbf{I} + \epsilon(\nabla_{\mathbf{y}}\mathbf{v}^\epsilon + (\nabla_{\mathbf{y}}\mathbf{v}^\epsilon)^{\rm T}) + \epsilon^2(\nabla_{\mathbf{x}}\mathbf{v}^\epsilon + (\nabla_{\mathbf{x}}\mathbf{v}^\epsilon)^{\rm T}) \tag{3.70}$$

$$\epsilon\mathsf{T}_{\rm I}^\epsilon = \mathbb{C}_{\rm I}\xi_{\mathbf{y}}(\mathbf{u}_{\rm I}^\epsilon) + \epsilon\mathbb{C}_{\rm I}\xi_{\mathbf{x}}(\mathbf{u}_{\rm I}^\epsilon) \tag{3.71}$$

$$\epsilon\mathsf{T}_{\rm II}^\epsilon = \mathbb{C}_{\rm II}\xi_{\mathbf{y}}(\mathbf{u}_{\rm II}^\epsilon) + \epsilon\mathbb{C}_{\rm II}\xi_{\mathbf{x}}(\mathbf{u}_{\rm II}^\epsilon), \tag{3.72}$$

while the balance equations in terms of the elastic displacement, fluid velocity and pressure $\mathbf{u}_{\rm II}^\epsilon$, $\mathbf{u}_{\rm I}^\epsilon$, $\mathbf{v}^\epsilon$, p^ϵ read

$$\begin{aligned}&\nabla_{\mathbf{y}}\cdot(\mathbb{C}_{\rm I}\xi_{\mathbf{y}}(\mathbf{u}_{\rm I}^\epsilon)) + \epsilon\nabla_{\mathbf{y}}\cdot(\mathbb{C}_{\rm I}\xi_{\mathbf{x}}(\mathbf{u}_{\rm I}^\epsilon)) + \\ &\epsilon\nabla_{\mathbf{x}}\cdot(\mathbb{C}_{\rm I}\xi_{\mathbf{y}}(\mathbf{u}_{\rm I}^\epsilon)) + \epsilon^2\nabla_{\mathbf{x}}\cdot(\mathbb{C}_{\rm I}\xi_{\mathbf{x}}(\mathbf{u}_{\rm I}^\epsilon)) = 0 \quad \text{in} \quad \Omega_{\rm I}\end{aligned} \tag{3.73}$$

$$\begin{aligned}&\nabla_{\mathbf{y}}\cdot(\mathbb{C}_{\rm II}\xi_{\mathbf{y}}(\mathbf{u}_{\rm II}^\epsilon)) + \epsilon\nabla_{\mathbf{y}}\cdot(\mathbb{C}_{\rm II}\xi_{\mathbf{x}}(\mathbf{u}_{\rm II}^\epsilon)) + \\ &\epsilon\nabla_{\mathbf{x}}\cdot(\mathbb{C}_{\rm II}\xi_{\mathbf{y}}(\mathbf{u}_{\rm II}^\epsilon)) + \epsilon^2\nabla_{\mathbf{x}}\cdot(\mathbb{C}_{\rm II}\xi_{\mathbf{x}}(\mathbf{u}_{\rm II}^\epsilon)) = 0 \quad \text{in} \quad \Omega_{\rm II}\end{aligned} \tag{3.74}$$

$$\begin{aligned}&\epsilon^3\nabla_{\mathbf{x}}^2\mathbf{v}^\epsilon + \epsilon^2\nabla_{\mathbf{x}}\cdot(\nabla_{\mathbf{y}}\mathbf{v}^\epsilon) + \epsilon^2\nabla_{\mathbf{y}}\cdot(\nabla_{\mathbf{x}}\mathbf{v}^\epsilon) + \epsilon\nabla_{\mathbf{y}}^2\mathbf{v}^\epsilon \\ &= \nabla_{\mathbf{y}}p^\epsilon + \epsilon\nabla_{\mathbf{x}}p^\epsilon \quad \text{in} \quad \Omega_{\rm f}\end{aligned} \tag{3.75}$$

We can now substitute power series of the type (3.58) into the relevant fields in (3.60−3.75). Then by equating the coefficients of ϵ^l for $l = 0, 1, ...$ we derive the macroscale model for the material in terms of the relevant leading (zero-th) order fields. Whenever a component in the asymptotic expansion retains a dependence on the microscale, we can take the integral average, which we define as

$$\langle\varphi\rangle_i = \frac{1}{|\Omega|}\int_{\Omega_i}\varphi(\mathbf{x},\mathbf{y},t)\mathrm{d}\mathbf{y} \quad i = \mathrm{f}, \mathrm{I}, \mathrm{II} \tag{3.76}$$

where φ is a field, and also where the integral average can be performed over one representative cell due to $\mathbf{y}$-periodicity and $|\Omega|$ is the volume of the domain and the integration is performed over the microscale. We note that $|\Omega| = |\Omega_{\rm f}| + |\Omega_{\rm I}| + |\Omega_{\rm II}|$. Due to the assumption of $\mathbf{y}$-periodicity, the integral average can be performed over one representative cell. Therefore (3.76) represents a cell average. For the sake of brevity, we also introduce the notation

$$\langle\varphi_{\rm I} + \varphi_{\rm II}\rangle_{\rm s} = \frac{1}{|\Omega|}\left(\int_{\Omega_{\rm I}}\varphi_{\rm I}(\mathbf{x},\mathbf{y},t)\mathrm{d}\mathbf{y} + \int_{\Omega_{\rm II}}\varphi_{\rm II}(\mathbf{x},\mathbf{y},t)\mathrm{d}\mathbf{y}\right), \tag{3.77}$$

for fields φ with components $\varphi_{\rm I}$ and $\varphi_{\rm II}$ defined in the solid cell portions $\Omega_{\rm I}$ or $\Omega_{\rm II}$, respectively.

Equating coefficients of ϵ^0 in (3.60−3.69) we obtain

$$\nabla_{\mathbf{y}} \cdot \mathsf{T}_{\rm I}^{(0)} = 0 \qquad \text{in} \quad \Omega_{\rm I} \tag{3.78}$$

$$\nabla_{\mathbf{y}} \cdot \mathsf{T}_{\rm II}^{(0)} = 0 \qquad \text{in} \quad \Omega_{\rm II} \tag{3.79}$$

$$\nabla_{\mathbf{y}} \cdot \mathsf{T}_{\mathsf{f}}{}^{(0)} = 0 \qquad \text{in} \quad \Omega_{\rm f} \tag{3.80}$$

$$\nabla_{\mathbf{y}} \cdot \mathbf{v}^{(0)} = 0 \qquad \text{in} \quad \Omega_{\rm f} \tag{3.81}$$

$$\dot{\mathbf{u}}_{\rm I}^{(0)} = \mathbf{v}^{(0)} \qquad \text{on} \quad \Gamma_{\rm I} \tag{3.82}$$

$$\dot{\mathbf{u}}_{\rm II}^{(0)} = \mathbf{v}^{(0)} \qquad \text{on} \quad \Gamma_{\rm II} \tag{3.83}$$

$$\mathsf{T}_{\mathsf{f}}{}^{(0)}\mathbf{n}_{\rm I} = \mathsf{T}_{\rm I}^{(0)}\mathbf{n}_{\rm I} \qquad \text{on} \quad \Gamma_{\rm I} \tag{3.84}$$

$$\mathsf{T}_{\mathsf{f}}{}^{(0)}\mathbf{n}_{\rm II} = \mathsf{T}_{\rm II}^{(0)}\mathbf{n}_{\rm II} \qquad \text{on} \quad \Gamma_{\rm II} \tag{3.85}$$

$$\mathsf{T}_{\rm I}^{(0)}\mathbf{n}_{\rm III} = \mathsf{T}_{\rm II}^{(0)}\mathbf{n}_{\rm III} \qquad \text{on} \quad \Gamma_{\rm III} \tag{3.86}$$

$$\mathbf{u}_{\rm I}^{(0)} = \mathbf{u}_{\rm II}^{(0)} \qquad \text{on} \quad \Gamma_{\rm III} \tag{3.87}$$

and the constitutive equations (3.70−3.72) for $\mathsf{T}_{\mathsf{f}}{}^{\epsilon}$, $\mathsf{T}_{\rm I}^{\epsilon}$, $\mathsf{T}_{\rm II}^{\epsilon}$ have coefficients of ϵ^0

$$\mathsf{T}_{\mathsf{f}}{}^{(0)} = -p^{(0)}\mathbf{I} \qquad \text{in} \quad \Omega_{\rm f} \tag{3.88}$$

$$\mathbb{C}_{\rm I}\xi_{\mathbf{y}}(\mathbf{u}_{\rm I}^{(0)}) = 0 \qquad \text{in} \quad \Omega_{\rm I} \tag{3.89}$$

$$\mathbb{C}_{\rm II}\xi_{\mathbf{y}}(\mathbf{u}_{\rm II}^{(0)}) = 0 \qquad \text{in} \quad \Omega_{\rm II} \tag{3.90}$$

and the balance equations (3.73−3.75) have coefficients of ϵ^0

$$\nabla_{\mathbf{y}} \cdot (\mathbb{C}_{\rm I}\xi_{\mathbf{y}}(\mathbf{u}_{\rm I}^{(0)})) = 0 \qquad \text{in} \quad \Omega_{\rm I} \tag{3.91}$$

$$\nabla_{\mathbf{y}} \cdot (\mathbb{C}_{\rm II}\xi_{\mathbf{y}}(\mathbf{u}_{\rm II}^{(0)})) = 0 \qquad \text{in} \quad \Omega_{\rm II} \tag{3.92}$$

$$\nabla_{\mathbf{y}} p^{(0)} = 0 \qquad \text{in} \quad \Omega_{\rm f} \tag{3.93}$$

Similarly we now wish to equate the coefficients of ϵ^1 in equations (3.60−3.69) which gives

$$\nabla_{\mathbf{y}} \cdot \mathsf{T}_{\rm I}^{(1)} + \nabla_{\mathbf{x}} \cdot \mathsf{T}_{\rm I}^{(0)} = 0 \qquad \text{in} \quad \Omega_{\rm I} \tag{3.94}$$

$$\nabla_{\mathbf{y}} \cdot \mathsf{T}_{\rm II}^{(1)} + \nabla_{\mathbf{x}} \cdot \mathsf{T}_{\rm II}^{(0)} = 0 \qquad \text{in} \quad \Omega_{\rm II} \tag{3.95}$$

$$\nabla_{\mathbf{y}} \cdot \mathsf{T}_{\mathsf{f}}^{(1)} + \nabla_{\mathbf{x}} \cdot \mathsf{T}_{\mathsf{f}}^{(0)} = 0 \quad \text{in} \quad \Omega_{\mathrm{f}} \tag{3.96}$$

$$\nabla_{\mathbf{y}} \cdot \mathbf{v}^{(1)} + \nabla_{\mathbf{x}} \cdot \mathbf{v}^{(0)} = 0 \quad \text{in} \quad \Omega_{\mathrm{f}} \tag{3.97}$$

$$\dot{\mathbf{u}}_{\mathrm{I}}^{(1)} = \mathbf{v}^{(1)} \quad \text{on} \quad \Gamma_{\mathrm{I}} \tag{3.98}$$

$$\dot{\mathbf{u}}_{\mathrm{II}}^{(1)} = \mathbf{v}^{(1)} \quad \text{on} \quad \Gamma_{\mathrm{II}} \tag{3.99}$$

$$\mathsf{T}_{\mathsf{f}}^{(1)}\mathbf{n}_{\mathrm{I}} = \mathsf{T}_{\mathrm{I}}^{(1)}\mathbf{n}_{\mathrm{I}} \quad \text{on} \quad \Gamma_{\mathrm{I}} \tag{3.100}$$

$$\mathsf{T}_{\mathsf{f}}^{(1)}\mathbf{n}_{\mathrm{II}} = \mathsf{T}_{\mathrm{II}}^{(1)}\mathbf{n}_{\mathrm{II}} \quad \text{on} \quad \Gamma_{\mathrm{II}} \tag{3.101}$$

$$\mathsf{T}_{\mathrm{I}}^{(1)}\mathbf{n}_{\mathrm{III}} = \mathsf{T}_{\mathrm{II}}^{(1)}\mathbf{n}_{\mathrm{III}} \quad \text{on} \quad \Gamma_{\mathrm{III}} \tag{3.102}$$

$$\mathbf{u}_{\mathrm{I}}^{(1)} = \mathbf{u}_{\mathrm{II}}^{(1)} \quad \text{on} \quad \Gamma_{\mathrm{III}} \tag{3.103}$$

and the constitutive equations (3.70−3.72) for $\mathsf{T}_{\mathsf{f}}{}^{\epsilon}$, $\mathsf{T}_{\mathrm{I}}^{\epsilon}$, $\mathsf{T}_{\mathrm{II}}^{\epsilon}$ have coefficients of ϵ^1

$$\mathsf{T}_{\mathsf{f}}^{(1)} = -p^{(1)}\mathbf{I} + (\nabla_{\mathbf{y}}\mathbf{v}^{(0)} + (\nabla_{\mathbf{y}}\mathbf{v}^{(0)})^{\mathrm{T}}) \quad \text{in} \quad \Omega_{\mathrm{f}} \tag{3.104}$$

$$\mathsf{T}_{\mathrm{I}}^{(0)} = \mathbb{C}_{\mathrm{I}}\xi_{\mathbf{y}}(\mathbf{u}_{\mathrm{I}}^{(1)}) + \mathbb{C}_{\mathrm{I}}\xi_{\mathbf{x}}(\mathbf{u}_{\mathrm{I}}^{(0)}) \quad \text{in} \quad \Omega_{\mathrm{I}} \tag{3.105}$$

$$\mathsf{T}_{\mathrm{II}}^{(0)} = \mathbb{C}_{\mathrm{II}}\xi_{\mathbf{y}}(\mathbf{u}_{\mathrm{II}}^{(1)}) + \mathbb{C}_{\mathrm{II}}\xi_{\mathbf{x}}(\mathbf{u}_{\mathrm{II}}^{(0)}) \quad \text{in} \quad \Omega_{\mathrm{II}} \tag{3.106}$$

and the balance equations (3.73−3.75) have coefficients of ϵ^1

$$\nabla_{\mathbf{y}} \cdot (\mathbb{C}_{\mathrm{I}}\xi_{\mathbf{y}}(\mathbf{u}_{\mathrm{I}}^{(1)})) + \nabla_{\mathbf{y}} \cdot (\mathbb{C}_{\mathrm{I}}\xi_{\mathbf{x}}(\mathbf{u}_{\mathrm{I}}^{(0)})) + \nabla_{\mathbf{x}} \cdot (\mathbb{C}_{\mathrm{I}}\xi_{\mathbf{y}}(\mathbf{u}_{\mathrm{I}}^{(0)})) = 0 \quad \text{in} \quad \Omega_{\mathrm{I}} \tag{3.107}$$

$$\nabla_{\mathbf{y}} \cdot (\mathbb{C}_{\mathrm{II}}\xi_{\mathbf{y}}(\mathbf{u}_{\mathrm{II}}^{(1)})) + \nabla_{\mathbf{y}} \cdot (\mathbb{C}_{\mathrm{II}}\xi_{\mathbf{x}}(\mathbf{u}_{\mathrm{II}}^{(0)})) + \nabla_{\mathbf{x}} \cdot (\mathbb{C}_{\mathrm{II}}\xi_{\mathbf{y}}(\mathbf{u}_{\mathrm{II}}^{(0)})) = 0 \quad \text{in} \quad \Omega_{\mathrm{II}} \tag{3.108}$$

$$\nabla_{\mathbf{y}}^2\mathbf{v}^{(0)} = \nabla_{\mathbf{y}}p^{(1)} + \nabla_{\mathbf{x}}p^{(0)} \quad \text{in} \quad \Omega_{\mathrm{f}} \tag{3.109}$$

We can now see from (3.80) and (3.88) that the leading order pressure $p^{(0)}$ does not depend on the microscale $\mathbf{y}$. That is

$$p^{(0)} = p^{(0)}(\mathbf{x}, t). \tag{3.110}$$

We also have from (3.89) and (3.90) that $\mathbf{u}_{\mathrm{I}}^{(0)}$ and $\mathbf{u}_{\mathrm{II}}^{(0)}$, which are the leading order solid displacements, are rigid body motions and therefore, by $\mathbf{y}$-periodicity, do not depend on the microscale $\mathbf{y}$. That is

$$\mathbf{u}_{\mathrm{I}}^{(0)} = \mathbf{u}_{\mathrm{I}}^{(0)}(\mathbf{x}, t) \tag{3.111}$$

$$\mathbf{u}_{\mathrm{II}}^{(0)} = \mathbf{u}_{\mathrm{II}}^{(0)}(\mathbf{x}, t). \tag{3.112}$$

Since we have the boundary condition $\mathbf{u}_{\mathrm{I}}^{(0)} = \mathbf{u}_{\mathrm{II}}^{(0)}$ on Γ_{III} given by (3.87) we can define

$$\mathbf{u}^{(0)} = \mathbf{u}_{\mathrm{I}}^{(0)} = \mathbf{u}_{\mathrm{II}}^{(0)}, \tag{3.113}$$

which we will use throughout the following sections.

3.2.4 Fluid Flow on the Macroscale

We now wish to investigate the leading order of the velocity which we denoted $\mathbf{v}^{(0)}$. We can define the relative fluid-solid displacement, $\mathbf{w}$, by

$$\mathbf{w}(\mathbf{x}, \mathbf{y}, t) = \mathbf{v}^{(0)}(\mathbf{x}, \mathbf{y}, t) - \dot{\mathbf{u}}^{(0)}(\mathbf{x}, \mathbf{y}, t), \tag{3.114}$$

Using equations (3.88), (3.82), (3.83), (3.96) and (3.104), exploiting notation (3.113), we have a Stokes'-type boundary value problem which is given by

$$\nabla_{\mathbf{y}}^2 \mathbf{w} - \nabla_{\mathbf{y}} p^{(1)} - \nabla_{\mathbf{x}} p^{(0)} = \mathbf{0} \qquad \text{in} \quad \Omega_{\mathrm{f}} \tag{3.115}$$

$$\nabla_{\mathbf{y}} \cdot \mathbf{w} = \mathbf{0} \qquad \text{in} \quad \Omega_{\mathrm{f}} \tag{3.116}$$

$$\mathbf{w} = \mathbf{0} \qquad \text{on} \quad \Gamma_{\mathrm{I}} \cup \Gamma_{\mathrm{II}}. \tag{3.117}$$

Now exploiting linearity and using (3.110) we can propose the following ansatz for the stokes-type boundary value problem (3.115−3.117),

$$\mathbf{w} = -W \nabla_{\mathbf{x}} p^{(0)}, \tag{3.118}$$

$$p^{(1)} = -\boldsymbol{\Pi} \nabla_{\mathbf{x}} p^{(0)} + c(\mathbf{x}), \tag{3.119}$$

where $p^{(1)}$ is defined up to an arbitrary $\mathbf{y}$-constant function. Equation (3.119) is the solution to the problem (3.115−3.117) provided that second rank tensor W and vector $\boldsymbol{\Pi}$ satisfy the following cell problem

$$\begin{cases} \nabla_{\mathbf{y}}^2 W^{\mathrm{T}} - \nabla_{\mathbf{y}} \boldsymbol{\Pi} + \mathbf{I} = \mathbf{0} & \text{in} \quad \Omega_{\mathrm{f}} \\ \nabla_{\mathbf{y}} \cdot W^{\mathrm{T}} = \mathbf{0} & \text{in} \quad \Omega_{\mathrm{f}} \\ W = \mathbf{0} & \text{on} \quad \Gamma_{\mathrm{I}} \cup \Gamma_{\mathrm{II}}, \end{cases} \tag{3.120}$$

where periodic conditions apply on the boundary $\partial\Omega_{\mathrm{f}}\backslash\Gamma_{\mathrm{I}}\cup\Gamma_{\mathrm{II}}$ and a further condition is to be placed on $\mathbf{\Pi}$ for the solution to be unique (for example zero average on the fluid cell portion). Taking the integral average of (3.118) over the fluid domain leads to

$$\langle\mathbf{w}\rangle_{\mathrm{f}} = -\langle W\rangle_{\mathrm{f}}\nabla_{\mathbf{x}}p^{(0)}, \tag{3.121}$$

meaning that the fluid flow is described by Darcy's law in the macroscale. As expected, this is the same result as standard poroelasticity with only one solid phase.

3.2.5 Poroelasticity on the Macroscale

We now require the macroscale equations to close the system for the elastic displacement $\mathbf{u}^{(0)}$ and $p^{(0)}$. Summing up the integral averages of equations (3.94), (3.95) and (3.96) we have

$$\begin{aligned}&\int_{\Omega_{\mathrm{I}}}\nabla_{\mathbf{y}}\cdot\mathsf{T}_{\mathrm{I}}^{(1)}\mathrm{d}\mathbf{y}+\int_{\Omega_{\mathrm{II}}}\nabla_{\mathbf{y}}\cdot\mathsf{T}_{\mathrm{II}}^{(1)}\mathrm{d}\mathbf{y}+\int_{\Omega_{\mathrm{f}}}\nabla_{\mathbf{y}}\cdot\mathsf{T}_{\mathsf{f}}{}^{(1)}\mathrm{d}\mathbf{y}+\\&\int_{\Omega_{\mathrm{I}}}\nabla_{\mathbf{x}}\cdot\mathsf{T}_{\mathrm{I}}^{(0)}\mathrm{d}\mathbf{y}+\int_{\Omega_{\mathrm{II}}}\nabla_{\mathbf{x}}\cdot\mathsf{T}_{\mathrm{II}}^{(0)}\mathrm{d}\mathbf{y}+\int_{\Omega_{\mathrm{f}}}\nabla_{\mathbf{x}}\cdot\mathsf{T}_{\mathsf{f}}{}^{(0)}\mathrm{d}\mathbf{y}=0.\end{aligned} \tag{3.122}$$

Applying the divergence theorem to the first three integrals and rearranging the last three integrals by means of macroscopic uniformity (3.59) we obtain

$$\begin{aligned}&\int_{\partial\Omega_{\mathrm{I}}\backslash\Gamma_{\mathrm{I}}\cup\Gamma_{\mathrm{III}}}\mathsf{T}_{\mathrm{I}}^{(1)}\mathbf{n}_{\Omega_{\mathrm{I}}\backslash\Gamma_{\mathrm{I}}\cup\Gamma_{\mathrm{III}}}\mathrm{dS}+\int_{\Gamma_{\mathrm{I}}}\mathsf{T}_{\mathrm{I}}^{(1)}\mathbf{n}_{\mathrm{I}}\mathrm{dS}-\int_{\Gamma_{\mathrm{III}}}\mathsf{T}_{\mathrm{I}}^{(1)}\mathbf{n}_{\mathrm{III}}\mathrm{dS}+\\&\int_{\partial\Omega_{\mathrm{II}}\backslash\Gamma_{\mathrm{II}}\cup\Gamma_{\mathrm{III}}}\mathsf{T}_{\mathrm{II}}^{(1)}\mathbf{n}_{\Omega_{\mathrm{II}}\backslash\Gamma_{\mathrm{II}}\cup\Gamma_{\mathrm{III}}}\mathrm{dS}+\int_{\Gamma_{\mathrm{II}}}\mathsf{T}_{\mathrm{II}}^{(1)}\mathbf{n}_{\mathrm{II}}\mathrm{dS}+\int_{\Gamma_{\mathrm{III}}}\mathsf{T}_{\mathrm{II}}^{(1)}\mathbf{n}_{\mathrm{III}}\mathrm{dS}+\\&\int_{\partial\Omega_{\mathrm{f}}\backslash\Gamma_{\mathrm{I}}\cup\Gamma_{\mathrm{II}}}\mathsf{T}_{\mathsf{f}}{}^{(1)}\mathbf{n}_{\Omega_{\mathrm{f}}\backslash\Gamma_{\mathrm{I}}\cup\Gamma_{\mathrm{II}}}\mathrm{dS}-\int_{\Gamma_{\mathrm{II}}}\mathsf{T}_{\mathsf{f}}{}^{(1)}\mathbf{n}_{\mathrm{II}}\mathrm{dS}-\int_{\Gamma_{\mathrm{I}}}\mathsf{T}_{\mathsf{f}}{}^{(1)}\mathbf{n}_{\mathrm{I}}\mathrm{dS}+\\&\nabla_{\mathbf{x}}\cdot\int_{\Omega_{\mathrm{I}}}\mathsf{T}_{\mathrm{I}}^{(0)}\mathrm{d}\mathbf{y}+\nabla_{\mathbf{x}}\cdot\int_{\Omega_{\mathrm{II}}}\mathsf{T}_{\mathrm{II}}^{(0)}\mathrm{d}\mathbf{y}+\nabla_{\mathbf{x}}\cdot\int_{\Omega_{\mathrm{f}}}\mathsf{T}_{\mathsf{f}}{}^{(0)}\mathrm{d}\mathbf{y}=0,\end{aligned} \tag{3.123}$$

where $\mathbf{n}_{\mathrm{I}}$, $\mathbf{n}_{\mathrm{II}}$, $\mathbf{n}_{\mathrm{III}}$, $\mathbf{n}_{\Omega_{\mathrm{I}}\backslash\Gamma_{\mathrm{I}}\cup\Gamma_{\mathrm{III}}}$, $\mathbf{n}_{\Omega_{\mathrm{II}}\backslash\Gamma_{\mathrm{II}}\cup\Gamma_{\mathrm{III}}}$ and $\mathbf{n}_{\Omega_{\mathrm{f}}\backslash\Gamma_{\mathrm{I}}\cup\Gamma_{\mathrm{II}}}$ are the unit normals corresponding to Γ_{I}, Γ_{II}, Γ_{III}, $\partial\Omega_{\mathrm{I}}\setminus\Gamma_{\mathrm{I}}\cup\Gamma_{\mathrm{III}}$, $\partial\Omega_{\mathrm{II}}\setminus\Gamma_{\mathrm{II}}\cup\Gamma_{\mathrm{III}}$ and $\partial\Omega_{\mathrm{f}}\setminus\Gamma_{\mathrm{I}}\cup\Gamma_{\mathrm{II}}$. Since the contributions over the external boundaries of Ω_{I}, Ω_{II} and Ω_{f} cancel out due to $\mathbf{y}$-periodicity (3.123) becomes

$$\begin{aligned}&\int_{\Gamma_{\mathrm{I}}}\mathsf{T}_{\mathrm{I}}^{(1)}\mathbf{n}_{\mathrm{I}}\mathrm{dS}+\int_{\Gamma_{\mathrm{II}}}\mathsf{T}_{\mathrm{II}}^{(1)}\mathbf{n}_{\mathrm{II}}\mathrm{dS}-\int_{\Gamma_{\mathrm{I}}}\mathsf{T}_{\mathsf{f}}{}^{(1)}\mathbf{n}_{\mathrm{I}}\mathrm{dS}-\\&\int_{\Gamma_{\mathrm{II}}}\mathsf{T}_{\mathsf{f}}{}^{(1)}\mathbf{n}_{\mathrm{II}}\mathrm{dS}-\int_{\Gamma_{\mathrm{III}}}\mathsf{T}_{\mathrm{I}}^{(1)}\mathbf{n}_{\mathrm{III}}\mathrm{dS}+\int_{\Gamma_{\mathrm{III}}}\mathsf{T}_{\mathrm{II}}^{(1)}\mathbf{n}_{\mathrm{III}}\mathrm{dS}+\end{aligned}$$

$$\nabla_{\mathbf{x}} \cdot \int_{\Omega_{\mathrm{I}}} \mathsf{T}_{\mathrm{I}}^{(0)} \mathrm{d}\mathbf{y} + \nabla_{\mathbf{x}} \cdot \int_{\Omega_{\mathrm{II}}} \mathsf{T}_{\mathrm{II}}^{(0)} \mathrm{d}\mathbf{y} + \nabla_{\mathbf{x}} \cdot \int_{\Omega_{\mathrm{f}}} \mathsf{T}_{\mathrm{f}}{}^{(0)} \mathrm{d}\mathbf{y} = 0. \tag{3.124}$$

The first six integrals in (3.124) cancel out due to (3.100), (3.101) and (3.102) and the final three terms can be written as

$$\nabla_{\mathbf{x}} \cdot \langle \mathsf{T}_{\mathrm{I}}^{(0)} + \mathsf{T}_{\mathrm{II}}^{(0)} \rangle_{\mathrm{s}} - \phi \nabla_{\mathbf{x}} p^{(0)} = 0, \tag{3.125}$$

where $\phi := |\Omega_{\mathrm{f}}|/|\Omega|$ is the porosity of the material.

Exploiting (3.110) and (3.113) we can write the following problem for $\mathbf{u}_{\mathrm{I}}^{(1)}$ and $\mathbf{u}_{\mathrm{II}}^{(1)}$ using (3.78), (3.79), (3.84), (3.85), (3.86), (3.88), (3.103), (3.105) and (3.106)

$$\nabla_{\mathbf{y}} \cdot (\mathbb{C}_{\mathrm{I}} \xi_{\mathbf{y}}(\mathbf{u}_{\mathrm{I}}^{(1)})) + \nabla_{\mathbf{y}} \cdot (\mathbb{C}_{\mathrm{I}} \xi_{\mathbf{x}}(\mathbf{u}^{(0)})) = 0 \qquad \text{in} \quad \Omega_{\mathrm{I}} \tag{3.126}$$

$$\nabla_{\mathbf{y}} \cdot (\mathbb{C}_{\mathrm{II}} \xi_{\mathbf{y}}(\mathbf{u}_{\mathrm{II}}^{(1)})) + \nabla_{\mathbf{y}} \cdot (\mathbb{C}_{\mathrm{II}} \xi_{\mathbf{x}}(\mathbf{u}^{(0)})) = 0 \qquad \text{in} \quad \Omega_{\mathrm{II}} \tag{3.127}$$

$$\mathbb{C}_{\mathrm{I}} \xi_{\mathbf{y}}(\mathbf{u}_{\mathrm{I}}^{(1)}) \mathbf{n}_{\mathrm{III}} - \mathbb{C}_{\mathrm{II}} \xi_{\mathbf{y}}(\mathbf{u}_{\mathrm{II}}^{(1)}) \mathbf{n}_{\mathrm{III}} = (\mathbb{C}_{\mathrm{II}} - \mathbb{C}_{\mathrm{I}}) \xi_{\mathbf{x}}(\mathbf{u}^{(0)}) \mathbf{n}_{\mathrm{III}} \qquad \text{on} \quad \Gamma_{\mathrm{III}} \tag{3.128}$$

$$\mathbf{u}_{\mathrm{I}}^{(1)} = \mathbf{u}_{\mathrm{II}}^{(1)} \qquad \text{on} \quad \Gamma_{\mathrm{III}} \tag{3.129}$$

$$(\mathbb{C}_{\mathrm{I}} \xi_{\mathbf{y}}(\mathbf{u}_{\mathrm{I}}^{(1)}) + \mathbb{C}_{\mathrm{I}} \xi_{\mathbf{x}}(\mathbf{u}^{(0)})) \mathbf{n}_{\mathrm{I}} = -p^{(0)} \mathbf{n}_{\mathrm{I}} \qquad \text{on} \quad \Gamma_{\mathrm{I}} \tag{3.130}$$

$$(\mathbb{C}_{\mathrm{II}} \xi_{\mathbf{y}}(\mathbf{u}_{\mathrm{II}}^{(1)}) + \mathbb{C}_{\mathrm{II}} \xi_{\mathbf{x}}(\mathbf{u}^{(0)})) \mathbf{n}_{\mathrm{II}} = -p^{(0)} \mathbf{n}_{\mathrm{II}} \qquad \text{on} \quad \Gamma_{\mathrm{II}} \tag{3.131}$$

The solution to the problem given by (3.126−3.131), exploiting linearity is given as

$$\mathbf{u}_{\mathrm{I}}^{(1)} = A_{\mathrm{I}} \xi_{\mathbf{x}}(\mathbf{u}^{(0)}) + \mathbf{a}_{\mathrm{I}} p^{(0)} \tag{3.132}$$

$$\mathbf{u}_{\mathrm{II}}^{(1)} = A_{\mathrm{II}} \xi_{\mathbf{x}}(\mathbf{u}^{(0)}) + \mathbf{a}_{\mathrm{II}} p^{(0)} \tag{3.133}$$

where A_{I} and A_{II} are third rank tensors and $\mathbf{a}_{\mathrm{I}}$ and $\mathbf{a}_{\mathrm{II}}$ are vectors. The auxiliary fields A_{I}, A_{II}, $\mathbf{a}_{\mathrm{I}}$ and $\mathbf{a}_{\mathrm{II}}$ solve the following cell problems.

$$\nabla_{\mathbf{y}} \cdot (\mathbb{C}_{\mathrm{I}} \xi_{\mathbf{y}}(A_{\mathrm{I}})) = -\nabla_{\mathbf{y}} \cdot \mathbb{C}_{\mathrm{I}} \qquad \text{in} \quad \Omega_{\mathrm{I}} \tag{3.134}$$

$$\nabla_{\mathbf{y}} \cdot (\mathbb{C}_{\mathrm{II}} \xi_{\mathbf{y}}(A_{\mathrm{II}})) = -\nabla_{\mathbf{y}} \cdot \mathbb{C}_{\mathrm{II}} \qquad \text{in} \quad \Omega_{\mathrm{II}} \tag{3.135}$$

$$\mathbb{C}_{\mathrm{I}} \xi_{\mathbf{y}}(A_{\mathrm{I}}) \mathbf{n}_{\mathrm{III}} - \mathbb{C}_{\mathrm{II}} \xi_{\mathbf{y}}(A_{\mathrm{II}}) \mathbf{n}_{\mathrm{III}} = (\mathbb{C}_{\mathrm{II}} - \mathbb{C}_{\mathrm{I}}) \mathbf{n}_{\mathrm{III}} \qquad \text{on} \quad \Gamma_{\mathrm{III}} \tag{3.136}$$

$$A_{\mathrm{I}} = A_{\mathrm{II}} \qquad \text{on} \quad \Gamma_{\mathrm{III}} \tag{3.137}$$

$$(\mathbb{C}_{\mathrm{I}} \xi_{\mathbf{y}}(A_{\mathrm{I}})) \mathbf{n}_{\mathrm{I}} = -\mathbb{C}_{\mathrm{I}} \mathbf{n}_{\mathrm{I}} \qquad \text{on} \quad \Gamma_{\mathrm{I}} \tag{3.138}$$

$$(\mathbb{C}_{\mathrm{II}} \xi_{\mathbf{y}}(A_{\mathrm{II}})) \mathbf{n}_{\mathrm{II}} = -\mathbb{C}_{\mathrm{II}} \mathbf{n}_{\mathrm{II}} \qquad \text{on} \quad \Gamma_{\mathrm{II}} \tag{3.139}$$

and

$$\nabla_{\mathbf{y}} \cdot (\mathbb{C}_{\mathrm{I}} \xi_{\mathbf{y}}(\mathbf{a}_{\mathrm{I}})) = \mathbf{0} \qquad \text{in} \quad \Omega_{\mathrm{I}} \tag{3.140}$$

$$\nabla_{\mathbf{y}} \cdot (\mathbb{C}_{\mathrm{II}} \xi_{\mathbf{y}}(\mathbf{a}_{\mathrm{II}})) = \mathbf{0} \qquad \text{in} \quad \Omega_{\mathrm{II}} \tag{3.141}$$

$$(\mathbb{C}_{\mathrm{I}} \xi_{\mathbf{y}}(\mathbf{a}_{\mathrm{I}}))\mathbf{n}_{\mathrm{III}} = (\mathbb{C}_{\mathrm{II}} \xi_{\mathbf{y}}(\mathbf{a}_{\mathrm{II}}))\mathbf{n}_{\mathrm{III}} \qquad \text{on} \quad \Gamma_{\mathrm{III}} \tag{3.142}$$

$$\mathbf{a}_{\mathrm{I}} = \mathbf{a}_{\mathrm{II}} \qquad \text{on} \quad \Gamma_{\mathrm{III}} \tag{3.143}$$

$$(\mathbb{C}_{\mathrm{I}} \xi_{\mathbf{y}}(\mathbf{a}_{\mathrm{I}}))\mathbf{n}_{\mathrm{I}} + \mathbf{n}_{\mathrm{I}} = \mathbf{0} \qquad \text{on} \quad \Gamma_{\mathrm{I}} \tag{3.144}$$

$$(\mathbb{C}_{\mathrm{II}} \xi_{\mathbf{y}}(\mathbf{a}_{\mathrm{II}}))\mathbf{n}_{\mathrm{II}} + \mathbf{n}_{\mathrm{II}} = \mathbf{0} \qquad \text{on} \quad \Gamma_{\mathrm{II}} \tag{3.145}$$

To ensure the uniqueness of the solution, we also require a further condition on A_{I}, A_{II}, $\mathbf{a}_{\mathrm{I}}$ and $\mathbf{a}_{\mathrm{II}}$, for example:

$$\langle A_{\mathrm{I}} \rangle_{\mathrm{I}} + \langle A_{\mathrm{II}} \rangle_{\mathrm{II}} = 0 \quad \textit{and} \quad \langle \mathbf{a}_{\mathrm{I}} \rangle_{\mathrm{I}} + \langle \mathbf{a}_{\mathrm{II}} \rangle_{\mathrm{II}} = \mathbf{0}. \tag{3.146}$$

We can also write the cell problems for A_{I}, A_{II}, $\mathbf{a}_{\mathrm{I}}$ and $\mathbf{a}_{\mathrm{II}}$ with corresponding components A^{I}_{ikl}, A^{II}_{ikl}, a^{I}_{i} and a^{II}_{i} as

$$\frac{\partial}{\partial y_j}\left(C^{\mathrm{I}}_{ijpq} \xi^{kl}_{pq}(A^{\mathrm{I}}) \right) + \frac{\partial C^{\mathrm{I}}_{ijkl}}{\partial y_j} = 0 \qquad \text{in} \quad \Omega_{\mathrm{I}} \tag{3.147}$$

$$\frac{\partial}{\partial y_j}\left(C^{\mathrm{II}}_{ijpq} \xi^{kl}_{pq}(A^{\mathrm{II}}) \right) + \frac{\partial C^{\mathrm{II}}_{ijkl}}{\partial y_j} = 0 \qquad \text{in} \quad \Omega_{\mathrm{II}} \tag{3.148}$$

$$C^{\mathrm{I}}_{ijpq} \xi^{kl}_{pq}(A^{\mathrm{I}}) n^{\mathrm{III}}_{j} - C^{\mathrm{II}}_{ijpq} \xi^{kl}_{pq}(A^{\mathrm{II}}) n^{\mathrm{III}}_{j} = (C^{\mathrm{II}} - C^{\mathrm{I}})_{ijkl} n^{\mathrm{III}}_{j} \qquad \text{on} \quad \Gamma_{\mathrm{III}} \tag{3.149}$$

$$A^{\mathrm{I}}_{ikl} = A^{\mathrm{II}}_{ikl} \qquad \text{on} \quad \Gamma_{\mathrm{III}} \tag{3.150}$$

$$C^{\mathrm{I}}_{ijpq} \xi^{kl}_{pq}(A^{\mathrm{I}}) n^{\mathrm{I}}_{j} + C^{\mathrm{I}}_{ijpq} n^{\mathrm{I}}_{j} = 0 \qquad \text{on} \quad \Gamma_{\mathrm{I}} \tag{3.151}$$

$$C^{\mathrm{II}}_{ijpq} \xi^{kl}_{pq}(A^{\mathrm{II}}) n^{\mathrm{II}}_{j} + C^{\mathrm{II}}_{ijpq} n^{\mathrm{II}}_{j} = 0 \qquad \text{on} \quad \Gamma_{\mathrm{II}} \tag{3.152}$$

and

$$\frac{\partial}{\partial y_j}\left(C^{\mathrm{I}}_{ijpq} \xi_{pq}(\mathbf{a}^{\mathrm{I}}) \right) = 0 \qquad \text{in} \quad \Omega_{\mathrm{I}} \tag{3.153}$$

$$\frac{\partial}{\partial y_j}\left(C^{\mathrm{II}}_{ijpq} \xi_{pq}(\mathbf{a}^{\mathrm{II}}) \right) = 0 \qquad \text{in} \quad \Omega_{\mathrm{II}} \tag{3.154}$$

$$C^{\mathrm{I}}_{ijpq} \xi_{pq}(\mathbf{a}^{\mathrm{I}}) n^{\mathrm{III}}_{j} = C^{\mathrm{II}}_{ijpq} \xi_{pq}(\mathbf{a}^{\mathrm{II}}) n^{\mathrm{III}}_{j} \qquad \text{on} \quad \Gamma_{\mathrm{III}} \tag{3.155}$$

$$a^{\mathrm{I}}_{i} = a^{\mathrm{II}}_{i} \qquad \text{on} \quad \Gamma_{\mathrm{III}} \tag{3.156}$$

$$C^{\mathrm{I}}_{ijpq} \xi_{pq}(\mathbf{a}^{\mathrm{I}}) n^{\mathrm{I}}_{j} + n^{\mathrm{I}}_{j} = 0 \qquad \text{on} \quad \Gamma_{\mathrm{I}} \tag{3.157}$$

$$C^{\rm II}_{ijpq}\xi_{pq}(\mathbf{a}^{\rm II})n^{\rm II}_j + n^{\rm II}_j = 0 \qquad \text{on} \quad \Gamma_{\rm II} \tag{3.158}$$

where we have used the notation

$$\xi^{kl}_{pq}(A^{\rm I}) = \frac{1}{2}\Big(\frac{\partial A^{\rm I}_{pkl}}{\partial y_q} + \frac{\partial A^{\rm I}_{qkl}}{\partial y_p}\Big); \quad \xi^{kl}_{pq}(A^{\rm II}) = \frac{1}{2}\Big(\frac{\partial A^{\rm II}_{pkl}}{\partial y_q} + \frac{\partial A^{\rm II}_{qkl}}{\partial y_p}\Big). \tag{3.159}$$

We should note that the problems in terms of $\mathbf{a}_i$ and A_i, where $i = {\rm I}, {\rm II}$, are to be solved on the solid cell portion Ω_s, where $\bar{\Omega}_s := \bar{\Omega}_{\rm I} \cup \bar{\Omega}_{\rm II}$.

Remark 5 (Compatibility Condition for the Cell Problems)**.** *We have the Compatibility Condition (also known as the solvability condition) for the cell problems, see, e.g. [27]. We first take the integral average of the sum of the left hand sides of (3.134) and (3.135) and apply the divergence theorem. That is,*

$$\int_{\Omega_{\rm I}} \nabla_{\mathbf{y}} \cdot (\mathbb{C}_{\rm I}\xi_{\mathbf{y}}(A_{\rm I}))\, d\mathbf{y} + \int_{\Omega_{\rm II}} \nabla_{\mathbf{y}} \cdot (\mathbb{C}_{\rm II}\xi_{\mathbf{y}}(A_{\rm II}))\, d\mathbf{y} \tag{3.160}$$

$$\begin{aligned} &= \int_{\Gamma_{\rm I}} (\mathbb{C}_{\rm I}\xi_{\mathbf{y}}(A_{\rm I}))\mathbf{n}_{\rm I}\, dS + \int_{\Gamma_{\rm III}} (\mathbb{C}_{\rm I}\xi_{\mathbf{y}}(A_{\rm I}))\mathbf{n}_{\rm III}\, dS + \int_{\partial\Omega_{\rm I}\setminus\Gamma_{\rm I}\cup\Gamma_{\rm III}} (\mathbb{C}_{\rm I}\xi_{\mathbf{y}}(A_{\rm I}))\mathbf{n}_{\Omega_{\rm I}\setminus\Gamma_{\rm I}\cup\Gamma_{\rm III}}\, dS \\ &+ \int_{\Gamma_{\rm II}} (\mathbb{C}_{\rm II}\xi_{\mathbf{y}}(A_{\rm II}))\mathbf{n}_{\rm II}\, dS - \int_{\Gamma_{\rm III}} (\mathbb{C}_{\rm II}\xi_{\mathbf{y}}(A_{\rm II}))\mathbf{n}_{\rm III}\, dS + \int_{\partial\Omega_{\rm II}\setminus\Gamma_{\rm II}\cup\Gamma_{\rm III}} (\mathbb{C}_{\rm II}\xi_{\mathbf{y}}(A_{\rm II}))\mathbf{n}_{\Omega_{\rm II}\setminus\Gamma_{\rm II}\cup\Gamma_{\rm III}}\, dS \end{aligned} \tag{3.161}$$

where $\mathbf{n}_{\rm I}$, $\mathbf{n}_{\rm II}$, $\mathbf{n}_{\rm III}$, $\mathbf{n}_{\Omega_{\rm I}\setminus\Gamma_{\rm I}\cup\Gamma_{\rm III}}$ *and* $\mathbf{n}_{\Omega_{\rm II}\setminus\Gamma_{\rm II}\cup\Gamma_{\rm III}}$ *are the unit normals corresponding to* $\Gamma_{\rm I}$, $\Gamma_{\rm II}$, $\Gamma_{\rm III}$, $\partial\Omega_{\rm I} \setminus \Gamma_{\rm I} \cup \Gamma_{\rm III}$ *and* $\partial\Omega_{\rm II} \setminus \Gamma_{\rm II} \cup \Gamma_{\rm III}$*. Terms on the external boundaries of* $\Omega_{\rm I}$ *and* $\Omega_{\rm II}$ *cancel due to* $\mathbf{y}$*-periodicity. So (3.161) becomes*

$$= \int_{\Gamma_{\rm I}} (\mathbb{C}_{\rm I}\xi_{\mathbf{y}}(A_{\rm I}))\mathbf{n}_{\rm I}\, dS + \int_{\Gamma_{\rm II}} (\mathbb{C}_{\rm II}\xi_{\mathbf{y}}(A_{\rm II}))\mathbf{n}_{\rm II}\, dS + \int_{\Gamma_{\rm III}} (\mathbb{C}_{\rm II} - \mathbb{C}_{\rm I})\mathbf{n}_{\rm III}\, dS \tag{3.162}$$

where we have used the interface condition (3.136) *and we can now also use* (3.138) *and* (3.139) *to write (3.162) as*

$$= \int_{\Gamma_{\rm III}} (\mathbb{C}_{\rm II} - \mathbb{C}_{\rm I})\mathbf{n}_{\rm III}\, dS - \int_{\Gamma_{\rm I}} \mathbb{C}_{\rm I} \cdot \mathbf{n}_{\rm I}\, dS - \int_{\Gamma_{\rm II}} \mathbb{C}_{\rm II} \cdot \mathbf{n}_{\rm II}\, dS. \tag{3.163}$$

On the other hand we are able to re-write (3.160) *using* (3.134) *and* (3.135) *as*

$$\int_{\Omega_{\rm I}} \nabla_{\mathbf{y}} \cdot (\mathbb{C}_{\rm I}\xi_{\mathbf{y}}(A_{\rm I}))\, d\mathbf{y} + \int_{\Omega_{\rm II}} \nabla_{\mathbf{y}} \cdot (\mathbb{C}_{\rm II}\xi_{\mathbf{y}}(A_{\rm II}))\, d\mathbf{y} \tag{3.164}$$

$$= -\int_{\Omega_{\rm I}} \nabla_{\mathbf{y}} \cdot \mathbb{C}_{\rm I}\, d\mathbf{y} - \int_{\Omega_{\rm II}} \nabla_{\mathbf{y}} \cdot \mathbb{C}_{\rm II}\, d\mathbf{y} \tag{3.165}$$

We can then apply the divergence theorem to obtain

$$\begin{aligned}&= -\int_{\Gamma_{\mathrm{I}}} \mathbb{C}_{\mathrm{I}} \cdot \mathbf{n}_{\mathrm{I}}\, dS - \int_{\Gamma_{\mathrm{III}}} \mathbb{C}_{\mathrm{I}} \cdot \mathbf{n}_{\mathrm{III}}\, dS - \int_{\partial\Omega_{\mathrm{I}}\setminus\Gamma_{\mathrm{I}}\cup\Gamma_{\mathrm{III}}} \mathbb{C}_{\mathrm{I}} \cdot \mathbf{n}_{\Omega_{\mathrm{I}}\setminus\Gamma_{\mathrm{I}}\cup\Gamma_{\mathrm{III}}}\, dS \\ &- \int_{\Gamma_{\mathrm{II}}} \mathbb{C}_{\mathrm{II}} \cdot \mathbf{n}_{\mathrm{II}}\, dS + \int_{\Gamma_{\mathrm{III}}} \mathbb{C}_{\mathrm{II}} \cdot \mathbf{n}_{\mathrm{III}}\, dS - \int_{\partial\Omega_{\mathrm{II}}\setminus\Gamma_{\mathrm{II}}\cup\Gamma_{\mathrm{III}}} \mathbb{C}_{\mathrm{II}} \cdot \mathbf{n}_{\Omega_{\mathrm{II}}\setminus\Gamma_{\mathrm{II}}\cup\Gamma_{\mathrm{III}}}\, dS\end{aligned}$$

where the unit normals are as above. The contributions over the periodic boundaries cancel to give

$$= -\int_{\Gamma_{\mathrm{I}}} \mathbb{C}_{\mathrm{I}} \cdot \mathbf{n}_{\mathrm{I}}\, dS - \int_{\Gamma_{\mathrm{II}}} \mathbb{C}_{\mathrm{II}} \cdot \mathbf{n}_{\mathrm{II}}\, dS + \int_{\Gamma_{\mathrm{III}}} (\mathbb{C}_{\mathrm{II}} - \mathbb{C}_{\mathrm{I}})\mathbf{n}_{\mathrm{III}}\, dS. \tag{3.166}$$

We can see that (3.163) *and* (3.166) *are equal, and therefore this proves the compatibility condition which is necessary for the problem to admit a solution, which can be made unique by imposing an additional condition, such as zero average of the auxiliary variables on the periodic cell.*

We now consider the leading order solid stress tensors. Since from (3.105) and (3.106) we have that $\mathbf{u}_{\mathrm{I}}^{(1)}$ and $\mathbf{u}_{\mathrm{II}}^{(1)}$ are related to $\mathsf{T}_{\mathrm{I}}^{(0)}$ and $\mathsf{T}_{\mathrm{II}}^{(0)}$ respectively we can exploit (3.132) and (3.133) to write

$$\mathsf{T}_{\mathrm{I}}^{(0)} = \mathbb{C}_{\mathrm{I}}\mathbb{M}_{\mathrm{I}}\xi_{\mathbf{x}}(\mathbf{u}^{(0)}) + \mathbb{C}_{\mathrm{I}}Q_{\mathrm{I}}p^{(0)} + \mathbb{C}_{\mathrm{I}}\xi_{\mathbf{x}}(\mathbf{u}^{(0)}) \tag{3.167}$$

and

$$\mathsf{T}_{\mathrm{II}}^{(0)} = \mathbb{C}_{\mathrm{II}}\mathbb{M}_{\mathrm{II}}\xi_{\mathbf{x}}(\mathbf{u}^{(0)}) + \mathbb{C}_{\mathrm{II}}Q_{\mathrm{II}}p^{(0)} + \mathbb{C}_{\mathrm{II}}\xi_{\mathbf{x}}(\mathbf{u}^{(0)}) \tag{3.168}$$

where we define

$$\begin{aligned}\mathbb{M}_{\mathrm{I}} = \xi_{\mathbf{y}}(A_{\mathrm{I}}), \quad \mathbb{M}_{\mathrm{II}} = \xi_{\mathbf{y}}(A_{\mathrm{II}}), \\ Q_{\mathrm{I}} = \xi_{\mathbf{y}}(\mathbf{a}_{\mathrm{I}}), \quad Q_{\mathrm{II}} = \xi_{\mathbf{y}}(\mathbf{a}_{\mathrm{II}}).\end{aligned} \tag{3.169}$$

Adding (3.167) and (3.168) and taking the integral average over the solid domain gives

$$\langle \mathsf{T}_{\mathrm{I}}^{(0)} + \mathsf{T}_{\mathrm{II}}^{(0)} \rangle_{\mathrm{s}} = \langle \mathbb{C}_{\mathrm{I}}\mathbb{M}_{\mathrm{I}} + \mathbb{C}_{\mathrm{I}} + \mathbb{C}_{\mathrm{II}}\mathbb{M}_{\mathrm{II}} + \mathbb{C}_{\mathrm{II}} \rangle_{\mathrm{s}} \xi_{\mathbf{x}}(\mathbf{u}^{(0)}) + \langle \mathbb{C}_{\mathrm{I}}Q_{\mathrm{I}} + \mathbb{C}_{\mathrm{II}}Q_{\mathrm{II}} \rangle_{\mathrm{s}} p^{(0)}. \tag{3.170}$$

From (3.125) we have that

$$\nabla_{\mathbf{x}} \cdot \hat{\mathsf{T}}_{\mathrm{Eff}} = 0 \tag{3.171}$$

where

$$\begin{aligned}\hat{\mathsf{T}}_{\text{Eff}} &= \langle \mathsf{T}_{\text{I}}^{(0)} + \mathsf{T}_{\text{II}}^{(0)} \rangle_{\text{s}} - \phi p^{(0)} \mathbf{I} \\ &= \langle \mathbb{C}_{\text{I}} \mathbb{M}_{\text{I}} + \mathbb{C}_{\text{I}} + \mathbb{C}_{\text{II}} \mathbb{M}_{\text{II}} + \mathbb{C}_{\text{II}} \rangle_{\text{s}} \xi_{\mathbf{x}}(\mathbf{u}^{(0)}) \\ &+ (\langle \mathbb{C}_{\text{I}} Q_{\text{I}} + \mathbb{C}_{\text{II}} Q_{\text{II}} \rangle_{\text{s}} - \phi \mathbf{I}) p^{(0)}. \end{aligned} \tag{3.172}$$

Equations (3.171)-(3.172) represent the average force balance equations for our poroelastic composite material.

We now return to (3.97), the incompressibility condition and integrate to obtain

$$0 = \int_{\Omega_{\text{f}}} \nabla_{\mathbf{y}} \cdot v^{(1)} \mathrm{d}\mathbf{y} + \int_{\Omega_{\text{f}}} \nabla_{\mathbf{x}} \cdot v^{(0)} \mathrm{d}\mathbf{y}. \tag{3.173}$$

Applying the divergence theorem twice to the first integral and using (3.98) and (3.99) and also rearranging the second integral we obtain

$$0 = -\int_{\Omega_{\text{I}}} \nabla_{\mathbf{y}} \cdot \dot{\mathbf{u}}_{\text{I}}^{(1)} \mathrm{d}\mathbf{y} - \int_{\Omega_{\text{II}}} \nabla_{\mathbf{y}} \cdot \dot{\mathbf{u}}_{\text{II}}^{(1)} \mathrm{d}\mathbf{y} + \nabla_{\mathbf{x}} \cdot \langle v^{(0)} \rangle_{\text{f}} \tag{3.174}$$

$$= -\int_{\Omega_{\text{I}}} \mathrm{Tr}(\xi_{\mathbf{y}}(\dot{\mathbf{u}}_{\text{I}}^{(1)})) \mathrm{d}\mathbf{y} - \int_{\Omega_{\text{II}}} \mathrm{Tr}(\xi_{\mathbf{y}}(\dot{\mathbf{u}}_{\text{II}}^{(1)})) \mathrm{d}\mathbf{y} + \nabla_{\mathbf{x}} \cdot \langle v^{(0)} \rangle_{\text{f}}. \tag{3.175}$$

Therefore we have

$$\langle \mathrm{Tr}(\xi_{\mathbf{y}}(\dot{\mathbf{u}}_{\text{I}}^{(1)}) + \xi_{\mathbf{y}}(\dot{\mathbf{u}}_{\text{II}}^{(1)})) \rangle_{\text{s}} = \nabla_{\mathbf{x}} \cdot \langle v^{(0)} \rangle_{\text{f}}. \tag{3.176}$$

Using (3.132) and (3.133) with (3.169) we have that

$$\xi_{\mathbf{y}}(\dot{\mathbf{u}}_{\text{I}}^{(1)}) + \xi_{\mathbf{y}}(\dot{\mathbf{u}}_{\text{II}}^{(1)}) = (\mathbb{M}_{\text{I}} + \mathbb{M}_{\text{II}}) \xi_{\mathbf{x}}(\dot{\mathbf{u}}^{(0)}) + (Q_{\text{I}} + Q_{\text{II}}) \dot{p}^{(0)}. \tag{3.177}$$

So using (3.177) then equation (3.176) becomes

$$\nabla_{\mathbf{x}} \cdot \langle v^{(0)} \rangle_{\text{f}} = \langle \mathrm{Tr}(\mathbb{M}_{\text{I}} + \mathbb{M}_{\text{II}}) \rangle_{\text{s}} : \xi_{\mathbf{x}}(\dot{\mathbf{u}}^{(0)}) + \langle \mathrm{Tr}(Q_{\text{I}} + Q_{\text{II}}) \rangle_{\text{s}} \dot{p}^{(0)}. \tag{3.178}$$

Now returning to (3.114), the expression for relative fluid-solid displacement, and taking the integral average over the fluid domain we obtain

$$\langle \mathbf{w} \rangle_{\text{f}} = \langle \mathbf{v}^{(0)} \rangle_{\text{f}} - \phi \dot{\mathbf{u}}^{(0)}, \tag{3.179}$$

where ϕ is the porosity of the material. Then rearranging we obtain

$$\langle \mathbf{v}^{(0)} \rangle_{\mathrm{f}} = \langle \mathbf{w} \rangle_{\mathrm{f}} + \phi \dot{\mathbf{u}}^{(0)}. \tag{3.180}$$

We then use this relation to rewrite (3.178) as

$$\nabla_{\mathbf{x}} \cdot (\langle \mathbf{w} \rangle_{\mathrm{f}} + \phi \dot{\mathbf{u}}^{(0)}) = \langle \mathrm{Tr}(\mathbb{M}_{\mathrm{I}} + \mathbb{M}_{\mathrm{II}}) \rangle_{\mathrm{s}} : \xi_{\mathbf{x}}(\dot{\mathbf{u}}^{(0)}) + \langle \mathrm{Tr}(Q_{\mathrm{I}} + Q_{\mathrm{II}}) \rangle_{\mathrm{s}} \dot{p}^{(0)}. \tag{3.181}$$

We can expand the left hand side of (3.181) and then rearrange to obtain the following expression for $\dot{p}^{(0)}$. We note that we are able to express $\phi \nabla_{\mathbf{x}} \cdot \dot{\mathbf{u}}^{(0)}$ as $\phi \mathbf{I} : \xi_{\mathbf{x}}(\dot{\mathbf{u}}^{(0)})$. Then

$$\dot{p}^{(0)} = \frac{1}{\langle \mathrm{Tr}(Q_{\mathrm{I}} + Q_{\mathrm{II}}) \rangle_{\mathrm{s}}} \Big(\nabla_{\mathbf{x}} \cdot \langle \mathbf{w} \rangle_{\mathrm{f}} + (\phi \mathbf{I} - \langle \mathrm{Tr}(\mathbb{M}_{\mathrm{I}} + \mathbb{M}_{\mathrm{II}}) \rangle_{\mathrm{s}}) : \xi_{\mathbf{x}}(\dot{\mathbf{u}}^{(0)}) \Big). \tag{3.182}$$

We can then define

$$\hat{M} := \frac{-1}{\langle \mathrm{Tr}(Q_{\mathrm{I}} + Q_{\mathrm{II}}) \rangle_{\mathrm{s}}} \quad \text{and} \quad \hat{\boldsymbol{\alpha}} := \phi \mathbf{I} - \langle \mathrm{Tr}(\mathbb{M}_{\mathrm{I}} + \mathbb{M}_{\mathrm{II}}) \rangle_{\mathrm{s}} \tag{3.183}$$

and then we can use (3.183) to write (3.182) as

$$\dot{p}^{(0)} = -\hat{M}(\nabla_{\mathbf{x}} \cdot \langle \mathbf{w} \rangle_{\mathrm{f}} + \hat{\boldsymbol{\alpha}} : \xi_{\mathbf{x}}(\dot{\mathbf{u}}^{(0)})). \tag{3.184}$$

Finally dividing through by $\hat{M}$ we obtain

$$\frac{\dot{p}^{(0)}}{\hat{M}} = -\nabla_{\mathbf{x}} \cdot \langle \mathbf{w} \rangle_{\mathrm{f}} - \hat{\boldsymbol{\alpha}} : \xi_{\mathbf{x}}(\dot{\mathbf{u}}^{(0)}). \tag{3.185}$$

We have now derived all the equations required to be able to state our macroscale model for a poroelastic composite. Within the next section we will state our novel macroscale model for poroelastic composites and will then prove properties of the effective coefficients of this model.

3.3 The macroscale result and properties of the effective coefficients

The equations in the macroscale model describe the effective poroelastic behaviour of the material in terms of the pore pressure, the average fluid velocity and the elastic displace-

ment. The macroscale model is then given by

$$\begin{cases} \langle \mathbf{w} \rangle_{\mathrm{f}} = -\langle W \rangle_{\mathrm{f}} \nabla_{\mathbf{x}} p^{(0)}, \\ \nabla_{\mathbf{x}} \cdot \hat{\mathsf{T}}_{\mathrm{Eff}} = 0, \\ \hat{\mathsf{T}}_{\mathrm{Eff}} = \langle \mathbb{C}_{\mathrm{I}} \mathbb{M}_{\mathrm{I}} + \mathbb{C}_{\mathrm{I}} + \mathbb{C}_{\mathrm{II}} \mathbb{M}_{\mathrm{II}} + \mathbb{C}_{\mathrm{II}} \rangle_{\mathrm{s}} \xi_{\mathbf{x}}(\mathbf{u}^{(0)}) + (\langle \mathbb{C}_{\mathrm{I}} Q_{\mathrm{I}} + \mathbb{C}_{\mathrm{II}} Q_{\mathrm{II}} \rangle_{\mathrm{s}} - \phi \mathbf{I}) p^{(0)}, \\ \dfrac{\dot{p}^{(0)}}{\hat{M}} = -\nabla_{\mathbf{x}} \cdot \langle \mathbf{w} \rangle_{\mathrm{f}} - \hat{\boldsymbol{\alpha}} : \xi_{\mathbf{x}}(\dot{\mathbf{u}}^{(0)}), \end{cases} \tag{3.186}$$

where we have that $p^{(0)}$ is the macroscale pressure, $\mathbf{u}^{(0)}$ is the solid displacement, $\dot{\mathbf{u}}^{(0)}$ is the solid velocity and $\mathbf{w}$ is the leading order relative fluid-solid velocity. The first equation of the macroscale model represents Darcy's law for $\mathbf{w}$, where $\mathbf{w}$ is the relative fluid-solid velocity. This is the same equation that we would obtain for standard poroelasticity. The second of the macroscale system of PDEs is the stress balance equation for the poroelastic composite material. The constitutive equation is of poroelastic type, with drained effective elasticity tensor given by

$$\widehat{\mathbb{C}} = \langle \mathbb{C}_{\mathrm{I}} \mathbb{M}_{\mathrm{I}} + \mathbb{C}_{\mathrm{I}} + \mathbb{C}_{\mathrm{II}} \mathbb{M}_{\mathrm{II}} + \mathbb{C}_{\mathrm{II}} \rangle_{s}. \tag{3.187}$$

The final equation in our macroscale model describes the conservation of mass for a poroelastic material and relates changes in the fluid pressure to changes in the fluid and solid volumes. We therefore have that the mechanical behaviour of the poroelastic composite material can be fully described by the effective elasticity tensor $\widehat{\mathbb{C}}$, the hydraulic conductivity tensor $\langle W \rangle_{\mathrm{f}}$, the tensor $\hat{\boldsymbol{\alpha}}$ and the scalar coefficient $\hat{M}$.

Our new model has a key difference from the model of classical poroelasticity. That is, our model is able to account for multiple elastic phases interacting at the porescale, whereas the model for classical poroelasticity is applicable when the matrix can be approximated as homogeneous at the porescale. The addition to the model of the extra interactions between multiple phases particularly beneficial to physical applications. For example, in bones water is interplaying with both collagen and mineral at the finest hierarchical levels. It is useful to be able to account for the mineral and collagen fibres separately in the model, especially for numerical simulations, as both constituents have very different elastic and mechanical properties. The differences in elastic and mechanical properties are accounted for by the multiple elasticity tensors $\mathbb{C}_{\mathrm{I}}$, $\mathbb{C}_{\mathrm{II}}$ and by $\mathbb{M}_{\mathrm{I}}$, $\mathbb{M}_{\mathrm{II}}$, Q_{I} and Q_{II}

in the coefficients of the model. A similar argument is applicable to biological tissues such as the interstitial matrix, which is a composite consisting of different types of cells and collagen fibres with fluid flowing in the interstitial space, we again believe that we would obtain a much more representative description of the behaviour of the material by accounting for the multiple constituents and their varying properties in the model. Another key difference between the model in our work and classical poroelasticity is the model coefficients. Here we propose novel cell problems from which the model coefficients are calculated. The cell problems given in our work are different from the cell problems in classical poroelasticity and also the cell problems for elastic composites. Overall our new model reads as a comprehensive frame work to describe materials where their constituents cannot be assumed to be homogeneous at the porescale.

Remark 6 (Limit cases for the macroscale model)**.** *It is important to note that our macroscale model* (3.186) *reduces to previously obtained results when we consider the following limit cases. In the limit of only one elastic phase then this macroscale model reduces to the macroscale model for a standard poroelastic material (See the no growth limit in [87], as well as [19, 68]). In this case our model would retain all four equations presented in (3.186) however, the coefficient of* $p^{(0)}$ *in the third equation, the effective elasticity tensor* $\widehat{\mathbb{C}}$*, the tensor* $\hat{\boldsymbol{\alpha}}$ *and the scalar coefficient* $\hat{M}$ *would reduce to only one elastic phase. This is because the contributions on the interface between the different elastic phases are no longer present in this case. We also note that in the limit of zero fluid (no pores) then this macroscale model reduces to the macroscale model for a standard elastic composite (See [89]). In this case, the mechanical behaviour of the system is entirely described by the equations for the balance in the solid phase, the pressures and fluid velocity reduces to zero, and the cell problem do not comprise any contribution related to the fluid phase, i.e. the only relevant cell problem (i.e. which results in non-trivial solutions) is the one involving the discontinuity in the elastic constants (3.134-3.139). That is, the model would coincide with the standard one described in the literature for elastic composites, see, e.g. [89].*

Next we rigorously prove the following properties of the effective coefficients. We prove a) the symmetries of the effective elasticity tensor, b) an analytical identity that allows us to identify the tensor $\hat{\boldsymbol{\alpha}}$ with Biot's coefficient tensor, and c) the positive definiteness of the $\hat{M}$, which can therefore be identified with the Biot's modulus for the whole material. These proofs generalize those proposed in [68] for standard poroelastic materials.

Theorem 1 (Symmetries of $\widehat{\mathbb{C}}$)**.** *The fourth rank effective elasticity tensor* $\widehat{\mathbb{C}}$ *defined by*

$$\widehat{\mathbb{C}} = \langle \mathbb{C}_{\mathrm{I}}\mathbb{M}_{\mathrm{I}} + \mathbb{C}_{\mathrm{I}} + \mathbb{C}_{\mathrm{II}}\mathbb{M}_{\mathrm{II}} + \mathbb{C}_{\mathrm{II}} \rangle_{\mathrm{s}}, \tag{3.188}$$

is major and minor symmetric.

Proof. We wish to show that the effective elasticity tensor $\widehat{\mathbb{C}}$ is major and minor symmetric. That is,

$$\widehat{C}_{ijkl} = \widehat{C}_{jikl} = \widehat{C}_{ijlk} = \widehat{C}_{klij}. \tag{3.189}$$

We know that the elasticity tensor $\mathbb{C}_\upsilon$ for $\upsilon = \mathrm{I}, \mathrm{II}$ is major and minor symmetric. We have that the first two equalities in (3.189) follow by definition. That is, $\mathbb{C}_\upsilon\mathbb{M}_\upsilon$ for $\upsilon = \mathrm{I}, \mathrm{II}$, is both left and right minor symmetric since we have the left minor symmetry of $\mathbb{C}_\upsilon$ and the right minor symmetry of $\mathbb{M}_\upsilon$. In order to prove major symmetry we have to show that

$$\langle C^{\mathrm{I}}_{klpq}\xi^{rs}_{pq}(A^{\mathrm{I}}) + C^{\mathrm{II}}_{klpq}\xi^{rs}_{pq}(A^{\mathrm{II}})\rangle_{\mathrm{s}} = \langle C^{\mathrm{I}}_{rspq}\xi^{kl}_{pq}(A^{\mathrm{I}}) + C^{\mathrm{II}}_{rspq}\xi^{kl}_{pq}(A^{\mathrm{II}})\rangle_{\mathrm{s}} \tag{3.190}$$

To show this we begin with the cell problems (3.147) and (3.148) and multiplying by A^{I}_{irs}, A^{II}_{irs} respectively and then integrating these terms over Ω_{I} and Ω_{II} respectively. We have

$$\begin{aligned}
&\int_{\Omega_{\mathrm{I}}} \frac{\partial}{\partial y_j}(C^{\mathrm{I}}_{ijpq}\xi^{kl}_{pq}(A^{\mathrm{I}}))A^{\mathrm{I}}_{irs}\mathrm{d}\mathbf{y} + \int_{\Omega_{\mathrm{I}}} \frac{\partial}{\partial y_j}(C^{\mathrm{I}}_{ijkl})A^{\mathrm{I}}_{irs}\mathrm{d}\mathbf{y} \\
&+ \int_{\Omega_{\mathrm{II}}} \frac{\partial}{\partial y_j}(C^{\mathrm{II}}_{ijpq}\xi^{kl}_{pq}(A^{\mathrm{II}}))A^{\mathrm{II}}_{irs}\mathrm{d}\mathbf{y} + \int_{\Omega_{\mathrm{II}}} \frac{\partial}{\partial y_j}(C^{\mathrm{II}}_{ijkl})A^{\mathrm{II}}_{irs}\mathrm{d}\mathbf{y} = 0.
\end{aligned} \tag{3.191}$$

Then integrating by parts we obtain

$$\begin{aligned}
&\int_{\Omega_{\mathrm{I}}} \frac{\partial}{\partial y_j}(C^{\mathrm{I}}_{ijpq}\xi^{kl}_{pq}(A^{\mathrm{I}})A^{\mathrm{I}}_{irs})\mathrm{d}\mathbf{y} - \int_{\Omega_{\mathrm{I}}} C^{\mathrm{I}}_{ijpq}\xi^{kl}_{pq}(A^{\mathrm{I}})\frac{\partial A^{\mathrm{I}}_{irs}}{\partial y_j}\mathrm{d}\mathbf{y} \\
&+ \int_{\Omega_{\mathrm{I}}} \frac{\partial}{\partial y_j}(C^{\mathrm{I}}_{ijkl}A^{\mathrm{I}}_{irs})\mathrm{d}\mathbf{y} - \int_{\Omega_{\mathrm{I}}} C^{\mathrm{I}}_{ijkl}\frac{\partial A^{\mathrm{I}}_{irs}}{\partial y_j}\mathrm{d}\mathbf{y} \\
&+ \int_{\Omega_{\mathrm{II}}} \frac{\partial}{\partial y_j}(C^{\mathrm{II}}_{ijpq}\xi^{kl}_{pq}(A^{\mathrm{II}})A^{\mathrm{II}}_{irs})\mathrm{d}\mathbf{y} - \int_{\Omega_{\mathrm{II}}} C^{\mathrm{II}}_{ijpq}\xi^{kl}_{pq}(A^{\mathrm{II}})\frac{\partial A^{\mathrm{II}}_{irs}}{\partial y_j}\mathrm{d}\mathbf{y} \\
&+ \int_{\Omega_{\mathrm{II}}} \frac{\partial}{\partial y_j}(C^{\mathrm{II}}_{ijkl}A^{\mathrm{II}}_{irs})\mathrm{d}\mathbf{y} - \int_{\Omega_{\mathrm{II}}} C^{\mathrm{II}}_{ijkl}\frac{\partial A^{\mathrm{II}}_{irs}}{\partial y_j}\mathrm{d}\mathbf{y} = 0.
\end{aligned} \tag{3.192}$$

Applying the divergence theorem we obtain

$$\int_{\Gamma_{\mathrm{I}}} C^{\mathrm{I}}_{ijpq}\xi^{kl}_{pq}(A^{\mathrm{I}})A^{\mathrm{I}}_{irs}\cdot n^{\mathrm{I}}_j\mathrm{dS} - \int_{\Gamma_{\mathrm{III}}} C^{\mathrm{I}}_{ijpq}\xi^{kl}_{pq}(A^{\mathrm{I}})A^{\mathrm{I}}_{irs}\cdot n^{\mathrm{III}}_j\mathrm{dS}$$

$$
\begin{aligned}
&+\int_{\partial\Omega_{\mathrm{I}}\setminus\Gamma_{\mathrm{I}}\cup\Gamma_{\mathrm{III}}} C^{\mathrm{I}}_{ijpq}\xi^{kl}_{pq}(A^{\mathrm{I}})A^{\mathrm{I}}_{irs}\cdot n_j^{\Omega_{\mathrm{I}}\setminus\Gamma_{\mathrm{I}}\cup\Gamma_{\mathrm{III}}}\mathrm{dS}-\int_{\Omega_{\mathrm{I}}} C^{\mathrm{I}}_{ijpq}\xi^{kl}_{pq}(A^{\mathrm{I}})\xi^{rs}_{ij}(A^{\mathrm{I}})\mathrm{d}\mathbf{y}\\
&+\int_{\Gamma_{\mathrm{I}}} C^{\mathrm{I}}_{ijkl}A^{\mathrm{I}}_{irs}\cdot n^{\mathrm{I}}_j\mathrm{dS}-\int_{\Gamma_{\mathrm{III}}} C^{\mathrm{I}}_{ijkl}A^{\mathrm{I}}_{irs}\cdot n^{\mathrm{III}}_j\mathrm{dS}\\
&+\int_{\partial\Omega_{\mathrm{I}}\setminus\Gamma_{\mathrm{I}}\cup\Gamma_{\mathrm{III}}} C^{\mathrm{I}}_{ijkl}A^{\mathrm{I}}_{irs}\cdot n_j^{\Omega_{\mathrm{I}}\setminus\Gamma_{\mathrm{I}}\cup\Gamma_{\mathrm{III}}}\mathrm{dS}-\int_{\Omega_{\mathrm{I}}} C^{\mathrm{I}}_{ijkl}\xi^{rs}_{ij}(A^{\mathrm{I}})\mathrm{d}\mathbf{y}\\
&+\int_{\Gamma_{\mathrm{II}}} C^{\mathrm{II}}_{ijpq}\xi^{kl}_{pq}(A^{\mathrm{II}})A^{\mathrm{II}}_{irs}\cdot n^{\mathrm{II}}_j\mathrm{dS}+\int_{\Gamma_{\mathrm{III}}} C^{\mathrm{II}}_{ijpq}\xi^{kl}_{pq}(A^{\mathrm{II}})A^{\mathrm{II}}_{irs}\cdot n^{\mathrm{III}}_j\mathrm{dS}\\
&+\int_{\partial\Omega_{\mathrm{II}}\setminus\Gamma_{\mathrm{II}}\cup\Gamma_{\mathrm{III}}} C^{\mathrm{II}}_{ijpq}\xi^{kl}_{pq}(A^{\mathrm{II}})A^{\mathrm{II}}_{irs}\cdot n_j^{\Omega_{\mathrm{II}}\setminus\Gamma_{\mathrm{II}}\cup\Gamma_{\mathrm{III}}}\mathrm{dS}-\int_{\Omega_{\mathrm{II}}} C^{\mathrm{II}}_{ijpq}\xi^{kl}_{pq}(A^{\mathrm{II}})\xi^{rs}_{ij}(A^{\mathrm{II}})\mathrm{d}\mathbf{y}\\
&+\int_{\Gamma_{\mathrm{II}}} C^{\mathrm{II}}_{ijkl}A^{\mathrm{II}}_{irs}\cdot n^{\mathrm{II}}_j\mathrm{dS}+\int_{\Gamma_{\mathrm{III}}} C^{\mathrm{II}}_{ijkl}A^{\mathrm{II}}_{irs}\cdot n^{\mathrm{III}}_j\mathrm{dS}\\
&+\int_{\partial\Omega_{\mathrm{II}}\setminus\Gamma_{\mathrm{II}}\cup\Gamma_{\mathrm{III}}} C^{\mathrm{II}}_{ijkl}A^{\mathrm{I}}_{irs}\cdot n_j^{\Omega_{\mathrm{II}}\setminus\Gamma_{\mathrm{II}}\cup\Gamma_{\mathrm{III}}}\mathrm{dS}-\int_{\Omega_{\mathrm{II}}} C^{\mathrm{II}}_{ijkl}\xi^{rs}_{ij}(A^{\mathrm{II}})\mathrm{d}\mathbf{y}=0
\end{aligned}
\tag{3.193}
$$

where $\mathbf{n}_{\mathrm{I}}$, $\mathbf{n}_{\mathrm{II}}$, $\mathbf{n}_{\mathrm{III}}$, $\mathbf{n}_{\Omega_{\mathrm{I}}\setminus\Gamma_{\mathrm{I}}\cup\Gamma_{\mathrm{III}}}$ and $\mathbf{n}_{\Omega_{\mathrm{II}}\setminus\Gamma_{\mathrm{II}}\cup\Gamma_{\mathrm{III}}}$ are the unit normals corresponding to Γ_{I}, Γ_{II}, Γ_{III}, $\partial\Omega_{\mathrm{I}}\setminus\Gamma_{\mathrm{I}}\cup\Gamma_{\mathrm{III}}$ and $\partial\Omega_{\mathrm{II}}\setminus\Gamma_{\mathrm{II}}\cup\Gamma_{\mathrm{III}}$. The terms on the boundaries $\partial\Omega_{\mathrm{I}}\setminus\Gamma_{\mathrm{I}}\cup\Gamma_{\mathrm{III}}$ and $\partial\Omega_{\mathrm{II}}\setminus\Gamma_{\mathrm{II}}\cup\Gamma_{\mathrm{III}}$ cancel due to periodicity and we can rewrite (3.193) as

$$
\begin{aligned}
&\int_{\Omega_{\mathrm{I}}} C^{\mathrm{I}}_{ijpq}\xi^{kl}_{pq}(A^{\mathrm{I}})\xi^{rs}_{ij}(A^{\mathrm{I}})\mathrm{d}\mathbf{y}+\int_{\Omega_{\mathrm{II}}} C^{\mathrm{II}}_{ijpq}\xi^{kl}_{pq}(A^{\mathrm{II}})\xi^{rs}_{ij}(A^{\mathrm{II}})\mathrm{d}\mathbf{y}\\
&+\Big[\int_{\Gamma_{\mathrm{III}}} C^{\mathrm{I}}_{ijpq}\xi^{kl}_{pq}(A^{\mathrm{I}})A^{\mathrm{I}}_{irs}\cdot n^{\mathrm{III}}_j\mathrm{dS}-\int_{\Gamma_{\mathrm{I}}} C^{\mathrm{I}}_{ijpq}\xi^{kl}_{pq}(A^{\mathrm{I}})A^{\mathrm{I}}_{irs}\cdot n^{\mathrm{I}}_j\mathrm{dS}\\
&+\int_{\Gamma_{\mathrm{III}}} C^{\mathrm{I}}_{ijkl}A^{\mathrm{I}}_{irs}\cdot n^{\mathrm{III}}_j\mathrm{dS}-\int_{\Gamma_{\mathrm{I}}} C^{\mathrm{I}}_{ijkl}A^{\mathrm{I}}_{irs}\cdot n^{\mathrm{I}}_j\mathrm{dS}\\
&-\int_{\Gamma_{\mathrm{II}}} C^{\mathrm{II}}_{ijpq}\xi^{kl}_{pq}(A^{\mathrm{II}})A^{\mathrm{II}}_{irs}\cdot n^{\mathrm{II}}_j\mathrm{dS}-\int_{\Gamma_{\mathrm{III}}} C^{\mathrm{II}}_{ijpq}\xi^{kl}_{pq}(A^{\mathrm{II}})A^{\mathrm{II}}_{irs}\cdot n^{\mathrm{III}}_j\mathrm{dS}\\
&-\int_{\Gamma_{\mathrm{II}}} C^{\mathrm{II}}_{ijkl}A^{\mathrm{II}}_{irs}\cdot n^{\mathrm{II}}_j\mathrm{dS}-\int_{\Gamma_{\mathrm{III}}} C^{\mathrm{II}}_{ijkl}A^{\mathrm{II}}_{irs}\cdot n^{\mathrm{III}}_j\mathrm{dS}\Big]\\
&+\int_{\Omega_{\mathrm{I}}} C^{\mathrm{I}}_{ijkl}\xi^{rs}_{ij}(A^{\mathrm{I}})\mathrm{d}\mathbf{y}+\int_{\Omega_{\mathrm{II}}} C^{\mathrm{II}}_{ijkl}\xi^{rs}_{ij}(A^{\mathrm{II}})\mathrm{d}\mathbf{y}=0.
\end{aligned}
\tag{3.194}
$$

The terms in the bracket cancel due to the cell problems (3.149) and (3.151−3.152) and we obtain

$$
\begin{aligned}
&\int_{\Omega_{\mathrm{I}}} C^{\mathrm{I}}_{ijpq}\xi^{kl}_{pq}(A^{\mathrm{I}})\xi^{rs}_{ij}(A^{\mathrm{I}})\mathrm{d}\mathbf{y}+\int_{\Omega_{\mathrm{II}}} C^{\mathrm{II}}_{ijpq}\xi^{kl}_{pq}(A^{\mathrm{II}})\xi^{rs}_{ij}(A^{\mathrm{II}})\mathrm{d}\mathbf{y}\\
&+\int_{\Omega_{\mathrm{I}}} C^{\mathrm{I}}_{ijkl}\xi^{rs}_{ij}(A^{\mathrm{I}})\mathrm{d}\mathbf{y}+\int_{\Omega_{\mathrm{II}}} C^{\mathrm{II}}_{ijkl}\xi^{rs}_{ij}(A^{\mathrm{II}})\mathrm{d}\mathbf{y}=0,
\end{aligned}
\tag{3.195}
$$

which we can rearrange to obtain

$$\begin{aligned}
&\int_{\Omega_s} \xi_{ij}^{rs}(A^{\mathrm{I}})C_{ijpq}^{\mathrm{I}}\xi_{pq}^{kl}(A^{\mathrm{I}}) + \xi_{ij}^{rs}(A^{\mathrm{II}})C_{ijpq}^{\mathrm{II}}\xi_{pq}^{kl}(A^{\mathrm{II}})\mathrm{d}\mathbf{y} \\
&= -\bigg(\int_{\Omega_s} \xi_{ij}^{rs}(A^{\mathrm{I}})C_{ijkl}^{\mathrm{I}} + \xi_{ij}^{rs}(A^{\mathrm{II}})C_{ijkl}^{\mathrm{II}}\mathrm{d}\mathbf{y}\bigg) \\
&= -\bigg(\int_{\Omega_s} C_{klij}^{\mathrm{I}}\xi_{ij}^{rs}(A^{\mathrm{I}}) + C_{klij}^{\mathrm{II}}\xi_{ij}^{rs}(A^{\mathrm{II}})\mathrm{d}\mathbf{y}\bigg). \qquad (3.196)
\end{aligned}$$

Rewriting the second equality in (3.196) interchanging r and s and k and l and using the symmetry $C_{ijpq} = C_{pqij}$ we obtain

$$\begin{aligned}
&\int_{\Omega_s} \xi_{ij}^{kl}(A^{\mathrm{I}})C_{pqij}^{\mathrm{I}}\xi_{pq}^{rs}(A^{\mathrm{I}}) + \xi_{ij}^{kl}(A^{\mathrm{II}})C_{pqij}^{\mathrm{II}}\xi_{pq}^{rs}(A^{\mathrm{II}})\mathrm{d}\mathbf{y} \\
&= -\bigg(\int_{\Omega_s} C_{rsij}^{\mathrm{I}}\xi_{ij}^{kl}(A^{\mathrm{I}}) + C_{rsij}^{\mathrm{II}}\xi_{ij}^{kl}(A^{\mathrm{II}})\mathrm{d}\mathbf{y}\bigg). \qquad (3.197)
\end{aligned}$$

Since the left hand sides of (3.196) and (3.197) are the same then so to are the right hand sides. Taking ij as pq in (3.196) and (3.197) we have that

$$\langle C_{klpq}^{\mathrm{I}}\xi_{pq}^{rs}(A^{\mathrm{I}}) + C_{klpq}^{\mathrm{II}}\xi_{pq}^{rs}(A^{\mathrm{II}})\rangle_{\mathrm{s}} = \langle C_{rspq}^{\mathrm{I}}\xi_{pq}^{kl}(A^{\mathrm{I}}) + C_{rspq}^{\mathrm{II}}\xi_{pq}^{kl}(A^{\mathrm{II}})\rangle_{\mathrm{s}} \qquad (3.198)$$

as required. Therefore $\widehat{\mathbb{C}}$ posessess major and minor symmetries. □

The following two Theorems relate to the resulting Biot's tensor of coefficients and Biot's modulus of the macroscale model. The coefficients of the macroscale model can be defined as

$$\hat{\boldsymbol{\alpha}} := \phi\mathbf{I} - \langle \mathrm{Tr}(\mathbb{M}_{\mathrm{I}} + \mathbb{M}_{\mathrm{II}})\rangle_{\mathrm{s}}, \qquad (3.199)$$

$$\boldsymbol{\gamma} := \langle \mathbb{C}_{\mathrm{I}}Q_{\mathrm{I}} + \mathbb{C}_{\mathrm{II}}Q_{\mathrm{II}}\rangle_{\mathrm{s}} - \phi\mathbf{I}, \qquad (3.200)$$

$$\beta := \mathrm{Tr}\langle Q_{\mathrm{I}} + Q_{\mathrm{II}}\rangle_{\mathrm{s}}, \qquad (3.201)$$

where $\hat{\boldsymbol{\alpha}}$ is from (3.183) and β is the denominator of the Biot's Modulus $\hat{M}$ also in (3.183). We obtain $\boldsymbol{\gamma}$ from (3.172), where $\boldsymbol{\gamma}$ is the coefficient of the leading order pressure in the effective stress, $\hat{\mathsf{T}}_{\mathrm{Eff}}$. We are able to give a physical interpretation of these coefficients following the descriptions given in [91]. The coefficient β (denominator of $\hat{M}$) can be thought of as a variation in the fluid volume in response to a variation in pore pressure. $\hat{M}$ is a poroelastic coefficient that depends on the pore scale geometry and porosity and

on the properties of the elastic matrix [19]. We can describe $\hat{\boldsymbol{\alpha}}$ as the ratio of change in interstitial fluid volume to changes in solid volume.

We can now state the following theorem that will provide an analytical identity allowing us to define an effective Biot's coefficient.

Theorem 2 (Biot's Coefficient)**.** *We have the following analytical identity*

$$\gamma_{ij} = -\hat{\alpha}_{ij} \tag{3.202}$$

which allows us to define an effective poroelastic Biot's coefficient tensor.

Proof. In index notation we can write $\boldsymbol{\gamma}$ and $\hat{\boldsymbol{\alpha}}$ as

$$\gamma_{ij} = \langle C^{\mathrm{I}}_{ijkl}\xi_{kl}(a^{\mathrm{I}}) + C^{\mathrm{II}}_{ijkl}\xi_{kl}(a^{\mathrm{II}})\rangle_{\mathrm{s}} - \phi\delta_{ij} \tag{3.203}$$

$$\hat{\alpha}_{ij} = \phi\delta_{ij} - \langle \xi^{kl}_{ij}(A^{\mathrm{I}}) + \xi^{kl}_{ij}(A^{\mathrm{II}})\rangle_{\mathrm{s}}\delta_{kl}. \tag{3.204}$$

We use (3.147) and (3.148) from the cell problems and multiply by a^{I}_i, a^{II}_i respectively. We then integrate these expressions over Ω_{I} and Ω_{II}, respectively, to obtain

$$\begin{aligned}&\int_{\Omega_{\mathrm{I}}} \frac{\partial}{\partial y_j}(C^{\mathrm{I}}_{ijpq}\xi^{kl}_{pq}(A^{\mathrm{I}}))a^{\mathrm{I}}_i \mathrm{d}\mathbf{y} + \int_{\Omega_{\mathrm{I}}} \frac{\partial}{\partial y_j}(C^{\mathrm{I}}_{ijkl})a^{\mathrm{I}}_i \mathrm{d}\mathbf{y}\\ &+ \int_{\Omega_{\mathrm{II}}} \frac{\partial}{\partial y_j}(C^{\mathrm{II}}_{ijpq}\xi^{kl}_{pq}(A^{\mathrm{II}}))a^{\mathrm{II}}_i \mathrm{d}\mathbf{y} + \int_{\Omega_{\mathrm{II}}} \frac{\partial}{\partial y_j}(C^{\mathrm{II}}_{ijkl})a^{\mathrm{II}}_i \mathrm{d}\mathbf{y} = 0.\end{aligned} \tag{3.205}$$

Then integrating by parts we obtain

$$\begin{aligned}&\int_{\Omega_{\mathrm{I}}} \frac{\partial}{\partial y_j}(C^{\mathrm{I}}_{ijpq}\xi^{kl}_{pq}(A^{\mathrm{I}})a^{\mathrm{I}}_i)\mathrm{d}\mathbf{y} - \int_{\Omega_{\mathrm{I}}} C^{\mathrm{I}}_{ijpq}\xi^{kl}_{pq}(A^{\mathrm{I}})\frac{\partial a^{\mathrm{I}}_i}{\partial y_j}\mathrm{d}\mathbf{y} + \int_{\Omega_{\mathrm{I}}} \frac{\partial}{\partial y_j}(C^{\mathrm{I}}_{ijkl}a^{\mathrm{I}}_i)\mathrm{d}\mathbf{y}\\ &- \int_{\Omega_{\mathrm{I}}} C^{\mathrm{I}}_{ijkl}\frac{\partial a^{\mathrm{I}}_i}{\partial y_j}\mathrm{d}\mathbf{y} + \int_{\Omega_{\mathrm{II}}} \frac{\partial}{\partial y_j}(C^{\mathrm{II}}_{ijpq}\xi^{kl}_{pq}(A^{\mathrm{II}})a^{\mathrm{II}}_i)\mathrm{d}\mathbf{y} - \int_{\Omega_{\mathrm{II}}} C^{\mathrm{II}}_{ijpq}\xi^{kl}_{pq}(A^{\mathrm{II}})\frac{\partial a^{\mathrm{II}}_i}{\partial y_j}\mathrm{d}\mathbf{y}\\ &+ \int_{\Omega_{\mathrm{II}}} \frac{\partial}{\partial y_j}(C^{\mathrm{II}}_{ijkl}a^{\mathrm{II}}_i)\mathrm{d}\mathbf{y} - \int_{\Omega_{\mathrm{II}}} C^{\mathrm{II}}_{ijkl}\frac{\partial a^{\mathrm{II}}_i}{\partial y_j}\mathrm{d}\mathbf{y} = 0.\end{aligned} \tag{3.206}$$

Applying the divergence theorem we have

$$\begin{aligned}&\int_{\Gamma_{\mathrm{I}}} C^{\mathrm{I}}_{ijpq}\xi^{kl}_{pq}(A^{\mathrm{I}})a^{\mathrm{I}}_i \cdot n^{\mathrm{I}}_j \mathrm{dS} - \int_{\Gamma_{\mathrm{III}}} C^{\mathrm{I}}_{ijpq}\xi^{kl}_{pq}(A^{\mathrm{I}})a^{\mathrm{I}}_i \cdot n^{\mathrm{III}}_j \mathrm{dS}\\ &+ \int_{\partial\Omega_{\mathrm{I}}\setminus\Gamma_{\mathrm{I}}\cup\Gamma_{\mathrm{III}}} C^{\mathrm{I}}_{ijpq}\xi^{kl}_{pq}(A^{\mathrm{I}})a^{\mathrm{I}}_i \cdot n^{\Omega_{\mathrm{I}}\setminus\Gamma_{\mathrm{I}}\cup\Gamma_{\mathrm{III}}}_j \mathrm{dS} - \int_{\Omega_{\mathrm{I}}} C^{\mathrm{I}}_{ijpq}\xi^{kl}_{pq}(A^{\mathrm{I}})\xi_{ij}(a^{\mathrm{I}})\mathrm{d}\mathbf{y}\\ &+ \int_{\Gamma_{\mathrm{I}}} C^{\mathrm{I}}_{ijkl}a^{\mathrm{I}}_i \cdot n^{\mathrm{I}}_j \mathrm{dS} - \int_{\Gamma_{\mathrm{III}}} C^{\mathrm{I}}_{ijkl}a^{\mathrm{I}}_i \cdot n^{\mathrm{III}}_j \mathrm{dS} + \int_{\partial\Omega_{\mathrm{I}}\setminus\Gamma_{\mathrm{I}}\cup\Gamma_{\mathrm{III}}} C^{\mathrm{I}}_{ijkl}a^{\mathrm{I}}_i \cdot n^{\Omega_{\mathrm{I}}\setminus\Gamma_{\mathrm{I}}\cup\Gamma_{\mathrm{III}}}_j \mathrm{dS}\end{aligned}$$

$$
\begin{aligned}
&- \int_{\Omega_{\rm I}} C^{\rm I}_{ijkl}\xi_{ij}(a^{\rm I})\mathrm{d}\mathbf{y} + \int_{\Gamma_{\rm II}} C^{\rm II}_{ijpq}\xi^{kl}_{pq}(A^{\rm II})a^{\rm II}_i\cdot n^{\rm II}_j\mathrm{dS} + \int_{\Gamma_{\rm III}} C^{\rm II}_{ijpq}\xi^{kl}_{pq}(A^{\rm II})a^{\rm II}_i\cdot n^{\rm III}_j\mathrm{dS}\\
&+ \int_{\partial\Omega_{\rm II}\setminus\Gamma_{\rm II}\cup\Gamma_{\rm III}} C^{\rm II}_{ijpq}\xi^{kl}_{pq}(A^{\rm II})a^{\rm II}_i\cdot n^{\Omega_{\rm II}\setminus\Gamma_{\rm II}\cup\Gamma_{\rm III}}_j\mathrm{dS} - \int_{\Omega_{\rm II}} C^{\rm II}_{ijpq}\xi^{kl}_{pq}(A^{\rm II})\xi_{ij}(a^{\rm II})\mathrm{d}\mathbf{y}\\
&+ \int_{\Gamma_{\rm II}} C^{\rm II}_{ijkl}a^{\rm II}_i\cdot n^{\rm II}_j\mathrm{dS} + \int_{\Gamma_{\rm III}} C^{\rm II}_{ijkl}a^{\rm II}_i\cdot n^{\rm III}_j\mathrm{dS} + \int_{\partial\Omega_{\rm II}\setminus\Gamma_{\rm II}\cup\Gamma_{\rm III}} C^{\rm II}_{ijkl}a^{\rm I}_i\cdot n^{\Omega_{\rm II}\setminus\Gamma_{\rm II}\cup\Gamma_{\rm III}}_j\mathrm{dS}\\
&- \int_{\Omega_{\rm II}} C^{\rm II}_{ijkl}\xi_{ij}(a^{\rm II})\mathrm{d}\mathbf{y} = 0
\end{aligned}
\tag{3.207}
$$

where $\mathbf{n}_{\rm I}$, $\mathbf{n}_{\rm II}$, $\mathbf{n}_{\rm III}$, $\mathbf{n}_{\Omega_{\rm I}\setminus\Gamma_{\rm I}\cup\Gamma_{\rm III}}$ and $\mathbf{n}_{\Omega_{\rm II}\setminus\Gamma_{\rm II}\cup\Gamma_{\rm III}}$ are the unit normals corresponding to $\Gamma_{\rm I}$, $\Gamma_{\rm II}$, $\Gamma_{\rm III}$, $\partial\Omega_{\rm I}\setminus\Gamma_{\rm I}\cup\Gamma_{\rm III}$ and $\partial\Omega_{\rm II}\setminus\Gamma_{\rm II}\cup\Gamma_{\rm III}$, and cancelling terms on the periodic boundaries due to $\mathbf{y}$-periodicity and accounting for the interface conditions (3.149) and (3.151-3.152) we obtain

$$
\begin{aligned}
&\int_{\Omega_{\rm I}} \xi_{ij}(a^{\rm I})C^{\rm I}_{ijpq}\xi^{kl}_{pq}(A^{\rm I})\mathrm{d}\mathbf{y} + \int_{\Omega_{\rm I}} C^{\rm I}_{klij}\xi_{ij}(a^{\rm I})\mathrm{d}\mathbf{y} + \int_{\Omega_{\rm II}} \xi_{ij}(a^{\rm II})C^{\rm II}_{ijpq}\xi^{kl}_{pq}(A^{\rm II})\mathrm{d}\mathbf{y}\\
&+ \int_{\Omega_{\rm II}} C^{\rm II}_{klij}\xi_{ij}(a^{\rm I})\mathrm{d}\mathbf{y} = 0.
\end{aligned}
\tag{3.208}
$$

Hence we have

$$
\langle \xi_{ij}(a^{\rm I})C^{\rm I}_{ijpq}\xi^{kl}_{pq}(A^{\rm I}) + \xi_{ij}(a^{\rm II})C^{\rm II}_{ijpq}\xi^{kl}_{pq}(A^{\rm II})\rangle_{\rm s} = -\langle C^{\rm I}_{klij}\xi_{ij}(a^{\rm I}) + C^{\rm II}_{klij}\xi_{ij}(a^{\rm II})\rangle_{\rm s}. \tag{3.209}
$$

We now wish to multiply (3.140) and (3.141) from the cell problems by $A^{\rm I}_{ikl}$, $A^{\rm II}_{ikl}$ respectively and then integrate over $\Omega_{\rm I}$ and $\Omega_{\rm II}$ respectively. Integrating by parts we obtain

$$
\begin{aligned}
&\int_{\Omega_{\rm I}} \frac{\partial}{\partial y_j}(C^{\rm I}_{ijpq}\xi_{pq}(a^{\rm I})A^{\rm I}_{ikl})\mathrm{d}\mathbf{y} - \int_{\Omega_{\rm I}} C^{\rm I}_{ijpq}\xi_{pq}(a^{\rm I})\frac{\partial A^{\rm I}_{ikl}}{\partial y_j}\mathrm{d}\mathbf{y}\\
&+ \int_{\Omega_{\rm II}} \frac{\partial}{\partial y_j}(C^{\rm II}_{ijpq}\xi_{pq}(a^{\rm II})A^{\rm II}_{ikl})\mathrm{d}\mathbf{y} - \int_{\Omega_{\rm II}} C^{\rm II}_{ijpq}\xi_{pq}(a^{\rm II})\frac{\partial A^{\rm II}_{ikl}}{\partial y_j}\mathrm{d}\mathbf{y} = 0.
\end{aligned}
\tag{3.210}
$$

Applying the divergence theorem and using (3.144) and (3.145) we obtain

$$
\begin{aligned}
&- \int_{\Gamma_{\rm I}} A^{\rm I}_{ikl}n^{\rm I}_i\mathrm{dS} - \int_{\Omega_{\rm I}} \frac{1}{2}\left(\frac{\partial A^{\rm I}_{ikl}}{\partial y_j} + \frac{\partial A^{\rm I}_{jkl}}{\partial y_i}\right)C^{\rm I}_{ijpq}\xi_{pq}(a^{\rm I})\mathrm{d}\mathbf{y}\\
&- \int_{\Gamma_{\rm II}} A^{\rm II}_{ikl}n^{\rm II}_i\mathrm{dS} - \int_{\Omega_{\rm II}} \frac{1}{2}\left(\frac{\partial A^{\rm II}_{ikl}}{\partial y_j} + \frac{\partial A^{\rm II}_{jkl}}{\partial y_i}\right)C^{\rm II}_{ijpq}\xi_{pq}(a^{\rm II})\mathrm{d}\mathbf{y} = 0
\end{aligned}
\tag{3.211}
$$

where terms on the boundaries have cancelled due to periodicity. Then reversing the

divergence theorem we have

$$-\int_{\Omega_{\rm I}} \frac{\partial A^{\rm I}_{ikl}}{\partial y_i}{\rm d}\mathbf{y} - \int_{\Omega_{\rm II}} \frac{\partial A^{\rm II}_{ikl}}{\partial y_i}{\rm d}\mathbf{y} - \int_{\Omega_{\rm I}} \xi^{kl}_{ij}(A^{\rm I}) C^{\rm I}_{ijpq}\xi_{pq}(a^{\rm I}){\rm d}\mathbf{y}$$
$$-\int_{\Omega_{\rm II}} \xi^{kl}_{ij}(A^{\rm II}) C^{\rm II}_{ijpq}\xi_{pq}(a^{\rm II}){\rm d}\mathbf{y} = 0. \tag{3.212}$$

Hence

$$-\left\langle \frac{\partial A^{\rm I}_{ikl}}{\partial y_i} + \frac{\partial A^{\rm II}_{ikl}}{\partial y_i} \right\rangle_{\rm s} = \langle \xi_{ij}(a^{\rm I}) C^{\rm I}_{ijpq}\xi^{kl}_{pq}(A^{\rm I}) + \xi_{ij}(a^{\rm II}) C^{\rm II}_{ijpq}\xi^{kl}_{pq}(A^{\rm II})\rangle_{\rm s}. \tag{3.213}$$

Using (3.209) and (3.213) we have that $\mathrm{Tr}\langle(\mathbb{M}_{\rm I} + \mathbb{M}_{\rm II})\rangle_{\rm s} = \langle \mathbb{C}_{\rm I} Q_{\rm I} + \mathbb{C}_{\rm II} Q_{\rm II}\rangle_{\rm s}$. Therefore using this in the definitions of $\hat{\alpha}_{ij}$ and γ_{ij} we have that $\gamma_{ij} = -\hat{\alpha}_{ij}$ as required. □

We should note here that the coefficients $\hat{\boldsymbol{\alpha}}$ and $\boldsymbol{\gamma}$ are defined by different cell problems for $A_{\rm I}$, $A_{\rm II}$ and for $\mathbf{a}_{\rm I}$, $\mathbf{a}_{\rm II}$ respectively. By having an analytical identity as in Theorem. 2 we can reduce computations as the numerics then do not have to be carried out for the cell problems involving $\mathbf{a}_{\rm I}$, $\mathbf{a}_{\rm II}$.

Now that we have proved this analytical identity we can use it to restate the macroscale model for a poroelastic composite material. We have

$$\begin{cases} \langle \mathbf{w}\rangle_{\rm f} = -\langle W\rangle_{\rm f} \nabla_{\mathbf{x}} p^{(0)}, \\ \nabla_{\mathbf{x}} \cdot \hat{\mathsf{T}}_{\rm Eff} = 0, \\ \hat{\mathsf{T}}_{\rm Eff} = \widehat{\mathbb{C}}\xi_{\mathbf{x}}(\mathbf{u}^{(0)}) - \hat{\boldsymbol{\alpha}} p^{(0)}, \\ \dfrac{\dot{p}^{(0)}}{\hat{M}} = -\nabla_{\mathbf{x}} \cdot \langle \mathbf{w}\rangle_{\rm f} - \hat{\boldsymbol{\alpha}} : \xi_{\mathbf{x}}(\dot{\mathbf{u}}^{(0)}). \end{cases} \tag{3.214}$$

We will now state our final theorem relating to the Biot's Modulus of our system.

Theorem 3 (Biot's Modulus)**.** *We have that the Biot's Modulus defined by*

$$\hat{M} := \frac{-1}{\langle Tr(Q_{\rm I} + Q_{\rm II})\rangle_{\rm s}}$$

is positive definite. That is

$$\hat{M} > 0. \tag{3.215}$$

Proof. In order to prove this we only need to prove that the denominator of $\hat{M}$ which we defined as β is less than zero. We can begin by recalling β from (3.201) and then in index

notation

$$\beta = \mathrm{Tr}\langle Q_{\mathrm{I}} + Q_{\mathrm{II}}\rangle_{\mathrm{s}} = \left\langle \frac{\partial a_i^{\mathrm{I}}}{\partial y_i} + \frac{\partial a_i^{\mathrm{II}}}{\partial y_i} \right\rangle_{\mathrm{s}}. \tag{3.216}$$

We can then multiply equations (3.140) and (3.141) from the cell problems by a_i^{I}, a_i^{II} and integrate over Ω_{I}, Ω_{II} respectively. That is,

$$\int_{\Omega_{\mathrm{I}}} a_i^{\mathrm{I}} \frac{\partial}{\partial y_j}(C_{ijkl}^{\mathrm{I}}\xi_{kl}(a^{\mathrm{I}}))\mathrm{d}\mathbf{y} + \int_{\Omega_{\mathrm{II}}} a_i^{\mathrm{II}} \frac{\partial}{\partial y_j}(C_{ijkl}^{\mathrm{II}}\xi_{kl}(a^{\mathrm{II}}))\mathrm{d}\mathbf{y} = 0. \tag{3.217}$$

Integrating by parts we obtain

$$\begin{aligned}
&\int_{\Omega_{\mathrm{I}}} \frac{\partial}{\partial y_j}(C_{ijkl}^{\mathrm{I}}\xi_{kl}(a^{\mathrm{I}})a_i^{\mathrm{I}})\mathrm{d}\mathbf{y} - \int_{\Omega_{\mathrm{I}}} C_{ijkl}^{\mathrm{I}}\xi_{kl}(a^{\mathrm{I}})\frac{\partial a_i^{\mathrm{I}}}{\partial y_j}\mathrm{d}\mathbf{y} \\
&+ \int_{\Omega_{\mathrm{II}}} \frac{\partial}{\partial y_j}(C_{ijkl}^{\mathrm{II}}\xi_{kl}(a^{\mathrm{II}})a_i^{\mathrm{II}})\mathrm{d}\mathbf{y} - \int_{\Omega_{\mathrm{II}}} C_{ijkl}^{\mathrm{II}}\xi_{kl}(a^{\mathrm{II}})\frac{\partial a_i^{\mathrm{II}}}{\partial y_j}\mathrm{d}\mathbf{y} = 0.
\end{aligned} \tag{3.218}$$

Then applying the divergence theorem we obtain

$$\begin{aligned}
&\int_{\Gamma_{\mathrm{I}}} C_{ijkl}^{\mathrm{I}}\xi_{kl}(a^{\mathrm{I}})a_i^{\mathrm{I}}\cdot n_j^{\mathrm{I}}\mathrm{dS} - \int_{\Gamma_{\mathrm{III}}} C_{ijkl}^{\mathrm{I}}\xi_{kl}(a^{\mathrm{I}})a_i^{\mathrm{I}}\cdot n_j^{\mathrm{III}}\mathrm{dS} \\
&+ \int_{\partial\Omega_{\mathrm{I}}\setminus\Gamma_{\mathrm{I}}\cup\Gamma_{\mathrm{III}}} C_{ijkl}^{\mathrm{I}}\xi_{kl}(a^{\mathrm{I}})a_i^{\mathrm{I}}\cdot n_j^{\Omega_{\mathrm{I}}\setminus\Gamma_{\mathrm{I}}\cup\Gamma_{\mathrm{III}}}\mathrm{dS} - \int_{\Omega_{\mathrm{I}}} C_{ijkl}^{\mathrm{I}}\xi_{kl}(a^{\mathrm{I}})\xi_{ij}(a^{\mathrm{I}})\mathrm{d}\mathbf{y} \\
&+ \int_{\Gamma_{\mathrm{II}}} C_{ijkl}^{\mathrm{II}}\xi_{kl}(a^{\mathrm{II}})a_i^{\mathrm{II}}\cdot n_j^{\mathrm{II}}\mathrm{dS} + \int_{\Gamma_{\mathrm{III}}} C_{ijkl}^{\mathrm{II}}\xi_{kl}(a^{\mathrm{II}})a_i^{\mathrm{II}}\cdot n_j^{\mathrm{III}}\mathrm{dS} \\
&+ \int_{\partial\Omega_{\mathrm{II}}\setminus\Gamma_{\mathrm{II}}\cup\Gamma_{\mathrm{III}}} C_{ijkl}^{\mathrm{II}}\xi_{kl}(a^{\mathrm{II}})a_i^{\mathrm{II}}\cdot n_j^{\Omega_{\mathrm{II}}\setminus\Gamma_{\mathrm{II}}\cup\Gamma_{\mathrm{III}}}\mathrm{dS} - \int_{\Omega_{\mathrm{II}}} C_{ijkl}^{\mathrm{II}}\xi_{kl}(a^{\mathrm{II}})\xi_{ij}(a^{\mathrm{II}})\mathrm{d}\mathbf{y} = 0
\end{aligned} \tag{3.219}$$

where $\mathbf{n}_{\mathrm{I}}$, $\mathbf{n}_{\mathrm{II}}$, $\mathbf{n}_{\mathrm{III}}$, $\mathbf{n}_{\Omega_{\mathrm{I}}\setminus\Gamma_{\mathrm{I}}\cup\Gamma_{\mathrm{III}}}$ and $\mathbf{n}_{\Omega_{\mathrm{II}}\setminus\Gamma_{\mathrm{II}}\cup\Gamma_{\mathrm{III}}}$ are the unit normals corresponding to Γ_{I}, Γ_{II}, Γ_{III}, $\partial\Omega_{\mathrm{I}}\setminus\Gamma_{\mathrm{I}}\cup\Gamma_{\mathrm{III}}$ and $\partial\Omega_{\mathrm{II}}\setminus\Gamma_{\mathrm{II}}\cup\Gamma_{\mathrm{III}}$. The terms on the boundaries cancel due to periodicity and then using equations (3.142), (3.144) and (3.145) from the cell problems we obtain

$$\begin{aligned}
&-\int_{\Gamma_{\mathrm{I}}} a_i^{\mathrm{I}} n_i^{\mathrm{I}}\mathrm{dS} - \int_{\Omega_{\mathrm{I}}} \xi_{ij}(a^{\mathrm{I}})C_{ijkl}^{\mathrm{I}}\xi_{kl}(a^{\mathrm{I}})\mathrm{d}\mathbf{y} \\
&-\int_{\Gamma_{\mathrm{II}}} a_i^{\mathrm{II}} n_i^{\mathrm{II}}\mathrm{dS} - \int_{\Omega_{\mathrm{II}}} \xi_{ij}(a^{\mathrm{II}})C_{ijkl}^{\mathrm{II}}\xi_{kl}(a^{\mathrm{II}})\mathrm{d}\mathbf{y} = 0.
\end{aligned} \tag{3.220}$$

Accounting for $\mathbf{y}$-periodicity and relationship (3.143), the sum of the first and third integrals above are equal to the sum of the corresponding integrals (with corresponding normals) on the boundaries $\partial\Omega_{\mathrm{I}}$ and $\partial\Omega_{\mathrm{II}}$, so that we can apply the divergence theorem in

reverse to obtain

$$-\int_{\Omega_s}\left(\frac{\partial a_i^{\mathrm{I}}}{\partial y_i}+\frac{\partial a_i^{\mathrm{II}}}{\partial y_i}\right)\mathrm{d}\mathbf{y}-\int_{\Omega_{\mathrm{I}}}\xi_{ij}(a^{\mathrm{I}})C_{ijkl}^{\mathrm{I}}\xi_{kl}(a^{\mathrm{I}})\mathrm{d}\mathbf{y}$$
$$-\int_{\Omega_{\mathrm{II}}}\xi_{ij}(a^{\mathrm{II}})C_{ijkl}^{\mathrm{II}}\xi_{kl}(a^{\mathrm{II}})\mathrm{d}\mathbf{y}=0. \tag{3.221}$$

We can write this as

$$-\int_{\Omega_s}\left(\frac{\partial a_i^{\mathrm{I}}}{\partial y_i}+\frac{\partial a_i^{\mathrm{II}}}{\partial y_i}\right)\mathrm{d}\mathbf{y}=\int_{\Omega_{\mathrm{I}}}\xi_{ij}(a^{\mathrm{I}})C_{ijkl}^{\mathrm{I}}\xi_{kl}(a^{\mathrm{I}})\mathrm{d}\mathbf{y}$$
$$+\int_{\Omega_{\mathrm{II}}}\xi_{ij}(a^{\mathrm{II}})C_{ijkl}^{\mathrm{II}}\xi_{kl}(a^{\mathrm{II}})\mathrm{d}\mathbf{y}. \tag{3.222}$$

Since the two terms on the right hand side are positive, we therefore have that

$$\int_{\Omega_s}\left(\frac{\partial a_i^{\mathrm{I}}}{\partial y_i}+\frac{\partial a_i^{\mathrm{II}}}{\partial y_i}\right)\mathrm{d}\mathbf{y}<0 \tag{3.223}$$

and so using the integral average notation we have

$$\beta=\left\langle\frac{\partial a_i^{\mathrm{I}}}{\partial y_i}+\frac{\partial a_i^{\mathrm{II}}}{\partial y_i}\right\rangle_{\mathrm{s}}<0. \tag{3.224}$$

Since $\beta<0$ we therefore have that $\hat{M}>0$. That is, the Biot's modulus is positive definite. □

3.4 Concluding Remarks

We have presented a poroelastic system of PDEs with novel model coefficients which describe the effective behaviour of poroelastic composites. In section 3.1 we have begun by considering the quasi-static multiphase fluid-structure interaction problem which describes the mechanics of a number of linear elastic inclusions/fibres embedded in a porous, linear elastic matrix, filled by a slowly-flowing incompressible Newtonian fluid. In Section 3.2 we have then enforced the length scale separation between the microscale and the macroscale to upscale the non-dimensionalized system of PDEs via asymptotic homogenization. In particular, we have assumed that both the pores and the elastic subphases (i.e. inclusions or fibres) are clearly resolved on the microscale, while the macroscale represents the average size of the macroscale domain. In Section 3.3 we show that the new model is both formally and substantially of poroelastic-type, by proving minor and major symmetries

of the effective elasticity tensor, positive definiteness of the macroscale Biot's modulus, and existence of a global macroscale Biot's coefficient tensor. The new model encodes the properties of the microstructure in the coefficients of the model, i.e. the effective hydraulic conductivity tensor, elasticity tensor, Biot's modulus and Biot's tensor of coefficients, which are to be computed by solving appropriate periodic cell problems. The latter comprise both a stress jump condition on the solid-solid interface (as in the cell problems for elastic composites), and inhomogeneous Neumann-type conditions on the fluid-solid interface (typical of the cell problems arising in poroelasticity).

The results are derived by assuming periodicity of the microstructure, and are presented by assuming that only one elastic subphase is contained in the representative periodic cell for the sake of simplicity. The new model is a natural generalization of the standard formulations for poroelastic media and composite materials derived via asymptotic homogenization, which are both recovered as particular cases.

Our model is relevant to the description of physical scenarios where the interactions between multiple elastic constituents take place at the porescale. The standard formulation of poroelasticity is appropriate when the interactions between the individual constituents of the solid phase and the fluid can be ignored, i.e. when the solid phase can be geometrically approximated as a homogeneous matrix at the porescale.

Our model also has some limitations and is open to a number of improvements that could enhance its range of applicability. The present formulation provides the effective governing equations in a quasi-static, linearized setting, and accounting for incompressibility of the fluid phase.

Generalization of our model to linearized inertia and compressibility of fluid is in principle straightforward, as it could be carried out as in [19], thus resulting in the corresponding changes on the macroscale. Leading order linearized inertia would appear in the effective balance equations for the poroelastic stress. Furthermore, the definition of the effective Biot's modulus would comprise the fluid bulk modulus, while the former depends only on the properties of the microstructure when the fluid phase is incompressible, see also [87]. However, the functional form of the elastic cell problems would not be affected by such changes, while the fluid cell problem is actually not affected by considering multiple elastic phases, and is simply the same as in standard poroelasticity in both cases. A relevant system where such an extension could provide a more accurate poroelastic modelling framework is the lung, where the investigation of the acoustic properties can be used in

the context of non-invasive diagnosis for pulmonary diseases, see, e.g., [107].

Mathematical modelling of nonlinear constitutive behaviour of the individual constituents is challenging in the context of asymptotic homogenization. However, there have been recent theoretical developments concerning both multiphase elastoplastic composites [99], and hyperelastic growing porous media, see [28]. Combining these approaches to extend our formulation would provide a comprehensive multiscale modelling framework for nonlinear poroelastic composites. The latter could then be used to formulate realistic predictions when large strains are relevant, as in the case of soft tissues such as arteries, see, e.g. [18, 49].

The results that we have illustrated here can also serve as a basis towards a more realistic modelling of hierarchical materials characterized by multiple separated scales (see, e.g. [100, 101] in the context of elastic composites). In this case, as the coefficients are to be computed at the porescale, our results could be exploited as a starting point to model the interaction between a poroelastic matrix and another fluid or elastic compartment, as done in the recent works [91, 123], [24, 105] for vascularized and fibre/inclusion reinforced poroelastic materials, respectively.

The next natural step is to obtain solutions of the model on the basis of a given microstructure, ideally parameterized by real-world images, for example related to biological tissues or artificial constructs, as described in the Introduction. For instance, three-dimensional numerical simulations of the asymptotic homogenization cell problems for elastic composites and poroelastic materials have been recently performed in [35, 88], respectively. As such, strategies developed therein could be adapted to compute the poroelastic coefficients presented here, which are obtained by solving cell problems which generalize those solved in [35, 88]. This way, predictions of the model could be validated against experimental data and/or used to optimize the design of poroelastic artificial constructs.

In the next chapter we continue with our aim to strengthen the applicability of poroelastic models to real world applications by deriving the model for poroelastic composites assuming that the elastic behaviour of the constituents is nonlinear. By incorporating the nonlinear behaviour in the model it will make it much more applicable to biological soft tissues such as the heart, arteries and the lungs. This generalisation is in general difficult in the context of asymptotic homogenization however, the following chapter is among the first few works that have been able to present a novel model that includes the nonlinear deformations and proposes a scheme that could be used to solve the model numerically.

Chapter 4

Homogenized balance equations for nonlinear poroelastic composites

We investigate materials that are subject to large deformations that have the underlying microstructure comprised of both a hyperelastic-fluid-filled porous matrix and a number of embedded hyperelastic subphases (fibres or inclusions). We then assume that both the matrix and the subphases interact with each other and the fluid at the porescale. This type of structure can be described as a poroelastic composite material that undergoes large deformations. For example, this is applicable to artery walls, which can be considered as a composite nonlinear elastic material consisting of a matrix with two families of symmetrically arranged embedded collagen and elastin fibres as well as fibroblast cells that interact with the fluid that is flowing in the pores [18, 49, 56, 58, 121]. If we wish to consider the artery walls in our framework, then the matrix can be identified with our matrix in the model, and the fibres and fibroblast cells could all be considered as the elastic subphases that are embedded in the matrix. The fluid in this setting would be the water that flows in the pores of the matrix. This modelling approach is applicable to the myocardium in the heart, which is a nonlinear elastic porous structure that consists of a matrix with muscle cells, fibroblasts, collagen fibres and embedded blood vessels [22, 29, 66]. Again, here, the various muscle cells, fibroblasts and fibres would all be the elastic subphases embedded in the matrix. By considering these systems as poroelastic composites, we are able to account for the mechanical contribution of each of the various phases individually.

Here, we generalise [69], Chapter 3, to account for nonlinear deformations by using the asymptotic homogenization technique to upscale the interaction between a hyperelastic porous matrix where there is an incompressible Newtonian fluid flowing in the pores and a number of embedded hyperelastic subphases. We make the assumption that both the hyperelastic matrix and subphases interact with the fluid that is flowing in the pores. We assume that the length scale where the individual hyperelastic subphases are clearly visible from the surrounding matrix is comparable to the pore size. We therefore determine that this scale will be the *porescale* of the material, that is the distance between adjacent subphases is comparable with the size of the pores. This length is assumed to be much smaller than the size of the whole domain, which is denoted the *macroscale*. The upscaling process is then used taking into account the continuity of the tractions and elastic displacements across the interfaces between the matrix and the subphases, as well as the continuity of the tractions and velocities across the interfaces between the fluid and solid domains. Furthermore, an appropriate coordinate transformation is carried out on some quantities to formulate the full problem in the undeformed/reference configuration, i.e., by solely using Lagrangian coordinates. The resulting system of governing equations is of poroelastic type and is a generalization of the formulations for (a) multiphase elastoplastic composites [102] in the limit of no plastic distortions and (b) the formulations for hyperelastic porous media [17] in the limit of only one elastic phase. It is also a natural extension to the formulation for linear poroelastic composites [69]. All three of these formulations are recovered as particular cases by assuming that: (a) our matrix is not porous; (b) that no elastic phase other than the matrix is present; and (c) by performing a linearisation. The coefficients of the model encode the properties of the microstructure and are computed by solving local differential problems.

The paper is organised as follows. In Section 4.1, we formulate the fluid–structure interaction problem that characterises the behaviour of the hyperelastic porous matrix, the hyperelastic subphases and the fluid flowing in the pores. We also perform a change of coordinates, which allows the fluid–structure interaction problem to be formulated in the reference configuration. In Section 4.2, we apply the asymptotic homogenization technique to the system of PDEs that were described in Section 4.1 and determine the new model that describes the effective macroscale mechanical behaviour of nonlinear poroelastic composites. In Section 4.3, we discuss the general nonlinear macroscale model before prescribing a specific strain energy function, namely the de Saint-Venant, for the material

and then give a physical interpretation of the novel terms. We also consider particular cases for our new model and are able to obtain previously known models from the literature. Section 4.4 concludes our work by highlighting and discussing the limitations of the current model and by providing further directions in which the model could be extended for particular biological applications.

4.1 Formulation of the Fluid–Structure Interaction Problem

We assume that we have a continuum body that is not subject to any surface or body forces to have a reference configuration, which we denote by $\mathscr{B}_0 \in \mathbb{R}^3$. The body $\mathscr{B}_0$ has a periodic microstructure that consists of the union of a porous hyperelastic matrix Ω^0_{II}, an interconnected fluid compartment Ω^0_{f} and a set Ω^0_{I} of N disjoint hyperelastic subphases Ω^0_α, where:

$$\Omega^0_{\text{I}} = \bigcup_{\alpha=1}^{N} \Omega^0_\alpha, \tag{4.1}$$

and $\bar{\Omega}^0 = \bar{\Omega}^0_{\text{I}} \cup \bar{\Omega}^0_{\text{II}} \cup \bar{\Omega}^0_{\text{f}}$, where $\bar{\ }$ denotes that the domain includes the interface. We note that when any domain, interface or normal vector has the superscript 0 then it is in the reference configuration. We provide a sketch of this structure as shown in Figure 4.1. The body undergoes a deformation described by the deformation function χ, and the deformed body is denoted by $\mathscr{B}_t$. Each point $\mathbf{x} \in \mathscr{B}_t$ is such that $\mathbf{x} = \chi(\mathbf{X}, t)$ with $\mathbf{X} \in \mathscr{B}_0$ being the point in the reference configuration. We assume that the periodicity of the body's microstructure is preserved during the deformation, and we now denote the deformed solid porous matrix as Ω^t_{II}, the deformed connected fluid compartment as Ω^t_{f} and the set of N disjoint deformed subphases Ω^t_α as Ω^t_{I} in $\mathscr{B}_t$. The assumption that the microstructure retains its periodicity is of course just one possible assumption. This option has been embraced for comparison with previous works e.g. [102] and also for the application to biological tissues where cells remain intact and with the same structures even when undergoing deformation. When any domain, interface or normal vector has the superscript t, this denotes the current configuration. The deformation from $\mathscr{B}_0$ to $\mathscr{B}_t$ is described by the deformation gradient $\mathbf{F} = \text{Grad}\chi$. Figure 4.1 highlights the description of this structure pictorially.

We now wish to describe the equations for the fluid and the solid compartments and the interface conditions in our structure. These equations however are not all in the same coordinate systems. We wish to work in the reference configuration so we have to perform

a pull back to some of the equations that are described in the current configuration. We begin by describing all equations in their natural coordinate systems before discussing the coordinate transformations.

The balance equations for the various hyperelastic domains Ω_α and Ω_{II} can be written as, $\forall \alpha = 1, \ldots, N$,

$$\nabla_{\mathbf{X}} \cdot \mathbf{P}_\alpha = 0 \quad \text{in} \quad \Omega_\alpha^0, \tag{4.2}$$

and:

$$\nabla_{\mathbf{X}} \cdot \mathbf{P}_{\text{II}} = 0 \quad \text{in} \quad \Omega_{\text{II}}^0, \tag{4.3}$$

where we neglect any volume forces and inertia. The tensors $\mathbf{P}_\alpha$ and $\mathbf{P}_{\text{II}}$ are the first Piola stresses. Each subphase Ω_α has the Piola stress tensor $\mathbf{P}_\alpha$, and the porous matrix Ω_{II} has Piola stress tensor $\mathbf{P}_{\text{II}}$. The matrix and the subphases are anisotropic, hyperelastic solids, and therefore, the constitutive laws for $\mathbf{P}_\alpha$ and $\mathbf{P}_{\text{II}}$ are given in terms of strain energy functions,

$$\mathbf{P}_\alpha = \frac{\partial \psi_\alpha}{\partial \mathbf{F}_\alpha} \quad \text{in} \quad \Omega_\alpha^0, \tag{4.4}$$

$$\mathbf{P}_{\text{II}} = \frac{\partial \psi_{\text{II}}}{\partial \mathbf{F}_{\text{II}}} \quad \text{in} \quad \Omega_{\text{II}}^0, \tag{4.5}$$

where $\mathbf{F}_\alpha$ and $\mathbf{F}_{\text{II}}$ are the deformation gradients in the subphases and the matrix, respectively, and ψ_α and ψ_{II} are the strain energy functions in the subphases and matrix, respectively. We do not define a specific strain energy function at this stage and wait until Section 4.3.1 to specify it.

We also require equations for the fluid phase. The balance equation is given as:

$$\nabla_{\mathbf{x}} \cdot \mathsf{T}_{\text{f}} = 0 \quad \text{in} \quad \Omega_{\text{f}}^t, \tag{4.6}$$

where we denoted the fluid stress tensor by T_{f}. The fluid is assumed to be an incompressible Newtonian fluid and, so, has the constitutive law:

$$\mathsf{T}_{\text{f}} = -p\mathbf{I} + \mu((\nabla_{\mathbf{x}}\mathbf{v}) + (\nabla_{\mathbf{x}}\mathbf{v})^{\text{T}}) \quad \text{in} \quad \Omega_{\text{f}}^t, \tag{4.7}$$

where $\mathbf{v}$ is the fluid velocity, p is the fluid pressure and μ is the fluid viscosity. As we

consider an incompressible fluid, the incompressibility condition reads:

$$\nabla_{\mathbf{x}} \cdot \mathbf{v} = 0 \quad \text{in} \quad \Omega_{\mathrm{f}}^t. \tag{4.8}$$

We can substitute the constitutive law (4.7) into the balance Equation (4.6), and then, by using (4.8), we obtain the Stokes problem:

$$0 = -\nabla_{\mathbf{x}} p + \mu \nabla_{\mathbf{x}} \cdot ((\nabla_{\mathbf{x}} \mathbf{v}) + (\nabla_{\mathbf{x}} \mathbf{v})^{\mathrm{T}}) \quad \text{in} \quad \Omega_{\mathrm{f}}^t. \tag{4.9}$$

In order to set up an appropriate fluid–structure interaction problem, we require interface conditions between the fluid and the various solid phases and also interface conditions between the various solid subphases and the matrix. The conditions we impose are the continuity of velocities, the continuity of tractions and the continuity of displacements. This presents an issue since the fluid and solid equations are described in different coordinate systems. The fluid equations are currently presented in Eulerian coordinates and the solid equations in Lagrangian coordinates. It is not possible to properly express continuity on the interface between the fluid and solid whilst the governing equations are in different coordinate systems. For this reason, we only describe the interface conditions between the elastic subphases and the matrix here and wait until Section 4.1.1 to describe the interface conditions between the fluid and solids once we have formulated all equations in Lagrangian coordinates. We define the interface between each elastic subphase and the matrix as $\Gamma_{\alpha\mathrm{II}}^0 := \partial\Omega_\alpha^0 \cap \partial\Omega_{\mathrm{II}}^0$ and impose continuity of tractions and displacements, namely:

$$\mathbf{P}_\alpha \mathbf{n}_{\alpha\mathrm{II}}^0 = \mathbf{P}_{\mathrm{II}} \mathbf{n}_{\alpha\mathrm{II}}^0 \quad \text{on} \quad \Gamma_{\alpha\mathrm{II}}^0, \tag{4.10}$$

$$\mathbf{u}_\alpha = \mathbf{u}_{\mathrm{II}} \quad \text{on} \quad \Gamma_{\alpha\mathrm{II}}^0, \tag{4.11}$$

$\forall \alpha = 1, \ldots, N$, where we define the unit vector normal to the interface $\Gamma_{\alpha\mathrm{II}}^0$ as $\mathbf{n}_{\alpha\mathrm{II}}^0$, and it is pointing into the subphase Ω_α^0 and where $\mathbf{u}_\alpha$ and $\mathbf{u}_{\mathrm{II}}$ are the elastic displacements in each subphase and the matrix, respectively.

We describe the deformation from $\mathscr{B}_0$ to $\mathscr{B}_t$ by the deformation gradient $\mathbf{F} = \mathrm{Grad}\chi$.

For convenience, we use the notation:

$$\mathbf{F} = \begin{cases} \mathbf{F}_\alpha & \text{in} \quad \Omega^0_\alpha, \\ \mathbf{F}_{\text{II}} & \text{in} \quad \Omega^0_{\text{II}}, \\ \mathbf{F}_{\text{f}} & \text{in} \quad \Omega^0_{\text{f}}, \end{cases} \tag{4.12}$$

where we have the deformation gradient in the α-th subphase, the matrix and the fluid respectively.

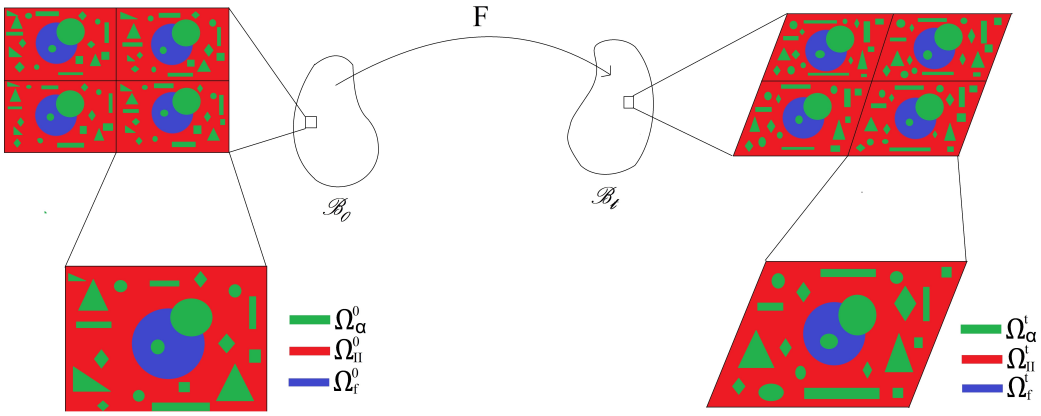

Figure 4.1: A 2D sketch that shows the poroelastic composite microstructure of the body in the reference configuration $\mathscr{B}_0$. It also shows the deformation $\mathbf{F}$ and gives the resulting microstructure of the deformed/current configuration $\mathscr{B}_t$. In both configurations, the porous matrix is shown in red, the subphases in green and the fluid in blue.

We note that our deformation gradient is in general discontinuous. It is however useful here to consider the definition of the deformation gradient in terms of the elastic deformations:

$$\mathbf{F} = \mathbf{I} + \text{Grad}\mathbf{u}, \tag{4.13}$$

where $\mathbf{I}$ is the identity tensor and Grad$\mathbf{u}$ is the gradient operator of the elastic displacement. We use the notation Grad with a capital G to denote the gradient in Lagrangian coordinates and grad for Eulerian coordinates. We can specialise relationship (4.13) in each of the reference elastic subphases as follows:

$$\mathbf{F} = \begin{cases} \mathbf{F}_\alpha = \mathbf{I} + \text{Grad}\mathbf{u}_\alpha & \text{in} \quad \Omega^0_\alpha, \\ \mathbf{F}_{\text{II}} = \mathbf{I} + \text{Grad}\mathbf{u}_{\text{II}} & \text{in} \quad \Omega^0_{\text{II}}. \end{cases} \tag{4.14}$$

We should note that the sketch here highlights a number of possible arrangements for the subphases. We can have subphases fully embedded in the matrix, fully embedded in

the fluid or in contact with both the matrix and the fluid. We set up our fluid–structure interaction with the assumption that all elastic phases are in contact with each other and the fluid.

4.1.1 Fluid–Structure Interaction in Lagrangian Coordinates

Within this section, we apply a coordinate transformation to the equations in the fluid–structure interaction (FSI) in order to obtain a full system of PDEs that describe the structure in the reference configuration. We do this in order to preserve the local periodicity of the microstructure, as was done in [28]. We define the Piola transformation, G, and the Jacobian, J, by:

$$J = \det\mathbf{F} \qquad \text{and} \qquad \mathsf{G} = J\mathbf{F}^{-1}, \tag{4.15}$$

where we have that:

$$\mathsf{G} = \begin{cases} \mathsf{G}_\alpha = J_\alpha \mathbf{F}_\alpha^{-1} & \text{in} \quad \Omega_\alpha^0, \\ \mathsf{G}_{\text{II}} = J_{\text{II}} \mathbf{F}_{\text{II}}^{-1} & \text{in} \quad \Omega_{\text{II}}^0, \\ \mathsf{G}_{\text{f}} = J_{\text{f}} \mathbf{F}_{\text{f}}^{-1} & \text{in} \quad \Omega_{\text{f}}^0. \end{cases} \tag{4.16}$$

Here, we wish to make a remark regarding the continuity of the Piola transformation.

Remark 7 (Continuity of G^{T})**.** *Here, we wish to explain the continuity of* G^{T} *across the various interfaces appearing in our structure. We begin with Nanson's formula:*

$$\mathbf{n}\text{da} = J\mathbf{F}^{-\text{T}}\mathbf{N}\text{dA}, \tag{4.17}$$

where $\mathbf{n}$ *is a general unit normal and* da *is a general area element in the current configuration and* $\mathbf{N}$ *is a general unit normal and* dA *is a general area element in the reference configuration. Using our notation for the Piola transform, we can rewrite this as:*

$$\mathbf{n}\text{da} = \mathsf{G}^{\text{T}}\mathbf{N}\text{dA}. \tag{4.18}$$

By using this relationship, we are able to deduce the continuities on our various interfaces Γ_α*,* Γ_{II} *and* $\Gamma_{\alpha\text{II}}$*, that is,*

$$\begin{gathered} \mathsf{G}_\alpha^{\text{T}}\mathbf{n}_\alpha^0 = \mathsf{G}_{\text{f}}^{\text{T}}\mathbf{n}_\alpha^0 \quad \textit{on} \quad \Gamma_\alpha, \qquad \mathsf{G}_{\text{II}}^{\text{T}}\mathbf{n}_{\text{II}}^0 = \mathsf{G}_{\text{f}}^{\text{T}}\mathbf{n}_{\text{II}}^0 \quad \textit{on} \quad \Gamma_{\text{II}}, \\ \textit{and} \quad \mathsf{G}_\alpha^{\text{T}}\mathbf{n}_{\alpha\text{II}}^0 = \mathsf{G}_{\text{II}}^{\text{T}}\mathbf{n}_{\alpha\text{II}}^0 \quad \textit{on} \quad \Gamma_{\alpha\text{II}}. \end{gathered} \tag{4.19}$$

These formulas are used in later sections of this work.

We use the following formulas to make the change of the coordinate systems. For a scalar ζ, a vector $\mathbf{z}$ and a tensor Z, we have:

$$\nabla_{\mathbf{x}}\zeta = \mathbf{F}^{-\mathrm{T}}\nabla_{\mathbf{X}}\zeta \qquad \text{and} \qquad \nabla_{\mathbf{x}}\mathbf{z} = (\nabla_{\mathbf{X}}\mathbf{z})\mathbf{F}^{-1}. \tag{4.20}$$

By again using Nanson's formula:

$$\mathbf{n}\mathrm{da} = J\mathbf{F}^{-\mathrm{T}}\mathbf{N}\mathrm{dA}, \tag{4.21}$$

the transformation rule for a general volume element:

$$\mathrm{d}v = J\mathrm{d}V, \tag{4.22}$$

and by applying the divergence theorem, we obtain the coordinate changes:

$$\nabla_{\mathbf{x}}\cdot\mathbf{z} = \frac{1}{J}\nabla_{\mathbf{X}}\cdot(\mathsf{G}\mathbf{z}) \qquad \text{and} \qquad \nabla_{\mathbf{x}}\cdot Z = \frac{1}{J}\nabla_{\mathbf{X}}\cdot(Z\mathsf{G}^{\mathrm{T}}). \tag{4.23}$$

We are now able to use (4.20) and (4.23) to write our FSI problem in the reference configuration. The equations governing the fluid in the reference configuration are therefore given by:

$$\nabla_{\mathbf{X}}\cdot(\mathsf{T}_{\mathrm{f}}\mathsf{G}_{\mathrm{f}}^{\mathrm{T}}) = 0 \quad \text{in} \quad \Omega_{\mathrm{f}}^{0}, \tag{4.24}$$

with the fluid stress tensor T_{f} transformed as:

$$\mathsf{T}_{\mathrm{f}}\mathsf{G}_{\mathrm{f}}^{\mathrm{T}} = -p\mathsf{G}_{\mathrm{f}}^{\mathrm{T}} + \mu((\nabla_{\mathbf{X}}\mathbf{V})\mathbf{F}_{\mathrm{f}}^{-1}\mathsf{G}_{\mathrm{f}}^{\mathrm{T}} + \mathbf{F}_{\mathrm{f}}^{-\mathrm{T}}(\nabla_{\mathbf{X}}\mathbf{V})^{\mathrm{T}}\mathsf{G}_{\mathrm{f}}^{\mathrm{T}}) \quad \text{in} \quad \Omega_{\mathrm{f}}^{0}, \tag{4.25}$$

to correspond to the fluid balance equation, where $\mathbf{V}$ is the fluid velocity in the reference configuration. The incompressibility condition also transforms as follows:

$$\nabla_{\mathbf{X}}\cdot(\mathsf{G}_{\mathrm{f}}\mathbf{V}) = 0 \quad \text{in} \quad \Omega_{\mathrm{f}}^{0}. \tag{4.26}$$

The Stokes' problem in the reference configuration is obtained by substituting (4.25) into (4.24) and using (4.26), that is,

$$0 = -\mathsf{G}_{\mathrm{f}}^{\mathrm{T}}\nabla_{\mathbf{X}}p + \mu\nabla_{\mathbf{X}}\cdot((\nabla_{\mathbf{X}}\mathbf{V})\mathsf{G}_{\mathrm{f}}\mathbf{F}_{\mathrm{f}}^{-\mathrm{T}} + \mathsf{G}_{\mathrm{f}}^{\mathrm{T}}(\nabla_{\mathbf{X}}\mathbf{V})^{\mathrm{T}}\mathbf{F}_{\mathrm{f}}^{-\mathrm{T}}) \quad \text{in} \quad \Omega_{\mathrm{f}}^{0}. \tag{4.27}$$

Now that all our governing equations are described in the Lagrangian framework, we are able to describe the interface conditions between the fluid and solid phases that we require to set up an appropriate FSI problem. We note that these interface conditions take place on the interfaces between the fluid and the elastic subphases in the reference configuration. Defining the interfaces between the fluid phase and each of the α subphases in the reference configuration as $\Gamma^0_\alpha := \partial\Omega^0_\alpha \cap \partial\Omega^0_{\mathrm{f}}$ and defining the interface between the matrix and the fluid phase, again in the reference configuration, as $\Gamma^0_{\mathrm{II}} := \partial\Omega^0_{\mathrm{II}} \cap \partial\Omega^0_{\mathrm{f}}$, we can impose the continuity of the velocities and tractions on the various interfaces. We therefore have:

$$\frac{\partial \mathbf{u}_\alpha}{\partial t} = \mathbf{V} \qquad \text{on} \qquad \Gamma^0_\alpha, \tag{4.28}$$

$$\mathsf{T}_{\mathrm{f}}\mathsf{G}_{\mathrm{f}}^{\mathrm{T}}\mathbf{n}^0_\alpha = \mathbf{P}_\alpha \mathbf{n}^0_\alpha \qquad \text{on} \qquad \Gamma^0_\alpha, \tag{4.29}$$

$$\frac{\partial \mathbf{u}_{\mathrm{II}}}{\partial t} = \mathbf{V} \qquad \text{on} \qquad \Gamma^0_{\mathrm{II}}, \tag{4.30}$$

$$\mathsf{T}_{\mathrm{f}}\mathsf{G}_{\mathrm{f}}^{\mathrm{T}}\mathbf{n}^0_{\mathrm{II}} = \mathbf{P}_{\mathrm{II}} \mathbf{n}^0_{\mathrm{II}} \qquad \text{on} \qquad \Gamma^0_{\mathrm{II}}, \tag{4.31}$$

$\forall \alpha = 1, \ldots, N$. We have that $\partial \mathbf{u}_\alpha / \partial t$ and $\partial \mathbf{u}_{\mathrm{II}} / \partial t$ are the solid velocities in each of the subphases and the matrix, respectively. We have that $\mathbf{n}^0_\alpha$ and $\mathbf{n}^0_{\mathrm{II}}$ are the unit outward normals to the interfaces Γ^0_α and Γ^0_{II}, respectively.

Our complete FSI problem in the reference configuration is therefore given by (4.2)–(4.5), (4.10)–(4.11), (4.14) and (4.24)–(4.31).

Within the next section, we carry out our analysis by first nondimensionalising the system of partial differential equations (PDEs) that we formulate in the reference configuration within this section. We introduce two well-separated length scales that allow us to apply the two-scale asymptotic homogenization technique to the nondimensionalised PDEs. This allows the derivation of the macroscale governing equations.

4.2 The Asymptotic Homogenization Method

Here, we summarise the fluid–structure interaction problem in the reference configuration that we introduced in the previous section. We will then be ready to perform a multiscale analysis.

$$\nabla_{\mathbf{X}} \cdot \mathbf{P}_\alpha = 0 \qquad \text{in} \qquad \Omega^0_\alpha, \tag{4.32}$$

$$\nabla_{\mathbf{X}} \cdot \mathbf{P}_{\text{II}} = 0 \qquad \text{in} \qquad \Omega^0_{\text{II}}, \tag{4.33}$$

$$\nabla_{\mathbf{X}} \cdot (\mathsf{T}_{\text{f}}\mathsf{G}_{\text{f}}^{\text{T}}) = 0 \qquad \text{in} \qquad \Omega^0_{\text{f}}, \tag{4.34}$$

$$\nabla_{\mathbf{X}} \cdot (\mathsf{G}_{\text{f}}\mathbf{V}) = 0 \qquad \text{in} \qquad \Omega^0_{\text{f}}, \tag{4.35}$$

$$\frac{\partial \mathbf{u}_\alpha}{\partial t} = \mathbf{V} \qquad \text{on} \qquad \Gamma^0_\alpha, \tag{4.36}$$

$$\frac{\partial \mathbf{u}_{\text{II}}}{\partial t} = \mathbf{V} \qquad \text{on} \qquad \Gamma^0_{\text{II}}, \tag{4.37}$$

$$\mathsf{T}_{\text{f}}\mathsf{G}_{\text{f}}^{\text{T}}\mathbf{n}^0_\alpha = \mathbf{P}_\alpha \mathbf{n}^0_\alpha \qquad \text{on} \qquad \Gamma^0_\alpha, \tag{4.38}$$

$$\mathsf{T}_{\text{f}}\mathsf{G}_{\text{f}}^{\text{T}}\mathbf{n}^0_{\text{II}} = \mathbf{P}_{\text{II}} \mathbf{n}^0_{\text{II}} \qquad \text{on} \qquad \Gamma^0_{\text{II}}, \tag{4.39}$$

$$\mathbf{P}_\alpha \mathbf{n}^0_{\alpha\text{II}} = \mathbf{P}_{\text{II}} \mathbf{n}^0_{\alpha\text{II}} \qquad \text{on} \qquad \Gamma^0_{\alpha\text{II}}. \tag{4.40}$$

$$\mathbf{u}_\alpha = \mathbf{u}_{\text{II}} \qquad \text{on} \qquad \Gamma^0_{\alpha\text{II}}, \tag{4.41}$$

We have that the constitutive relationships for the fluid and the multiple solid phases are given as:

$$\mathsf{T}_{\text{f}}\mathsf{G}_{\text{f}}^{\text{T}} = -p\mathsf{G}_{\text{f}}^{\text{T}} + \mu((\nabla_{\mathbf{X}}\mathbf{V})\mathbf{F}_{\text{f}}^{-1}\mathsf{G}_{\text{f}}^{\text{T}} + \mathbf{F}_{\text{f}}^{-\text{T}}(\nabla_{\mathbf{X}}\mathbf{V})^{\text{T}}\mathsf{G}_{\text{f}}^{\text{T}}) \qquad \text{in} \qquad \Omega^0_{\text{f}}, \tag{4.42}$$

$$\mathbf{P}_\alpha = \frac{\partial \psi_\alpha}{\partial \mathbf{F}_\alpha} \qquad \text{in} \qquad \Omega^0_\alpha, \tag{4.43}$$

$$\mathbf{P}_{\text{II}} = \frac{\partial \psi_{\text{II}}}{\partial \mathbf{F}_{\text{II}}} \qquad \text{in} \qquad \Omega^0_{\text{II}}. \tag{4.44}$$

We then use the constitutive relationship (4.42) with the incompressibility constraint (4.35) in the balance Equation (4.34) to obtain:

$$0 = -\mathsf{G}_{\text{f}}^{\text{T}}\nabla_{\mathbf{X}}p + \mu\nabla_{\mathbf{X}} \cdot ((\nabla_{\mathbf{X}}\mathbf{V})\mathsf{G}_{\text{f}}\mathbf{F}_{\text{f}}^{-\text{T}} + \mathsf{G}_{\text{f}}^{\text{T}}(\nabla_{\mathbf{X}}\mathbf{V})^{\text{T}}\mathbf{F}_{\text{f}}^{-\text{T}}) \qquad \text{in} \qquad \Omega^0_{\text{f}}. \tag{4.45}$$

We also have the deformation gradients for each of the solid phases:

$$\mathbf{F}_\alpha = \mathbf{I} + \nabla_{\mathbf{X}}\mathbf{u}_\alpha \qquad \text{in} \qquad \Omega^0_\alpha, \tag{4.46}$$

$$\mathbf{F}_{\text{II}} = \mathbf{I} + \nabla_{\mathbf{X}}\mathbf{u}_{\text{II}} \qquad \text{in} \qquad \Omega^0_{\text{II}}, \tag{4.47}$$

$\forall \alpha = 1, \ldots, N$. We assume that the system possesses two distinct length scales. The whole domain has a length scale, which we denote by L, and this is referred to as the macroscale. There also exists a second length scale, which we denote by d, and this describes the porescale. The length d is comparable to the intersubphase distance and the size of the pores. Therefore, to capture the true difference between the two scales, it is useful to

perform a nondimensional analysis of the system of PDEs (4.32)–(4.47). This nondimensionalisation is carried out in the next section.

We should note that this fluid–structure interaction is the nonlinear counterpart to the one found in [69] for linear poroelastic composites. We also highlight that this FSI problem is formulated with the intention that all elastic phases are in contact with each other and the fluid.

4.2.1 Non-dimensionalisation

We carry out the non-dimensionalisation process by relying on the standard parabolic fluid velocity in the pores, which is quadratic in the pore-scale d and proportional to a given pressure gradient C_p. This scaling is the classical one, which ensures that a Newtonian fluid flowing in the pores is macroscopically governed by porous media flow equations (e.g., of Darcy's type) (see [87], where this is discussed). There are of course alternative scalings available for the fluid velocity; however, these scalings do not account for the appropriate effective behaviour of a fluid flow in porous media.

Therefore, we choose the scalings:

$$\mathbf{x} = L\mathbf{x}', \quad \mathbf{u}_\alpha = L\mathbf{u}'_\alpha, \quad \mathbf{u}_{\text{II}} = L\mathbf{u}'_{\text{II}}, \quad \mathbf{V} = \frac{C_p d^2}{\mu}\mathbf{V}', \quad p = C_p L p', \quad \mathbf{P}_\alpha = C_p L \mathbf{P}'_\alpha,$$
$$\mathbf{P}_{\text{II}} = C_p L \mathbf{P}'_{\text{II}}. \tag{4.48}$$

We then use (4.48), and the gradient operator becomes:

$$\nabla = \frac{1}{L}\nabla', \tag{4.49}$$

and the nondimensionalised form of the system of the PDEs (4.32)–(4.41) is given by,

$$\nabla_{\mathbf{X}} \cdot \mathbf{P}_\alpha = 0 \qquad \text{in} \qquad \Omega^0_\alpha, \tag{4.50}$$
$$\nabla_{\mathbf{X}} \cdot \mathbf{P}_{\text{II}} = 0 \qquad \text{in} \qquad \Omega^0_{\text{II}}, \tag{4.51}$$
$$\nabla_{\mathbf{X}} \cdot (\mathsf{T}_{\text{f}}\mathsf{G}_{\text{f}}^{\text{T}}) = 0 \qquad \text{in} \qquad \Omega^0_{\text{f}}, \tag{4.52}$$
$$\nabla_{\mathbf{X}} \cdot (\mathsf{G}_{\text{f}}\mathbf{V}) = 0 \qquad \text{in} \qquad \Omega^0_{\text{f}}, \tag{4.53}$$
$$\frac{\partial \mathbf{u}_\alpha}{\partial t} = \mathbf{V} \qquad \text{on} \qquad \Gamma^0_\alpha, \tag{4.54}$$
$$\frac{\partial \mathbf{u}_{\text{II}}}{\partial t} = \mathbf{V} \qquad \text{on} \qquad \Gamma^0_{\text{II}}, \tag{4.55}$$

$$\mathsf{T}_{\mathrm{f}}\mathsf{G}_{\mathrm{f}}^{\mathrm{T}}\mathbf{n}_{\alpha}^{0} = \mathbf{P}_{\alpha}\mathbf{n}_{\alpha}^{0} \qquad \text{on} \qquad \Gamma_{\alpha}^{0}, \tag{4.56}$$

$$\mathsf{T}_{\mathrm{f}}\mathsf{G}_{\mathrm{f}}^{\mathrm{T}}\mathbf{n}_{\mathrm{II}}^{0} = \mathbf{P}_{\mathrm{II}}\mathbf{n}_{\mathrm{II}}^{0} \qquad \text{on} \qquad \Gamma_{\mathrm{II}}^{0}, \tag{4.57}$$

$$\mathbf{P}_{\alpha}\mathbf{n}_{\alpha\mathrm{II}}^{0} = \mathbf{P}_{\mathrm{II}}\mathbf{n}_{\alpha\mathrm{II}}^{0} \qquad \text{on} \qquad \Gamma_{\alpha\mathrm{II}}^{0}, \tag{4.58}$$

$$\mathbf{u}_{\alpha} = \mathbf{u}_{\mathrm{II}} \qquad \text{on} \qquad \Gamma_{\alpha\mathrm{II}}^{0}. \tag{4.59}$$

We also non-dimensionalise the constitutive relationships for the fluid and the solid, and these are given by:

$$\mathsf{T}_{\mathrm{f}}\mathsf{G}_{\mathrm{f}}^{\mathrm{T}} = -p\mathsf{G}_{\mathrm{f}}^{\mathrm{T}} + \epsilon^{2}((\nabla_{\mathbf{X}}\mathbf{V})\mathbf{F}_{\mathrm{f}}^{-1}\mathsf{G}_{\mathrm{f}}^{\mathrm{T}} + \mathbf{F}_{\mathrm{f}}^{-\mathrm{T}}(\nabla_{\mathbf{X}}\mathbf{V})^{\mathrm{T}}\mathsf{G}_{\mathrm{f}}^{\mathrm{T}}) \qquad \text{in} \qquad \Omega_{\mathrm{f}}^{0}, \tag{4.60}$$

$$\mathbf{P}_{\alpha} = \frac{\partial\psi_{\alpha}}{\partial\mathbf{F}_{\alpha}} \qquad \text{in} \qquad \Omega_{\alpha}^{0}, \tag{4.61}$$

$$\mathbf{P}_{\mathrm{II}} = \frac{\partial\psi_{\mathrm{II}}}{\partial\mathbf{F}_{\mathrm{II}}} \qquad \text{in} \qquad \Omega_{\mathrm{II}}^{0}. \tag{4.62}$$

We also have the non-dimensionalised fluid balance equation and solid deformation gradients given by:

$$0 = -\mathsf{G}_{\mathrm{f}}^{\mathrm{T}}\nabla_{\mathbf{X}}p + \epsilon^{2}\nabla_{\mathbf{X}}\cdot((\nabla_{\mathbf{X}}\mathbf{V})\mathsf{G}_{\mathrm{f}}\mathbf{F}_{\mathrm{f}}^{-\mathrm{T}} + \mathsf{G}_{\mathrm{f}}^{\mathrm{T}}(\nabla_{\mathbf{X}}\mathbf{V})^{\mathrm{T}}\mathbf{F}_{\mathrm{f}}^{-\mathrm{T}}) \qquad \text{in} \qquad \Omega_{\mathrm{f}}^{0}, \tag{4.63}$$

$$\mathbf{F}_{\alpha} = \mathbf{I} + \nabla_{\mathbf{X}}\mathbf{u}_{\alpha} \qquad \text{in} \qquad \Omega_{\alpha}^{0}, \tag{4.64}$$

$$\mathbf{F}_{\mathrm{II}} = \mathbf{I} + \nabla_{\mathbf{X}}\mathbf{u}_{\mathrm{II}} \qquad \text{in} \qquad \Omega_{\mathrm{II}}^{0}, \tag{4.65}$$

where in (4.50)–(4.65), we drop the primes for the sake of a simpler notation, and we have the parameter:

$$\epsilon = \frac{d}{L}. \tag{4.66}$$

Within the next section, we introduce the two-scale asymptotic homogenization technique, which we then use to upscale our system (4.50)–(4.65) in order to obtain our macroscale model.

4.2.2 The Two-Scale Asymptotic Homogenization Method

Here, we now introduce the asymptotic homogenization technique, which we will use to derive the effective macroscale governing equations for our structure. As described above, we have the porescale, denoted by d, and the macroscale, which is the average size of the

whole material, denoted by L. We assume that these scales are well separated, i.e.,

$$\epsilon = \frac{d}{L} \ll 1. \tag{4.67}$$

We can describe ϵ as the scale separation parameter. We require a local scale spatial variable, which will capture the porescale variations of each of the fields appearing in (4.50)–(4.65), that is,

$$\bar{\mathbf{Y}} = \frac{\mathbf{X}}{\epsilon}. \tag{4.68}$$

We also have the macroscale variable:

$$\bar{\mathbf{X}} = \mathbf{X}. \tag{4.69}$$

The newly introduced spatial variables $\bar{\mathbf{X}}$ and $\bar{\mathbf{Y}}$ represent the macroscale and the porescale respectively and are to be considered formally independent. The gradient operator also transforms, by the application of the chain rule, to become an operator of both scales, which we can write as:

$$\nabla_{\mathbf{X}} \to \nabla_{\bar{\mathbf{X}}} + \frac{1}{\epsilon}\nabla_{\bar{\mathbf{Y}}}. \tag{4.70}$$

We also make the assumption that all the fields in (4.50)–(4.65), $\forall \alpha = 1, ..., N$, are functions of the two spatial variables $\bar{\mathbf{X}}$ and $\bar{\mathbf{Y}}$ and that every field can be written as a power series expansion in ϵ:

$$\varphi^{\epsilon}(\bar{\mathbf{X}}, \bar{\mathbf{Y}}, t) = \sum_{l=0}^{\infty} \varphi^{(l)}(\bar{\mathbf{X}}, \bar{\mathbf{Y}}, t)\epsilon^{l}, \tag{4.71}$$

where φ is used to denote a general field in (4.50)–(4.65).

Remark 8 (Porescale periodicity)**.** *We assume that every field $\varphi^{(l)}$ in our analysis is $\bar{\mathbf{Y}}$-periodic, and this allows us to focus our attention on a single periodic cell in our structure. This is a technical assumption that is related solely to the microscale. The fields can still vary with respect to the macroscale. Making this assumption means that we formulate the porescale differential problems on this periodic cell, and it is these problems that are to be solved to determine the macroscale model coefficients. In [35], the authors assumed that all the fields are periodic in the porescale variable and are able to compute the coefficients of the model of standard poroelasticity obtained via asymptotic homogenization. In comparison, in [34], the macroscale model of poroelasticity was solved. As such,*

although the effective coefficients used are those computed by following the methodology described in [35], the illustrated solution solely depends on the macroscale and is in general not periodic. It is possible to relax this assumption that all fields are $\bar{\mathbf{Y}}$*-periodic and assume instead that all the fields are locally bounded. This assumption is less strict than local periodicity and means that all the fields are finite with respect to the porescale variable* $\bar{\mathbf{Y}}$ *when* $\epsilon \to 0$*, but not necessarily periodic. This assumption however only permits the functional form of the macroscale model to be derived and does not in general allow for the model coefficients to be computed without further assumptions (see [48, 90] for further details) in multidimensional problems [90].*

We have that our periodic cell could potentially contain a variety of subphases and these subphases could possess various geometries and elastic properties. This assumption is particularly useful as it allows us to solve the differential problems obtained from the asymptotic homogenization technique on a single periodic cell instead of the whole material domain, therefore reducing the computational complexity. This periodic cell where we solve the differential problems is shown in Figure 4.2.

Remark 9 (Macroscopic uniformity)**.** *We know that the porescale structure of a material can vary with respect to the macroscale position (see [19, 32, 48, 86, 87]). In general, this dependence is neglected in the literature due to wanting to simplify the analysis. Here, we assume that the porescale geometry does not depend on the macroscale variable* $\bar{\mathbf{X}}$*, i.e., the material is macroscopically uniform. This assumption allows for simple differentiation under the integral sign to take place, that is:*

$$\int_{\Omega} \nabla_{\bar{\mathbf{x}}} \cdot (\bullet)\, d\bar{\mathbf{Y}} = \nabla_{\bar{\mathbf{x}}} \cdot \int_{\Omega} (\bullet)\, d\bar{\mathbf{Y}}. \tag{4.72}$$

If we do not assume macroscopic uniformity, then (4.72) is not satisfied, and in this case, the application of the Reynolds' transport theorem is required. This may lead to additional terms appearing in the macroscale governing equations.

Remark 10 (Porescale geometry)**.** *In our description so far, we assume that there are various different subphases included within our periodic cell; however, without loss of generality, we can focus our attention on the case where each periodic cell contains only one hyperelastic subphase. This structure is shown in Figure 4.3. Therefore, we do not require the index* α*, and the notation can be adjusted as follows. We have the continuum body* $\mathscr{B}_0$*, which has a periodic microstructure. Within* $\mathscr{B}_0$*, we have many periodic cells; how-*

ever, due to periodicity, we can identify the domain Ω^0 *with the periodic cell, which has a hyperelastic subphase, hyperelastic matrix and fluid portions denoted by* $\Omega^0_{\rm I}$, $\Omega^0_{\rm II}$ *and* $\Omega^0_{\rm f}$, *respectively. We are also able to simplify the notation we use for the different interfaces. The interface between the subphase and the fluid is* $\Gamma^0_{\rm I} := \partial\Omega^0_{\rm I} \cap \partial\Omega^0_{\rm f}$; *the interface between the matrix and the fluid is* $\Gamma^0_{\rm II} := \partial\Omega^0_{\rm II} \cap \partial\Omega^0_{\rm f}$; *the interface between our two hyperelastic solid phases is* $\Gamma^0_{\rm III} := \partial\Omega^0_{\rm I} \cap \partial\Omega^0_{\rm II}$, *with corresponding unit normal vectors* $\mathbf{n}^0_{\rm I}$, $\mathbf{n}^0_{\rm II}$ *and* $\mathbf{n}^0_{\rm III}$. *If a specific application required multiple subphases to be contained in the periodic cell, then it would be simple to extend the formulation, as has been done in the case of elastic composites [88].*

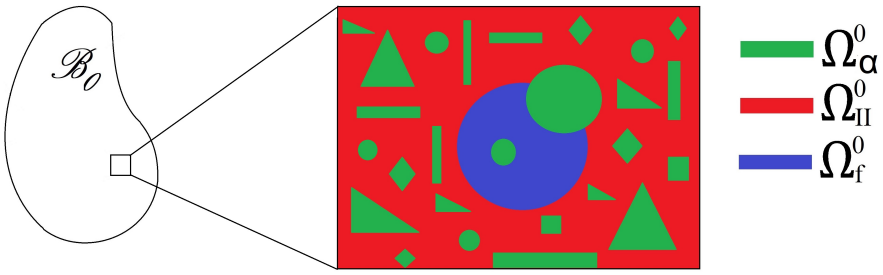

Figure 4.2: A 2D cross-section of a single periodic cell in our structure. We have the fluid represented in blue, the hyperelastic porous matrix in red and the hyperelastic subphases in green. We highlight that the subphases Ω_α for $\alpha = 1, \ldots, N$ can interact with both the matrix and the fluid or be fully embedded in the either the matrix or the fluid.

We should note that our periodic structure is 3D, that is, the fluid flow is in three interconnected cylinders. For an example of the geometry of our 3D structure see Fig. 3.2 in Chapter 3, where we are considering the same microstructure but for small (linear) deformations.

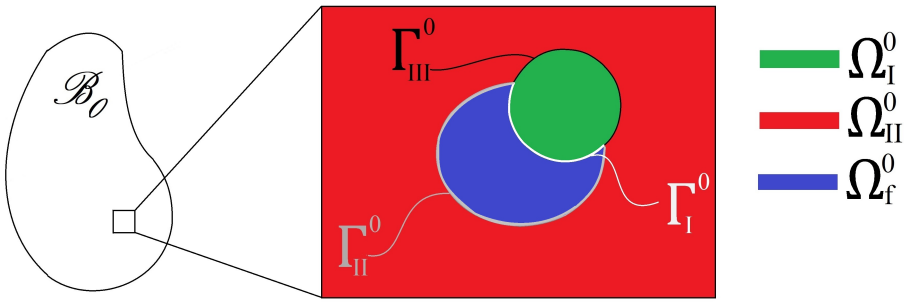

Figure 4.3: This is a sketch of a 2D cross-section of the periodic cell on which we focus. We have one hyperelastic subphase shown in green that is in contact with the hyperelastic matrix shown in red and the fluid shown in blue. We also highlight the interfaces $\Gamma_{\rm I}$, $\Gamma_{\rm II}$ and $\Gamma_{\rm III}$ between the phases.

4.2.3 The Macroscale Results

The assumptions (4.70) and (4.71) of the asymptotic homogenization technique can be applied to Equations (4.50)–(4.65). We then obtain the following multiscale system of PDEs:

$$\nabla_{\bar{\mathbf{Y}}} \cdot \mathbf{P}_{\mathrm{I}}^{\epsilon} + \epsilon \nabla_{\bar{\mathbf{X}}} \cdot \mathbf{P}_{\mathrm{I}}^{\epsilon} = 0 \qquad \text{in} \qquad \Omega_{\mathrm{I}}^{0}, \tag{4.73}$$

$$\nabla_{\bar{\mathbf{Y}}} \cdot \mathbf{P}_{\mathrm{II}}^{\epsilon} + \epsilon \nabla_{\bar{\mathbf{X}}} \cdot \mathbf{P}_{\mathrm{II}}^{\epsilon} = 0 \qquad \text{in} \qquad \Omega_{\mathrm{II}}^{0}, \tag{4.74}$$

$$\nabla_{\bar{\mathbf{Y}}} \cdot (\mathsf{T}_{\mathrm{f}}{}^{\epsilon}(\mathsf{G}_{\mathrm{f}}^{\epsilon})^{\mathrm{T}}) + \epsilon \nabla_{\bar{\mathbf{X}}} \cdot (\mathsf{T}_{\mathrm{f}}{}^{\epsilon}(\mathsf{G}_{\mathrm{f}}^{\epsilon})^{\mathrm{T}}) = 0 \qquad \text{in} \qquad \Omega_{\mathrm{f}}^{0}, \tag{4.75}$$

$$\nabla_{\bar{\mathbf{Y}}} \cdot (\mathsf{G}_{\mathrm{f}}^{\epsilon}\mathbf{V}^{\epsilon}) + \epsilon \nabla_{\bar{\mathbf{X}}} \cdot (\mathsf{G}_{\mathrm{f}}^{\epsilon}\mathbf{V}^{\epsilon}) = 0 \qquad \text{in} \qquad \Omega_{\mathrm{f}}^{0}, \tag{4.76}$$

$$\frac{\partial \mathbf{u}_{\mathrm{I}}^{\epsilon}}{\partial t} = \mathbf{V}^{\epsilon} \qquad \text{on} \qquad \Gamma_{\mathrm{I}}^{0}, \tag{4.77}$$

$$\frac{\partial \mathbf{u}_{\mathrm{II}}^{\epsilon}}{\partial t} = \mathbf{V}^{\epsilon} \qquad \text{on} \qquad \Gamma_{\mathrm{II}}^{0}, \tag{4.78}$$

$$\mathsf{T}_{\mathrm{f}}{}^{\epsilon}(\mathsf{G}_{\mathrm{f}}^{\epsilon})^{\mathrm{T}}\mathbf{n}_{\mathrm{I}}^{0} = \mathbf{P}_{\mathrm{I}}^{\epsilon}\mathbf{n}_{\mathrm{I}}^{0} \qquad \text{on} \qquad \Gamma_{\mathrm{I}}^{0}, \tag{4.79}$$

$$\mathsf{T}_{\mathrm{f}}{}^{\epsilon}(\mathsf{G}_{\mathrm{f}}^{\epsilon})^{\mathrm{T}}\mathbf{n}_{\mathrm{II}}^{0} = \mathbf{P}_{\mathrm{II}}^{\epsilon}\mathbf{n}_{\mathrm{II}}^{0} \qquad \text{on} \qquad \Gamma_{\mathrm{II}}^{0}, \tag{4.80}$$

$$\mathbf{P}_{\mathrm{I}}^{\epsilon}\mathbf{n}_{\mathrm{III}}^{0} = \mathbf{P}_{\mathrm{II}}^{\epsilon}\mathbf{n}_{\mathrm{III}}^{0} \qquad \text{on} \qquad \Gamma_{\mathrm{III}}^{0}, \tag{4.81}$$

$$\mathbf{u}_{\mathrm{I}}^{\epsilon} = \mathbf{u}_{\mathrm{II}}^{\epsilon} \qquad \text{on} \qquad \Gamma_{\mathrm{III}}^{0}, \tag{4.82}$$

as well as the multiscale constitutive equations for $\mathsf{T}_{\mathrm{f}}{}^{\epsilon}(\mathsf{G}_{\mathrm{f}}^{\epsilon})^{\mathrm{T}}$, $\mathbf{P}_{\mathrm{I}}^{\epsilon}$ and $\mathbf{P}_{\mathrm{II}}^{\epsilon}$, which are given by:

$$\begin{aligned}\mathsf{T}_{\mathrm{f}}{}^{\epsilon}(\mathsf{G}_{\mathrm{f}}^{\epsilon})^{\mathrm{T}} = &- p^{\epsilon}(\mathsf{G}_{\mathrm{f}}^{\epsilon})^{\mathrm{T}} + \epsilon((\nabla_{\bar{\mathbf{Y}}}\mathbf{V}^{\epsilon})(\mathbf{F}_{\mathrm{f}}^{\epsilon})^{-1}(\mathsf{G}_{\mathrm{f}}^{\epsilon})^{\mathrm{T}} + (\mathbf{F}_{\mathrm{f}}^{\epsilon})^{-\mathrm{T}}(\nabla_{\bar{\mathbf{Y}}}\mathbf{V}^{\epsilon})^{\mathrm{T}}(\mathsf{G}_{\mathrm{f}}^{\epsilon})^{\mathrm{T}}) \\ &+ \epsilon^{2}((\nabla_{\bar{\mathbf{X}}}\mathbf{V}^{\epsilon})(\mathbf{F}_{\mathrm{f}}^{\epsilon})^{-1}(\mathsf{G}_{\mathrm{f}}^{\epsilon})^{\mathrm{T}} + (\mathbf{F}_{\mathrm{f}}^{\epsilon})^{-\mathrm{T}}(\nabla_{\bar{\mathbf{X}}}\mathbf{V}^{\epsilon})^{\mathrm{T}}(\mathsf{G}_{\mathrm{f}}^{\epsilon})^{\mathrm{T}}) \qquad \text{in} \qquad \Omega_{\mathrm{f}}^{0},\end{aligned} \tag{4.83}$$

$$\mathbf{P}_{\mathrm{I}}^{\epsilon} = \frac{\partial \psi_{\mathrm{I}}^{\epsilon}}{\partial \mathbf{F}_{\mathrm{I}}^{\epsilon}} \qquad \text{in} \qquad \Omega_{\mathrm{I}}^{0}, \tag{4.84}$$

$$\mathbf{P}_{\mathrm{II}}^{\epsilon} = \frac{\partial \psi_{\mathrm{II}}^{\epsilon}}{\partial \mathbf{F}_{\mathrm{II}}^{\epsilon}} \qquad \text{in} \qquad \Omega_{\mathrm{II}}^{0}, \tag{4.85}$$

and the fluid balance equation and the solid deformation gradients are given by:

$$\begin{aligned}0 = &-(\mathsf{G}_{\mathrm{f}}^{\epsilon})^{\mathrm{T}}(\epsilon\nabla_{\bar{\mathbf{X}}}p^{\epsilon} + \nabla_{\bar{\mathbf{Y}}}p^{\epsilon}) + \epsilon\nabla_{\bar{\mathbf{Y}}} \cdot ((\nabla_{\bar{\mathbf{Y}}}\mathbf{V}^{\epsilon})\mathsf{G}_{\mathrm{f}}^{\epsilon}(\mathbf{F}_{\mathrm{f}}^{\epsilon})^{-\mathrm{T}} \\ &+ (\mathsf{G}_{\mathrm{f}}^{\epsilon})^{\mathrm{T}}(\nabla_{\bar{\mathbf{Y}}}\mathbf{V}^{\epsilon})^{\mathrm{T}}(\mathbf{F}_{\mathrm{f}}^{\epsilon})^{-\mathrm{T}}) + O(\epsilon^{2}) \qquad \text{in} \qquad \Omega_{\mathrm{f}}^{0},\end{aligned} \tag{4.86}$$

$$\epsilon\mathbf{F}_{\mathrm{I}}^{\epsilon} = \epsilon\mathbf{I} + \epsilon\nabla_{\bar{\mathbf{X}}}\mathbf{u}_{\mathrm{I}}^{\epsilon} + \nabla_{\bar{\mathbf{Y}}}\mathbf{u}_{\mathrm{I}}^{\epsilon} \qquad \text{in} \qquad \Omega_{\mathrm{I}}^{0}, \tag{4.87}$$

$$\epsilon\mathbf{F}_{\mathrm{II}}^{\epsilon} = \epsilon\mathbf{I} + \epsilon\nabla_{\bar{\mathbf{X}}}\mathbf{u}_{\mathrm{II}}^{\epsilon} + \nabla_{\bar{\mathbf{Y}}}\mathbf{u}_{\mathrm{II}}^{\epsilon} \qquad \text{in} \qquad \Omega_{\mathrm{II}}^{0}, \tag{4.88}$$

where the power series representation (4.71) is implied in Equations (4.73)–(4.88) through the use of the superscript ϵ. We then proceed with the technique by equating the coefficients of ϵ^l for $l = 0, 1, ...$, and this way, we derive the effective macroscale model in terms of the relevant zeroth-order fields. Following the asymptotic expansion, if any term still retains a dependence on the porescale, then we can apply the integral average formula. The integral average can be defined as:

$$\langle\varphi\rangle_i = \frac{1}{|\Omega^0|}\int_{\Omega_i^0}\varphi(\bar{\mathbf{X}},\bar{\mathbf{Y}},t)\mathrm{d}\bar{\mathbf{Y}} \quad i = \mathrm{f},\mathrm{I},\mathrm{II}, \tag{4.89}$$

and again, φ is a general field. The integral average is performed over one representative cell due to the assumption of $\bar{\mathbf{Y}}$-periodicity, as discussed in Remark 8, so it is therefore a cell average. We have that the volume of the domain is given by $|\Omega^0| = |\Omega_{\mathrm{f}}^0| + |\Omega_{\mathrm{I}}^0| + |\Omega_{\mathrm{II}}^0|$.

We can equate the coefficients of ϵ^0 in (4.73)–(4.82) to obtain:

$$\nabla_{\bar{\mathbf{Y}}}\cdot\mathbf{P}_{\mathrm{I}}^{(0)} = 0 \qquad \text{in} \qquad \Omega_{\mathrm{I}}^0, \tag{4.90}$$

$$\nabla_{\bar{\mathbf{Y}}}\cdot\mathbf{P}_{\mathrm{II}}^{(0)} = 0 \qquad \text{in} \qquad \Omega_{\mathrm{II}}^0, \tag{4.91}$$

$$\nabla_{\bar{\mathbf{Y}}}\cdot(\mathsf{T}_{\mathrm{f}}{}^{(0)}(\mathsf{G}_{\mathrm{f}}^{(0)})^{\mathrm{T}}) = 0 \qquad \text{in} \qquad \Omega_{\mathrm{f}}^0, \tag{4.92}$$

$$\nabla_{\bar{\mathbf{Y}}}\cdot(\mathsf{G}_{\mathrm{f}}^{(0)}\mathbf{V}^{(0)}) = 0 \qquad \text{in} \qquad \Omega_{\mathrm{f}}^0, \tag{4.93}$$

$$\frac{\partial\mathbf{u}_{\mathrm{I}}^{(0)}}{\partial t} = \mathbf{V}^{(0)} \qquad \text{on} \qquad \Gamma_{\mathrm{I}}^0, \tag{4.94}$$

$$\frac{\partial\mathbf{u}_{\mathrm{II}}^{(0)}}{\partial t} = \mathbf{V}^{(0)} \qquad \text{on} \qquad \Gamma_{\mathrm{II}}^0, \tag{4.95}$$

$$\mathsf{T}_{\mathrm{f}}{}^{(0)}(\mathsf{G}_{\mathrm{f}}^{(0)})^{\mathrm{T}}\mathbf{n}_{\mathrm{I}}^0 = \mathbf{P}_{\mathrm{I}}^{(0)}\mathbf{n}_{\mathrm{I}}^0 \qquad \text{on} \qquad \Gamma_{\mathrm{I}}^0, \tag{4.96}$$

$$\mathsf{T}_{\mathrm{f}}{}^{(0)}(\mathsf{G}_{\mathrm{f}}^{(0)})^{\mathrm{T}}\mathbf{n}_{\mathrm{II}}^0 = \mathbf{P}_{\mathrm{II}}^{(0)}\mathbf{n}_{\mathrm{II}}^0 \qquad \text{on} \qquad \Gamma_{\mathrm{II}}^0, \tag{4.97}$$

$$\mathbf{P}_{\mathrm{I}}^{(0)}\mathbf{n}_{\mathrm{III}}^0 = \mathbf{P}_{\mathrm{II}}^{(0)}\mathbf{n}_{\mathrm{III}}^0 \qquad \text{on} \qquad \Gamma_{\mathrm{III}}^0, \tag{4.98}$$

$$\mathbf{u}_{\mathrm{I}}^{(0)} = \mathbf{u}_{\mathrm{II}}^{(0)} \qquad \text{on} \qquad \Gamma_{\mathrm{III}}^0. \tag{4.99}$$

The constitutive Equations (4.83)–(4.85) have coefficients of ϵ^0 given by:

$$\mathsf{T}_{\mathrm{f}}{}^{(0)}(\mathsf{G}_{\mathrm{f}}^{(0)})^{\mathrm{T}} = -p^{(0)}(\mathsf{G}_{\mathrm{f}}^{(0)})^{\mathrm{T}} \qquad \text{in} \qquad \Omega_{\mathrm{f}}^0, \tag{4.100}$$

$$\mathbf{P}_{\mathrm{I}}^{(0)} = \frac{\partial\psi_{\mathrm{I}}^{(0)}}{\partial\mathbf{F}_{\mathrm{I}}^{(0)}} \qquad \text{in} \qquad \Omega_{\mathrm{I}}^0, \tag{4.101}$$

$$\mathbf{P}_{\mathrm{II}}^{(0)} = \frac{\partial\psi_{\mathrm{II}}^{(0)}}{\partial\mathbf{F}_{\mathrm{II}}^{(0)}} \qquad \text{in} \qquad \Omega_{\mathrm{II}}^0, \tag{4.102}$$

and the fluid balance equation and the deformation gradients (4.86)–(4.88) have coefficients of ϵ^0:

$$(\mathsf{G}_{\mathrm{f}}^{(0)})^{\mathrm{T}}\nabla_{\bar{\mathbf{Y}}}p^{(0)}=0 \qquad \text{in} \qquad \Omega_{\mathrm{f}}^0, \tag{4.103}$$

$$\nabla_{\bar{\mathbf{Y}}}\mathbf{u}_{\mathrm{I}}^{(0)}=0 \qquad \text{in} \qquad \Omega_{\mathrm{I}}^0, \tag{4.104}$$

$$\nabla_{\bar{\mathbf{Y}}}\mathbf{u}_{\mathrm{II}}^{(0)}=0 \qquad \text{in} \qquad \Omega_{\mathrm{II}}^0. \tag{4.105}$$

Now, equating the coefficients of ϵ^1 in Equations (4.73)–(4.82) gives:

$$\nabla_{\bar{\mathbf{Y}}}\cdot\mathbf{P}_{\mathrm{I}}^{(1)}+\nabla_{\bar{\mathbf{X}}}\cdot\mathbf{P}_{\mathrm{I}}^{(0)}=0 \quad \text{in} \qquad \Omega_{\mathrm{I}}^0, \tag{4.106}$$

$$\nabla_{\bar{\mathbf{Y}}}\cdot\mathbf{P}_{\mathrm{II}}^{(1)}+\nabla_{\bar{\mathbf{X}}}\cdot\mathbf{P}_{\mathrm{II}}^{(0)}=0 \quad \text{in} \qquad \Omega_{\mathrm{II}}^0, \tag{4.107}$$

$$\nabla_{\bar{\mathbf{Y}}}\cdot(\mathsf{T}_{\mathrm{f}}{}^{(1)}(\mathsf{G}_{\mathrm{f}}^{(0)})^{\mathrm{T}})+\nabla_{\bar{\mathbf{Y}}}\cdot(\mathsf{T}_{\mathrm{f}}{}^{(0)}(\mathsf{G}_{\mathrm{f}}^{(1)})^{\mathrm{T}})+\nabla_{\bar{\mathbf{X}}}\cdot(\mathsf{T}_{\mathrm{f}}{}^{(0)}(\mathsf{G}_{\mathrm{f}}^{(0)})^{\mathrm{T}})=0 \quad \text{in} \qquad \Omega_{\mathrm{f}}^0, \tag{4.108}$$

$$\nabla_{\bar{\mathbf{Y}}}\cdot(\mathsf{G}_{\mathrm{f}}^{(0)}\mathbf{V}^{(1)})+\nabla_{\bar{\mathbf{Y}}}\cdot(\mathsf{G}_{\mathrm{f}}^{(1)}\mathbf{v}^{(0)})+\nabla_{\bar{\mathbf{X}}}\cdot(\mathsf{G}_{\mathrm{f}}^{(0)}\mathbf{V}^{(0)})=0 \quad \text{in} \qquad \Omega_{\mathrm{f}}^0, \tag{4.109}$$

$$\frac{\partial\mathbf{u}_{\mathrm{I}}^{(1)}}{\partial t}=\mathbf{V}^{(1)} \quad \text{on} \qquad \Gamma_{\mathrm{I}}^0, \tag{4.110}$$

$$\frac{\partial\mathbf{u}_{\mathrm{II}}^{(1)}}{\partial t}=\mathbf{V}^{(1)} \quad \text{on} \qquad \Gamma_{\mathrm{II}}^0, \tag{4.111}$$

$$(\mathsf{T}_{\mathrm{f}}{}^{(1)}(\mathsf{G}_{\mathrm{f}}^{(0)})^{\mathrm{T}}+\mathsf{T}_{\mathrm{f}}{}^{(0)}(\mathsf{G}_{\mathrm{f}}^{(1)})^{\mathrm{T}})\mathbf{n}_{\mathrm{I}}^0=\mathbf{P}_{\mathrm{I}}^{(1)}\mathbf{n}_{\mathrm{I}}^0 \quad \text{on} \qquad \Gamma_{\mathrm{I}}^0, \tag{4.112}$$

$$(\mathsf{T}_{\mathrm{f}}{}^{(1)}(\mathsf{G}_{\mathrm{f}}^{(0)})^{\mathrm{T}}+\mathsf{T}_{\mathrm{f}}{}^{(0)}(\mathsf{G}_{\mathrm{f}}^{(1)})^{\mathrm{T}})\mathbf{n}_{\mathrm{II}}^0=\mathbf{P}_{\mathrm{II}}^{(1)}\mathbf{n}_{\mathrm{II}}^0 \quad \text{on} \qquad \Gamma_{\mathrm{II}}^0, \tag{4.113}$$

$$\mathbf{P}_{\mathrm{I}}^{(1)}\mathbf{n}_{\mathrm{III}}^0=\mathbf{P}_{\mathrm{II}}^{(1)}\mathbf{n}_{\mathrm{III}}^0 \quad \text{on} \qquad \Gamma_{\mathrm{III}}^0, \tag{4.114}$$

$$\mathbf{u}_{\mathrm{I}}^{(1)}=\mathbf{u}_{\mathrm{II}}^{(1)} \quad \text{on} \qquad \Gamma_{\mathrm{III}}^0, \tag{4.115}$$

and the coefficients of ϵ^1 in the constitutive Equations (4.83)–(4.85) are:

$$\begin{aligned}\mathsf{T}_{\mathrm{f}}{}^{(1)}(\mathsf{G}_{\mathrm{f}}^{(0)})^{\mathrm{T}}+\mathsf{T}_{\mathrm{f}}{}^{(0)}(\mathsf{G}_{\mathrm{f}}^{(1)})^{\mathrm{T}}&=-p^{(1)}(\mathsf{G}_{\mathrm{f}}^{(0)})^{\mathrm{T}}-p^{(0)}(\mathsf{G}_{\mathrm{f}}^{(1)})^{\mathrm{T}}\\ +((\nabla_{\bar{\mathbf{Y}}}\mathbf{V}^{(0)})(\mathbf{F}_{\mathrm{f}}^{(0)})^{-1}(\mathsf{G}_{\mathrm{f}}^{(0)})^{\mathrm{T}}&+(\mathbf{F}_{\mathrm{f}}^{(0)})^{-\mathrm{T}}(\nabla_{\bar{\mathbf{Y}}}\mathbf{V}^{(0)})^{\mathrm{T}}(\mathsf{G}_{\mathrm{f}}^{(0)})^{\mathrm{T}}) \qquad \text{in} \qquad \Omega_{\mathrm{f}}^0,\end{aligned} \tag{4.116}$$

$$\mathbf{P}_{\mathrm{I}}^{(1)}=\frac{\partial\psi_{\mathrm{I}}^{(1)}}{\partial\mathbf{F}_{\mathrm{I}}^{(1)}} \qquad \text{in} \qquad \Omega_{\mathrm{I}}^0, \tag{4.117}$$

$$\mathbf{P}_{\mathrm{II}}^{(1)}=\frac{\partial\psi_{\mathrm{II}}^{(1)}}{\partial\mathbf{F}_{\mathrm{II}}^{(1)}} \qquad \text{in} \qquad \Omega_{\mathrm{II}}^0, \tag{4.118}$$

while the fluid balance equation and the deformation gradients (4.86)–(4.88) have coefficients of ϵ^1:

$$0=-(\mathsf{G}_{\mathrm{f}}^{(0)})^{\mathrm{T}}(\nabla_{\bar{\mathbf{X}}}p^{(0)}+\nabla_{\bar{\mathbf{Y}}}p^{(1)})+\nabla_{\bar{\mathbf{Y}}}\cdot((\nabla_{\bar{\mathbf{Y}}}\mathbf{V}^{(0)})\mathsf{G}_{\mathrm{f}}^{(0)}(\mathbf{F}_{\mathrm{f}}^{(0)})^{-\mathrm{T}}$$

$$+(\mathsf{G}_{\mathrm{f}}^{(0)})^{\mathrm{T}}(\nabla_{\bar{\mathbf{Y}}}\mathbf{V}^{(0)})^{\mathrm{T}}(\mathbf{F}_{\mathrm{f}}^{(0)})^{-\mathrm{T}}) \quad \text{in} \qquad \Omega_{\mathrm{f}}^{0}, \tag{4.119}$$

$$\mathbf{F}_{\mathrm{I}}^{(0)} = \mathbf{I} + \nabla_{\bar{\mathbf{X}}}\mathbf{u}_{\mathrm{I}}^{(0)} + \nabla_{\bar{\mathbf{Y}}}\mathbf{u}_{\mathrm{I}}^{(1)} \quad \text{in} \qquad \Omega_{\mathrm{I}}^{0}, \tag{4.120}$$

$$\mathbf{F}_{\mathrm{II}}^{(0)} = \mathbf{I} + \nabla_{\bar{\mathbf{X}}}\mathbf{u}_{\mathrm{II}}^{(0)} + \nabla_{\bar{\mathbf{Y}}}\mathbf{u}_{\mathrm{II}}^{(1)} \quad \text{in} \qquad \Omega_{\mathrm{II}}^{0}. \tag{4.121}$$

We can show that the Piola transformation $(\mathsf{G}^{\epsilon})^{\mathrm{T}}$, where we exploit the notation (4.16), is divergence free and derive some useful identities. We have:

$$\begin{aligned}\int_{\mathscr{B}_0} \nabla_{\mathbf{X}} \cdot \mathsf{G}^{\mathrm{T}} \mathrm{dV}_{\mathbf{X}} &= \int_{\partial\mathscr{B}_0} \mathsf{G}^{\mathrm{T}} \cdot \mathbf{N} \mathrm{dA} = \int_{\partial\mathscr{B}_0} \mathrm{JF}^{-\mathrm{T}}\mathbf{N} \mathrm{dA} = \int_{\partial\mathscr{B}_t} \mathbf{I} \cdot \mathbf{n} \mathrm{da} \\ &= \int_{\mathscr{B}_t} \nabla_{\mathbf{x}} \cdot \mathbf{I} \mathrm{dV}_{\mathbf{x}} = 0,\end{aligned} \tag{4.122}$$

where we have used Nanson's formula (4.21) and $\mathbf{N}$ is normal to the boundary of the reference body and $\mathbf{n}$ is normal to the boundary of the current body and so, $(\mathsf{G}^{\epsilon})^{\mathrm{T}}$ is divergence free. We can also consider the expansion of $(\mathsf{G}^{\epsilon})^{\mathrm{T}}$, which is:

$$(\mathsf{G}^{\epsilon})^{\mathrm{T}} = (\mathsf{G}^{(0)})^{\mathrm{T}} + \epsilon(\mathsf{G}^{(1)})^{\mathrm{T}} + o(\epsilon^2), \tag{4.123}$$

and the expansion of $\nabla_{\mathbf{X}} \cdot (\mathsf{G}^{\epsilon})^{\mathrm{T}}$ is:

$$(\epsilon\nabla_{\bar{\mathbf{X}}} + \nabla_{\bar{\mathbf{Y}}}) \cdot ((\mathsf{G}^{(0)})^{\mathrm{T}} + \epsilon(\mathsf{G}^{(1)})^{\mathrm{T}} + o(\epsilon^2)) = 0. \tag{4.124}$$

Then, equating the coefficient of ϵ^0 gives:

$$\nabla_{\bar{\mathbf{Y}}} \cdot (\mathsf{G}^{(0)})^{\mathrm{T}} = 0, \tag{4.125}$$

and equating the coefficient of ϵ^1 gives:

$$\nabla_{\bar{\mathbf{X}}} \cdot (\mathsf{G}^{(0)})^{\mathrm{T}} + \nabla_{\bar{\mathbf{Y}}} \cdot (\mathsf{G}^{(1)})^{\mathrm{T}} = 0 \implies \nabla_{\bar{\mathbf{X}}} \cdot (\mathsf{G}^{(0)})^{\mathrm{T}} = -\nabla_{\bar{\mathbf{Y}}} \cdot (\mathsf{G}^{(1)})^{\mathrm{T}}. \tag{4.126}$$

We can use the notation (4.16) to write (4.125) and (4.126) as their counterparts in each of the solid domains and the fluid domain as:

$$\nabla_{\bar{\mathbf{Y}}} \cdot (\mathsf{G}_{\mathrm{I}}^{(0)})^{\mathrm{T}} = 0, \quad \nabla_{\bar{\mathbf{Y}}} \cdot (\mathsf{G}_{\mathrm{II}}^{(0)})^{\mathrm{T}} = 0, \quad \nabla_{\bar{\mathbf{Y}}} \cdot (\mathsf{G}_{\mathrm{f}}^{(0)})^{\mathrm{T}} = 0, \tag{4.127}$$

and:

$$\nabla_{\bar{\mathbf{X}}} \cdot (\mathsf{G}_{\mathrm{I}}^{(0)})^{\mathrm{T}} = -\nabla_{\bar{\mathbf{Y}}} \cdot (\mathsf{G}_{\mathrm{I}}^{(1)})^{\mathrm{T}}, \quad \nabla_{\bar{\mathbf{X}}} \cdot (\mathsf{G}_{\mathrm{II}}^{(0)})^{\mathrm{T}} = -\nabla_{\bar{\mathbf{Y}}} \cdot (\mathsf{G}_{\mathrm{II}}^{(1)})^{\mathrm{T}},$$
$$\nabla_{\bar{\mathbf{X}}} \cdot (\mathsf{G}_{\mathrm{f}}^{(0)})^{\mathrm{T}} = -\nabla_{\bar{\mathbf{Y}}} \cdot (\mathsf{G}_{\mathrm{f}}^{(1)})^{\mathrm{T}}. \tag{4.128}$$

Here, we also wish to perform the multiscale expansion of (4.19). We have:

$$(\mathsf{G}_{\mathrm{I}}^{\epsilon})^{\mathrm{T}}\mathbf{n}_{\mathrm{I}}^{0} = (\mathsf{G}_{\mathrm{f}}^{\epsilon})^{\mathrm{T}}\mathbf{n}_{\mathrm{I}}^{0} \quad \text{on} \quad \Gamma_{\mathrm{I}}, \qquad (\mathsf{G}_{\mathrm{II}}^{\epsilon})^{\mathrm{T}}\mathbf{n}_{\mathrm{II}}^{0} = (\mathsf{G}_{\mathrm{f}}^{\epsilon})^{\mathrm{T}}\mathbf{n}_{\mathrm{II}}^{0} \quad \text{on} \quad \Gamma_{\mathrm{II}},$$
$$(\mathsf{G}_{\mathrm{I}}^{\epsilon})^{\mathrm{T}}\mathbf{n}_{\mathrm{III}}^{0} = (\mathsf{G}_{\mathrm{II}}^{\epsilon})^{\mathrm{T}}\mathbf{n}_{\mathrm{III}}^{0} \quad \text{on} \quad \Gamma_{\mathrm{III}}, \tag{4.129}$$

and equating the coefficients of ϵ^0 gives:

$$(\mathsf{G}_{\mathrm{I}}^{(0)})^{\mathrm{T}}\mathbf{n}_{\mathrm{I}}^{0} = (\mathsf{G}_{\mathrm{f}}^{(0)})^{\mathrm{T}}\mathbf{n}_{\mathrm{I}}^{0} \quad \text{on} \quad \Gamma_{\mathrm{I}}, \quad (\mathsf{G}_{\mathrm{II}}^{(0)})^{\mathrm{T}}\mathbf{n}_{\mathrm{II}}^{0} = (\mathsf{G}_{\mathrm{f}}^{(0)})^{\mathrm{T}}\mathbf{n}_{\mathrm{II}}^{0} \quad \text{on} \quad \Gamma_{\mathrm{II}},$$
$$(\mathsf{G}_{\mathrm{I}}^{(0)})^{\mathrm{T}}\mathbf{n}_{\mathrm{III}}^{0} = (\mathsf{G}_{\mathrm{II}}^{(0)})^{\mathrm{T}}\mathbf{n}_{\mathrm{III}}^{0} \quad \text{on} \quad \Gamma_{\mathrm{III}}. \tag{4.130}$$

Similarly, equating the coefficients of ϵ^1 gives:

$$(\mathsf{G}_{\mathrm{I}}^{(1)})^{\mathrm{T}}\mathbf{n}_{\mathrm{I}}^{0} = (\mathsf{G}_{\mathrm{f}}^{(1)})^{\mathrm{T}}\mathbf{n}_{\mathrm{I}}^{0} \quad \text{on} \quad \Gamma_{\mathrm{I}}, \quad (\mathsf{G}_{\mathrm{II}}^{(1)})^{\mathrm{T}}\mathbf{n}_{\mathrm{II}}^{0} = (\mathsf{G}_{\mathrm{f}}^{(1)})^{\mathrm{T}}\mathbf{n}_{\mathrm{II}}^{0} \quad \text{on} \quad \Gamma_{\mathrm{II}},$$
$$(\mathsf{G}_{\mathrm{I}}^{(1)})^{\mathrm{T}}\mathbf{n}_{\mathrm{III}}^{0} = (\mathsf{G}_{\mathrm{II}}^{(1)})^{\mathrm{T}}\mathbf{n}_{\mathrm{III}}^{0} \quad \text{on} \quad \Gamma_{\mathrm{III}}. \tag{4.131}$$

Equating higher powers of epsilon leads to the continuity at higher orders also. We use these expressions in later sections.

We can see using (4.92), (4.100) and (4.125) that $(\mathsf{G}_{\mathrm{f}}^{(0)})^{\mathrm{T}}\nabla_{\bar{\mathbf{Y}}}p^{(0)} = 0$. This implies that $p^{(0)}$ does not depend on the pore-scale $\bar{\mathbf{Y}}$, that is:

$$p^{(0)} = p^{(0)}(\bar{\mathbf{X}}, t) \tag{4.132}$$

We can deduce from (4.104) and (4.105) that $\mathbf{u}_{\mathrm{I}}^{(0)}$ and $\mathbf{u}_{\mathrm{II}}^{(0)}$ do not depend on the pore-scale $\bar{\mathbf{Y}}$, that is,

$$\mathbf{u}_{\mathrm{I}}^{(0)} = \mathbf{u}_{\mathrm{I}}^{(0)}(\bar{\mathbf{X}}, t), \tag{4.133}$$
$$\mathbf{u}_{\mathrm{II}}^{(0)} = \mathbf{u}_{\mathrm{II}}^{(0)}(\bar{\mathbf{X}}, t), \tag{4.134}$$

and since we have the boundary condition (4.99), we can write:

$$\mathbf{u}^{(0)} = \mathbf{u}_{\mathrm{I}}^{(0)} = \mathbf{u}_{\mathrm{II}}^{(0)}. \tag{4.135}$$

We use (4.132) and (4.135) throughout the remainder of this work.

4.2.4 The Macroscale Fluid Flow

We can investigate the leading order velocity, which we denote by $\mathbf{v}^{(0)}$. We begin by defining the relative fluid–solid velocity, $\mathbf{w}$, as:

$$\mathbf{w} := \mathbf{V}^{(0)} - \frac{\partial \mathbf{u}^{(0)}}{\partial t}. \tag{4.136}$$

We can rearrange (4.136) to obtain:

$$\mathbf{V}^{(0)} = \mathbf{w} + \dot{\mathbf{u}}^{(0)} \tag{4.137}$$

We are then able to use (4.137) and Equations (4.93), (4.94), (4.95), (4.100), (4.108) and (4.116) to form a Stokes'-type boundary value problem given by:

$$\begin{aligned} -(\mathsf{G}_{\mathrm{f}}^{(0)})^{\mathrm{T}}(\nabla_{\bar{\mathbf{X}}} p^{(0)} + \nabla_{\bar{\mathbf{Y}}} p^{(1)}) + \nabla_{\bar{\mathbf{Y}}} \cdot \big(& (\nabla_{\bar{\mathbf{Y}}} \mathbf{w}) \mathsf{G}_{\mathrm{f}}^{(0)} (\mathbf{F}_{\mathrm{f}}^{(0)})^{-\mathrm{T}} \\ & + (\mathsf{G}_{\mathrm{f}}^{(0)})^{\mathrm{T}} (\nabla_{\bar{\mathbf{Y}}} \mathbf{w})^{\mathrm{T}} (\mathbf{F}_{\mathrm{f}}^{(0)})^{-\mathrm{T}} \big) = \mathbf{0} \qquad \text{in} \qquad \Omega_{\mathrm{f}}^{0}, \end{aligned} \tag{4.138}$$

$$\nabla_{\bar{\mathbf{Y}}} \cdot (\mathsf{G}_{\mathrm{f}}^{(0)} \mathbf{w}) = \mathbf{0} \qquad \text{in} \qquad \Omega_{\mathrm{f}}^{0}, \tag{4.139}$$

$$\mathbf{w} = \mathbf{0} \qquad \text{on} \qquad \Gamma_{\mathrm{I}}^{0} \cup \Gamma_{\mathrm{II}}^{0}. \tag{4.140}$$

The boundary value problem (4.138)–(4.140) admits a solution. Exploiting linearity, the solution is given by:

$$\mathbf{w} = -\hat{W} \nabla_{\bar{\mathbf{X}}} p^{(0)}, \tag{4.141}$$

$$p^{(1)} = -\hat{\mathbf{\Pi}} \nabla_{\bar{\mathbf{X}}} p^{(0)} + c(\bar{X}), \tag{4.142}$$

where $p^{(1)}$ is defined up to an arbitrary $\bar{\mathbf{Y}}$-constant function given by $c(\bar{X})$. The second rank tensor $\hat{W}$ and the vector $\hat{\mathbf{\Pi}}$ are the solution to the cell problem given by:

$$\begin{aligned} \nabla_{\bar{\mathbf{Y}}} \cdot \big(& (\nabla_{\bar{\mathbf{Y}}} \hat{W}) \mathsf{G}_{\mathrm{f}}^{(0)} (\mathbf{F}_{\mathrm{f}}^{(0)})^{-\mathrm{T}} + (\mathsf{G}_{\mathrm{f}}^{(0)})^{\mathrm{T}} (\nabla_{\bar{\mathbf{Y}}} \hat{W})^{\mathrm{T}} (\mathbf{F}_{\mathrm{f}}^{(0)})^{-\mathrm{T}} \big) \\ & + (\mathsf{G}_{\mathrm{f}}^{(0)})^{\mathrm{T}} (\mathbf{I} - \nabla_{\bar{\mathbf{Y}}} \hat{\mathbf{\Pi}}) = \mathbf{0} \qquad \text{in} \qquad \Omega_{\mathrm{f}}^{0}, \end{aligned} \tag{4.143}$$

$$\nabla_{\bar{\mathbf{Y}}} \cdot (\mathsf{G}_{\mathrm{f}}^{(0)} \hat{W}) = \mathbf{0} \qquad \text{in} \qquad \Omega_{\mathrm{f}}^{0}, \tag{4.144}$$

$$\hat{W} = \mathbf{0} \qquad \text{on} \qquad \Gamma_{\mathrm{I}}^{0} \cup \Gamma_{\mathrm{II}}^{0}, \tag{4.145}$$

This cell problem is to be supplemented by periodic conditions on the boundary $\partial\Omega_{\mathrm{f}}^{0} \backslash (\Gamma_{\mathrm{I}}^{0} \cup \Gamma_{\mathrm{II}}^{0})$, and for the uniqueness of the solution, a further condition on the aux-

iliary variable $\hat{\mathbf{\Pi}}\mathbf{I}$ is required, i.e., $\langle\hat{\mathbf{\Pi}}\mathbf{I}\rangle_{\mathrm{f}} = 0$. Since the quantity $\hat{W}$ retains a dependence on the porescale, we take the integral average of (4.141) over the fluid domain, which leads to:

$$\langle\mathbf{w}\rangle_{\mathrm{f}} = -\langle\hat{W}\rangle_{\mathrm{f}}\nabla_{\bar{\mathbf{x}}}p^{(0)} \tag{4.146}$$

Therefore, the macroscale fluid flow is described by Darcy's law.

We also consider the incompressibility constraint (4.109), and we integrate over the fluid domain to obtain:

$$\int_{\Omega_{\mathrm{f}}^0}\nabla_{\bar{\mathbf{x}}}\cdot(\mathsf{G}_{\mathrm{f}}^{(0)}\mathbf{V}^{(0)})\mathrm{d}\bar{\mathbf{Y}} + \int_{\Omega_{\mathrm{f}}^0}\nabla_{\bar{\mathbf{Y}}}\cdot(\mathsf{G}_{\mathrm{f}}^{(1)}\mathbf{V}^{(0)} + \mathsf{G}_{\mathrm{f}}^{(0)}\mathbf{V}^{(1)})\mathrm{d}\bar{\mathbf{Y}} = 0. \tag{4.147}$$

Applying the divergence theorem to the second integral and using (4.94), (4.95), (4.110) and (4.111) give:

$$\begin{aligned}&\int_{\Omega_{\mathrm{f}}^0}\nabla_{\bar{\mathbf{x}}}\cdot(\mathsf{G}_{\mathrm{f}}^{(0)}\mathbf{V}^{(0)})\mathrm{d}\bar{\mathbf{Y}} + \int_{\Gamma_{\mathrm{I}}^0}(\mathsf{G}_{\mathrm{f}}^{(1)}\dot{\mathbf{u}}^{(0)} + \mathsf{G}_{\mathrm{f}}^{(0)}\dot{\mathbf{u}}_{\mathrm{I}}^{(1)})\mathbf{n}_{\mathrm{I}}^0\mathrm{dS}\\ &+ \int_{\Gamma_{\mathrm{II}}^0}(\mathsf{G}_{\mathrm{f}}^{(1)}\dot{\mathbf{u}}^{(0)} + \mathsf{G}_{\mathrm{f}}^{(0)}\dot{\mathbf{u}}_{\mathrm{II}}^{(1)})\mathbf{n}_{\mathrm{II}}^0\mathrm{dS} = 0.\end{aligned} \tag{4.148}$$

We are able to rewrite this as:

$$\begin{aligned}&\int_{\Omega_{\mathrm{f}}^0}\nabla_{\bar{\mathbf{x}}}\cdot(\mathsf{G}_{\mathrm{f}}^{(0)}\mathbf{V}^{(0)})\mathrm{d}\bar{\mathbf{Y}} + \int_{\Gamma_{\mathrm{I}}^0}(\dot{\mathbf{u}}^{(0)}(\mathsf{G}_{\mathrm{f}}^{(1)})^{\mathrm{T}} + \dot{\mathbf{u}}_{\mathrm{I}}^{(1)}(\mathsf{G}_{\mathrm{f}}^{(0)})^{\mathrm{T}})\mathbf{n}_{\mathrm{I}}^0\mathrm{dS} + \int_{\Gamma_{\mathrm{II}}^0}(\dot{\mathbf{u}}^{(0)}(\mathsf{G}_{\mathrm{f}}^{(1)})^{\mathrm{T}}\\ &+ \dot{\mathbf{u}}_{\mathrm{II}}^{(1)}(\mathsf{G}_{\mathrm{f}}^{(0)})^{\mathrm{T}})\mathbf{n}_{\mathrm{II}}^0\mathrm{dS} = 0,\end{aligned} \tag{4.149}$$

and accounting for the continuity of the transpose of the Piola transformations applied to the normal (4.130) and (4.131) gives:

$$\begin{aligned}&\int_{\Omega_{\mathrm{f}}^0}\nabla_{\bar{\mathbf{x}}}\cdot(\mathsf{G}_{\mathrm{f}}^{(0)}\mathbf{V}^{(0)})\mathrm{d}\bar{\mathbf{Y}} + \int_{\Gamma_{\mathrm{I}}^0}(\dot{\mathbf{u}}^{(0)}(\mathsf{G}_{\mathrm{I}}^{(1)})^{\mathrm{T}} + \dot{\mathbf{u}}_{\mathrm{I}}^{(1)}(\mathsf{G}_{\mathrm{I}}^{(0)})^{\mathrm{T}})\mathbf{n}_{\mathrm{I}}^0\mathrm{dS}\\ &+ \int_{\Gamma_{\mathrm{II}}^0}(\dot{\mathbf{u}}^{(0)}(\mathsf{G}_{\mathrm{II}}^{(1)})^{\mathrm{T}} + \dot{\mathbf{u}}_{\mathrm{II}}^{(1)}(\mathsf{G}_{\mathrm{II}}^{(0)})^{\mathrm{T}})\mathbf{n}_{\mathrm{II}}^0\mathrm{dS} = 0.\end{aligned} \tag{4.150}$$

This can be rewritten as:

$$\begin{aligned}&\int_{\Omega_{\mathrm{f}}^0}\nabla_{\bar{\mathbf{x}}}\cdot(\mathsf{G}_{\mathrm{f}}^{(0)}\mathbf{V}^{(0)})\mathrm{d}\bar{\mathbf{Y}} + \int_{\Gamma_{\mathrm{I}}^0}(\mathsf{G}_{\mathrm{I}}^{(1)}\dot{\mathbf{u}}^{(0)} + \mathsf{G}_{\mathrm{I}}^{(0)}\dot{\mathbf{u}}_{\mathrm{I}}^{(1)})\mathbf{n}_{\mathrm{I}}^0\mathrm{dS}\\ &+ \int_{\Gamma_{\mathrm{II}}^0}(\mathsf{G}_{\mathrm{II}}^{(1)}\dot{\mathbf{u}}^{(0)} + \mathsf{G}_{\mathrm{II}}^{(0)}\dot{\mathbf{u}}_{\mathrm{II}}^{(1)})\mathbf{n}_{\mathrm{II}}^0\mathrm{dS} = 0,\end{aligned} \tag{4.151}$$

where we use the notation that $\dot{()} = \partial()/\partial t$. We wish to apply the divergence theorem again; however, to do this, we must include the terms on the interface Γ_{III}, that is:

$$\begin{aligned}
&\int_{\Omega_{\text{f}}^0} \nabla_{\bar{\mathbf{X}}} \cdot (\mathsf{G}_{\text{f}}^{(0)} \mathbf{V}^{(0)}) \mathrm{d}\bar{\mathbf{Y}} + \int_{\Gamma_{\text{I}}^0} (\mathsf{G}_{\text{I}}^{(1)} \dot{\mathbf{u}}^{(0)} + \mathsf{G}_{\text{I}}^{(0)} \dot{\mathbf{u}}_{\text{I}}^{(1)}) \mathbf{n}_{\text{I}}^0 \mathrm{dS} \\
&+ \int_{\Gamma_{\text{II}}^0} (\mathsf{G}_{\text{II}}^{(1)} \dot{\mathbf{u}}^{(0)} + \mathsf{G}_{\text{II}}^{(0)} \dot{\mathbf{u}}_{\text{II}}^{(1)}) \mathbf{n}_{\text{II}}^0 \mathrm{dS} + \int_{\Gamma_{\text{III}}^0} (\dot{\mathbf{u}}^{(0)} (\mathsf{G}_{\text{I}}^{(1)})^{\text{T}} + \dot{\mathbf{u}}_{\text{I}}^{(1)} (\mathsf{G}_{\text{I}}^{(0)})^{\text{T}}) \mathbf{n}_{\text{III}}^0 \mathrm{dS} \\
&- \int_{\Gamma_{\text{III}}^0} (\dot{\mathbf{u}}^{(0)} (\mathsf{G}_{\text{II}}^{(1)})^{\text{T}} + \dot{\mathbf{u}}_{\text{II}}^{(1)} (\mathsf{G}_{\text{II}}^{(0)})^{\text{T}}) \mathbf{n}_{\text{III}}^0 \mathrm{dS} = 0,
\end{aligned} \tag{4.152}$$

where we can add these terms on Γ_{III} because they are effectively zero because of the continuity of the transpose of the Piola transform (4.130) and (4.131). Applying the divergence theorem again gives:

$$\begin{aligned}
&\nabla_{\bar{\mathbf{X}}} \cdot \langle \mathsf{G}_{\text{f}}^{(0)} \mathbf{V}^{(0)} \rangle_{\text{f}} - \int_{\Omega_{\text{I}}^0} \nabla_{\bar{\mathbf{Y}}} \cdot (\mathsf{G}_{\text{I}}^{(1)} \dot{\mathbf{u}}^{(0)} + \mathsf{G}_{\text{I}}^{(0)} \dot{\mathbf{u}}_{\text{I}}^{(1)}) \mathrm{d}\bar{\mathbf{Y}} \\
&- \int_{\Omega_{\text{II}}^0} \nabla_{\bar{\mathbf{Y}}} \cdot (\mathsf{G}_{\text{II}}^{(1)} \dot{\mathbf{u}}^{(0)} + \mathsf{G}_{\text{II}}^{(0)} \dot{\mathbf{u}}_{\text{II}}^{(1)}) \mathrm{d}\bar{\mathbf{Y}} = 0.
\end{aligned} \tag{4.153}$$

Therefore, we can write this as:

$$\nabla_{\bar{\mathbf{X}}} \cdot \langle \mathsf{G}_{\text{f}}^{(0)} \mathbf{V}^{(0)} \rangle_{\text{f}} = \langle \nabla_{\bar{\mathbf{Y}}} \cdot (\mathsf{G}_{\text{I}}^{(1)} \dot{\mathbf{u}}^{(0)} + \mathsf{G}_{\text{I}}^{(0)} \dot{\mathbf{u}}_{\text{I}}^{(1)}) \rangle_{\text{I}} + \langle \nabla_{\bar{\mathbf{Y}}} \cdot (\mathsf{G}_{\text{II}}^{(1)} \dot{\mathbf{u}}^{(0)} + \mathsf{G}_{\text{II}}^{(0)} \dot{\mathbf{u}}_{\text{II}}^{(1)}) \rangle_{\text{II}}. \tag{4.154}$$

Since we have that $\mathbf{w} = \mathbf{V}^{(0)} - \dot{\mathbf{u}}^{(0)}$ from (4.136), then this can be rearranged, and multiplying by $\mathsf{G}_{\text{f}}^{(0)}$ gives $\mathsf{G}_{\text{f}}^{(0)} \mathbf{V}^{(0)} = \mathsf{G}_{\text{f}}^{(0)} \mathbf{w} + \mathsf{G}_{\text{f}}^{(0)} \dot{\mathbf{u}}^{(0)}$. We then take the integral average over the fluid domain, which gives $\langle \mathsf{G}_{\text{f}}^{(0)} \mathbf{V}^{(0)} \rangle_{\text{f}} = \langle \mathsf{G}_{\text{f}}^{(0)} \mathbf{w} \rangle_{\text{f}} + \langle \mathsf{G}_{\text{f}}^{(0)} \rangle_{\text{f}} \dot{\mathbf{u}}^{(0)}$, and this can be used to replace the LHS of (4.154). Therefore, we have:

$$\begin{aligned}
\nabla_{\bar{\mathbf{X}}} \cdot \left(\langle \mathsf{G}_{\text{f}}^{(0)} \mathbf{w} \rangle_{\text{f}} + \langle \mathsf{G}_{\text{f}}^{(0)} \rangle_{\text{f}} \dot{\mathbf{u}}^{(0)} \right) &= \langle \nabla_{\bar{\mathbf{Y}}} \cdot (\mathsf{G}_{\text{I}}^{(1)} \dot{\mathbf{u}}^{(0)} + \mathsf{G}_{\text{I}}^{(0)} \dot{\mathbf{u}}_{\text{I}}^{(1)}) \rangle_{\text{I}} \\
&+ \langle \nabla_{\bar{\mathbf{Y}}} \cdot (\mathsf{G}_{\text{II}}^{(1)} \dot{\mathbf{u}}^{(0)} + \mathsf{G}_{\text{II}}^{(0)} \dot{\mathbf{u}}_{\text{II}}^{(1)}) \rangle_{\text{II}}.
\end{aligned} \tag{4.155}$$

Then, we wish to expand the two terms on the RHS of (4.155), which gives:

$$\begin{aligned}
&\nabla_{\bar{\mathbf{Y}}} \cdot (\mathsf{G}_{\text{I}}^{(1)} \dot{\mathbf{u}}^{(0)} + \mathsf{G}_{\text{I}}^{(0)} \dot{\mathbf{u}}_{\text{I}}^{(1)}) + \nabla_{\bar{\mathbf{Y}}} \cdot (\mathsf{G}_{\text{II}}^{(1)} \dot{\mathbf{u}}^{(0)} + \mathsf{G}_{\text{II}}^{(0)} \dot{\mathbf{u}}_{\text{II}}^{(1)}) \\
&= \mathrm{Tr} \nabla_{\bar{\mathbf{Y}}} (\mathsf{G}_{\text{I}}^{(1)} \dot{\mathbf{u}}^{(0)} + \mathsf{G}_{\text{I}}^{(0)} \dot{\mathbf{u}}_{\text{I}}^{(1)}) + \mathrm{Tr} \nabla_{\bar{\mathbf{Y}}} (\mathsf{G}_{\text{II}}^{(1)} \dot{\mathbf{u}}^{(0)} + \mathsf{G}_{\text{II}}^{(0)} \dot{\mathbf{u}}_{\text{II}}^{(1)}) \\
&= (\nabla_{\bar{\mathbf{Y}}} \cdot (\mathsf{G}_{\text{I}}^{(1)})^{\text{T}}) \cdot \dot{\mathbf{u}}^{(0)} + (\nabla_{\bar{\mathbf{Y}}} \cdot (\mathsf{G}_{\text{II}}^{(1)})^{\text{T}}) \cdot \dot{\mathbf{u}}^{(0)} + \mathsf{G}_{\text{I}}^{(0)} : \nabla_{\bar{\mathbf{Y}}} \dot{\mathbf{u}}_{\text{I}}^{(1)} \\
&+ \mathsf{G}_{\text{II}}^{(0)} : \nabla_{\bar{\mathbf{Y}}} \dot{\mathbf{u}}_{\text{II}}^{(1)} + (\nabla_{\bar{\mathbf{Y}}} \cdot (\mathsf{G}_{\text{I}}^{(0)})^{\text{T}}) \cdot \dot{\mathbf{u}}_{\text{I}}^{(1)} + (\nabla_{\bar{\mathbf{Y}}} \cdot (\mathsf{G}_{\text{II}}^{(0)})^{\text{T}}) \cdot \dot{\mathbf{u}}_{\text{II}}^{(1)}
\end{aligned}$$

$$+ \mathsf{G}_{\mathrm{I}}^{(1)} : \nabla_{\bar{\mathbf{Y}}} \dot{\mathbf{u}}^{(0)} + \mathsf{G}_{\mathrm{II}}^{(0)} : \nabla_{\bar{\mathbf{Y}}} \dot{\mathbf{u}}^{(0)}. \tag{4.156}$$

We can cancel the terms in (4.156) due to $\mathbf{u}^{(0)} = \mathbf{u}^{(0)}(\bar{X}, t)$ and using (4.127) and then rewrite (4.155) using (4.156) as:

$$\begin{aligned}\nabla_{\bar{\mathbf{X}}} \cdot \left(\langle \mathsf{G}_{\mathrm{f}}^{(0)} \mathbf{w} \rangle_{\mathrm{f}} + \langle \mathsf{G}_{\mathrm{f}}^{(0)} \rangle_{\mathrm{f}} \dot{\mathbf{u}}^{(0)} \right) &= -\big(\langle \nabla_{\bar{\mathbf{X}}} \cdot (\mathsf{G}_{\mathrm{I}}^{(0)})^{\mathrm{T}} \rangle_{\mathrm{I}} + \langle \nabla_{\bar{\mathbf{X}}} \cdot (\mathsf{G}_{\mathrm{II}}^{(0)})^{\mathrm{T}} \rangle_{\mathrm{II}} \big) \cdot \dot{\mathbf{u}}^{(0)} \\ &\quad + \langle \mathsf{G}_{\mathrm{I}}^{(0)} : \nabla_{\bar{\mathbf{Y}}} \dot{\mathbf{u}}_{\mathrm{I}}^{(1)} \rangle_{\mathrm{I}} + \langle \mathsf{G}_{\mathrm{II}}^{(0)} : \nabla_{\bar{\mathbf{Y}}} \dot{\mathbf{u}}_{\mathrm{II}}^{(1)} \rangle_{\mathrm{II}},\end{aligned} \tag{4.157}$$

where we also use (4.128) to replace the first two terms in (4.156). We return to this expression in Section 4.3.

4.2.5 The Macroscale Poroelastic Relationships

We require the macroscale constitutive relationship. To begin, we sum up the integral averages of Equations (4.106), (4.107) and (4.108), that is,

$$\begin{aligned}&\int_{\Omega_{\mathrm{I}}^0} \nabla_{\bar{\mathbf{Y}}} \cdot \mathbf{P}_{\mathrm{I}}^{(1)} \mathrm{d}\bar{\mathbf{Y}} + \int_{\Omega_{\mathrm{II}}^0} \nabla_{\bar{\mathbf{Y}}} \cdot \mathbf{P}_{\mathrm{II}}^{(1)} \mathrm{d}\bar{\mathbf{Y}} + \int_{\Omega_{\mathrm{f}}^0} \nabla_{\bar{\mathbf{Y}}} \cdot (\mathsf{T}_{\mathrm{f}}{}^{(1)} (\mathsf{G}_{\mathrm{f}}^{(0)})^{\mathrm{T}}) \mathrm{d}\bar{\mathbf{Y}} \\ &+ \int_{\Omega_{\mathrm{f}}^0} \nabla_{\bar{\mathbf{Y}}} \cdot (\mathsf{T}_{\mathrm{f}}{}^{(0)} (\mathsf{G}_{\mathrm{f}}^{(1)})^{\mathrm{T}}) \mathrm{d}\bar{\mathbf{Y}} + \int_{\Omega_{\mathrm{I}}^0} \nabla_{\bar{\mathbf{X}}} \cdot \mathbf{P}_{\mathrm{I}}^{(0)} \mathrm{d}\bar{\mathbf{Y}} + \int_{\Omega_{\mathrm{II}}^0} \nabla_{\bar{\mathbf{X}}} \cdot \mathbf{P}_{\mathrm{II}}^{(0)} \mathrm{d}\bar{\mathbf{Y}} \\ &+ \int_{\Omega_{\mathrm{f}}^0} \nabla_{\bar{\mathbf{X}}} \cdot (\mathsf{T}_{\mathrm{f}}{}^{(0)} (\mathsf{G}_{\mathrm{f}}^{(0)})^{\mathrm{T}}) \mathrm{d}\bar{\mathbf{Y}} = 0.\end{aligned} \tag{4.158}$$

We apply the divergence theorem to the first four integrals and then rearrange the last three integrals due to the assumption of macroscopic uniformity (4.72) to obtain:

$$\begin{aligned}&\int_{\partial\Omega_{\mathrm{I}}^0 \setminus (\Gamma_{\mathrm{I}}^0 \cup \Gamma_{\mathrm{III}}^0)} \mathbf{P}_{\mathrm{I}}^{(1)} \mathbf{n}_{\Omega_{\mathrm{I}}^0 \setminus (\Gamma_{\mathrm{I}}^0 \cup \Gamma_{\mathrm{III}}^0)}^0 \mathrm{dS} + \int_{\Gamma_{\mathrm{I}}^0} \mathbf{P}_{\mathrm{I}}^{(1)} \mathbf{n}_{\mathrm{I}}^0 \mathrm{dS} - \int_{\Gamma_{\mathrm{III}}^0} \mathbf{P}_{\mathrm{I}}^{(1)} \mathbf{n}_{\mathrm{III}}^0 \mathrm{dS} + \\ &\int_{\partial\Omega_{\mathrm{II}}^0 \setminus (\Gamma_{\mathrm{II}}^0 \cup \Gamma_{\mathrm{III}}^0)} \mathbf{P}_{\mathrm{II}}^{(1)} \mathbf{n}_{\Omega_{\mathrm{II}}^0 \setminus (\Gamma_{\mathrm{II}}^0 \cup \Gamma_{\mathrm{III}}^0)}^0 \mathrm{dS} + \int_{\Gamma_{\mathrm{II}}^0} \mathbf{P}_{\mathrm{II}}^{(1)} \mathbf{n}_{\mathrm{II}}^0 \mathrm{dS} + \int_{\Gamma_{\mathrm{III}}^0} \mathbf{P}_{\mathrm{II}}^{(1)} \mathbf{n}_{\mathrm{III}}^0 \mathrm{dS} + \\ &\int_{\partial\Omega_{\mathrm{f}}^0 \setminus (\Gamma_{\mathrm{I}}^0 \cup \Gamma_{\mathrm{II}}^0)} \mathsf{T}_{\mathrm{f}}^{(1)} (\mathsf{G}_{\mathrm{f}}^{(0)})^{\mathrm{T}} \mathbf{n}_{\Omega_{\mathrm{f}}^0 \setminus (\Gamma_{\mathrm{I}}^0 \cup \Gamma_{\mathrm{II}}^0)}^0 \mathrm{dS} - \int_{\Gamma_{\mathrm{II}}^0} \mathsf{T}_{\mathrm{f}}^{(1)} (\mathsf{G}_{\mathrm{f}}^{(0)})^{\mathrm{T}} \mathbf{n}_{\mathrm{II}}^0 \mathrm{dS} - \int_{\Gamma_{\mathrm{I}}^0} \mathsf{T}_{\mathrm{f}}^{(1)} (\mathsf{G}_{\mathrm{f}}^{(0)})^{\mathrm{T}} \mathbf{n}_{\mathrm{I}}^0 \mathrm{dS} + \\ &\int_{\partial\Omega_{\mathrm{f}}^0 \setminus (\Gamma_{\mathrm{I}}^0 \cup \Gamma_{\mathrm{II}}^0)} \mathsf{T}_{\mathrm{f}}^{(0)} (\mathsf{G}_{\mathrm{f}}^{(1)})^{\mathrm{T}} \mathbf{n}_{\Omega_{\mathrm{f}}^0 \setminus (\Gamma_{\mathrm{I}}^0 \cup \Gamma_{\mathrm{II}}^0)}^0 \mathrm{dS} - \int_{\Gamma_{\mathrm{II}}^0} \mathsf{T}_{\mathrm{f}}^{(0)} (\mathsf{G}_{\mathrm{f}}^{(1)})^{\mathrm{T}} \mathbf{n}_{\mathrm{II}}^0 \mathrm{dS} - \int_{\Gamma_{\mathrm{I}}^0} \mathsf{T}_{\mathrm{f}}^{(0)} (\mathsf{G}_{\mathrm{f}}^{(1)})^{\mathrm{T}} \mathbf{n}_{\mathrm{I}}^0 \mathrm{dS} + \\ &\nabla_{\bar{\mathbf{X}}} \cdot \int_{\Omega_{\mathrm{I}}^0} \mathbf{P}_{\mathrm{I}}^{(0)} \mathrm{d}\bar{\mathbf{Y}} + \nabla_{\bar{\mathbf{X}}} \cdot \int_{\Omega_{\mathrm{II}}^0} \mathbf{P}_{\mathrm{II}}^{(0)} \mathrm{d}\bar{\mathbf{Y}} + \nabla_{\bar{\mathbf{X}}} \cdot \int_{\Omega_{\mathrm{f}}^0} \mathsf{T}_{\mathrm{f}}{}^{(0)} (\mathsf{G}_{\mathrm{f}}^{(0)})^{\mathrm{T}} \mathrm{d}\bar{\mathbf{Y}} = 0,\end{aligned} \tag{4.159}$$

where $\mathbf{n}_{\mathrm{I}}^0$, $\mathbf{n}_{\mathrm{II}}^0$, $\mathbf{n}_{\mathrm{III}}^0$, $\mathbf{n}_{\Omega_{\mathrm{I}}^0 \setminus (\Gamma_{\mathrm{I}}^0 \cup \Gamma_{\mathrm{III}}^0)}^0$, $\mathbf{n}_{\Omega_{\mathrm{II}}^0 \setminus (\Gamma_{\mathrm{II}}^0 \cup \Gamma_{\mathrm{III}}^0)}^0$ and $\mathbf{n}_{\Omega_{\mathrm{f}}^0 \setminus (\Gamma_{\mathrm{I}}^0 \cup \Gamma_{\mathrm{II}}^0)}^0$ are the unit normals corresponding to the interfaces Γ_{I}^0, Γ_{II}^0, Γ_{III}^0, $\partial\Omega_{\mathrm{I}}^0 \setminus (\Gamma_{\mathrm{I}}^0 \cup \Gamma_{\mathrm{III}}^0)$, $\partial\Omega_{\mathrm{II}}^0 \setminus (\Gamma_{\mathrm{II}}^0 \cup \Gamma_{\mathrm{III}}^0)$ and $\partial\Omega_{\mathrm{f}}^0 \setminus$

$(\Gamma^0_{\rm I} \cup \Gamma^0_{\rm II})$. The contributions over the external boundaries of $\Omega^0_{\rm I}$, $\Omega^0_{\rm II}$ and $\Omega^0_{\rm f}$ cancel due to $\bar{\mathbf{Y}}$-periodicity, so (4.159) becomes:

$$\int_{\Gamma^0_{\rm I}} \mathbf{P}^{(1)}_{\rm I}\mathbf{n}^0_{\rm I}{\rm dS} - \int_{\Gamma^0_{\rm I}} \mathsf{T}^{(1)}_{\rm f}(\mathsf{G}^{(0)}_{\rm f})^{\rm T}\mathbf{n}^0_{\rm I}{\rm dS} - \int_{\Gamma^0_{\rm I}} \mathsf{T}^{(0)}_{\rm f}(\mathsf{G}^{(1)}_{\rm f})^{\rm T}\mathbf{n}^0_{\rm I}{\rm dS} + \int_{\Gamma^0_{\rm II}} \mathbf{P}^{(1)}_{\rm II}\mathbf{n}^0_{\rm II}{\rm dS} -$$
$$\int_{\Gamma^0_{\rm II}} \mathsf{T}^{(1)}_{\rm f}(\mathsf{G}^{(0)}_{\rm f})^{\rm T}\mathbf{n}^0_{\rm II}{\rm dS} - \int_{\Gamma^0_{\rm II}} \mathsf{T}^{(0)}_{\rm f}(\mathsf{G}^{(1)}_{\rm f})^{\rm T}\mathbf{n}^0_{\rm II}{\rm dS} - \int_{\Gamma^0_{\rm III}} \mathbf{P}^{(1)}_{\rm I}\mathbf{n}^0_{\rm III}{\rm dS} + \int_{\Gamma^0_{\rm III}} \mathbf{P}^{(1)}_{\rm II}\mathbf{n}^0_{\rm III}{\rm dS} +$$
$$\nabla_{\bar{\mathbf{x}}} \cdot \int_{\Omega^0_{\rm I}} \mathbf{P}^{(0)}_{\rm I}{\rm d}\bar{\mathbf{Y}} + \nabla_{\bar{\mathbf{x}}} \cdot \int_{\Omega^0_{\rm II}} \mathbf{P}^{(0)}_{\rm II}{\rm d}\bar{\mathbf{Y}} + \nabla_{\bar{\mathbf{x}}} \cdot \int_{\Omega^0_{\rm f}} \mathsf{T}_{\rm f}{}^{(0)}(\mathsf{G}^{(0)}_{\rm f})^{\rm T}{\rm d}\bar{\mathbf{Y}} = 0. \tag{4.160}$$

The first eight integrals cancel using the continuity of tractions (4.112), (4.113) and (4.114), so we obtain:

$$\nabla_{\bar{\mathbf{x}}} \cdot \langle \mathbf{P}^{(0)}_{\rm I}\rangle_{\rm I} + \nabla_{\bar{\mathbf{x}}} \cdot \langle \mathbf{P}^{(0)}_{\rm II}\rangle_{\rm II} - \nabla_{\bar{\mathbf{x}}} \cdot \left(p^{(0)}\langle (\mathsf{G}^{(0)}_{\rm f})^{\rm T}\rangle_{\rm f}\right) = 0, \tag{4.161}$$

where we use (4.100). Then, we have that:

$$\nabla_{\bar{\mathbf{x}}} \cdot \bar{\mathsf{T}}_{\rm Eff} = 0, \tag{4.162}$$

where:

$$\bar{\mathsf{T}}_{\rm Eff} = \langle \mathbf{P}^{(0)}_{\rm I}\rangle_{\rm I} + \langle \mathbf{P}^{(0)}_{\rm II}\rangle_{\rm II} - p^{(0)}\langle (\mathsf{G}^{(0)}_{\rm f})^{\rm T}\rangle_{\rm f}. \tag{4.163}$$

We can describe (4.162) and (4.163) as the average stress balance and constitutive law for our nonlinear poroelastic composite material.

We can write the following problem for $\mathbf{u}^{(1)}_{\rm I}$ and $\mathbf{u}^{(1)}_{\rm II}$ using (4.90), (4.91), (4.96), (4.97), (4.98), (4.100) and (4.115):

$$\nabla_{\bar{\mathbf{Y}}} \cdot \mathbf{P}^{(0)}_{\rm I} = 0 \qquad \text{in} \qquad \Omega^0_{\rm I}, \tag{4.164}$$
$$\nabla_{\bar{\mathbf{Y}}} \cdot \mathbf{P}^{(0)}_{\rm II} = 0 \qquad \text{in} \qquad \Omega^0_{\rm II}, \tag{4.165}$$
$$\mathbf{u}^{(1)}_{\rm I} = \mathbf{u}^{(1)}_{\rm II} \qquad \text{on} \qquad \Gamma^0_{\rm III}, \tag{4.166}$$
$$\mathbf{P}^{(0)}_{\rm I}\mathbf{n}^0_{\rm III} = \mathbf{P}^{(0)}_{\rm II}\mathbf{n}^0_{\rm III} \qquad \text{on} \qquad \Gamma^0_{\rm III}, \tag{4.167}$$
$$\mathbf{P}^{(0)}_{\rm I}\mathbf{n}^0_{\rm I} = -(p^{(0)}(\mathsf{G}^{(0)}_{\rm f})^{\rm T})\mathbf{n}^0_{\rm I} \qquad \text{on} \qquad \Gamma^0_{\rm I}, \tag{4.168}$$
$$\mathbf{P}^{(0)}_{\rm II}\mathbf{n}^0_{\rm II} = -(p^{(0)}(\mathsf{G}^{(0)}_{\rm f})^{\rm T})\mathbf{n}^0_{\rm II} \qquad \text{on} \qquad \Gamma^0_{\rm II}. \tag{4.169}$$

Since our solid stress tensors $\mathbf{P}_{\rm I}$ and $\mathbf{P}_{\rm II}$ are described by a constitutive law, our problem here is the general case. It is possible to state a generalised ansatz to this problem and

state the cell problems. However, we wait to do this until the constitutive law has been specified. Within the next section, we state the macroscale model for this general case and then specify this problem for a specific choice of the constitutive law.

4.3 The Macroscale Model and Particular Cases

We begin by stating the general nonlinear macroscale model for poroelastic composite materials undergoing large deformations where the specific constitutive law for the material has not yet been specified, that is,

$$\begin{cases} \langle \mathbf{w} \rangle_{\mathrm{f}} = -\langle \hat{W} \rangle_{\mathrm{f}} \nabla_{\bar{\mathbf{x}}} p^{(0)}, \\ \nabla_{\bar{\mathbf{x}}} \cdot \bar{\mathsf{T}}_{\mathrm{Eff}} = 0, \\ \bar{\mathsf{T}}_{\mathrm{Eff}} = \left\langle \dfrac{\partial \psi_{\mathrm{I}}^{(0)}}{\partial \mathbf{F}_{\mathrm{I}}^{(0)}} \right\rangle_{\mathrm{I}} + \left\langle \dfrac{\partial \psi_{\mathrm{II}}^{(0)}}{\partial \mathbf{F}_{\mathrm{II}}^{(0)}} \right\rangle_{\mathrm{II}} - p^{(0)} \langle (\mathsf{G}_{\mathrm{f}}^{(0)})^{\mathrm{T}} \rangle_{\mathrm{f}}, \\ \nabla_{\bar{\mathbf{x}}} \cdot \langle \mathsf{G}_{\mathrm{f}}^{(0)} \mathbf{w} \rangle_{\mathrm{f}} = -\big(\langle \nabla_{\bar{\mathbf{x}}} \cdot (\mathsf{G}_{\mathrm{I}}^{(0)})^{\mathrm{T}} \rangle_{\mathrm{I}} + \langle \nabla_{\bar{\mathbf{x}}} \cdot (\mathsf{G}_{\mathrm{II}}^{(0)})^{\mathrm{T}} \rangle_{\mathrm{II}} + \langle \nabla_{\bar{\mathbf{x}}} \cdot (\mathsf{G}_{\mathrm{f}}^{(0)})^{\mathrm{T}} \rangle_{\mathrm{f}} \big) \cdot \dot{\mathbf{u}}^{(0)} \\ + \langle \mathsf{G}_{\mathrm{I}}^{(0)} : \nabla_{\bar{\mathbf{Y}}} \dot{\mathbf{u}}_{\mathrm{I}}^{(1)} \rangle_{\mathrm{I}} + \langle \mathsf{G}_{\mathrm{II}}^{(0)} : \nabla_{\bar{\mathbf{Y}}} \dot{\mathbf{u}}_{\mathrm{II}}^{(1)} \rangle_{\mathrm{II}} - \langle \mathsf{G}_{\mathrm{f}}^{(0)} \rangle_{\mathrm{f}} : \nabla_{\bar{\mathbf{x}}} \dot{\mathbf{u}}^{(0)}, \end{cases}$$

where ψ_{I} and ψ_{II} are the strain energy functions for the material in the subphase and matrix, respectively. This model comprises Darcy's law for the relative fluid–solid velocity. The second and third equations are the stress balance and the constitutive law for the nonlinear poroelastic composite material. The constitutive law is to be specified further by choosing a specific strain energy function for the matrix and the subphase, relevant to the intended application. The final equation is the conservation of mass equation. This equation is also be influenced by the choice of strain energy function for the matrix and the subphase. Within the next subsection, we prescribe a particular constitutive law for the elastic materials, and this leads to a specified model that reduces to three previously known models under appropriate simplifying assumptions.

4.3.1 Constitutive Law

Within this section we specialise the model for a choosen constitutive law. We choose the very simple de Saint-Venant strain energy function given by:

$$\psi_v = \frac{1}{2} \mathbf{E}_v : \mathbb{C}_v : \mathbf{E}_v \qquad \text{in} \qquad \Omega_v^0 \quad \text{where} \quad v = \mathrm{I}, \mathrm{II}, \tag{4.170}$$

where ψ_v is described by different parameters depending on the solid domain that it is describing and $\mathbf{E}_v$ is the Green-Lagrangian strain tensor for each solid domain, that is,

$$\psi_v = \begin{cases} \psi_{\text{I}} = \dfrac{1}{2}\mathbf{E}_{\text{I}} : \mathbb{C}_{\text{I}} : \mathbf{E}_{\text{I}} \qquad \text{in} \quad \Omega^0_{\text{I}}, \\ \psi_{\text{II}} = \dfrac{1}{2}\mathbf{E}_{\text{II}} : \mathbb{C}_{\text{II}} : \mathbf{E}_{\text{II}} \quad \text{in} \quad \Omega^0_{\text{II}}. \end{cases} \tag{4.171}$$

We make this choice since it will allow us to recover the linear elastic case and the other few works in the literature that have used asymptotic homogenization in the nonlinear setting.

We adopt the notation that:

$$\mathbb{C} = \begin{cases} \mathbb{C}_{\text{I}} \quad \text{in} \quad \Omega^0_{\text{I}} \\ \mathbb{C}_{\text{II}} \quad \text{in} \quad \Omega^0_{\text{II}} \end{cases} \tag{4.172}$$

and the subscript $v = \text{I}, \text{II}$, where I is the subphase and II is the matrix throughout this section. We have that the expansion of ψ_v is given by:

$$\psi^\epsilon_v = \frac{1}{2}\mathbf{E}^\epsilon_v : \mathbb{C} : \mathbf{E}^\epsilon_v, \tag{4.173}$$

and we note that $\mathbb{C}$ is the fourth rank elasticity tensor with major and minor symmetries, namely:

$$C_{ijkl} = C_{jikl} = C_{ijlk} = C_{klij}. \tag{4.174}$$

We can now determine $\mathbf{E}_v$. We have:

$$\begin{aligned} \mathbf{E}_v &= \frac{1}{2}((\mathbf{F}_v)^{\text{T}}\mathbf{F}_v - \mathbf{I}) = \frac{1}{2}((\nabla_{\mathbf{X}}\mathbf{u}_v + \mathbf{I})^{\text{T}}(\nabla_{\mathbf{X}}\mathbf{u}_v + \mathbf{I}) - \mathbf{I}) \\ &= \frac{1}{2}((\nabla_{\mathbf{X}}\mathbf{u}_v)^{\text{T}}\nabla_{\mathbf{X}}\mathbf{u}_v + (\nabla_{\mathbf{X}}\mathbf{u}_v)^{\text{T}} + \nabla_{\mathbf{X}}\mathbf{u}_v), \end{aligned} \tag{4.175}$$

where the subscript $v = \text{I}, \text{II}$ denotes the subphase and the matrix. We now apply the asymptotic homogenization technique to (4.175). Using the transformation of the gradient operator (4.70):

$$\nabla_{\mathbf{X}} \to \nabla_{\bar{\mathbf{x}}} + \frac{1}{\epsilon}\nabla_{\bar{\mathbf{Y}}}, \tag{4.176}$$

we can write $\mathbf{E}_v^\epsilon$ as:

$$\begin{aligned}\mathbf{E}_v^\epsilon =&\frac{1}{2}\Big[(\nabla_{\bar{\mathbf{X}}}\mathbf{u}_v^\epsilon+\frac{1}{\epsilon}\nabla_{\bar{\mathbf{Y}}}\mathbf{u}_v^\epsilon)^{\mathrm{T}}(\nabla_{\bar{\mathbf{X}}}\mathbf{u}_v^\epsilon+\frac{1}{\epsilon}\nabla_{\bar{\mathbf{Y}}}\mathbf{u}_v^\epsilon)+(\nabla_{\bar{\mathbf{X}}}\mathbf{u}_v^\epsilon+\frac{1}{\epsilon}\nabla_{\bar{\mathbf{Y}}}\mathbf{u}_v^\epsilon)^{\mathrm{T}}+(\nabla_{\bar{\mathbf{X}}}\mathbf{u}_v^\epsilon+\frac{1}{\epsilon}\nabla_{\bar{\mathbf{Y}}}\mathbf{u}_v^\epsilon)\Big]\\ =&\frac{1}{2}\Big[(\nabla_{\bar{\mathbf{X}}}\mathbf{u}_v^\epsilon)^{\mathrm{T}}\nabla_{\bar{\mathbf{X}}}\mathbf{u}_v^\epsilon+\frac{1}{\epsilon}(\nabla_{\bar{\mathbf{X}}}\mathbf{u}_v^\epsilon)^{\mathrm{T}}\nabla_{\bar{\mathbf{Y}}}\mathbf{u}_v^\epsilon+\frac{1}{\epsilon}(\nabla_{\bar{\mathbf{Y}}}\mathbf{u}_v^\epsilon)^{\mathrm{T}}\nabla_{\bar{\mathbf{X}}}\mathbf{u}_v^\epsilon+\frac{1}{\epsilon^2}(\nabla_{\bar{\mathbf{Y}}}\mathbf{u}_v^\epsilon)^{\mathrm{T}}(\nabla_{\bar{\mathbf{Y}}}\mathbf{u}_v^\epsilon)\\ &+\nabla_{\bar{\mathbf{X}}}\mathbf{u}_v^\epsilon+\frac{1}{\epsilon}\nabla_{\bar{\mathbf{Y}}}\mathbf{u}_v^\epsilon+(\nabla_{\bar{\mathbf{X}}}\mathbf{u}_v^\epsilon)^{\mathrm{T}}+\frac{1}{\epsilon}(\nabla_{\bar{\mathbf{Y}}}\mathbf{u}_v^\epsilon)^{\mathrm{T}}\Big].\end{aligned}\tag{4.177}$$

Then, using (4.177), we are able to write the expansion of the strain energy function ψ_v^ϵ as:

$$\begin{aligned}\psi_v^\epsilon =&\frac{1}{8}\Big[\Big((\nabla_{\bar{\mathbf{X}}}\mathbf{u}_v^\epsilon)^{\mathrm{T}}\nabla_{\bar{\mathbf{X}}}\mathbf{u}_v^\epsilon+\frac{1}{\epsilon}(\nabla_{\bar{\mathbf{X}}}\mathbf{u}_v^\epsilon)^{\mathrm{T}}\nabla_{\bar{\mathbf{Y}}}\mathbf{u}_v^\epsilon+\frac{1}{\epsilon}(\nabla_{\bar{\mathbf{Y}}}\mathbf{u}_v^\epsilon)^{\mathrm{T}}\nabla_{\bar{\mathbf{X}}}\mathbf{u}_v^\epsilon+\frac{1}{\epsilon^2}(\nabla_{\bar{\mathbf{Y}}}\mathbf{u}_v^\epsilon)^{\mathrm{T}}(\nabla_{\bar{\mathbf{Y}}}\mathbf{u}_v^\epsilon)\\ &+\nabla_{\bar{\mathbf{X}}}\mathbf{u}_v^\epsilon+\frac{1}{\epsilon}\nabla_{\bar{\mathbf{Y}}}\mathbf{u}_v^\epsilon+(\nabla_{\bar{\mathbf{X}}}\mathbf{u}_v^\epsilon)^{\mathrm{T}}+\frac{1}{\epsilon}(\nabla_{\bar{\mathbf{Y}}}\mathbf{u}_v^\epsilon)^{\mathrm{T}}\Big):\mathbb{C}:\Big((\nabla_{\bar{\mathbf{X}}}\mathbf{u}_v^\epsilon)^{\mathrm{T}}\nabla_{\bar{\mathbf{X}}}\mathbf{u}_v^\epsilon\\ &+\frac{1}{\epsilon}(\nabla_{\bar{\mathbf{X}}}\mathbf{u}_v^\epsilon)^{\mathrm{T}}\nabla_{\bar{\mathbf{Y}}}\mathbf{u}_v^\epsilon+\frac{1}{\epsilon}(\nabla_{\bar{\mathbf{Y}}}\mathbf{u}_v^\epsilon)^{\mathrm{T}}\nabla_{\bar{\mathbf{X}}}\mathbf{u}_v^\epsilon+\frac{1}{\epsilon^2}(\nabla_{\bar{\mathbf{Y}}}\mathbf{u}_v^\epsilon)^{\mathrm{T}}(\nabla_{\bar{\mathbf{Y}}}\mathbf{u}_v^\epsilon)\\ &+\nabla_{\bar{\mathbf{X}}}\mathbf{u}_v^\epsilon+\frac{1}{\epsilon}\nabla_{\bar{\mathbf{Y}}}\mathbf{u}_v^\epsilon+(\nabla_{\bar{\mathbf{X}}}\mathbf{u}_v^\epsilon)^{\mathrm{T}}+\frac{1}{\epsilon}(\nabla_{\bar{\mathbf{Y}}}\mathbf{u}_v^\epsilon)^{\mathrm{T}}\Big)\Big].\end{aligned}\tag{4.178}$$

Multiplying (4.178) by ϵ^2, we obtain:

$$\begin{aligned}\epsilon^2\psi_v^\epsilon =&\frac{1}{8}\Big[\Big(\epsilon^2(\nabla_{\bar{\mathbf{X}}}\mathbf{u}_v^\epsilon)^{\mathrm{T}}\nabla_{\bar{\mathbf{X}}}\mathbf{u}_v^\epsilon+\epsilon(\nabla_{\bar{\mathbf{X}}}\mathbf{u}_v^\epsilon)^{\mathrm{T}}\nabla_{\bar{\mathbf{Y}}}\mathbf{u}_v^\epsilon+\epsilon(\nabla_{\bar{\mathbf{Y}}}\mathbf{u}_v^\epsilon)^{\mathrm{T}}\nabla_{\bar{\mathbf{X}}}\mathbf{u}_v^\epsilon+(\nabla_{\bar{\mathbf{Y}}}\mathbf{u}_v^\epsilon)^{\mathrm{T}}\nabla_{\bar{\mathbf{Y}}}\mathbf{u}_v^\epsilon\\ &+\epsilon^2\nabla_{\bar{\mathbf{X}}}\mathbf{u}_v^\epsilon+\epsilon\nabla_{\bar{\mathbf{Y}}}\mathbf{u}_v^\epsilon+\epsilon^2(\nabla_{\bar{\mathbf{X}}}\mathbf{u}_v^\epsilon)^{\mathrm{T}}+\epsilon(\nabla_{\bar{\mathbf{Y}}}\mathbf{u}_v^\epsilon)^{\mathrm{T}}\Big):\epsilon^2\mathbb{C}:\Big(\epsilon^2(\nabla_{\bar{\mathbf{X}}}\mathbf{u}_v^\epsilon)^{\mathrm{T}}\nabla_{\bar{\mathbf{X}}}\mathbf{u}_v^\epsilon\\ &+\epsilon(\nabla_{\bar{\mathbf{X}}}\mathbf{u}_v^\epsilon)^{\mathrm{T}}\nabla_{\bar{\mathbf{Y}}}\mathbf{u}_v^\epsilon+\epsilon(\nabla_{\bar{\mathbf{Y}}}\mathbf{u}_v^\epsilon)^{\mathrm{T}}\nabla_{\bar{\mathbf{X}}}\mathbf{u}_v^\epsilon+(\nabla_{\bar{\mathbf{Y}}}\mathbf{u}_v^\epsilon)^{\mathrm{T}}\nabla_{\bar{\mathbf{Y}}}\mathbf{u}_v^\epsilon+\epsilon^2\nabla_{\bar{\mathbf{X}}}\mathbf{u}_v^\epsilon\\ &+\epsilon\nabla_{\bar{\mathbf{Y}}}\mathbf{u}_v^\epsilon+\epsilon^2(\nabla_{\bar{\mathbf{X}}}\mathbf{u}_v^\epsilon)^{\mathrm{T}}+\epsilon(\nabla_{\bar{\mathbf{Y}}}\mathbf{u}_v^\epsilon)^{\mathrm{T}}\Big)\Big].\end{aligned}\tag{4.179}$$

We can then equate the coefficients of ϵ^0, ϵ^1 and ϵ^2 in (4.179). For ϵ^0, we have:

$$0=\frac{1}{8}\Big[\Big((\nabla_{\bar{\mathbf{Y}}}\mathbf{u}^{(0)})^{\mathrm{T}}\nabla_{\bar{\mathbf{Y}}}\mathbf{u}^{(0)}\Big):\Big((\nabla_{\bar{\mathbf{Y}}}\mathbf{u}^{(0)})^{\mathrm{T}}\nabla_{\bar{\mathbf{Y}}}\mathbf{u}^{(0)}\Big)\Big]=0.\tag{4.180}$$

Equating the coefficients of ϵ^1 gives:

$$\begin{aligned}0=&\frac{1}{8}\Big[\Big((\nabla_{\bar{\mathbf{X}}}\mathbf{u}^{(0)})^{\mathrm{T}}\nabla_{\bar{\mathbf{Y}}}\mathbf{u}^{(0)}+(\nabla_{\bar{\mathbf{Y}}}\mathbf{u}^{(0)})^{\mathrm{T}}\nabla_{\bar{\mathbf{X}}}\mathbf{u}^{(0)}+(\nabla_{\bar{\mathbf{Y}}}\mathbf{u}_v^{(1)})^{\mathrm{T}}\nabla_{\bar{\mathbf{Y}}}\mathbf{u}^{(0)}+(\nabla_{\bar{\mathbf{Y}}}\mathbf{u}^{(0)})^{\mathrm{T}}\nabla_{\bar{\mathbf{Y}}}\mathbf{u}_v^{(1)}\\ &+\nabla_{\bar{\mathbf{Y}}}\mathbf{u}^{(0)}+(\nabla_{\bar{\mathbf{Y}}}\mathbf{u}^{(0)})^{\mathrm{T}}\Big):\Big((\nabla_{\bar{\mathbf{X}}}\mathbf{u}^{(0)})^{\mathrm{T}}\nabla_{\bar{\mathbf{Y}}}\mathbf{u}^{(0)}+(\nabla_{\bar{\mathbf{Y}}}\mathbf{u}^{(0)})^{\mathrm{T}}\nabla_{\bar{\mathbf{X}}}\mathbf{u}^{(0)}+(\nabla_{\bar{\mathbf{Y}}}\mathbf{u}_v^{(1)})^{\mathrm{T}}\nabla_{\bar{\mathbf{Y}}}\mathbf{u}^{(0)}\\ &+(\nabla_{\bar{\mathbf{Y}}}\mathbf{u}^{(0)})^{\mathrm{T}}\nabla_{\bar{\mathbf{Y}}}\mathbf{u}_v^{(1)}+\nabla_{\bar{\mathbf{Y}}}\mathbf{u}^{(0)}+(\nabla_{\bar{\mathbf{Y}}}\mathbf{u}^{(0)})^{\mathrm{T}}\Big)\Big]=0,\end{aligned}\tag{4.181}$$

and finally, equating the coefficients of ϵ^2 gives:

$$\begin{aligned}\psi_v^{(0)} =&\frac{1}{8}\Bigg[\Bigg((\nabla_{\bar{\mathbf{X}}}\mathbf{u}^{(0)})^{\mathrm{T}}\nabla_{\bar{\mathbf{X}}}\mathbf{u}^{(0)} + (\nabla_{\bar{\mathbf{X}}}\mathbf{u}^{(0)})^{\mathrm{T}}\nabla_{\bar{\mathbf{Y}}}\mathbf{u}_v^{(1)} + (\nabla_{\bar{\mathbf{Y}}}\mathbf{u}_v^{(1)})^{\mathrm{T}}\nabla_{\bar{\mathbf{X}}}\mathbf{u}^{(0)} + (\nabla_{\bar{\mathbf{Y}}}\mathbf{u}_v^{(1)})^{\mathrm{T}}\nabla_{\bar{\mathbf{Y}}}\mathbf{u}_v^{(1)}\\ &+ \nabla_{\bar{\mathbf{X}}}\mathbf{u}^{(0)} + \nabla_{\bar{\mathbf{Y}}}\mathbf{u}_v^{(1)} + (\nabla_{\bar{\mathbf{X}}}\mathbf{u}^{(0)})^{\mathrm{T}} + (\nabla_{\bar{\mathbf{Y}}}\mathbf{u}_v^{(1)})^{\mathrm{T}}\Bigg) : \mathbb{C} : \Bigg((\nabla_{\bar{\mathbf{X}}}\mathbf{u}^{(0)})^{\mathrm{T}}\nabla_{\bar{\mathbf{X}}}\mathbf{u}^{(0)}\\ &+ (\nabla_{\bar{\mathbf{X}}}\mathbf{u}^{(0)})^{\mathrm{T}}\nabla_{\bar{\mathbf{Y}}}\mathbf{u}_v^{(1)} + (\nabla_{\bar{\mathbf{Y}}}\mathbf{u}_v^{(1)})^{\mathrm{T}}\nabla_{\bar{\mathbf{X}}}\mathbf{u}^{(0)} + (\nabla_{\bar{\mathbf{Y}}}\mathbf{u}_v^{(1)})^{\mathrm{T}}\nabla_{\bar{\mathbf{Y}}}\mathbf{u}_v^{(1)} + \nabla_{\bar{\mathbf{X}}}\mathbf{u}^{(0)} + \nabla_{\bar{\mathbf{Y}}}\mathbf{u}_v^{(1)}\\ &+ (\nabla_{\bar{\mathbf{X}}}\mathbf{u}^{(0)})^{\mathrm{T}} + (\nabla_{\bar{\mathbf{Y}}}\mathbf{u}_v^{(1)})^{\mathrm{T}}\Bigg)\Bigg]\\ =&\frac{1}{2}\mathbf{E}_v^{(0)} : \mathbb{C} : \mathbf{E}_v^{(0)},\end{aligned} \tag{4.182}$$

where we have that:

$$\begin{aligned}\mathbf{E}_v^{(0)} =& (\nabla_{\bar{\mathbf{X}}}\mathbf{u}^{(0)})^{\mathrm{T}}\nabla_{\bar{\mathbf{X}}}\mathbf{u}^{(0)} + (\nabla_{\bar{\mathbf{X}}}\mathbf{u}^{(0)})^{\mathrm{T}}\nabla_{\bar{\mathbf{Y}}}\mathbf{u}_v^{(1)} + (\nabla_{\bar{\mathbf{Y}}}\mathbf{u}_v^{(1)})^{\mathrm{T}}\nabla_{\bar{\mathbf{X}}}\mathbf{u}^{(0)}\\ &+ (\nabla_{\bar{\mathbf{Y}}}\mathbf{u}_v^{(1)})^{\mathrm{T}}\nabla_{\bar{\mathbf{Y}}}\mathbf{u}_v^{(1)} + \nabla_{\bar{\mathbf{X}}}\mathbf{u}^{(0)} + \nabla_{\bar{\mathbf{Y}}}\mathbf{u}_v^{(1)} + (\nabla_{\bar{\mathbf{X}}}\mathbf{u}^{(0)})^{\mathrm{T}} + (\nabla_{\bar{\mathbf{Y}}}\mathbf{u}_v^{(1)})^{\mathrm{T}}.\end{aligned} \tag{4.183}$$

Therefore, we have that the leading order term of the constitutive law in the subphase and the matrix respectively are:

$$\psi_{\mathrm{I}}^{(0)} = \frac{1}{2}\mathbf{E}_{\mathrm{I}}^{(0)} : \mathbb{C}_{\mathrm{I}} : \mathbf{E}_{\mathrm{I}}^{(0)} \quad \text{and} \quad \psi_{\mathrm{II}}^{(0)} = \frac{1}{2}\mathbf{E}_{\mathrm{II}}^{(0)} : \mathbb{C}_{\mathrm{II}} : \mathbf{E}_{\mathrm{II}}^{(0)}. \tag{4.184}$$

Now that we have an expression for $\psi_v^{(0)}$, we can use this to find the leading order term of the second Piola–Kirchoff stress, that is we take the derivatives of (4.184) with respect to $\mathbf{E}_{\mathrm{I}}^{(0)}$ and $\mathbf{E}_{\mathrm{II}}^{(0)}$, respectively. Therefore, we have:

$$\mathbf{S}_v^{(0)} = \frac{\partial \psi_v^{(0)}}{\partial \mathbf{E}_v^{(0)}} = \mathbb{C} : \mathbf{E}_v^{(0)}, \tag{4.185}$$

where we have a different second Piola–Kirchoff stress for both the subphase and the matrix, respectively, that is,

$$\mathbf{S}_v^{(0)} = \begin{cases}\mathbf{S}_{\mathrm{I}}^{(0)} = \mathbb{C}_{\mathrm{I}} : \mathbf{E}_{\mathrm{I}}^{(0)} & \text{in} \quad \Omega_{\mathrm{I}}^0,\\ \mathbf{S}_{\mathrm{II}}^{(0)} = \mathbb{C}_{\mathrm{II}} : \mathbf{E}_{\mathrm{II}}^{(0)} & \text{in} \quad \Omega_{\mathrm{II}}^0.\end{cases} \tag{4.186}$$

We now wish to linearise the second Piola–Kirchoff stress $\mathbf{S}_v^{(0)}$. To do this, we can use

the expression $\mathbf{F}_v^{(0)} = \mathbf{I} + \mathbf{H}$ where:

$$\mathbf{H} = \begin{cases} \mathbf{H}_{\text{I}} = \nabla_{\bar{\mathbf{X}}}\mathbf{u}^{(0)} + \nabla_{\bar{\mathbf{Y}}}\mathbf{u}_{\text{I}}^{(1)} & \text{in} \quad \Omega_{\text{I}}^0, \\ \mathbf{H}_{\text{II}} = \nabla_{\bar{\mathbf{X}}}\mathbf{u}^{(0)} + \nabla_{\bar{\mathbf{Y}}}\mathbf{u}_{\text{II}}^{(1)} & \text{in} \quad \Omega_{\text{II}}^0. \end{cases} \tag{4.187}$$

Therefore, carrying out the linearisation, we have that:

$$\begin{aligned} \mathbf{S}_v^{(0)} =& \mathbb{C} : \mathbf{E}_v^{(0)} \\ =& \mathbb{C} : \left(\frac{1}{2}((\mathbf{F}_v^{(0)})^{\text{T}}\mathbf{F}_v^{(0)} - \mathbf{I})\right) \\ =& \mathbb{C} : \left(\frac{1}{2}((\mathbf{I} + \mathbf{H})^{\text{T}}(\mathbf{I} + \mathbf{H}) - \mathbf{I})\right) \qquad (4.188) \\ =& \mathbb{C} : \left(\frac{1}{2}(\mathbf{H} + \mathbf{H}^{\text{T}} + \mathbf{H}^{\text{T}}\mathbf{H})\right). \qquad (4.189) \end{aligned}$$

We will now ignore the nonlinear terms to obtain:

$$(\mathbf{S}_v^{(0)})_{\text{lin}} = \mathbb{C} : \left(\frac{1}{2}(\mathbf{H} + \mathbf{H}^{\text{T}})\right) = \mathbb{C} : \text{Sym}\mathbf{H}. \tag{4.190}$$

We are now able to use the second Piola–Kirchoff stress $\mathbf{S}_v^{(0)}$ to find the first Piola–Kirchoff stress:

$$\begin{aligned} \mathbf{P}_v^{(0)} &= \mathbf{F}_v^{(0)}\mathbf{S}_v^{(0)} \\ &= (\mathbf{I} + \mathbf{H})\mathbb{C} : \mathbf{E}_v^{(0)}, \end{aligned} \tag{4.191}$$

where we can define the first Piola stress $\mathbf{P}^{(0)}$ in both of the solid constituents, the subphase and matrix, as:

$$\mathbf{P}_v^{(0)} = \begin{cases} \mathbf{P}_{\text{I}}^{(0)} = (\mathbf{I} + \mathbf{H}_{\text{I}})\mathbb{C}_{\text{I}} : \mathbf{E}_{\text{I}}^{(0)} & \text{in} \quad \Omega_{\text{I}}^0, \\ \mathbf{P}_{\text{II}}^{(0)} = (\mathbf{I} + \mathbf{H}_{\text{II}})\mathbb{C}_{\text{II}} : \mathbf{E}_{\text{II}}^{(0)} & \text{in} \quad \Omega_{\text{II}}^0. \end{cases} \tag{4.192}$$

We can also linearise the first Piola–Kirchoff stress $\mathbf{P}_v^{(0)}$. Therefore, we have:

$$(\mathbf{P}_v^{(0)})_{\text{lin}} = \mathbb{C} : \text{Sym}\mathbf{H}, \tag{4.193}$$

and since we have that $\mathbb{C}$ is major and minor symmetric, then we can write this as:

$$(\mathbf{P}_v^{(0)})_{\text{lin}} = \mathbb{C} : \mathbf{H}. \tag{4.194}$$

We perform these linearisations of the stresses as this will allow us to reach a differential problem that can be solved by a linear ansatz. This allows us to obtain a final model with cell problems that are solvable yet we will still retain the non-linearity in the coefficients and in the arising additional terms in the model.

We therefore can define the solid stresses in the subphase and matrix as:

$$(\mathbf{P}_{\mathrm{I}}^{(0)})_{\mathrm{lin}} = \mathbb{C}_{\mathrm{I}} : (\nabla_{\bar{\mathbf{X}}}\mathbf{u}^{(0)} + \nabla_{\bar{\mathbf{Y}}}\mathbf{u}_{\mathrm{I}}^{(1)}) \qquad \text{in} \quad \Omega_{\mathrm{I}}^{0}, \tag{4.195}$$

$$(\mathbf{P}_{\mathrm{II}}^{(0)})_{\mathrm{lin}} = \mathbb{C}_{\mathrm{II}} : (\nabla_{\bar{\mathbf{X}}}\mathbf{u}^{(0)} + \nabla_{\bar{\mathbf{Y}}}\mathbf{u}_{\mathrm{II}}^{(1)}) \qquad \text{in} \quad \Omega_{\mathrm{II}}^{0}, \tag{4.196}$$

respectively, for our chosen constitutive law. These stresses are reminiscent of the stresses found in Chapter 3 for the linear poroelastic composites, however the following problem still contains the non-linear transformations $(\mathsf{G}_{\mathrm{f}}^{(0)})^{\mathrm{T}}$ which mean that when this problem is solved to find the model coefficients then the non-linearity is still encoded.

We can then use these expressions (4.195) in the problem for $\mathbf{u}_{\mathrm{I}}^{(1)}$ and $\mathbf{u}_{\mathrm{II}}^{(1)}$ given by Equations (4.164)–(4.169), that is,

$$\nabla_{\bar{\mathbf{Y}}} \cdot (\mathbb{C}_{\mathrm{I}}\nabla_{\bar{\mathbf{Y}}}(\mathbf{u}_{\mathrm{I}}^{(1)})) + \nabla_{\bar{\mathbf{Y}}} \cdot (\mathbb{C}_{\mathrm{I}}\nabla_{\bar{\mathbf{X}}}(\mathbf{u}^{(0)})) = 0 \qquad \text{in} \quad \Omega_{\mathrm{I}}^{0}, \tag{4.197}$$

$$\nabla_{\bar{\mathbf{Y}}} \cdot (\mathbb{C}_{\mathrm{II}}\nabla_{\bar{\mathbf{Y}}}(\mathbf{u}_{\mathrm{II}}^{(1)})) + \nabla_{\bar{\mathbf{Y}}} \cdot (\mathbb{C}_{\mathrm{II}}\nabla_{\bar{\mathbf{X}}}(\mathbf{u}^{(0)})) = 0 \qquad \text{in} \quad \Omega_{\mathrm{II}}^{0}, \tag{4.198}$$

$$\mathbf{u}_{\mathrm{I}}^{(1)} = \mathbf{u}_{\mathrm{II}}^{(1)} \qquad \text{on} \quad \Gamma_{\mathrm{III}}^{0}, \tag{4.199}$$

$$\mathbb{C}_{\mathrm{I}}\nabla_{\bar{\mathbf{Y}}}(\mathbf{u}_{\mathrm{I}}^{(1)})\mathbf{n}_{\mathrm{III}}^{0} - \mathbb{C}_{\mathrm{II}}\nabla_{\bar{\mathbf{Y}}}(\mathbf{u}_{\mathrm{II}}^{(1)})\mathbf{n}_{\mathrm{III}}^{0} = (\mathbb{C}_{\mathrm{II}} - \mathbb{C}_{\mathrm{I}})\nabla_{\bar{\mathbf{X}}}(\mathbf{u}^{(0)})\mathbf{n}_{\mathrm{III}}^{0} \qquad \text{on} \quad \Gamma_{\mathrm{III}}^{0}, \tag{4.200}$$

$$(\mathbb{C}_{\mathrm{I}}\nabla_{\bar{\mathbf{Y}}}(\mathbf{u}_{\mathrm{I}}^{(1)}) + \mathbb{C}_{\mathrm{I}}\nabla_{\bar{\mathbf{X}}}(\mathbf{u}^{(0)}))\mathbf{n}_{\mathrm{I}}^{0} = -(p^{(0)}(\mathsf{G}_{\mathrm{f}}^{(0)})^{\mathrm{T}})\mathbf{n}_{\mathrm{I}}^{0} \qquad \text{on} \quad \Gamma_{\mathrm{I}}^{0}, \tag{4.201}$$

$$(\mathbb{C}_{\mathrm{II}}\nabla_{\bar{\mathbf{Y}}}(\mathbf{u}_{\mathrm{II}}^{(1)}) + \mathbb{C}_{\mathrm{II}}\nabla_{\bar{\mathbf{X}}}(\mathbf{u}^{(0)}))\mathbf{n}_{\mathrm{II}}^{0} = -(p^{(0)}(\mathsf{G}_{\mathrm{f}}^{(0)})^{\mathrm{T}})\mathbf{n}_{\mathrm{II}}^{0} \qquad \text{on} \quad \Gamma_{\mathrm{II}}^{0}. \tag{4.202}$$

This differential problem again reminds of the differential problem presented in Chapter 3 however, here we see that in (4.201) and (4.202) we have the tensor $(\mathsf{G}_{\mathrm{f}}^{(0)})^{\mathrm{T}}$ appearing. This is a nonlinear transformation that is based on the deformation gradient of the materials and it is through this quantity that the model coefficients will still retain the non-linear character post linearisation.

The problem given by (4.197)–(4.202) admits a unique solution up to a $\bar{\mathbf{Y}}$-constant function. Exploiting the imposed linearity, the solution is given as:

$$\mathbf{u}_{\mathrm{I}}^{(1)} = \hat{A}_{\mathrm{I}}\nabla_{\bar{\mathbf{X}}}(\mathbf{u}^{(0)}) + \hat{\mathbf{a}}_{\mathrm{I}}p^{(0)} + c_1(\bar{\mathbf{X}}), \tag{4.203}$$

$$\mathbf{u}_{\mathrm{II}}^{(1)} = \hat{A}_{\mathrm{II}}\nabla_{\bar{\mathbf{X}}}(\mathbf{u}^{(0)}) + \hat{\mathbf{a}}_{\mathrm{II}}p^{(0)} + c_2(\bar{\mathbf{X}}), \tag{4.204}$$

where $c_1(\bar{\mathbf{X}})$ and $c_2(\bar{\mathbf{X}})$ are $\bar{\mathbf{Y}}$-constant functions. The third rank tensors $\hat{A}_{\mathrm{I}}$ and $\hat{A}_{\mathrm{II}}$ are the solutions of the porescale problems given by:

$$\nabla_{\bar{\mathbf{Y}}} \cdot (\mathbb{C}_{\mathrm{I}} \nabla_{\bar{\mathbf{Y}}}(\hat{A}_{\mathrm{I}})) + \nabla_{\bar{\mathbf{Y}}} \cdot \mathbb{C}_{\mathrm{I}} = 0 \qquad \text{in} \qquad \Omega^0_{\mathrm{I}}, \tag{4.205}$$

$$\nabla_{\bar{\mathbf{Y}}} \cdot (\mathbb{C}_{\mathrm{II}} \nabla_{\bar{\mathbf{Y}}}(\hat{A}_{\mathrm{II}})) + \nabla_{\bar{\mathbf{Y}}} \cdot \mathbb{C}_{\mathrm{II}} = 0 \qquad \text{in} \qquad \Omega^0_{\mathrm{II}}, \tag{4.206}$$

$$\hat{A}_{\mathrm{I}} = \hat{A}_{\mathrm{II}} \qquad \text{on} \qquad \Gamma^0_{\mathrm{III}}, \tag{4.207}$$

$$\mathbb{C}_{\mathrm{I}} \nabla_{\bar{\mathbf{Y}}}(\hat{A}_{\mathrm{I}}) \mathbf{n}^0_{\mathrm{III}} - \mathbb{C}_{\mathrm{II}} \nabla_{\bar{\mathbf{Y}}}(\hat{A}_{\mathrm{II}}) \mathbf{n}^0_{\mathrm{III}} = (\mathbb{C}_{\mathrm{II}} - \mathbb{C}_{\mathrm{I}}) \mathbf{n}^0_{\mathrm{III}} \qquad \text{on} \qquad \Gamma^0_{\mathrm{III}}, \tag{4.208}$$

$$(\mathbb{C}_{\mathrm{I}} \nabla_{\bar{\mathbf{Y}}}(\hat{A}_{\mathrm{I}})) \mathbf{n}^0_{\mathrm{I}} + \mathbb{C}_{\mathrm{I}} \mathbf{n}^0_{\mathrm{I}} = 0 \qquad \text{on} \qquad \Gamma^0_{\mathrm{I}} \tag{4.209}$$

$$(\mathbb{C}_{\mathrm{II}} \nabla_{\bar{\mathbf{Y}}}(\hat{A}_{\mathrm{II}})) \mathbf{n}^0_{\mathrm{II}} + \mathbb{C}_{\mathrm{II}} \mathbf{n}^0_{\mathrm{II}} = 0 \qquad \text{on} \qquad \Gamma^0_{\mathrm{II}}, \tag{4.210}$$

and the vectors $\hat{\mathbf{a}}_{\mathrm{I}}$ and $\hat{\mathbf{a}}_{\mathrm{II}}$ are the solution to this porescale problem:

$$\nabla_{\bar{\mathbf{Y}}} \cdot (\mathbb{C}_{\mathrm{I}} \nabla_{\bar{\mathbf{Y}}}(\hat{\mathbf{a}}_{\mathrm{I}})) = \mathbf{0} \qquad \text{in} \qquad \Omega^0_{\mathrm{I}}, \tag{4.211}$$

$$\nabla_{\bar{\mathbf{Y}}} \cdot (\mathbb{C}_{\mathrm{II}} \nabla_{\bar{\mathbf{Y}}}(\hat{\mathbf{a}}_{\mathrm{II}})) = \mathbf{0} \qquad \text{in} \qquad \Omega^0_{\mathrm{II}}, \tag{4.212}$$

$$\hat{\mathbf{a}}_{\mathrm{I}} = \hat{\mathbf{a}}_{\mathrm{II}} \qquad \text{on} \qquad \Gamma^0_{\mathrm{III}}, \tag{4.213}$$

$$(\mathbb{C}_{\mathrm{I}} \nabla_{\bar{\mathbf{Y}}}(\hat{\mathbf{a}}_{\mathrm{I}})) \mathbf{n}^0_{\mathrm{III}} = (\mathbb{C}_{\mathrm{II}} \nabla_{\bar{\mathbf{Y}}}(\hat{\mathbf{a}}_{\mathrm{II}})) \mathbf{n}^0_{\mathrm{III}} \qquad \text{on} \qquad \Gamma^0_{\mathrm{III}}, \tag{4.214}$$

$$(\mathbb{C}_{\mathrm{I}} \nabla_{\bar{\mathbf{Y}}}(\hat{\mathbf{a}}_{\mathrm{I}}) + (\mathsf{G}^{(0)}_{\mathrm{f}})^{\mathrm{T}}) \mathbf{n}^0_{\mathrm{I}} = \mathbf{0} \qquad \text{on} \qquad \Gamma^0_{\mathrm{I}}, \tag{4.215}$$

$$(\mathbb{C}_{\mathrm{II}} \nabla_{\bar{\mathbf{Y}}}(\hat{\mathbf{a}}_{\mathrm{II}}) + (\mathsf{G}^{(0)}_{\mathrm{f}})^{\mathrm{T}}) \mathbf{n}^0_{\mathrm{II}} = \mathbf{0} \qquad \text{on} \qquad \Gamma^0_{\mathrm{II}}. \tag{4.216}$$

Both (4.205)–(4.210) and (4.211)–(4.216) are to be solved on the periodic cell. To ensure the uniqueness of the solution, we also require a further condition on $\hat{A}_{\mathrm{I}}$, $\hat{A}_{\mathrm{II}}$, $\hat{\mathbf{a}}_{\mathrm{I}}$ and $\hat{\mathbf{a}}_{\mathrm{II}}$, for example:

$$\langle \hat{A}_{\mathrm{I}} \rangle_{\mathrm{I}} + \langle \hat{A}_{\mathrm{II}} \rangle_{\mathrm{II}} = 0 \quad \text{and} \quad \langle \hat{\mathbf{a}}_{\mathrm{I}} \rangle_{\mathrm{I}} + \langle \hat{\mathbf{a}}_{\mathrm{II}} \rangle_{\mathrm{II}} = \mathbf{0}. \tag{4.217}$$

Here, we wish to discuss in detail the cell problems (4.143)–(4.145), (4.205)–(4.210) and (4.211)–(4.216) and how they can potentially be solved. These porescale periodic cell problems are to be solved to determine the model coefficients of the final macroscale model. It is through these model coefficients that the complexity of the materials microstructure is encoded in the final model.

In general, with the asymptotic homogenization technique, these cell problems would only depend on the pore-scale and therefore can be solved in a straight-forward way. For example, solving the porescale asymptotic homogenization cell problems for linear elastic composites was carried out in [88], and for linear poroelasticity, the problems were

solved in [35]. Similarly, it would be possible to solve the cell problems arising from linear poroelastic composites by combining the techniques used in both of these previous works. In the linear case, we have the problems (4.143)–(4.145), (4.205)–(4.210) and (4.211)–(4.216) with the simplification that $(\mathsf{G}_{\mathrm{f}}^{(0)})^{\mathrm{T}}$ approaches the identity. This simplification means that the two scales are fully decoupled, and we can solve the fluid and the elastic-type cell problems.

However, due to the nonlinearity of the system we consider here, the two scales are coupled, meaning that the porescale periodic cell problems have a dependence on the macroscale and therefore cannot be easily solved. This dependence is through the quantity $(\mathsf{G}_{\mathrm{f}}^{(0)})^{\mathrm{T}}$ appearing in (4.143)–(4.145) and (4.215)–(4.216). This quantity is the Piola transform, which involves the leading order deformation gradient $\mathbf{F}^{(0)}$. This depends on both the porescale and the macroscale, as can be seen in Equations (4.120) and (4.121). This means that the two scales are not fully decoupled, and therefore, this dramatically increases the computational complexity.

It is however crucial for a realistic analysis of the scenarios of interest (such as biological tissues) to be able to solve problems of this type. Despite the complexity, there are some potential emerging techniques that may mean it would be possible to solve this model numerically in the future. A recent example of a proposed method that could be potentially used to solve the types of problems arising in this work is found in [36]. This work investigated the potential of using Artificial Neural Networks (ANNs) for quick, accurate upscaling and localisation of problems. The method involves an incremental numerical approach where there is a rearrangement of the cell properties relating to the current deformation, and this means that there is a remodelling of the macroscopic model after each incremental time step. This method is applicable to finite strain and large deformation problems, whilst there will only be infinitesimal deformation within each incremental time step. Reference [36] investigated the full effects of the coupling between the macroscale and microscale for the first time in the analysis of fluid-saturated porous media. We believe that by following an approach similar to the one set out in [36], we could obtain a solution to our model numerically.

We can use our expressions (4.203) and (4.204) for $\mathbf{u}_{\mathrm{I}}^{(1)}$ and $\mathbf{u}_{\mathrm{II}}^{(1)}$ to rewrite $(\mathbf{P}_{\mathrm{I}}^{(0)})_{\mathrm{lin}}$ and $(\mathbf{P}_{\mathrm{II}}^{(0)})_{\mathrm{lin}}$. We have:

$$(\mathbf{P}_{\mathrm{I}}^{(0)})_{\mathrm{lin}} = \mathbb{C}_{\mathrm{I}}\nabla_{\bar{\mathbf{Y}}}(\hat{A}_{\mathrm{I}}\nabla_{\bar{\mathbf{X}}}\mathbf{u}^{(0)} + \hat{\mathbf{a}}_{\mathrm{I}}p^{(0)}) + \mathbb{C}_{\mathrm{I}}\nabla_{\bar{\mathbf{X}}}\mathbf{u}^{(0)}$$

$$
\begin{aligned}
&= \mathbb{C}_{\mathrm{I}} \nabla_{\bar{\mathbf{Y}}} \hat{A}_{\mathrm{I}} \nabla_{\bar{\mathbf{X}}} \mathbf{u}^{(0)} + \mathbb{C}_{\mathrm{I}} \nabla_{\bar{\mathbf{Y}}} \hat{\mathbf{a}}_{\mathrm{I}} p^{(0)} + \mathbb{C}_{\mathrm{I}} \nabla_{\bar{\mathbf{X}}} \mathbf{u}^{(0)} \\
&= \mathbb{C}_{\mathrm{I}} \mathbb{M}_{\mathrm{I}} \nabla_{\bar{\mathbf{X}}} \mathbf{u}^{(0)} + \mathbb{C}_{\mathrm{I}} \nabla_{\bar{\mathbf{X}}} \mathbf{u}^{(0)} + \mathbb{C}_{\mathrm{I}} \mathbf{Q}_{\mathrm{I}} p^{(0)} \\
&= (\mathbb{C}_{\mathrm{I}} \mathbb{M}_{\mathrm{I}} + \mathbb{C}_{\mathrm{I}}) \nabla_{\bar{\mathbf{X}}} \mathbf{u}^{(0)} + \mathbb{C}_{\mathrm{I}} \mathbf{Q}_{\mathrm{I}} p^{(0)},
\end{aligned} \tag{4.218}
$$

and:

$$
\begin{aligned}
(\mathbf{P}_{\mathrm{II}}^{(0)})_{\mathrm{lin}} &= \mathbb{C}_{\mathrm{II}} \nabla_{\bar{\mathbf{Y}}} (\hat{A}_{\mathrm{II}} \nabla_{\bar{\mathbf{X}}} \mathbf{u}^{(0)} + \hat{\mathbf{a}}_{\mathrm{II}} p^{(0)}) + \mathbb{C}_{\mathrm{II}} \nabla_{\bar{\mathbf{X}}} \mathbf{u}^{(0)} \\
&= \mathbb{C}_{\mathrm{II}} \nabla_{\bar{\mathbf{Y}}} \hat{A}_{\mathrm{II}} \nabla_{\bar{\mathbf{X}}} \mathbf{u}^{(0)} + \mathbb{C}_{\mathrm{II}} \nabla_{\bar{\mathbf{Y}}} \hat{\mathbf{a}}_{\mathrm{II}} p^{(0)} + \mathbb{C}_{\mathrm{II}} \nabla_{\bar{\mathbf{X}}} \mathbf{u}^{(0)} \\
&= \mathbb{C}_{\mathrm{II}} \mathbb{M}_{\mathrm{II}} \nabla_{\bar{\mathbf{X}}} \mathbf{u}^{(0)} + \mathbb{C}_{\mathrm{II}} \nabla_{\bar{\mathbf{X}}} \mathbf{u}^{(0)} + \mathbb{C}_{\mathrm{II}} \mathbf{Q}_{\mathrm{II}} p^{(0)} \\
&= (\mathbb{C}_{\mathrm{II}} \mathbb{M}_{\mathrm{II}} + \mathbb{C}_{\mathrm{II}}) \nabla_{\bar{\mathbf{X}}} \mathbf{u}^{(0)} + \mathbb{C}_{\mathrm{II}} \mathbf{Q}_{\mathrm{II}} p^{(0)},
\end{aligned} \tag{4.219}
$$

where we define the porescale gradients of the auxiliary variables as:

$$
\hat{\mathbb{M}}_{\mathrm{I}} = \nabla_{\bar{\mathbf{Y}}} \hat{A}_{\mathrm{I}}, \quad \hat{\mathbb{M}}_{\mathrm{II}} = \nabla_{\bar{\mathbf{Y}}} \hat{A}_{\mathrm{II}}, \quad \hat{\mathbf{Q}}_{\mathrm{I}} = \nabla_{\bar{\mathbf{Y}}} \hat{\mathbf{a}}_{\mathrm{I}}, \quad \hat{\mathbf{Q}}_{\mathrm{II}} = \nabla_{\bar{\mathbf{Y}}} \hat{\mathbf{a}}_{\mathrm{II}}. \tag{4.220}
$$

Then, we can return to (4.163) and use our linearised solid stresses to find the effective stress:

$$
\begin{aligned}
\bar{\mathsf{T}}_{\mathrm{Eff}} &= \langle (\mathbf{P}_{\mathrm{I}}^{(0)})_{\mathrm{lin}} \rangle_{\mathrm{I}} + \langle (\mathbf{P}_{\mathrm{II}}^{(0)})_{\mathrm{lin}} \rangle_{\mathrm{II}} - p^{(0)} \langle (\mathsf{G}_{\mathrm{f}}^{(0)})^{\mathrm{T}} \rangle_{\mathrm{f}} \\
&= \big(\langle \mathbb{C}_{\mathrm{I}} \hat{\mathbb{M}}_{\mathrm{I}} + \mathbb{C}_{\mathrm{I}} \rangle_{\mathrm{I}} + \langle \mathbb{C}_{\mathrm{II}} \hat{\mathbb{M}}_{\mathrm{II}} + \mathbb{C}_{\mathrm{II}} \rangle_{\mathrm{II}} \big) \nabla_{\bar{\mathbf{X}}} \mathbf{u}^{(0)} + \big(\langle \mathbb{C}_{\mathrm{I}} \hat{\mathbf{Q}}_{\mathrm{I}} \rangle_{\mathrm{I}} + \langle \mathbb{C}_{\mathrm{II}} \hat{\mathbf{Q}}_{\mathrm{II}} \rangle_{\mathrm{II}} \\
&\quad - \langle (\mathsf{G}_{\mathrm{f}}^{(0)})^{\mathrm{T}} \rangle_{\mathrm{f}} \big) p^{(0)}.
\end{aligned} \tag{4.221}
$$

Again this effective stress will remind of the effective stress in the linear case Chapter 3. Here however we see that it contains the tensor $(\mathsf{G}_{\mathrm{f}}^{(0)})^{\mathrm{T}}$ which is the nonlinear transformation and also the quantities $\hat{\mathbb{M}}_{\mathrm{I}}$, $\hat{\mathbb{M}}_{\mathrm{II}}$, $\hat{\mathbf{Q}}_{\mathrm{I}}$ and $\hat{\mathbf{Q}}_{\mathrm{II}}$. These are to be found by solving cell problems (4.205)–(4.210) and (4.211)–(4.216) which again contain nonlinear transformations.

As mentioned in Section 4.2.4, we return to the expression (4.157), restated here for convenience,

$$
\begin{aligned}
\nabla_{\bar{\mathbf{x}}} \cdot \left(\langle \mathsf{G}_{\mathrm{f}}^{(0)} \mathbf{w} \rangle_{\mathrm{f}} + \langle \mathsf{G}_{\mathrm{f}}^{(0)} \rangle_{\mathrm{f}} \dot{\mathbf{u}}^{(0)} \right) &= - \big(\langle \nabla_{\bar{\mathbf{x}}} \cdot (\mathsf{G}_{\mathrm{I}}^{(0)})^{\mathrm{T}} \rangle_{\mathrm{I}} + \langle \nabla_{\bar{\mathbf{x}}} \cdot (\mathsf{G}_{\mathrm{II}}^{(0)})^{\mathrm{T}} \rangle_{\mathrm{II}} \big) \cdot \dot{\mathbf{u}}^{(0)} \\
&\quad + \langle \mathsf{G}_{\mathrm{I}}^{(0)} : \nabla_{\bar{\mathbf{Y}}} \dot{\mathbf{u}}_{\mathrm{I}}^{(1)} \rangle_{\mathrm{I}} + \langle \mathsf{G}_{\mathrm{II}}^{(0)} : \nabla_{\bar{\mathbf{Y}}} \dot{\mathbf{u}}_{\mathrm{II}}^{(1)} \rangle_{\mathrm{II}}
\end{aligned} \tag{4.222}
$$

We obtain expressions for $\dot{\mathbf{u}}_{\mathrm{I}}^{(1)}$ and $\dot{\mathbf{u}}_{\mathrm{II}}^{(1)}$ by taking the time derivative of (4.203) and (4.204), and we then substitute these expressions into (4.222) to obtain:

$$\begin{aligned}\nabla_{\bar{\mathbf{x}}}\cdot\left(\langle \mathsf{G}_{\mathrm{f}}^{(0)}\mathbf{w}\rangle_{\mathrm{f}}+\langle \mathsf{G}_{\mathrm{f}}^{(0)}\rangle_{\mathrm{f}}\dot{\mathbf{u}}^{(0)}\right)&=\langle \mathsf{G}_{\mathrm{I}}^{(0)}:\nabla_{\bar{\mathbf{Y}}}\hat{A}_{\mathrm{I}}\rangle_{\mathrm{I}}:\nabla_{\bar{\mathbf{x}}}\dot{\mathbf{u}}^{(0)}+\langle \mathsf{G}_{\mathrm{I}}^{(0)}:\nabla_{\bar{\mathbf{Y}}}\hat{\mathbf{a}}_{\mathrm{I}}\rangle_{\mathrm{I}}\dot{p}^{(0)}\\&\quad+\langle \mathsf{G}_{\mathrm{II}}^{(0)}:\nabla_{\bar{\mathbf{Y}}}\hat{A}_{\mathrm{II}}\rangle_{\mathrm{II}}:\nabla_{\bar{\mathbf{x}}}\dot{\mathbf{u}}^{(0)}+\langle \mathsf{G}_{\mathrm{II}}^{(0)}:\nabla_{\bar{\mathbf{Y}}}\hat{\mathbf{a}}_{\mathrm{II}}\rangle_{\mathrm{II}}\dot{p}^{(0)}\\&\quad-\left(\langle\nabla_{\bar{\mathbf{x}}}\cdot(\mathsf{G}_{\mathrm{I}}^{(0)})^{\mathrm{T}}\rangle_{\mathrm{I}}+\langle\nabla_{\bar{\mathbf{x}}}\cdot(\mathsf{G}_{\mathrm{II}}^{(0)})^{\mathrm{T}}\rangle_{\mathrm{II}}\right)\cdot\dot{\mathbf{u}}^{(0)}.\end{aligned}\tag{4.223}$$

Expanding the LHS in (4.223) and using (4.220), we obtain:

$$\begin{aligned}\nabla_{\bar{\mathbf{x}}}\cdot\langle \mathsf{G}_{\mathrm{f}}^{(0)}\mathbf{w}\rangle_{\mathrm{f}}+\nabla_{\bar{\mathbf{x}}}\cdot\left(\langle \mathsf{G}_{\mathrm{f}}^{(0)}\rangle_{\mathrm{f}}\dot{\mathbf{u}}^{(0)}\right)&=\langle \mathsf{G}_{\mathrm{I}}^{(0)}:\hat{\mathbb{M}}_{\mathrm{I}}\rangle_{\mathrm{I}}:\nabla_{\bar{\mathbf{x}}}\dot{\mathbf{u}}^{(0)}+\langle \mathsf{G}_{\mathrm{I}}^{(0)}:\hat{\mathbf{Q}}_{\mathrm{I}}\rangle_{\mathrm{I}}\dot{p}^{(0)}\\&\quad+\langle \mathsf{G}_{\mathrm{II}}^{(0)}:\hat{\mathbb{M}}_{\mathrm{II}}\rangle_{\mathrm{II}}:\nabla_{\bar{\mathbf{x}}}\dot{\mathbf{u}}^{(0)}+\langle \mathsf{G}_{\mathrm{II}}^{(0)}:\hat{\mathbf{Q}}_{\mathrm{II}}\rangle_{\mathrm{II}}\dot{p}^{(0)}\\&\quad-\left(\langle\nabla_{\bar{\mathbf{x}}}\cdot(\mathsf{G}_{\mathrm{I}}^{(0)})^{\mathrm{T}}\rangle_{\mathrm{I}}+\langle\nabla_{\bar{\mathbf{x}}}\cdot(\mathsf{G}_{\mathrm{II}}^{(0)})^{\mathrm{T}}\rangle_{\mathrm{II}}\right)\cdot\dot{\mathbf{u}}^{(0)}.\end{aligned}\tag{4.224}$$

Expanding the second term on the LHS further and rearranging, we obtain:

$$\begin{aligned}\nabla_{\bar{\mathbf{x}}}\cdot\langle \mathsf{G}_{\mathrm{f}}^{(0)}\mathbf{w}\rangle_{\mathrm{f}}+\langle \mathsf{G}_{\mathrm{f}}^{(0)}\rangle_{\mathrm{f}}:\nabla_{\bar{\mathbf{x}}}\dot{\mathbf{u}}^{(0)}=&\langle \mathsf{G}_{\mathrm{I}}^{(0)}:\hat{\mathbb{M}}_{\mathrm{I}}\rangle_{\mathrm{I}}:\nabla_{\bar{\mathbf{x}}}\dot{\mathbf{u}}^{(0)}+\langle \mathsf{G}_{\mathrm{I}}^{(0)}:\hat{\mathbf{Q}}_{\mathrm{I}}\rangle_{\mathrm{I}}\dot{p}^{(0)}\\&+\langle \mathsf{G}_{\mathrm{II}}^{(0)}:\hat{\mathbb{M}}_{\mathrm{II}}\rangle_{\mathrm{II}}:\nabla_{\bar{\mathbf{x}}}\dot{\mathbf{u}}^{(0)}+\langle \mathsf{G}_{\mathrm{II}}^{(0)}:\hat{\mathbf{Q}}_{\mathrm{II}}\rangle_{\mathrm{II}}\dot{p}^{(0)}-\left(\langle\nabla_{\bar{\mathbf{x}}}\cdot(\mathsf{G}_{\mathrm{I}}^{(0)})^{\mathrm{T}}\rangle_{\mathrm{I}}\right.\\&\left.+\langle\nabla_{\bar{\mathbf{x}}}\cdot(\mathsf{G}_{\mathrm{II}}^{(0)})^{\mathrm{T}}\rangle_{\mathrm{II}}+\langle\nabla_{\bar{\mathbf{x}}}\cdot(\mathsf{G}_{\mathrm{f}}^{(0)})^{\mathrm{T}}\rangle_{\mathrm{f}}\right)\cdot\dot{\mathbf{u}}^{(0)}.\end{aligned}\tag{4.225}$$

Rearranging and collecting $\dot{p}^{(0)}$ terms gives:

$$\begin{aligned}\dot{p}^{(0)}=\frac{1}{\langle \mathsf{G}_{\mathrm{I}}^{(0)}:\hat{\mathbf{Q}}_{\mathrm{I}}\rangle_{\mathrm{I}}+\langle \mathsf{G}_{\mathrm{II}}^{(0)}:\hat{\mathbf{Q}}_{\mathrm{II}}\rangle_{\mathrm{II}}}&\left[\nabla_{\bar{\mathbf{x}}}\cdot\langle \mathsf{G}_{\mathrm{f}}^{(0)}\mathbf{w}\rangle_{\mathrm{f}}+\left(\langle \mathsf{G}_{\mathrm{f}}^{(0)}\rangle_{\mathrm{f}}-\langle \mathsf{G}_{\mathrm{I}}^{(0)}:\hat{\mathbb{M}}_{\mathrm{I}}\rangle_{\mathrm{I}}\right.\right.\\&\left.-\langle \mathsf{G}_{\mathrm{II}}^{(0)}:\hat{\mathbb{M}}_{\mathrm{II}}\rangle_{\mathrm{II}}\right):\nabla_{\bar{\mathbf{x}}}\dot{\mathbf{u}}^{(0)}+\left(\langle\nabla_{\bar{\mathbf{x}}}\cdot(\mathsf{G}_{\mathrm{I}}^{(0)})^{\mathrm{T}}\rangle_{\mathrm{I}}+\langle\nabla_{\bar{\mathbf{x}}}\cdot(\mathsf{G}_{\mathrm{II}}^{(0)})^{\mathrm{T}}\rangle_{\mathrm{II}}\right.\\&\left.\left.+\langle\nabla_{\bar{\mathbf{x}}}\cdot(\mathsf{G}_{\mathrm{f}}^{(0)})^{\mathrm{T}}\rangle_{\mathrm{f}}\right)\cdot\dot{\mathbf{u}}^{(0)}\right].\end{aligned}\tag{4.226}$$

We define:

$$\bar{M}:=\frac{-1}{\langle \mathsf{G}_{\mathrm{I}}^{(0)}:\hat{\mathbf{Q}}_{\mathrm{I}}\rangle_{\mathrm{I}}+\langle \mathsf{G}_{\mathrm{II}}^{(0)}:\hat{\mathbf{Q}}_{\mathrm{II}}\rangle_{\mathrm{II}}},\tag{4.227}$$

and:

$$\bar{\boldsymbol{\alpha}}:=\langle \mathsf{G}_{\mathrm{f}}^{(0)}\rangle_{\mathrm{f}}-\langle \mathsf{G}_{\mathrm{I}}^{(0)}:\hat{\mathbb{M}}_{\mathrm{I}}\rangle_{\mathrm{I}}-\langle \mathsf{G}_{\mathrm{II}}^{(0)}:\hat{\mathbb{M}}_{\mathrm{II}}\rangle_{\mathrm{II}},\tag{4.228}$$

and we can then use (4.227) and (4.228) to rewrite (4.226) as:

$$\dot{p}^{(0)} = -\bar{M}\big[\nabla_{\bar{\mathbf{x}}}\cdot\langle \mathsf{G}_{\mathrm{f}}^{(0)}\mathbf{w}\rangle_{\mathrm{f}} + \bar{\boldsymbol{\alpha}} : \nabla_{\bar{\mathbf{x}}}\dot{\mathbf{u}}^{(0)} + \big(\langle\nabla_{\bar{\mathbf{x}}}\cdot(\mathsf{G}_{\mathrm{I}}^{(0)})^{\mathrm{T}}\rangle_{\mathrm{I}} + \langle\nabla_{\bar{\mathbf{x}}}\cdot(\mathsf{G}_{\mathrm{II}}^{(0)})^{\mathrm{T}}\rangle_{\mathrm{II}} + \langle\nabla_{\bar{\mathbf{x}}}\cdot(\mathsf{G}_{\mathrm{f}}^{(0)})^{\mathrm{T}}\rangle_{\mathrm{f}}\big)\cdot\dot{\mathbf{u}}^{(0)}\big]. \tag{4.229}$$

Finally, we can divide by $\bar{M}$ to obtain:

$$\frac{\dot{p}^{(0)}}{\bar{M}} = -\nabla_{\bar{\mathbf{x}}}\cdot\langle \mathsf{G}_{\mathrm{f}}^{(0)}\mathbf{w}\rangle_{\mathrm{f}} - \bar{\boldsymbol{\alpha}} : \nabla_{\bar{\mathbf{x}}}\dot{\mathbf{u}}^{(0)} - \big(\langle\nabla_{\bar{\mathbf{x}}}\cdot(\mathsf{G}_{\mathrm{I}}^{(0)})^{\mathrm{T}}\rangle_{\mathrm{I}} + \langle\nabla_{\bar{\mathbf{x}}}\cdot(\mathsf{G}_{\mathrm{II}}^{(0)})^{\mathrm{T}}\rangle_{\mathrm{II}} + \langle\nabla_{\bar{\mathbf{x}}}\cdot(\mathsf{G}_{\mathrm{f}}^{(0)})^{\mathrm{T}}\rangle_{\mathrm{f}}\big)\cdot\dot{\mathbf{u}}^{(0)}. \tag{4.230}$$

We therefore have now derived the effective macroscale governing equations for a nonlinear poroelastic composite that has the constitutive law given by the de Saint-Venant strain energy function. We state our novel macroscale model and then consider limit cases for the model where we obtain previously known results from the literature. The equations in the macroscale model represent a poroelastic-type system of PDEs. Therefore, the macroscale model is given by:

$$\langle\mathbf{w}\rangle_{\mathrm{f}} = -\langle\hat{W}\rangle_{\mathrm{f}}\nabla_{\bar{\mathbf{x}}}p^{(0)}, \tag{4.231}$$

$$\nabla_{\bar{\mathbf{x}}}\cdot\bar{\mathsf{T}}_{\mathrm{Eff}} = 0, \tag{4.232}$$

$$\bar{\mathsf{T}}_{\mathrm{Eff}} = \big(\langle\mathbb{C}_{\mathrm{I}}\hat{\mathbb{M}}_{\mathrm{I}} + \mathbb{C}_{\mathrm{I}}\rangle_{\mathrm{I}} + \langle\mathbb{C}_{\mathrm{II}}\hat{\mathbb{M}}_{\mathrm{II}} + \mathbb{C}_{\mathrm{II}}\rangle_{\mathrm{II}}\big) : \nabla_{\bar{\mathbf{x}}}\mathbf{u}^{(0)} + \big(\langle\mathbb{C}_{\mathrm{I}}\hat{\mathbf{Q}}_{\mathrm{I}}\rangle_{\mathrm{I}} + \langle\mathbb{C}_{\mathrm{II}}\hat{\mathbf{Q}}_{\mathrm{II}}\rangle_{\mathrm{II}} - \langle(\mathsf{G}_{\mathrm{f}}^{(0)})^{\mathrm{T}}\rangle_{\mathrm{f}}\big)p^{(0)}, \tag{4.233}$$

$$\dot{p}^{(0)} = \frac{1}{\langle\mathsf{G}_{\mathrm{I}}^{(0)} : \hat{\mathbf{Q}}_{\mathrm{I}}\rangle_{\mathrm{I}} + \langle\mathsf{G}_{\mathrm{II}}^{(0)} : \hat{\mathbf{Q}}_{\mathrm{II}}\rangle_{\mathrm{II}}}\Bigg[\nabla_{\bar{\mathbf{x}}}\cdot\langle\mathsf{G}_{\mathrm{f}}^{(0)}\mathbf{w}\rangle_{\mathrm{f}} + \Big(\langle\mathsf{G}_{\mathrm{f}}^{(0)}\rangle_{\mathrm{f}} - \langle\mathsf{G}_{\mathrm{I}}^{(0)} : \hat{\mathbb{M}}_{\mathrm{I}}\rangle_{\mathrm{I}} - \langle\mathsf{G}_{\mathrm{II}}^{(0)} : \hat{\mathbb{M}}_{\mathrm{II}}\rangle_{\mathrm{II}}\Big) : \nabla_{\bar{\mathbf{x}}}\dot{\mathbf{u}}^{(0)} + \Big(\langle\nabla_{\bar{\mathbf{x}}}\cdot(\mathsf{G}_{\mathrm{I}}^{(0)})^{\mathrm{T}}\rangle_{\mathrm{I}} + \langle\nabla_{\bar{\mathbf{x}}}\cdot(\mathsf{G}_{\mathrm{II}}^{(0)})^{\mathrm{T}}\rangle_{\mathrm{II}} + \langle\nabla_{\bar{\mathbf{x}}}\cdot(\mathsf{G}_{\mathrm{f}}^{(0)})^{\mathrm{T}}\rangle_{\mathrm{f}}\Big)\cdot\dot{\mathbf{u}}^{(0)}\Bigg], \tag{4.234}$$

where the macroscale pressure is denoted by $p^{(0)}$, $\mathbf{u}^{(0)}$ is the leading order elastic displacement, the solid velocity is represented by $\dot{\mathbf{u}}^{(0)}$ and, finally, $\mathbf{w}$ is the leading order relative fluid–solid velocity. Equation (4.231) in the macroscale model is Darcy's law for $\mathbf{w}$. Equation (4.232) of the macroscale model is the stress balance equation with the effective stress tensor $\bar{\mathsf{T}}_{\mathrm{Eff}}$. The constitutive equation given by (4.233) is of poroelastic type; however, it contains a nonlinear coordinate transformation. The effective elasticity tensor for the

material is given by:

$$\widetilde{\mathbb{C}} = \langle \mathbb{C}_{\mathrm{I}} \hat{\mathbb{M}}_{\mathrm{I}} + \mathbb{C}_{\mathrm{I}} \rangle_{\mathrm{I}} + \langle \mathbb{C}_{\mathrm{II}} \hat{\mathbb{M}}_{\mathrm{II}} + \mathbb{C}_{\mathrm{II}} \rangle_{\mathrm{II}} \tag{4.235}$$

Finally, (4.234) is the conservation of mass for a nonlinear poroelastic composite material. The three terms in our expression for $\dot{p}^{(0)}$ that are the divergence of the Piola transforms in the subphase, matrix and fluid, respectively, describe the volume changes related to the deformation and can be viewed as a correction term that maintains the conservation of mass despite the nonlinear coordinate transformations.

We can say that the effective mechanical behaviour of our nonlinear poroelastic composite material can be fully described by the model coefficients, that is the effective elasticity tensor $\widetilde{\mathbb{C}}$, the hydraulic conductivity tensor $\langle \hat{W} \rangle_{\mathrm{f}}$, the transformed Biot's tensor of coefficients, $\bar{\boldsymbol{\alpha}}$ and the transformed Biot's modulus, $\bar{M}$. We note that although, structurally, this model is similar to that of linear poroelasticity, the key novelty resides in the model coefficients that capture the nonlinear deformations and the additional terms. These model coefficients are to be obtained by solving the novel cell problems (4.143)–(4.145), (4.205)–(4.210) and (4.211)–(4.216)

It would indeed be possible to make the choice of other strain energy functions and follow a similar process as we have just carried out to obtain a model with different coefficients and additional terms that would also describe nonlinear poroelastic composites. We emphasise here that the choice of strain energy function influences the cinstitutive law and the conservation of mass equations in the final macroscale model.

Next, we consider particular cases for our model and are able to derive previously known models that were developed using the asymptotic homogenization technique.

4.3.2 Comparison with Linear Poroelastic Composites

We begin with the case where the poroelastic composite solids that we are considering are linearly elastic. This setting is applicable to many situations including the interstitial matrix of biological tissues and when describing hard hierarchical materials such as bones and tendons where deformations are very small. We note that to reduce to the linear elastic case, we have that $\mathsf{G}^{(0)} \to \mathbf{I}$. We also introduce the notation:

$$\langle \varphi_{\mathrm{I}} \rangle_{\mathrm{I}} + \langle \varphi_{\mathrm{II}} \rangle_{\mathrm{II}} = \langle \varphi_{\mathrm{I}} + \varphi_{\mathrm{II}} \rangle_{\mathrm{s}}, \tag{4.236}$$

for fields φ with components φ_{I} and φ_{II} defined in the solid cell portions Ω^0_{I} or Ω^0_{II}, respectively. This means that the model (4.231)-(4.234) reduces to:

$$\begin{cases} \langle \mathbf{w} \rangle_{\mathrm{f}} = -\langle \hat{W} \rangle_{\mathrm{f}} \nabla_{\bar{\mathbf{x}}} p^{(0)}, \\ \nabla_{\bar{\mathbf{x}}} \cdot \bar{\mathsf{T}}_{\mathrm{Eff}} = 0, \\ \bar{\mathsf{T}}_{\mathrm{Eff}} = \langle \mathbb{C}_{\mathrm{I}} \hat{\mathbb{M}}_{\mathrm{I}} + \mathbb{C}_{\mathrm{I}} + \mathbb{C}_{\mathrm{II}} \hat{\mathbb{M}}_{\mathrm{II}} + \mathbb{C}_{\mathrm{II}} \rangle_s \nabla_{\bar{\mathbf{x}}} \mathbf{u}^{(0)} + (\langle \mathbb{C}_{\mathrm{I}} \hat{\mathbf{Q}}_{\mathrm{I}} + \mathbb{C}_{\mathrm{II}} \hat{\mathbf{Q}}_{\mathrm{II}} \rangle_s - \phi \mathbf{I}) p^{(0)}, \\ \dot{p}^{(0)} = \dfrac{1}{\langle \mathrm{Tr}(\hat{\mathbf{Q}}_{\mathrm{I}} + \hat{\mathbf{Q}}_{\mathrm{II}}) \rangle_s} \left(\nabla_{\bar{\mathbf{x}}} \cdot \langle \mathbf{w} \rangle_{\mathrm{f}} + (\phi \mathbf{I} - \langle \mathrm{Tr}(\hat{\mathbb{M}}_{\mathrm{I}} + \hat{\mathbb{M}}_{\mathrm{II}}) \rangle_s) : \nabla_{\bar{\mathbf{x}}} \dot{\mathbf{u}}^{(0)} \right), \end{cases} \tag{4.237}$$

This is identically the model for linear poroelastic composites presented in [69] and Chapter 3 (3.186) (up to the difference in notation). We note that the integral average over the fluid domain of the identity tensor, $\langle \mathbf{I} \rangle_{\mathrm{f}}$, is $\phi \mathbf{I}$. We also have that $\langle \mathsf{G}^{(0)}_{\upsilon} : \mathbf{Q}_{\upsilon} \rangle_{\upsilon}$, where $\upsilon = \mathrm{I}, \mathrm{II}$ becomes $\langle \mathrm{Tr} \mathbf{Q}_{\upsilon} \rangle_{\upsilon}$ in the limit $\mathsf{G}^{(0)} \to \mathbf{I}$. Similarly, $\langle \mathsf{G}^{(0)}_{\upsilon} : \mathbb{M}_{\upsilon} \rangle_{\upsilon} : \nabla_{\bar{\mathbf{x}}} \dot{\mathbf{u}}^{(0)}$ becomes $\langle \mathrm{Tr} \mathbb{M}_{\upsilon} \rangle_{\upsilon} : \nabla_{\bar{\mathbf{x}}} \dot{\mathbf{u}}^{(0)}$. As a result of taking the limit $\mathsf{G}^{(0)} \to \mathbf{I}$, we also have that $\mathbf{F}^{(0)} \to \mathbf{I}$, and using this in the cell problems (4.143)–(4.145), (4.205)–(4.210) and (4.211)–(4.216), we recover the same cell problems as in [69] and therefore obtain exactly the same model coefficients under this limit and therefore we can equate the notation used in both models.

We also note, as remarked in [69], that if we consider only one elastic phase, then the model reduces to the macroscale model for a standard poroelastic material (see the no growth limit in [87], as well as [19, 68]). Furthermore, in the limit of zero fluid (no pores), then this macroscale model reduces to the model for an elastic composite [89].

4.3.3 Comparison with Nonlinear Poroelasticity

We now wish to recover previous work on nonlinear poroelasticity. For this, we assume that our material has only one hyperelastic phase, the matrix that we denote by Ω_{II}, with fluid flowing in the pores. We wish to compare our equation (4.225) under the assumption of only one elastic phase (the matrix) with the generalised Biot fluid equation found in [17]. We can rewrite our equation with only one elastic phase as:

$$\begin{aligned} -\nabla_{\bar{\mathbf{x}}} \cdot \langle \mathsf{G}^{(0)}_{\mathrm{f}} \hat{W} \rangle_{\mathrm{f}} \nabla_{\bar{\mathbf{x}}} p^{(0)} = \langle \mathsf{G}^{(0)}_{\mathrm{II}} : \hat{\mathbb{M}}_{\mathrm{II}} \rangle_{\mathrm{II}} : \nabla_{\bar{\mathbf{x}}} \dot{\mathbf{u}}^{(0)} + \langle \mathsf{G}^{(0)}_{\mathrm{II}} : \hat{\mathbf{Q}}_{\mathrm{II}} \rangle_{\mathrm{II}} \dot{p}^{(0)} - \langle \nabla_{\bar{\mathbf{x}}} \cdot (\mathsf{G}^{(0)}_{\mathrm{II}})^{\mathrm{T}} \rangle_{\mathrm{II}} \cdot \dot{\mathbf{u}}^{(0)} \\ - \nabla_{\bar{\mathbf{x}}} \cdot (\langle \mathsf{G}^{(0)}_{\mathrm{f}} \rangle_{\mathrm{f}} \dot{\mathbf{u}}^{(0)}). \end{aligned} \tag{4.238}$$

We note that we do not consider any body forces, so the f appearing in [17] equals zero

here. A general ansatz for $\mathbf{u}^{(1)}$ was also used in [17], but we are still able to make some identifications between the terms in our equation (4.238) and the terms in their generalised Biot fluid equation. We note that the model coefficients of [17] all involve $(\mathsf{G}^{(0)})^{\mathrm{T}}$, so we should point out that due to a different choice in the definition of the Piola transformation between this work and [17], we have that $(\mathsf{G}^{(0)})^{\mathrm{T}}$ in [17] equals $\mathsf{G}^{(0)}$ in this work. We also use a modified (4.16) where we only have $\mathsf{G}^{(0)} = \mathsf{G}^{(0)}_{\mathrm{II}}$ in Ω^0_{II} and $\mathsf{G}^{(0)} = \mathsf{G}^{(0)}_{\mathrm{f}}$ in Ω^0_{f}. This means that we can identify the coefficients:

$$\begin{aligned} K^* = -\langle \mathsf{G}^{(0)} \hat{W} \rangle_{\mathrm{f}}, \qquad A^* = \langle \nabla_{\bar{\mathbf{Y}}} (\mathsf{G}^{(0)}_{\mathrm{II}} \hat{A}_{\mathrm{II}}) \rangle_{\mathrm{II}} = \langle \mathsf{G}^{(0)}_{\mathrm{II}} : \hat{\mathbb{M}}_{\mathrm{II}} \rangle_{\mathrm{II}}, \\ B^* = \langle \nabla_{\bar{\mathbf{Y}}} (\mathsf{G}^{(0)}_{\mathrm{II}} \hat{\mathbf{a}}_{\mathrm{II}}) \rangle_{\mathrm{II}} = \langle \mathsf{G}^{(0)}_{\mathrm{II}} : \hat{\mathbf{Q}}_{\mathrm{II}} \rangle_{\mathrm{II}}, \qquad D^* = \langle \mathsf{G}^{(0)} \rangle_{\Omega}. \end{aligned} \tag{4.239}$$

The difference in sign between K^* and $\hat{W}$ is due to the difference in the choice of ansatz for the fluid problem. We therefore can recover the generalised Biot fluid equation from our equation (4.238).

We now wish to compare the macroscale elasticity equation in [17] with our macroscale balance equation and constitutive law (4.232) and (4.233). We first should note that in our work, we are not considering any body forces, and therefore, we can assume that the f and b appearing in [17] are both zero. Using (4.233) in (4.232) and reducing to only one elastic phase (the matrix), we obtain:

$$\nabla_{\bar{\mathbf{x}}} \cdot \left(\langle \mathbb{C}_{\mathrm{II}} \mathbb{M}_{\mathrm{II}} + \mathbb{C}_{\mathrm{II}} \rangle_{\mathrm{II}} : \nabla_{\bar{\mathbf{x}}} \mathbf{u}^{(0)} + \big(\langle \mathbb{C}_{\mathrm{II}} \mathbf{Q}_{\mathrm{II}} \rangle_{\mathrm{II}} - \langle (\mathsf{G}^{(0)}_{\mathrm{f}})^{\mathrm{T}} \rangle_{\mathrm{f}} \big) p^{(0)} \right) = 0 \tag{4.240}$$

We are able to make the identifications between the macroscale elasticity equation of [17] using a generalised ansatz and our equation (4.240), where a specific ansatz is used. The term $Ce_x(u_0)$ can be identified with our term $\mathbb{C}_{\mathrm{II}} : \nabla_{\bar{\mathbf{x}}} \mathbf{u}^{(0)}$. Similarly, the term $Ce_y(N(p_0, \nabla_x u_0))$ can lead to our terms $\mathbb{C}_{\mathrm{II}} \mathbb{M}_{\mathrm{II}} : \nabla_{\bar{\mathbf{x}}} \mathbf{u}^{(0)} + \mathbb{C}_{\mathrm{II}} \mathbf{Q} p^{(0)}$ when using our ansatz. Finally, we need to compare the term $\phi_1(p_0, \nabla_x u_0) \nabla_x p_0$ appearing in [17] with the final term in (4.240). The final term in (4.240) can be expanded as:

$$-\nabla_{\bar{\mathbf{x}}} \cdot \big(\langle (\mathsf{G}^{(0)}_{\mathrm{f}})^{\mathrm{T}} \rangle_{\mathrm{f}} p^{(0)} \big) = -\langle (\mathsf{G}^{(0)}_{\mathrm{f}})^{\mathrm{T}} \rangle_{\mathrm{f}} \nabla_{\bar{\mathbf{x}}} p^{(0)} - (\nabla_{\bar{\mathbf{x}}} \cdot \langle \mathsf{G}^{(0)}_{\mathrm{f}} \rangle_{\mathrm{f}}) p^{(0)} \tag{4.241}$$

The term $\phi_1(p_0, \nabla_x u_0) \nabla_x p_0$ can be identified with the first term in (4.241), and when we assume that $\mathsf{G}^{(0)}_{\mathrm{f}}$ is a constant, then we recover exactly the macroscale elasticity equation of [17].

We also wish to make a comparison between the cell problems found in [17] and our cell problems. The fluid cell problem (4.143)–(4.145) matches exactly the first cell problem found in [17]. We however do not require the second cell problem found in [17] as we do not include any forces in our formulation, so $f = 0$. We also have the two elastic cell problems (4.205)–(4.210) and (4.211)–(4.216), and these cannot be directly compared with the cell problems found in [17] as these arise after the application of a specific ansatz. We can however compare the elastic problem of [17] with (4.165) and (4.169), and it is clear that if (4.165) and (4.169) are identical, up to a choice of sign, to the balance equation of [17]' and continuity of tractions, then the same ansatz would produce the same cell problems.

4.3.4 Comparison with Nonlinear Elastic Composites

We now consider the case that our structure has no pores and therefore can be described as a composite comprised of two hyperelastic materials. We can instantly reduce our model (4.231)-(4.234) by removing the equations that govern the fluid. We are able to obtain the model derived in [102], where we make the assumption that plastic distortions are absent, that is assuming $\mathbf{F}_p = \mathbf{I}$ in [102].

When we assume that $\mathbf{F}_p = \mathbf{I}$ in [102], then we have that the plastic Green–Lagrange strain tensor $\mathbf{E}_p^{(0)} = \frac{1}{2}((\mathbf{F}_p^{(0)})^{\mathrm{T}}\mathbf{F}_p^{(0)} - \mathbf{I}) = \frac{1}{2}(\mathbf{I} - \mathbf{I}) = 0$. This means the first Piola stress obtained in [102] becomes:

$$T_{\mathrm{lin}}^{(0)} = \mathscr{C}_{\mathrm{R}} : \mathbf{H}, \tag{4.242}$$

and we can make the identifications in the notation that $\mathscr{C}_{\mathrm{R}} = \mathbb{C}$ and $T_{\mathrm{lin}}^{(0)} = (\mathbf{P}_v^{(0)})_{\mathrm{lin}}$ in our case. Therefore, the first Piola stress tensor (4.194), that we obtained here matches the first Piola stress obtained by [102].

We should note that within this work, we use notation to specifically identify the two constituents of the composite, whereas [102] kept the different constituents implicit. We can modify our problem (4.197)–(4.202) to remove the involvement of the fluid. We therefore end up with the problem for elastic composites, which is given by:

$$\nabla_{\bar{\mathbf{Y}}} \cdot (\mathbb{C}_{\mathrm{I}} \nabla_{\bar{\mathbf{Y}}}(\mathbf{u}_{\mathrm{I}}^{(1)})) + \nabla_{\bar{\mathbf{Y}}} \cdot (\mathbb{C}_{\mathrm{I}} \nabla_{\bar{\mathbf{X}}}(\mathbf{u}^{(0)})) = 0 \qquad \text{in} \quad \Omega_{\mathrm{I}}^0, \tag{4.243}$$

$$\nabla_{\bar{\mathbf{Y}}} \cdot (\mathbb{C}_{\mathrm{II}} \nabla_{\bar{\mathbf{Y}}}(\mathbf{u}_{\mathrm{II}}^{(1)})) + \nabla_{\bar{\mathbf{Y}}} \cdot (\mathbb{C}_{\mathrm{II}} \nabla_{\bar{\mathbf{X}}}(\mathbf{u}^{(0)})) = 0 \qquad \text{in} \quad \Omega_{\mathrm{II}}^0, \tag{4.244}$$

$$\mathbf{u}_{\mathrm{I}}^{(1)} = \mathbf{u}_{\mathrm{II}}^{(1)} \qquad \text{on} \quad \Gamma_{\mathrm{III}}^0, \tag{4.245}$$

$$\mathbb{C}_{\mathrm{I}} \nabla_{\bar{\mathbf{Y}}}(\mathbf{u}_{\mathrm{I}}^{(1)}) \mathbf{n}_{\mathrm{III}}^0 - \mathbb{C}_{\mathrm{II}} \nabla_{\bar{\mathbf{Y}}}(\mathbf{u}_{\mathrm{II}}^{(1)}) \mathbf{n}_{\mathrm{III}}^0 = (\mathbb{C}_{\mathrm{II}} - \mathbb{C}_{\mathrm{I}}) \nabla_{\bar{\mathbf{X}}}(\mathbf{u}^{(0)}) \mathbf{n}_{\mathrm{III}}^0 \qquad \text{on} \quad \Gamma_{\mathrm{III}}^0. \tag{4.246}$$

When using the notation of [102], we can write (4.243)–(4.246) as:

$$\mathrm{Div}_{\bar{Y}} T^{(0)} = \mathbf{0}, \tag{4.247}$$

$$[[\mathbf{u}^{(1)}]] = \mathbf{0}, \tag{4.248}$$

$$[[T^{(0)} \cdot \mathbf{N}]] = \mathbf{0}. \tag{4.249}$$

This matches identically the problem given by [102]. The reduced problem (4.243)–(4.246) has the ansatz:

$$\mathbf{u}_{\mathrm{I}}^{(1)} = \hat{A}_{\mathrm{I}} \nabla_{\bar{\mathbf{X}}} \mathbf{u}^{(0)} \qquad \text{and} \qquad \mathbf{u}_{\mathrm{II}}^{(1)} = \hat{A}_{\mathrm{II}} \nabla_{\bar{\mathbf{X}}} \mathbf{u}^{(0)}, \tag{4.250}$$

where $\hat{A}_{\mathrm{I}}$ and $\hat{A}_{\mathrm{II}}$ are third rank tensors. This is the ansatz (4.203) and (4.204) where we take $p^{(0)} = 0$. This leads to the cell problem for $\hat{A}_{\mathrm{I}}$ and $\hat{A}_{\mathrm{II}}$:

$$\begin{cases} \nabla_{\bar{\mathbf{Y}}} \cdot (\mathbb{C}_{\mathrm{I}} \nabla_{\bar{\mathbf{Y}}} (\hat{A}_{\mathrm{I}})) + \nabla_{\bar{\mathbf{Y}}} \cdot \mathbb{C}_{\mathrm{I}} = 0, \\ \nabla_{\bar{\mathbf{Y}}} \cdot (\mathbb{C}_{\mathrm{II}} \nabla_{\bar{\mathbf{Y}}} (\hat{A}_{\mathrm{II}})) + \nabla_{\bar{\mathbf{Y}}} \cdot \mathbb{C}_{\mathrm{II}} = 0, \\ \hat{A}_{\mathrm{I}} = \hat{A}_{\mathrm{II}}, \\ \mathbb{C}_{\mathrm{I}} \nabla_{\bar{\mathbf{Y}}} (\hat{A}_{\mathrm{I}}) \mathbf{n}_{\mathrm{III}}^0 - \mathbb{C}_{\mathrm{II}} \nabla_{\bar{\mathbf{Y}}} (\hat{A}_{\mathrm{II}}) \mathbf{n}_{\mathrm{III}}^0 = (\mathbb{C}_{\mathrm{II}} - \mathbb{C}_{\mathrm{I}}) \mathbf{n}_{\mathrm{III}}^0, \end{cases} \tag{4.251}$$

which is again cell problem (4.205)–(4.210) reduced under the assumption that our material has no pores. In [102], they remarked about the case of no plastic distortions occurring and stated the cell problem they obtained under those circumstances, and this is identical to the cell problem (4.251) where we make the identification that $T\mathrm{Grad}_{\bar{Y}} \xi = \nabla_{\bar{\mathbf{Y}}} \hat{A} = \hat{\mathbb{M}}$ in our work and where we use the implicit notation that:

$$\hat{\mathbb{M}} = \begin{cases} \hat{\mathbb{M}}_{\mathrm{I}} & \text{in} \quad \Omega_{\mathrm{I}}^0, \\ \hat{\mathbb{M}}_{\mathrm{II}} & \text{in} \quad \Omega_{\mathrm{II}}^0. \end{cases} \tag{4.252}$$

Therefore, the cell problem from [102] that matches (4.251) is given by:

$$\begin{cases} \mathrm{Div}_{\bar{Y}} (\mathscr{C} + \mathscr{C} : T\mathrm{Grad}_{\bar{Y}} \xi) = \mathbf{0}, \\ [[\xi]] = \mathbf{0}, \\ [[(\mathscr{C} + \mathscr{C} : T\mathrm{Grad}_{\bar{Y}} \xi) \cdot \mathbf{N}]] = \mathbf{0}. \end{cases} \tag{4.253}$$

Finally, under the assumption of no fluid-filled pores, our macroscale model (4.231-

(4.234)) can be reduced to:

$$\begin{cases} \nabla_{\bar{\mathbf{x}}} \cdot \bar{\mathsf{T}}_{\mathrm{Eff}} = 0, \\ \bar{\mathsf{T}}_{\mathrm{Eff}} = \langle \mathbb{C}_{\mathrm{I}}\mathbb{M}_{\mathrm{I}} + \mathbb{C}_{\mathrm{I}} + \mathbb{C}_{\mathrm{II}}\mathbb{M}_{\mathrm{II}} + \mathbb{C}_{\mathrm{II}} \rangle_{\mathrm{s}} \nabla_{\bar{\mathbf{x}}} \mathbf{u}^{(0)}. \end{cases} \tag{4.254}$$

We can make the identification that $\bar{\mathsf{T}}_{\mathrm{Eff}} = \hat{\mathscr{C}} : \mathrm{Grad}_{\bar{X}} \mathbf{u}^{(0)}$, then we can see that (4.254) matches the model obtained in [102] in the absence of plastic distortions. This is given by:

$$\begin{cases} \mathrm{Div}_{\bar{X}} \langle \hat{\mathscr{C}} : \mathrm{Grad}_{\bar{X}} \mathbf{u}^{(0)} \rangle_{\mathrm{s}} = 0, \\ \langle \hat{\mathscr{C}} : \mathrm{Grad}_{\bar{X}} \mathbf{u}^{(0)} \rangle_{\mathrm{s}} = \langle \mathscr{C} : T\mathrm{Grad}_{\bar{Y}} \xi + \mathscr{C} \rangle_{s} \mathrm{Grad}_{\bar{X}} \mathbf{u}^{(0)}. \end{cases} \tag{4.255}$$

Therefore, we can conclude that our model for nonlinear poroelastic composites can reduce to the model of [102] under the assumption of no plastic distortions.

4.4 Concluding Remarks

We derived a novel framework consisting of partial differential equations that describe the effective mechanical behaviour of nonlinear poroelastic composites. These structures are comprised of a porous hyperelastic matrix with embedded hyperelastic subphases, both of which interact with the fluid flowing in the pores. This type of structure is applicable to many real-world situations, including modelling of soft biological tissues. We began by considering the multiphase fluid–structure interaction (FSI) problem among all the constituents. The problem is closed by appropriate interface conditions arising from the continuity of tractions, displacements and velocities. We also performed a coordinate transformation on certain quantities in the FSI problem in order to obtain a formulation in the reference configuration. We exploited the length scale separation between the porescale (where the pores and elastic subphases are clearly visible) and the macroscale (average size of the material domain) to apply the asymptotic homogenization technique to the non-dimensionalised system of PDEs in order to obtain a macroscale system of governing equations. We were able to recover previously known results in the literature by considering particular limit cases of our model. The new model encodes the detailed properties of the microstructure in its coefficients, that is the microstructural details are encoded in the effective hydraulic conductivity tensor, the Biot modulus and Biot's tensor of coefficients. These are computed by solving the arising differential problems on the periodic cell.

The model obtained here is a generalisation of the formulations for multiphase elastoplastic composites [102] in the limit of no plastic distortions and the formulations of hyperelastic porous media [17]. The model is also a natural extension to the formulation for linear poroelastic composites [69]. All three of these models are recovered as particular cases of our new macroscale model.

The key novelty of this work is the ability to describe a scenario where the hyperelastic matrix is inhomogeneous at the porescale, that is we are able to account for the interactions between various hyperelastic phases and the fluid flowing in the pores. This is generally the case in biological tissues. This means that this model is applicable to a wide range of biological scenarios including modelling lungs. The lungs have previously been approached in a biphasic (tissue and air) manner [9]. However, the lung microstructure is more complex, and there exist collagen and elastin fibres embedded in the matrix and in the fluid, so it could therefore be beneficial to use a nonlinear poroelastic composite approach to modelling. Another example is [121], where the interaction between pulsatile blood flow and the arterial wall mechanics was modelled. The blood flow was modelled as an incompressible viscous fluid, confined by Biot's equations of poroelasticity for the artery wall. This model could be generalised by considering the wall as a nonlinear poroelastic composite of the type we modelled in this work.

The formulation of standard nonlinear poroelasticity is applicable when the solid phase can be approximated as a homogeneous matrix. The linear formulation of poroelastic composites is applicable to situations where the deformations are small such as in hard hierarchical material such as bones (see, e.g., [83, 117]). Our novel model provides a formulation that bridges a gap that has not previously been considered and can be grouped with those found in [37] for strength homogenization, nonsaturated microporomechanics, microporoplasticity and microporofracture and microporodamage theory as an extension to the nonlinear homogenization of porous media.

There are some limitations of the current model, and there are a number possible theoretical extensions that could potentially improve its applicability to certain biological systems. At present, the macroscale model is derived by accounting for a quasi-static regime and only considering the incompressibility of the fluid. Within this work, we used the de Saint-Venant strain energy function for the sake of simplicity. To study a wider range of scenarios, we would need to select a variety of more detailed constitutive laws and then use those to formulate the problem before finding the corresponding cell prob-

lems and the homogenized macroscale model. Strain energy functions specific to certain applications could be used in our formulation, for example the Holzapfel–Ogden Law for the myocardium. Another possible extension, which would be of particular interest, is to incorporate growth and remodelling in our framework. Growth and remodelling are of particular importance to settings such as arteries or heart subject to disease or ageing. Finally, a third theoretical extension we could consider would be the assumption that the solid matrix and the subphases are both incompressible, in addition to the fluid incompressibility, which was already assumed in this work. This would require the incompressibility constraint to be imposed when defining the strain energy function and when determining the Piola stresses in the material. This would lead to alternative cell problems and macroscale model. Moreover, it would be possible to assume that the fluid was in fact compressible, and this would lead to the appearance of the fluid bulk modulus in the resulting Biot's modulus of our system. This modification could be particularly useful to modelling applications in lungs where acoustic properties can be used to aid the diagnosis of respiratory diseases [9,107]. It would also be possible to consider a three-scale approach where there would exist an intermediate *local scale* between the porescale and macroscale that is still well separated. To do this, we could follow the approach taken in [103] and [101] for fibre-reinforced composites.

There are a number of potential next steps for this work; however, potentially the most important of these is to investigate the model by numerical simulations. Recently, the numerical simulations of the cell problems arising from the asymptotic homogenization technique when studying linear elastic composites and linear poroelasticity were carried out by [35, 88]. The simulations for a linear poroelastic composite could be obtained by using the techniques in [35, 88] to compute the poroelastic coefficients in the linear problem. Obtaining numerical results for the nonlinear macroscale model is significantly more complex due to the coupling between the macroscale variables and the cell problems. Developing suitable computational schemes is a current active area of research. A recent example of a proposed method that could be potentially used to solve the types of problems arising in this work is found in [36]. It is important to note that the potential results of any simulations should be validated by experimental data, which could be related to biological tissues.

In the next chapter we propose a novel theoretical model for hierarchical multiscale porous materials. This is another development in the aim to create accurate real world

poroelastic models. We derive the effective governing equations for double poroelastic materials i.e. a poroelastic matrix with embedded poroelastic subphases. By addressing this type of microstructure we can incorporate structural details from three scales into our model meaning that we can produce more detailed results for applications.

Chapter 5

Double poroelasticity derived from the microstructure

Within this work we will focus specifically on multiscale deformable porous media, in particular we consider materials which have three different length scales. These materials have a porous structure and the interactions that occur between the fluid and the solid take place on a scale (the *porescale*), which is much smaller than the size of the whole material (the *global scale*). However, a hierarchical porous medium is in general also characterised by intermediate length scale(s). For example, it is possible to identify a *local scale* related to poroelastic heterogeneities (see Fig. 5.1) and it is this scale and the global scale that are focused on here. In this work, we are not addressing a full three-scale modelling approach, see, e.g. [100] for an example related to elastic composites. We refer to the underlying porescale microstructure as the equations used here are those that would arise from upscaling of the porescale fluid-structure interaction between the fluid and solid phases, see [19], [92]. These equations are Biot's anisotropic, heterogeneous, compressible equations for poroelasticity. This is the most general formulation and is not usually taken into account, as most of the works in the literature typically refer to isotropic, and also incompressible poroelasticity. It would be possible to indeed incorporate a third scale (porescale) into this work where we would see the fluid flowing in the pores, however it would not change the theoretical model derivation.

In this work we aim to determine the effective behaviour of a material which has the underlying microstructure comprising both a poroelastic matrix and a number of embedded poroelastic subphases (i.e. fibres, inclusions and strata) which are interacting with each

other. We assume that the various phases are, in general, anisotropic and heterogeneous. The main motivation behind this work is to study the behaviour of materials which comprise multiple poroelastic phases which are interacting on the local scale. This structure has been considered by [85] where the authors study a poroelastic extracellular matrix in which poroelastic cells are embedded. They develop a set of equations describing such a material and use these equations to study the consolidation of a one-dimensional sample of tissue. The interstitial matrix of biological tissues, which comprises many poroelastic subphases such as cells and different types of collagen fibres embedded in the matrix [61], is an example of this type of structure. In [105] and [24], the authors use the asymptotic homogenization technique to provide an analysis of a system comprising a poroelastic matrix with an embedded subphase. In these cases the simplification that the subphase is purely elastic is made, which provides a model with different applications to which we wish to consider here.

In the present work we generalise [105] and [24] by using the asymptotic homogenization technique to upscale the interaction between the matrix and the subphases, where each phase is described by Biot's anisotropic, heterogeneous, compressible poroelasticity. We assume the scale at which the various subphases are clearly resolved, denoted by the local scale, is much smaller than the size of the whole domain, denoted global scale. The upscaling can then be carried out, accounting for continuity of tractions, displacements, pressures and fluxes across the interface between the phases. The resulting global scale model is of Biot-type. The coefficients of the model encode the properties of the microstructure and are to be computed by solving differential problems on a finite subset of the domain. The model recovers the works [105] and [24] under a set of consistent simplifying assumptions.

The chapter is organised as follows. In Sec. 5.1 we consider the quasi-static, multiphase problem consisting of the governing equations for both the poroelastic matrix and the poroelastic subphases and the appropriate interface conditions. The governing equations for the matrix and the subphases are the equations of Biot's anisotropic, heterogeneous, compressible poroelasticity. In Sec. 5.2 we introduce the two-scale asymptotic homogenization method. In Sec. 5.3 we enforce the length scale separation that occurs between, the inter-subphase distance (*the local scale*) and the overall size of the domain (*the global scale*) to apply the asymptotic homogenization technique to upscale the problem to a system of global scale PDEs. In Sec. 5.4 we provide a detailed description of the effective

coefficients of our novel global scale model. We then prove that our novel global scale model is both formally and substantially of poroelastic type by proving a) the existence of a global scale Biot's tensor of coefficients and b) that the effective Biot's Modulus of the system is positive. Sec. 5.5 concludes our work by discussing limitations of the model and by providing further perspectives. We also provide an appendix in which we recover previously known models by taking appropriate limiting cases of our global scale model and provide an explicit computational scheme for solving the global scale model.

5.1 Formulation of the problem

We have a set $\Omega \in \mathbb{R}^3$, where Ω is the union of a poroelastic matrix Ω_{M} and a collection of K disjoint embedded poroelastic subphases Ω_{Sub}, where we can write

$$\Omega_{\mathrm{Sub}} = \bigcup_{\eta=1}^{N} \Omega_\eta. \tag{5.1}$$

We have that $\bar{\Omega} = \bar{\Omega}_{\mathrm{M}} \cup \bar{\Omega}_{\mathrm{Sub}}$ and $\Omega_{\mathrm{M}} \cap \Omega_{\mathrm{Sub}} = \emptyset$. A sketch of a cross section of the domain Ω is shown in Fig. 5.1, where we highlight the hierarchical structure of the material we are considering. At the local scale, Fig. 5.1 b), we have the various subdomains Ω_{M} and Ω_η for $\eta = 1, \ldots, N$. When zooming in on each of these subdomains separately, Fig. 5.1 c), we find that Ω_{M} and Ω_η have a standard poroelastic structure (see [19], [92]).

To set up an appropriate problem we require the governing equations for each of the subdomains and interface conditions. The balance equations in the matrix and each of the subphases are given by

$$\nabla \cdot \boldsymbol{\sigma}_{\mathrm{M}} = 0 \qquad \text{in} \quad \Omega_{\mathrm{M}}, \tag{5.2}$$

$$\nabla \cdot \boldsymbol{\sigma}_\eta = 0 \qquad \text{in} \quad \Omega_\eta, \tag{5.3}$$

respectively. We have $\boldsymbol{\sigma}_{\mathrm{M}}$ and $\boldsymbol{\sigma}_\eta$ appearing in (5.2-5.3), these are the effective stress tensors in the matrix and subphases respectively. These are given by

$$\boldsymbol{\sigma}_{\mathrm{M}} = \mathbb{C}_{\mathrm{M}} : \xi \mathbf{u}_{\mathrm{M}} - \boldsymbol{\alpha}_{\mathrm{M}} \vartheta_{\mathrm{M}} \qquad \text{in} \quad \Omega_{\mathrm{M}}, \tag{5.4}$$

$$\boldsymbol{\sigma}_\eta = \mathbb{C}_\eta : \xi \mathbf{u}_\eta - \boldsymbol{\alpha}_\eta \vartheta_\eta \qquad \text{in} \quad \Omega_\eta, \tag{5.5}$$

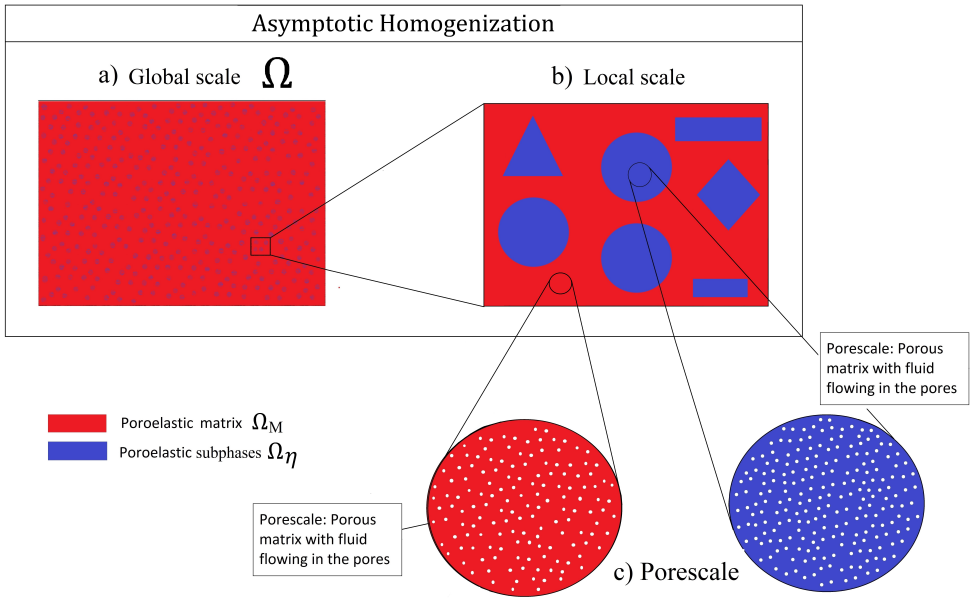

Figure 5.1: A schematic representing a cross section of the domain Ω showing the poroelastic matrix Ω_{M} in red and the various subphases Ω_η in blue at the local scale. We highlight the local scale periodic cell with embedded subphases and highlight the hierarchical structure of the materials we are considering here by also showing their porescale structures.

where

$$\xi(\bullet) = \frac{\nabla(\bullet) + (\nabla(\bullet))^{\mathrm{T}}}{2}, \tag{5.6}$$

is the symmetric part of the gradient operator. We have that $\mathbf{u}_{\mathrm{M}}$ and $\mathbf{u}_\eta$ are the elastic displacements in the matrix and each of the subphases respectively and ϑ_{M} and ϑ_η are the pressures in the matrix and the subphases respectively. The $\mathbb{C}_{\mathrm{M}}$ and $\mathbb{C}_\eta$ are the effective elasticity tensors which would be obtained from the homogenization at the finer hierarchical level. $\mathbb{C}_{\mathrm{M}}$ and $\mathbb{C}_\eta$ are the effective elasticity tensors obtained in ([19], [92]) for a standard poroelastic material. These effective elasticity tensors also possess major and minor symmetries as proved in [68]. We can therefore write the fourth rank effective elasticity tensors in components as $\mathcal{C}^{\mathrm{M}}_{ijkl}$ and $\mathcal{C}^{\eta}_{ijkl}$, for $i, j, k, l = 1, 2, 3$. Therefore we have

$$\mathcal{C}^{\mathrm{M}}_{ijkl} = \mathcal{C}^{\mathrm{M}}_{jikl} = \mathcal{C}^{\mathrm{M}}_{ijlk} = \mathcal{C}^{\mathrm{M}}_{klij}, \tag{5.7}$$

$$\mathcal{C}^{\eta}_{ijkl} = \mathcal{C}^{\eta}_{jikl} = \mathcal{C}^{\eta}_{ijlk} = \mathcal{C}^{\eta}_{klij}. \tag{5.8}$$

The $\boldsymbol{\alpha}_{\mathrm{M}}$ and $\boldsymbol{\alpha}_\eta$ appearing in (5.4-5.5) are the effective Biot's tensors of coefficients in the matrix and the subphases respectively, which have been obtained from the homogenization at finer hierarchical scales. The second rank tensors $\boldsymbol{\alpha}_{\mathrm{M}}$ and $\boldsymbol{\alpha}_\eta$ are related to the ratio of fluid to solid volume changes at constant pressure in their respective poroelastic phases.

We also have Darcy's law for both the matrix and the subphases. That is,

$$\mathbf{w}_{\mathrm{M}} = -\mathsf{K}_{\mathrm{M}}\nabla\vartheta_{\mathrm{M}} \qquad \text{in} \quad \Omega_{\mathrm{M}}, \tag{5.9}$$

$$\mathbf{w}_{\eta} = -\mathsf{K}_{\eta}\nabla\vartheta_{\eta} \qquad \text{in} \quad \Omega_{\eta}, \tag{5.10}$$

where K_{M} and K_{η} are the hydraulic conductivities in the matrix and the subphases respectively and the $\mathbf{w}_{\mathrm{M}}$ and $\mathbf{w}_{\eta}$ are the relative fluid-solid velocities in the matrix and subphases respectively[1].

The last governing equation of each compartment is the conservation of mass equations given by

$$\frac{\dot{\vartheta}_{\mathrm{M}}}{\mathcal{M}_{\mathrm{M}}} = -\boldsymbol{\alpha}_{\mathrm{M}} : \xi\dot{\mathbf{u}}_{\mathrm{M}} - \nabla\cdot\mathbf{w}_{\mathrm{M}} \qquad \text{in} \quad \Omega_{\mathrm{M}}, \tag{5.11}$$

$$\frac{\dot{\vartheta}_{\eta}}{\mathcal{M}_{\eta}} = -\boldsymbol{\alpha}_{\eta} : \xi\dot{\mathbf{u}}_{\eta} - \nabla\cdot\mathbf{w}_{\eta} \qquad \text{in} \quad \Omega_{\eta}, \tag{5.12}$$

for the matrix and subphases respectively. The coefficients $\mathcal{M}_{\mathrm{M}}$ and $\mathcal{M}_{\eta}$ are the Biot's moduli in each compartment, which can as well be obtained from the homogenization process at finer hierarchical scales. $\mathcal{M}_{\mathrm{M}}$ and $\mathcal{M}_{\eta}$ can be described physically as poroelastic coefficients that depend on the porescale geometry, porosity and the fluid bulk modulus. They also depend on the elastic properties of the matrix and subphases respectively. We can interpret $\mathcal{M}_{\mathrm{M}}$ and $\mathcal{M}_{\eta}$ as the inverse of the variation of fluid volume in response to a variation in pore pressure. $\mathcal{M}_{\mathrm{M}}$ and $\mathcal{M}_{\eta}$ are positive definite (see [68], for proof of this property).

In order to close the problem in the whole domain Ω we require interface conditions between the matrix and each of the embedded subphases. We define the interfaces as $\Upsilon_{\eta} := \partial\Omega_{\mathrm{M}} \cap \partial\Omega_{\eta}$ for $\eta = 1, .., N$. Then we impose continuity of tractions, displacements, pressures and fluxes. That is,

$$\boldsymbol{\sigma}_{\mathrm{M}}\mathbf{n}_{\eta} = \boldsymbol{\sigma}_{\eta}\mathbf{n}_{\eta} \qquad \text{on} \qquad \Upsilon_{\eta}, \tag{5.13}$$

$$\mathbf{u}_{\mathrm{M}} = \mathbf{u}_{\eta} \qquad \text{on} \qquad \Upsilon_{\eta}. \tag{5.14}$$

$$\vartheta_{\mathrm{M}} = \vartheta_{\eta} \qquad \text{on} \qquad \Upsilon_{\eta}, \tag{5.15}$$

$$\mathbf{w}_{\mathrm{M}}\cdot\mathbf{n}_{\eta} = \mathbf{w}_{\eta}\cdot\mathbf{n}_{\eta} \qquad \text{on} \qquad \Upsilon_{\eta}, \tag{5.16}$$

[1]They should be in principle multiplied by the porosities, however, the latter can be incorporated in the definition of each hydraulic conductivity tensor

where the unit outward vectors (i.e pointing into the subphase Ω_η) normal to the interfaces Υ_η are denoted by $\mathbf{n}_\eta$ for $\eta = 1, \ldots, N$.

The problem is also to be closed by appropriate boundary conditions on the external boundary $\partial\Omega$. The latter could be, for example, of Dirichlet-Neumann type, as noted in [99]. The conditions on the external boundary typically do not play a role in the derivation of results carried out by formal asymptotic homogenization.

Within the next section we decouple spatial variations by introducing two distinct variables, we then introduce the two-scale asymptotic homogenization method and discuss the assumptions made to carry out the required analysis in the sections that follow.

5.2 The two-scale asymptotic homogenization method

Here we summarise the problem that we introduced in the previous section and now wish to perform a multiscale analysis of this system,

$$\nabla \cdot \boldsymbol{\sigma}_{\mathrm{M}} = 0 \qquad \text{in} \quad \Omega_{\mathrm{M}}, \tag{5.17}$$

$$\nabla \cdot \boldsymbol{\sigma}_{\eta} = 0 \qquad \text{in} \quad \Omega_{\eta}, \tag{5.18}$$

$$\boldsymbol{\sigma}_{\mathrm{M}} = \mathbb{C}_{\mathrm{M}} : \xi \mathbf{u}_{\mathrm{M}} - \boldsymbol{\alpha}_{\mathrm{M}} \vartheta_{\mathrm{M}} \qquad \text{in} \quad \Omega_{\mathrm{M}}, \tag{5.19}$$

$$\boldsymbol{\sigma}_{\eta} = \mathbb{C}_{\eta} : \xi \mathbf{u}_{\eta} - \boldsymbol{\alpha}_{\eta} \vartheta_{\eta} \qquad \text{in} \quad \Omega_{\eta}, \tag{5.20}$$

$$\mathbf{w}_{\mathrm{M}} = -\mathsf{K}_{\mathrm{M}} \nabla \vartheta_{\mathrm{M}} \qquad \text{in} \quad \Omega_{\mathrm{M}}, \tag{5.21}$$

$$\mathbf{w}_{\eta} = -\mathsf{K}_{\eta} \nabla \vartheta_{\eta} \qquad \text{in} \quad \Omega_{\eta}, \tag{5.22}$$

$$\frac{\dot{\vartheta}_{\mathrm{M}}}{\mathcal{M}_{\mathrm{M}}} = -\boldsymbol{\alpha}_{\mathrm{M}} : \xi \dot{\mathbf{u}}_{\mathrm{M}} - \nabla \cdot \mathbf{w}_{\mathrm{M}} \qquad \text{in} \quad \Omega_{\mathrm{M}}, \tag{5.23}$$

$$\frac{\dot{\vartheta}_{\eta}}{\mathcal{M}_{\eta}} = -\boldsymbol{\alpha}_{\eta} : \xi \dot{\mathbf{u}}_{\eta} - \nabla \cdot \mathbf{w}_{\eta} \qquad \text{in} \quad \Omega_{\eta}, \tag{5.24}$$

$$\boldsymbol{\sigma}_{\mathrm{M}} \mathbf{n}_{\eta} = \boldsymbol{\sigma}_{\eta} \mathbf{n}_{\eta} \qquad \text{on} \quad \Upsilon_{\eta}, \tag{5.25}$$

$$\mathbf{u}_{\mathrm{M}} = \mathbf{u}_{\eta} \qquad \text{on} \quad \Upsilon_{\eta}, \tag{5.26}$$

$$\vartheta_{\mathrm{M}} = \vartheta_{\eta} \qquad \text{on} \quad \Upsilon_{\eta}, \tag{5.27}$$

$$\mathbf{w}_{\mathrm{M}} \cdot \mathbf{n}_{\eta} = \mathbf{w}_{\eta} \cdot \mathbf{n}_{\eta} \qquad \text{on} \quad \Upsilon_{\eta}, \tag{5.28}$$

up to conditions on the external boundary $\partial\Omega$. We assume that the system can be characterised by two different length scales. The whole domain Ω has the average size denoted by D. This is the global scale. We assume the second length scale, L, to be the inter-subphase

distance. This is the local scale.

We will now introduce the asymptotic homogenization technique which we will use to upscale (5.17-5.28) to a system of global scale PDEs. We make the assumption that the local length scale (this is where the individual subphases are distinctly visible from the surrounding matrix) denoted by L, is small compared to the average size of the global scale domain denoted by D. That is,

$$\epsilon := \frac{L}{D} \ll 1. \tag{5.29}$$

We also must introduce a spatial variable $\mathbf{y}$. This variable captures local scale variations of the fields, that is

$$\mathbf{y} = \frac{\mathbf{x}}{\epsilon}. \tag{5.30}$$

The global scale and local scale have corresponding spatial variables $\mathbf{x}$ and $\mathbf{y}$ respectively. These variables are formally independent. The gradient operator with the corresponding two-scales becomes

$$\nabla \to \nabla_{\mathbf{x}} + \frac{1}{\epsilon}\nabla_{\mathbf{y}}. \tag{5.31}$$

We assume that all fields in the system of equations (5.17-5.28) as well as $\mathbb{C}_{\mathrm{M}}$, $\mathbb{C}_{\eta}$, K_{M}, K_{η}, $\mathcal{M}_{\mathrm{M}}$, $\mathcal{M}_{\eta}$, $\boldsymbol{\alpha}_{\mathrm{M}}$ and $\boldsymbol{\alpha}_{\eta}$ for $\eta = 1, \ldots, N$ are functions of both the spatial variables $\mathbf{x}$ and $\mathbf{y}$. We also assume that each of the fields can be written as a power series in ϵ. That is,

$$\varphi^{\epsilon}(\mathbf{x}, \mathbf{y}, t) = \varphi^{(0)}(\mathbf{x}, \mathbf{y}, t) + \epsilon\varphi^{(1)}(\mathbf{x}, \mathbf{y}, t) + \epsilon^2\varphi^{(2)}(\mathbf{x}, \mathbf{y}, t) + \cdots \tag{5.32}$$

where formally the series comprises an infinite number of terms and φ represents a typical field in the current work.

Remark 11. *(Local scale Periodicity) We assume that every field $\varphi^{(l)}$ in (5.17-5.28), $\mathbb{C}_{\mathrm{M}}$, $\mathbb{C}_{\eta}$, K_{M}, K_{η}, $\mathcal{M}_{\mathrm{M}}$, $\mathcal{M}_{\eta}$, $\boldsymbol{\alpha}_{\mathrm{M}}$ and $\boldsymbol{\alpha}_{\eta}$ are $\mathbf{y}$-periodic. This allows the analysis of the microstructure to be carried out on a single periodic cell. We make this assumption as it allows us to solve the local scale problems that we will obtain from the asymptotic homogenization technique on a finite subset of the domain. However, the analysis that follows could be carried out by assuming local boundedness of fields only (see, for example, [19] and [90]).*

Remark 12. *(Uniformity on the global scale) It is clear that in principle the local scale geometry can vary with respect to the global scale (See [87], [19], [48], [88], [32]). This*

dependence is however, in general neglected for the sake of simplicity. This means that the material can be described as macroscopically uniform, i.e the local scale geometry does not depend on the global scale variable $\mathbf{x}$*. We make this assumption here. This means that we have the simple differentiation under the integral sign given by*

$$\int_{\Omega} \nabla_{\mathbf{x}} \cdot (\bullet)\, d\mathbf{y} = \nabla_{\mathbf{x}} \cdot \int_{\Omega} (\bullet)\, d\mathbf{y}, \tag{5.33}$$

where $(\bullet)$ *denotes a tensor or a vector quantity.*

Remark 13. *(Local scale Geometry) Up to this point we have assumed that there are many different subphases in each periodic cell, this is highlighted in Fig. 5.1 (b). In general the microstructure of biological tissues is very heterogeneous and will have many local scale subphases. Therefore, by beginning the formulation with many subphases we are relating our problem to this type of microstructure. However, for the sake of simplicity and without loss of generality it is possible to restrict our analysis to the situation where there is only one subphase embedded within each periodic cell. This is shown in Fig. 5.2 below. It would be simple to extend the model to account for a number of subphases contained in the periodic cell if this was appropriate for a specific application (See [88] where this has been done for simple elastic composites). Therefore the subscript* η *is no longer needed. Due to periodicity, we can identify the domain* Ω *with the periodic cell, which has matrix and subphase sections denoted by* Ω_{M} *and* Ω_{Sub} *respectively. The interface and corresponding normal can be defined by* $\Upsilon := \partial\Omega_{\mathrm{M}} \cap \partial\Omega_{\mathrm{Sub}}$ *and* $\mathbf{n}_{\Upsilon}$*.*

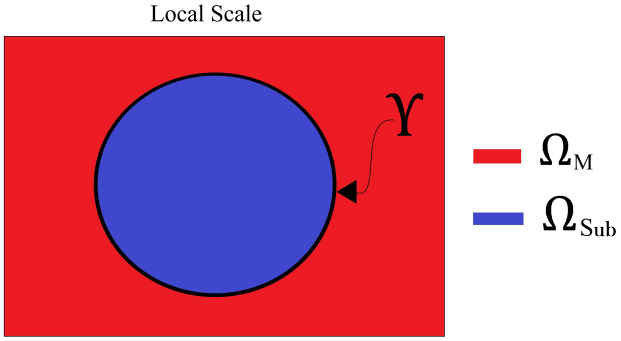

Figure 5.2: A 2D sketch of the simplified microstructure where we assume that there is only one subphase included in each periodic cell. The poroelastic matrix is shown in red and the poroelastic subphase is shown in blue. The interface Υ between the phases is shown in black.

Remark 14. *(Strain gradient effects) In this work we embrace the traditional, zeroth-order*

asymptotic homogenization method (also used for example in the derivation of the standard Biot's equations in [19]), which means that we focus on obtaining a closed system of PDEs for the zero-th order fields. We therefore formally derive the global scale model in the limit $\epsilon \to 0$. *The homogenised, zero-th order solution, (provided that the condition* (5.29) *is met) is supposed to be accurate assuming that strain gradient effects, which would be taken into account by fully considering further terms in the power series expansion* (5.32)*, are negligible. In this work, this condition is deemed acceptable as we are assuming that there exists a sharp length scale separation in the system and we are considering a quasi-static scenario (i.e. inertia is neglected), so that rates are supposed to be small. However, it is possible not to enforce the strict limit as* $\epsilon \to 0$ *(motivated by either the presence of non-negligible strain gradients triggered by fast rates and/or by* ϵ *not being sufficiently small for higher order terms to be ignored) and to extend the macroscopic stress-strain relation to include strain gradients in the formulation. For a clear derivation of this extended macroscopic stress-strain relation for periodic elastic media see [42]. Additionally, for further details see [109], [111] and [2], and the large number of references therein, where strain gradient effects are discussed in detail for a variety of physical scenarios of interest.*

Next, we exploit the two-scale asymptotic homogenization method to obtain the global scale equations describing the behaviour of the double poroelastic material.

5.3 The global double poroelastic results

The assumptions (5.31) and (5.32) of the two-scale asymptotic homogenization technique can now be applied to the system of equations (5.17-5.28). This gives the following multiscale PDEs

$$\epsilon \nabla_{\mathbf{x}} \cdot \boldsymbol{\sigma}^{\epsilon}_{\mathrm{M}} + \nabla_{\mathbf{y}} \cdot \boldsymbol{\sigma}^{\epsilon}_{\mathrm{M}} = 0 \qquad \text{in} \quad \Omega_{\mathrm{M}}, \tag{5.34}$$

$$\epsilon \nabla_{\mathbf{x}} \cdot \boldsymbol{\sigma}^{\epsilon}_{\mathrm{S}} + \nabla_{\mathbf{y}} \cdot \boldsymbol{\sigma}^{\epsilon}_{\mathrm{S}} = 0 \qquad \text{in} \quad \Omega_{\mathrm{Sub}}, \tag{5.35}$$

$$\epsilon \boldsymbol{\sigma}^{\epsilon}_{\mathrm{M}} = \mathbb{C}_{\mathrm{M}} : \xi_{\mathbf{y}} \mathbf{u}^{\epsilon}_{\mathrm{M}} + \epsilon \mathbb{C}_{\mathrm{M}} : \xi_{\mathbf{x}} \mathbf{u}^{\epsilon}_{\mathrm{M}} - \epsilon \boldsymbol{\alpha}_{\mathrm{M}} \vartheta^{\epsilon}_{\mathrm{M}} \qquad \text{in} \quad \Omega_{\mathrm{M}}, \tag{5.36}$$

$$\epsilon \boldsymbol{\sigma}^{\epsilon}_{\mathrm{S}} = \mathbb{C}_{\mathrm{S}} : \xi_{\mathbf{y}} \mathbf{u}^{\epsilon}_{\mathrm{S}} + \epsilon \mathbb{C}_{\mathrm{S}} : \xi_{\mathbf{x}} \mathbf{u}^{\epsilon}_{\mathrm{S}} - \epsilon \boldsymbol{\alpha}_{\mathrm{S}} \vartheta^{\epsilon}_{\mathrm{S}} \qquad \text{in} \quad \Omega_{\mathrm{Sub}}, \tag{5.37}$$

$$\epsilon \mathbf{w}^{\epsilon}_{\mathrm{M}} = -\mathsf{K}_{\mathrm{M}} \nabla_{\mathbf{y}} \vartheta^{\epsilon}_{\mathrm{M}} - \epsilon \mathsf{K}_{\mathrm{M}} \nabla_{\mathbf{x}} \vartheta^{\epsilon}_{\mathrm{M}} \qquad \text{in} \quad \Omega_{\mathrm{M}}, \tag{5.38}$$

$$\epsilon \mathbf{w}^{\epsilon}_{\mathrm{S}} = -\mathsf{K}_{\mathrm{S}} \nabla_{\mathbf{y}} \vartheta^{\epsilon}_{\mathrm{S}} - \epsilon \mathsf{K}_{\mathrm{S}} \nabla_{\mathbf{x}} \vartheta^{\epsilon}_{\mathrm{S}} \qquad \text{in} \quad \Omega_{\mathrm{Sub}}, \tag{5.39}$$

$$\epsilon \frac{\dot{\vartheta}^{\epsilon}_{\mathrm{M}}}{\mathcal{M}_{\mathrm{M}}} = -\boldsymbol{\alpha}_{\mathrm{M}} : \xi_{\mathbf{y}} \dot{\mathbf{u}}^{\epsilon}_{\mathrm{M}} - \epsilon \boldsymbol{\alpha}_{\mathrm{M}} : \xi_{\mathbf{x}} \dot{\mathbf{u}}^{\epsilon}_{\mathrm{M}} - \nabla_{\mathbf{y}} \cdot \mathbf{w}^{\epsilon}_{\mathrm{M}} - \epsilon \nabla_{\mathbf{x}} \cdot \mathbf{w}^{\epsilon}_{\mathrm{M}} \qquad \text{in} \quad \Omega_{\mathrm{M}}, \tag{5.40}$$

$$\epsilon\frac{\dot{\vartheta}_{\rm S}^{\epsilon}}{\mathcal{M}_{\rm S}} = -\boldsymbol{\alpha}_{\rm S} : \xi_{\mathbf{y}}\dot{\mathbf{u}}_{\rm S}^{\epsilon} - \epsilon\boldsymbol{\alpha}_{\rm S} : \xi_{\mathbf{x}}\dot{\mathbf{u}}_{\rm S}^{\epsilon} - \nabla_{\mathbf{y}}\cdot\mathbf{w}_{\rm S}^{\epsilon} - \epsilon\nabla_{\mathbf{x}}\cdot\mathbf{w}_{\rm S}^{\epsilon} \quad \text{in} \quad \Omega_{\rm Sub}, \tag{5.41}$$

$$\boldsymbol{\sigma}_{\rm M}^{\epsilon}\mathbf{n}_{\Upsilon} = \boldsymbol{\sigma}_{\rm S}^{\epsilon}\mathbf{n}_{\Upsilon} \quad \text{on} \quad \Upsilon, \tag{5.42}$$

$$\mathbf{u}_{\rm M}^{\epsilon} = \mathbf{u}_{\rm S}^{\epsilon} \quad \text{on} \quad \Upsilon, \tag{5.43}$$

$$\vartheta_{\rm M}^{\epsilon} = \vartheta_{\rm S}^{\epsilon} \quad \text{on} \quad \Upsilon, \tag{5.44}$$

$$\mathbf{w}_{\rm M}^{\epsilon}\cdot\mathbf{n}_{\Upsilon} = \mathbf{w}_{\rm S}^{\epsilon}\cdot\mathbf{n}_{\Upsilon} \quad \text{on} \quad \Upsilon, \tag{5.45}$$

where representation (5.32) is implied in relationships (5.34-5.45) and indicated by the superscript ϵ. We also have periodic conditions on the cell boundary $\partial\Omega \setminus \Upsilon$. We then proceed by equating the same terms multiplying the various powers of ϵ^l, $l = 0, 1, \ldots$. This way, we derive the global double poroelastic model in terms of the zero-th order variables.

We can equate the coefficients of ϵ^0 in equations (5.34-5.45), which gives,

$$\nabla_{\mathbf{y}}\cdot\boldsymbol{\sigma}_{\rm M}^{(0)} = 0 \quad \text{in} \quad \Omega_{\rm M}, \tag{5.46}$$

$$\nabla_{\mathbf{y}}\cdot\boldsymbol{\sigma}_{\rm S}^{(0)} = 0 \quad \text{in} \quad \Omega_{\rm Sub}, \tag{5.47}$$

$$\mathbb{C}_{\rm M} : \xi_{\mathbf{y}}\mathbf{u}_{\rm M}^{(0)} = 0 \quad \text{in} \quad \Omega_{\rm M}, \tag{5.48}$$

$$\mathbb{C}_{\rm S} : \xi_{\mathbf{y}}\mathbf{u}_{\rm S}^{(0)} = 0 \quad \text{in} \quad \Omega_{\rm Sub}, \tag{5.49}$$

$$\nabla_{\mathbf{y}}\vartheta_{\rm M}^{(0)} = 0 \quad \text{in} \quad \Omega_{\rm M}, \tag{5.50}$$

$$\nabla_{\mathbf{y}}\vartheta_{\rm S}^{(0)} = 0 \quad \text{in} \quad \Omega_{\rm Sub}, \tag{5.51}$$

$$\boldsymbol{\alpha}_{\rm M} : \xi_{\mathbf{y}}\dot{\mathbf{u}}_{\rm M}^{(0)} + \nabla_{\mathbf{y}}\cdot\mathbf{w}_{\rm M}^{(0)} = 0 \quad \text{in} \quad \Omega_{\rm M}, \tag{5.52}$$

$$\boldsymbol{\alpha}_{\rm S} : \xi_{\mathbf{y}}\dot{\mathbf{u}}_{\rm S}^{(0)} + \nabla_{\mathbf{y}}\cdot\mathbf{w}_{\rm S}^{(0)} = 0 \quad \text{in} \quad \Omega_{\rm Sub}, \tag{5.53}$$

$$\boldsymbol{\sigma}_{\rm M}^{(0)}\mathbf{n}_{\Upsilon} = \boldsymbol{\sigma}_{\rm S}^{(0)}\mathbf{n}_{\Upsilon} \quad \text{on} \quad \Upsilon, \tag{5.54}$$

$$\mathbf{u}_{\rm M}^{(0)} = \mathbf{u}_{\rm S}^{(0)} \quad \text{on} \quad \Upsilon, \tag{5.55}$$

$$\vartheta_{\rm M}^{(0)} = \vartheta_{\rm S}^{(0)} \quad \text{on} \quad \Upsilon, \tag{5.56}$$

$$\mathbf{w}_{\rm M}^{(0)}\cdot\mathbf{n}_{\Upsilon} = \mathbf{w}_{\rm S}^{(0)}\cdot\mathbf{n}_{\Upsilon} \quad \text{on} \quad \Upsilon. \tag{5.57}$$

From (5.48) and (5.49) we can see that $\mathbf{u}_{\rm M}^{(0)}$ and $\mathbf{u}_{\rm S}^{(0)}$ are rigid body motions in $\mathbf{y}$ for each $\mathbf{x}$ and so by $\mathbf{y}$-periodicity we deduce that

$$\mathbf{u}_{\rm M}^{(0)} = \mathbf{u}_{\rm M}^{(0)}(\mathbf{x}, t) \quad \text{and} \quad \mathbf{u}_{\rm S}^{(0)} = \mathbf{u}_{\rm S}^{(0)}(\mathbf{x}, t), \tag{5.58}$$

respectively. Since we also have the continuity of leading order displacements (5.55) then

we can define

$$\mathbf{u}^{(0)}(\mathbf{x},t) := \mathbf{u}_{\mathrm{M}}^{(0)} = \mathbf{u}_{\mathrm{S}}^{(0)}. \tag{5.59}$$

From (5.50) and (5.51) we have that

$$\vartheta_{\mathrm{M}}^{(0)} = \vartheta_{\mathrm{M}}^{(0)}(\mathbf{x},t) \quad \text{and} \quad \vartheta_{\mathrm{S}}^{(0)} = \vartheta_{\mathrm{S}}^{(0)}(\mathbf{x},t), \tag{5.60}$$

respectively. Again since we also have the continuity of leading order pressures (5.56) then we can define

$$\vartheta^{(0)}(\mathbf{x},t) := \vartheta_{\mathrm{M}}^{(0)} = \vartheta_{\mathrm{S}}^{(0)}. \tag{5.61}$$

We will use the new notations (5.59) and (5.61) in the remainder of this work.

Now equating the coefficients of ϵ^1 in the system of PDEs (5.34-5.45) we obtain,

$$\nabla_{\mathbf{x}} \cdot \boldsymbol{\sigma}_{\mathrm{M}}^{(0)} + \nabla_{\mathbf{y}} \cdot \boldsymbol{\sigma}_{\mathrm{M}}^{(1)} = 0 \qquad \text{in} \quad \Omega_{\mathrm{M}}, \tag{5.62}$$

$$\nabla_{\mathbf{x}} \cdot \boldsymbol{\sigma}_{\mathrm{S}}^{(0)} + \nabla_{\mathbf{y}} \cdot \boldsymbol{\sigma}_{\mathrm{S}}^{(1)} = 0 \qquad \text{in} \quad \Omega_{\mathrm{Sub}}, \tag{5.63}$$

$$\boldsymbol{\sigma}_{\mathrm{M}}^{(0)} = \mathbb{C}_{\mathrm{M}} : \xi_{\mathbf{y}} \mathbf{u}_{\mathrm{M}}^{(1)} + \mathbb{C}_{\mathrm{M}} : \xi_{\mathbf{x}} \mathbf{u}^{(0)} - \boldsymbol{\alpha}_{\mathrm{M}} \vartheta^{(0)} \qquad \text{in} \quad \Omega_{\mathrm{M}}, \tag{5.64}$$

$$\boldsymbol{\sigma}_{\mathrm{S}}^{(0)} = \mathbb{C}_{\mathrm{S}} : \xi_{\mathbf{y}} \mathbf{u}_{\mathrm{S}}^{(1)} + \mathbb{C}_{\mathrm{S}} : \xi_{\mathbf{x}} \mathbf{u}^{(0)} - \boldsymbol{\alpha}_{\mathrm{S}} \vartheta^{(0)} \qquad \text{in} \quad \Omega_{\mathrm{Sub}}, \tag{5.65}$$

$$\mathbf{w}_{\mathrm{M}}^{(0)} = -\mathsf{K}_{\mathrm{M}} \nabla_{\mathbf{y}} \vartheta_{\mathrm{M}}^{(1)} - \mathsf{K}_{\mathrm{M}} \nabla_{\mathbf{x}} \vartheta^{(0)} \qquad \text{in} \quad \Omega_{\mathrm{M}}, \tag{5.66}$$

$$\mathbf{w}_{\mathrm{S}}^{(0)} = -\mathsf{K}_{\mathrm{S}} \nabla_{\mathbf{y}} \vartheta_{\mathrm{S}}^{(1)} - \mathsf{K}_{\mathrm{S}} \nabla_{\mathbf{x}} \vartheta^{(0)} \qquad \text{in} \quad \Omega_{\mathrm{Sub}}, \tag{5.67}$$

$$\frac{\dot{\vartheta}^{(0)}}{\mathcal{M}_{\mathrm{M}}} = -\boldsymbol{\alpha}_{\mathrm{M}} : \xi_{\mathbf{y}} \dot{\mathbf{u}}_{\mathrm{M}}^{(1)} - \boldsymbol{\alpha}_{\mathrm{M}} : \xi_{\mathbf{x}} \dot{\mathbf{u}}_{\mathrm{M}}^{(0)} - \nabla_{\mathbf{y}} \cdot \mathbf{w}_{\mathrm{M}}^{(1)} - \nabla_{\mathbf{x}} \cdot \mathbf{w}_{\mathrm{M}}^{(0)} \qquad \text{in} \quad \Omega_{\mathrm{M}}, \tag{5.68}$$

$$\frac{\dot{\vartheta}^{(0)}}{\mathcal{M}_{\mathrm{S}}} = -\boldsymbol{\alpha}_{\mathrm{S}} : \xi_{\mathbf{y}} \dot{\mathbf{u}}_{\mathrm{S}}^{(1)} - \boldsymbol{\alpha}_{\mathrm{S}} : \xi_{\mathbf{x}} \dot{\mathbf{u}}_{\mathrm{S}}^{(0)} - \nabla_{\mathbf{y}} \cdot \mathbf{w}_{\mathrm{S}}^{(1)} - \nabla_{\mathbf{x}} \cdot \mathbf{w}_{\mathrm{S}}^{(0)} \qquad \text{in} \quad \Omega_{\mathrm{Sub}}, \tag{5.69}$$

$$\boldsymbol{\sigma}_{\mathrm{M}}^{(1)} \mathbf{n}_{\Upsilon} = \boldsymbol{\sigma}_{\mathrm{S}}^{(1)} \mathbf{n}_{\Upsilon} \qquad \text{on} \quad \Upsilon, \tag{5.70}$$

$$\mathbf{u}_{\mathrm{M}}^{(1)} = \mathbf{u}_{\mathrm{S}}^{(1)} \qquad \text{on} \quad \Upsilon, \tag{5.71}$$

$$\vartheta_{\mathrm{M}}^{(1)} = \vartheta_{\mathrm{S}}^{(1)} \qquad \text{on} \quad \Upsilon, \tag{5.72}$$

$$\mathbf{w}_{\mathrm{M}}^{(1)} \cdot \mathbf{n}_{\Upsilon} = \mathbf{w}_{\mathrm{S}}^{(1)} \cdot \mathbf{n}_{\Upsilon} \qquad \text{on} \quad \Upsilon. \tag{5.73}$$

We also define the specific cell average operator as

$$\langle \varphi \rangle_v = \frac{1}{|\Omega|} \int_{\Omega_v} \varphi_v(\mathbf{x},\mathbf{y},t)\, \mathrm{d}\mathbf{y} \qquad v = \mathrm{M},\, \mathrm{S}. \tag{5.74}$$

Here, φ_v is any of the components of the fields involved in our analysis in their respective

subdomains, and $|\Omega|$ represents the volume of the periodic cell. As such we have

$$|\Omega| = |\Omega_{\rm M}| + |\Omega_{\rm Sub}|. \tag{5.75}$$

The cell average over the whole periodic cell is defined as

$$\langle \varphi_{\rm M} + \varphi_{\rm S} \rangle_{\Omega} = \frac{1}{|\Omega|}\bigg(\int_{\Omega_{\rm M}} \varphi_{\rm M}(\mathbf{x},\mathbf{y},t)\,{\rm d}\mathbf{y} + \int_{\Omega_{\rm Sub}} \varphi_{\rm S}(\mathbf{x},\mathbf{y},t)\,{\rm d}\mathbf{y}\bigg). \tag{5.76}$$

5.3.1 The global scale poroelastic constitutive relationship

Using equations (5.46), (5.47), (5.64), (5.65), (5.54) and (5.71) we can write the problem for $\mathbf{u}_{\rm M}^{(1)}$ and $\mathbf{u}_{\rm S}^{(1)}$. That is,

$$\nabla_{\mathbf{y}} \cdot (\mathbb{C}_{\rm M}\xi_{\mathbf{y}}\mathbf{u}_{\rm M}^{(1)}) = -\nabla_{\mathbf{y}} \cdot (\mathbb{C}_{\rm M}\xi_{\mathbf{x}}\mathbf{u}^{(0)}) + \nabla_{\mathbf{y}} \cdot (\vartheta^{(0)}\boldsymbol{\alpha}_{\rm M}) \ \text{ in } \Omega_{\rm M}, \tag{5.77}$$

$$\nabla_{\mathbf{y}} \cdot (\mathbb{C}_{\rm S}\xi_{\mathbf{y}}\mathbf{u}_{\rm S}^{(1)}) = -\nabla_{\mathbf{y}} \cdot (\mathbb{C}_{\rm S}\xi_{\mathbf{x}}\mathbf{u}^{(0)}) + \nabla_{\mathbf{y}} \cdot (\vartheta^{(0)}\boldsymbol{\alpha}_{\rm S}) \ \text{ in } \ \Omega_{\rm Sub}, \tag{5.78}$$

$$(\mathbb{C}_{\rm M}\xi_{\mathbf{y}}\mathbf{u}_{\rm M}^{(1)} - \mathbb{C}_{\rm S}\xi_{\mathbf{y}}\mathbf{u}_{\rm S}^{(1)})\mathbf{n}_{\Upsilon} = ((\mathbb{C}_{\rm S} - \mathbb{C}_{\rm M})\xi_{\mathbf{x}}\mathbf{u}^{(0)} - (\boldsymbol{\alpha}_{\rm S} - \boldsymbol{\alpha}_{\rm M})\vartheta^{(0)})\mathbf{n}_{\Upsilon} \ \text{ on } \ \Upsilon, \tag{5.79}$$

$$\mathbf{u}_{\rm M}^{(1)} = \mathbf{u}_{\rm S}^{(1)} \ \text{ on } \ \Upsilon. \tag{5.80}$$

The problem (5.77-5.80) admits a unique solution up to a $\mathbf{y}$ constant function. The solution, exploiting linearity, is given as,

$$\mathbf{u}_{\rm M}^{(1)} = \mathsf{B}_{\rm M}\xi_{\mathbf{x}}\mathbf{u}^{(0)} + \mathbf{b}_{\rm M}\vartheta^{(0)} + c_1(\mathbf{x}), \tag{5.81}$$

$$\mathbf{u}_{\rm S}^{(1)} = \mathsf{B}_{\rm S}\xi_{\mathbf{x}}\mathbf{u}^{(0)} + \mathbf{b}_{\rm S}\vartheta^{(0)} + c_2(\mathbf{x}), \tag{5.82}$$

where $c_1(\mathbf{x})$ and $c_2(\mathbf{x})$ are $\mathbf{y}$ constant functions. The third order tensors $\mathsf{B}_{\rm M}$ and $\mathsf{B}_{\rm S}$ are the solutions of the local scale problems given below

$$\nabla_{\mathbf{y}} \cdot (\mathbb{C}_{\rm M}\xi_{\mathbf{y}}\mathsf{B}_{\rm M}) = -\nabla_{\mathbf{y}} \cdot \mathbb{C}_{\rm M} \qquad \text{in} \quad \Omega_{\rm M}, \tag{5.83}$$

$$\nabla_{\mathbf{y}} \cdot (\mathbb{C}_{\rm S}\xi_{\mathbf{y}}\mathsf{B}_{\rm S}) = -\nabla_{\mathbf{y}} \cdot \mathbb{C}_{\rm S} \qquad \text{in} \quad \Omega_{\rm Sub}, \tag{5.84}$$

$$(\mathbb{C}_{\rm M}\xi_{\mathbf{y}}\mathsf{B}_{\rm M} - \mathbb{C}_{\rm S}\xi_{\mathbf{y}}\mathsf{B}_{\rm S})\mathbf{n}_{\Upsilon} = (\mathbb{C}_{\rm S} - \mathbb{C}_{\rm M})\mathbf{n}_{\Upsilon} \qquad \text{on} \quad \Upsilon, \tag{5.85}$$

$$\mathsf{B}_{\rm M} = \mathsf{B}_{\rm S} \qquad \text{on} \quad \Upsilon. \tag{5.86}$$

The vectors $\mathbf{b}_{\mathrm{M}}$ and $\mathbf{b}_{\mathrm{S}}$ satisfy the elastic-type problem given by

$$\nabla_{\mathbf{y}} \cdot (\mathbb{C}_{\mathrm{M}} \xi_{\mathbf{y}} \mathbf{b}_{\mathrm{M}}) = \nabla_{\mathbf{y}} \cdot \boldsymbol{\alpha}_{\mathrm{M}} \qquad \text{in} \quad \Omega_{\mathrm{M}}, \tag{5.87}$$

$$\nabla_{\mathbf{y}} \cdot (\mathbb{C}_{\mathrm{S}} \xi_{\mathbf{y}} \mathbf{b}_{\mathrm{S}}) = \nabla_{\mathbf{y}} \cdot \boldsymbol{\alpha}_{\mathrm{S}} \qquad \text{in} \quad \Omega_{\mathrm{Sub}}, \tag{5.88}$$

$$(\mathbb{C}_{\mathrm{M}} \xi_{\mathbf{y}} \mathbf{b}_{\mathrm{M}} - \mathbb{C}_{\mathrm{S}} \xi_{\mathbf{y}} \mathbf{b}_{\mathrm{S}}) \mathbf{n}_{\Upsilon} = -(\boldsymbol{\alpha}_{\mathrm{S}} - \boldsymbol{\alpha}_{\mathrm{M}}) \mathbf{n}_{\Upsilon} \qquad \text{on} \quad \Upsilon, \tag{5.89}$$

$$\mathbf{b}_{\mathrm{M}} = \mathbf{b}_{\mathrm{S}} \qquad \text{on} \quad \Upsilon. \tag{5.90}$$

Both the problems (5.83-5.86) and (5.87-5.90) are to be solved on the cell and be equipped with periodic conditions on $\partial\Omega \setminus \Upsilon$. We also require one further condition on the auxiliary variables B_{M}, B_{S}, $\mathbf{b}_{\mathrm{M}}$ and $\mathbf{b}_{\mathrm{S}}$ to ensure uniqueness, for example

$$\langle \mathsf{B}_{\mathrm{M}} + \mathsf{B}_{\mathrm{S}} \rangle_{\Omega} = 0 \quad \text{and} \quad \langle \mathbf{b}_{\mathrm{M}} + \mathbf{b}_{\mathrm{S}} \rangle_{\Omega} = 0. \tag{5.91}$$

For the cell problems (5.83-5.86) and (5.87-5.90) in components see Appendix A.2.

We can use (5.81-5.82) to write the leading order effective stress tensors in both the matrix and the subphase respectively as

$$\begin{aligned} \boldsymbol{\sigma}_{\mathrm{M}}^{(0)} &= \mathbb{C}_{\mathrm{M}} \xi_{\mathbf{y}} (\mathsf{B}_{\mathrm{M}} \xi_{\mathbf{x}} \mathbf{u}^{(0)} + \mathbf{b}_{\mathrm{M}} \vartheta^{(0)}) + \mathbb{C}_{\mathrm{M}} \xi_{\mathbf{x}} \mathbf{u}^{(0)} - \boldsymbol{\alpha}_{\mathrm{M}} \vartheta^{(0)} \\ &= (\mathbb{C}_{\mathrm{M}} \mathbb{L}_{\mathrm{M}} + \mathbb{C}_{\mathrm{M}}) \xi_{\mathbf{x}} \mathbf{u}^{(0)} + (\mathbb{C}_{\mathrm{M}} \boldsymbol{\tau}_{\mathrm{M}} - \boldsymbol{\alpha}_{\mathrm{M}}) \vartheta^{(0)}, \end{aligned} \tag{5.92}$$

where we have the auxiliary tensors

$$\mathbb{L}_{\mathrm{M}} = \xi_{\mathbf{y}} \mathsf{B}_{\mathrm{M}} \qquad \text{and} \qquad \boldsymbol{\tau}_{\mathrm{M}} = \xi_{\mathbf{y}} \mathbf{b}_{\mathrm{M}}, \tag{5.93}$$

and

$$\begin{aligned} \boldsymbol{\sigma}_{\mathrm{S}}^{(0)} &= \mathbb{C}_{\mathrm{S}} \xi_{\mathbf{y}} (\mathsf{B}_{\mathrm{S}} \xi_{\mathbf{x}} \mathbf{u}^{(0)} + \mathbf{b}_{\mathrm{S}} \vartheta^{(0)}) + \mathbb{C}_{\mathrm{S}} \xi_{\mathbf{x}} \mathbf{u}^{(0)} - \boldsymbol{\alpha}_{\mathrm{S}} \vartheta^{(0)} \\ &= (\mathbb{C}_{\mathrm{S}} \mathbb{L}_{\mathrm{S}} + \mathbb{C}_{\mathrm{S}}) \xi_{\mathbf{x}} \mathbf{u}^{(0)} + (\mathbb{C}_{\mathrm{S}} \boldsymbol{\tau}_{\mathrm{S}} - \boldsymbol{\alpha}_{\mathrm{S}}) \vartheta^{(0)}, \end{aligned} \tag{5.94}$$

where we have the auxiliary tensors

$$\mathbb{L}_{\mathrm{S}} = \xi_{\mathbf{y}} \mathsf{B}_{\mathrm{S}} \qquad \text{and} \qquad \boldsymbol{\tau}_{\mathrm{S}} = \xi_{\mathbf{y}} \mathbf{b}_{\mathrm{S}}. \tag{5.95}$$

Summing up the integral averages of (5.62) and (5.63) gives

$$\int_{\Omega_{\mathrm{M}}} \nabla_{\mathbf{y}} \cdot \boldsymbol{\sigma}_{\mathrm{M}}^{(1)} \mathrm{d}\mathbf{y} + \int_{\Omega_{\mathrm{Sub}}} \nabla_{\mathbf{y}} \cdot \boldsymbol{\sigma}_{\mathrm{S}}^{(1)} \mathrm{d}\mathbf{y} + \int_{\Omega_{\mathrm{M}}} \nabla_{\mathbf{x}} \cdot \boldsymbol{\sigma}_{\mathrm{M}}^{(0)} \mathrm{d}\mathbf{y} + \int_{\Omega_{\mathrm{Sub}}} \nabla_{\mathbf{x}} \cdot \boldsymbol{\sigma}_{\mathrm{S}}^{(0)} \mathrm{d}\mathbf{y} = 0. \quad (5.96)$$

Application of the divergence theorem to the first two integrals and applying the assumption of macroscopic uniformity to the last two integrals gives

$$\begin{aligned} &\int_{\partial\Omega_{\mathrm{M}}\setminus\Upsilon} \boldsymbol{\sigma}_{\mathrm{M}}^{(1)} \mathbf{n}_{\Upsilon}^{\Omega_{\mathrm{M}}\setminus\Upsilon} \mathrm{dS} + \int_{\Upsilon} \boldsymbol{\sigma}_{\mathrm{M}}^{(1)} \mathbf{n}_{\Upsilon} \mathrm{dS} + \int_{\partial\Omega_{\mathrm{Sub}}\setminus\Upsilon} \boldsymbol{\sigma}_{\mathrm{S}}^{(1)} \mathbf{n}_{\Upsilon}^{\Omega_{\mathrm{Sub}}\setminus\Upsilon} \mathrm{dS} - \int_{\Upsilon} \boldsymbol{\sigma}_{\mathrm{S}}^{(1)} \mathbf{n}_{\Upsilon} \mathrm{dS} \\ &+ \nabla_{\mathbf{x}} \cdot \int_{\Omega_{\mathrm{M}}} \boldsymbol{\sigma}_{\mathrm{M}}^{(0)} \mathrm{d}\mathbf{y} + \nabla_{\mathbf{x}} \cdot \int_{\Omega_{\mathrm{Sub}}} \boldsymbol{\sigma}_{\mathrm{S}}^{(0)} \mathrm{d}\mathbf{y} = 0, \end{aligned} \quad (5.97)$$

where $\mathbf{n}_{\Upsilon}$, $\mathbf{n}_{\Upsilon}^{\Omega_{\mathrm{M}}\setminus\Upsilon}$ and $\mathbf{n}_{\Upsilon}^{\Omega_{\mathrm{Sub}}\setminus\Upsilon}$ are the unit normals corresponding to Υ, $\partial\Omega_{\mathrm{M}} \setminus \Upsilon$ and $\partial\Omega_{\mathrm{Sub}} \setminus \Upsilon$. The terms on the boundaries $\partial\Omega_{\mathrm{M}} \setminus \Upsilon$ and $\partial\Omega_{\mathrm{Sub}} \setminus \Upsilon$ cancel due to periodicity and the terms on Υ cancel due to (5.70). So we have

$$\nabla_{\mathbf{x}} \cdot \langle \boldsymbol{\sigma}_{\mathrm{M}}^{(0)} \rangle_{\mathrm{M}} + \nabla_{\mathbf{x}} \cdot \langle \boldsymbol{\sigma}_{\mathrm{S}}^{(0)} \rangle_{\mathrm{S}} = 0, \quad (5.98)$$

which can be written as

$$\nabla_{\mathbf{x}} \cdot \langle \boldsymbol{\sigma}_{\mathrm{M}}^{(0)} + \boldsymbol{\sigma}_{\mathrm{S}}^{(0)} \rangle_{\Omega} = 0, \quad (5.99)$$

by exploiting notation (5.76). We therefore have

$$\nabla_{\mathbf{x}} \cdot \boldsymbol{\sigma}_{\mathrm{eff}} = 0, \quad (5.100)$$

where

$$\begin{aligned} \boldsymbol{\sigma}_{\mathrm{eff}} &= \langle \boldsymbol{\sigma}_{\mathrm{M}}^{(0)} + \boldsymbol{\sigma}_{\mathrm{S}}^{(0)} \rangle_{\Omega} \quad (5.101) \\ &= \langle \mathbb{C}_{\mathrm{M}} \mathbb{L}_{\mathrm{M}} + \mathbb{C}_{\mathrm{M}} + \mathbb{C}_{\mathrm{S}} \mathbb{L}_{\mathrm{S}} + \mathbb{C}_{\mathrm{S}} \rangle_{\Omega} : \xi_{\mathbf{x}} \mathbf{u}^{(0)} + \langle \mathbb{C}_{\mathrm{M}} \boldsymbol{\tau}_{\mathrm{M}} + \mathbb{C}_{\mathrm{S}} \boldsymbol{\tau}_{\mathrm{S}} - \boldsymbol{\alpha}_{\mathrm{M}} - \boldsymbol{\alpha}_{\mathrm{S}} \rangle_{\Omega} \vartheta^{(0)}. \end{aligned}$$

Relationship (5.101) represents the global scale constitutive equation for the double poroelastic material, where the effective drained elasticity tensor is defined as

$$\bar{\mathbb{C}} = \langle \mathbb{C}_{\mathrm{M}} \mathbb{L}_{\mathrm{M}} + \mathbb{C}_{\mathrm{M}} + \mathbb{C}_{\mathrm{S}} \mathbb{L}_{\mathrm{S}} + \mathbb{C}_{\mathrm{S}} \rangle_{\Omega}. \quad (5.102)$$

Next, we derive the effective Darcy's law and close the global scale system of PDEs.

5.3.2 The effective Darcy's law

We can use (5.52), (5.53), (5.72) and (5.57) to write the following problem for $\vartheta_{\mathrm{M}}^{(1)}$ and $\vartheta_{\mathrm{S}}^{(1)}$

$$\nabla_{\mathbf{y}} \cdot \mathbf{w}_{\mathrm{M}}^{(0)} = \mathbf{0} \qquad \text{in} \quad \Omega_{\mathrm{M}}, \tag{5.103}$$

$$\nabla_{\mathbf{y}} \cdot \mathbf{w}_{\mathrm{S}}^{(0)} = \mathbf{0} \qquad \text{in} \quad \Omega_{\mathrm{Sub}}, \tag{5.104}$$

$$\vartheta_{\mathrm{M}}^{(1)} = \vartheta_{\mathrm{S}}^{(1)} \qquad \text{on} \quad \Upsilon, \tag{5.105}$$

$$\mathbf{w}_{\mathrm{M}}^{(0)} \cdot \mathbf{n}_{\Upsilon} = \mathbf{w}_{\mathrm{S}}^{(0)} \cdot \mathbf{n}_{\Upsilon} \qquad \text{on} \quad \Upsilon. \tag{5.106}$$

Using the expressions (5.66) and (5.67) for $\mathbf{w}_{\mathrm{M}}^{(0)}$ and $\mathbf{w}_{\mathrm{S}}^{(0)}$ we can rewrite the problem (5.103-5.106) as

$$\nabla_{\mathbf{y}} \cdot (\mathsf{K}_{\mathrm{M}} \nabla_{\mathbf{y}} \vartheta_{\mathrm{M}}^{(1)}) = -\nabla_{\mathbf{y}} \cdot (\mathsf{K}_{\mathrm{M}} \nabla_{\mathbf{x}} \vartheta^{(0)}) \qquad \text{in} \quad \Omega_{\mathrm{M}}, \tag{5.107}$$

$$\nabla_{\mathbf{y}} \cdot (\mathsf{K}_{\mathrm{S}} \nabla_{\mathbf{y}} \vartheta_{\mathrm{S}}^{(1)}) = -\nabla_{\mathbf{y}} \cdot (\mathsf{K}_{\mathrm{S}} \nabla_{\mathbf{x}} \vartheta^{(0)}) \qquad \text{in} \quad \Omega_{\mathrm{Sub}}, \tag{5.108}$$

$$\vartheta_{\mathrm{M}}^{(1)} = \vartheta_{\mathrm{S}}^{(1)} \qquad \text{on} \quad \Upsilon, \tag{5.109}$$

$$(\mathsf{K}_{\mathrm{M}} \nabla_{\mathbf{y}} \vartheta_{\mathrm{M}}^{(1)} - \mathsf{K}_{\mathrm{S}} \nabla_{\mathbf{y}} \vartheta_{\mathrm{S}}^{(1)}) \cdot \mathbf{n}_{\Upsilon} = ((\mathsf{K}_{\mathrm{S}} - \mathsf{K}_{\mathrm{M}}) \nabla_{\mathbf{x}} \vartheta^{(0)}) \cdot \mathbf{n}_{\Upsilon} \qquad \text{on} \quad \Upsilon. \tag{5.110}$$

The problem given by (5.107-5.110) admits a unique solution up to a $\mathbf{y}$ constant function (see [27], [7]). Exploiting linearity we have,

$$\vartheta_{\mathrm{M}}^{(1)} = \hat{\boldsymbol{\vartheta}}_{\mathrm{M}} \cdot \nabla_{\mathbf{x}} \vartheta^{(0)} + c_3(\mathbf{x}), \tag{5.111}$$

$$\vartheta_{\mathrm{S}}^{(1)} = \hat{\boldsymbol{\vartheta}}_{\mathrm{S}} \cdot \nabla_{\mathbf{x}} \vartheta^{(0)} + c_4(\mathbf{x}), \tag{5.112}$$

where $c_3(\mathbf{x})$ and $c_4(\mathbf{x})$ are $\mathbf{y}$ constant functions and $\hat{\boldsymbol{\vartheta}}_{\mathrm{M}}$ and $\hat{\boldsymbol{\vartheta}}_{\mathrm{S}}$ are vectors which satisfy the following cell problem

$$\nabla_{\mathbf{y}} \cdot (\nabla_{\mathbf{y}} \hat{\boldsymbol{\vartheta}}_{\mathrm{M}} \mathsf{K}_{\mathrm{M}}^{\mathrm{T}}) = -\nabla_{\mathbf{y}} \cdot \mathsf{K}_{\mathrm{M}}^{\mathrm{T}} \qquad \text{in} \quad \Omega_{\mathrm{M}}, \tag{5.113}$$

$$\nabla_{\mathbf{y}} \cdot (\nabla_{\mathbf{y}} \hat{\boldsymbol{\vartheta}}_{\mathrm{S}} \mathsf{K}_{\mathrm{S}}^{\mathrm{T}}) = -\nabla_{\mathbf{y}} \cdot \mathsf{K}_{\mathrm{S}}^{\mathrm{T}} \qquad \text{in} \quad \Omega_{\mathrm{Sub}}, \tag{5.114}$$

$$\hat{\boldsymbol{\vartheta}}_{\mathrm{M}} = \hat{\boldsymbol{\vartheta}}_{\mathrm{S}} \qquad \text{on} \quad \Upsilon, \tag{5.115}$$

$$(\nabla_{\mathbf{y}} \hat{\boldsymbol{\vartheta}}_{\mathrm{M}} \mathsf{K}_{\mathrm{M}}^{\mathrm{T}} - \nabla_{\mathbf{y}} \hat{\boldsymbol{\vartheta}}_{\mathrm{S}} \mathsf{K}_{\mathrm{S}}^{\mathrm{T}}) \mathbf{n}_{\Upsilon} = (\mathsf{K}_{\mathrm{S}} - \mathsf{K}_{\mathrm{M}})^{\mathrm{T}} \mathbf{n}_{\Upsilon} \qquad \text{on} \quad \Upsilon. \tag{5.116}$$

The anisotropic Poisson's-type cell problem (5.113-5.116) is to be supplemented by periodic conditions on the boundary $\partial\Omega \setminus \Upsilon$ and a further condition has to be placed on $\hat{\boldsymbol{\vartheta}}_{\mathrm{M}}$ and

$\hat{\boldsymbol{\vartheta}}_{\mathrm{S}}$ to ensure the solution is unique, for example

$$\langle \hat{\boldsymbol{\vartheta}}_{\mathrm{M}} + \hat{\boldsymbol{\vartheta}}_{\mathrm{S}} \rangle_{\Omega} = 0. \tag{5.117}$$

For cell problem (5.113-5.116) in components see Appendix A.1.

Using the expressions (5.111) and (5.112) for $\vartheta_{\mathrm{M}}^{(1)}$ and $\vartheta_{\mathrm{S}}^{(1)}$ in (5.66) and (5.67) and taking the integral average (5.74) gives

$$\begin{aligned} \langle \mathbf{w}_{\mathrm{M}}^{(0)} \rangle_{\mathrm{M}} &= -\langle \mathsf{K}_{\mathrm{M}} (\nabla_{\mathbf{y}} \hat{\boldsymbol{\vartheta}}_{\mathrm{M}})^{\mathrm{T}} \rangle_{\mathrm{M}} \nabla_{\mathbf{x}} \vartheta^{(0)} - \langle \mathsf{K}_{\mathrm{M}} \rangle_{\mathrm{M}} \nabla_{\mathbf{x}} \vartheta^{(0)} \\ &= -\langle \mathsf{K}_{\mathrm{M}} \mathsf{R}_{\mathrm{M}} + \mathsf{K}_{\mathrm{M}} \rangle_{\mathrm{M}} \nabla_{\mathbf{x}} \vartheta^{(0)}, \end{aligned} \tag{5.118}$$

where we have used the notation

$$\mathsf{R}_{\mathrm{M}} = (\nabla_{\mathbf{y}} \hat{\boldsymbol{\vartheta}}_{\mathrm{M}})^{\mathrm{T}}, \tag{5.119}$$

and

$$\begin{aligned} \langle \mathbf{w}_{\mathrm{S}}^{(0)} \rangle_{\mathrm{S}} &= -\langle \mathsf{K}_{\mathrm{S}} (\nabla_{\mathbf{y}} \hat{\boldsymbol{\vartheta}}_{\mathrm{S}})^{\mathrm{T}} \rangle_{\mathrm{S}} \nabla_{\mathbf{x}} \vartheta^{(0)} - \langle \mathsf{K}_{\mathrm{S}} \rangle_{\mathrm{S}} \nabla_{\mathbf{x}} \vartheta^{(0)} \\ &= -\langle \mathsf{K}_{\mathrm{S}} \mathsf{R}_{\mathrm{S}} + \mathsf{K}_{\mathrm{S}} \rangle_{\mathrm{S}} \nabla_{\mathbf{x}} \vartheta^{(0)}, \end{aligned} \tag{5.120}$$

where we have used the notation

$$\mathsf{R}_{\mathrm{S}} = (\nabla_{\mathbf{y}} \hat{\boldsymbol{\vartheta}}_{\mathrm{S}})^{\mathrm{T}}. \tag{5.121}$$

Then we have the effective Darcy's law

$$\mathbf{w}_{\mathrm{eff}} := \langle \mathbf{w}_{\mathrm{M}}^{(0)} + \mathbf{w}_{\mathrm{S}}^{(0)} \rangle_{\Omega} = -\langle \mathsf{K}_{\mathrm{M}} \mathsf{R}_{\mathrm{M}} + \mathsf{K}_{\mathrm{M}} + \mathsf{K}_{\mathrm{S}} \mathsf{R}_{\mathrm{S}} + \mathsf{K}_{\mathrm{S}} \rangle_{\Omega} \nabla_{\mathbf{x}} \vartheta^{(0)}. \tag{5.122}$$

We can define the hydraulic conductivity tensor for this structure as

$$\mathsf{W} = \langle \mathsf{K}_{\mathrm{M}} \mathsf{R}_{\mathrm{M}} + \mathsf{K}_{\mathrm{M}} + \mathsf{K}_{\mathrm{S}} \mathsf{R}_{\mathrm{S}} + \mathsf{K}_{\mathrm{S}}, \rangle_{\Omega} \tag{5.123}$$

and rewrite Darcy's Law as

$$\mathbf{w}_{\mathrm{eff}} = -\mathsf{W} \nabla_{\mathbf{x}} \vartheta^{(0)}. \tag{5.124}$$

We now wish to obtain the conservation of mass equation. We integrate the expressions

(5.68) and (5.69) in Ω_{M} and Ω_{Sub} respectively. That is

$$\begin{aligned}\int_{\Omega_{\mathrm{M}}}\frac{\dot{\vartheta}^{(0)}}{\mathcal{M}_{\mathrm{M}}}\mathrm{d}\mathbf{y}+\int_{\Omega_{\mathrm{Sub}}}\frac{\dot{\vartheta}^{(0)}}{\mathcal{M}_{\mathrm{S}}}\mathrm{d}\mathbf{y}&=-\int_{\Omega_{\mathrm{M}}}\boldsymbol{\alpha}_{\mathrm{M}}:\xi_{\mathbf{x}}\dot{\mathbf{u}}^{(0)}\mathrm{d}\mathbf{y}-\nabla_{\mathbf{x}}\cdot\int_{\Omega_{\mathrm{M}}}\mathbf{w}_{\mathrm{M}}^{(0)}\mathrm{d}\mathbf{y}\\&-\int_{\Omega_{\mathrm{Sub}}}\boldsymbol{\alpha}_{\mathrm{S}}:\xi_{\mathbf{x}}\dot{\mathbf{u}}^{(0)}\mathrm{d}\mathbf{y}-\nabla_{\mathbf{x}}\cdot\int_{\Omega_{\mathrm{Sub}}}\mathbf{w}_{\mathrm{S}}^{(0)}\mathrm{d}\mathbf{y}-\int_{\Omega_{\mathrm{M}}}\boldsymbol{\alpha}_{\mathrm{M}}:\xi_{\mathbf{y}}\dot{\mathbf{u}}_{\mathrm{M}}^{(1)}\mathrm{d}\mathbf{y}\\&-\int_{\Omega_{\mathrm{Sub}}}\boldsymbol{\alpha}_{\mathrm{S}}:\xi_{\mathbf{y}}\dot{\mathbf{u}}_{\mathrm{S}}^{(1)}\mathrm{d}\mathbf{y}-\int_{\Omega_{\mathrm{M}}}\nabla_{\mathbf{y}}\cdot\mathbf{w}_{\mathrm{M}}^{(1)}\mathrm{d}\mathbf{y}-\int_{\Omega_{\mathrm{Sub}}}\nabla_{\mathbf{y}}\cdot\mathbf{w}_{\mathrm{S}}^{(1)}\mathrm{d}\mathbf{y}.\end{aligned}\tag{5.125}$$

Applying the divergence theorem and using (5.73) cancels the final two integrals and we can rewrite the remaining terms as

$$\begin{aligned}\left(\frac{\langle\mathcal{M}_{\mathrm{M}}+\mathcal{M}_{\mathrm{S}}\rangle_{\Omega}}{\langle\mathcal{M}_{\mathrm{M}}\rangle_{\mathrm{M}}\langle\mathcal{M}_{\mathrm{S}}\rangle_{\mathrm{S}}}\right)\dot{\vartheta}^{(0)}&=-\langle\boldsymbol{\alpha}_{\mathrm{M}}+\boldsymbol{\alpha}_{\mathrm{S}}\rangle_{\Omega}\xi_{\mathbf{x}}\dot{\mathbf{u}}^{(0)}-\nabla_{\mathbf{x}}\cdot\langle\mathbf{w}_{\mathrm{M}}^{(0)}+\mathbf{w}_{\mathrm{S}}^{(0)}\rangle_{\Omega}\\&\quad-\langle\boldsymbol{\alpha}_{\mathrm{M}}:\xi_{\mathbf{y}}\dot{\mathbf{u}}_{\mathrm{M}}^{(1)}+\boldsymbol{\alpha}_{\mathrm{S}}:\xi_{\mathbf{y}}\dot{\mathbf{u}}_{\mathrm{S}}^{(1)}\rangle_{\Omega}.\end{aligned}\tag{5.126}$$

We can use the expressions for $\mathbf{u}_{\mathrm{M}}^{(1)}$ and $\mathbf{u}_{\mathrm{S}}^{(1)}$ from (5.81) and (5.82) to obtain $\dot{\mathbf{u}}_{\mathrm{M}}^{(1)}$ and $\dot{\mathbf{u}}_{\mathrm{S}}^{(1)}$ and using these in (5.126) we obtain

$$\left(\frac{\langle\mathcal{M}_{\mathrm{M}}+\mathcal{M}_{\mathrm{S}}\rangle_{\Omega}}{\langle\mathcal{M}_{\mathrm{M}}\rangle_{\mathrm{M}}\langle\mathcal{M}_{\mathrm{S}}\rangle_{\mathrm{S}}}\right)\dot{\vartheta}^{(0)}=-\Big(\langle\boldsymbol{\alpha}_{\mathrm{M}}+\boldsymbol{\alpha}_{\mathrm{S}}\rangle_{\Omega}:\xi_{\mathbf{x}}\dot{\mathbf{u}}^{(0)}+\nabla_{\mathbf{x}}\cdot\mathbf{w}_{\mathrm{eff}}\tag{5.127}$$

$$+\langle\mathbb{L}_{\mathrm{M}}^{\mathrm{T}}:\boldsymbol{\alpha}_{\mathrm{M}}+\mathbb{L}_{\mathrm{S}}^{\mathrm{T}}:\boldsymbol{\alpha}_{\mathrm{S}}\rangle_{\Omega}:\xi_{\mathbf{x}}\dot{\mathbf{u}}^{(0)}+\langle\boldsymbol{\alpha}_{\mathrm{M}}:\boldsymbol{\tau}_{\mathrm{M}}+\boldsymbol{\alpha}_{\mathrm{S}}:\boldsymbol{\tau}_{\mathrm{S}}\rangle_{\Omega}\dot{\vartheta}^{(0)}\Big).\tag{5.128}$$

Rearranging (5.127) to obtain an expression for $\dot{\vartheta}^{(0)}$ we obtain

$$\dot{\vartheta}^{(0)}=-\bar{\mathcal{M}}\Big(\nabla_{\mathbf{x}}\cdot\mathbf{w}_{\mathrm{eff}}+\langle\boldsymbol{\alpha}_{\mathrm{M}}+\boldsymbol{\alpha}_{\mathrm{S}}+\mathbb{L}_{\mathrm{M}}^{\mathrm{T}}:\boldsymbol{\alpha}_{\mathrm{M}}+\mathbb{L}_{\mathrm{S}}^{\mathrm{T}}:\boldsymbol{\alpha}_{\mathrm{S}}\rangle_{\Omega}:\xi_{\mathbf{x}}\dot{\mathbf{u}}^{(0)}\Big),\tag{5.129}$$

where we define

$$\bar{\mathcal{M}}:=\frac{\langle\mathcal{M}_{\mathrm{M}}\rangle_{\mathrm{M}}\langle\mathcal{M}_{\mathrm{S}}\rangle_{\mathrm{S}}}{\langle\mathcal{M}_{\mathrm{M}}\rangle_{\mathrm{M}}+\langle\mathcal{M}_{\mathrm{S}}\rangle_{\mathrm{S}}+\langle\mathcal{M}_{\mathrm{M}}\rangle_{\mathrm{M}}\langle\mathcal{M}_{\mathrm{S}}\rangle_{\mathrm{S}}(\langle\boldsymbol{\alpha}_{\mathrm{M}}:\boldsymbol{\tau}_{\mathrm{M}}\rangle_{\mathrm{M}}+\langle\boldsymbol{\alpha}_{\mathrm{S}}:\boldsymbol{\tau}_{\mathrm{S}}\rangle_{\mathrm{S}})},\tag{5.130}$$

which reminds of the Biot's modulus for the system. We can also define the tensor

$$\widetilde{\boldsymbol{\alpha}}:=\langle\boldsymbol{\alpha}_{\mathrm{M}}+\boldsymbol{\alpha}_{\mathrm{S}}+\mathbb{L}_{\mathrm{M}}^{\mathrm{T}}:\boldsymbol{\alpha}_{\mathrm{M}}+\mathbb{L}_{\mathrm{S}}^{\mathrm{T}}:\boldsymbol{\alpha}_{\mathrm{S}}\rangle_{\Omega},\tag{5.131}$$

which has the form of an effective Biot's tensor of coefficients.

Equations (5.100), (5.101), (5.122), (5.129), collectively represent, from a formal standpoint, a poroelastic-type system of PDEs in terms of the zero-th order displacement, ve-

locity, and pressure fields, i.e.

$$\nabla_{\mathbf{x}} \cdot \boldsymbol{\sigma}_{\text{eff}} = 0, \tag{5.132a}$$

$$\boldsymbol{\sigma}_{\text{eff}} = \langle \mathbb{C}_{\text{M}}\mathbb{L}_{\text{M}} + \mathbb{C}_{\text{M}} + \mathbb{C}_{\text{S}}\mathbb{L}_{\text{S}} + \mathbb{C}_{\text{S}} \rangle_{\Omega} : \xi_{\mathbf{x}}\mathbf{u}^{(0)} + \langle \mathbb{C}_{\text{M}}\boldsymbol{\tau}_{\text{M}} + \mathbb{C}_{\text{S}}\boldsymbol{\tau}_{\text{S}} - \boldsymbol{\alpha}_{\text{M}} - \boldsymbol{\alpha}_{\text{S}} \rangle_{\Omega}\vartheta^{(0)}, \tag{5.132b}$$

$$\mathbf{w}_{\text{eff}} = -\langle \mathsf{K}_{\text{M}}\mathsf{R}_{\text{M}} + \mathsf{K}_{\text{M}} + \mathsf{K}_{\text{S}}\mathsf{R}_{\text{S}} + \mathsf{K}_{\text{S}} \rangle_{\Omega} \nabla_{\mathbf{x}}\vartheta^{(0)}, \tag{5.132c}$$

$$\dot{\vartheta}^{(0)} = -\bar{\mathcal{M}}\big(\nabla_{\mathbf{x}} \cdot \mathbf{w}_{\text{eff}} + \widetilde{\boldsymbol{\alpha}} : \xi_{\mathbf{x}}\dot{\mathbf{u}}^{(0)}\big), \tag{5.132d}$$

where we have that $\vartheta^{(0)}$ is the global scale pressure, $\mathbf{w}_{\text{eff}}$ comprises the average of $\mathbf{w}_{\text{M}}^{(0)}$ and $\mathbf{w}_{\text{S}}^{(0)}$ which are the leading order relative fluid velocities in the matrix and subphase respectively, $\mathbf{u}^{(0)}$ is the solid displacement and $\dot{\mathbf{u}}^{(0)}$ is the solid velocity. Our model (5.132) is formally of poroelastic-type. We can conclude from our global scale model that the mechanical behaviour of a double poroelastic material can be fully described by the material's effective elasticity tensor $\bar{\mathbb{C}}$, the hydraulic conductivity tensor W, the tensor $\widetilde{\boldsymbol{\alpha}}$ which is reminiscent of the classical Biot's tensor of coefficients and the scalar quantity $\bar{\mathcal{M}}$ which can be identified with the Biot's modulus. For a step-by-step guide to solving the global scale model (5.132) see Appendix A.2.

It is important to note that our global scale model (5.132) reduces to previously obtained results when we consider the following limit cases. The first case is in the limit of no fluid present in either our matrix or subphases. In this case the model reduces to that of elastic composites (see [89]). When we assume that the subphase is purely elastic and the matrix remains poroelastic we recover the works of [105] and [24]. We provide a more detailed description and recover these limits in the appendix A.1.

Within the next section we will discuss each of the global scale coefficients in detail as well as discussing the key novelties of the new model. We will then prove that our model is both formally and substantially of poroelastic type by defining a global Biot's tensor of coefficients and proving the resulting Biot's modulus is positive.

5.4 Properties of the coefficients on the global scale

The coefficients of the global scale model (5.132) that fully characterize the mechanical behaviour of the double poroelastic material are the effective elasticity tensor $\bar{\mathbb{C}}$, the hydraulic conductivity tensor W, the Biot's tensor of coefficients $\widetilde{\boldsymbol{\alpha}}$ and the scalar Biot's

modulus $\bar{\mathcal{M}}$. These can be interpreted physically as follows. The constitutive law, which is of poroelastic-type, has the drained effective elasticity tensor given by

$$\bar{\mathbb{C}} = \langle \mathbb{C}_{\mathrm{M}}\mathbb{L}_{\mathrm{M}} + \mathbb{C}_{\mathrm{M}} + \mathbb{C}_{\mathrm{S}}\mathbb{L}_{\mathrm{S}} + \mathbb{C}_{\mathrm{S}} \rangle_{\Omega}. \tag{5.133}$$

We should note here that the $\mathbb{C}_{\mathrm{M}}$ and $\mathbb{C}_{\mathrm{S}}$ are actually the effective elasticity tensors from carrying out the homogenization process at the finer scale. These effective elasticity tensors are positive semi-definite and possess both major and minor symmetries. The hydraulic conductivity tensor is given by

$$\mathsf{W} = \langle \mathsf{K}_{\mathrm{M}}\mathsf{R}_{\mathrm{M}} + \mathsf{K}_{\mathrm{M}} + \mathsf{K}_{\mathrm{S}}\mathsf{R}_{\mathrm{S}} + \mathsf{K}_{\mathrm{S}} \rangle_{\Omega}. \tag{5.134}$$

This hydraulic conductivity tensor comprises the hydraulic conductivities K_{M} and K_{S} from the matrix and subphase respectively, as well as two additional terms $\mathsf{K}_{\mathrm{M}}\mathsf{R}_{\mathrm{M}}$ and $\mathsf{K}_{\mathrm{S}}\mathsf{R}_{\mathrm{S}}$ which account for the differences in the hydraulic conductivities of the subphase and the matrix at different points on the local scale. This hydraulic conductivity tensor can be found by solving the cell problem (5.113-5.116).

We can consider the effective Biot's tensor of coefficients $\widetilde{\boldsymbol{\alpha}}$.

Remark 15. *(Effective Biot's tensor of coefficients $\widetilde{\boldsymbol{\alpha}}$) We have the effective Biot's tensor of coefficients given by*

$$\widetilde{\boldsymbol{\alpha}} := \langle \boldsymbol{\alpha}_{\mathrm{M}} + \boldsymbol{\alpha}_{\mathrm{S}} + \mathbb{L}_{\mathrm{M}}^{\mathrm{T}} : \boldsymbol{\alpha}_{\mathrm{M}} + \mathbb{L}_{\mathrm{S}}^{\mathrm{T}} : \boldsymbol{\alpha}_{\mathrm{S}} \rangle_{\Omega}. \tag{5.135}$$

The first two terms are the Biot's tensors from the matrix and subphase respectively and we should view the third and fourth terms of this expression as the contributions arising from considering the changing compressibility at different points on the microstructure. These final two terms can be thought of as a correction term to the typical cell average (see (5.74)). We should note however, that when $\boldsymbol{\alpha}_{\mathrm{M}} = \boldsymbol{\alpha}_{\mathrm{S}} = \alpha$, where α is a constant then we can write $\widetilde{\boldsymbol{\alpha}}$ as

$$\widetilde{\boldsymbol{\alpha}} = \langle \alpha + \alpha + \alpha(\mathbb{L}_{\mathrm{M}} + \mathbb{L}_{\mathrm{S}}) \rangle_{\Omega}. \tag{5.136}$$

We have that $\langle \mathbb{L}_{\mathrm{M}} + \mathbb{L}_{\mathrm{S}} \rangle_{\Omega} = 0$, as proved in [89], where the notation $\mathbb{M}$ has been used by [89] instead of $\mathbb{L}$ to denote the same auxiliary tensor. This holds here since the cell problem (5.83 - 5.86) for $\mathbb{L}_{\mathrm{M}}$ and $\mathbb{L}_{\mathrm{S}}$ is the cell problem for composites found in [89]. Therefore in this specific case $\widetilde{\boldsymbol{\alpha}}$ is the proper cell average of the Biot's tensor of coefficients from the

individual phases given by

$$\widetilde{\boldsymbol{\alpha}} = \langle \alpha + \alpha \rangle_{\Omega} = \langle \alpha \rangle_{\mathrm{M}} + \langle \alpha \rangle_{\mathrm{S}}. \tag{5.137}$$

Finally, the resulting Biot's modulus $\bar{\mathcal{M}}$ comprises the coefficients $\mathcal{M}_{\mathrm{M}}$ and $\mathcal{M}_{\mathrm{S}}$ as well as other terms involving $\boldsymbol{\alpha}_{\mathrm{M}}$, $\boldsymbol{\alpha}_{\mathrm{S}}$, $\boldsymbol{\tau}_{\mathrm{M}}$ and $\boldsymbol{\tau}_{\mathrm{S}}$. We can consider the physical interpretations of $\bar{\mathcal{M}}$ for two possible scenarios. When $\boldsymbol{\alpha}_{\mathrm{M}}$ and $\boldsymbol{\alpha}_{\mathrm{S}}$ are not equal or constants then $\bar{\mathcal{M}}$ comprises the average of $\mathcal{M}_{\mathrm{M}}$ and $\mathcal{M}_{\mathrm{S}}$ and two other terms that account for local changes in the compressibility occurring on the microstructure. When $\boldsymbol{\alpha}_{\mathrm{M}} = \boldsymbol{\alpha}_{\mathrm{S}} = \alpha$, where α is a constant then the effective Biot's modulus $\bar{\mathcal{M}}$ is given by the harmonic mean. The effective Biot's modulus $\bar{\mathcal{M}}$ is the inverse of a storage coefficient. Under constant volumetric strain, it can be defined as the increase in the amount of fluid as a result of a unit increase in pore pressure.

Our new model has key features that make it differ substantially from other models of poroelasticity, poroelastic composites or composite materials. That is, this model is able to account for the behaviour of two different poroelastic compartments and the interactions between them. We are therefore able to address the scenario where there exists a difference in the poroelastic properties of the material which could potentially be dictated by a difference in the elastic, fluid and geometrical properties at the local scale. This model is of particular benefit to physiological applications. For example, in the cardiac muscle the interstitial matrix with embedded fibroblast cells can be considered using this model (see [74]). The interstitial matrix is clearly poroelastic and so too are the fibroblast cells, so using our novel model in this situation would allow the poroelastic behaviour of each of these phases to be considered individually leading to a much more realistic description of the material. The key distinction between the current model and previous models in the literature is the fact that our model coefficients can encode the difference in a full set of poroelastic parameters. These coefficients are to be calculated by solving differential problems on a finite subset of the given microstructure. The cell problem (5.87-5.90), is novel and is the key feature that encodes the changes in compressibility, stiffness and geometry of the two phases in the model coefficients. This means that these local scale variations in compressibility, stiffness and geometry are encoded in the global scale coefficients such as the average Biot's modulus and the Biot's tensor of coefficients, which provides a precise description of the effective material behaviour. Overall our novel model

reads as a comprehensive framework to describe materials that are composites comprising of two different poroelastic structures.

Within the next subsection we will prove properties of the effective coefficients of the model which allow us to conclude that our novel global scale model is truly of poroelastic type.

5.4.1 Biot's tensor of coefficients and Biot's modulus

In this Section we demonstrate a) the existence of a tensor which plays the role of the classical Biot's tensor of coefficients via a suitable analytical identity and b) the global scale coefficient $\bar{\mathcal{M}}$ is positive, which then qualifies as the global Biot's modulus for the double poroelastic material. Throughout the proofs of these properties we will use the cell problems in components which can be found in Appendix A.2. We will also make use of Gauss' (divergence) theorem. The following two theorems involve the global scale model coefficients which we summarise here, for convenience, as

$$\widetilde{\boldsymbol{\alpha}} := \langle \boldsymbol{\alpha}_{\mathrm{M}} + \boldsymbol{\alpha}_{\mathrm{S}} + \mathbb{L}_{\mathrm{M}}^{\mathrm{T}} : \boldsymbol{\alpha}_{\mathrm{M}} + \mathbb{L}_{\mathrm{S}}^{\mathrm{T}} : \boldsymbol{\alpha}_{\mathrm{S}} \rangle_{\Omega}, \tag{5.138}$$

$$\bar{\boldsymbol{\gamma}} := \langle \mathbb{C}_{\mathrm{M}} \boldsymbol{\tau}_{\mathrm{M}} + \mathbb{C}_{\mathrm{S}} \boldsymbol{\tau}_{\mathrm{S}} - \boldsymbol{\alpha}_{\mathrm{M}} - \boldsymbol{\alpha}_{\mathrm{S}} \rangle_{\Omega}, \tag{5.139}$$

$$\bar{\mathcal{M}} := \frac{\langle \mathcal{M}_{\mathrm{M}} \rangle_{\mathrm{M}} \langle \mathcal{M}_{\mathrm{S}} \rangle_{\mathrm{S}}}{\langle \mathcal{M}_{\mathrm{M}} \rangle_{\mathrm{M}} + \langle \mathcal{M}_{\mathrm{S}} \rangle_{\mathrm{S}} + \langle \mathcal{M}_{\mathrm{M}} \rangle_{\mathrm{M}} \langle \mathcal{M}_{\mathrm{S}} \rangle_{\mathrm{S}} (\langle \boldsymbol{\alpha}_{\mathrm{M}} : \boldsymbol{\tau}_{\mathrm{M}} \rangle_{\mathrm{M}} + \langle \boldsymbol{\alpha}_{\mathrm{S}} : \boldsymbol{\tau}_{\mathrm{S}} \rangle_{\mathrm{S}})}, \tag{5.140}$$

where $\widetilde{\boldsymbol{\alpha}}$ and $\bar{\mathcal{M}}$ are from (5.130) and (5.131) respectively. The coefficient $\bar{\boldsymbol{\gamma}}$ multiplies the global scale pressure $\vartheta^{(0)}$ in the constitutive equation (5.101). We now state and prove the first theorem. We start by focusing on the Biot's tensor of coefficients.

Theorem 4 (Biot's tensor of coefficients)**.** *The global scale coefficients $\bar{\boldsymbol{\gamma}}$ and $\widetilde{\boldsymbol{\alpha}}$ are related by the following relationship*

$$\bar{\boldsymbol{\gamma}} = -\widetilde{\boldsymbol{\alpha}}. \tag{5.141}$$

The existence of this equality guarantees that the tensor $\widetilde{\boldsymbol{\alpha}}$ can be regarded as the Biot's tensor of coefficients for the double poroelastic material on the global scale.

Proof. We begin by writing $\bar{\boldsymbol{\gamma}}$ and $\widetilde{\boldsymbol{\alpha}}$ in components as

$$\bar{\gamma}_{ij} = \langle \mathcal{C}_{ijkl}^{\mathrm{M}} \xi_{kl}(b^{\mathrm{M}}) + \mathcal{C}_{ijkl}^{\mathrm{S}} \xi_{kl}(b^{\mathrm{S}}) - \alpha_{ij}^{\mathrm{M}} - \alpha_{ij}^{\mathrm{S}} \rangle_{\Omega}, \tag{5.142}$$

$$\widetilde{\alpha}_{ij} = \langle \alpha_{ij}^{\mathrm{M}} + \alpha_{ij}^{\mathrm{S}} + \xi_{kl}^{ij}(B^{\mathrm{M}}) \alpha_{kl}^{\mathrm{M}} + \xi_{kl}^{ij}(B^{\mathrm{S}}) \alpha_{kl}^{\mathrm{S}} \rangle_{\Omega}. \tag{5.143}$$

We use (5.83) and (5.84) from the cell problems, in components, and multiply by b_i^{M}, b_i^{S} (which are the cell problem solutions) respectively. Integrating over Ω_{M} and Ω_{Sub}, respectively, yields

$$\begin{aligned}&\int_{\Omega_{\mathrm{M}}}\frac{\partial}{\partial y_j}(\mathcal{C}^{\mathrm{M}}_{ijpq}\xi^{kl}_{pq}(B^{\mathrm{M}}))b_i^{\mathrm{M}}\mathrm{d}\mathbf{y}+\int_{\Omega_{\mathrm{M}}}\frac{\partial}{\partial y_j}(\mathcal{C}^{\mathrm{M}}_{ijkl})b_i^{\mathrm{M}}\mathrm{d}\mathbf{y}\\&+\int_{\Omega_{\mathrm{Sub}}}\frac{\partial}{\partial y_j}(\mathcal{C}^{\mathrm{S}}_{ijpq}\xi^{kl}_{pq}(B^{\mathrm{S}}))b_i^{\mathrm{S}}\mathrm{d}\mathbf{y}+\int_{\Omega_{\mathrm{Sub}}}\frac{\partial}{\partial y_j}(\mathcal{C}^{\mathrm{S}}_{ijkl})b_i^{\mathrm{S}}\mathrm{d}\mathbf{y}=0.\end{aligned}\tag{5.144}$$

We perform integration by parts to obtain

$$\begin{aligned}&\int_{\Omega_{\mathrm{M}}}\frac{\partial}{\partial y_j}(\mathcal{C}^{\mathrm{M}}_{ijpq}\xi^{kl}_{pq}(B^{\mathrm{M}})b_i^{\mathrm{M}})\mathrm{d}\mathbf{y}-\int_{\Omega_{\mathrm{M}}}\mathcal{C}^{\mathrm{M}}_{ijpq}\xi^{kl}_{pq}(B^{\mathrm{M}})\frac{\partial b_i^{\mathrm{M}}}{\partial y_j}\mathrm{d}\mathbf{y}+\int_{\Omega_{\mathrm{M}}}\frac{\partial}{\partial y_j}(\mathcal{C}^{\mathrm{M}}_{ijkl}b_i^{\mathrm{M}})\mathrm{d}\mathbf{y}\\&-\int_{\Omega_{\mathrm{M}}}\mathcal{C}^{\mathrm{M}}_{ijkl}\frac{\partial b_i^{\mathrm{M}}}{\partial y_j}\mathrm{d}\mathbf{y}+\int_{\Omega_{\mathrm{Sub}}}\frac{\partial}{\partial y_j}(\mathcal{C}^{\mathrm{S}}_{ijpq}\xi^{kl}_{pq}(B^{\mathrm{S}})b_i^{\mathrm{S}})\mathrm{d}\mathbf{y}-\int_{\Omega_{\mathrm{Sub}}}\mathcal{C}^{\mathrm{S}}_{ijpq}\xi^{kl}_{pq}(B^{\mathrm{S}})\frac{\partial b_i^{\mathrm{S}}}{\partial y_j}\mathrm{d}\mathbf{y}\\&+\int_{\Omega_{\mathrm{Sub}}}\frac{\partial}{\partial y_j}(\mathcal{C}^{\mathrm{S}}_{ijkl}b_i^{\mathrm{S}})\mathrm{d}\mathbf{y}-\int_{\Omega_{\mathrm{Sub}}}\mathcal{C}^{\mathrm{S}}_{ijkl}\frac{\partial b_i^{\mathrm{S}}}{\partial y_j}\mathrm{d}\mathbf{y}=0.\end{aligned}\tag{5.145}$$

Enforcing Gauss' theorem and using minor symmetries of $\mathbb{C}_{\mathrm{M}}$ and $\mathbb{C}_{\mathrm{S}}$ we have

$$\begin{aligned}&\int_{\Upsilon}\mathcal{C}^{\mathrm{M}}_{ijpq}\xi^{kl}_{pq}(B^{\mathrm{M}})b_i^{\mathrm{M}}\cdot n_j\mathrm{dS}+\int_{\partial\Omega_{\mathrm{M}}\setminus\Upsilon}\mathcal{C}^{\mathrm{M}}_{ijpq}\xi^{kl}_{pq}(B^{\mathrm{M}})b_i^{\mathrm{M}}\cdot n_j^{\Omega_{\mathrm{M}}\setminus\Upsilon}\mathrm{dS}\\&-\int_{\Omega_{\mathrm{M}}}\mathcal{C}^{\mathrm{M}}_{ijpq}\xi^{kl}_{pq}(B^{\mathrm{M}})\xi_{ij}(b^{\mathrm{M}})\mathrm{d}\mathbf{y}+\int_{\Upsilon}\mathcal{C}^{\mathrm{M}}_{ijkl}b_i^{\mathrm{M}}\cdot n_j\mathrm{dS}+\int_{\partial\Omega_{\mathrm{M}}\setminus\Upsilon}\mathcal{C}^{\mathrm{M}}_{ijkl}b_i^{\mathrm{M}}\cdot n_j^{\Omega_{\mathrm{M}}\setminus\Upsilon}\mathrm{dS}\\&-\int_{\Omega_{\mathrm{M}}}\mathcal{C}^{\mathrm{M}}_{klij}\xi_{ij}(b^{\mathrm{M}})\mathrm{d}\mathbf{y}-\int_{\Upsilon}\mathcal{C}^{\mathrm{S}}_{ijpq}\xi^{kl}_{pq}(B^{\mathrm{S}})b_i^{\mathrm{S}}\cdot n_j\mathrm{dS}\\&+\int_{\partial\Omega_{\mathrm{Sub}}\setminus\Upsilon}\mathcal{C}^{\mathrm{S}}_{ijpq}\xi^{kl}_{pq}(B^{\mathrm{S}})b_i^{\mathrm{S}}\cdot n_j^{\Omega_{\mathrm{Sub}}\setminus\Upsilon}\mathrm{dS}-\int_{\Omega_{\mathrm{Sub}}}\mathcal{C}^{\mathrm{S}}_{ijpq}\xi^{kl}_{pq}(B^{\mathrm{S}})\xi_{ij}(b^{\mathrm{S}})\mathrm{d}\mathbf{y}\\&-\int_{\Upsilon}\mathcal{C}^{\mathrm{S}}_{ijkl}b_i^{\mathrm{S}}\cdot n_j\mathrm{dS}+\int_{\partial\Omega_{\mathrm{Sub}}\setminus\Upsilon}\mathcal{C}^{\mathrm{S}}_{ijkl}b_i^{\mathrm{S}}\cdot n_j^{\Omega_{\mathrm{Sub}}\setminus\Upsilon}\mathrm{dS}-\int_{\Omega_{\mathrm{Sub}}}\mathcal{C}^{\mathrm{S}}_{klij}\xi_{ij}(b^{\mathrm{S}})\mathrm{d}\mathbf{y}=0,\end{aligned}\tag{5.146}$$

where $\mathbf{n}_\Upsilon$, $\mathbf{n}_\Upsilon^{\Omega_{\mathrm{M}}\setminus\Upsilon}$ and $\mathbf{n}_\Upsilon^{\Omega_{\mathrm{Sub}}\setminus\Upsilon}$ are the unit normals corresponding to Υ, $\partial\Omega_{\mathrm{M}}\setminus\Upsilon$ and $\partial\Omega_{\mathrm{Sub}}\setminus\Upsilon$, and cancelling terms on the periodic boundaries due to $\mathbf{y}$-periodicity and accounting for the interface conditions (5.85) we obtain

$$\begin{aligned}&\int_{\Omega_{\mathrm{M}}}\xi_{ij}(b^{\mathrm{M}})\mathcal{C}^{\mathrm{M}}_{ijpq}\xi^{kl}_{pq}(B^{\mathrm{M}})\mathrm{d}\mathbf{y}+\int_{\Omega_{\mathrm{M}}}\mathcal{C}^{\mathrm{M}}_{klij}\xi_{ij}(b^{\mathrm{M}})\mathrm{d}\mathbf{y}+\int_{\Omega_{\mathrm{Sub}}}\xi_{ij}(b^{\mathrm{S}})\mathcal{C}^{\mathrm{S}}_{ijpq}\xi^{kl}_{pq}(B^{\mathrm{S}})\mathrm{d}\mathbf{y}\\&+\int_{\Omega_{\mathrm{Sub}}}\mathcal{C}^{\mathrm{S}}_{klij}\xi_{ij}(b^{\mathrm{S}})\mathrm{d}\mathbf{y}=0.\end{aligned}\tag{5.147}$$

Therefore we have

$$\langle \xi_{ij}(b^{\mathrm{M}})\mathcal{C}^{\mathrm{M}}_{ijpq}\xi^{kl}_{pq}(B^{\mathrm{M}}) + \xi_{ij}(b^{\mathrm{S}})\mathcal{C}^{\mathrm{S}}_{ijpq}\xi^{kl}_{pq}(B^{\mathrm{S}})\rangle_{\Omega} = -\langle \mathcal{C}^{\mathrm{M}}_{klij}\xi_{ij}(b^{\mathrm{M}}) + \mathcal{C}^{\mathrm{S}}_{klij}\xi_{ij}(b^{\mathrm{S}})\rangle_{\Omega}. \quad (5.148)$$

We now wish to multiply (5.87) and (5.88), in components, by the cell problem solutions B^{M}_{ikl}, B^{S}_{ikl} respectively and then integrate over Ω_{M} and Ω_{Sub} respectively to obtain

$$\begin{aligned}&\int_{\Omega_{\mathrm{M}}} \frac{\partial}{\partial y_j}(\mathcal{C}^{\mathrm{M}}_{ijpq}\xi_{pq}(b^{\mathrm{M}}))B^{\mathrm{M}}_{ikl}\mathrm{d}\mathbf{y} - \int_{\Omega_{\mathrm{M}}} \frac{\partial \alpha^{\mathrm{M}}_{ij}}{\partial y_j}B^{\mathrm{M}}_{ikl}\mathrm{d}\mathbf{y}\\ &+ \int_{\Omega_{\mathrm{Sub}}} \frac{\partial}{\partial y_j}(\mathcal{C}^{\mathrm{S}}_{ijpq}\xi_{pq}(b^{\mathrm{S}}))B^{\mathrm{S}}_{ikl}\mathrm{d}\mathbf{y} - \int_{\Omega_{\mathrm{Sub}}} \frac{\partial \alpha^{\mathrm{S}}_{ij}}{\partial y_j}B^{\mathrm{S}}_{ikl}\mathrm{d}\mathbf{y} = 0. \end{aligned} \quad (5.149)$$

We perform integration by parts

$$\begin{aligned}&\int_{\Omega_{\mathrm{M}}} \frac{\partial}{\partial y_j}(\mathcal{C}^{\mathrm{M}}_{ijpq}\xi_{pq}(b^{\mathrm{M}})B^{\mathrm{M}}_{ikl})\mathrm{d}\mathbf{y} - \int_{\Omega_{\mathrm{M}}} \mathcal{C}^{\mathrm{M}}_{ijpq}\xi_{pq}(b^{\mathrm{M}})\frac{\partial B^{\mathrm{M}}_{ikl}}{\partial y_j}\mathrm{d}\mathbf{y} - \int_{\Omega_{\mathrm{M}}} \frac{\partial}{\partial y_j}(\alpha^{\mathrm{M}}_{ij}B^{\mathrm{M}}_{ikl})\mathrm{d}\mathbf{y}\\ &+ \int_{\Omega_{\mathrm{M}}} \alpha^{\mathrm{M}}_{ij}\frac{\partial B^{\mathrm{M}}_{ikl}}{\partial y_j}\mathrm{d}\mathbf{y} + \int_{\Omega_{\mathrm{Sub}}} \frac{\partial}{\partial y_j}(\mathcal{C}^{\mathrm{S}}_{ijpq}\xi_{pq}(b^{\mathrm{S}})B^{\mathrm{S}}_{ikl})\mathrm{d}\mathbf{y} - \int_{\Omega_{\mathrm{Sub}}} \mathcal{C}^{\mathrm{S}}_{ijpq}\xi_{pq}(b^{\mathrm{S}})\frac{\partial B^{\mathrm{S}}_{ikl}}{\partial y_j}\mathrm{d}\mathbf{y}\\ &- \int_{\Omega_{\mathrm{Sub}}} \frac{\partial}{\partial y_j}(\alpha^{\mathrm{S}}_{ij}B^{\mathrm{S}}_{ikl})\mathrm{d}\mathbf{y} + \int_{\Omega_{\mathrm{Sub}}} \alpha^{\mathrm{S}}_{ij}\frac{\partial B^{\mathrm{S}}_{ikl}}{\partial y_j}\mathrm{d}\mathbf{y} = 0. \end{aligned} \quad (5.150)$$

We apply Gauss' theorem and using both minor and major symmetries of $\mathbb{C}_{\mathrm{M}}$ and $\mathbb{C}_{\mathrm{S}}$ we have

$$\begin{aligned}&\int_{\Upsilon}(\mathcal{C}^{\mathrm{M}}_{ijpq}\xi_{pq}(b^{\mathrm{M}})B^{\mathrm{M}}_{ikl})\cdot n_j\mathrm{dS} + \int_{\partial\Omega_{\mathrm{M}}\setminus\Upsilon}(\mathcal{C}^{\mathrm{M}}_{ijpq}\xi_{pq}(b^{\mathrm{M}})B^{\mathrm{M}}_{ikl})\cdot n_j^{\Omega_{\mathrm{M}}\setminus\Upsilon}\mathrm{dS}\\ &- \int_{\Omega_{\mathrm{M}}} \xi_{ij}(b^{\mathrm{M}})\mathcal{C}^{\mathrm{M}}_{ijpq}\xi^{kl}_{pq}(B^{\mathrm{M}})\mathrm{d}\mathbf{y} - \int_{\Upsilon}(\alpha^{\mathrm{M}}_{ij}B^{\mathrm{M}}_{ikl})\cdot n_j\mathrm{dS} - \int_{\partial\Omega_{\mathrm{M}}\setminus\Upsilon}(\alpha^{\mathrm{M}}_{ij}B^{\mathrm{M}}_{ikl})\cdot n_j^{\Omega_{\mathrm{M}}\setminus\Upsilon}\mathrm{dS}\\ &+ \int_{\Omega_{\mathrm{M}}} \alpha^{\mathrm{M}}_{ij}\frac{\partial B^{\mathrm{M}}_{ikl}}{\partial y_j}\mathrm{d}\mathbf{y} - \int_{\Upsilon}(\mathcal{C}^{\mathrm{S}}_{ijpq}\xi_{pq}(b^{\mathrm{S}})B^{\mathrm{S}}_{ikl})\cdot n_j\mathrm{dS} + \int_{\partial\Omega_{\mathrm{Sub}}\setminus\Upsilon}(\mathcal{C}^{\mathrm{S}}_{ijpq}\xi_{pq}(b^{\mathrm{S}})B^{\mathrm{S}}_{ikl})\cdot n_j^{\Omega_{\mathrm{Sub}}\setminus\Upsilon}\mathrm{dS}\\ &- \int_{\Omega_{\mathrm{Sub}}} \xi_{ij}(b^{\mathrm{S}})\mathcal{C}^{\mathrm{S}}_{ijpq}\xi^{kl}_{pq}(B^{\mathrm{S}})\mathrm{d}\mathbf{y} + \int_{\Upsilon}(\alpha^{\mathrm{S}}_{ij}B^{\mathrm{S}}_{ikl})\cdot n_j\mathrm{dS} - \int_{\partial\Omega_{\mathrm{Sub}}\setminus\Upsilon}(\alpha^{\mathrm{S}}_{ij}B^{\mathrm{S}}_{ikl})\cdot n_j^{\Omega_{\mathrm{Sub}}\setminus\Upsilon}\mathrm{dS}\\ &+ \int_{\Omega_{\mathrm{Sub}}} \alpha^{\mathrm{S}}_{ij}\frac{\partial B^{\mathrm{S}}_{ikl}}{\partial y_j}\mathrm{d}\mathbf{y} = 0, \end{aligned} \quad (5.151)$$

where $\mathbf{n}_{\Upsilon}$, $\mathbf{n}_{\Upsilon}^{\Omega_{\mathrm{M}}\setminus\Upsilon}$ and $\mathbf{n}_{\Upsilon}^{\Omega_{\mathrm{Sub}}\setminus\Upsilon}$ are the unit normals corresponding to Υ, $\partial\Omega_{\mathrm{M}}\setminus\Upsilon$ and $\partial\Omega_{\mathrm{Sub}}\setminus\Upsilon$. Cancelling terms on the periodic boundaries due to $\mathbf{y}$-periodicity and accounting for the interface conditions (5.89) and (5.86) the terms of Υ cancel. So we can write (5.151)

as

$$\int_{\Omega_{\mathrm{M}}} \alpha_{ij}^{\mathrm{M}} \frac{\partial B_{ikl}^{\mathrm{M}}}{\partial y_j} \mathrm{d}\mathbf{y} + \int_{\Omega_{\mathrm{Sub}}} \alpha_{ij}^{\mathrm{S}} \frac{\partial B_{ikl}^{\mathrm{S}}}{\partial y_j} \mathrm{d}\mathbf{y} = \int_{\Omega_{\mathrm{M}}} \xi_{ij}(b^{\mathrm{M}}) \mathcal{C}_{ijpq}^{\mathrm{M}} \xi_{pq}^{kl}(B^{\mathrm{M}}) \mathrm{d}\mathbf{y} + \int_{\Omega_{\mathrm{Sub}}} \xi_{ij}(b^{\mathrm{S}}) \mathcal{C}_{ijpq}^{\mathrm{S}} \xi_{pq}^{kl}(B^{\mathrm{S}}) \mathrm{d}\mathbf{y}. \tag{5.152}$$

Hence we have

$$\langle \xi_{ij}(b^{\mathrm{M}}) \mathcal{C}_{ijpq}^{\mathrm{M}} \xi_{pq}^{kl}(B^{\mathrm{M}}) + \xi_{ij}(b^{\mathrm{S}}) \mathcal{C}_{ijpq}^{\mathrm{S}} \xi_{pq}^{kl}(B^{\mathrm{S}}) \rangle_{\Omega} = \langle \alpha_{ij}^{\mathrm{M}} \xi_{ij}^{kl}(B^{\mathrm{M}}) + \alpha_{ij}^{\mathrm{S}} \xi_{ij}^{kl}(B^{\mathrm{S}}) \rangle_{\Omega}. \tag{5.153}$$

From (5.153) and (5.148) we have that $\langle \mathbb{C}_{\mathrm{M}} \boldsymbol{\tau}_{\mathrm{M}} + \mathbb{C}_{\mathrm{S}} \boldsymbol{\tau}_{\mathrm{S}} \rangle_{\Omega} = -\langle \mathbb{L}_{\mathrm{M}}^{\mathrm{T}} : \boldsymbol{\alpha}_{\mathrm{M}} + \mathbb{L}_{\mathrm{S}}^{\mathrm{T}} : \boldsymbol{\alpha}_{\mathrm{S}} \rangle_{\Omega}$. Therefore using this in the definitions of $\bar{\boldsymbol{\gamma}}$ and $\widetilde{\boldsymbol{\alpha}}$, we have that $\bar{\boldsymbol{\gamma}} = -\widetilde{\boldsymbol{\alpha}}$ as required. □

The model (5.132) can be recast to show its genuine poroelastic character by means of the identity we proved, namely:

$$\begin{cases} \nabla_{\mathbf{x}} \cdot \boldsymbol{\sigma}_{\mathrm{eff}} = 0, \\ \boldsymbol{\sigma}_{\mathrm{eff}} = \bar{\mathbb{C}} : \xi_{\mathbf{x}} \mathbf{u}^{(0)} - \widetilde{\boldsymbol{\alpha}} \vartheta^{(0)}, \\ \mathbf{w}_{\mathrm{eff}} = -\mathsf{W} \nabla_{\mathbf{x}} \vartheta^{(0)}, \\ \dot{\vartheta}^{(0)} = -\bar{\mathcal{M}} \big(\nabla_{\mathbf{x}} \cdot \mathbf{w}_{\mathrm{eff}} + \widetilde{\boldsymbol{\alpha}} : \xi_{\mathbf{x}} \dot{\mathbf{u}}^{(0)} \big), \end{cases} \tag{5.154}$$

where we have

$$\bar{\mathbb{C}} = \langle \mathbb{C}_{\mathrm{M}} \mathbb{L}_{\mathrm{M}} + \mathbb{C}_{\mathrm{M}} + \mathbb{C}_{\mathrm{S}} \mathbb{L}_{\mathrm{S}} + \mathbb{C}_{\mathrm{S}} \rangle_{\Omega} \quad \text{and} \quad \mathsf{W} = \langle \mathsf{K}_{\mathrm{M}} \mathsf{R}_{\mathrm{M}} + \mathsf{K}_{\mathrm{M}} + \mathsf{K}_{\mathrm{S}} \mathsf{R}_{\mathrm{S}} + \mathsf{K}_{\mathrm{S}} \rangle_{\Omega}. \tag{5.155}$$

We can now state and prove our second theorem relating to our global scale coefficients

Theorem 5 (The Biot's Modulus is positive)**.** *The Biot's modulus that arises from our system, defined by*

$$\bar{\mathcal{M}} := \frac{\langle \mathcal{M}_{\mathrm{M}} \rangle_{\mathrm{M}} \langle \mathcal{M}_{\mathrm{S}} \rangle_{\mathrm{S}}}{\langle \mathcal{M}_{\mathrm{M}} \rangle_{\mathrm{M}} + \langle \mathcal{M}_{\mathrm{S}} \rangle_{\mathrm{S}} + \langle \mathcal{M}_{\mathrm{M}} \rangle_{\mathrm{M}} \langle \mathcal{M}_{\mathrm{S}} \rangle_{\mathrm{S}} (\langle \boldsymbol{\alpha}_{\mathrm{M}} : \boldsymbol{\tau}_{\mathrm{M}} \rangle_{\mathrm{M}} + \langle \boldsymbol{\alpha}_{\mathrm{S}} : \boldsymbol{\tau}_{\mathrm{S}} \rangle_{\mathrm{S}})}, \tag{5.156}$$

is positive i.e.

$$\bar{\mathcal{M}} > 0. \tag{5.157}$$

Proof. To show that $\bar{\mathcal{M}} > 0$, we need to show that the denominator of (5.156) is positive.

So we rearrange the denominator and we then need to show that

$$\langle \boldsymbol{\alpha}_{\mathrm{M}} : \boldsymbol{\tau}_{\mathrm{M}} \rangle_{\mathrm{M}} + \langle \boldsymbol{\alpha}_{\mathrm{S}} : \boldsymbol{\tau}_{\mathrm{S}} \rangle_{\mathrm{S}} > -\left(\frac{1}{\langle \mathcal{M}_{\mathrm{M}} \rangle_{\mathrm{M}}} + \frac{1}{\langle \mathcal{M}_{\mathrm{S}} \rangle_{\mathrm{S}}} \right), \tag{5.158}$$

where $\mathcal{M}_{\mathrm{M}}$ and $\mathcal{M}_{\mathrm{S}}$ are positive definite from the homogenization process at the finer scale. We are able to show that

$$\langle \boldsymbol{\alpha}_{\mathrm{M}} : \boldsymbol{\tau}_{\mathrm{M}} \rangle_{\mathrm{M}} + \langle \boldsymbol{\alpha}_{\mathrm{S}} : \boldsymbol{\tau}_{\mathrm{S}} \rangle_{\mathrm{S}} = \langle \boldsymbol{\alpha}_{\mathrm{M}} : \boldsymbol{\tau}_{\mathrm{M}} + \boldsymbol{\alpha}_{\mathrm{S}} : \boldsymbol{\tau}_{\mathrm{S}} \rangle_{\Omega} \geq 0, \tag{5.159}$$

which means that (5.158) will be satisfied. To do this we begin by multiplying (5.87) and (5.88) by b_i^{M} and b_i^{S} respectively and integrate over Ω_{M} and Ω_{Sub}. That is

$$\begin{aligned} &\int_{\Omega_{\mathrm{M}}} \frac{\partial}{\partial y_j} (\mathcal{C}_{ijpq}^{\mathrm{M}} \xi_{pq}(b^{\mathrm{M}})) b_i^{\mathrm{M}} \mathrm{d}\mathbf{y} - \int_{\Omega_{\mathrm{M}}} \frac{\partial \alpha_{ij}^{\mathrm{M}}}{\partial y_j} b_i^{\mathrm{M}} \mathrm{d}\mathbf{y} \\ &+ \int_{\Omega_{\mathrm{Sub}}} \frac{\partial}{\partial y_j} (\mathcal{C}_{ijpq}^{\mathrm{S}} \xi_{pq}(b^{\mathrm{S}})) b_i^{\mathrm{S}} \mathrm{d}\mathbf{y} - \int_{\Omega_{\mathrm{Sub}}} \frac{\partial \alpha_{ij}^{\mathrm{S}}}{\partial y_j} b_i^{\mathrm{S}} \mathrm{d}\mathbf{y} = 0. \end{aligned} \tag{5.160}$$

Performing integration by parts

$$\begin{aligned} &\int_{\Omega_{\mathrm{M}}} \frac{\partial}{\partial y_j} (\mathcal{C}_{ijpq}^{\mathrm{M}} \xi_{pq}(b^{\mathrm{M}}) b_i^{\mathrm{M}}) \mathrm{d}\mathbf{y} - \int_{\Omega_{\mathrm{M}}} \mathcal{C}_{ijpq}^{\mathrm{M}} \xi_{pq}(b^{\mathrm{M}}) \frac{\partial b_i^{\mathrm{M}}}{\partial y_j} \mathrm{d}\mathbf{y} - \int_{\Omega_{\mathrm{M}}} \frac{\partial}{\partial y_j} (\alpha_{ij}^{\mathrm{M}} b_i^{\mathrm{M}}) \mathrm{d}\mathbf{y} \\ &+ \int_{\Omega_{\mathrm{M}}} \alpha_{ij}^{\mathrm{M}} \frac{\partial b_i^{\mathrm{M}}}{\partial y_j} \mathrm{d}\mathbf{y} + \int_{\Omega_{\mathrm{Sub}}} \frac{\partial}{\partial y_j} (\mathcal{C}_{ijpq}^{\mathrm{S}} \xi_{pq}(b^{\mathrm{S}}) b_i^{\mathrm{S}}) \mathrm{d}\mathbf{y} - \int_{\Omega_{\mathrm{Sub}}} \mathcal{C}_{ijpq}^{\mathrm{S}} \xi_{pq}(b^{\mathrm{S}}) \frac{\partial b_i^{\mathrm{S}}}{\partial y_j} \mathrm{d}\mathbf{y} \\ &- \int_{\Omega_{\mathrm{Sub}}} \frac{\partial}{\partial y_j} (\alpha_{ij}^{\mathrm{S}} b_i^{\mathrm{S}}) \mathrm{d}\mathbf{y} + \int_{\Omega_{\mathrm{Sub}}} \alpha_{ij}^{\mathrm{S}} \frac{\partial b_i^{\mathrm{S}}}{\partial y_j} \mathrm{d}\mathbf{y} = 0. \end{aligned} \tag{5.161}$$

By enforcing Gauss' theorem and using minor symmetries of $\mathbb{C}_{\mathrm{M}}$ and $\mathbb{C}_{\mathrm{S}}$ we have

$$\begin{aligned} &\int_{\Upsilon} (\mathcal{C}_{ijpq}^{\mathrm{M}} \xi_{pq}(b^{\mathrm{M}}) b_i^{\mathrm{M}}) \cdot n_j \mathrm{dS} + \int_{\partial\Omega_{\mathrm{M}} \setminus \Upsilon} (\mathcal{C}_{ijpq}^{\mathrm{M}} \xi_{pq}(b^{\mathrm{M}}) b_i^{\mathrm{M}}) \cdot n_j^{\Omega_{\mathrm{M}} \setminus \Upsilon} \mathrm{dS} \\ &- \int_{\Omega_{\mathrm{M}}} \xi_{ij}(b^{\mathrm{M}}) \mathcal{C}_{ijpq}^{\mathrm{M}} \xi_{pq}(b^{\mathrm{M}}) \mathrm{d}\mathbf{y} - \int_{\partial\Omega_{\mathrm{M}} \setminus \Upsilon} (\alpha_{ij}^{\mathrm{M}} b_i^{\mathrm{M}}) \cdot n_j^{\Omega_{\mathrm{M}} \setminus \Upsilon} \mathrm{dS} - \int_{\Upsilon} (\alpha_{ij}^{\mathrm{M}} b_i^{\mathrm{M}}) \cdot n_j \mathrm{dS} \\ &+ \int_{\Omega_{\mathrm{M}}} \alpha_{ij}^{\mathrm{M}} \frac{\partial b_i^{\mathrm{M}}}{\partial y_j} \mathrm{d}\mathbf{y} - \int_{\Upsilon} (\mathcal{C}_{ijpq}^{\mathrm{S}} \xi_{pq}(b^{\mathrm{S}}) b_i^{\mathrm{S}}) \cdot n_j \mathrm{dS} + \int_{\partial\Omega_{\mathrm{Sub}} \setminus \Upsilon} (\mathcal{C}_{ijpq}^{\mathrm{S}} \xi_{pq}(b^{\mathrm{S}}) b_i^{\mathrm{S}}) \cdot n_j^{\Omega_{\mathrm{Sub}} \setminus \Upsilon} \mathrm{dS} \\ &- \int_{\Omega_{\mathrm{Sub}}} \xi_{ij}(b^{\mathrm{S}}) \mathcal{C}_{ijpq}^{\mathrm{S}} \xi_{pq}(b^{\mathrm{S}}) \mathrm{d}\mathbf{y} + \int_{\Upsilon} (\alpha_{ij}^{\mathrm{S}} b_i^{\mathrm{S}}) \cdot n_j \mathrm{dS} - \int_{\partial\Omega_{\mathrm{Sub}} \setminus \Upsilon} (\alpha_{ij}^{\mathrm{S}} b_i^{\mathrm{S}}) \cdot n_j^{\Omega_{\mathrm{Sub}} \setminus \Upsilon} \mathrm{dS} \\ &+ \int_{\Omega_{\mathrm{Sub}}} \alpha_{ij}^{\mathrm{S}} \frac{\partial b_i^{\mathrm{S}}}{\partial y_j} \mathrm{d}\mathbf{y} = 0, \end{aligned} \tag{5.162}$$

where $\mathbf{n}_{\Upsilon}$, $\mathbf{n}_{\Upsilon}^{\Omega_{\mathrm{M}} \setminus \Upsilon}$ and $\mathbf{n}_{\Upsilon}^{\Omega_{\mathrm{Sub}} \setminus \Upsilon}$ are the unit normals corresponding to Υ, $\partial\Omega_{\mathrm{M}} \setminus \Upsilon$ and $\partial\Omega_{\mathrm{Sub}} \setminus \Upsilon$. Cancelling terms on the periodic boundaries due to $\mathbf{y}$-periodicity and using

(5.89) and (5.90) the terms on Υ cancel and so we can write (5.162) as

$$\int_{\Omega_{\mathrm{M}}} \alpha_{ij}^{\mathrm{M}} \frac{1}{2}\left(\frac{\partial b_i^{\mathrm{M}}}{\partial y_j} + \frac{\partial b_j^{\mathrm{M}}}{\partial y_i}\right) \mathrm{d}\mathbf{y} + \int_{\Omega_{\mathrm{Sub}}} \alpha_{ij}^{\mathrm{S}} \frac{1}{2}\left(\frac{\partial b_i^{\mathrm{S}}}{\partial y_j} + \frac{\partial b_j^{\mathrm{S}}}{\partial y_i}\right) \mathrm{d}\mathbf{y}$$
$$= \int_{\Omega_{\mathrm{M}}} \xi_{ij}(b^{\mathrm{M}}) \mathcal{C}_{ijpq}^{\mathrm{M}} \xi_{pq}(b^{\mathrm{M}}) \mathrm{d}\mathbf{y} + \int_{\Omega_{\mathrm{Sub}}} \xi_{ij}(b^{\mathrm{S}}) \mathcal{C}_{ijpq}^{\mathrm{S}} \xi_{pq}(b^{\mathrm{S}}) \mathrm{d}\mathbf{y}. \tag{5.163}$$

The two terms on the RHS of (5.163) are positive, so we therefore have that

$$\int_{\Omega} (\alpha_{ij}^{\mathrm{M}} \xi_{ij}(b^{\mathrm{M}}) + \alpha_{ij}^{\mathrm{S}} \xi_{ij}(b^{\mathrm{S}})) \mathrm{d}\mathbf{y} > 0. \tag{5.164}$$

Equivalently,

$$\langle \boldsymbol{\alpha}_{\mathrm{M}} : \boldsymbol{\tau}_{\mathrm{M}} + \boldsymbol{\alpha}_{\mathrm{S}} : \boldsymbol{\tau}_{\mathrm{S}} \rangle_{\Omega} > 0. \tag{5.165}$$

In the case where $\boldsymbol{\alpha}_{\mathrm{M}} = \boldsymbol{\alpha}_{\mathrm{S}} =$ constant then

$$\langle \boldsymbol{\alpha}_{\mathrm{M}} : \boldsymbol{\tau}_{\mathrm{M}} + \boldsymbol{\alpha}_{\mathrm{S}} : \boldsymbol{\tau}_{\mathrm{S}} \rangle_{\Omega} = 0. \tag{5.166}$$

Therefore we have that $\bar{\mathcal{M}} > 0$ and the proof is complete. □

We have now proved both these properties for our model coefficients. This means that our novel global scale model is both formally and substantially of poroelastic type.

5.5 Conclusion

We have presented the poroelastic system of PDEs with novel coefficients that describe the effective behaviour of double poroelastic materials, i.e. a poroelastic matrix with embedded poroelastic subphases. This type of structure represents many real-world scenarios including biological soft tissues (e.g. cardiac muscle, artery walls and tumours), soil and porous rocks. We have considered a quasi-static, multiphase problem, in the absence of body forces, consisting of the governing equations for both the poroelastic matrix and the poroelastic subphases (5.17-5.24). The governing equations for the matrix and the subphases are the equations of Biot's poroelasticity assuming anisotropy. The problem is closed by the application of the appropriate interface conditions (5.25-5.28) that arise from the continuity of tractions, displacements, pressures and fluxes across the boundary between each of the subphases and the matrix. We have then enforced the length scale separation that occurs between, the inter-subphase distance (*the local scale*) and the over-

all size of the domain (*the global scale*) to apply the asymptotic homogenization technique to upscale the structure-structure interaction problem to the system of global scale PDEs (5.132). We prove that our novel global scale model (5.132) is both formally and substantially of poroelastic type by proving a) the existence of a global scale Biot's tensor of coefficients and b) the effective Biot's Modulus is positive.

The model obtained in this work generalises [105] and [24] and is also a next natural step in the modelling of hierarchical multiscale materials. The key novelty of this work resides in taking into account the difference in a full set of poroelastic parameters characterising the matrix and the subphases. This is reflected in the new cell problem (5.87-5.90). This cell problem is driven by the changes in compressibility of the matrix and the subphase at different points in the microstructure. Solving this cell problem encodes this detail of the varying compressibility, stiffness and geometry of the microstructure in the quantities $\boldsymbol{\tau}_{\mathrm{M}}$ and $\boldsymbol{\tau}_{\mathrm{S}}$, which appear in the coefficients of the global scale model. This means that the local scale complexity is accounted for even at the global scale within the average Biot's modulus and the Biot's tensor of coefficients. We have therefore addressed the scenario where there exists a difference in the poroelastic properties of the material which could potentially be dictated by a difference in the elastic, fluid and geometrical properties of the material at the local scale. For these reasons our new formulation provides a robust framework for fully describing double poroelastic materials effectively.

The current model assumes two standard poroelastic phases at the local scale, however, it is possible to assume that one or both phases are a poroelastic composite [69]. This situation would not change the overall global scale model however, different properties would be encoded in the model coefficients due to the different porescale microstructure. The problem detailed in Sec. 5.1 would instead use the global scale model derived in [69] as the governing equations for the matrix compartment and continue with the upscaling as carried out here. The effective elasticity tensor would encode the properties of the inhomogeneous porescale material in the contributions $\mathbb{C}_{\mathrm{M}}$ and $\mathbb{C}_{\mathrm{S}}$. A situation like this could provide a more realistic setup for biological applications.

Our current model has some limitations and there are possible extensions to this current work that would extend the applicability to a wider range of scenarios. At present the model has been formulated to provide the global scale model in a quasi-static, linearized setting.

It would be straight-forward to generalise our model to include linearized inertia and

would result in additional terms in our global scale model. These changes would include the appearance of leading order linearized inertia in the effective balance equation for the effective stress (5.132a). The addition of these terms could help provide a more realistic poroelastic modelling framework for biological tissues such as organs. For example, in the lungs, this model with the addition of the inertia could lead to advances in the understanding of the acoustic properties of the lungs and be of use in non-invasive diagnosis of pulmonary diseases [107]. The extension of this work to a nonlinear elasticity setting is more challenging whilst using the two-scale asymptotic homogenization technique. There have however, been recent advances in the literature (see, for example [99] and [28]).

The natural next step would be to obtain solutions to the model on the basis of a specific microstructure with parameters specified by real-world data. This data could relate to a wide variety of biological examples. In the literature there have been three-dimensional numerical simulations carried out on the cell problems obtained from asymptotic homogenization for elastic composites and poroelastic/porous materials ([88], [35], [101]). The numerical simulations for the cell problems associated with this model would combine the strategies used within the literature. It would be possible to indeed incorporate a third scale (porescale) into this work through the computational results. With experimental data that characterised our material on the porescale and the local scale then we would be able to produce numerical simulations for our model on three scales. The porescale problems, where the fluid is flowing in the pores, would first be solved and this information would then be used as the input data in the local scale cell problems. The local scale cell problems would then be solved to provide the global scale model coefficients.

In the next chapter we carry out numerical simulations to highlight the advantages of using our novel model for poroelastic composites, detailed in Chapter 3 [69], compared with a standard Biot's poroelastic approach when investigating the elastic parameters of poroelastic materials. The results of this emphasise the necessity for the development of poroelastic models with detailed microstructures such as that of poroelastic composites.

Chapter 6

Micromechanical analysis of the effective stiffness of poroelastic composites

Within this chapter we will compare the resulting elastic parameters arising from solving the *LMRP model* [L. Miller and R. Penta, Effective Balance Equations for Poroelastic Composites, Continuum Mechanics and Thermodynamics, 32, 1533-1557 (2020)] [69], which is derived in Chapter 3, for poroelastic composites compared to the parameters that arise from solving a model for an elastic composite where the matrix is poroelastic. In other words we determine the effect of considering the interactions of three different phases (two elastic and one fluid) at the porescale compared to considering the interactions of two elastic phases one of which results from a further homogenization problem at a finer scale [19], [35]. When a material's microstructure comprises a matrix, embedded elastic subphases and fluid filled pores then using the models that are currently available in the literature (excluding the LMRP model) gives two choices. These are making the assumption that the matrix is homogeneous (ignore the subphases) or carry out a two-step process. The two-step process involves first solving the Biot's porous matrix problem and then solving the elastic composite problem that comprises the subphases and the results of the porous matrix simulations (the so-called standard poroelastic approach in this work). This second approach means that even when considering the three phases, these are not all at the same scale, which is what the intended application actually possesses as a microstructure. This means that estimations of the parameters cannot be fully reliable.

We therefore developed the LMRP model to remove this issue. This analysis will highlight under which circumstances the LMRP model provides a more accurate description of the effective elastic parameters of a poroelastic material. We can describe our computational platform for the LMRP model as robust, in the sense that it is very applicable to a variety of situations. That is, the platform can be altered for a variety of geometries including short fibres, various directions of fluid flow, a variety of different shaped inclusions and a wide range of constitutive properties of the constituents.

The chapter is organised as follows. In Sec. 6.1, we introduce the LMRP model for poroelastic composites, derived in [69], and also introduce a comparative setup that focusses on a standard poroelastic (Biot's poroelasticity) approach. In Sec. 6.2 we have a variety of subsections each individually aimed at introducing the computational setup that would be required to solve the 3D and also the reduced 2D cell problems that arise from both models introduced in Sec. 6.1. In Sec. 6.3, we provide the results of our 2D simulations and give an example of the applicability of the model to investigating the elastic parameters of the human heart. In Sec. 6.4 we carry out 3D simulations for a different geometrical setup, namely the case of short fibre elastic inclusions, and obtain the elastic parameters. In Sec. 6.5, we conclude this chapter by discussing the limitations of the current simulations and provide further perspectives of the types of problems that the model could investigate and the biological scenarios where it would be best applied. We also have an appendix which contains a detailed 2D reduction of the cell problems for the LMRP model for poroelastic composites for orthotropic constituents. This cases is the most general and under simplifying assumptions it can also be used as a framework for the 2D cell problems for standard poroelasticity and elastic composites with elastic properties with any possible symmetries.

6.1 Governing Equations

In this section we describe the governing equations for a poroelastic composite, the LMRP model [69] which is derved in Chapter 3, and the governing equations for standard Biot's poroelastic materials with elastic inclusions. In Fig. 6.1 we can see a comparison of the microstructure of each model setup. We note that in order to exemplify the difference that being able to account for multiple elastic and fluid phases all at the same scale has in comparison to the existing computational frameworks we have chosen the simplest

geometry that considers uniaxial flow and uniaxial fibre/subphase elongation. Also for the sake of symmetry we arrange the fluid flow as four cylinders in the corners of the cell. This means that we will use a modified version of the LMRP model presented in Chapter 3 where only one solid phase is in contact with the fluid. We also chose this microstructure as it allows for the reduction of the microstructural cell problems to 2D, which we present clearly in the appendix in a way that can be used as guidance to the reader who would also like to reduce to 2D their own different cell problems.

On the right-hand side of Fig. 6.1 we have the porescale microstructure (periodic cell) of the LMRP model for poroelastic composites. We can see that this structure comprises a porous matrix Ω_{II}, and elastic inclusion Ω_{I} and fluid filled pores Ω_{f}. The interface between the matrix and the inclusion is denoted Γ_{III} and the interface between the matrix and the fluid is denoted Γ_{II}.

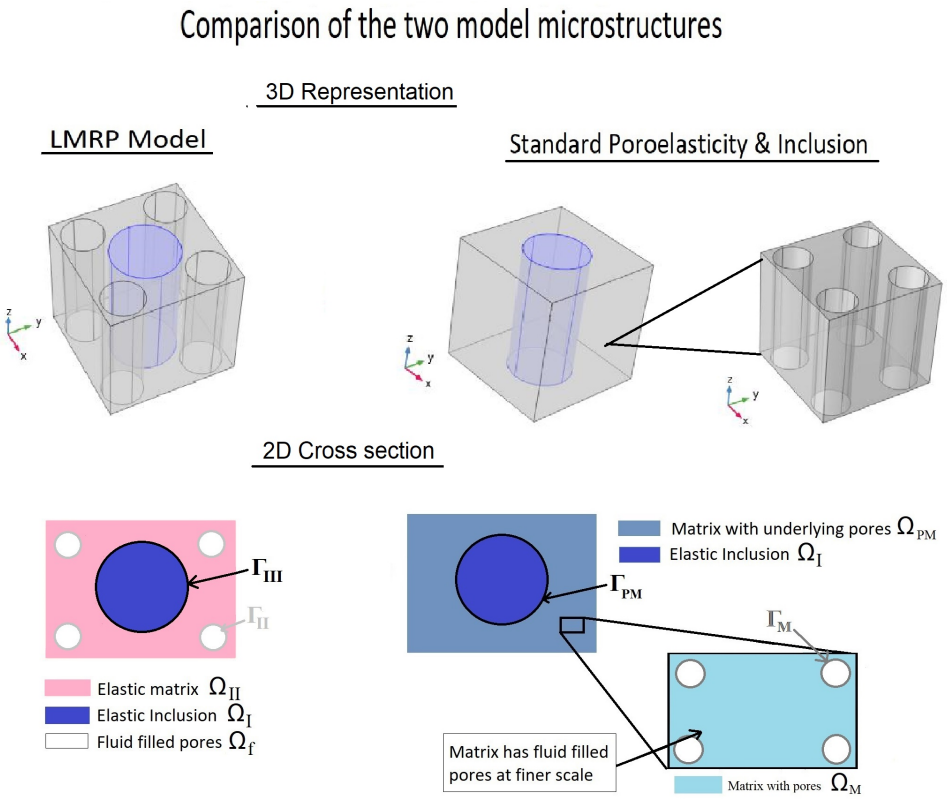

Figure 6.1: Comparison of the two models microstructures 2D sketch of the 3D domains

In Fig. 6.1 we have presented the different choices for the microstructures showing both the 3D and a 2D cross section of the domain.

Here we will introduce the effective balance equations for a poroelastic composite derived by the asymptotic homogenization technique in [69]. The model is derived by con-

sidering the fluid-structure interaction between a linear elastic porous matrix, Ω_{II}, with embedded linear elastic subphases, Ω_{I}, with a Newtonian fluid, Ω_{f}, flowing in the pores. The fluid structure interaction problem consists of balance equations for each elastic domain and the fluid domain, as well as constitutive laws. We also have the incompressibility contraint for the fluid and interface conditions such as continuity of tractions, elastic displacements and velocities. We make the assumption that the size of the materials pores (the porescale) is comparable with the distance between the adjacent subphases. This length is then taken to be much smaller than the size of the whole domain (the macroscale). This allows us to decouple the spatial scales, embracing the asymptotic homogenization technique, and we derive the new macroscale model. The asymptotic homogenization technique applies the assumption that all fields in the fluid structure interaction problem can be written as a power series of the scale sepatation parameter and then performing a multiple scale expansion we can derive the cell problems that determine the model coefficients. The system of partial differential equations that arises from applying the technique is of poroelastic-type. The coefficients of the model encode the properties of the microstructure, and can be computed by solving appropriate cell problems which reflect the complexity of the underlying material microstructure. The macroscale model comprises the balance of linear momentum

$$\nabla_{\mathbf{x}} \cdot \mathsf{T}_{\mathrm{Eff}}^{\mathrm{LMRP}} = 0, \tag{6.1}$$

and the conservation of mass equation

$$\frac{\dot{p}^{(0)}}{M^{\mathrm{LMRP}}} = -\nabla_{\mathbf{x}} \cdot \langle \mathbf{w} \rangle_{\mathrm{f}} - \boldsymbol{\alpha}^{\mathrm{LMRP}} : \xi_{\mathbf{x}} \dot{\mathbf{u}}^{(0)}, \tag{6.2}$$

where we have that ∇_x is the macroscale gradient operator, (we note that with the subscript y this would be the microscale gradient operator), $\mathsf{T}_{\mathrm{Eff}}^{\mathrm{LMRP}}$ is the stress tensor (the superscript LMRP is used to show that this is the stress that arises specifically from this model), $p^{(0)}$ is the macroscale pressure, $\xi_{\mathbf{x}}$ is the symmetric part of the macroscale gradient operator, $\dot{\mathbf{u}}^{(0)}$ is the leading order solid velocity, $\mathbf{w}$ is the average fluid velocity, M^{LMRP} and $\boldsymbol{\alpha}^{\mathrm{LMRP}}$ are the resulting Biot's modulus and tensor associated with the system respectively. The conservation of mass equation relates changes in the fluid pressure to changes in the fluid and solid volumes. The macroscale model also comprises Darcy's law

$$\langle \mathbf{w} \rangle_{\mathrm{f}} = -\langle W \rangle_{\mathrm{f}} \nabla_{\mathbf{x}} p^{(0)}, \tag{6.3}$$

where $\langle W \rangle_{\mathrm{f}}$ is the hydraulic conductivity tensor, and the constitutive law

$$\mathsf{T}_{\mathrm{Eff}}^{\mathrm{LMRP}} = \langle \mathbb{C}_{\mathrm{I}}\mathbb{M}_{\mathrm{I}} + \mathbb{C}_{\mathrm{I}} + \mathbb{C}_{\mathrm{II}}\mathbb{M}_{\mathrm{II}} + \mathbb{C}_{\mathrm{II}} \rangle_s \xi_{\mathbf{x}} \mathbf{u}^{(0)} + \boldsymbol{\gamma}^{\mathrm{LMRP}} p^{(0)}, \tag{6.4}$$

where $\mathbb{C}_v$ where $v = \mathrm{I}, \mathrm{II}$ is the elasticity tensor for the inclusion and matrix respectively. We can define the effective elasticity tensor $\widetilde{\mathbb{C}}^{\mathrm{LMRP}}$ as

$$\widetilde{\mathbb{C}}^{\mathrm{LMRP}} = \langle \mathbb{C}_{\mathrm{I}}\mathbb{M}_{\mathrm{I}} + \mathbb{C}_{\mathrm{I}} + \mathbb{C}_{\mathrm{II}}\mathbb{M}_{\mathrm{II}} + \mathbb{C}_{\mathrm{II}} \rangle_s. \tag{6.5}$$

We should note that our effective elasticity tensor possesses tetragonal symmetry, that is, possessing six distinct elastic entries. The reason for this is that, while if we began with the orthotropic elasticity tensor, we would have 9 different elastic entries, as the geometry we selected is a cube with embedded cylinders with circular bases, then the x and y directions are equivalent, and hence the reduction to 6 independent elastic parameters.

We therefore have that the behaviour of the poroelastic composite material can be fully described by the effective elasticity tensor $\widetilde{\mathbb{C}}^{\mathrm{LMRP}}$, the hydraulic conductivity $\langle W \rangle_{\mathrm{f}}$, the Biot's tensor of coefficients $\boldsymbol{\alpha}^{\mathrm{LMRP}}$ and the Biot's coefficient M^{LMRP}. We have that these macroscale coefficients read

$$\boldsymbol{\alpha}^{\mathrm{LMRP}} = \phi\mathbf{I} - \langle \mathrm{Tr}(\mathbb{M}_{\mathrm{II}}) \rangle_s, \quad M^{\mathrm{LMRP}} = \frac{-1}{\langle \mathrm{Tr}(Q_{\mathrm{II}}) \rangle_s}, \quad \boldsymbol{\gamma}^{\mathrm{LMRP}} = \langle \mathbb{C}_{\mathrm{II}} Q_{\mathrm{II}} \rangle_s - \phi\mathbf{I}, \tag{6.6}$$

where the fourth rank tensors $\mathbb{M}_{\mathrm{I}}$, $\mathbb{M}_{\mathrm{II}}$ and the second rank tensor Q_{II} are to be computed by solving the microscale cell problems that will be discussed in the next section.

We note that the notation $\langle \varphi \rangle$ is a cell average defined as

$$\langle \varphi \rangle_k = \frac{1}{|\Omega|} \int_{\Omega_k} \varphi(\mathbf{x}, \mathbf{y}, t) \mathrm{d}\mathbf{y} \quad k = \mathrm{f}, \mathrm{s} \tag{6.7}$$

where φ is a general field in our system and $|\Omega|$ is the volume of the domain and the integration is taken over the porescale.

Now we wish to consider the governing equations for our alternative comparison setup. That is, the governing equations for a poroelastic material containing an elastic inclusion derived via the asymptotic homogenization technique. This standard poroelastic setup is merely created to act as a comparison highlighting how to approach a material that possesses a microstructure comprising a matrix, embedded elastic subphases and fluid filled pores using the computational models already available in the literature (assuming we had

not yet created the LMRP model). This approach uses Biot's poroelasticity plus elastic composites however doesn't allow for the multiple elastic and fluid phase all to be considered at the same scale, hence firstly justifying the introduction of the LMRP model as well as showing that calculating the elastic parameters via this standard poroelastic approach cannot be entirely appropriate. We emphasise that this work focuses on the comparison between the drained elasticity tensors computed via the LMRP and SP approaches, respectively, see also Remark 16.

We can determine that this microstructure is a limit case of the double poroelasticity model [70] when there is no fluid in the inclusion. This is also the geometry considered in [24] and [105]. This means that we are considering a linear elastic problem where the interactions take place between a matrix (that is porous at a finer scale), Ω_{PM}, and an embedded linear elastic inclusion Ω_{I}. We should note that the elastic inclusion Ω_{I} is the same in both model setups, that is, it possesses exactly the same elastic properties and volume fraction, and it is only the scale at which the matrix is porous that varies between this setup and the LMRP model. This structure is shown in Fig. 6.1. The interface between the inclusion and the porous matrix is denoted Γ_{PM}. We assume that the distance between the embedded subphases (the microscale) is small compared with the size of the whole domain (the macroscale). By enforcing this scale separation we can decouple the spatial scales and and derive the effective governing equations for the poroelastic material with an elastic inclusion. The governing equations are those presented in the appendix of [70] in the limit of only fluid in one phase. The stress balance is given by

$$\nabla_{\mathbf{x}} \cdot \mathsf{T}^{\mathrm{SP}}_{\mathrm{Eff}} = 0, \tag{6.8}$$

with the constitutive law

$$\mathsf{T}^{\mathrm{SP}}_{\mathrm{Eff}} = \langle \mathbb{C}^{\mathrm{SP}}_{\mathrm{I}} \mathbb{M}^{\mathrm{SP}}_{\mathrm{I}} + \mathbb{C}^{\mathrm{SP}}_{\mathrm{I}} + \mathbb{C}_{\mathrm{PM}} \mathbb{M}^{\mathrm{SP}}_{\mathrm{II}} + \mathbb{C}_{\mathrm{PM}} \rangle_s \xi_{\mathbf{x}} \hat{\mathbf{u}}^{(0)} + \boldsymbol{\gamma}^{\mathrm{SP}} \hat{p}^{(0)}. \tag{6.9}$$

where $\hat{p}^{(0)}$ is the macroscale pressure, $\hat{\mathbf{u}}^{(0)}$ is the leading order elastic displacement and

$$\boldsymbol{\gamma}^{\mathrm{SP}} = \langle \mathbb{C}^{\mathrm{SP}}_{\mathrm{I}} Q^{\mathrm{SP}}_{\mathrm{I}} + \mathbb{C}_{\mathrm{PM}} Q^{\mathrm{SP}}_{\mathrm{II}} \rangle_s - \boldsymbol{\alpha}_{\mathrm{M}}. \tag{6.10}$$

We have used the superscript SP to denote that this approach compares with Standard Poroelasticity. The second rank tensors $Q^{\mathrm{SP}}_{\mathrm{I}}$, $Q^{\mathrm{SP}}_{\mathrm{II}}$ are to be computed by solving microscale

cell problems that encode details of the materials microstructure and the second rank tensor $\boldsymbol{\alpha}_{\mathrm{M}}$ is the Biot's tensor of coefficients that arises from the homogenization of the porous matrix at the finer scale. We can define the effective elasticity tensor $\widetilde{\mathbb{C}}^{\mathrm{SP}}$ as

$$\widetilde{\mathbb{C}}^{\mathrm{SP}} = \langle \mathbb{C}_{\mathrm{I}}^{\mathrm{SP}} \mathbb{M}_{\mathrm{I}}^{\mathrm{SP}} + \mathbb{C}_{\mathrm{I}}^{\mathrm{SP}} + \mathbb{C}_{\mathrm{PM}} \mathbb{M}_{\mathrm{II}}^{\mathrm{SP}} + \mathbb{C}_{\mathrm{PM}} \rangle_s. \tag{6.11}$$

Where we have that $\mathbb{C}_{\mathrm{PM}}$ is the effective elasticity tensor that arises from carrying out the asymptotic homogenization technique on the porous matrix, $\mathbb{C}_{\mathrm{I}}^{\mathrm{SP}}$ is the elasticity tensor for the inclusion in this model setup, and is equal to $\mathbb{C}_{\mathrm{I}}$ from the LMRP model. The fourth rank tensors $\mathbb{M}_{\mathrm{I}}^{\mathrm{SP}}$, $\mathbb{M}_{\mathrm{II}}^{\mathrm{SP}}$ are to be computed by solving the microscale cell problems that will be discussed in the next section. We should note that our effective elasticity tensor possesses tetragonal symmetry for the same geometrical reasons as described for $\widetilde{\mathbb{C}}^{\mathrm{LMRP}}$ previously.

The macroscale model also comprises the conservation of mass equation given by

$$\frac{\dot{\hat{p}}^{(0)}}{M^{\mathrm{SP}}} = -\nabla_{\mathbf{x}} \cdot \langle \mathbf{w}'_{\mathrm{eff}} \rangle_{\mathrm{f}} - \boldsymbol{\alpha}^{\mathrm{SP}} : \xi_{\mathbf{x}} \dot{\hat{\mathbf{u}}}^{(\mathbf{0})}, \tag{6.12}$$

where $\dot{\hat{\mathbf{u}}}^{(\mathbf{0})}$ is the leading order solid velocity, M^{SP} and $\boldsymbol{\alpha}^{\mathrm{SP}}$ are the resulting Biot's modulus and tensor associated with the system respectively and are given by

$$\boldsymbol{\alpha}^{\mathrm{SP}} = \langle \boldsymbol{\alpha}_{\mathrm{M}} + (\mathbb{M}_{\mathrm{II}}^{\mathrm{SP}})^{\mathrm{T}} : \boldsymbol{\alpha}_{\mathrm{M}} \rangle_s, \quad M^{\mathrm{SP}} = \frac{\langle \mathcal{M}_{\mathrm{PM}} \rangle_s}{1 + \langle \mathcal{M}_{\mathrm{PM}} (\boldsymbol{\alpha}_{\mathrm{M}} : Q_{\mathrm{II}}^{\mathrm{SP}}) \rangle_s} \tag{6.13}$$

where $\mathcal{M}_{\mathrm{PM}}$ is the Biot's modulus of the porous matrix and the $\mathbf{w}'_{\mathrm{eff}}$ is given as the final macroscale equation (Darcy's law)

$$\langle \mathbf{w}'_{\mathrm{eff}} \rangle_{\mathrm{f}} = -\langle W' \rangle_{\mathrm{f}} \nabla_{\mathbf{x}} \hat{p}^{(0)}, \tag{6.14}$$

where the second rank tensor W' is a modified hydraulic conductivity tensor that accounts for the differences in hydraulic conductivities at different points in the microstructure.

Remark 16 (Undrained Effective Elasticity tensors)**.** *We have presented a brief summary of the LMRP model [69] and the comparative setup SP that combines standard poroelasticity with elastic composites. We have presented the whole model for each of these setups for the sake of completeness however, the simulations focus on only computing the effective drained elasticity tensor. However, it would be possible to also compute the equivalent*

tensors for the undrained case. To do this first for the LMRP model we would assume that we had a static fluid filling phase and the undrained elasticity tensor could be obtained using a static (6.2) *in* (6.4)*. This gives the undrained effective elasticity tensor*

$$\widetilde{\mathbb{C}}^{\mathrm{LMRP}}_{\mathrm{undrained}} = \widetilde{\mathbb{C}}^{\mathrm{LMRP}} + \boldsymbol{\alpha}\boldsymbol{\alpha} M. \tag{6.15}$$

In exactly the same way we would assume a static (6.12) *and use in* (6.9) *to obtain the undrained elasticity tensor for the standard poroelastic with elastic inclusion approach.*

$$\widetilde{\mathbb{C}}^{\mathrm{SP}}_{\mathrm{undrained}} = \widetilde{\mathbb{C}}^{\mathrm{SP}} + \widetilde{\boldsymbol{\alpha}}\widetilde{\boldsymbol{\alpha}}\mathcal{M}. \tag{6.16}$$

By carrying out further simulations (which are beyond the scope of this particular work), we could also compute this undrained effective elasticity tensor for each of these setups.

We also note that despite it not being a focus of this particular work that all the poroelastic coefficients of both model setups are able to be obtained. The additional problems which are not presented here and that would need to be solved to compute the Biot's modulus and tensor of coefficients and hydraulic conductivity can be found in [69].

6.2 Computational setup

Within this section we consider the numerical setups and describe the 3D cell problems required to compute the effective elasticity tensor for both the LMRP model and the standard poroelasticity with an elastic inclusion. We then also provide the 2D reduction for each of the cell problems by simplifying the framework for a 2D reduction of a poroelastic composite with orthotropic elastic phases that is provided in detail in the appendix. B.1.

Here we summarise the specific equations for each of the 9 particular cell problems that we present in detail in the following 4 subsections. For the 3D LMRP model cell problem see (6.19)-(6.23) and for the 2D equivalent of the LMRP model see (B.23)-(B.27) (in-plane) and (6.50)-(6.54) (anti-plane). For the standard poroelastic with inclusion setup we have two steps, first the standard cell problem for poroelasticity in 3D is given by (6.73)-(6.74) and the 2D equivalent of this is given by (B.24) and (B.27) (in-plane) and (6.95) and (6.96) (anti-plane). We then have the second step where the 3D elastic composite problem is given by (6.77)-(6.80) and the 2D equivalent of this is given by (B.23)-(B.26) (in-plane) and (6.105)-(6.108) (anti-plane).

6.2.1 3D Cell Problems for LMRP model

We are able to compute the fourth rank effective elasticity tensor $\widetilde{\mathbb{C}}^{\text{LMRP}}$ for the LMRP model and by using its components calculate the two Young's moduli and two shear moduli corresponding to our model. The effective elasticity tensor is given by

$$\widetilde{\mathbb{C}}^{\text{LMRP}} = \langle \mathbb{C}_{\text{I}}\mathbb{M}_{\text{I}} + \mathbb{C}_{\text{I}} + \mathbb{C}_{\text{II}}\mathbb{M}_{\text{II}} + \mathbb{C}_{\text{II}} \rangle_s. \tag{6.17}$$

We can see that this comprises the fourth rank tensor $\mathbb{M}_i$, where $i = \text{I}, \text{II}$, which can be defined as

$$\mathbb{M}_{\text{I}} = \xi^{kl}_{pq}(A^{\text{I}}) = \frac{1}{2}\left(\frac{\partial A^{\text{I}}_{pkl}}{\partial y_q} + \frac{\partial A^{\text{I}}_{qkl}}{\partial y_p}\right); \quad \mathbb{M}_{\text{II}} = \xi^{kl}_{pq}(A^{\text{II}}) = \frac{1}{2}\left(\frac{\partial A^{\text{II}}_{pkl}}{\partial y_q} + \frac{\partial A^{\text{II}}_{qkl}}{\partial y_p}\right). \tag{6.18}$$

We can then write the cell problems for third rank tensors A_{I} and A_{II}, found in [69] and Chapter 3, with corresponding components A^{I}_{ikl} and A^{II}_{ikl} as

$$\frac{\partial}{\partial y_j}\left(C^{\text{I}}_{ijpq}\xi^{kl}_{pq}(A^{\text{I}})\right) + \frac{\partial C^{\text{I}}_{ijkl}}{\partial y_j} = 0 \qquad \text{in} \quad \Omega_{\text{I}} \tag{6.19}$$

$$\frac{\partial}{\partial y_j}\left(C^{\text{II}}_{ijpq}\xi^{kl}_{pq}(A^{\text{II}})\right) + \frac{\partial C^{\text{II}}_{ijkl}}{\partial y_j} = 0 \qquad \text{in} \quad \Omega_{\text{II}} \tag{6.20}$$

$$C^{\text{I}}_{ijpq}\xi^{kl}_{pq}(A^{\text{I}})n^{\text{III}}_j - C^{\text{II}}_{ijpq}\xi^{kl}_{pq}(A^{\text{II}})n^{\text{III}}_j = (C^{\text{II}} - C^{\text{I}})_{ijkl}n^{\text{III}}_j \qquad \text{on} \quad \Gamma_{\text{III}} \tag{6.21}$$

$$A^{\text{I}}_{ikl} = A^{\text{II}}_{ikl} \qquad \text{on} \quad \Gamma_{\text{III}} \tag{6.22}$$

$$C^{\text{II}}_{ijpq}\xi^{kl}_{pq}(A^{\text{II}})n^{\text{II}}_j + C^{\text{II}}_{ijkl}n^{\text{II}}_j = 0 \qquad \text{on} \quad \Gamma_{\text{II}}. \tag{6.23}$$

The solutions to the problem (6.19)-(6.23), $\xi^{kl}_{pq}(A^{\text{I}})$ and $\xi^{kl}_{pq}(A^{\text{II}})$, are found by solving six elastic-type cell problems by fixing the couple of indices (k, l). By doing this the $\xi^{kl}_{pq}(A^{\text{I}})$ and $\xi^{kl}_{pq}(A^{\text{II}})$ that appear in (6.19)-(6.23) represent a strain. Then for every fixed couple (k, l) we have a linear elastic problem which has the following forces driving each of the six cell problems (6.19)-(6.23) which depend on the jump in the elastic constants between the matrix and the subphase and on the geometry of the subphase, that is encoded in the normal $\mathbf{n}^{\text{III}}$ to the interface between the matrix and inclusion Γ_{III}

$$\begin{aligned} &kl = 11 \qquad C^{\text{I}}_{ijpq}\xi^{11}_{pq}(A^{\text{I}})n^{\text{III}}_j - C^{\text{II}}_{ijpq}\xi^{11}_{pq}(A^{\text{II}})n^{\text{III}}_j = (C^{\text{II}} - C^{\text{I}})_{ij11}n^{\text{III}}_j, \\ &\text{where} \quad f^{\Gamma_{\text{III}}}_i = (C^{\text{II}} - C^{\text{I}})_{ij11}n^{\text{III}}_j \\ &kl = 22 \qquad C^{\text{I}}_{ijpq}\xi^{22}_{pq}(A^{\text{I}})n^{\text{III}}_j - C^{\text{II}}_{ijpq}\xi^{22}_{pq}(A^{\text{II}})n^{\text{III}}_j = (C^{\text{II}} - C^{\text{I}})_{ij22}n^{\text{III}}_j, \end{aligned} \tag{6.24}$$

$$\text{where} \quad f_i^{\Gamma_{\text{III}}} = (C^{\text{II}} - C^{\text{I}})_{ij22} n_j^{\text{III}} \tag{6.25}$$

$$kl = 33 \qquad C^{\text{I}}_{ijpq}\xi^{33}_{pq}(A^{\text{I}})n_j^{\text{III}} - C^{\text{II}}_{ijpq}\xi^{33}_{pq}(A^{\text{II}})n_j^{\text{III}} = (C^{\text{II}} - C^{\text{I}})_{ij33} n_j^{\text{III}},$$

$$\text{where} \quad f_i^{\Gamma_{\text{III}}} = (C^{\text{II}} - C^{\text{I}})_{ij33} n_j^{\text{III}} \tag{6.26}$$

$$kl = 23 \qquad C^{\text{I}}_{ijpq}\xi^{23}_{pq}(A^{\text{I}})n_j^{\text{III}} - C^{\text{II}}_{ijpq}\xi^{23}_{pq}(A^{\text{II}})n_j^{\text{III}} = (C^{\text{II}} - C^{\text{I}})_{ij23} n_j^{\text{III}},$$

$$\text{where} \quad f_i^{\Gamma_{\text{III}}} = (C^{\text{II}} - C^{\text{I}})_{ij23} n_j^{\text{III}} \tag{6.27}$$

$$kl = 13 \qquad C^{\text{I}}_{ijpq}\xi^{13}_{pq}(A^{\text{I}})n_j^{\text{III}} - C^{\text{II}}_{ijpq}\xi^{13}_{pq}(A^{\text{II}})n_j^{\text{III}} = (C^{\text{II}} - C^{\text{I}})_{ij13} n_j^{\text{III}},$$

$$\text{where} \quad f_i^{\Gamma_{\text{III}}} = (C^{\text{II}} - C^{\text{I}})_{ij13} n_j^{\text{III}} \tag{6.28}$$

$$kl = 12 \qquad C^{\text{I}}_{ijpq}\xi^{12}_{pq}(A^{\text{I}})n_j^{\text{III}} - C^{\text{II}}_{ijpq}\xi^{12}_{pq}(A^{\text{II}})n_j^{\text{III}} = (C^{\text{II}} - C^{\text{I}})_{ij12} n_j^{\text{III}},$$

$$\text{where} \quad f_i^{\Gamma_{\text{III}}} = (C^{\text{II}} - C^{\text{I}})_{ij12} n_j^{\text{III}} \tag{6.29}$$

where $\mathbf{n}^{\text{III}}$ is the unit outward normal corresponding to the interface Γ_{III}. In order to solve (6.19)-(6.23) we also have interface conditions between the matrix and the fluid, Γ_{II}. We are still fixing every couple (k, l) to find the following forces that account for the difference between the elastic matrix and the void where the fluid has been removed since we are computing the drained coefficients. The normal $\mathbf{n}^{\text{II}}$ encodes the geometry of the voids as it is the normal to the interface Γ_{II}. The forces therefore are

$$kl = 11 \qquad C^{\text{II}}_{ijpq}\xi^{11}_{pq}(A^{\text{II}})n_j^{\text{II}} = -C^{\text{II}}_{ij11} n_j^{\text{II}}, \quad \text{where} \quad f_i^{\Gamma_{\text{II}}} = C^{\text{II}}_{ij11} n_j^{\text{II}} \tag{6.30}$$

$$kl = 22 \qquad C^{\text{II}}_{ijpq}\xi^{22}_{pq}(A^{\text{II}})n_j^{\text{II}} = -C^{\text{II}}_{ij22} n_j^{\text{II}}, \quad \text{where} \quad f_i^{\Gamma_{\text{II}}} = C^{\text{II}}_{ij22} n_j^{\text{II}} \tag{6.31}$$

$$kl = 33 \qquad C^{\text{II}}_{ijpq}\xi^{33}_{pq}(A^{\text{II}})n_j^{\text{II}} = -C^{\text{II}}_{ij33} n_j^{\text{II}}, \quad \text{where} \quad f_i^{\Gamma_{\text{II}}} = C^{\text{II}}_{ij33} n_j^{\text{II}} \tag{6.32}$$

$$kl = 23 \qquad C^{\text{II}}_{ijpq}\xi^{23}_{pq}(A^{\text{II}})n_j^{\text{II}} = -C^{\text{II}}_{ij23} n_j^{\text{II}}, \quad \text{where} \quad f_i^{\Gamma_{\text{II}}} = C^{\text{II}}_{ij23} n_j^{\text{II}} \tag{6.33}$$

$$kl = 13 \qquad C^{\text{II}}_{ijpq}\xi^{13}_{pq}(A^{\text{II}})n_j^{\text{II}} = -C^{\text{II}}_{ij13} n_j^{\text{II}}, \quad \text{where} \quad f_i^{\Gamma_{\text{II}}} = C^{\text{II}}_{ij13} n_j^{\text{II}} \tag{6.34}$$

$$kl = 12 \qquad C^{\text{II}}_{ijpq}\xi^{12}_{pq}(A^{\text{II}})n_j^{\text{II}} = -C^{\text{II}}_{ij12} n_j^{\text{II}}, \quad \text{where} \quad f_i^{\Gamma_{\text{II}}} = C^{\text{II}}_{ij12} n_j^{\text{II}} \tag{6.35}$$

where $\mathbf{n}^{\text{II}}$ is the unit outward normal corresponding to the interface Γ_{II}. We assume that the fourth rank elasticity tensors C^{I}_{ijpq} and C^{II}_{ijpq} are isotropic at the porescale. That is

$$C^{\text{I}}_{ijpq} = \lambda^{\text{I}}\delta_{ij}\delta_{pq} + \mu^{\text{I}}(\delta_{ip}\delta_{jq} + \delta_{iq}\delta_{jp}) \tag{6.36}$$

$$C^{\text{II}}_{ijpq} = \lambda^{\text{II}}\delta_{ij}\delta_{pq} + \mu^{\text{II}}(\delta_{ip}\delta_{jq} + \delta_{iq}\delta_{jp}) \tag{6.37}$$

We can then use (6.36) and (6.37) in the interface loads to determine the forces $f_i^{\Gamma_{\text{III}}}$ on Γ_{III} and the forces $f_i^{\Gamma_{\text{II}}}$ on Γ_{II}. We note that for the forces f_i the superscript given refers

to the interface on which the force is applied, we will use this convention throughout this chapter. Firstly the forces on the matrix inclusion interface Γ_{III}

$$kl = 11 \qquad \mathbf{f}^{\Gamma_{\text{III}}} = (\lambda^{\text{II}} - \lambda^{\text{I}})\mathbf{n}^{\text{III}} + 2(\mu^{\text{II}} - \mu^{\text{I}})n_1^{\text{III}}\mathbf{e}_1 \tag{6.38}$$

$$kl = 22 \qquad \mathbf{f}^{\Gamma_{\text{III}}} = (\lambda^{\text{II}} - \lambda^{\text{I}})\mathbf{n}^{\text{III}} + 2(\mu^{\text{II}} - \mu^{\text{I}})n_2^{\text{III}}\mathbf{e}_2 \tag{6.39}$$

$$kl = 33 \qquad \mathbf{f}^{\Gamma_{\text{III}}} = (\lambda^{\text{II}} - \lambda^{\text{I}})\mathbf{n}^{\text{III}} + 2(\mu^{\text{II}} - \mu^{\text{I}})n_3^{\text{III}}\mathbf{e}_3 \tag{6.40}$$

$$kl = 23 \qquad \mathbf{f}^{\Gamma_{\text{III}}} = (\mu^{\text{II}} - \mu^{\text{I}})(n_3^{\text{III}}\mathbf{e}_2 + n_2^{\text{III}}\mathbf{e}_3) \tag{6.41}$$

$$kl = 13 \qquad \mathbf{f}^{\Gamma_{\text{III}}} = (\mu^{\text{II}} - \mu^{\text{I}})(n_3^{\text{III}}\mathbf{e}_1 + n_1^{\text{III}}\mathbf{e}_3) \tag{6.42}$$

$$kl = 12 \qquad \mathbf{f}^{\Gamma_{\text{III}}} = (\mu^{\text{II}} - \mu^{\text{I}})(n_2^{\text{III}}\mathbf{e}_1 + n_1^{\text{III}}\mathbf{e}_2) \tag{6.43}$$

where we have used n_1^{III}, n_2^{III} and n_3^{III} to mean the components of the unit vector normal to the interface Γ_{III} and we have used the standard unit vectors in the Cartesian coordinate system $\mathbf{e}_1$, $\mathbf{e}_2$ and $\mathbf{e}_3$. Similarly for the fluid-matrix interface, Γ_{II} we have the forces

$$kl = 11 \qquad \mathbf{f}^{\Gamma_{\text{II}}} = \lambda^{\text{II}}\mathbf{n}^{\text{II}} + 2\mu^{\text{II}}n_1^{\text{II}}\mathbf{e}_1 \tag{6.44}$$

$$kl = 22 \qquad \mathbf{f}^{\Gamma_{\text{II}}} = \lambda^{\text{II}}\mathbf{n}^{\text{II}} + 2\mu^{\text{II}}n_2^{\text{II}}\mathbf{e}_2 \tag{6.45}$$

$$kl = 33 \qquad \mathbf{f}^{\Gamma_{\text{II}}} = \lambda^{\text{II}}\mathbf{n}^{\text{II}} + 2\mu^{\text{II}}n_3^{\text{II}}\mathbf{e}_3 \tag{6.46}$$

$$kl = 23 \qquad \mathbf{f}^{\Gamma_{\text{II}}} = \mu^{\text{II}}(n_3^{\text{II}}\mathbf{e}_2 + n_2^{\text{II}}\mathbf{e}_3) \tag{6.47}$$

$$kl = 13 \qquad \mathbf{f}^{\Gamma_{\text{II}}} = \mu^{\text{II}}(n_3^{\text{II}}\mathbf{e}_1 + n_1^{\text{II}}\mathbf{e}_3) \tag{6.48}$$

$$kl = 12 \qquad \mathbf{f}^{\Gamma_{\text{II}}} = \mu^{\text{II}}(n_2^{\text{II}}\mathbf{e}_1 + n_1^{\text{II}}\mathbf{e}_2) \tag{6.49}$$

where we have used n_1^{II}, n_2^{II} and n_3^{II} to mean the components of the unit vector normal to the interface Γ_{II} and we have used the standard unit vectors in the Cartesian coordinate system $\mathbf{e}_1$, $\mathbf{e}_2$ and $\mathbf{e}_3$. We note that because of the geometry that we have chosen for the periodic cell (see Fig. 6.1) that we only have two interfaces so this is a limit case of the cell problems shown in Chapter 3 where we have all inclusions interacting with the fluid.

The cell problem (6.19)-(6.23) is a three dimensional problem. Our interface conditions (6.38)-(6.43) and (6.44)-(6.49) are also 3D. For each pair of boundary loads given in (6.38)-(6.43) and (6.44)-(6.49) we compute a corresponding numerical solution of the elastic-type problem (6.19)-(6.23). This can be done using the finite element software Comsol Multiphysics employing its Structural Mechanics Module. We wish to perform 2D simulations so we must reduce our cell problems.

The cell problem (6.19)-(6.23) is a three dimensional problem. Our interface conditions (6.38)-(6.43) and (6.44)-(6.49) are also 3D. We wish to perform 2D simulations so we must reduce our cell problems.

6.2.2 2D Cell Problems for LMRP model

We now wish to consider the 2D reduction of the cell problems. The geometry of our periodic cell is such that we have a cube with a cylindrical elastic inclusion extending in the $\mathbf{e}_3$ direction from the top to the bottom of the cell as well as 4 cylindrical voids placed in each of the corners of the cube also extending from the top to the bottom of the cell in the $\mathbf{e}_3$ direction. This means that at every cross-section in the $\mathbf{e}_3$ direction gives a square with a circular inclusion and 4 circular voids. This geometry is shown in the 2D sketch Fig. 6.2.

Figure 6.2: Schematic of the 2D domain for LMRP model microstructure

We can consider the 2D reduction presented in the appendix and assume that both the inclusion and the matrix are isotropic materials. This means that we have that $C^i_{1111} = C^i_{2222} = C^i_{3333} = \lambda^i + 2\mu^i$, $C^i_{2323} = C^i_{1313} = C^i_{1212} = \mu^i$ and $C^i_{1122} = C^i_{2211} = C^i_{1133} = C^i_{3311} = C^i_{2233} = C^i_{3322} = \lambda^i$ where $i = \mathrm{I}, \mathrm{II}$. Using this in the anti-plane problem (B.18)-(B.22) we obtain

$$\mu^{\mathrm{I}} \frac{\partial A^{\mathrm{I}}_{3kl}}{\partial y_1^2} + \mu^{\mathrm{I}} \frac{\partial A^{\mathrm{I}}_{3kl}}{\partial y_2^2} = 0 \qquad \text{in} \quad D_{\mathrm{I}} \tag{6.50}$$

$$\mu^{\mathrm{II}} \frac{\partial A^{\mathrm{II}}_{3kl}}{\partial y_1^2} + \mu^{\mathrm{II}} \frac{\partial A^{\mathrm{II}}_{3kl}}{\partial y_2^2} = 0 \qquad \text{in} \quad D_{\mathrm{II}} \tag{6.51}$$

$$\begin{aligned} \mu^{\mathrm{I}} \frac{\partial A^{\mathrm{I}}_{3kl}}{\partial y_1} n_1^{\mathrm{III}} + \mu^{\mathrm{I}} \frac{\partial A^{\mathrm{I}}_{3kl}}{\partial y_2} n_2^{\mathrm{III}} - \left(\mu^{\mathrm{II}} \frac{\partial A^{\mathrm{II}}_{3kl}}{\partial y_1} n_1^{\mathrm{III}} + \mu^{\mathrm{II}} \frac{\partial A^{\mathrm{II}}_{3kl}}{\partial y_2} n_2^{\mathrm{III}}\right) \\ = (C^{\mathrm{II}}_{31kl} n_1^{\mathrm{III}} + C^{\mathrm{II}}_{32kl} n_2^{\mathrm{III}}) - (C^{\mathrm{I}}_{31kl} n_1^{\mathrm{III}} + C^{\mathrm{I}}_{32kl} n_2^{\mathrm{III}}) \qquad \text{on} \quad \partial D_{\mathrm{I}} \cap \partial D_{\mathrm{II}} \end{aligned} \tag{6.52}$$

$$A^{\mathrm{I}}_{3kl} = A^{\mathrm{II}}_{3kl} \qquad \text{on} \quad \partial D_{\mathrm{I}} \cap \partial D_{\mathrm{II}} \tag{6.53}$$

$$\mu^{\mathrm{II}} \frac{\partial A^{\mathrm{II}}_{3kl}}{\partial y_1} n_1^{\mathrm{II}} + \mu^{\mathrm{II}} \frac{\partial A^{\mathrm{II}}_{3kl}}{\partial y_2} n_2^{\mathrm{II}} + C^{\mathrm{II}}_{31kl} n_1^{\mathrm{II}} + C^{\mathrm{II}}_{32kl} n_2^{\mathrm{II}} = 0 \qquad \text{on} \quad \partial D_{\mathrm{f}} \tag{6.54}$$

where the notation $D_{\rm I}$, $D_{\rm II}$ are the corresponding 2D slices of $\Omega_{\rm I}$ and $\Omega_{\rm II}$. The interfaces in 2D are represented as $\partial D_{\rm I} \cap \partial D_{\rm II}$ for the matrix inclusion interface and $\partial D_{\rm f}$ for the fluid-matrix interface. We also note that our normals to the interfaces $\partial D_{\rm I} \cap \partial D_{\rm II}$ and $\partial D_{\rm f}$ are the same normals (but with only two components) as in the 3D case as these were normals to cylindrical surfaces so are still the normals to the curved surfaces of the circular voids and inclusion.

The solutions to the problem (6.50)-(6.54) are found by solving the two anti-plane problems by fixing the couple (k,l)=(1,3)=(3,1), (2,3)=(3,2). Then for every fixed couple we have the Poisson problem with the following interface conditions. The first force we require to solve (6.50)-(6.54) is on the matrix inclusion interface, $\partial D_{\rm I} \cap \partial D_{\rm II}$, and it is, for each fixed couple,

$$\begin{aligned}
kl = 23 \quad & \mu^{\rm I} \frac{\partial A^{\rm I}_{323}}{\partial y_1} n_1^{\rm III} + \mu^{\rm I} \frac{\partial A^{\rm I}_{323}}{\partial y_2} n_2^{\rm III} - \big(\mu^{\rm II} \frac{\partial A^{\rm II}_{323}}{\partial y_1} n_1^{\rm III} + \mu^{\rm II} \frac{\partial A^{\rm II}_{323}}{\partial y_2} n_2^{\rm III}\big) \\
& = (C^{\rm II}_{3123} n_1^{\rm III} + C^{\rm II}_{3223} n_2^{\rm III}) - (C^{\rm I}_{3123} n_1^{\rm III} + C^{\rm I}_{3223} n_2^{\rm III}), \\
\text{where} \quad & f^{\partial D_{\rm I} \cap \partial D_{\rm II}}_{\rm anti} = (C^{\rm II}_{3123} n_1^{\rm III} + C^{\rm II}_{3223} n_2^{\rm III}) - (C^{\rm I}_{3123} n_1^{\rm III} + C^{\rm I}_{3223} n_2^{\rm III}) \qquad (6.55) \\
kl = 13 \quad & \mu^{\rm I} \frac{\partial A^{\rm I}_{313}}{\partial y_1} n_1^{\rm III} + \mu^{\rm I} \frac{\partial A^{\rm I}_{313}}{\partial y_2} n_2^{\rm III} - \big(\mu^{\rm II} \frac{\partial A^{\rm II}_{313}}{\partial y_1} n_1^{\rm III} + \mu^{\rm II} \frac{\partial A^{\rm II}_{313}}{\partial y_2} n_2^{\rm III}\big) \\
& = (C^{\rm II}_{3113} n_1^{\rm III} + C^{\rm II}_{3213} n_2^{\rm III}) - (C^{\rm I}_{3113} n_1^{\rm III} + C^{\rm I}_{3213} n_2^{\rm III}), \\
\text{where} \quad & f^{\partial D_{\rm I} \cap \partial D_{\rm II}}_{\rm anti} = (C^{\rm II}_{3113} n_1^{\rm III} + C^{\rm II}_{3213} n_2^{\rm III}) - (C^{\rm I}_{3113} n_1^{\rm III} + C^{\rm I}_{3213} n_2^{\rm III}) \qquad (6.56)
\end{aligned}$$

where the forces can be written using the assumption of isotropy of both phases as

$$\begin{aligned}
kl = 23 \quad & f^{\partial D_{\rm I} \cap \partial D_{\rm II}}_{\rm anti} = C^{\rm II}_{3223} n_2^{\rm III} - C^{\rm I}_{3223} n_2^{\rm III} = \mu^{\rm II} n_2^{\rm III} - \mu^{\rm I} n_2^{\rm III} \qquad (6.57) \\
kl = 13 \quad & f^{\partial D_{\rm I} \cap \partial D_{\rm II}}_{\rm anti} = C^{\rm II}_{3113} n_1^{\rm III} - C^{\rm I}_{3113} n_1^{\rm III} = \mu^{\rm II} n_1^{\rm III} - \mu^{\rm I} n_1^{\rm III}. \qquad (6.58)
\end{aligned}$$

The second force we require to solve (6.50)-(6.54) is on the matrix fluid interface, $\partial D_{\rm f}$, and we have

$$\begin{aligned}
kl = 23 \quad & \mu^{\rm II} \frac{\partial A^{\rm II}_{323}}{\partial y_1} n_1^{\rm II} + \mu^{\rm II} \frac{\partial A^{\rm II}_{323}}{\partial y_2} n_2^{\rm II} = -(C^{\rm II}_{3123} n_1^{\rm II} + C^{\rm II}_{3223} n_2^{\rm II}), \\
& \text{where} \quad f^{\partial D_{\rm f}}_{\rm anti} = C^{\rm II}_{3123} n_1^{\rm II} + C^{\rm II}_{3223} n_2^{\rm II} \qquad (6.59) \\
kl = 13 \quad & \mu^{\rm II} \frac{\partial A^{\rm II}_{313}}{\partial y_1} n_1^{\rm II} + \mu^{\rm II} \frac{\partial A^{\rm II}_{313}}{\partial y_2} n_2^{\rm II} = -(C^{\rm II}_{3113} n_1^{\rm II} + C^{\rm II}_{3213} n_2^{\rm II}), \\
& \text{where} \quad f^{\partial D_{\rm f}}_{\rm anti} = C^{\rm II}_{3113} n_1^{\rm II} + C^{\rm II}_{3213} n_2^{\rm II} \qquad (6.60)
\end{aligned}$$

where the forces can be written using the assumption of isotropy of both phases as

$$kl = 23 \quad f_{\text{anti}}^{\partial D_{\text{f}}} = C_{3223}^{\text{II}} n_2^{\text{II}} = \mu^{\text{II}} n_2^{\text{II}} \tag{6.61}$$

$$kl = 13 \quad f_{\text{anti}}^{\partial D_{\text{f}}} = C_{3113}^{\text{II}} n_1^{\text{II}} = \mu^{\text{II}} n_1^{\text{II}}. \tag{6.62}$$

We now need to consider the in-plane problems. Using (B.23)-(B.27) from the appendix we can consider the interface loads on both the matrix inclusion interface $\partial D_{\text{I}} \cap \partial D_{\text{II}}$ and on the matrix fluid interface and ∂D_{f}. In the LMRP model we assume that both elastic phases are isotropic. Each interface load is a vector with two components, due to $i = 1, 2$. We fix the couple (k,l) and obtain on the matrix inclusion interface $\partial D_{\text{I}} \cap \partial D_{\text{II}}$

$$\begin{aligned} kl = 11 \quad \mathbf{f}_{11}^{\partial D_{\text{I}} \cap \partial D_{\text{II}}} &= (C_{i111}^{\text{II}} n_1^{\text{III}} + C_{i211}^{\text{II}} n_2^{\text{III}}) - (C_{i111}^{\text{I}} n_1^{\text{III}} + C_{i211}^{\text{I}} n_2^{\text{III}}) \\ &= \begin{bmatrix} C_{11}^{\text{II}} n_1^{\text{III}} - C_{11}^{\text{I}} n_1^{\text{III}} \\ C_{12}^{\text{II}} n_2^{\text{III}} - C_{12}^{\text{I}} n_2^{\text{III}} \end{bmatrix} \\ &= \begin{bmatrix} (\lambda_{\text{II}} - \lambda_{\text{I}} + 2(\mu_{\text{II}} - \mu_{\text{I}})) n_1^{\text{III}} \\ (\lambda_{\text{II}} - \lambda_{\text{I}}) n_2^{\text{III}} \end{bmatrix} \end{aligned} \tag{6.63}$$

$$\begin{aligned} kl = 22 \quad \mathbf{f}_{22}^{\partial D_{\text{I}} \cap \partial D_{\text{II}}} &= (C_{i122}^{\text{II}} n_1^{\text{III}} + C_{i222}^{\text{II}} n_2^{\text{III}}) - (C_{i122}^{\text{I}} n_1^{\text{III}} + C_{i222}^{\text{I}} n_2^{\text{III}}) \\ &= \begin{bmatrix} C_{12}^{\text{II}} n_1^{\text{III}} - C_{12}^{\text{I}} n_1^{\text{III}} \\ C_{22}^{\text{II}} n_2^{\text{III}} - C_{22}^{\text{I}} n_2^{\text{III}} \end{bmatrix} \\ &= \begin{bmatrix} (\lambda_{\text{II}} - \lambda_{\text{I}}) n_1^{\text{III}} \\ (\lambda_{\text{II}} - \lambda_{\text{I}} + 2(\mu_{\text{II}} - \mu_{\text{I}})) n_2^{\text{III}} \end{bmatrix} \end{aligned} \tag{6.64}$$

$$\begin{aligned} kl = 33 \quad \mathbf{f}_{33}^{\partial D_{\text{I}} \cap \partial D_{\text{II}}} &= (C_{i133}^{\text{II}} n_1^{\text{III}} + C_{i233}^{\text{II}} n_2^{\text{III}}) - (C_{i133}^{\text{I}} n_1^{\text{III}} + C_{i233}^{\text{I}} n_2^{\text{III}}) \\ &= \begin{bmatrix} C_{13}^{\text{II}} n_1^{\text{III}} - C_{13}^{\text{I}} n_1^{\text{III}} \\ C_{23}^{\text{II}} n_2^{\text{III}} - C_{23}^{\text{I}} n_2^{\text{III}} \end{bmatrix} \\ &= \begin{bmatrix} (\lambda_{\text{II}} - \lambda_{\text{I}}) n_1^{\text{III}} \\ (\lambda_{\text{II}} - \lambda_{\text{I}}) n_2^{\text{III}} \end{bmatrix} \end{aligned} \tag{6.65}$$

$$\begin{aligned} kl = 12 \quad \mathbf{f}_{12}^{\partial D_{\text{I}} \cap \partial D_{\text{II}}} &= (C_{i112}^{\text{II}} n_1^{\text{III}} + C_{i212}^{\text{II}} n_2^{\text{III}}) - (C_{i112}^{\text{I}} n_1^{\text{III}} + C_{i212}^{\text{I}} n_2^{\text{III}}) \\ &= \begin{bmatrix} C_{66}^{\text{II}} n_1^{\text{III}} - C_{66}^{\text{I}} n_1^{\text{III}} \\ C_{66}^{\text{II}} n_2^{\text{III}} - C_{66}^{\text{I}} n_2^{\text{III}} \end{bmatrix} \\ &= \begin{bmatrix} (\mu_{\text{II}} - \mu_{\text{I}}) n_1^{\text{III}} \\ (\mu_{\text{II}} - \mu_{\text{I}}) n_2^{\text{III}} \end{bmatrix}, \end{aligned} \tag{6.66}$$

where we have used voigt notation for the entries as in [88]. We will use interchangeably the standard index notation for a fourth rank tensor and the Voigt notation representation throughout the remainder of this work and the associated appendix. We also need the interface loads on the fluid matrix interface ∂D_{f}. We have that

$$kl = 11 \quad \mathbf{f}_{11}^{\partial D_{\mathrm{f}}} = C_{i111}^{\mathrm{II}} n_1^{\mathrm{II}} + C_{i211}^{\mathrm{II}} n_2^{\mathrm{II}} = \begin{bmatrix} (\lambda_{\mathrm{II}} + 2\mu_{\mathrm{II}}) n_1^{\mathrm{II}} \\ \lambda_{\mathrm{II}} n_2^{\mathrm{II}} \end{bmatrix} \tag{6.67}$$

$$kl = 22 \quad \mathbf{f}_{22}^{\partial D_{\mathrm{f}}} = C_{i122}^{\mathrm{II}} n_1^{\mathrm{II}} + C_{i222}^{\mathrm{II}} n_2^{\mathrm{II}} = \begin{bmatrix} \lambda_{\mathrm{II}} n_1^{\mathrm{II}} \\ (\lambda_{\mathrm{II}} + 2\mu_{\mathrm{II}}) n_2^{\mathrm{II}} \end{bmatrix} \tag{6.68}$$

$$kl = 33 \quad \mathbf{f}_{33}^{\partial D_{\mathrm{f}}} = C_{i133}^{\mathrm{II}} n_1^{\mathrm{II}} + C_{i233}^{\mathrm{II}} n_2^{\mathrm{II}} = \begin{bmatrix} \lambda_{\mathrm{II}} n_1^{\mathrm{II}} \\ \lambda_{\mathrm{II}} n_2^{\mathrm{II}} \end{bmatrix} \tag{6.69}$$

$$kl = 12 \quad \mathbf{f}_{12}^{\partial D_{\mathrm{f}}} = C_{i112}^{\mathrm{II}} n_1^{\mathrm{II}} + C_{i212}^{\mathrm{II}} n_2^{\mathrm{II}} = \begin{bmatrix} \mu_{\mathrm{II}} n_1^{\mathrm{II}} \\ \mu_{\mathrm{II}} n_2^{\mathrm{II}} \end{bmatrix}. \tag{6.70}$$

6.2.3 3D Cell problems for standard poroelasticity with elastic inclusion

Here we wish to compute the fourth rank effective elasticity tensor $\widetilde{\mathbb{C}}^{\mathrm{SP}}$ for the poroelastic material with elastic inclusion and by using its components calculate the two Young's moduli and two shear moduli corresponding to this setup.

This model requires two steps. We begin by finding the effective elasticity tensor for a poroelastic material and we use components of that tensor as the parameters for the matrix Ω_{PM} at the next scale. The problem we consider is for a porous matrix Ω_{M} with fluid flowing in the pores, shown in the zoomed in area of Fig. 6.1, and we wish to find the effective elasticity tensor $\mathbb{C}_{\mathrm{PM}}$ (porous matrix). That is

$$\mathbb{C}_{\mathrm{PM}} = \langle \mathbb{C}_{\mathrm{Mat}} \mathbb{M}_{\mathrm{Mat}} + \mathbb{C}_{\mathrm{Mat}} \rangle_s, \tag{6.71}$$

where $\mathbb{C}_{\mathrm{Mat}}$ is the elasticity tensor for the elastic matrix and the fourth rank tensor $\mathbb{M}_{\mathrm{Mat}}$ is defined as

$$\mathbb{M}_{\mathrm{Mat}} = \nabla_{\mathbf{y}} B = \frac{1}{2}\left(\frac{\partial B_{pkl}}{\partial y_q} + \frac{\partial B_{qkl}}{\partial y_p} \right). \tag{6.72}$$

We have that the third rank tensor B solves the following cell problem. We have

$$\nabla_{\mathbf{y}} \cdot (\mathbb{C}_{\mathrm{Mat}} \nabla_{\mathbf{y}} B) + \nabla_{\mathbf{y}} \cdot \mathbb{C}_{\mathrm{Mat}} = 0 \quad \text{in} \quad \Omega_s \tag{6.73}$$

$$(\mathbb{C}_{\mathrm{Mat}} \nabla_{\mathbf{y}} B)\mathbf{n} + \mathbb{C}_{\mathrm{Mat}} \mathbf{n} = 0 \quad \text{on} \quad \Gamma_{\mathrm{M}}, \tag{6.74}$$

where $\mathbf{n}$ is the unit normal pointing into the fluid. This problem can be solved as done in [35]. The solution of the problem, which is the fourth rank tensor $\mathbb{M}_{\text{Mat}}$, can be obtained by solving six elastic-type cell problems by fixing the couple of indices in the component wise representation of problem (6.73)-(6.74). This allows each component of $\mathbb{M}_{\text{Mat}}$ to be interpreted as a strain and this means that for each couple of indices that are fixed we have a linear elastic problem with inhomogeneous Neumann interface conditions. The component wise cell problem and the corresponding interface conditions can be found in [35].

The second problem within this setup that we consider is for a composite comprising a matrix that is poroelastic at a finer scale, with parameters supplied from the effective elasticity tensor $\mathbb{C}_{\text{PM}}$, and an isotropic elastic inclusion. We begin by formulating the 3D problems.

Here we will be obtaining the effective elasticity tensor, $\widetilde{\mathbb{C}}^{\text{SP}}$, for our standard poroelastic material with inclusion. That is

$$\widetilde{\mathbb{C}}^{\text{SP}} = \langle \mathbb{C}_{\text{I}}^{\text{SP}} \mathbb{M}_{\text{I}}^{\text{SP}} + \mathbb{C}_{\text{I}}^{\text{SP}} + \mathbb{C}_{\text{PM}} \mathbb{M}_{\text{II}}^{\text{SP}} + \mathbb{C}_{\text{PM}} \rangle_s. \tag{6.75}$$

We can see that this comprises the fourth rank tensor $\mathbb{M}_i^{\text{SP}}$, where $i = \text{I}, \text{II}$, which can be defined as

$$\mathbb{M}_{\text{I}}^{\text{SP}} = \xi_{pq}^{kl}(F^{\text{I}}) = \frac{1}{2}\left(\frac{\partial F_{pkl}^{\text{I}}}{\partial y_q} + \frac{\partial F_{qkl}^{\text{I}}}{\partial y_p}\right); \quad \mathbb{M}_{\text{II}}^{\text{SP}} = \xi_{pq}^{kl}(F^{\text{II}}) = \frac{1}{2}\left(\frac{\partial F_{pkl}^{\text{II}}}{\partial y_q} + \frac{\partial F_{qkl}^{\text{II}}}{\partial y_p}\right). \tag{6.76}$$

We can then write the cell problems for third rank tensors F_{I} and F_{II} with corresponding components F_{ikl}^{I} and F_{ikl}^{II} as

$$\frac{\partial}{\partial y_j}\left(C_{ijpq}^{\text{I}^{\text{SP}}} \xi_{pq}^{kl}(F^{\text{I}})\right) + \frac{\partial C_{ijkl}^{\text{I}^{\text{SP}}}}{\partial y_j} = 0 \qquad \text{in} \quad \Omega_{\text{I}} \tag{6.77}$$

$$\frac{\partial}{\partial y_j}\left(C_{ijpq}^{\text{PM}} \xi_{pq}^{kl}(F^{\text{II}})\right) + \frac{\partial C_{ijkl}^{\text{PM}}}{\partial y_j} = 0 \qquad \text{in} \quad \Omega_{\text{PM}} \tag{6.78}$$

$$C_{ijpq}^{\text{I}^{\text{SP}}} \xi_{pq}^{kl}(F^{\text{I}}) n_j^{\text{PM}} - C_{ijpq}^{\text{PM}} \xi_{pq}^{kl}(F^{\text{II}}) n_j^{\text{PM}} = (C^{\text{PM}} - C^{\text{I}^{\text{SP}}})_{ijkl} n_j^{\text{PM}} \qquad \text{on} \quad \Gamma_{\text{PM}} \tag{6.79}$$

$$F_{ikl}^{\text{I}} = F_{ikl}^{\text{II}} \qquad \text{on} \quad \Gamma_{\text{PM}} \tag{6.80}$$

where $\mathbf{n}^{\text{PM}}$ is the unit normal to the interface Γ_{PM}. We also have introduced the notation $C_{ijkl}^{\text{I}^{\text{SP}}}$, this is the component representation of $\mathbb{C}_{\text{I}}^{\text{SP}}$ and the notation C_{ijkl}^{PM} which is the component wise representation of $\mathbb{C}^{\text{PM}}$. The solutions to the problem (6.77)-(6.80), $\xi_{pq}^{kl}(F^{\text{I}})$

and $\xi^{kl}_{pq}(F^{\mathrm{II}})$, are found by solving six elastic-type cell problems by fixing the couple of indices (k,l). By doing this the $\xi^{kl}_{pq}(F^{\mathrm{I}})$ and $\xi^{kl}_{pq}(F^{\mathrm{II}})$ that appear in (6.19) and (6.23) represent a strain, Then for every fixed couple (k, l) we have a linear elastic problem which has the following interface conditions

$$\begin{aligned}
kl=11 \quad & C^{\mathrm{I^{SP}}}_{ijpq}\xi^{11}_{pq}(F^{\mathrm{I}})n^{\mathrm{PM}}_j - C^{\mathrm{PM}}_{ijpq}\xi^{11}_{pq}(F^{\mathrm{II}})n^{\mathrm{PM}}_j = (C^{\mathrm{PM}} - C^{\mathrm{I^{SP}}})_{ij11}n^{\mathrm{PM}}_j, \\
& \text{where } f^{\Gamma_{\mathrm{PM}}}_i = (C^{\mathrm{PM}} - C^{\mathrm{I^{SP}}})_{ij11}n^{\mathrm{PM}}_j \qquad (6.81) \\
kl=22 \quad & C^{\mathrm{I^{SP}}}_{ijpq}\xi^{22}_{pq}(F^{\mathrm{I}})n^{\mathrm{PM}}_j - C^{\mathrm{PM}}_{ijpq}\xi^{22}_{pq}(F^{\mathrm{II}})n^{\mathrm{PM}}_j = (C^{\mathrm{PM}} - C^{\mathrm{I^{SP}}})_{ij22}n^{\mathrm{PM}}_j, \\
& \text{where } f^{\Gamma_{\mathrm{PM}}}_i = (C^{\mathrm{PM}} - C^{\mathrm{I^{SP}}})_{ij22}n^{\mathrm{PM}}_j \qquad (6.82) \\
kl=33 \quad & C^{\mathrm{I^{SP}}}_{ijpq}\xi^{33}_{pq}(F^{\mathrm{I}})n^{\mathrm{PM}}_j - C^{\mathrm{PM}}_{ijpq}\xi^{33}_{pq}(F^{\mathrm{II}})n^{\mathrm{PM}}_j = (C^{\mathrm{PM}} - C^{\mathrm{I^{SP}}})_{ij33}n^{\mathrm{PM}}_j, \\
& \text{where } f^{\Gamma_{\mathrm{PM}}}_i = (C^{\mathrm{PM}} - C^{\mathrm{I^{SP}}})_{ij33}n^{\mathrm{PM}}_j \qquad (6.83) \\
kl=23 \quad & C^{\mathrm{I^{SP}}}_{ijpq}\xi^{23}_{pq}(F^{\mathrm{I}})n^{\mathrm{PM}}_j - C^{\mathrm{PM}}_{ijpq}\xi^{23}_{pq}(F^{\mathrm{II}})n^{\mathrm{PM}}_j = (C^{\mathrm{PM}} - C^{\mathrm{I^{SP}}})_{ij23}n^{\mathrm{PM}}_j, \\
& \text{where } f^{\Gamma_{\mathrm{PM}}}_i = (C^{\mathrm{PM}} - C^{\mathrm{I^{SP}}})_{ij23}n^{\mathrm{PM}}_j \qquad (6.84) \\
kl=13 \quad & C^{\mathrm{I^{SP}}}_{ijpq}\xi^{13}_{pq}(F^{\mathrm{I}})n^{\mathrm{PM}}_j - C^{\mathrm{PM}}_{ijpq}\xi^{13}_{pq}(F^{\mathrm{II}})n^{\mathrm{PM}}_j = (C^{\mathrm{PM}} - C^{\mathrm{I^{SP}}})_{ij13}n^{\mathrm{PM}}_j, \\
& \text{where } f^{\Gamma_{\mathrm{PM}}}_i = (C^{\mathrm{PM}} - C^{\mathrm{I^{SP}}})_{ij13}n^{\mathrm{PM}}_j \qquad (6.85) \\
kl=12 \quad & C^{\mathrm{I^{SP}}}_{ijpq}\xi^{12}_{pq}(F^{\mathrm{I}})n^{\mathrm{PM}}_j - C^{\mathrm{PM}}_{ijpq}\xi^{12}_{pq}(F^{\mathrm{II}})n^{\mathrm{PM}}_j = (C^{\mathrm{PM}} - C^{\mathrm{I^{SP}}})_{ij12}n^{\mathrm{PM}}_j, \\
& \text{where } f^{\Gamma_{\mathrm{PM}}}_i = (C^{\mathrm{PM}} - C^{\mathrm{I^{SP}}})_{ij12}n^{\mathrm{PM}}_j. \qquad (6.86)
\end{aligned}$$

In this case we assume that the fourth rank elasticity tensor $C^{\mathrm{I^{SP}}}_{ijpq}$ is isotropic at the microscale and C^{PM}_{ijpq} has components calculated by solving the poroelastic problem (6.73)-(6.74) above. That is

$$C^{\mathrm{I^{SP}}}_{ijpq} = \lambda^{\mathrm{I^{SP}}}\delta_{ij}\delta_{pq} + \mu^{\mathrm{I^{SP}}}(\delta_{ip}\delta_{jq} + \delta_{iq}\delta_{jp}) \qquad (6.87)$$

and

$$\mathbb{C}_{\mathrm{PM}} = \begin{bmatrix}
C^{\mathrm{PM}}_{11} & C^{\mathrm{PM}}_{12} & C^{\mathrm{PM}}_{13} & 0 & 0 & 0 \\
C^{\mathrm{PM}}_{12} & C^{\mathrm{PM}}_{11} & C^{\mathrm{PM}}_{13} & 0 & 0 & 0 \\
C^{\mathrm{PM}}_{13} & C^{\mathrm{PM}}_{13} & C^{\mathrm{PM}}_{33} & 0 & 0 & 0 \\
0 & 0 & 0 & C^{\mathrm{PM}}_{44} & 0 & 0 \\
0 & 0 & 0 & 0 & C^{\mathrm{PM}}_{44} & 0 \\
0 & 0 & 0 & 0 & 0 & C^{\mathrm{PM}}_{66}
\end{bmatrix} \qquad (6.88)$$

where we have used Voigt notation to represent the components of the tenor $\mathbb{C}_{\mathrm{PM}}$. We

should note that this effective elasticity tensor possesses tetragonal symmetry, that is, possessing six distinct elastic entries. The reason for the six entries is due to our choice of geometry (see Fig. 6.1 cube with cylindrical voids) which means that our x and y directions are equivalent hence the reduction from the nine entries in the orthotropic case to the six entries we have here.

We can then use (6.87) and (6.88) in the interface loads to determine the $f_i^{\Gamma_{\rm PM}}$. That is

$$kl = 11 \quad \mathbf{f}^{\Gamma_{\rm PM}} = \text{diag}\begin{bmatrix} C_{11}^{\rm PM} \\ C_{12}^{\rm PM} \\ C_{13}^{\rm PM} \end{bmatrix} \mathbf{n}^{\rm PM} - \lambda^{\rm I^{SP}} \mathbf{n}^{\rm PM} - 2\mu^{\rm I^{SP}} n_1^{\rm PM} \mathbf{e}_1 \tag{6.89}$$

$$kl = 22 \quad \mathbf{f}^{\Gamma_{\rm PM}} = \text{diag}\begin{bmatrix} C_{12}^{\rm PM} \\ C_{11}^{\rm PM} \\ C_{13}^{\rm PM} \end{bmatrix} \mathbf{n}^{\rm PM} - \lambda^{\rm I^{SP}} \mathbf{n}^{\rm PM} - 2\mu^{\rm I^{SP}} n_2^{\rm PM} \mathbf{e}_2 \tag{6.90}$$

$$kl = 33 \quad \mathbf{f}^{\Gamma_{\rm PM}} = \text{diag}\begin{bmatrix} C_{13}^{\rm PM} \\ C_{13}^{\rm PM} \\ C_{33}^{\rm PM} \end{bmatrix} \mathbf{n}^{\rm PM} - \lambda^{\rm I^{SP}} \mathbf{n}^{\rm PM} - 2\mu^{\rm I^{SP}} n_3^{\rm PM} \mathbf{e}_3 \tag{6.91}$$

$$kl = 23 \quad \mathbf{f}^{\Gamma_{\rm PM}} = \text{diag}\begin{bmatrix} -\mu^{\rm I^{SP}} \\ C_{44}^{\rm PM} - \mu^{\rm I^{SP}} \\ C_{44}^{\rm PM} - \mu^{\rm I^{SP}} \end{bmatrix} (n_3^{\rm PM} \mathbf{e}_2 + n_2^{\rm PM} \mathbf{e}_3) \tag{6.92}$$

$$kl = 13 \quad \mathbf{f}^{\Gamma_{\rm PM}} = \text{diag}\begin{bmatrix} C_{44}^{\rm PM} - \mu^{\rm I^{SP}} \\ -\mu^{\rm I^{SP}} \\ C_{44}^{\rm PM} - \mu^{\rm I^{SP}} \end{bmatrix} (n_3^{\rm PM} \mathbf{e}_1 + n_1^{\rm PM} \mathbf{e}_3) \tag{6.93}$$

$$kl = 12 \quad \mathbf{f}^{\Gamma_{\rm PM}} = \text{diag}\begin{bmatrix} C_{66}^{\rm PM} - \mu^{\rm I^{SP}} \\ C_{66}^{\rm PM} - \mu^{\rm I^{SP}} \\ -\mu^{\rm I^{SP}} \end{bmatrix} (n_2^{\rm PM} \mathbf{e}_1 + n_1^{\rm PM} \mathbf{e}_2) \tag{6.94}$$

where we have used $n_1^{\rm PM}$, $n_2^{\rm PM}$ and $n_3^{\rm PM}$ to mean the components of the unit vector normal to the interface $\Gamma_{\rm PM}$ and we have used the standard unit vectors in the Cartesian coordinate system $\mathbf{e}_1$, $\mathbf{e}_2$ and $\mathbf{e}_3$.

This current setup is for solving the 3D problem. We are again able to perform a reduction so that we instead study the 2D problem.

6.2.4 2D Cell problems for standard poroelasticity with elastic inclusion

We now wish to consider the 2D reduction of the cell problems that have been presented in the previous subsection. Within this model set up we have two different cell problems to solve. The first is the cell problem for a porous matrix. The geometry of our periodic cell in this case is such that we have a cube with 4 cylindrical voids placed in each of the corners of the cube extending from the top to the bottom of the cell in the $\mathbf{e}_3$ direction. This means that at every cross-section in the $\mathbf{e}_3$ direction gives a square with 4 circular voids.

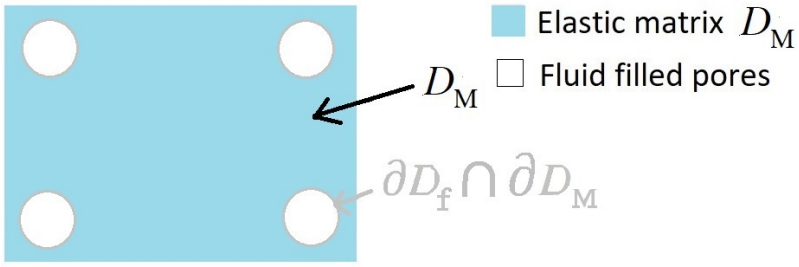

Figure 6.3: 2D domain for Porous matrix microstructure

We can consider the 2D reduction presented in the appendix where we assume that there is only the matrix D_{M} and the voids and assuming the matrix is isotropic. This means that we have that $C_{1111} = C_{2222} = C_{3333} = \lambda_{\mathrm{M}} + 2\mu_{\mathrm{M}}$, $C_{2323} = C_{1313} = C_{1212} = \mu_{\mathrm{M}}$ and $C_{1122} = C_{2211} = C_{1133} = C_{3311} = C_{2233} = C_{3322} = \lambda_{\mathrm{M}}$. Using these assumptions in the anti-plane problem (B.18)-(B.22), where we only require (B.19) and (B.22)

$$\mu^{\mathrm{M}} \frac{\partial B_{3kl}}{\partial y_1^2} + \mu^{\mathrm{M}} \frac{\partial B_{3kl}}{\partial y_2^2} = 0 \qquad \text{in} \quad D_{\mathrm{M}} \tag{6.95}$$

$$\mu^{\mathrm{M}} \frac{\partial B_{3kl}}{\partial y_1} n_1 + \mu^{\mathrm{M}} \frac{\partial B_{3kl}}{\partial y_2} n_2 + C^{\mathrm{M}}_{31kl} n_1 + C^{\mathrm{M}}_{32kl} n_2 = 0 \qquad \text{on} \quad \partial D_{\mathrm{f}} \cap \partial D_{\mathrm{M}} \tag{6.96}$$

where the notation D_{M} is the corresponding 2D slice of Ω_{M} and the interface $\partial D_{\mathrm{f}} \cap \partial D_{\mathrm{M}}$ is the 2D projection of Γ_{M}. We also note that the normal to the interface $\mathbf{n}$ is the same normal in 3D as in 2D since it is the outward normal to a cylinder in 3D and is the same to the circle in the 2D slices but with only components n_1 and n_2.

The solutions to the problem (6.95) and (6.96) are found by solving the two anti-plane problems by fixing the couple $(k, l) = (1, 3) = (3, 1), (2, 3) = (3, 2)$. Then for every fixed

couple we have the Poisson problem with the following interface conditions.

$$\begin{aligned} kl = 23 \quad & \mu^{\mathrm{M}} \frac{\partial B_{323}}{\partial y_1} n_1 + \mu^{\mathrm{M}} \frac{\partial B_{323}}{\partial y_2} n_2 = -(C^{\mathrm{M}}_{3123} n_1 + C^{\mathrm{M}}_{3223} n_2), \\ \text{where} \quad & f^{\partial D_{\mathrm{f}} \cap \partial D_{\mathrm{M}}}_{\mathrm{anti}} = C^{\mathrm{M}}_{3123} n_1 + C^{\mathrm{M}}_{3223} n_2 \end{aligned} \tag{6.97}$$

$$\begin{aligned} kl = 13 \quad & \mu^{\mathrm{M}} \frac{\partial B_{313}}{\partial y_1} n_1 + \mu^{\mathrm{M}} \frac{\partial B_{313}}{\partial y_2} n_2 = -(C^{\mathrm{M}}_{3113} n_1 + C^{\mathrm{M}}_{3213} n_2), \\ \text{where} \quad & f^{\partial D_{\mathrm{f}} \cap \partial D_{\mathrm{M}}}_{\mathrm{anti}} = C^{\mathrm{M}}_{3113} n_1 + C^{\mathrm{M}}_{3213} n_2 \end{aligned} \tag{6.98}$$

where the forces can be written using the assumption of isotropy of both phases as

$$kl = 23 \qquad f^{\partial D_{\mathrm{f}} \cap \partial D_{\mathrm{M}}}_{\mathrm{anti}} = C^{\mathrm{M}}_{3223} n_2 = \mu^{\mathrm{M}} n_2 \tag{6.99}$$

$$kl = 13 \qquad f^{\partial D_{\mathrm{f}} \cap \partial D_{\mathrm{M}}}_{\mathrm{anti}} = C^{\mathrm{M}}_{3113} n_1 = \mu^{\mathrm{M}} n_1. \tag{6.100}$$

We now need to consider the in-plane problems. We have the problem (B.23)-(B.27) from the appendix, however for the case of a porous matrix we only require (B.23) and (B.27). We can consider the interface loads on the matrix fluid interface (B.29). We assume that the matrix material is isotropic. Each interface load is a vector with two components, due to $i = 1, 2$. We fix the couple (k, l) and obtain

$$kl = 11 \qquad \mathbf{f}^{\partial D_{\mathrm{f}} \cap \partial D_{\mathrm{M}}}_{11} = C^{\mathrm{M}}_{i111} n_1 + C^{\mathrm{M}}_{i211} n_2 = \begin{bmatrix} (\lambda_{\mathrm{M}} + 2\mu_{\mathrm{M}}) n_1 \\ \lambda_{\mathrm{M}} n_2 \end{bmatrix} \tag{6.101}$$

$$kl = 22 \qquad \mathbf{f}^{\partial D_{\mathrm{f}} \cap \partial D_{\mathrm{M}}}_{22} = C^{\mathrm{M}}_{i122} n_1 + C^{\mathrm{M}}_{i222} n_2 = \begin{bmatrix} \lambda_{\mathrm{M}} n_1 \\ (\lambda_{\mathrm{M}} + 2\mu_{\mathrm{M}}) n_2 \end{bmatrix} \tag{6.102}$$

$$kl = 33 \qquad \mathbf{f}^{\partial D_{\mathrm{f}} \cap \partial D_{\mathrm{M}}}_{33} = C^{\mathrm{M}}_{i133} n_1 + C^{\mathrm{M}}_{i233} n_2 = \begin{bmatrix} \lambda_{\mathrm{M}} n_1 \\ \lambda_{\mathrm{M}} n_2 \end{bmatrix} \tag{6.103}$$

$$kl = 12 \qquad \mathbf{f}^{\partial D_{\mathrm{f}} \cap \partial D_{\mathrm{M}}}_{12} = C^{\mathrm{M}}_{i112} n_1 + C^{\mathrm{M}}_{i212} n_2 = \begin{bmatrix} \mu_{\mathrm{M}} n_1 \\ \mu_{\mathrm{M}} n_2 \end{bmatrix} \tag{6.104}$$

The second cell problem is for an elastic composite that comprises the porous matrix and the elastic inclusion. The geometry of our periodic cell in this case is a cube with an embedded cylinder placed in the centre extending from the top to the bottom of the cell in the $\mathbf{e}_3$ direction. This means that at every cross-section in the $\mathbf{e}_3$ direction gives a square with an embedded circle in the centre.

We can consider the 2D reduction presented in the appendix in the case where there

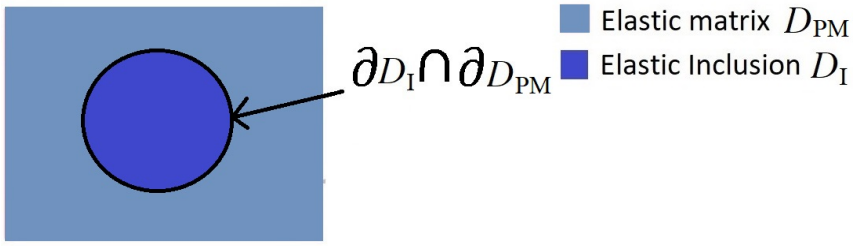

Figure 6.4: 2D domain for Standard Poroelastic setup microstructure

is no void. We assume that the inclusion is isotropic $C^{\mathrm{SP}}_{1111} = C^{\mathrm{SP}}_{2222} = C^{\mathrm{SP}}_{3223} = \lambda^{\mathrm{SP}}_{\mathrm{I}} + 2\mu^{\mathrm{SP}}_{\mathrm{I}}$, $C^{\mathrm{SP}}_{2323} = C^{\mathrm{SP}}_{1313} = C^{\mathrm{SP}}_{1212} = \mu^{\mathrm{SP}}_{\mathrm{I}}$ and $C^{\mathrm{SP}}_{1122} = C^{\mathrm{SP}}_{2211} = C^{\mathrm{SP}}_{1133} = C^{\mathrm{SP}}_{3311} = C^{\mathrm{SP}}_{2233} = C^{\mathrm{SP}}_{3322} = \lambda^{\mathrm{SP}}_{\mathrm{I}}$, and the matrix has its input from $\mathbb{C}_{\mathrm{PM}}$. Using this in the anti-plane problem, where we require only (B.18)-(B.21) we obtain

$$\mu^{\mathrm{I^{SP}}} \frac{\partial F^{\mathrm{I}}_{3kl}}{\partial y_1^2} + \mu^{\mathrm{I^{SP}}} \frac{\partial F^{\mathrm{I}}_{3kl}}{\partial y_2^2} = 0 \qquad \text{in} \quad D_{\mathrm{I}} \tag{6.105}$$

$$C^{\mathrm{PM}}_{3131} \frac{\partial F^{\mathrm{II}}_{3kl}}{\partial y_1^2} + C^{\mathrm{PM}}_{3232} \frac{\partial F^{\mathrm{II}}_{3kl}}{\partial y_2^2} = 0 \qquad \text{in} \quad D_{\mathrm{PM}} \tag{6.106}$$

$$\begin{aligned} &\mu^{\mathrm{I^{SP}}} \frac{\partial F^{\mathrm{I}}_{3kl}}{\partial y_1} n_1^{\mathrm{PM}} + \mu^{\mathrm{I^{SP}}} \frac{\partial F^{\mathrm{I}}_{3kl}}{\partial y_2} n_2^{\mathrm{PM}} - \big(C^{\mathrm{PM}}_{3131} \frac{\partial F^{\mathrm{PM}}_{3kl}}{\partial y_1} n_1^{\mathrm{PM}} + C^{\mathrm{PM}}_{3232} \frac{\partial F^{\mathrm{PM}}_{3kl}}{\partial y_2} n_2^{\mathrm{PM}}\big) \\ &= (C^{\mathrm{PM}}_{31kl} n_1^{\mathrm{PM}} + C^{\mathrm{PM}}_{32kl} n_2^{\mathrm{PM}}) - (C^{\mathrm{I}}_{31kl} n_1^{\mathrm{PM}} + C^{\mathrm{I}}_{32kl} n_2^{\mathrm{PM}}) \qquad \text{on} \quad \partial D_{\mathrm{I}} \cap \partial D_{\mathrm{PM}} \end{aligned} \tag{6.107}$$

$$F^{\mathrm{I}}_{3kl} = F^{\mathrm{II}}_{3kl} \qquad \text{on} \quad \partial D_{\mathrm{I}} \cap \partial D_{\mathrm{PM}} \tag{6.108}$$

where D_{I}, D_{PM} are the 2D slices of Ω_{I} and Ω_{PM} and the interface $\partial D_{\mathrm{I}} \cap \partial D_{\mathrm{PM}}$ is the 2D projection of Γ_{PM} and n_1^{PM} and n_2^{PM} are the two components of the normal $\mathbf{n}^{\mathrm{PM}}$ that are used in the 2D cell problem.

The solutions to the problem (6.105)-(6.108) are found by solving the two anti-plane problems by fixing the couple (k,l)=(1,3)=(3,1), (2,3)=(3,2). Then for every fixed couple we have the Poisson problem with the following interface conditions. On the matrix inclusion interface we have

$$\begin{aligned} kl = 23 \qquad &\mu^{\mathrm{I^{SP}}} \frac{\partial F^{\mathrm{I}}_{323}}{\partial y_1} n_1^{\mathrm{PM}} + \mu^{\mathrm{I^{SP}}} \frac{\partial F^{\mathrm{I}}_{323}}{\partial y_2} n_2^{\mathrm{PM}} - \big(C^{\mathrm{PM}}_{3131} \frac{\partial F^{\mathrm{PM}}_{323}}{\partial y_1} n_1^{\mathrm{PM}} + C^{\mathrm{PM}}_{3232} \frac{\partial F^{\mathrm{PM}}_{323}}{\partial y_2} n_2^{\mathrm{PM}}\big) \\ &= (C^{\mathrm{PM}}_{3123} n_1^{\mathrm{PM}} + C^{\mathrm{PM}}_{3223} n_2^{\mathrm{PM}}) - (C^{\mathrm{I}}_{3123} n_1^{\mathrm{PM}} + C^{\mathrm{I}}_{3223} n_2^{\mathrm{PM}}), \\ &\text{where,} \\ &f^{\partial D_{\mathrm{I}} \cap \partial D_{\mathrm{PM}}}_{\mathrm{anti}} = (C^{\mathrm{PM}}_{3123} n_1^{\mathrm{PM}} + C^{\mathrm{PM}}_{3223} n_2^{\mathrm{PM}}) - (C^{\mathrm{I}}_{3123} n_1^{\mathrm{PM}} + C^{\mathrm{I}}_{3223} n_2^{\mathrm{PM}}) \end{aligned} \tag{6.109}$$

$$kl = 13 \qquad \mu^{\mathrm{I^{SP}}} \frac{\partial F^{\mathrm{I}}_{313}}{\partial y_1} n_1^{\mathrm{PM}} + \mu^{\mathrm{I^{SP}}} \frac{\partial F^{\mathrm{I}}_{313}}{\partial y_2} n_2^{\mathrm{PM}} - \big(C^{\mathrm{PM}}_{3131} \frac{\partial F^{\mathrm{PM}}_{313}}{\partial y_1} n_1^{\mathrm{PM}} + C^{\mathrm{PM}}_{3232} \frac{\partial F^{\mathrm{PM}}_{313}}{\partial y_2} n_2^{\mathrm{PM}}\big)$$

$$= (C^{\mathrm{PM}}_{3113} n^{\mathrm{PM}}_1 + C^{\mathrm{PM}}_{3213} n^{\mathrm{PM}}_2) - (C^{\mathrm{I}}_{3113} n^{\mathrm{PM}}_1 + C^{\mathrm{I}}_{3213} n^{\mathrm{PM}}_2),$$

where,

$$f^{\partial D_{\mathrm{I}} \cap \partial D_{\mathrm{PM}}}_{\mathrm{anti}} = (C^{\mathrm{PM}}_{3113} n^{\mathrm{PM}}_1 + C^{\mathrm{PM}}_{3213} n^{\mathrm{PM}}_2) - (C^{\mathrm{I}}_{3113} n^{\mathrm{PM}}_1 + C^{\mathrm{I}}_{3213} n^{\mathrm{PM}}_2) \tag{6.110}$$

where the forces $f^{\partial D_{\mathrm{I}} \cap \partial D_{\mathrm{PM}}}_{\mathrm{anti}}$ on the interface $\partial D_{\mathrm{I}} \cap \partial D_{\mathrm{PM}}$ can be written using the assumption of isotropy of the inclusion and using the entries of $\mathbb{C}^{\mathrm{PM}}$ for the matrix

$$kl = 23 \qquad f^{\partial D_{\mathrm{I}} \cap \partial D_{\mathrm{PM}}}_{\mathrm{anti}} = C^{\mathrm{PM}}_{3223} n^{\mathrm{PM}}_2 - C^{\mathrm{I}}_{3223} n^{\mathrm{PM}}_2 = C^{\mathrm{PM}}_{44} n^{\mathrm{PM}}_2 - \mu^{\mathrm{I}^{\mathrm{SP}}} n^{\mathrm{PM}}_2 \tag{6.111}$$

$$kl = 13 \qquad f^{\partial D_{\mathrm{I}} \cap \partial D_{\mathrm{PM}}}_{\mathrm{anti}} = C^{\mathrm{PM}}_{3113} n^{\mathrm{PM}}_1 - C^{\mathrm{I}}_{3113} n^{\mathrm{PM}}_1 = C^{\mathrm{PM}}_{55} n^{\mathrm{PM}}_1 - \mu^{\mathrm{I}^{\mathrm{SP}}} n^{\mathrm{PM}}_1. \tag{6.112}$$

We now need to consider the in-plane problems. Using (B.23)-(B.26) from the appendix where we assume that the inclusion is isotropic and we use the values of $\mathbb{C}_{\mathrm{PM}}$. Each interface load is a vector with two components, due to $i = 1, 2$. We fix the couple (k,l) and obtain on the matrix inclusion interface

$$\begin{aligned} kl = 11 \qquad \mathbf{f}^{\partial D_{\mathrm{I}} \cap \partial D_{\mathrm{PM}}}_{11} &= (C^{\mathrm{PM}}_{i111} n^{\mathrm{PM}}_1 + C^{\mathrm{PM}}_{i211} n^{\mathrm{PM}}_2) - (C^{\mathrm{I}}_{i111} n^{\mathrm{PM}}_1 + C^{\mathrm{I}}_{i211} n^{\mathrm{PM}}_2) \\ &= \begin{bmatrix} C^{\mathrm{PM}}_{11} n^{\mathrm{PM}}_1 - C^{\mathrm{I}}_{11} n^{\mathrm{PM}}_1 \\ C^{\mathrm{PM}}_{12} n^{\mathrm{PM}}_2 - C^{\mathrm{I}}_{12} n^{\mathrm{PM}}_2 \end{bmatrix} \\ &= \begin{bmatrix} (C^{\mathrm{PM}}_{11} - \lambda^{\mathrm{SP}}_{\mathrm{I}} - 2\mu^{\mathrm{SP}}_{\mathrm{I}}) n^{\mathrm{PM}}_1 \\ (C^{\mathrm{PM}}_{12} - \lambda^{\mathrm{SP}}_{\mathrm{I}}) n^{\mathrm{PM}}_2 \end{bmatrix} \end{aligned} \tag{6.113}$$

$$\begin{aligned} kl = 22 \qquad \mathbf{f}^{\partial D_{\mathrm{I}} \cap \partial D_{\mathrm{PM}}}_{22} &= (C^{\mathrm{PM}}_{i122} n^{\mathrm{PM}}_1 + C^{\mathrm{PM}}_{i222} n^{\mathrm{PM}}_2) - (C^{\mathrm{I}}_{i122} n^{\mathrm{PM}}_1 + C^{\mathrm{I}}_{i222} n^{\mathrm{PM}}_2) \\ &= \begin{bmatrix} C^{\mathrm{PM}}_{12} n^{\mathrm{PM}}_1 - C^{\mathrm{I}}_{12} n^{\mathrm{PM}}_1 \\ C^{\mathrm{PM}}_{22} n^{\mathrm{PM}}_2 - C^{\mathrm{I}}_{22} n^{\mathrm{PM}}_2 \end{bmatrix} \\ &= \begin{bmatrix} (C^{\mathrm{PM}}_{12} - \lambda^{\mathrm{SP}}_{\mathrm{I}}) n^{\mathrm{PM}}_1 \\ (C^{\mathrm{PM}}_{22} - \lambda^{\mathrm{SP}}_{\mathrm{I}} - 2\mu^{\mathrm{SP}}_{\mathrm{I}}) n^{\mathrm{PM}}_2 \end{bmatrix} \end{aligned} \tag{6.114}$$

$$\begin{aligned} kl = 33 \qquad \mathbf{f}^{\partial D_{\mathrm{I}} \cap \partial D_{\mathrm{PM}}}_{33} &= (C^{\mathrm{PM}}_{i133} n^{\mathrm{PM}}_1 + C^{\mathrm{PM}}_{i233} n^{\mathrm{PM}}_2) - (C^{\mathrm{I}}_{i133} n^{\mathrm{PM}}_1 + C^{\mathrm{I}}_{i233} n^{\mathrm{PM}}_2) \\ &= \begin{bmatrix} C^{\mathrm{PM}}_{13} n^{\mathrm{PM}}_1 - C^{\mathrm{I}}_{13} n^{\mathrm{PM}}_1 \\ C^{\mathrm{PM}}_{23} n^{\mathrm{PM}}_2 - C^{\mathrm{I}}_{23} n^{\mathrm{PM}}_2 \end{bmatrix} \\ &= \begin{bmatrix} (C^{\mathrm{PM}}_{13} - \lambda^{\mathrm{SP}}_{\mathrm{I}}) n^{\mathrm{PM}}_1 \\ (C^{\mathrm{PM}}_{23} - \lambda^{\mathrm{SP}}_{\mathrm{I}}) n^{\mathrm{PM}}_2 \end{bmatrix} \end{aligned} \tag{6.115}$$

$$kl = 12 \qquad \mathbf{f}^{\partial D_{\mathrm{I}} \cap \partial D_{\mathrm{PM}}}_{12} = (C^{\mathrm{PM}}_{i112} n^{\mathrm{PM}}_1 + C^{\mathrm{PM}}_{i212} n^{\mathrm{PM}}_2) - (C^{\mathrm{I}}_{i112} n^{\mathrm{PM}}_1 + C^{\mathrm{I}}_{i212} n^{\mathrm{PM}}_2)$$

$$
\begin{aligned}
&= \begin{bmatrix} C_{66}^{\mathrm{PM}} n_1^{\mathrm{PM}} - C_{66}^{\mathrm{I}} n_1^{\mathrm{PM}} \\ C_{66}^{\mathrm{PM}} n_2^{\mathrm{PM}} - C_{66}^{\mathrm{I}} n_2^{\mathrm{PM}} \end{bmatrix} \\
&= \begin{bmatrix} (C_{66}^{\mathrm{PM}} - \mu_{\mathrm{I}}^{\mathrm{SP}}) n_1^{\mathrm{PM}} \\ (C_{66}^{\mathrm{PM}} - \mu_{\mathrm{I}}^{\mathrm{SP}}) n_2^{\mathrm{PM}} \end{bmatrix}
\end{aligned} \tag{6.116}
$$

6.3 Applications & Results

Within this section we present the results of solving the 2D cell problems that were presented for each of the two different setups described in Sec. 6.1 using COMSOL Multiphysics 4.3. The solution is computed by following the procedures detailed in Sec. 6.2. We present the difference in the elastic parameters, Young's and Shear moduli, for the two different model setups. We interpret under which scenarios each model should be used. We also highlight how this framework could be applied to modelling of the heart.

6.3.1 2D Simulation Results

Within this section we solve the 2D cell problems setup in the previous sections Sec. 6.2.2 and Sec. 6.2.4. We set up our problems on a unit square cell with the circular elastic subphase accounting for 20% volume fraction and the porosity varying from 2% - 30% divided among the four cylinders.

We solve the cell problems using the following parameters. For the LMRP model we have the matrix D_{II} with Poisson ratio 0.4 and Young's modulus 80 kPa, we have the elastic inclusion D_{I} with volume fraction 20% with Poisson ratio 0.49 and Young's modulus 35 kPa. These values have been selected at random to have a difference in stiffness and compressibility between the two elstic phases yet keeping them on the same order of magnitude.

For the standard poroelastic material with elastic inclusion we have two steps, the first is the porous matrix problem where we have the matrix D_{M} with Poisson ratio 0.4 and Young's modulus 80 kPa, and for the second step we have the problem between the inclusion and the porous matrix, where we have the matrix informed by the results from the porous matrix simulations and the elastic inclusion D_{I} with volume fraction 20% with Poisson ratio 0.49 and Young's modulus 35 kPa. This keeps the parameters consistent between the two model setups.

We begin by considering the comparison of the two Young's moduli E_1 transverse and

E_3 axial for the LMRP model and the standard poroelasticity with inclusion setup. Using the components of the effective elasticity tensors that we compute for each of the models at varying porosities we have the formulas for the Young's moduli given by

$$E_1^\theta = \frac{(C_{12}^\theta - C_{11}^\theta)(2C_{13}^{2^\theta} - C_{12}^\theta C_{33}^\theta - C_{11}^\theta C_{33}^\theta)}{(-C_{13}^{\theta^2} + C_{11}^\theta C_{33}^\theta)} \tag{6.117}$$

$$E_3^\theta = \frac{(2C_{13}^{2^\theta} - C_{12}^\theta C_{33}^\theta - C_{11}^\theta C_{33}^\theta)}{(-C_{12}^\theta - C_{11}^\theta)} \tag{6.118}$$

where the superscript $\theta = \text{LMRP}, \text{SP}$ determines which model we are using. We have plotted the results of these Young's moduli with a range of porosities from $2\% - 30\%$ in the figures Fig. 6.5a and Fig. 6.5b

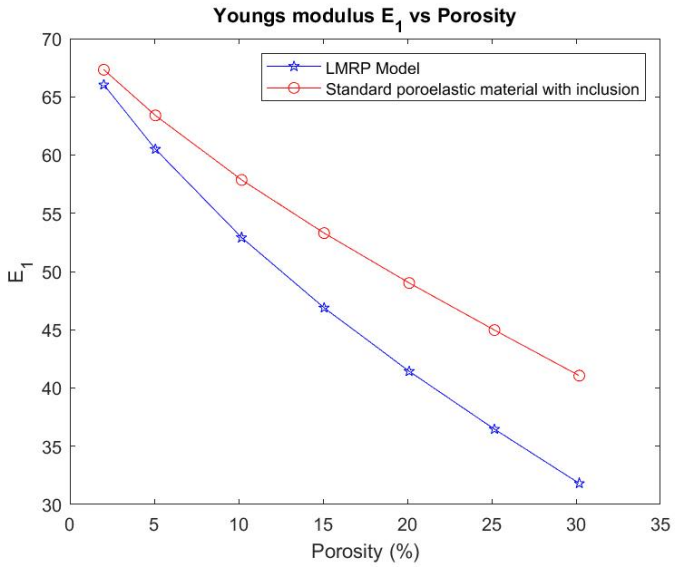

(a) E_1 versus porosity

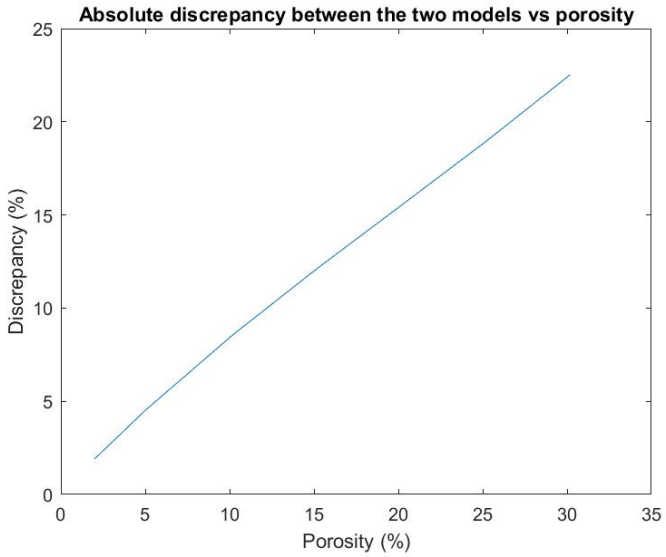

(b) The difference between the two models vs porosity

Figure 6.5: Results of Young's Modulus E_1 simulations

By considering Fig. 6.5a we can see that the Young's modulus E_1 (transverse) decreases with increasing porosity. We can also see that the transverse Young's modulus is lower for the LMRP model. For this reason we have plotted the difference between the LMRP model and the standard poroelastic with inclusion setup in Fig. 6.5b. From this plot we can see that at approx 5% porosity there is already a difference of 5 % between the two different model setups. This difference between the models increases to approx 22% at 30% porosity. This means that the influence that the porosity has on the overall material stiffness, when directly being considered with the other phases, is considerably more prominant than when

considering the porosity at the finer scale.

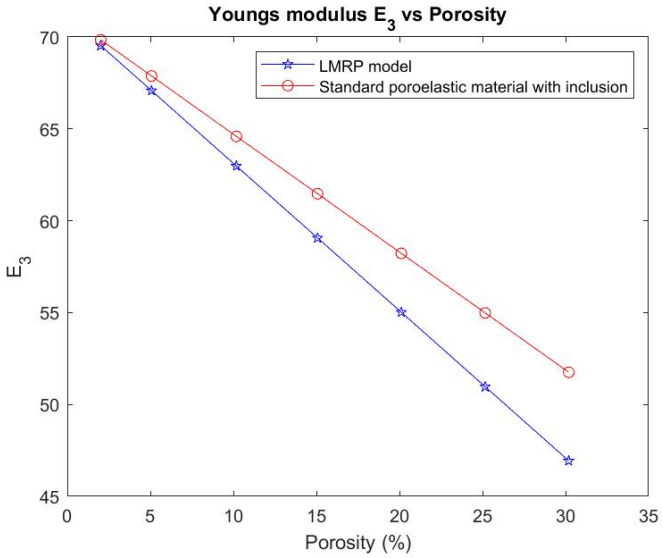

(a) E_3 versus porosity

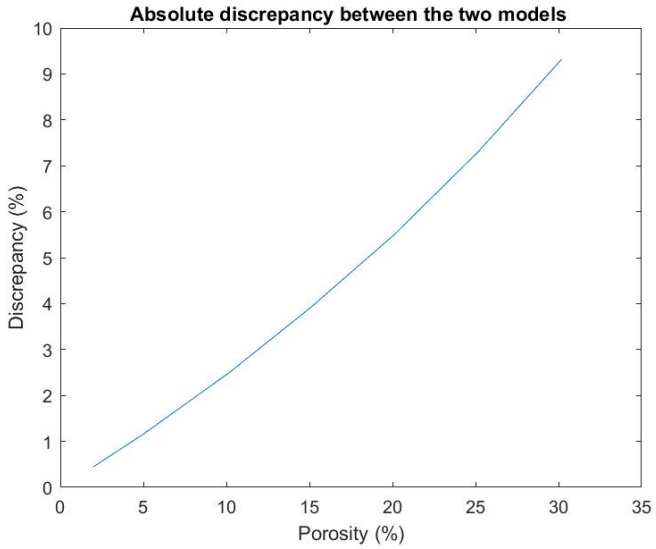

(b) Absolute difference between the two models vs porosity

Figure 6.6: Results of Young's Modulus E_3 simulations

We can now consider Fig. 6.6a and we can see that the Young's modulus E_3 (axial) also decreases with increasing porosity. Similarly to the transverse Young's modulus, we can see that the axial Young's modulus is also lower for the LMRP model. We have again plotted the absolute difference between the LMRP model and the standard poroelastic setup in Fig. 6.6b. From this plot we can see that at approx 10% porosity there is already a difference of 2.5 % between the two different model setups, rising to almost 10% at 30% porosity. This again means that the influence that the porosity has on the overall

material stiffness when directly being considered with the other phases is considerably more prominent than when considering the porosity at the finer scale. However, the effect is slightly less prominent on the axial Young's modulus than the transverse one.

The other two elastic parameters that we compare for the two different model setups are the shear moduli C_{44}^{θ} and C_{66}^{θ}, where $\theta = \text{LMRP}, \text{SP}$. These parameters are taken directly from the computed effective elasticity tensor for each of the models. We have plotted the comparison of the shear moduli over a range of porosities from $2\% - 30\%$.

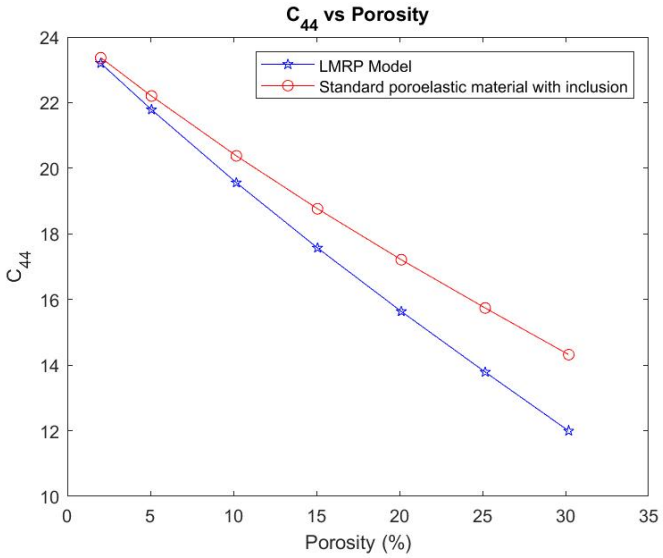

(a) Shear C_{44} versus porosity

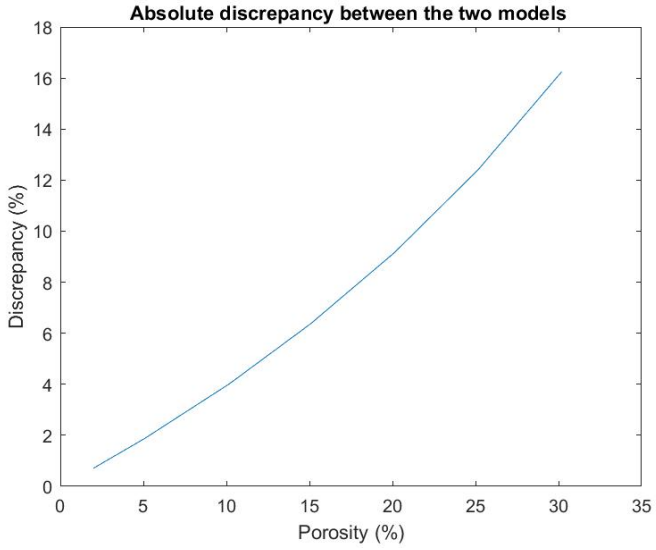

(b) Absolute difference between the two models vs porosity

Figure 6.7: Results of Shear Modulus C_{44} simulations

In Fig. 6.7a we see that the shear C_{44} decreases with increasing porosity and that the

LMRP model decreases more than the standard poroelastic type setup. For C_{44} the force is being applied in the axial direction which is the direction in which the inclusion and the voids elongate. This means that when the force is applied the material deforms and the voids flatten out, the voids just make it softer allowing for the decrease in shear with increasing porosity. The standard poroelastic type model has less of a decrease in shear due to the fact that is does not have the voids present at this scale but accounts for the increasing porosity of the matrix at a finer scale (where the voids are present). We also see that the difference between the two models is increasing with increasing porosity. For these reasons we wish to consider the absolute difference between the two model setups, and this has been done in Fig. 6.7b. We can see that for 5% porosity we have approximately a 2% difference between the two model setups. This increases to a 16% discrepancy for a 30% porosity. This means that when the porosity exceeds 5% it is more useful and accurate to use the LMRP model to describe the behaviour of the material parameter C_{44}. For porosities below 5% then the standard poroelastic setup can be realistically used.

In Fig. 6.8a we can see that there is very little difference between the in-plane shear for both models when the porosity is less than 20%, however after this point the difference becomes more pronounced. This is confirmed by the absolute difference plot, see Fig. 6.8b, where we can see that up to 20% porosity the discrepancy between the models does not exceed 2%, however after this point it reaches 13% when porosity is 30%. For C_{66} the force is being applied in the x-direction (transverse). Therefore for the LMRP model the force is being applied taking a cross section of structure which contains the voids and inclusions. At higher porosities this makes the material weaker as the larger voids deform and hence the larger decrease in shear compared with C_{44}. Up until approx 20% porosity the difference in the two models is negligible ($< 2\%$), this is explained by a critical level of porosity where the scale at which the porosity is being considered becomes important with this direction of shear. When the porosity is low, the pores in the LMRP structure are small and do not influence the shear. When the porosity is higher the pores are much larger so the distance between the voids and the inclusion becomes less and then the difference this make to the shear value become apparent. This critical level of porosity where we begin to see the difference between the models is also influenced by the length of the embedded fibre. The shorter the fibre the more pronounced the difference between the models is at a lower porosity. We can see this is the case in the following section Sec. 6.4 where we consider a variety of fibre lengths.

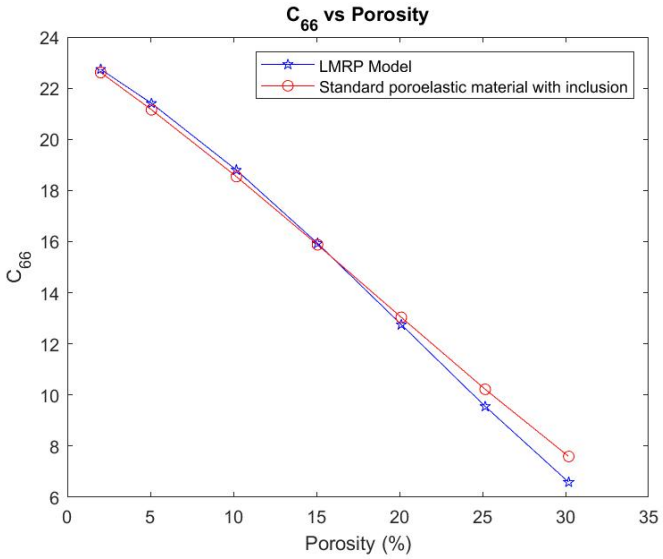

(a) Shear C_{66} versus porosity

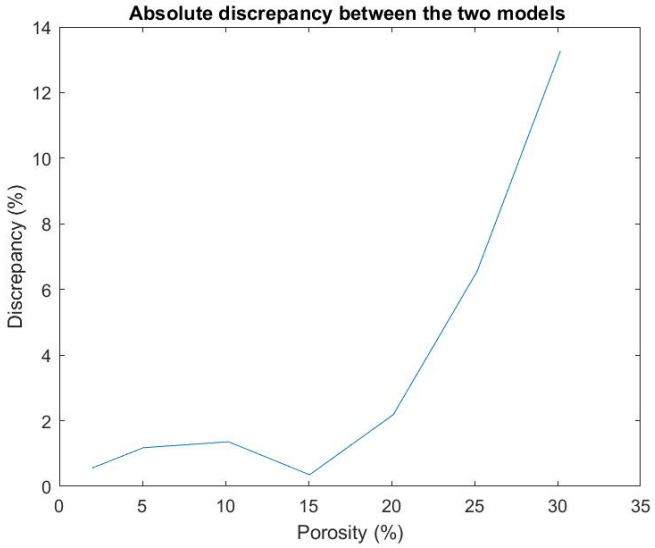

(b) Absolute difference between the two models vs porosity

Figure 6.8: Results of Shear Modulus C_{66} simulations

We can now summarise the findings and explain exactly how they should be interpreted. When a material possesses a microstructure comprising a matrix, embedded elastic subphases and fluid filled pores then using the models that are currently available in the literature (excluding the LMRP model) offers two approaches. These are either make the assumption that the matrix is homogeneous (ignore the subphases) which is not true, or carry out a two-step process first solving the Biot's porous matrix problem and then solving a composite that comprises the subphases and the results of the porous matrix simulations. This second approach means that even though we are considering the three

phases, we are not considering them all at the same scale which is what the intended application actually possesses as a microstructure. This means that the estimations of the parameters cannot be fully reliable. We therefore developed the LMRP model to remove this issue. With this novel model it is possible to account for multiple elastic phases all with different properties as well as the fluid all at the same scale. It is for this reason that the LMRP model results can be thought to be more accurate for these types of applications as we are truly capturing the correct microstructure by using our model. These are the results that we have shown in the previous plots, where we assume 2% discrepancy as a threshold for determining when the LMRP model should be used. We indeed see that when using the two-step approach, the stresses are much higher (especially for large porosities) than the LMRP model.

After considering all four of our elastic parameters we can now summarise our findings in Table 6.1, where we have set the critical model discrepancy percentage to be 2%. We find that at porosities exceeding 20% then the LMRP model is the more effective at determining the true elastic parameters. However, even at lower porosities ($< 20\%$) the LMRP model is more effective at determining E_1, E_3 and C_{44} and is equally effective at determining C_{66} as the standard poroelastic type model.

Table 6.1: Threshold porosities for when model discrepancy exceeds 2% (long fibres)

model	E_1	E_3	C_{44}	C_{66}
LMRP	$> 2\%$	$>8\%$	$>5\%$	$>20\%$
SP	$<2\%$	$<8\%$	$<5\%$	$<20\%$

6.3.2 Applicability of these results to heart modelling

We now wish to give a brief insight into a potential application where the LMRP model can be more efficient at determining the elastic parameters than a standard poroelastic approach.

The human heart has four chambers each of which has a muscular wall with three distinct layers, the endocardium, the myocardium, and the epicardium. The endocardium and epicardium are the thin inner and outer layers, whereas the myocardium is the middle contractile layer. It is supplied by the coronary arteries and is the layer most affected by a variety of diseases, e.g., myocardial infarction, angina and the effects of ageing. For this

reason the modelling approach can be focussed on the myocardium [120], [118], [98].

The myocardium has a structure where there are cardiac myocytes (muscle cells) embedded in a collagen matrix, which is produced by the cardiac fibroblasts, with an interconnected fluid (blood) flow through permeating vasculature. These structures are visible on a microscale length which is much smaller than the size of the heart muscle. The myocardium microstructure is complex geometrically and is strongly impacted by a variety of diseases, in particular myocardial infarction (heart attack). In the case of myocardial infarction blood flow is reduced to an area of myocardium tissue, this results in the death of the cardiac myocytes and in their place, we find collagen rich scar tissue produced by the fibroblasts to retain the structural integrity of the myocardium. The size and amount of scar tissue affects the heart's functionality post recovery [39], [54].

We wish to model the bundles of myocytes found in the myocardium, both healthy and diseased, and can identify the structural components with the different phases considered in the LMRP model. Firstly in the healthy case, the collagen matrix corresponds to the matrix domain, the single myocyte and fibroblast cells can be treated as individual elastic inclusions and the permeating vasculature is the fluid flow through the matrix. The volume fraction of the cardiac myocyte and the fluid volume fraction (porosity) in each cell should be equivalent to be realistic to the structure found in the myocardium. This volume fraction is approximately 20% using the parameters found in [63]. This means that we want to consider all the plots in the previous section (Sec. 6.3.1) for porosities above 20% to determine if the LMRP model will provide a more realistic result for the elastic parameters than standard poroelasticity. We can see from Fig. 6.5b − Fig. 6.8b above that when the porosity is 20% or above then the two Young's moduli and the two shear moduli are likely better to be calculated by the LMRP model as it will better encode the complicated structural geometry and this can be validated using experimental data.

In the case of diseases such as myocardial infarction, the LMRP model can also be used. In this case we could perform a parametric analysis where the inclusion volume fraction and geometry are changed to simulate the loss of myocytes and the replacement with fibrous collagen matrix scar tissue. This would simulate the behaviour of the heart during the myocardial infarction.

We note that of course our model here uses linear elasticity and the heart is of course nonlinear. However, we can obtain results by using a piecewise linear approach as done in [52], [53]. By doing this we can approximate the nonlinear behaviour using simple,

computationally cheap simulations. We should also remark that of course the hearts overall behaviour is nonlinear but by considering the microstructure as individual cells (where the LMRP model could be applied to the different cellular components) the deformations will be much smaller and even linear.

6.4 3D Application - short fibres

Within this section we discuss the comparison of elastic parameters for short fibre models. This can be an interesting application since the difference in the elastic parameters varies depending on whether or not the subphases are connected between the cells. It can also be useful for biological applications where specific cells are inclusions and not subphases. Here we must use a 3D framework since our embedded inclusion does not run from the top of our periodic cell to the bottom but is in fact fully embedded (i.e. a short fibre), therefore the fibres do not connect between cells. In this case we cannot use the 2D simulations since some of the slices in the e_3 direction would not include the fibre. We therefore perform 3D simulations to solve the 3D cell problems (6.19)-(6.23) for LMRP, and for the comparative standard poroelastic model (6.73)-(6.74) and (6.77)-(6.80), presented in the previous sections Sec. 6.2.1 and Sec. 6.2.3. We can justify that our 3D simulations are accurate by considering the absolute error plots between the 2D and 3D long fibres simulations presented in the appendix B.3, where we see that there is less than 1% error for all parameters considered.

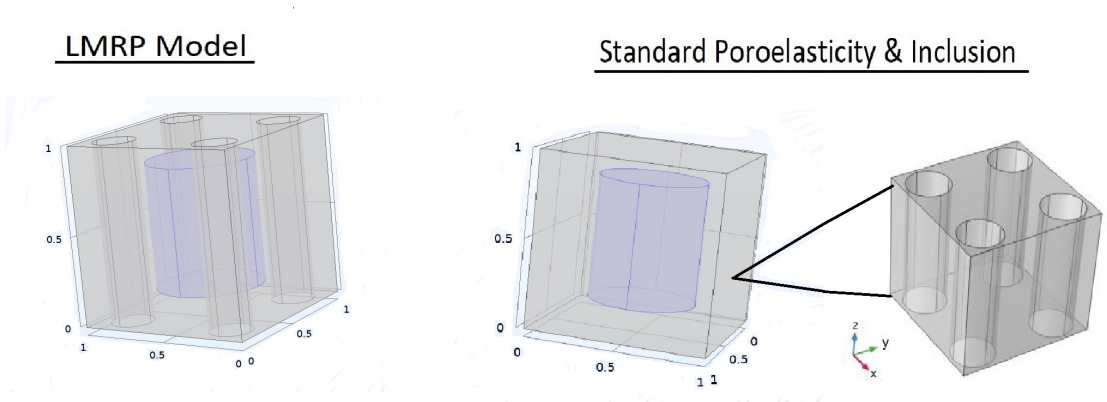

Figure 6.9: Short fibres periodic cell

For the short fibre case we will again be considering the Young's moduli E_1 transverse and E_3 axial as well as the two shears C_{44} and C_{66}. We begin by considering the difference in the Young's Moduli between the two model setups. In this case we choose that

the cylindrical fibres are length 0.8 out of a length one cube and are placed in the centre. For further details about how the model is setup in COMSOL Multiphysics see the Appendix B.2 for the short fibres. In Fig. 6.10 we have carried out the 3D simulations to give

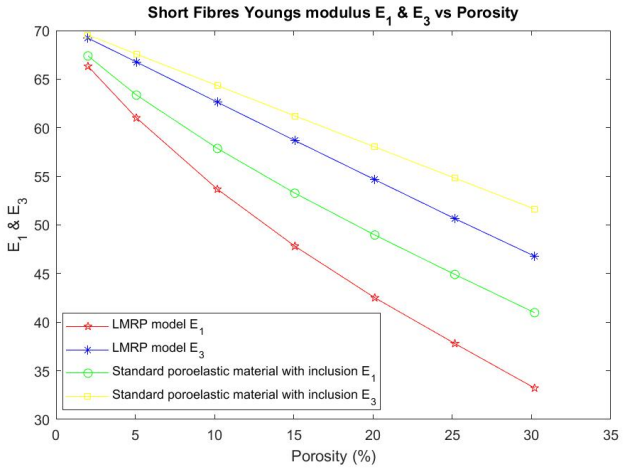

Figure 6.10: short fibres E_1 and E_3 versus porosity

a comparison between our two different computational setups for both the Young's moduli E_1 and E_3 for short fibres. We see that both E_1 and E_3 are lower for the LMRP model. This can be explained by the fact that using the LMRP model explicitly considers the fluid contribution at the porescale along with the matrix and the inclusion. In particular, the LMRP model fully considers the influence of the porosity (which appears as a void in the microscale geometry) thus leading to a lower value of the stiffness moduli.

To confirm our deductions we have plotted the absolute difference between the model setups for both of the Young's moduli.

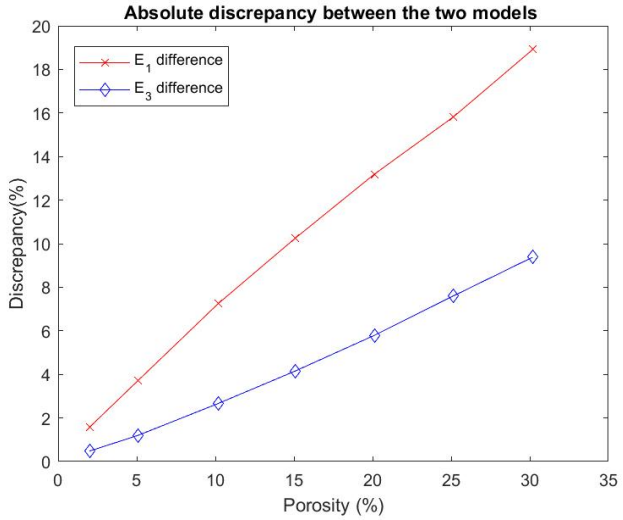

Figure 6.11: Absolute difference between the two models

In Fig. 6.11 we can see that the discrepancy between the two models for E_1 increases from 1.5% to 19% with increasing porosity. This means that for very low porosities then both LMRP and Standard poroelastic type model both produce similar results, but for materials with higher porosities the LMRP model will provide the most accurate representation of the parameters. Similarly for E_3 the absolute difference increases from 0.5% to 9% with increasing porosity. This means that for low porosities (less than 10%) then both LMRP and Standard poroelastic type model both produce similar results. When the materials however, have higher porosities then again the LMRP model will provide the most accurate representation of the parameters.

We also wish to consider the difference in the shear moduli. In Fig. 6.12a and Fig. 6.13a we have carried out the 3D simulations to give a comparison between our two different computational setups for both the Shear moduli C_{44} and C_{66} for short fibres. Here we are again using the 3D framework since our embedded inclusion does not run from the top of our periodic cell to the bottom but is in fact fully embedded (i.e. a short fibre).

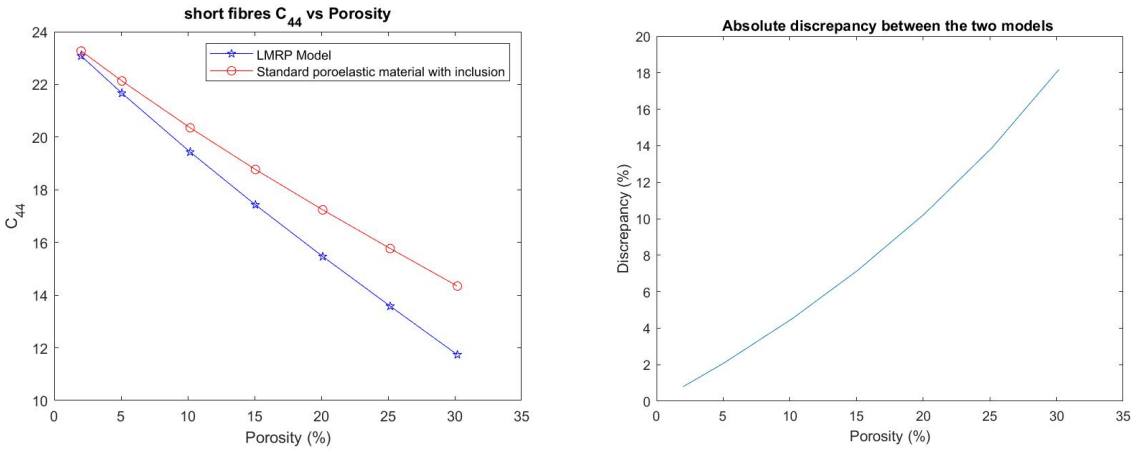

(a) Short fibre C_{44} versus porosity (b) Absolute difference between the models

Figure 6.12: Results of short fibre Shear Modulus C_{44} simulations

In Fig. 6.12a we see that for shear C_{44} that the LMRP model decreases more than the standard poroelastic type model and that the difference between the two models is increasing with increasing porosity. The LMRP model considers the voids and the two elastic phases at the same scale and this contributes to the greater decrease in shear. The standard poroelastic material with inclusion has less of a decrease in shear due to the fact that is does not have the voids present at this scale but accounts for the increasing porosity of the matrix at a finer scale. We also plot the absolute difference between the two models. In Fig. 6.12b we see that for very low porosities that the difference between

the two models is less than 2%, however, for increasing porosities the discrepancy reaches 18%. This means that if we have a material with a porosity greater than 5% then the standard poroelastic approach will not capture the true elastic parameter and it would be much more appropriate to use the LMRP model. Yet still for materials with very low porosities both models will produce similar results.

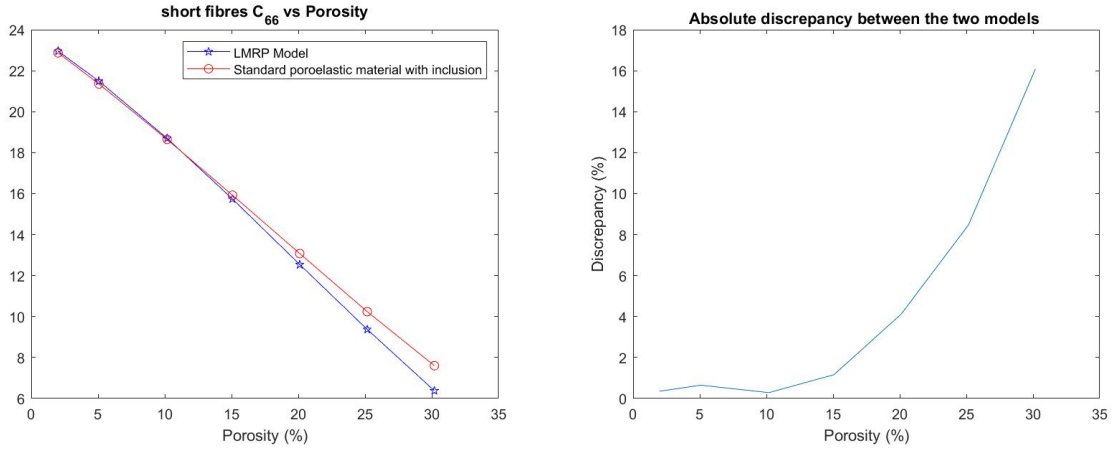

(a) Short fibre C_{66} versus porosity (b) Absolute difference between the models

Figure 6.13: Results of short fibre Shear Modulus C_{66} simulations

For short fibre C_{66} the physical description of the deformation is the same as the long fibre case. In Fig. 6.13a we can see that up until approx 15% porosity the difference in the two models is negligible, this could be explained by a critical level of porosity where the scale at which the porosity is being considered becomes important with this direction of shear. This is because at low porosities the size of the voids is very small in the LMRP model and so therefore do not influence the shear more than the pores at a finer scale. However, once the porosity exceeds 15% then the pores are large enough to influence the shear. This is confirmed by Fig. 6.13b where we can see that for porosities up to 15% that the difference between the models is less than 2%. This means that up to this level of porosity the standard poroelastic approach or the LMRP model are capturing the behaviour similarly. However for porosities greater than 15% then the discrepancy between the models approaches 16% this highlights than in this case it would be more realistic to use the LMRP model. This critical level of porosity where we begin to see the difference between the models is influenced by the length of the embedded fibre. The shorter the fibre the difference between the models becomes more pronounced at a lower porosity. This is due to us keeping the volume of the fibre consistent even though the length is decreasing, so the fibre becomes shorter but thicker meaning the distance between the voids and the

fibres is smaller in the shorter fibre models and this means that the voids can have an influence on the shear at a lower porosity. Note that this idea can be further enforced by the plot of C_{66} Fig. 6.8a where we see that up until approx 20% porosity the difference in the two models is negligible. We further confirm this idea by performing the simulations for a range of fibre lengths from 0.6-1 , results shown in Table 6.2 and Fig. 6.14.

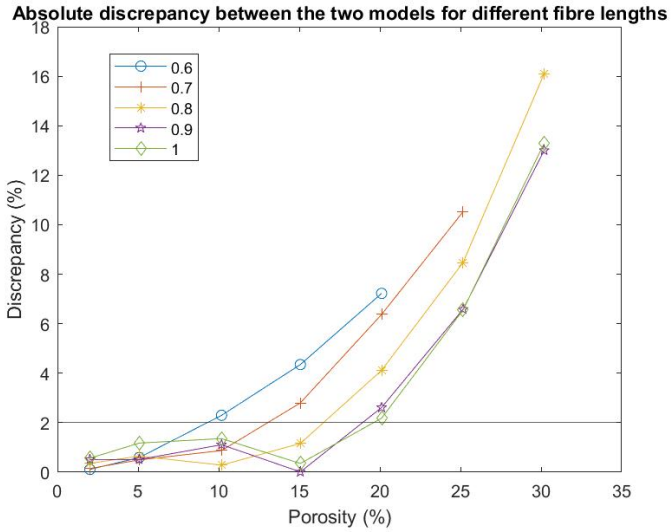

Figure 6.14: Absolute difference between the two models for a variety of fibre lengths with line at error threshold 2%

Table 6.2: Threshold porosities for when model discrepancy exceeds 2% for C_{66} for a variety of fibre lengths

Fibre length	1	0.9	0.8	0.7	0.6
Porosity	19.6%	18.9%	16.5%	13%	9.3%

From considering all four elastic parameters we can now summarise or findings for the short fibre simulations in Table. 6.3. We find that at porosities exceeding 15% then the LMRP model is the more effective at encoding the complex microstructural detail in the elastic parameters and may indeed be more effective at determining the elastic parameters where this second point can be reinforced using experimental data. However, even at low porosities ($< 15\%$) the LMRP model is more effective at determining E_1, E_3 and C_{44} and is equally effective at determining C_{66} as the standard poroelastic type model. We also note that the range of the discrepancy between the models with increasing porosity is higher for the short fibre than the long fibre setting.

Table 6.3: Threshold porosities for when model discrepancy exceeds 2% (short fibres 0.8 length)

model	E_1	E_3	C_{44}	C_{66}
LMRP	>5%	>10%	>5%	>15%
SP	<5%	<10%	<5%	<15%

6.5 Conclusions and Future Perspectives

Within this chapter we have created a robust computational platform that has allowed for a valid comparison between the LMRP model for poroelastic composites and an approach that uses standard poroelasticity with elastic inclusions. We describe our platform as robust due to the wide range of situations where it can be used for computations. That is, the platform can be altered for a variety of geometries including short fibres, various directions of fluid flow, a variety of differently shaped inclusions and a wide range of constitutive properties of the constituents. We investigated a variety of elastic parameters obtained by solving the 2D cell problems, which were derived in the appendix accompanying this chapter, to determine under which circumstances the approach by the LMRP model is most appropriate to be used.

We begin our analysis by providing a summary of the macroscale LMRP model for poroelastic composites that has been derived via asymptotic homogenization in [69]. We then present the 3D cell problem (6.19)-(6.23) that is to be solved to obtain the model coefficients such as the effective elasticity tensor. From this problem we write down explicitly the boundary loads that are required to solve the problem numerically. In order to be computationally less expensive we carry out, and present, the reduction of the cell problems to 2D, where we again present the appropriate boundary loads. Since the aim of this chapter is to have a valid comparison that uses a standard poroelastic approach we then derive the comparison model setup using asymptotic homogenization. The comparison standard poroelastic with inclusion model has two steps, firstly the porous matrix and then a composite between the porous matrix and an elastic inclusion. This means that we have two 3D cell problems (6.73)-(6.74) and (6.77)-(6.80) that are to be solved to provide the model coefficients. We again write down explicitly the boundary loads that are required to solve these two problems numerically. Again in keeping with the comparison, we

carry out and present the reduction of both of these cell problems to 2D, again presenting the appropriate boundary loads. We are then able to solve numerically the cell problems for a simplified geometry where we have unidirectional flow and only one fibre direction. We then plot and compare the elastic parameters Young's moduli and shear moduli.

We also present a discussion on how our current modelling approach can be applicable to modelling of the heart, in particular the myocardium. We then present an example of our computational platform solving the 3D cell problems, justified by the error plots between the 3D and 2D simulations showing less than 1% error.

The results of our numerical simulations show that whenever investigating a poroelastic composite material with porosity exceeding 5% then the LMRP model should be used to compute the Youngs moduli E_1 and E_3 and the shear C_{44} and when the porosity exceeds 20% it should also be used to investigate the shear C_{66}. We find that for material with less than 5% porosity a standard poroelastic approach or the LMRP model produce the same results.

The model simulations have the current limitations and are subject to the following extensions. Within this chapter we have only focussed on the parameters of the elastic matrix. It is also of interest to investigate the fluid flow and solve the cell problem in order to obtain the hydraulic conductivity tensor for the material.

The simulations in this chapter have also only been carried out for a simplified geometry (unidirectional flow and fibre direction) so as to show the difference in the two models in the simplest possible case. It would however be possible, due to the robustness of the 3D computational platform highlighted by the 3D example, to consider a much more complex geometry consisting of additional fibres and also fibre angles and fluid flow in many directions.

We should also note that in this work we are focussing solely on solving the microscale cell problems that determine the model coefficients. It would however, be posible to solve the complete macroscale model that is presented in Sec. 6.1.

The derivation and numerical simulations have focussed on a general set of parameters since we we aiming just to capture the effects of the LMRP model and the settings where it is most applicable. The next step would be to apply the LMRP model to a realistic set of parameters and geometry and this will allow for model validation by comparing with experimental data, as done for example by [24]. Another important aspect which is to be considered is the model validation in terms of how well it converges to the actual behaviour

of the physical system whenever scales become more and more separated. This is indeed a problematic issue primarily due to the required computational cost, although one next natural step is indeed the development of direct numerical simulations (for example performed on reference heterogeneous geometries in two-dimensions). This approach (which is carried out for example in [31] in the context of three-scale asymptotic homogenisation for a one-dimensional example) would increase the reliability of these results, and in general, of any model derived via homogenisation techniques, and will become more and more realistic following advances in computational resources available. This specific validation will also better elucidate the role of the heterogeneities as a discriminant in determining which homogenised model better represents the actual physical system at hand.

Finally, the simulations could be extended to investigate changing the volume fraction and/or geometry of the inclusion. This could have many relevant biological applications. Such as to myocardial infarction where the cardiac myocytes die and become replaced by fibrous collagen matrix.

In the next chapter we use the model for poroelastic composites, derived in Chapter 3, to describe the microstructure of the myocardium. Using the model we investigate how physiologically observed microstructural changes induced by myocardial infarction impact the elastic parameters of the heart. This is a first study to show how useful detailed microstructural poroelastic models can be at modelling the response of biological tissues [72].

Chapter 7

Investigating the effects of microstructural changes induced by myocardial infarction on the elastic parameters of the heart

The human heart has four chambers each of which have a muscular wall with three distinct layers, the endocardium, the myocardium, and the epicardium. The endocardium and epicardium are the thin inner and outer layers, whereas the myocardium is the middle and most dominant layer. It is supplied by the coronary arteries and is the layer most affected by a variety of diseases, e.g., myocardial infarction, angina and the effects of ageing [120], [118].

The myocardium has a structure where there are cardiac myocytes (muscle cells) embedded in a collagen matrix, which is produced by the cardiac fibroblasts, with an interconnected fluid (blood) flow through permeating vasculature. These structures are visible on a microscale length which is much smaller than the size of the heart muscle. The myocardium microstructure is complex geometrically and is strongly impacted by a variety of diseases, in particular myocardial infarction (heart attack). In the case of myocardial infarction blood flow is reduced to an area of myocardium tissue, this results in the death of the cardiac myocytes and in their place, we find collagen rich scar tissue produced by the fibroblasts to retain the structural integrity of the myocardium [39], [54]. The size and amount of scar tissue affects the heart's functionality post recovery [38]. As a result of

the loss of cardiac myocytes, the remaining myocytes in the area surrounding the infarct increase in volume to attempt to retain homeostasis in the heart [59]. The growth and remodelling of the surviving myocytes corresponds to the infarct size [79], [78], [3].

Within this work we aim to investigate the effects of microstructural changes induced by myocardial infarction (MI) on the elastic parameters of the heart. In Sec. 7.1 we summarise the LMRP [69] (see Chapter 3) model for poroelastic composites which we will use to model the microstructure of the myocardium. Within the sections that follow we will investigate a variety of changes to the parameters and geometry of the microstructure in order to simulate a variety of phenomena observed post myocardial infarction. We account for the anisotropy of the heart microstructure through the inclusion of the myocytes in one direction. In Sec. 7.2 we will investigate the comparison between healthy elastic parameters and the parameters obtained in the post myocardial infarction setting of loss of myocyte and increased fibrosis. Then in Sec. 7.3 we consider the effect that the increase in myocyte volume fraction has on the elastic parameters of the myocardium post myocardial infarction. Finally in Sec. 7.4 we propose a 3D frame work to model the myocytes connected via intercalated discs. We conclude this work by providing the future prospects of developing this model and its potential as a diagnostic tool to aid clinicians.

7.1 The Mathematical Model

We use the LMRP model for poroelastic composites [69] (see Chapter 3) to describe the microstructure of the myocardium tissue. The myocardium is predominantly comprised of an extracellular matrix with embedded blood vessels and cardiac myocyte cells. We therefore have two elastic phases and a fluid interacting on the microscale.

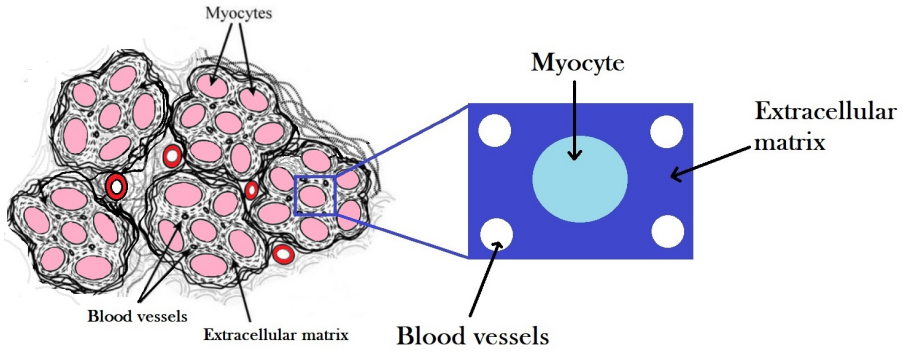

Figure 7.1: Image of heart microstructure and the assumed microstructural geometry of our model. LHS of diagram redrawn taking inspiration from [44]

Here we summarise the mathematical model for a poroelastic composite derived by the asymptotic homogenization technique in [69] and Chapter 3 that we will use to describe the myocardium microstructure. The model derivation is carried out by setting up an appropriate fluid-structure interaction problem between a linear elastic porous matrix, Ω_{II}, with embedded linear elastic subphases, Ω_{I}, with a Newtonian fluid, Ω_{f}, flowing in the pores. When applying this to the myocardium we make the identifications that Ω_{II} is the extracellular matrix, Ω_{I} is the myocyte and Ω_{f} is the permeating vasculature of the heart. We make the assumption that the radius of the blood vessels (the porescale) is comparable with the distance between the adjacent myocytes [97], [112]. Overall this length is much smaller than the size of the entire myocardium (the macroscale). Having this difference in lengths allows us to decouple the spatial scales and apply the asymptotic homogenization technique to derive the macroscale model. The new system of partial differential equations is of poroelastic-type. The model equations contain coefficients that encode the properties of the underlying material microstructure, and can be computed by solving appropriate cell problems. Here we summarise the four governing equations. We are using the LMRP model of Chapter 3, summarised in Chapter 6, with some small differences in subscripts to clearly show the application to the myocardium modelling. The first macroscale equation is the balance of linear momentum

$$\nabla_{\mathbf{x}} \cdot \mathsf{T}_{\text{Eff}}^{\text{LMRP}} = 0, \tag{7.1}$$

where we have the constitutive law

$$\mathsf{T}_{\text{Eff}}^{\text{LMRP}} = \langle \mathbb{C}_{\text{Myo}} \mathbb{M}_{\text{Myo}} + \mathbb{C}_{\text{Myo}} + \mathbb{C}_{\text{IM}} \mathbb{M}_{\text{IM}} + \mathbb{C}_{\text{IM}} \rangle_s \xi_{\mathbf{x}} \mathbf{u}^{(0)} + \boldsymbol{\gamma}^{\text{LMRP}} p^{(0)}, \tag{7.2}$$

where $\mathbb{C}_v$ with $v = \text{Myo}, \text{IM}$ is the elasticity tensor for the myocyte and interstitial matrix respectively. We can define the effective elasticity tensor $\widetilde{\mathbb{C}}^{\text{LMRP}}$ as

$$\widetilde{\mathbb{C}}^{\text{LMRP}} = \langle \mathbb{C}_{\text{Myo}} \mathbb{M}_{\text{Myo}} + \mathbb{C}_{\text{Myo}} + \mathbb{C}_{\text{IM}} \mathbb{M}_{\text{IM}} + \mathbb{C}_{\text{IM}} \rangle_s, \tag{7.3}$$

The system also comprises the conservation of mass equation

$$\frac{\dot{p}^{(0)}}{M^{\text{LMRP}}} = -\nabla_{\mathbf{x}} \cdot \langle \mathbf{w} \rangle_{\text{f}} - \boldsymbol{\alpha}^{\text{LMRP}} : \xi_{\mathbf{x}} \dot{\mathbf{u}}^{(0)}, \tag{7.4}$$

where we have that $p^{(0)}$ is the macroscale pressure, $\dot{\mathbf{u}}^{(0)}$ is the leading order solid velocity,

$\mathbf{w}$ is the average fluid-solid velocity, M^{LMRP} and $\boldsymbol{\alpha}^{\text{LMRP}}$ are the resulting Biot's modulus and tensor of coefficients associated with the system respectively. The final macroscale equation is Darcy's law

$$\langle \mathbf{w} \rangle_{\text{f}} = -\langle W \rangle_{\text{f}} \nabla_{\mathbf{x}} p^{(0)}, \tag{7.5}$$

where $\langle W \rangle_{\text{f}}$ is the hydraulic conductivity tensor.

From our governing equations we have that the behaviour of the poroelastic composite material (myocardium) can be fully characterised by the model coefficients, that is, by the effective elasticity tensor $\widetilde{\mathbb{C}}^{\text{LMRP}}$, the hydraulic conductivity $\langle W \rangle_{\text{f}}$, the Biot's tensor of coefficients $\boldsymbol{\alpha}^{\text{LMRP}}$ and the Biot's coefficient M^{LMRP}. These coefficients can be written as

$$\boldsymbol{\alpha}^{\text{LMRP}} = \phi \mathbf{I} - \langle \text{Tr}(\mathbb{M}_{\text{IM}}) \rangle_s, \quad M^{\text{LMRP}} = \frac{-1}{\langle \text{Tr}(Q_{\text{IM}}) \rangle_s}, \quad \boldsymbol{\gamma}^{\text{LMRP}} = \langle \mathbb{C}_{\text{IM}} Q_{\text{IM}} \rangle_s - \phi \mathbf{I}, \tag{7.6}$$

where the fourth rank tensors $\mathbb{M}_{\text{Myo}}$, $\mathbb{M}_{\text{IM}}$ and the second rank tensor Q_{IM} are to be computed by solving the microscale cell problems arising from the application of asymptotic homogenization. The asymptotic homogenization technique provides six elastic type cell problems that are to be solved to compute the strains $\mathbb{M}_{\text{Myo}}$, $\mathbb{M}_{\text{IM}}$. These can then be used, along with the original input elasticity tensors for the material $\mathbb{C}_{\text{Myo}}$, $\mathbb{C}_{\text{IM}}$ to compute the effective elasticity tensor. To see these elastic type problems explicitly see Appendix C.1 and for even further details consider the references therein. The asymptotic homogenization technique also gives rise to a further vector problem that can be solved to obtain the tensor Q_{IM}. By solving the seven problems we obtain the three tensors required that we can compute all the coefficients of our novel macroscale model.

Within this work since our analysis will focus predominantly on the elastic parameters of the myocardium in both healthy and diseased scenarios we will only compute the necessary components of the effective elasticity tensor $\widetilde{\mathbb{C}}^{\text{LMRP}}$.

Lastly we note the notation $\langle \varphi \rangle$, which is a cell average defined as

$$\langle \varphi \rangle_k = \frac{1}{|\Omega|} \int_{\Omega_k} \varphi(\mathbf{x}, \mathbf{y}, t) \text{d}\mathbf{y} \quad k = \text{f}, \text{s} \tag{7.7}$$

where $\langle \varphi \rangle_{\text{s}} = \langle \varphi \rangle_{\text{IM}} + \langle \varphi \rangle_{\text{Myo}}$, and where φ is a general field in our system and $|\Omega|$ is the volume of the domain and the integration is taken over the porescale.

7.2 Loss of myocytes and increased fibrosis

Within this section we wish to compare the elastic parameters (Young's and shear moduli) for the healthy myocardium versus the infarcted myocardium. The healthy myocardium is proposed to consist of a number of cardiac myocytes embedded in an extracellular matrix surrounded by a network of blood vessels supplying the myocytes. This structure is shown in Fig. 7.2. In the infarct region we have a loss of myocytes due to the interruption in the blood flow supplying them which causes them to die or become damaged. In order to retain the structural integrity of the heart the extracellular matrix forms a collagen rich scar to replace the damaged and lost myocytes. In order to provide a first approximation to this myocyte damage we have created the below geometry, Fig. 7.3 where the myocyte is missing a section and in its place we increase the stiffness of the extracellular matrix.

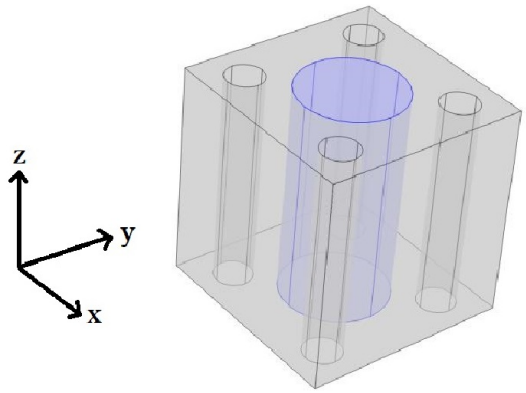

Figure 7.2: 3D geometry healthy intact myocyte embedded in soft extracellular matrix with four blood vessels

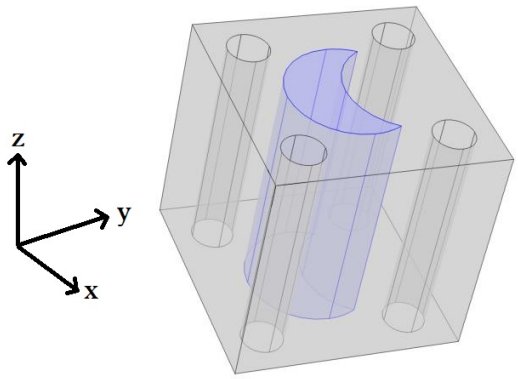

Figure 7.3: 3D geometry myocyte that has been injured as a result of infarction embedded in the stiffer collagen rich extracellular matrix with four blood vessels

Within this section we make the assumption that both the healthy and the damaged myocytes run from the top of the cell to the bottom as a single fibre. This means that we can cut the plane and perform 2D simulations to solve the cell problems of LMRP. The details of the 3D cell problems can be found in the Appendix C.1 and the reduction of these problems to 2D can be found in [73] and Appendix B.1. We show the assumed equivalent 2D geometry in Fig. 7.4 and Fig. 7.5.

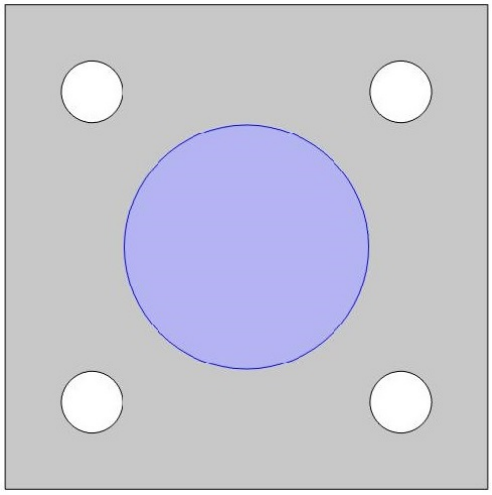

Figure 7.4: 2D geometry for healthy myocyte embedded in the healthy extracellular matrix with four blood vessels

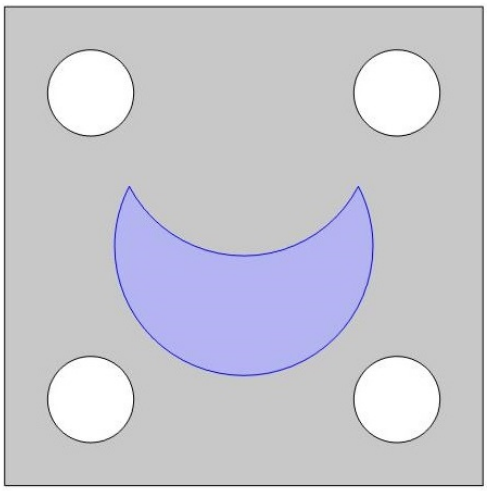

Figure 7.5: 2D cross-section showing a myocyte that has been injured as a result of infarction embedded in the stiffer collagen rich extracellular matrix with four blood vessels

We use the following input parameters to carry out our simulations. These parameters come from a variety of sources [1], [26], [63]. We require a Young's modulus E and a Poisson ratio ν for both the interstitial matrix and the myocyte in both the healthy and the infarcted state.

Table 7.1: Input parameters for the following simulations obtained from [1], [26], [63]

Model	E_{myo} (kPa)	E_{matrix} (kPa)	ν_{myo}	ν_{matrix}
Healthy	35	40	0.49	0.4
Infarcted	35	80	0.49	0.4

Due to the geometry we are assuming for the microstructure we are including the effects of anisotropy of the myocardium tissue in our results. This means that we have more than one independent shear and more than one independent Young's modulus. Our healthy material is not fully orthotropic with three Young's moduli and three shears since there is a symmetry in $\mathbf{x}$ and $\mathbf{y}$. Therefore due to the symmetries imposed by our choice of healthy geometry we should note that the shear C_{44} is the same as the shear C_{55}, so we consider shears C_{44} and C_{66}. We also only have the two Young's moduli E_1 and E_3, since E_1 is the same as E_2. Even though we do not possess the symmetry in $\mathbf{x}$ and $\mathbf{y}$ for the infarcted case, since we wish to make a comparison with the healthy case we chose to

present only the parameters Young's moduli E_1 and E_3 and shears C_{44} and C_{66}. However, it is clear from the geometry that the infarcted case will also have a different E_2 and C_{55}.

Here we compare the shear modulus C_{44} for a healthy myocyte embedded in the extracellular matrix with a setup where there has been loss of myocyte volume fraction and increased fibrosis of the matrix designed to represent the case of myocardial infarction. The parameter C_{44} is taken directly from the computed effective elasticity tensor for the model. We have plotted the comparison of the shear moduli for the healthy and infarcted cases over a range of porosities from $2\% - 30\%$. This is shown in the figures below.

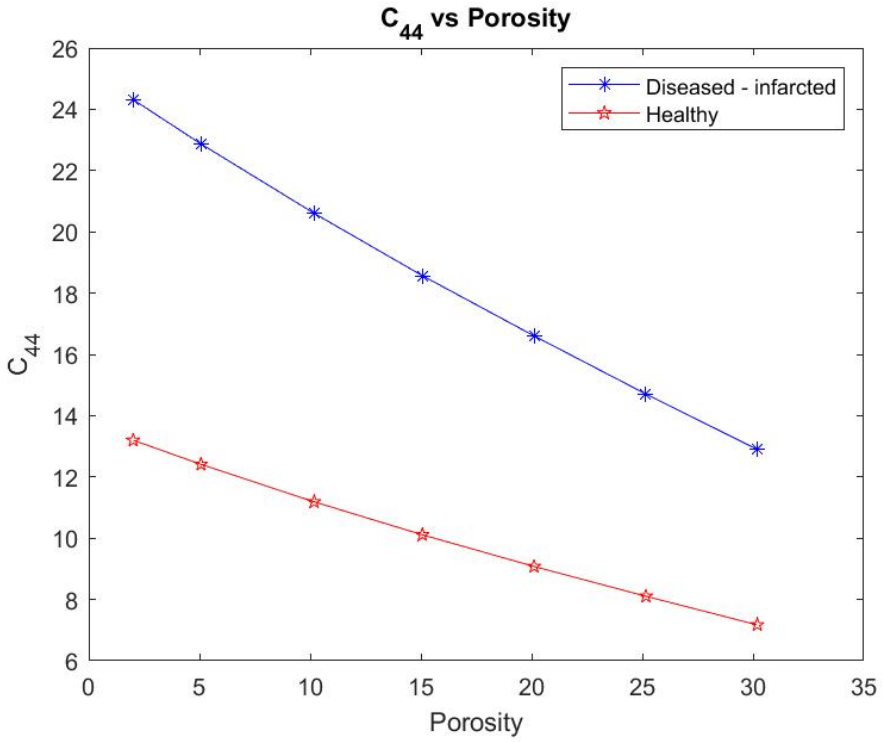

Figure 7.6: Shear C_{44} versus porosity for both the healthy heart and the infarcted case.

We see in Fig. 7.6 that the healthy setup has much lower values for shear and produces an overall smaller decrease in shear with increasing porosity than the diseased case. The shear is being applied in the axial direction (where the myocytes and voids elongate) so the material deforms into the voids and they flatten out allowing for the decrease in shear as the voids increase in size (larger porosity). The diseased case has a higher initial value for shear due to the increased stiffness of the matrix and the unusual geometry of the damaged myocyte, compared to the healthy case which has the normal soft extracellular matrix and regular myocyte. The higher the shear the stiffer the overall material, this means in the case of infarction even with reperfusion (increase in porosity) the stiffness of

the myocardium still does not return to the normal healthy value. However, the increased porosity does improve the overall compliance of the diseased material.

We also carry out the same comparison for the shear modulus C_{66}.

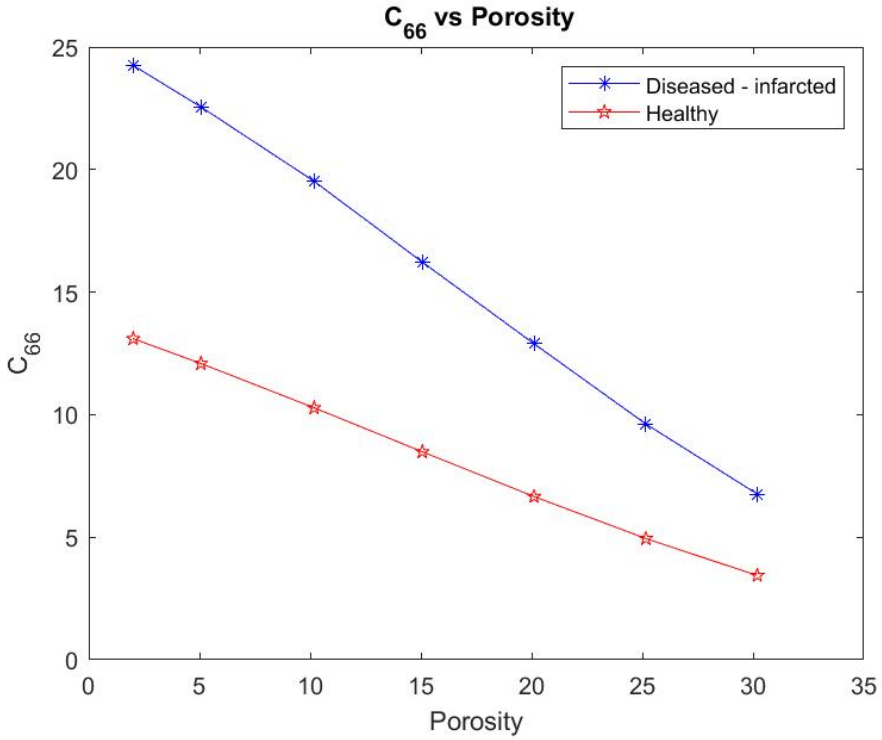

Figure 7.7: Shear C_{66} versus porosity for both the healthy heart and the infarcted case.

In Fig. 7.7 we see that the healthy setup begins with a much lower shear value even at small porosities compared with the infarcted case. The healthy case produces an overall much smaller decrease in shear with increasing porosity than the diseased case. The shear is being applied in the x-direction (transverse). Therefore for both the diseased and healthy cases the force is being applied taking a cross section of structure which contains the voids and the myocyte. At higher porosities this makes the material weaker as the larger voids deform more easily hence why the decrease in shear is observed in both cases. The diseased case has a higher initial value for shear C_{66} due to the increased stiffness of the matrix and the unusual geometry of the damaged myocyte, compared to the healthy case which has the normal soft extracellular matrix and regular myocyte. Again the increase in porosity (to mimic reperfusion) in the diseased case does reduced to overall stiffness of the material to attempt to return to a similar stiffness as the healthy. Comparing the shear C_{66} with shear C_{44} we can see that C_{66} has higher initial values but with increasing porosity actually becomes lower than C_{44}. This can be explained by the geometry and the direction in which

the myocytes elongate and the presence of the voids. The voids have the larger influence on shear when applying in the C_{66} direction as they deform easily with less influence from the myocyte.

We also wish to consider the comparison between the two Young's moduli E_1 (transverse) and E_3 (axial) for the healthy and the infarcted heart using the LMRP model. We compute the components of the effective elasticity tensor for both the healthy and infarcted cases and use in the formulas for the Young's moduli. These formulas, which can be derived via inverting the elasticity tensor and comparing with the material compliance tensor, such as in [114], are given by

$$E_1 = \frac{(C_{12} - C_{11})(2C_{13}^2 - C_{12}C_{33} - C_{11}C_{33})}{(-C_{13}^2 + C_{11}C_{33})} \tag{7.8}$$

$$E_3 = \frac{(2C_{13}^2 - C_{12}C_{33} - C_{11}C_{33})}{(-C_{12} - C_{11})}. \tag{7.9}$$

We plot the comparison of Young's moduli between the healthy and infarcted cases.

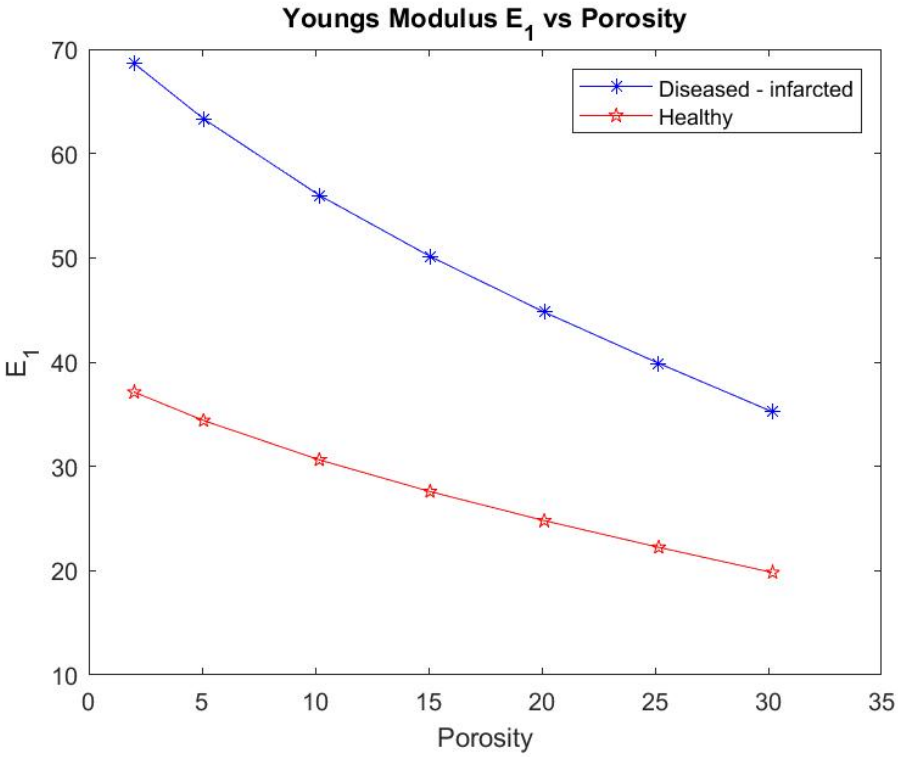

Figure 7.8: E_1 versus porosity for both the healthy heart and the infarcted case.

Fig. 7.8 shows that the infarcted myocardium has a much higher transverse Young's modulus than the healthy case (almost double the stiffness). This is explained by the fact

that the matrix in the infarcted case is much stiffer than in the healthy case and therefore influences the overall stiffness of the material to a large extent. The infarcted case also has the damaged myocyte which has lost volume and been replaced by the stiffer matrix which also influences the overall stiffness of the myocardium. We see that the stiffness of the infarcted case reduces dramatically with increasing porosity of the material. This means that with reperfusion of the infarcted tissue then the stiffness of the myocardium can be reduced with the benefit that the overall compliance of the tissue will then improve, thus improving heart function. We do see however that even at the highest porosities the diseased case never reaches the standard healthy E_1 value that would be approximately 30kPA. The difference between these two cases is two-fold and is due to both the additional complexity in the geometry and the increased stiffness in the matrix. By changing just one of these factors in the healthy case would not be enough to remove the discrepancy between the two cases and illustrates the necessity of model coefficients that incorporate geometry and material properties.

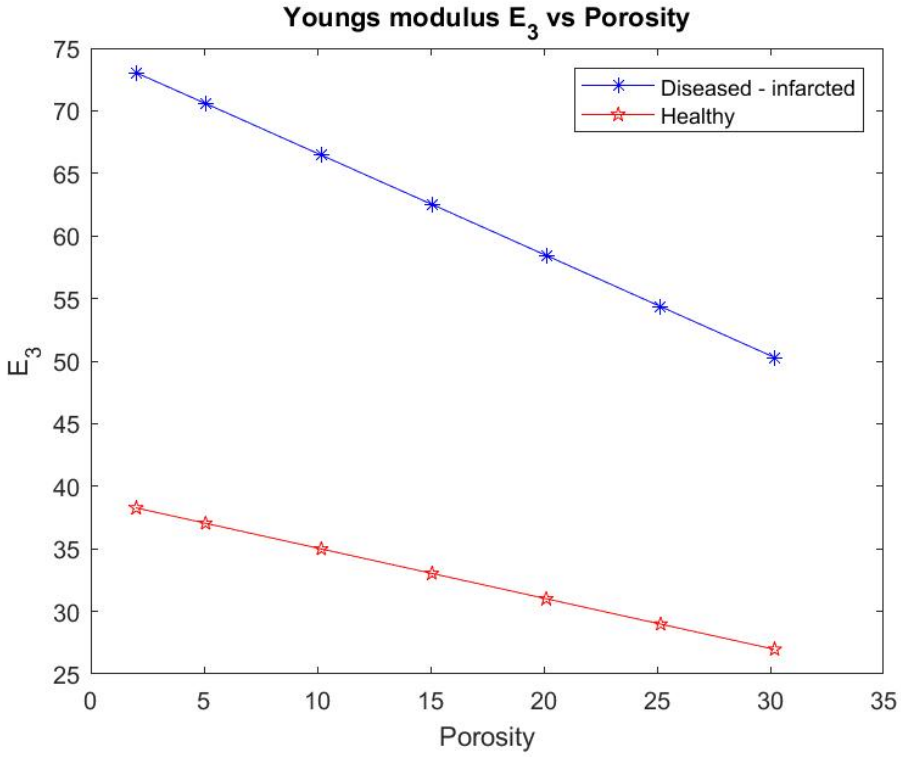

Figure 7.9: E_3 versus porosity for both the healthy heart and the infarcted case.

In Fig. 7.9 we consider the Young's modulus E_3. We can again see that the healthy myocardium has a much lower axial Young's modulus than the infarcted case. In fact the infarcted Young's modulus is approximately double that of the healthy case. Overall again

the increasing porosity does have an effect in reducing the overall stiffness in both cases with the effects of the increasing porosity being shown more clearly in the diseased case. The increasing porosity has a much greater effect on the infarcted case in an attempt to improve the compliance of the overall heart muscle.

We can compare E_3 with E_1. We find that both the healthy and infarcted axial Young's moduli (E_3) are initially higher than both the healthy and infarcted transverse Young's moduli (E_1). We can see that the infarcted E_3 is always higher than the infarcted E_1. We can also observe that the healthy E_3 is also always higher than the healthy E_1. This is due to the fact that the myocytes and voids elongate in the axial direction which is also considered a contributory factor to the stiffness in that direction.

7.3 Changing myocyte volume fraction

Following myocardial infarction we see a decrease in the volume fraction of myocytes in the infarct zone due to the death and damage of myocytes, however, in the regions surrounding the infarct zone the intact myocytes increase in volume to attempt to compensate for the section of damaged heart [79], [3]. We therefore wish to investigate the influence that this change in volume has on the overall elastic parameters of the heart. We assume our increase in myocyte volume fraction corresponds to different infarct sizes and not a time dependant increase following the infarction [78], [3].

Within this section we make the assumption that the myocytes run from the top of the cell to the bottom as a single cylindrical fibre. The myocytes here are intact cylinders since they have not been damaged by the infarction. This means that we can cut the plane and perform 2D simulations to solve the cell problems of LMRP. For a description of the cell problems see Appendix C.1 and for the complete 2D reduction of the model see [73] and Appendix B.1.

We solve the cell problems using the following parameters, found in [1], [26], [63], summarised in the table below.

Table 7.2: Input parameters for the following simulations obtained from [1], [26], [63]

Parameter	E_{myo} (kPa)	E_{matrix} (kPa)	ν_{myo}	ν_{matrix}
Value	35	80	0.49	0.4

We carry out the simulations for four fixed fluid volume fractions ϕ_f =

$5\%, 10\%, 15\%, 20\%$ and for each of these varying the myocyte volume fraction from $5\% - 30\%$. The fluid volume fractions have been chosen to represent the following settings; 5% reduced flow leading to infarction, 10%-15% normal range of healthy perfusion, 20% over perfused leading to myocardial injury.

We begin by considering the two Young's moduli E_1 and E_3 for the infarcted heart.

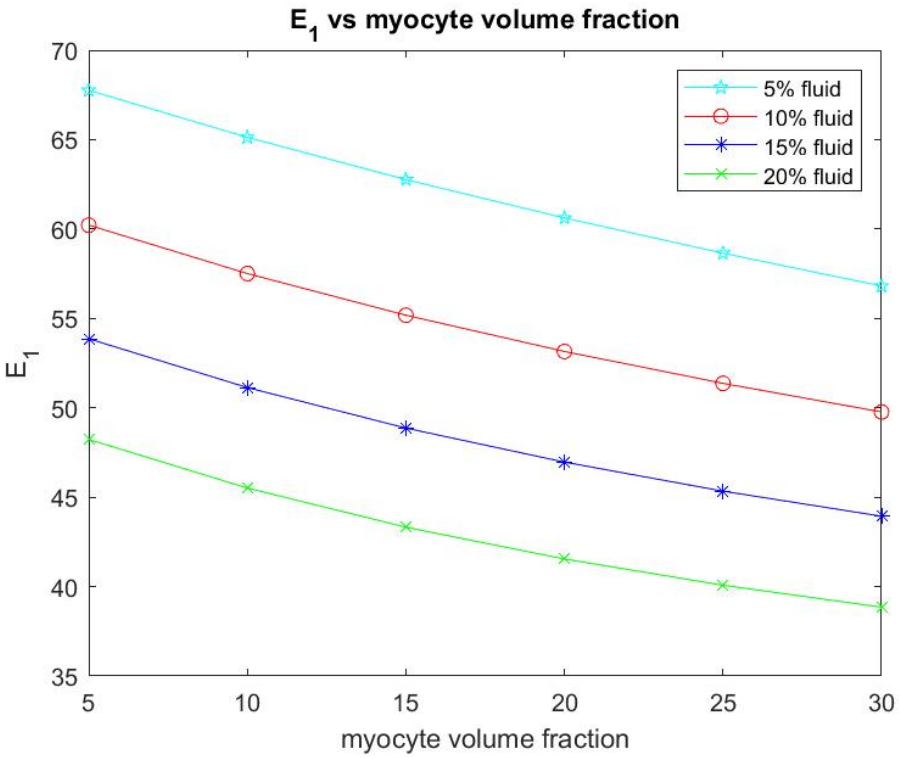

Figure 7.10: E_1 versus myocyte volume fraction for four different fixed fluid volume fractions.

In Fig. 7.10 we see that the transverse Young's modulus E_1 decreases with increasing myocyte volume fraction and this behaviour is consistent across the four fixed fluid volume fractions that we have considered. The Young's modulus can be thought of as a measure of material stiffness so in the case of low myocyte volume fraction the extracellular matrix is the dominating parameter in influencing the stiffness of the overall material. A stiffer material leads to less elastic compliance which can be detrimental for overall function of the heart. This is why in the regions surrounding a myocardial infarction the myocyte volume fractions increase as their increase in volume actually reduces the overall stiffness and hence improves the overall compliance of the material. This biological mechanism is highlighted in the results of our simulations. We also note that the fluid volume fractions contribute to the overall stiffness, with the stiffest setting being the one with only a 5%

fluid volume fraction with the material getting progressively more compliant with the increase in the fluid contribution.

We also wish to consider the axial Young's modulus E_3. This Young's modulus is in the same direction that the myocytes and voids elongate.

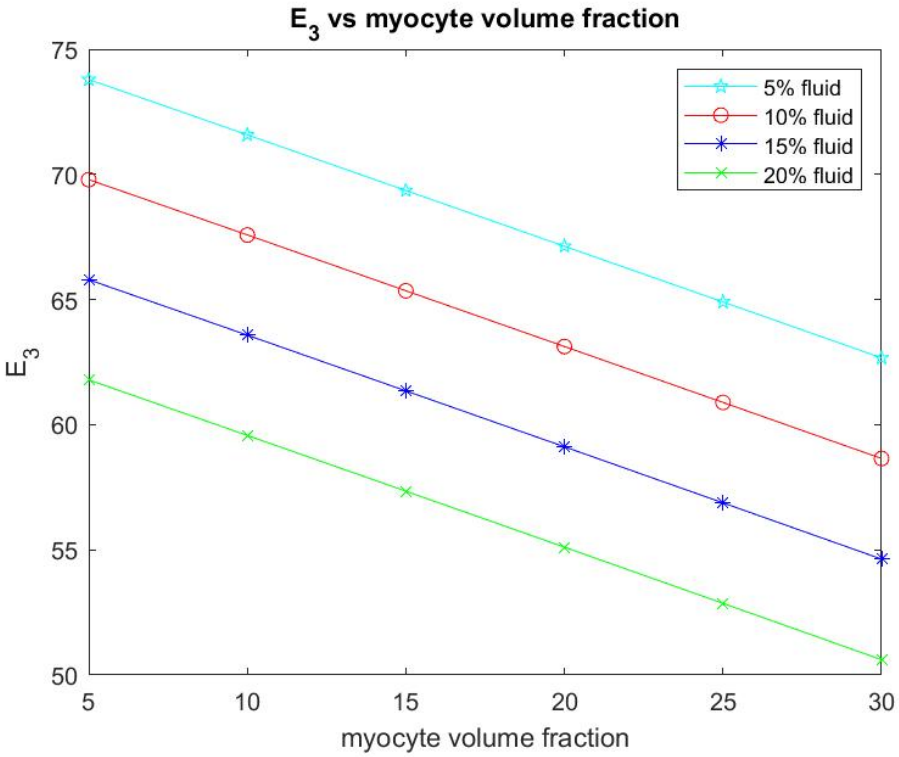

Figure 7.11: E_3 versus myocyte volume fraction for four different fixed fluid volume fractions.

In Fig. 7.11 we see that the axial Young's modulus E_3 also decreases with increasing myocyte volume fraction and this behaviour is consistent across the four fixed fluid volume fractions that we have considered. In the case of E_3 the values are higher for each of the fixed fluid volume fractions when compared to the transverse Young's modulus E_1. This is due to the fact that the myocytes elongate in this direction which adds to the increased stiffness. Again since the matrix is stiffer as a result of the myocardial infarction then the increase in myocyte volume fraction helps to reduce the stiffness and improve the compliance of the material, which again emphasises the observed physiological response.

The other two elastic parameters that we consider for varying myocyte volume fraction are the shear moduli C_{44} and C_{66}. These parameters are taken directly from the computed effective elasticity tensor for the model. In the same way as with the Young's moduli we have plotted the comparison of the shear moduli over a range of myocyte volume fractions

from $5\% - 35\%$ at the four fixed fluid volume fractions. This is shown in the figures below.

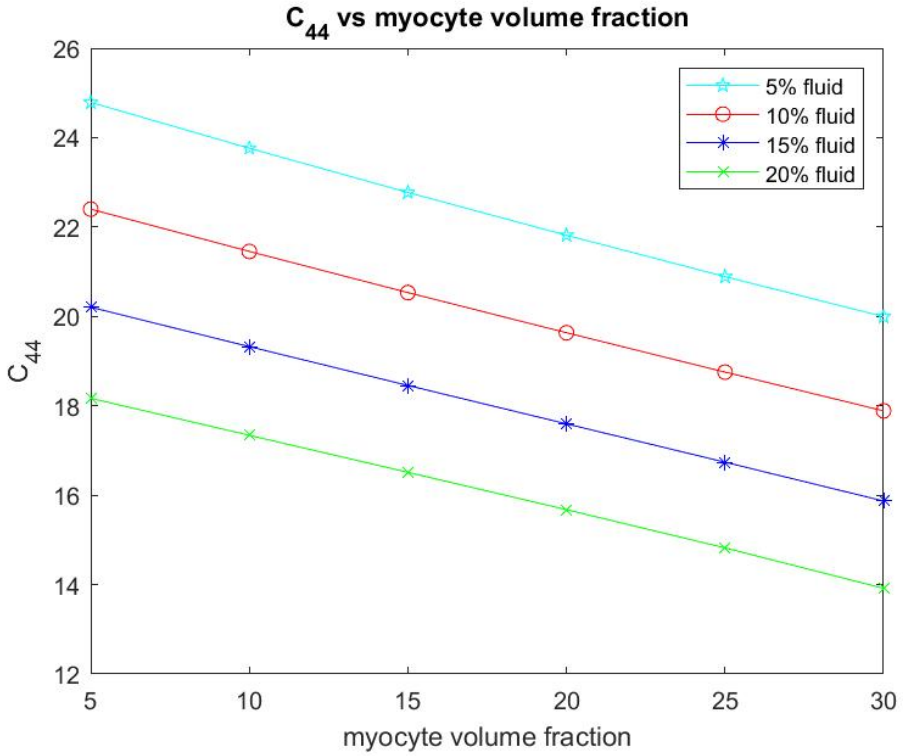

Figure 7.12: Shear C_{44} versus myocyte volume fraction for four different fixed fluid volume fractions.

From Fig. 7.12 we can see that the shear C_{44} decreases with increasing myocyte volume fraction. In the case of C_{44} the force is being applied in the axial direction, this is the direction in which the myocytes and blood vessels elongate. The blood vessels can be thought of as empty channels since we are considering the drained parameters. This means that when the force is applied to the material it deforms and the channels flatten out. This means that the empty channels just make it softer allowing for the decrease in shear with the increasing fluid volume fraction. When the myocytes have a low volume fraction, such as in the case where myocyte damage and death has occurred due to myocardial infarction, then we see that, for all four fixed fluid volumes, the shear values are higher than for a larger myocyte volume fraction. The stiffest scenario is for fixed 5% fluid volume and low myocyte volume fraction and this can be representative of the situation directly following myocardial infarction where fluid flow to the tissue has been dramatically reduced resulting in the loss of myocyte volume. We see that by increasing the myocyte volume fraction the shear decreases at all four fluid volumes, meaning that we have a softer more compliant material once the myocytes increase in size. Physiologically this occurs to

help the myocardium return to homeostasis after infarction and this mechanism is clearly observed from our simulations.

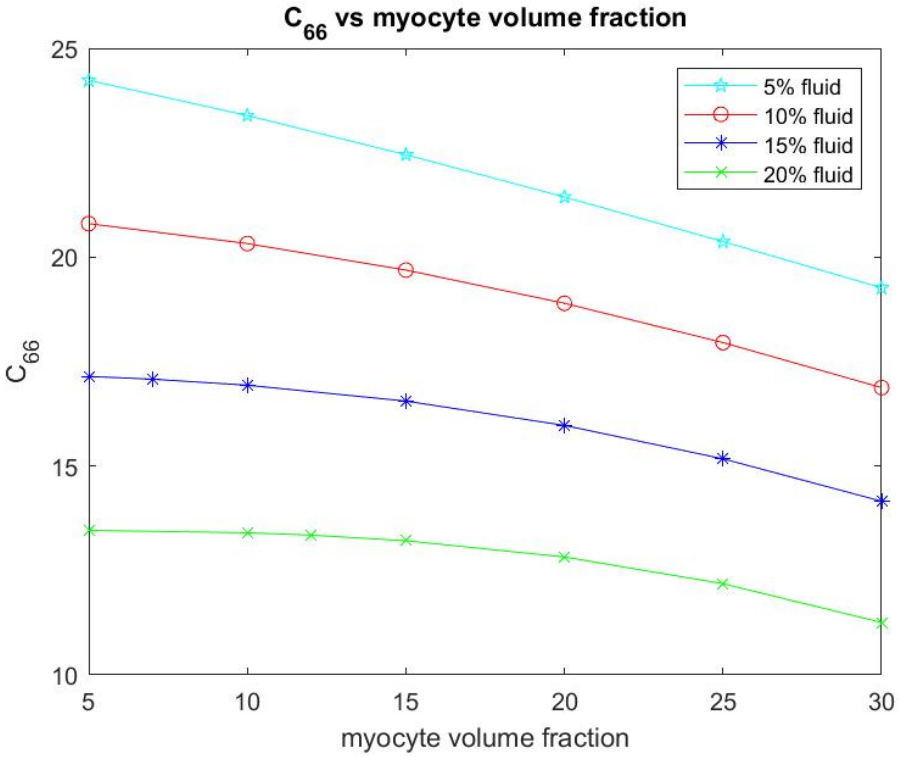

Figure 7.13: Shear C_{66} versus myocyte volume fraction for four different fixed fluid volume fractions.

In Fig. 7.13 the shear C_{66} decreases with increasing myocyte volume fraction for all four fixed fluid volumes. For C_{66} the force is being applied in the transverse direction, that is, the force is being applied taking a cross section of structure where we have the myocyte and the channels. At the lowest fluid volume fraction and smallest myocyte volume (the scenario representing immediately post myocardial infarction) we see that the shear is the largest, this means that under this setting the myocardium is very stiff. The typical healthy shear for the myocardium would be approx. 10kPa which is much lower that the 24.2kPa value we see for the infarcted setup. This motivates the myocardium's biological response to increase the myocyte volume fraction in order to try to return the tissue to the correct shear values so that the stiffness and compliance of the material is closer to the healthy case and leads to greater efficiency of the recovered muscle. If we compare C_{66} with C_{44} we see that C_{44} has the higher values across the increasing myocyte volume fraction. This is due to the fact that the shear C_{44} is being applied in the direction the myocyte elongates so the increase in its volume influences the material in that direction

making it stiffer. The behaviour we see here has a more 'nonlinear' appearance than the behaviour in the previos plots. This can be caused by the geometry and the direction we are taking the shear in. The distance between the myocyte and the voids gets closer as the myocyte volume increases and this smaller distance causes the slightly more non-linear drop in shear.

7.4 3D Simulations Results - Intercalated discs

Within this section we extend the current computational platform to 3D to allow us incorporate more structural details that will give us an even more detailed picture of the true elastic response of the heart. We now consider a setup where we have the myocyte with intercalated discs at either end embedded in the extracellular matrix with the four blood vessels in each corner. The intercalated disks are thin connecting plates found at either end of the myocytes that allow for connection to the next myocyte cell [75]. The more detailed 3D geometry we consider is shown in Fig. 7.14.

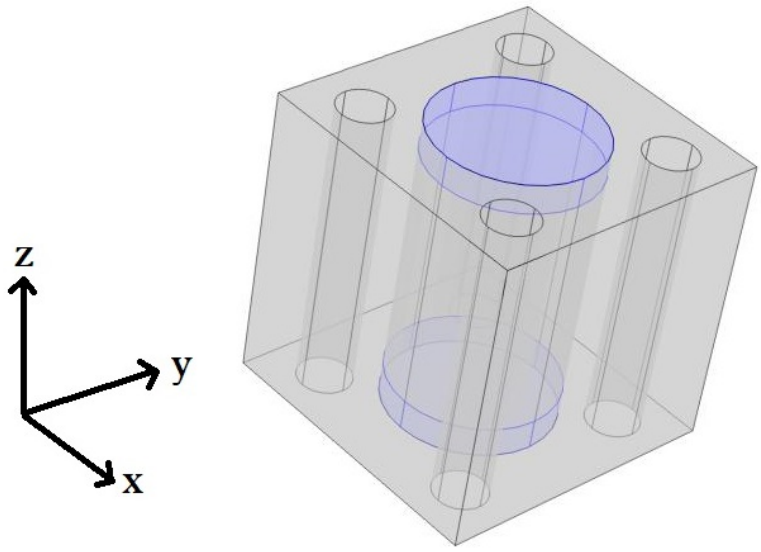

Figure 7.14: 3D geometry myocyte with intercalated disks at both ends embedded in the extracellular matrix with four blood vessels.

Here we make the assumption that the myocytes have a height of 0.8 in the unit cell of length 1. This is centred so there is a gap of 0.1 height between the myocyte ends and the top and bottom of the cell. In this gap we place the intercalated discs that connect the myocytes between cells. This means that we must perform 3D simulations to solve the cell problems of LMRP since for every slice in the z direction we do not have the same

microstructure so we cannot reduce to 2D.

We solve the cell problems using the following parameters, found in [1], [26] and [63]. As far as can be determined from the literature there is no clear Young's modulus for the intercalated disc, this can be attributed to the fact they are composed of a variety of different proteins all with different elastic parameters. However, we do know that the intercalated discs between myocytes are exposed to substantially higher forces than the equivalent cell-cell junctions in other organs [67]. This leads to the assumption that discs should be stiffer than the myocyte but on the same order of magnitude. We should note that given some experimental data on the effective elastic parameters of the material overall, it may be possible to perform an inverse analysis to obtain a value of say the Youngs moduli for the intercalated discs. We have the following parameters and the values we have selected for the intercalated discs.

Table 7.3: Input parameters 3D simulations found in [1], [26] and [63]

Parameter	E_{myo} (kPa)	E_{matrix} (kPa)	E_{disc} (kPa)	ν_{myo}	ν_{matrix}	ν_{disc}
Value	35	80	60	0.49	0.4	0.49

We carry out the simulations for four fixed fluid volume fractions $\phi_f = 5\%, 10\%, 15\%, 20\%$ and for each of these varying the myocyte volume fraction from $5\% - 25\%$. The fluid volume fractions have been chosen to represent the following settings; 5% reduced flow leading to infarction, 10%-15% normal range of healthy perfusion, 20% over perfused leading to myocardial injury. We should note that the intercalated disc is the connection between the myocytes, therefore we are assuming that the intercalated discs are growing with the myocytes so that the radii of both are consistently the same. This means that we are losing a larger percentage of the matrix with the increase in myocyte volume fraction at the expense of the larger discs.

We begin our analysis by considering the Young's moduli.

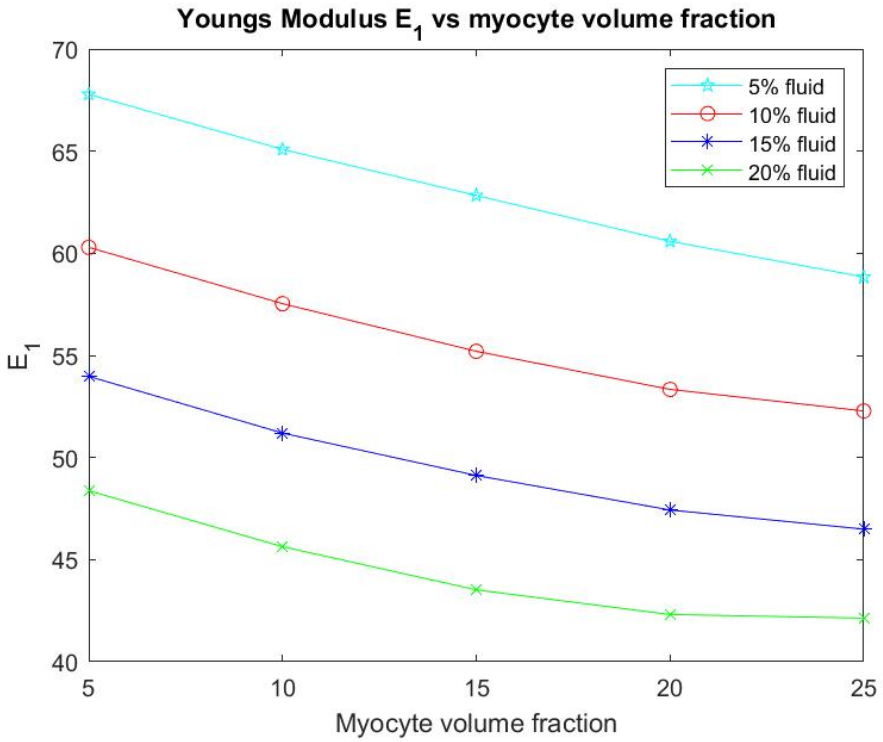

Figure 7.15: Young's Modulus E_1 versus myocyte volume fraction for four different fixed fluid volume fractions.

From Fig. 7.15 we can see that for each fixed fluid volume fraction that the Young's modulus E_1 decreases with increasing myocyte volume fraction. As before the Young's modulus is a measure of the material stiffness and therefore gives information about the overall elastic compliance of the heart. The heart should be soft and elastic when healthy with an overall Young's modulus of 35kPA [63]. This means we can determine a range of conclusions from the simulations that agree with physiological findings. Post myocardial infarction intact, surviving myocytes enlarge in an attempt to regulate the stiffness of the heart caused by the increasing stiffness of the extracellular matrix. Here we see exactly this phenomena, with the larger the myocyte volume and the greater the fluid volume fraction the closer the E_1 parameter gets to that of the healthy heart.

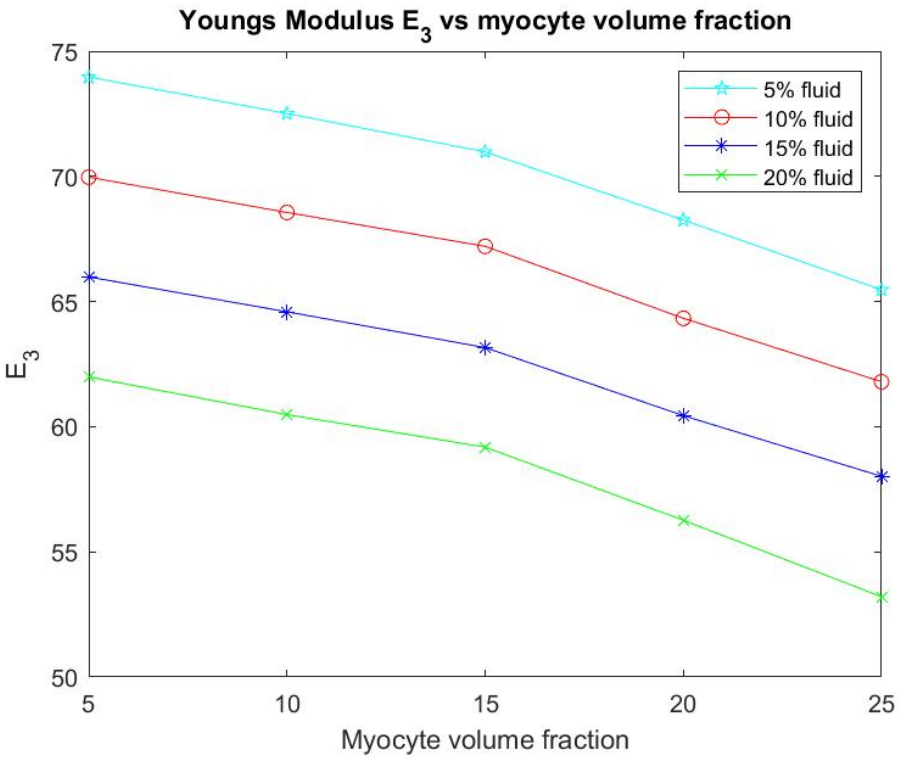

Figure 7.16: Young's Modulus E_3 versus myocyte volume fraction for four different fixed fluid volume fractions.

Here, in Fig. 7.16, we consider the axial Young's modulus E_3. We again can see that with increasing myocyte volume fraction the value of E_3 (the stiffness) decreases for all four fixed fluid volumes. We again see that this behaviour is again representative of what happens physiologically in the heart to try to maintain homeostasis post infarction. We also can compare E_3 with E_1. We see that E_3 changes more than E_1 when we compare line-by-line (for each fluid volume fraction) and that the starting values of E_3 are higher than that of E_1. This can be explained by the fact that since the myocytes elongate in E_3 this creates the stiffer Young's modulus in this direction compared with the E_1 Young's modulus.

We also wish to consider the two shear moduli C_{44} and C_{66} for the four fixed fluid volumes with increasing myocyte volume.

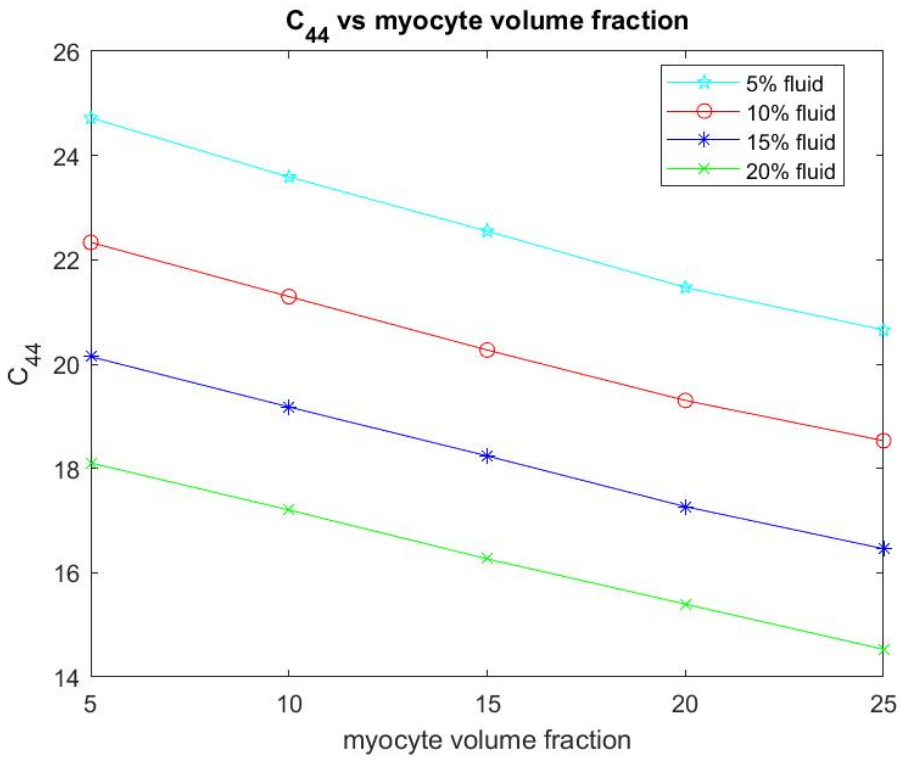

Figure 7.17: Shear C_{44} versus myocyte volume fraction for four different fixed fluid volume fractions.

In Fig. 7.17 we see that the shear C_{44} decreases with increasing myocyte volume fraction at all four fluid volumes. This shear is applied in the direction that the myocyte and channels elongate. This means that for small myocyte volume fractions the matrix and the specified fluid volume fraction have most influence on the stiffness of the material. When the myocytes and discs increase in volume they play a role in reducing the overall stiffness since they are softer than the matrix. The higher the value of the shear then the stiffer the overall material is. The results of our simulations again agree with the physiologically observed behaviour that the increased myocyte volume aims to reduce the overall stiffness of the myocardium caused by the infarct scar in an attempt to return to homeostasis.

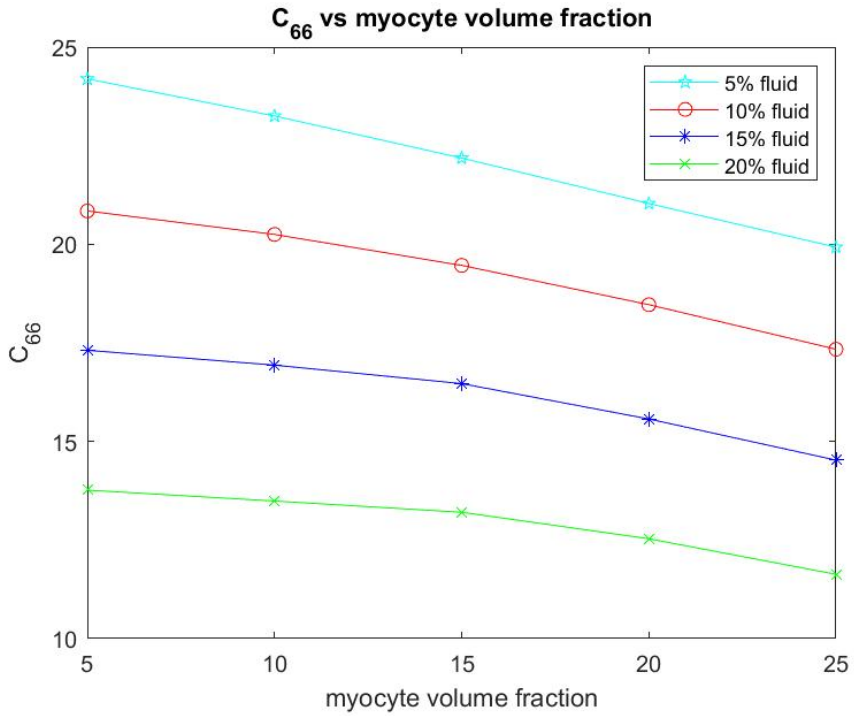

Figure 7.18: Shear C_{66} versus myocyte volume fraction for 4 different fixed fluid volume fractions.

The final parameter we have considered is the shear C_{66} as shown in Fig. 7.18. This shear is applied taking a cross-section of the material where we will see matrix, channels and intercalated disc. This shear again decreases with increasing myocyte volume. We can compare the behaviour with C_{44}. We see that for the 5% fluid volume fraction that C_{66} decreases more than C_{44}, however for 10%, 15% and 20% fluid volume fractions C_{44} shows the greater decrease with increasing myocyte volume fraction. We note that C_{44} has higher values across all myocyte volume fractions for all four fluid volume fractions than C_{66}. This can be explained by the different directions the shear is applied in. The increase in the myocyte volume does indeed decrease the overall stiffness since the myocyte and the discs are taking up a larger volume of the whole structure and are softer than the matrix. However C_{44} is being applied against the base of the disc/myocyte fibre and as the volume of this increases it has an influence when the force is applied. The voids with the C_{44} shear only flatten out rather than deforming with the shear. Both of these reasons are what keeps the value of the shear C_{44} higher that that of C_{66}.

7.5 Conclusions and future directions

Within this work we have created a robust computational platform that has allowed for a first study of how different microstructural features, that can be observed clinically following myocardial infarction, affect the elastic parameters of the heart. We have investigated a variety of elastic parameters obtained by solving the asymptotic homogenization cell problems of [69] and Chapter 3 for poroelastic composites.

We begin this work by firstly summarising the LMRP model for poroelastic composites. We provide an Appendix C.1 with the specific cell problems that we have solved to produce the results of this work, as well as references to inform the reader of the numerical procedures that are carried out. We then consider the first microstructural change that occurs as the result of myocardial infarction. That is, the loss of myocyte volume and increasing matrix fibrosis and we consider this versus porosity. For this microstructural change we make the comparison with the healthy heart for the four elastic parameters (Young's moduli E_1 and E_3 and shear moduli C_{44} and C_{66}). We find that in all cases the diseased/infarcted heart is much stiffer across the range of porosities considered. This is in line with the expected physiological response post infarction.

We continue our analysis by considering the effect of increasing the volume fraction of the myocyte with the extracellular matrix still being stiffer than in the healthy case. Physiologically this happens in the areas surrounding the infarct region in an attempt to counter balance the increased stiffness of the matrix with scar tissue. The results we obtain for all four elastic parameters, for all four different fixed fluid volume fractions, confirms this physiological phenomenon. For both of these cases it was possible to carry out the simulations in 2D since our geometry is identical for each z.

The final part of our analysis extends the previous section by the addition of the intercalated disks that are stiffer than the myocytes and connect myocytes cell-to-cell. The analysis carried out in this section requires 3D simulations since the microstructure varies with the z coordinate. In this setting it is again the increase in the myocyte volume fraction that is considered. We again see that with increasing myocyte volume all of the elastic parameters that we have considered here decrease, meaning the stiffness of the overall myocardium is decreasing. Once again our numerical results were replicating the physiological response (i.e. increasing myocyte volume in order to try to reduce the stiffness of the complete organ caused by the scar tissue).

The numerical simulations carried out in this work can be thought of as a first at-

tempt to model some basic microstructural changes that can be observed post myocardial infarction. The simulations here are computationally cheap (approximately 15 seconds computing time to obtain each data point) and can provide realistically observed phsiological responses.

Our current model does have some limitations and possible extensions. The model currently assumes a simplified microstructure. By increasing the complexity (i.e. the number of phases and shape of the interfaces) we would obtain differences in the overall elastic parameters but the generic behaviour would be similiar. We could for example extend the 3D simulations in Sec. 7.4 to include also the influence of the fibroblast cells on the parameters. It would also be possible to split the heart into regions such as infarct zone, the infarct border and the remaining unaffected tissue. By doing this we would obtain different macroscale coefficients for each of the regions that can be used to solve the overall macroscale model.

It is important to note that micromechanical modelling approaches other than asymptotic homogenization could also be of use to obtain reasonable approximations of these elastic parameters. Other methods such as effective medium theory and mixture theory are able to accommodate multiple phases and various shaped inclusions and various specific shaped pores (ellipsoidal, penny-shaped or shperical) however they cannot account for the unusual or complex geometries with the same precise prescription as asymptotic homogenization.

Currently this work has used linear elasticity however, we are able to make use of this computational platform to represent a more accurate nonlinear behaviour of the heart by using a piecewise approach to modelling as done in [52], [53]. By doing this we can approximate the nonlinear behaviour using simple, computationally cheap simulations.

Future extensions to this model that could allow it to be used as a predictive tool for clinicians would be adding additional microstructural features that have an influence on the overall behaviour of the heart. As well as obtaining additional data from medical imaging that would allow us to create a patient specific profile of the elastic parameters post infarction and in the recovery period. By solving the macroscale model, which is not done in this work, we would obtain values for pressure that could be compared with pressure-volume loop data obtained from patients.

Another useful source of data for model comparison and validation would come from elastography of the heart. The elastography technique uses vibrations applied to the

skin and measures the responses from the underlying tissues since stiffer tissue responds differently to softer tissue [119]. This can be used to assess changes in myocardial elasticity during the cardiac cycle [113]. These measurements along with our model predictions can provide valuable insight to clinicians on the stiffness of the heart and inform treatment choices.

Chapter 8

Summary and Conclusions

We have derived a variety of novel theoretical models that consist of partial differential equations that describe the effective mechanical behaviour of poroelastic materials with various different microstructures. This has been used to enhance the literature surrounding poroelasticity and has allowed for a range of choices of models when faced with real world applications that feature a detailed microstructure.

Our analysis begins firstly in Chapter 2 where we present a re-derivation of the quasi static governing equations of a porous elastic matrix with an incompressible Newtonian fluid flowing in the pores. We assume that the size of the pores is much smaller than the size of the whole domain and therefore embrace the asymptotic homogenization technique to derive the model. The governing equations are that of Biot's poroelasticity [12–15] which have previously been derived via homogenization by [19]. This chapter serves as a first example of the application of the asymptotic homogenization technique and as a standard for comparison with our novel models derived in later chapters that aim to improve upon the applicability of poroelastic models to real-world scenarios.

In Chapter 3 we derive the novel quasi-static governing equations for the macroscale behaviour of a linear elastic porous composite comprising a matrix interacting with inclusions and/or fibres, and an incompressible Newtonian fluid flowing in the pores. We assume that the size of the pores (the microscale) is comparable with the distance between adjacent subphases and is much smaller than the size of the whole domain (the macroscale). We then decouple spatial scales embracing the asymptotic (periodic) homogenization technique to derive the new macroscale model by upscaling the fluid–structure interaction problem between the elastic constituents and the fluid phase. The resulting system of partial differential equations is of poroelastic type and encodes the properties of

the microstructure in the coefficients of the model, which are to be computed by solving appropriate cell problems which reflect the complexity of the given microstructure. The model reduces to the limit case of simple composites when there are no pores [89], and standard Biot's poroelasticity whenever only the matrix–fluid interaction is considered [19] and [92]. We further prove rigorous properties of the coefficients, namely (a) major and minor symmetries of the effective elasticity tensor, (b) positive definiteness of the resulting Biot's modulus, and (c) analytical identities which allow us to define an effective Biot's coefficient.

In Chapter 4 we extend this work to a nonlinear framework. Within this work, we upscale the equations that describe the porescale behaviour of nonlinear porous elastic composites, using the asymptotic homogenization technique in order to derive the macroscale effective governing equations. A porous hyperelastic composite can be thought of as being comprised of a matrix interacting with a number of subphases and percolated by a fluid flowing in the pores (which is chosen to be Newtonian and incompressible here). A general nonlinear macroscale model is derived and is then specified for a particular choice of strain energy function, namely the de Saint-Venant function. This leads to a macroscale system of PDEs, which is of poroelastic type with additional terms and transformations to account for the nonlinear behaviour of the material. Our new porohyperelastic-type model describes the effective behaviour of nonlinear porous composites by prescribing the stress balance equations, the conservation of mass and Darcy's law. The coefficients of these macroscale equations encode the detailed microstructure of the material and are to be found by solving porescale differential problems. The model reduces to the following limit cases of (a) linear poroelastic composites when the deformation gradient approaches the identity [69], (b) nonlinear composites when there are no pores [102] and (c) nonlinear poroelasticity when only the matrix–fluid interaction is considered [17].

We further develop the poroelastic modelling literature with our novel model for double poroelastic materials, that is, materials with a poroelastic matrix with embedded poroelastic subphases. This is derived in Chapter 5. We assume that the distance between the subphases (the local scale) is much smaller than the size of the domain (the global scale). We assume that at the local scale both the matrix and subphases can be described by Biot's anisotropic, heterogeneous, compressible poroelasticity (i.e. the porescale is already smoothed out). We then decompose the spatial variations by means of the two-scale homogenization method to upscale the interaction between the poroelastic phases at the local

scale. This way, we derive the novel global scale model which is formally of poroelastic-type. The global scale coefficients account for the complexity of the given microstructure and heterogeneities. These effective poroelastic moduli are to be computed by solving appropriate differential periodic cell problems. The model coefficients possess properties that, once proved, allow us to determine that the model is both formally and substantially of poroelastic-type. The properties we prove are a) the existence of a tensor which plays the role of the classical Biot's tensor of coefficients via a suitable analytical identity and b) the global scale scalar coefficient $\bar{\mathcal{M}}$ is positive which then qualifies as the global Biot's modulus for the double poroelastic material.

We then begin our numerical analysis of our novel models. In Chapter 6 we investigate the role that the microstructure of a poroelastic material has on the resulting elastic parameters. We are considering the effect that multiple elastic and fluid phases at the same scale (LMRP model from Chapter 3) have on the estimation of the materials elastic parameters when compared with a standard poroelastic approach. We present a summary of both the LMRP model and the comparable standard poroelastic approach both derived via the asymptotic homogenization approach. We provide the 3D periodic cell problems with associated boundary loads that are required to be solved to obtain the effective elasticity tensor for both model setups. We then perform a 2D reduction of the cell problems, again presenting the 2D boundary loads that are required to solve the problems numerically. The results of our numerical simulations show that whenever investigating a poroelastic composite material with porosity exceeding 5% then the LMRP model should be used to compute the Young's moduli E_1 and E_3 and the shear C_{44} and when the porosity exceeds 20% it should also be used to investigate the shear C_{66}. We find that for materials with less than 5% porosity a standard poroelastic approach or the LMRP model produce the same results.

Finally in Chapter 7 we apply our novel model for poroelastic composites to investigating the elastic parameters of the heart post myocardial infarction. Within this work we investigate how physiologically observed microstructural changes induced by myocardial infarction impact the elastic parameters of the heart. We use the LMRP model for poroelastic composites [69] to describe the microstructure of the myocardium and investigate microstructural changes such as loss of myocyte volume and increased matrix fibrosis as well as increased myocyte volume fraction in the areas surrounding the infarct. We also consider a 3D framework to model the myocardial microstructure with the addition

of the intercalated disks, which provide the connections between adjacent myocytes. The results of our simulations agree with the physiological observations that can be made post-infarction. That is, the infarcted heart is much stiffer than the healthy heart but with reperfusion of the tissue it begins to soften. We also observe that with the increase in myocyte volume of the non-damaged myocytes the myocardium also begins to soften. With a measurable stiffness parameter the results of our model simulations could predict the range of porosity (reperfusion) that could help return the heart to the healthy stiffness. It would also be possible to predict the volume of the myocytes in the area surrounding the infarct from the overall stiffness measurements.

The current work has extended the literature surrounding poroelastic materials and has produced computationally feasible models. There are of course many extensions to the research lines that have been developed in this thesis and there have been specific comments made on these in the concluding remarks of the individual chapters. Overall there are a variety of novel models that could still be developed in order to extend and develop the understanding of perfusion and mechanics in real world poroelastic materials.

Appendix A

Appendix: Double poroelastic material model

A.1 Limit cases for the global scale model

It is important to note that our global scale model (5.132) reduces to previously obtained results when we consider the following limit cases. The first case is in the limit of no fluid present. This means that we are able to set $\vartheta^{(0)}$ to zero and therefore $\dot{\vartheta}^{(0)}$ is also zero and the relative fluid velocities $\mathbf{w}_{\mathrm{M}}$ and $\mathbf{w}_{\mathrm{S}}$ are both zero. In this case the mechanical behaviour of the material is described by only the balance equation with no pressure contribution in the effective stress, Therefore the model reduces to only two equations and has the form

$$\begin{cases} \nabla_{\mathbf{x}} \cdot \boldsymbol{\sigma}_{\mathrm{eff}} = 0, \\ \boldsymbol{\sigma}_{\mathrm{eff}} = \langle \mathbb{C}_{\mathrm{M}}\mathbb{L}_{\mathrm{M}} + \mathbb{C}_{\mathrm{M}} + \mathbb{C}_{\mathrm{S}}\mathbb{L}_{\mathrm{S}} + \mathbb{C}_{\mathrm{S}} \rangle_{\Omega} : \xi_{\mathbf{x}} \mathbf{u}^{(0)}. \end{cases} \tag{A.1}$$

This is the model for a simple elastic composite material. We also note that the only cell problem that is relevant in this case is (5.83-5.86). This model coincides with the models for elastic composites found in the literature [89].

The second limit case we consider is where our subphase has no fluid (i.e the subphase is purely elastic) and our matrix remains poroelastic. This is the setting considered by [105] and, assuming also incompressibility of the phases, [24]. To reduce our model to this case we assume that $\boldsymbol{\alpha}_{\mathrm{S}} = 0$, $\mathbf{w}_{\mathrm{S}} = \mathbf{0}$ and that $\vartheta_{\mathrm{S}} = 0$. Under this assumption our model looks

like

$$\begin{cases} \nabla_{\mathbf{x}} \cdot \boldsymbol{\sigma}'_{\text{eff}} = 0, \\ \boldsymbol{\sigma}'_{\text{eff}} = \bar{\mathbb{C}}' : \xi_{\mathbf{x}} \mathbf{u}^{(0)} + \bar{\boldsymbol{\gamma}}' \vartheta^{(0)}, \\ \mathbf{w}'_{\text{eff}} = -\mathsf{W}' \nabla_{\mathbf{x}} \vartheta^{(0)}, \\ \dot{\vartheta}^{(0)} = -\bar{\mathcal{M}}' \big(\nabla_{\mathbf{x}} \cdot \mathbf{w}_{\text{eff}} - \widetilde{\boldsymbol{\alpha}}' : \xi_{\mathbf{x}} \dot{\mathbf{u}}^{(0)} \big), \end{cases} \tag{A.2}$$

where

$$\bar{\mathcal{M}}' = \frac{\langle \mathcal{M}_{\text{M}} \rangle_{\text{M}}}{1 + \langle \mathcal{M}_{\text{M}} (\boldsymbol{\alpha}_{\text{M}} : \boldsymbol{\tau}_{\text{M}}) \rangle_{\text{M}}}, \quad \bar{\boldsymbol{\gamma}}' = \langle \mathbb{C}_{\text{M}} \boldsymbol{\tau}_{\text{M}} + \mathbb{C}_{\text{S}} \boldsymbol{\tau}_{\text{S}} - \boldsymbol{\alpha}_{\text{M}} \rangle_{\Omega}, \quad \mathbf{w}'_{\text{eff}} = \langle \mathbf{w}_{\text{M}}^{(0)} \rangle_{\Omega},$$
$$\mathsf{W}' = \langle \mathsf{K}_{\text{M}} \mathsf{R}_{\text{M}} + \mathsf{K}_{\text{M}} \rangle_{\Omega}, \quad \widetilde{\boldsymbol{\alpha}}' = \langle \boldsymbol{\alpha}_{\text{M}} + \mathbb{L}_{\text{M}}^{\text{T}} : \boldsymbol{\alpha}_{\text{M}} \rangle_{\Omega}, \tag{A.3}$$

and $\bar{\mathbb{C}}'$ is the same as in (5.133). The effective behaviour of our material under these assumptions is characterised by the coefficients $\bar{\mathbb{C}}'$, $\widetilde{\boldsymbol{\alpha}}'$, W', $\widetilde{\boldsymbol{\gamma}}'$ and $\bar{\mathcal{M}}'$. We can make the following identifications in our notation with the notation used in [105], where a weak formulation has also been used, which are

$$\bar{\mathbb{C}}' = C^{\text{eff}}, \quad \widetilde{\boldsymbol{\alpha}}' = G^{\text{eff}}, \quad -\bar{\boldsymbol{\gamma}}' = A^{\text{eff}}, \quad \frac{1}{\bar{\mathcal{M}}'} = B^{\text{eff}}, \quad \mathsf{W}' = K^{\text{eff}}. \tag{A.4}$$

We have that our $\bar{\boldsymbol{\gamma}}'$ is identifiable with [105]'s A^{eff} up to a change in sign due to the difference in sign used within the ansatz between their work and ours. As noted by [105] the effective elasticity tensor found here is that of elastic composites [89]. It is also possible to show that $A^{\text{eff}} = G^{\text{eff}}$ and that B^{eff} is positive as in [105]. We can also identify our coefficients with those used in [24]. We enforce the assumption that our material is incompressible in both phases to our coefficients in (A.3) and then we can make the following identifications

$$\bar{\mathbb{C}}' = \mathbb{C}^{\text{eff}}, \quad \widetilde{\boldsymbol{\alpha}}' = \mathbf{S}^{\text{eff}}, \quad \bar{\boldsymbol{\gamma}}' = \mathbf{G}^{\text{eff}}, \quad \frac{1}{\bar{\mathcal{M}}'} = \Gamma^{\text{eff}}, \quad \mathsf{W}' = \mathbf{K}^{\text{eff}}. \tag{A.5}$$

We can also find a correspondence the cell problems found in [105] and [24] and those found here. The cell problem (5.83-5.86) which is the cell problem for elastic composites is the cell problem found in [24] when the assumptions of isotropy and incompressibility are applied and the cell problem found in [105] where a weak formulation has been used. The second cell problem (5.87-5.90) reduces in this limit case. We have that $\boldsymbol{\alpha}_{\text{S}} = 0$ due

to there being no fluid in the subphase. The reduced cell problem is

$$\nabla_{\mathbf{y}} \cdot (\mathbb{C}_{\mathrm{M}} \xi_{\mathbf{y}} \mathbf{b}_{\mathrm{M}}) = \nabla_{\mathbf{y}} \cdot \boldsymbol{\alpha}_{\mathrm{M}} \quad \text{in} \quad \Omega_{\mathrm{M}}, \tag{A.6}$$

$$\nabla_{\mathbf{y}} \cdot (\mathbb{C}_{\mathrm{S}} \xi_{\mathbf{y}} \mathbf{b}_{\mathrm{S}}) = \mathbf{0} \quad \text{in} \quad \Omega_{\mathrm{S}}, \tag{A.7}$$

$$(\mathbb{C}_{\mathrm{M}} \xi_{\mathbf{y}} \mathbf{b}_{\mathrm{M}} - \mathbb{C}_{\mathrm{S}} \xi_{\mathbf{y}} \mathbf{b}_{\mathrm{S}}) \mathbf{n} = \boldsymbol{\alpha}_{\mathrm{M}} \mathbf{n} \quad \text{on} \quad \Upsilon, \tag{A.8}$$

$$\mathbf{b}_{\mathrm{M}} = \mathbf{b}_{\mathrm{S}} \quad \text{on} \quad \Upsilon. \tag{A.9}$$

When the assumptions of isotropy and incompressibility are made we also have that $\boldsymbol{\alpha}_{\mathrm{M}} = 1$. This means that the right hand side of (A.6) and (A.7) are both zero. This again coincides with the cell problems found in [24] and [105]. The anisotropic Poisson problem (5.113-5.116) reduces in this limit also. Since there is no fluid in the subphase from the commencement then there is no requirement for the continuity of pressure interface condition or for a Darcy's law equation in the subphase, that is $\mathbf{w}_{\mathrm{S}} = 0$. This means that the problem retains only two equations. The reduced cell problem is therefore

$$\nabla_{\mathbf{y}} \cdot (\nabla_{\mathbf{y}} \hat{\boldsymbol{\vartheta}}_{\mathrm{M}} \mathsf{K}_{\mathrm{M}}^{\mathrm{T}}) = -\nabla_{\mathbf{y}} \cdot \mathsf{K}_{\mathrm{M}}^{\mathrm{T}} \quad \text{in} \quad \Omega_{\mathrm{M}}, \tag{A.10}$$

$$(\nabla_{\mathbf{y}} \hat{\boldsymbol{\vartheta}}_{\mathrm{M}} \mathsf{K}_{\mathrm{M}}^{\mathrm{T}}) \mathbf{n} = -\mathsf{K}_{\mathrm{M}}^{\mathrm{T}} \mathbf{n} \quad \text{on} \quad \Upsilon. \tag{A.11}$$

This corresponds to the cell problem in [105] and the cell problem in [24] when again in this latter case the assumptions of isotropy and incompressibility are made as well as assuming the hydraulic conductivity tensor $\mathsf{K}_{\mathrm{M}} = 1$.

A.2 Computational scheme

We aim to provide a clear step-by-step guide to finding our effective coefficients and solving our global scale model (5.132) encoding structural details from three scales. We also provide, where available, particular references that would assist the reader with the type of numerical simulations that would need to be carried out. Since we have made the assumption of global scale uniformity of the material then we can propose the following steps to solve the model. The process is as follows:

1. We begin by fixing the original material properties of the poroelastic matrix and the poroelastic subphases at the local scale. We require the effective elasticity tensors $\mathbb{C}_{\mathrm{M}}$ and $\mathbb{C}_{\mathrm{S}}$, the Biot's tensors $\boldsymbol{\alpha}_{\mathrm{M}}$ and $\boldsymbol{\alpha}_{\mathrm{S}}$, the Biot's moduli $\mathcal{M}_{\mathrm{M}}$ and $\mathcal{M}_{\mathrm{S}}$ and finally

the hydraulic conductivities K_{M} and K_{S} from both the matrix and the subphases. Under the assumption of isotropy we are required to fix 5 parameters for the matrix and 5 parameters for the subphase. These parameters are two independent elastic constants e.g the Poisson ratio and Young's modulus (or alternatively the Lamé constants), hydraulic conductivity, Biot's coefficient and Biot's modulus.

2. The local scale geometry then must be defined and we fix a single periodic cell at this stage.

3. We would then be able to solve the elastic-type cell problems (5.83 - 5.86) and (5.87 - 5.90) to obtain the auxiliary tensors $\mathbb{L}_{\mathrm{M}}, \mathbb{L}_{\mathrm{S}}, \boldsymbol{\tau}_{\mathrm{M}}$ and $\boldsymbol{\tau}_{\mathrm{S}}$ which appear in the global scale model coefficients. The cell problems to be solved are, in components,

$$\frac{\partial}{\partial y_j}\big(\mathcal{C}^{\mathrm{M}}_{ijpq}\zeta^{kl}_{pq}(B^{\mathrm{M}})\big) + \frac{\partial \mathcal{C}^{\mathrm{M}}_{ijkl}}{\partial y_j} = 0 \qquad \text{in} \qquad \Omega_{\mathrm{M}}, \tag{A.12}$$

$$\frac{\partial}{\partial y_j}\big(\mathcal{C}^{\mathrm{S}}_{ijpq}\zeta^{kl}_{pq}(B^{\mathrm{S}})\big) + \frac{\partial \mathcal{C}^{\mathrm{S}}_{ijkl}}{\partial y_j} = 0 \qquad \text{in} \qquad \Omega_{\mathrm{Sub}}, \tag{A.13}$$

$$\mathcal{C}^{\mathrm{M}}_{ijpq}\zeta^{kl}_{pq}(B^{\mathrm{M}})n_j - \mathcal{C}^{\mathrm{S}}_{ijpq}\zeta^{kl}_{pq}(B^{\mathrm{S}})n_j = (\mathcal{C}^{\mathrm{M}} - \mathcal{C}^{\mathrm{S}})_{ijkl}n_j \qquad \text{on} \qquad \Upsilon, \tag{A.14}$$

$$B^{\mathrm{M}}_{ikl} = B^{\mathrm{S}}_{ikl} \qquad \text{on} \qquad \Upsilon, \tag{A.15}$$

as well as another elastic-type cell problem driven by variations in the constituents' compressibility

$$\frac{\partial}{\partial y_j}\big(\mathcal{C}^{\mathrm{M}}_{ijpq}\zeta_{pq}(b^{\mathrm{M}})\big) = \frac{\partial \alpha^{\mathrm{M}}_{ij}}{\partial y_j} \qquad \text{in} \qquad \Omega_{\mathrm{M}}, \tag{A.16}$$

$$\frac{\partial}{\partial y_j}\big(\mathcal{C}^{\mathrm{S}}_{ijpq}\zeta_{pq}(b^{\mathrm{S}})\big) = \frac{\partial \alpha^{\mathrm{S}}_{ij}}{\partial y_j} \qquad \text{in} \qquad \Omega_{\mathrm{Sub}}, \tag{A.17}$$

$$\mathcal{C}^{\mathrm{M}}_{ijpq}\zeta_{pq}(b^{\mathrm{M}})n_j - \mathcal{C}^{\mathrm{S}}_{ijpq}\zeta_{pq}(b^{\mathrm{S}})n_j = -(\alpha^{\mathrm{S}} - \alpha^{\mathrm{M}})_{ij}n_j \qquad \text{on} \qquad \Upsilon, \tag{A.18}$$

$$b^{\mathrm{M}}_{i} = b^{\mathrm{S}}_{i} \qquad \text{on} \qquad \Upsilon, \tag{A.19}$$

where we have used the notation

$$\zeta^{kl}_{pq}(B^{v}) = \frac{1}{2}\left(\frac{\partial B^{v}_{pkl}}{\partial y_q} + \frac{\partial B^{v}_{qkl}}{\partial y_p}\right) \quad \text{and} \quad \zeta_{pq}(\mathbf{b}^{v}) = \frac{1}{2}\left(\frac{\partial b^{v}_{p}}{\partial y_q} + \frac{\partial b^{v}_{q}}{\partial y_p}\right), \tag{A.20}$$

and the superscript $v = \mathrm{M}, \mathrm{S}$ refers to either the matrix or the subphase. The solution of the problem (A.12-A.15) can be obtained by solving six elastic-type cell problems by fixing the couple of indices $k, l = 1, 2, 3$. By doing this we can see

that $\zeta_{pq}^{kl}(B^v)$ represents a strain and that for each fixed couple of indices k, l we have a linear elastic problem. For an example of where this cell problem has been solved computationally, see the recent works [88] and [89]. The solution of problem (A.16-A.19) is obtained by solving 3 cell problems for each $i = 1, 2, 3$.

The auxiliary second rank tensors R_{M} and R_{S} can be computed by solving the vector cell problem given by (5.113-5.116). The latter corresponds to three scalar anisotropic Poisson's problems (for each $j = 1, 2, 3$) equipped with continuity and transmission interface conditions, component-wise. The cell problem in components is

$$\frac{\partial}{\partial y_i}\left(K_{il}^{\mathrm{M}}\frac{\partial \hat{\vartheta}_j^{\mathrm{M}}}{\partial y_l}\right) = -\frac{\partial K_{ij}^{\mathrm{M}}}{\partial y_i} \qquad \text{in} \qquad \Omega_{\mathrm{M}}, \tag{A.21}$$

$$\frac{\partial}{\partial y_i}\left(K_{il}^{\mathrm{S}}\frac{\partial \hat{\vartheta}_j^{\mathrm{S}}}{\partial y_l}\right) = -\frac{\partial K_{ij}^{\mathrm{S}}}{\partial y_i} \qquad \text{in} \qquad \Omega_{\mathrm{Sub}}, \tag{A.22}$$

$$\hat{\vartheta}_j^{\mathrm{M}} = \hat{\vartheta}_j^{\mathrm{S}} \qquad \text{on} \qquad \Upsilon, \tag{A.23}$$

$$\left(K_{il}^{\mathrm{M}}\frac{\partial \hat{\vartheta}_j^{\mathrm{M}}}{\partial y_l} - K_{il}^{\mathrm{S}}\frac{\partial \hat{\vartheta}_j^{\mathrm{S}}}{\partial y_l}\right)n_i = (K^{\mathrm{M}} - K^{\mathrm{S}})_{ij}n_i \qquad \text{on} \qquad \Upsilon. \tag{A.24}$$

This problem is the same as the classical problem that arises from applying the asymptotic homogenization technique to the diffusion problem and porous media problems, see [27], [7], and [93]

4. We also require one more condition to ensure uniqueness of solution. We can enforce that the cell averages of the cell problem solutions are zero. That is, $\langle \mathsf{B}_{\mathrm{M}} + \mathsf{B}_{\mathrm{S}} \rangle_\Omega = 0$, $\langle \mathbf{b}_{\mathrm{M}} + \mathbf{b}_{\mathrm{S}} \rangle_\Omega = 0$ and $\langle \hat{\boldsymbol{\vartheta}}_{\mathrm{M}} + \hat{\boldsymbol{\vartheta}}_{\mathrm{S}} \rangle_\Omega = 0$

5. The auxiliary tensors arising form the cell problems (i.e. the quantities $\mathbb{L}_{\mathrm{M}}$, $\mathbb{L}_{\mathrm{S}}$, $\boldsymbol{\tau}_{\mathrm{M}}$, $\boldsymbol{\tau}_{\mathrm{S}}$, R_{M} and R_{S}) can then be used to determine the global scale model coefficients.

6. The geometry at the global scale then must be prescribed. The boundary conditions for the homogenized cell boundary must also be given, and the system is to be supplemented with initial conditions for the global scale solid displacement and pressure.

7. Finally, the global scale model (5.132) for a double poroelastic material can then be solved.

Remark 17. *(Computational scheme on three scales) If porescale data was available for*

our material then we would be able to obtain a solution encoding structural detail on three scales. We would begin by fixing the original material properties on the porescale. This includes fixing the stiffness of the solid phase in both the matrix and subphase, defining the pore structures, and determining the fluid properties, which are, the viscosity and potentially the bulk moduli for compressible fluids. At this scale we are considering both these poroelastic materials separately. We then must define the porescale geometry for both the matrix and the subphases. This includes fixing a periodic cell in both the matrix and the subphases. We would then be able to solve the separate cell problems for the matrix and the subphase. These cell problems are the standard cell problems of poroelasticity found in [19] and with a step-by step computational scheme found in [92]. These cell problem solutions would then be used to determine the local scale coefficients such as the elasticity tensors $\mathbb{C}_{\mathrm{M}}$ *and* $\mathbb{C}_{\mathrm{S}}$*, the Biot's tensors of coefficients in the matrix and the subphases* $\boldsymbol{\alpha}_{\mathrm{M}}$ *and* $\boldsymbol{\alpha}_{\mathrm{S}}$*, the Biot's moduli* $\mathcal{M}_{\mathrm{M}}$ *and* $\mathcal{M}_{\mathrm{S}}$*, and the hydraulic conductivities* K_{M} *and* K_{S}*, which would then be used in Step 1 above. For an example of where these elastic and fluid cell problems have been solved numerically see the recent work [35].*

Appendix B

Appendix: Analysis of stiffness of poroelastic composites

This appendix contains firstly the 2D reduction of the cell problems for poroelastic composites shown in Sec. 6.2.1 with orthotropic elastic constituents. This reduction is the most general and can have different assumptions applied so it can be reduced to the 2D problems for the model in Sec. 6.2.3. The second function of this appendix is to provide details of the numerical setup and justification of our computational setup for 3D simulations.

B.1 2D reduction

Our 2D reduction of the problem will be carried out for the most general case, which in this work is the poroelastic composite where both elastic phases are orthotropic. From this problem which comprises five equations we can make some simplifying assumptions which allow the reduction to also be applicable to the porous matrix problem and to the composite comprising the porous matrix and the elastic inclusion. In order to carry out our 2D reduction we consider and build upon [82], [81], [88]

Since we are beginning with the case of poroelastic composites we will use the notation of the LMRP model in Sec. 6.2.1. We begin our reduction by making the assumption that the elasticity tensors $\mathbb{C}_{\mathrm{I}}$ and $\mathbb{C}_{\mathrm{II}}$ are constant with respect to both the porescale and macroscale. This will also be the case for $\mathbb{C}_{\mathrm{M}}$, $\mathbb{C}_{\mathrm{I}}^{\mathrm{SP}}$ and $\mathbb{C}_{\mathrm{PM}}$ for the other problems. This means that we can re-write the 3D cell problem (6.19)-(6.23) for third rank tensors A_{ikl}^{I}

and A^{II}_{ikl} as follows

$$C^{\text{I}}_{ijpq}\frac{\partial A^{\text{I}}_{pkl}}{\partial y_j \partial y_q} = 0 \qquad \text{in} \quad \Omega_{\text{I}} \tag{B.1}$$

$$C^{\text{II}}_{ijpq}\frac{\partial A^{\text{II}}_{pkl}}{\partial y_j \partial y_q} = 0 \qquad \text{in} \quad \Omega_{\text{II}} \tag{B.2}$$

$$C^{\text{I}}_{ijpq}\frac{\partial A^{\text{I}}_{pkl}}{\partial y_q} n^{\text{III}}_j - C^{\text{II}}_{ijpq}\frac{\partial A^{\text{II}}_{pkl}}{\partial y_q} n^{\text{III}}_j = (C^{\text{II}} - C^{\text{I}})_{ijkl} n^{\text{III}}_j \qquad \text{on} \quad \Gamma_{\text{III}} \tag{B.3}$$

$$A^{\text{I}}_{ikl} = A^{\text{II}}_{ikl} \qquad \text{on} \quad \Gamma_{\text{III}} \tag{B.4}$$

$$C^{\text{II}}_{ijpq}\frac{\partial A^{\text{II}}_{pkl}}{\partial y_q} n^{\text{II}}_j + C^{\text{II}}_{ijkl} n^{\text{II}}_j = 0 \qquad \text{on} \quad \Gamma_{\text{II}} \tag{B.5}$$

In the above cell problem the summation over repeated indices $j, p, q = 1, 2, 3$ is understood. We note that our unknown third rank tensors A^{I} and A^{II} do not depend on y_3 due to symmetry, neither do the third rank tensors B, F^{I} or F^{II} that we use in the other cell problems presented in Sec. 6.2.3. We also have that our normals to the interfaces are also only functions of y_1 and y_2. This, along with the elasticity tensors being $\mathbf{y}$-constant, means that A^{I} and A^{II} only depend on y_1 and y_2. The cell problem (B.1)-(B.5) can now be solved in two dimensions, so we can rewrite as

$$C^{\text{I}}_{i\alpha s\beta}\frac{\partial A^{\text{I}}_{skl}}{\partial y_\alpha \partial y_\beta} = 0 \qquad \text{in} \quad D_{\text{I}} \tag{B.6}$$

$$C^{\text{II}}_{i\alpha s\beta}\frac{\partial A^{\text{II}}_{skl}}{\partial y_j \partial y_q} = 0 \qquad \text{in} \quad D_{\text{II}} \tag{B.7}$$

$$C^{\text{I}}_{i\alpha s\beta}\frac{\partial A^{\text{I}}_{skl}}{\partial y_\beta} n^{\text{III}}_\alpha - C^{\text{II}}_{i\alpha s\beta}\frac{\partial A^{\text{II}}_{skl}}{\partial y_\beta} n^{\text{III}}_\alpha = (C^{\text{II}} - C^{\text{I}})_{i\alpha kl} n^{\text{III}}_\alpha \qquad \text{on} \quad \partial D_{\text{I}} \cap \partial D_{\text{II}} \tag{B.8}$$

$$A^{\text{I}}_{ikl} = A^{\text{II}}_{ikl} \qquad \text{on} \quad \partial D_{\text{I}} \cap \partial D_{\text{II}} \tag{B.9}$$

$$C^{\text{II}}_{i\alpha s\beta}\frac{\partial A^{\text{II}}_{skl}}{\partial y_\beta} n^{\text{II}}_\alpha + C^{\text{II}}_{i\alpha kl} n^{\text{II}}_\alpha = 0 \qquad \text{on} \quad \partial D_{\text{f}} \tag{B.10}$$

In the problem (B.1)-(B.5) the summation over repeated indices $s = 1, 2, 3$ and α, $\beta = 1, 2$ is understood. We also have the domains D_{I} and D_{II} which represent the two-dimensional cross section of the periodic cell where the subscripts I and II represent the inclusion and matrix respectively. We also have the interfaces $\partial D_{\text{I}} \cap \partial D_{\text{II}}$ which corresponds to a 2D cross section of Γ_{III} and ∂D_{f} is the 2D cross section of Γ_{I}.

We assume that our $C^{\text{I}}_{i\alpha s\beta}$ and $C^{\text{II}}_{i\alpha s\beta}$ are orthotropic, that is, the following represen-

tations for $\mathbb{C}^{\mathrm{I}}$ and $\mathbb{C}^{\mathrm{II}}$ holds

$$\mathbb{C}^{\mathrm{I}} = \begin{bmatrix} C^{\mathrm{I}}_{11} & C^{\mathrm{I}}_{12} & C^{\mathrm{I}}_{13} & 0 & 0 & 0 \\ C^{\mathrm{I}}_{12} & C^{\mathrm{I}}_{22} & C^{\mathrm{I}}_{13} & 0 & 0 & 0 \\ C^{\mathrm{I}}_{13} & C^{\mathrm{I}}_{13} & C^{\mathrm{I}}_{33} & 0 & 0 & 0 \\ 0 & 0 & 0 & C^{\mathrm{I}}_{44} & 0 & 0 \\ 0 & 0 & 0 & 0 & C^{\mathrm{I}}_{55} & 0 \\ 0 & 0 & 0 & 0 & 0 & C^{\mathrm{I}}_{66} \end{bmatrix} \tag{B.11}$$

$$\mathbb{C}^{\mathrm{II}} = \begin{bmatrix} C^{\mathrm{II}}_{11} & C^{\mathrm{II}}_{12} & C^{\mathrm{II}}_{13} & 0 & 0 & 0 \\ C^{\mathrm{II}}_{12} & C^{\mathrm{II}}_{22} & C^{\mathrm{II}}_{13} & 0 & 0 & 0 \\ C^{\mathrm{II}}_{13} & C^{\mathrm{II}}_{13} & C^{\mathrm{II}}_{33} & 0 & 0 & 0 \\ 0 & 0 & 0 & C^{\mathrm{II}}_{44} & 0 & 0 \\ 0 & 0 & 0 & 0 & C^{\mathrm{II}}_{55} & 0 \\ 0 & 0 & 0 & 0 & 0 & C^{\mathrm{II}}_{66} \end{bmatrix} \tag{B.12}$$

where we have used voigt notation for the entries as in [88].

We expand problem (B.1)-(B.5) using $s = 1, 2, 3$ and α, $\beta = 1, 2$. That is

$$\begin{aligned} &C^{\mathrm{I}}_{i111}\frac{\partial A^{\mathrm{I}}_{1kl}}{\partial y_1^2} + C^{\mathrm{I}}_{i121}\frac{\partial A^{\mathrm{I}}_{2kl}}{\partial y_1^2} + C^{\mathrm{I}}_{i131}\frac{\partial A^{\mathrm{I}}_{3kl}}{\partial y_1^2} + C^{\mathrm{I}}_{i112}\frac{\partial A^{\mathrm{I}}_{1kl}}{\partial y_1 \partial y_2} + C^{\mathrm{I}}_{i122}\frac{\partial A^{\mathrm{I}}_{2kl}}{\partial y_1 \partial y_2} \\ &+ C^{\mathrm{I}}_{i132}\frac{\partial A^{\mathrm{I}}_{3kl}}{\partial y_1 \partial y_2} + C^{\mathrm{I}}_{i211}\frac{\partial A^{\mathrm{I}}_{1kl}}{\partial y_2 \partial y_1} + C^{\mathrm{I}}_{i221}\frac{\partial A^{\mathrm{I}}_{2kl}}{\partial y_2 \partial y_1} + C^{\mathrm{I}}_{i231}\frac{\partial A^{\mathrm{I}}_{3kl}}{\partial y_2 \partial y_1} \\ &+ C^{\mathrm{I}}_{i212}\frac{\partial A^{\mathrm{I}}_{1kl}}{\partial y_2^2} + C^{\mathrm{I}}_{i222}\frac{\partial A^{\mathrm{I}}_{2kl}}{\partial y_2^2} + C^{\mathrm{I}}_{i232}\frac{\partial A^{\mathrm{I}}_{3kl}}{\partial y_2^2} = 0 \qquad \text{in} \quad D_{\mathrm{I}} \end{aligned} \tag{B.13}$$

$$\begin{aligned} &C^{\mathrm{II}}_{i111}\frac{\partial A^{\mathrm{II}}_{1kl}}{\partial y_1^2} + C^{\mathrm{II}}_{i121}\frac{\partial A^{\mathrm{II}}_{2kl}}{\partial y_1^2} + C^{\mathrm{II}}_{i131}\frac{\partial A^{\mathrm{II}}_{3kl}}{\partial y_1^2} + C^{\mathrm{II}}_{i112}\frac{\partial A^{\mathrm{II}}_{1kl}}{\partial y_1 \partial y_2} + C^{\mathrm{II}}_{i122}\frac{\partial A^{\mathrm{II}}_{2kl}}{\partial y_1 \partial y_2} \\ &+ C^{\mathrm{II}}_{i132}\frac{\partial A^{\mathrm{II}}_{3kl}}{\partial y_1 \partial y_2} + C^{\mathrm{II}}_{i211}\frac{\partial A^{\mathrm{II}}_{1kl}}{\partial y_2 \partial y_1} + C^{\mathrm{II}}_{i221}\frac{\partial A^{\mathrm{II}}_{2kl}}{\partial y_2 \partial y_1} + C^{\mathrm{II}}_{i231}\frac{\partial A^{\mathrm{II}}_{3kl}}{\partial y_2 \partial y_1} \\ &+ C^{\mathrm{II}}_{i212}\frac{\partial A^{\mathrm{II}}_{1kl}}{\partial y_2^2} + C^{\mathrm{II}}_{i222}\frac{\partial A^{\mathrm{II}}_{2kl}}{\partial y_2^2} + C^{\mathrm{II}}_{i232}\frac{\partial A^{\mathrm{II}}_{3kl}}{\partial y_2^2} = 0 \qquad \text{in} \quad D_{\mathrm{II}} \end{aligned} \tag{B.14}$$

$$\begin{aligned} &C^{\mathrm{I}}_{i111}\frac{\partial A^{\mathrm{I}}_{1kl}}{\partial y_1} n_1^{\mathrm{III}} + C^{\mathrm{I}}_{i121}\frac{\partial A^{\mathrm{I}}_{2kl}}{\partial y_1} n_1^{\mathrm{III}} + C^{\mathrm{I}}_{i131}\frac{\partial A^{\mathrm{I}}_{3kl}}{\partial y_1} n_1^{\mathrm{III}} + C^{\mathrm{I}}_{i112}\frac{\partial A^{\mathrm{I}}_{1kl}}{\partial y_2} n_1^{\mathrm{III}} + C^{\mathrm{I}}_{i122}\frac{\partial A^{\mathrm{I}}_{2kl}}{\partial y_2} n_1^{\mathrm{III}} \\ &+ C^{\mathrm{I}}_{i132}\frac{\partial A^{\mathrm{I}}_{3kl}}{\partial y_2} n_1^{\mathrm{III}} + C^{\mathrm{I}}_{i211}\frac{\partial A^{\mathrm{I}}_{1kl}}{\partial y_1} n_2^{\mathrm{III}} + C^{\mathrm{I}}_{i221}\frac{\partial A^{\mathrm{I}}_{2kl}}{\partial y_1} n_2^{\mathrm{III}} + C^{\mathrm{I}}_{i231}\frac{\partial A^{\mathrm{I}}_{3kl}}{\partial y_1} n_2^{\mathrm{III}} + C^{\mathrm{I}}_{i212}\frac{\partial A^{\mathrm{I}}_{1kl}}{\partial y_2} n_2^{\mathrm{III}} \\ &+ C^{\mathrm{I}}_{i222}\frac{\partial A^{\mathrm{I}}_{2kl}}{\partial y_2} n_2^{\mathrm{III}} + C^{\mathrm{I}}_{i232}\frac{\partial A^{\mathrm{I}}_{3kl}}{\partial y_2} n_2^{\mathrm{III}} - \Big(C^{\mathrm{II}}_{i111}\frac{\partial A^{\mathrm{II}}_{1kl}}{\partial y_1} n_1^{\mathrm{III}} + C^{\mathrm{II}}_{i121}\frac{\partial A^{\mathrm{II}}_{2kl}}{\partial y_1} n_1^{\mathrm{III}} + C^{\mathrm{II}}_{i131}\frac{\partial A^{\mathrm{II}}_{3kl}}{\partial y_1} n_1^{\mathrm{III}} \end{aligned}$$

$$+ C^{\text{II}}_{i112}\frac{\partial A^{\text{II}}_{1kl}}{\partial y_2}n^{\text{III}}_1 + C^{\text{II}}_{i122}\frac{\partial A^{\text{II}}_{2kl}}{\partial y_2}n^{\text{III}}_1 + C^{\text{II}}_{i132}\frac{\partial A^{\text{II}}_{3kl}}{\partial y_2}n^{\text{III}}_1 + C^{\text{II}}_{i211}\frac{\partial A^{\text{II}}_{1kl}}{\partial y_1}n^{\text{III}}_2 + C^{\text{II}}_{i221}\frac{\partial A^{\text{II}}_{2kl}}{\partial y_1}n^{\text{III}}_2$$
$$+ C^{\text{II}}_{i231}\frac{\partial A^{\text{II}}_{3kl}}{\partial y_1}n^{\text{III}}_2 + C^{\text{II}}_{i212}\frac{\partial A^{\text{II}}_{1kl}}{\partial y_2}n^{\text{III}}_2 + C^{\text{II}}_{i222}\frac{\partial A^{\text{II}}_{2kl}}{\partial y_2}n^{\text{III}}_2 + C^{\text{II}}_{i232}\frac{\partial A^{\text{II}}_{3kl}}{\partial y_2}n^{\text{III}}_2\Big)$$
$$= (C^{\text{II}}_{i1kl}n^{\text{III}}_1 + C^{\text{II}}_{i2kl}n^{\text{III}}_2) - (C^{\text{I}}_{i1kl}n^{\text{III}}_1 + C^{\text{I}}_{i2kl}n^{\text{III}}_2) \qquad \text{on} \quad \partial D_{\text{I}} \cap \partial D_{\text{II}} \tag{B.15}$$

$$A^{\text{I}}_{ikl} = A^{\text{II}}_{ikl} \qquad \text{on} \quad \partial D_{\text{I}} \cap \partial D_{\text{II}} \tag{B.16}$$

$$C^{\text{II}}_{i111}\frac{\partial A^{\text{II}}_{1kl}}{\partial y_1}n^{\text{II}}_1 + C^{\text{II}}_{i121}\frac{\partial A^{\text{II}}_{2kl}}{\partial y_1}n^{\text{II}}_1 + C^{\text{II}}_{i131}\frac{\partial A^{\text{II}}_{3kl}}{\partial y_1}n^{\text{II}}_1 + C^{\text{II}}_{i112}\frac{\partial A^{\text{II}}_{1kl}}{\partial y_2}n^{\text{II}}_1 + C^{\text{II}}_{i122}\frac{\partial A^{\text{II}}_{2kl}}{\partial y_2}n^{\text{II}}_1$$
$$+ C^{\text{II}}_{i132}\frac{\partial A^{\text{II}}_{3kl}}{\partial y_2}n^{\text{II}}_1 + C^{\text{II}}_{i211}\frac{\partial A^{\text{II}}_{1kl}}{\partial y_1}n^{\text{II}}_2 + C^{\text{II}}_{i221}\frac{\partial A^{\text{II}}_{2kl}}{\partial y_1}n^{\text{II}}_2 + C^{\text{II}}_{i231}\frac{\partial A^{\text{II}}_{3kl}}{\partial y_1}n^{\text{II}}_2 + C^{\text{II}}_{i212}\frac{\partial A^{\text{II}}_{1kl}}{\partial y_2}n^{\text{II}}_2$$
$$+ C^{\text{II}}_{i222}\frac{\partial A^{\text{II}}_{2kl}}{\partial y_2}n^{\text{II}}_2 + C^{\text{II}}_{i232}\frac{\partial A^{\text{II}}_{3kl}}{\partial y_2}n^{\text{II}}_2 + C^{\text{II}}_{i1kl}n^{\text{II}}_1 + C^{\text{II}}_{i2kl}n^{\text{II}}_2 = 0 \qquad \text{on} \quad \partial D_{\text{f}} \tag{B.17}$$

Now we have our problem we can set $i = 1, 2$ to get the in-plane problems and $i = 3$ for the anti-plane problems and use the entries from the matrices (B.11) and (B.12) to simplify. We have four in-plane problems and two anti-plane problems in total.

We first consider the anti-plane problem, so we put $i = 3$ in (B.13)-(B.17) and use the entries from the matrices (B.11) and (B.12), not in Voigt notation, to simplify. That is,

$$C^{\text{I}}_{3131}\frac{\partial A^{\text{I}}_{3kl}}{\partial y_1^2} + C^{\text{I}}_{3232}\frac{\partial A^{\text{I}}_{3kl}}{\partial y_2^2} = 0 \qquad \text{in} \quad D_{\text{I}} \tag{B.18}$$
$$C^{\text{II}}_{3131}\frac{\partial A^{\text{II}}_{3kl}}{\partial y_1^2} + C^{\text{II}}_{3232}\frac{\partial A^{\text{II}}_{3kl}}{\partial y_2^2} = 0 \qquad \text{in} \quad D_{\text{II}} \tag{B.19}$$
$$C^{\text{I}}_{3131}\frac{\partial A^{\text{I}}_{3kl}}{\partial y_1}n^{\text{III}}_1 + C^{\text{I}}_{3232}\frac{\partial A^{\text{I}}_{3kl}}{\partial y_2}n^{\text{III}}_2 - \big(C^{\text{II}}_{3131}\frac{\partial A^{\text{II}}_{3kl}}{\partial y_1}n^{\text{III}}_1 + C^{\text{II}}_{3232}\frac{\partial A^{\text{II}}_{3kl}}{\partial y_2}n^{\text{III}}_2\big)$$
$$= (C^{\text{II}}_{31kl}n^{\text{III}}_1 + C^{\text{II}}_{32kl}n^{\text{III}}_2) - (C^{\text{I}}_{31kl}n^{\text{III}}_1 + C^{\text{I}}_{32kl}n^{\text{III}}_2) \qquad \text{on} \quad \partial D_{\text{I}} \cap \partial D_{\text{II}} \tag{B.20}$$
$$A^{\text{I}}_{3kl} = A^{\text{II}}_{3kl} \qquad \text{on} \quad \partial D_{\text{I}} \cap \partial D_{\text{II}} \tag{B.21}$$
$$C^{\text{II}}_{3131}\frac{\partial A^{\text{II}}_{3kl}}{\partial y_1}n^{\text{II}}_1 + C^{\text{II}}_{3232}\frac{\partial A^{\text{II}}_{3kl}}{\partial y_2}n^{\text{II}}_2 + C^{\text{II}}_{31kl}n^{\text{II}}_1 + C^{\text{II}}_{32kl}n^{\text{II}}_2 = 0 \qquad \text{on} \quad \partial D_{\text{f}} \tag{B.22}$$

Now similarly for the in-plane problem, so we put $i = 1, 2$ simultaneously in (B.13)-(B.17) and use the entries from the matrices (B.11) and (B.12) to simplify to obtain a vector problem of the form

$$\nabla \cdot \big(\mathbb{C}^{\text{I}}\nabla \mathbf{A}^{\text{I}}_{kl}\big) = 0 \qquad \text{in} \quad D_{\text{I}} \tag{B.23}$$
$$\nabla \cdot \big(\mathbb{C}^{\text{II}}\nabla \mathbf{A}^{\text{II}}_{kl}\big) = 0 \qquad \text{in} \quad D_{\text{II}} \tag{B.24}$$

$$\left(\mathbb{C}^{\mathrm{I}}\nabla\mathbf{A}^{\mathrm{I}}_{kl} - \mathbb{C}^{\mathrm{II}}\nabla\mathbf{A}^{\mathrm{II}}_{kl}\right)\mathbf{n}^{\mathrm{III}} = \mathbf{f}_{kl} \qquad \text{on} \quad \partial D_{\mathrm{I}} \cap \partial D_{\mathrm{II}} \tag{B.25}$$

$$\mathbf{A}^{\mathrm{I}}_{kl} = \mathbf{A}^{\mathrm{II}}_{kl} \qquad \text{on} \quad \partial D_{\mathrm{I}} \cap \partial D_{\mathrm{II}} \tag{B.26}$$

$$\mathbb{C}^{\mathrm{II}}\nabla\mathbf{A}^{\mathrm{II}}_{kl}\mathbf{n}^{\mathrm{II}} + \mathbb{C}^{\mathrm{II}}\mathbf{n}^{\mathrm{II}} = 0 \qquad \text{on} \quad \partial D_{\mathrm{f}} \tag{B.27}$$

where $\mathbf{A}^{\mathrm{I}}_{kl}$ and $\mathbf{A}^{\mathrm{II}}_{kl}$ are vectors with two components $i = 1, 2$ for each fixed couple (k,l)=(1,1), (2,2), (3,3), (1,2). The force on the interface $\partial D_{\mathrm{I}} \cap \partial D_{\mathrm{II}}$ between the two elastic phases $\mathbf{f}^{\partial D_{\mathrm{I}} \cap \partial D_{\mathrm{II}}}_{kl}$ can be written as

$$\mathbf{f}^{\partial D_{\mathrm{I}} \cap \partial D_{\mathrm{II}}}_{kl} = (C^{\mathrm{II}}_{i1kl} n^{\mathrm{III}}_1 + C^{\mathrm{II}}_{i2kl} n^{\mathrm{III}}_2) - (C^{\mathrm{I}}_{i1kl} n^{\mathrm{III}}_1 + C^{\mathrm{I}}_{i2kl} n^{\mathrm{III}}_2) \tag{B.28}$$

We also have a second interface between the fluid and the matrix ∂D_{f} and this has the interface load

$$\mathbf{f}^{\partial D_{\mathrm{f}}}_{kl} = C^{\mathrm{II}}_{i1kl} n^{\mathrm{II}}_1 + C^{\mathrm{II}}_{i2kl} n^{\mathrm{II}}_2 \tag{B.29}$$

again for each fixed couple (k,l)=(1,1), (2,2), (3,3), (1,2).

We therefore have that the 2D problems to be solved are the two anti-plane (B.18)-(B.22) for (k,l)=(1,3), (2,3) and the four in-plane (B.23)-(B.27) for (k,l)=(1,1), (2,2), (3,3), (1,2). For the LMRP model we see these specified for isotropic elasticity tensors in Sec. 6.2.2. We can simplify these problems for the porous matrix problem by using only (B.19) and (B.22) for (k,l)=(1,3), (2,3) and (B.24) and (B.27) for (k,l)=(1,1), (2,2), (3,3), (1,2). We also assume that the matrix has an isotropic elasticity tensor which we illustrate in Sec. 6.2.4. Also for the problem between the inclusion and the porous matrix we require only (B.18)-(B.21) for (k,l)=(1,3), (2,3) and the four in-plane (B.23)-(B.26) for (k,l)=(1,1), (2,2), (3,3), (1,2). We also make the assumption that the inclusion is isotropic and use the results from the 2D porous matrix simulations to inform the elasticity tensor for the matrix. This can be seen in Sec. 6.2.4.

B.2 Numerical Simulations and Meshing

Within this section we aim to give an overview of the steps carried out in COMSOL Multiphysics to compute the results presented in this work. To do this in the most clear and useful way we will begin with the set up for the 3D simulations platform, and then explain the simplified 2D simulations which have results presented in Fig. 6.5a - 6.8a.

We can now discuss the 3D simulations that are applicable to long fibres embedded

in the matrix with the fluid cylinders. We can then mention the small modification for the case of short fibres, with results shown in Fig. 6.10 - 6.13a. For the LMRP model the cell problem (6.19)-(6.23) is a three dimensional problem. Our interface conditions (6.38)-(6.43) and (6.44)-(6.49) are also 3D. For each pair of boundary loads given in (6.38)-(6.43) and (6.44)-(6.49) we compute a corresponding numerical solution of the elastic-type problem (6.19)-(6.23). This can be done using the finite element software COMSOL Multiphysics employing its Structural Mechanics Module.

We use this software to compute the 36 entries of the tensors $\mathbb{M}_{\mathrm{I}}$ and $\mathbb{M}_{\mathrm{II}}$. Then once we have these results they can be used in (6.5) to obtain the entries of $\widetilde{\mathbb{C}}^{\mathrm{LMRP}}$. Once we have the complete tensor $\widetilde{\mathbb{C}}^{\mathrm{LMRP}}$ then we can use the components in the formulas for our elastic moduli E_1 and E_3 and take the shears directly from the tensor.

We will now give some details of how this process in COMSOL is carried out. The finite element software creates a mesh for the periodic cell Ω. It does so in such a way that it creates a surface mesh for the interfaces between the phases and around the voids. It then extends the surface mesh into a three-dimensional one for the entire periodic cell Ω. By using this method it allows for both interface conditions described by boundary pairs and interfaces on the drained fluid voids. This is beneficial since it allows for a particularly refined mesh on the interfaces (where the important physics takes place) and the surrounding area which gets gradually coarser the further away from the subphase and void interfaces that we are.

We know from the cell problem (6.19)-(6.23) that the stress-jump condition on the matrix-subphase interface as well as the condition on the interface between the matrix and fluid are the driving forces for the solution of the cell problems. This means that we require a sufficiently fine mesh on these interfaces to ensure we obtain an accurate numerical solution. Therefore, to capture these areas where the important physics is taking place, our mesh in Ω is set to be much more refined around the boundary pairs and voids representing the interfaces than in the remainder of the domain further away from these interfaces. It is important we mention that we can use a sequence of increasingly refined meshes of Ω. These meshes are predefined by COMSOL Multiphysics and range in refinement from extremely coarse to extremely fine.

In cell problem (6.19)-(6.23) the stress balance equations (6.19)-(6.20) are simple since we have zero volume forces and a constant, isotropic elasticity tensor for both the matrix Ω_{II} and the subphase Ω_{I}. The stress jump and the continuity of the auxiliary tensors A_{I}

and A_{II} (6.21)-(6.22) across the interface between the two elastic phases are encoded by conditions on each boundary pair. The condition between the matrix and the void (6.23) is encoded on the interface. We then impose periodic boundary conditions on the outer boundary $\partial\Omega$. By using this framework the solution of the elastic-type problem will be unique up to a constant. The constant here is unimportant since it will disappear when the partial derivatives of the solution are taken to allow us to determine $\mathbb{M}_{\text{I}}$ and $\mathbb{M}_{\text{II}}$. That being said, computationally we do require a unique solution of the elastic-type problems in our periodic cell. To obtain this we can add an additional constraint in COMSOL that fixes the auxiliary displacement to zero in one corner point of Ω. This fixes the constant that is obtained. COMSOL Multiphysics uses the principle of virtual work to implement the elastic-type problem described above in weak form.

As we do not have continuity of stresses the problem for the auxiliary variables A_{I} and A_{II} is solved in the geometrical setting in the Comsol feature assembly. If we were to use the union setting then the subdomains Ω_{II} and Ω_{I} would be merged to form a simple union with continuity which is not the case in our materials. By using the assembly feature we are able to retain the boundaries for each phase of the domain, which allows for the necessary flexibility in the application of the interface conditions.

The entries of the third rank tensors A_{I} and A_{II} are numerically approximated once the six elastic-type problems (6.19)-(6.23) corresponding to the six pairs of interface loads (6.38)-(6.43) and (6.44)-(6.49) have been solved. The derivatives of the entries of A_{I} and A_{II} are linear functions that can be evaluated without additional error and therefore so can all entries of the auxiliary fourth rank tensors $\mathbb{M}_{\text{I}}$ and $\mathbb{M}_{\text{II}}$. The entries of the effective elasticity tensor $\widetilde{\mathbb{C}}_{\text{LMRP}}$ are then computed using (6.5) by calculating the averages without additional errors. All the steps carried out such as the finite element approximations for A_{I} and A_{II} to the computation of the effective elasticity tensor $\widetilde{\mathbb{C}}_{\text{LMRP}}$ is obtained in COMSOL Multiphysics by using its integral post-processing tools.

For the short fibre simulations the same setup is used however, in this case the boundary pairs are on the full cylindrical surface (curved walls and circular ends) of the embedded subphase rather than just on the curved surface of the cylinder since it is fully embedded in the matrix. The rest of the setup and post-processing remains the same procedure.

A very similar setup can be employed for the standard poroelastic setting. Here we have created a platform comprising 3 phases (and many more could be added) but by assuming limit cases of the details just provided we can split this platform into the two

steps required by the standard poroelastic approach. We first have this setup assuming the subphase does not exist which would mean it would be a porous matrix set up with only the interface between matrix and void. Secondly the setup can be modified assuming the voids do not exist, for further details on this second step see the [88] where the numerical simulations for a composite have been carried out.

In terms of the 2D problems, the setup is almost identical although this time we are using a 2D domain and the interfaces are lines not surfaces. We again do not have continuity of stresses so the problem for the auxiliary variables A_{I} and A_{II} is still solved in the geometrical setting using the COMSOL feature assembly where the interface is just a circle. We have our voids on which the forces are placed on the interfaces. We have the corresponding periodic conditions which are applied on the external edges (lines) making the boundary. For uniqueness of solution a constraint in COMSOL is placed that fixes the auxiliary displacement to zero in one corner of the square domain. In the same way all the steps carried out such as the finite element approximations for A_{I} and A_{II} to the computation of the effective elasticity tensor $\widetilde{\mathbb{C}}_{\mathrm{LMRP}}$ are obtained in COMSOL Multiphysics by using its integral post-processing tools. This time using surface integration rather than volume integration.

B.3 Error Plots

Within this section of the appendix we show the plots of the error we obtained between carrying out the 3D and 2D simulations for both the LMRP model and the standard poroelasticity type model. All the plots have at most a 1% error between the 3D and 2D simulations which justifies the accuracy of the 3D simulations that we have carried out and justifies the results obtained for the short fibres in Sec. 6.4.

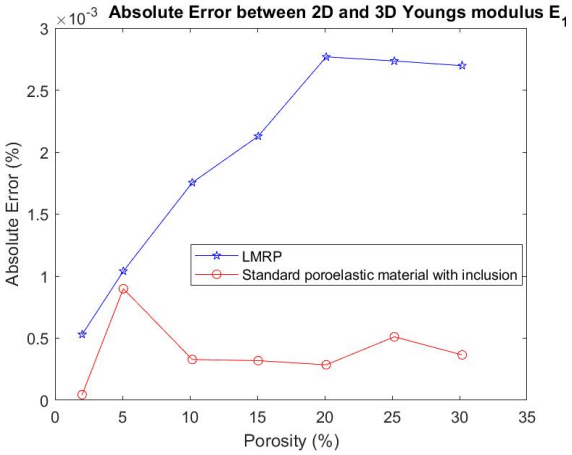

(a) Absolute error between 2D and 3D for E_1

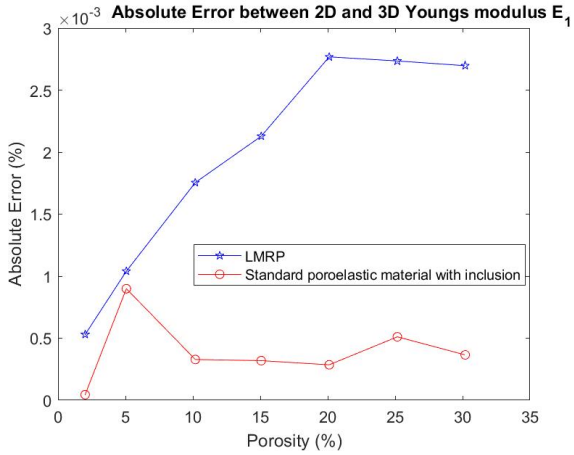

(b) Absolute error between 2D and 3D for E_3

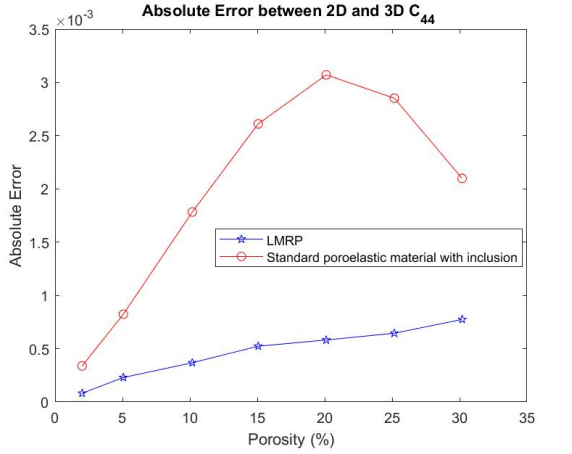

(a) Absolute error between 2D and 3D for C_{44}

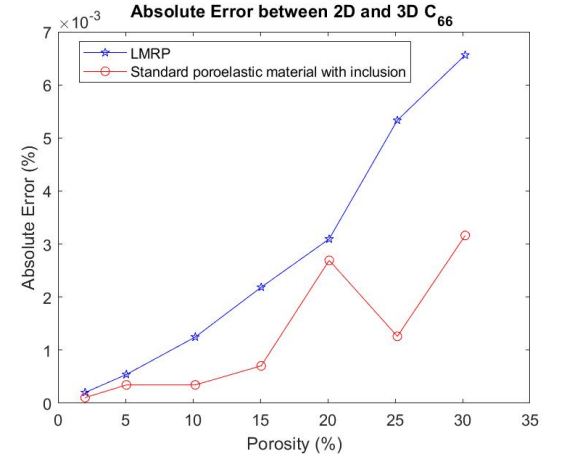

(b) Absolute error between 2D and 3D for C_{66}

Figure B.2: Error between 2D and 3D simulations

Appendix C

Appendix: Effects of MI on elastic parameters of the heart

C.1 Cell problems

Within this appendix we present the cell problems for poroelastic composites arising from the asymptotic homogenization technique as found in [69] and Chapter 3. These cell problems allow us to compute all of the macroscale model coefficients.

We are able to compute the fourth rank effective elasticity tensor $\widetilde{\mathbb{C}}$ for the LMRP model and by using its components calculate the two Young's moduli and two shear moduli. The effective elasticity tensor is given by

$$\widetilde{\mathbb{C}}^{\mathrm{LMRP}} = \langle \mathbb{C}_{\mathrm{Myo}}\mathbb{M}_{\mathrm{Myo}} + \mathbb{C}_{\mathrm{Myo}} + \mathbb{C}_{\mathrm{IM}}\mathbb{M}_{\mathrm{IM}} + \mathbb{C}_{\mathrm{IM}} \rangle_s. \tag{C.1}$$

We see this comprises the fourth rank tensor $\mathbb{M}_v$, where $v = \mathrm{Myo}, \mathrm{IM}$, which are defined as

$$\mathbb{M}_{\mathrm{Myo}} = \xi^{kl}_{pq}(A^{\mathrm{Myo}}) = \frac{1}{2}\left(\frac{\partial A^{\mathrm{Myo}}_{pkl}}{\partial y_q} + \frac{\partial A^{\mathrm{Myo}}_{qkl}}{\partial y_p}\right); \;\; \mathbb{M}_{\mathrm{IM}} = \xi^{kl}_{pq}(A^{\mathrm{IM}}) = \frac{1}{2}\left(\frac{\partial A^{\mathrm{IM}}_{pkl}}{\partial y_q} + \frac{\partial A^{\mathrm{IM}}_{qkl}}{\partial y_p}\right). \tag{C.2}$$

We can then write the cell problems for third rank tensors A_{Myo} and A_{IM}, found in [69], with corresponding components A^{Myo}_{ikl} and A^{IM}_{ikl} as

$$\frac{\partial}{\partial y_j}\left(C^{\mathrm{Myo}}_{ijpq}\xi^{kl}_{pq}(A^{\mathrm{Myo}})\right) + \frac{\partial C^{\mathrm{Myo}}_{ijkl}}{\partial y_j} = 0 \qquad \text{in} \quad \Omega_{\mathrm{I}} \tag{C.3}$$

$$\frac{\partial}{\partial y_j}\left(C^{\mathrm{IM}}_{ijpq}\xi^{kl}_{pq}(A^{\mathrm{IM}})\right) + \frac{\partial C^{\mathrm{IM}}_{ijkl}}{\partial y_j} = 0 \qquad \text{in} \quad \Omega_{\mathrm{II}} \tag{C.4}$$

$$C^{\text{Myo}}_{ijpq}\xi^{kl}_{pq}(A^{\text{Myo}})n^{\text{III}}_j - C^{\text{M}}_{ijpq}\xi^{kl}_{pq}(A^{\text{M}})n^{\text{III}}_j = (C^{\text{IM}} - C^{\text{Myo}})_{ijkl}n^{\text{III}}_j \qquad \text{on} \quad \Gamma_{\text{III}} \tag{C.5}$$

$$A^{\text{Myo}}_{ikl} = A^{\text{IM}}_{ikl} \qquad \text{on} \quad \Gamma_{\text{III}} \tag{C.6}$$

$$C^{\text{IM}}_{ijpq}\xi^{kl}_{pq}(A^{\text{IM}})n^{\text{II}}_j + C^{\text{IM}}_{ijkl}n^{\text{II}}_j = 0 \qquad \text{on} \quad \Gamma_{\text{II}} \tag{C.7}$$

The solutions to the problem (C.3)-(C.7), $\xi^{kl}_{pq}(A^{\text{Myo}})$ and $\xi^{kl}_{pq}(A^{\text{IM}})$, are found by solving six elastic-type cell problems by fixing the couple of indices (k, l). By doing this the $\xi^{kl}_{pq}(A^{\text{Myo}})$ and $\xi^{kl}_{pq}(A^{\text{IM}})$ that appear in (C.3)-(C.7) represent a strain, Then for every fixed couple (k, l) we have a linear elastic problem which has interface conditions between the matrix and inclusion determined by using the elasticity tensor in (C.5) and between the matrix and the fluid that can be determined using (C.7).

We also wish to be able to determine the other macroscale coefficients such as the Biot's modulus and the Biot's tensor of coefficients (see (7.6)). We see that these coefficients contain the tensors $\mathbb{Q}_{\text{Myo}}$ and $\mathbb{Q}_{\text{IM}}$. These can be defined as

$$\mathbb{Q}_{\text{Myo}} = \xi_{pq}(\mathbf{a}^{\text{Myo}}) = \frac{1}{2}\left(\frac{\partial a^{\text{Myo}}_p}{\partial y_q} + \frac{\partial a^{\text{Myo}}_q}{\partial y_p}\right); \quad \mathbb{Q}_{\text{IM}} = \xi_{pq}(\mathbf{a}^{\text{IM}}) = \frac{1}{2}\left(\frac{\partial a^{\text{IM}}_p}{\partial y_q} + \frac{\partial a^{\text{IM}}_q}{\partial y_p}\right). \tag{C.8}$$

We then have the cell problems for the vectors $\mathbf{a}^{\text{Myo}}$ and $\mathbf{a}^{\text{IM}}$, which is given by

$$\frac{\partial}{\partial y_j}\left(C^{\text{Myo}}_{ijpq}\xi_{pq}(\mathbf{a}^{\text{Myo}})\right) = 0 \qquad \text{in} \quad \Omega_{\text{I}} \tag{C.9}$$

$$\frac{\partial}{\partial y_j}\left(C^{\text{IM}}_{ijpq}\xi_{pq}(\mathbf{a}^{\text{IM}})\right) = 0 \qquad \text{in} \quad \Omega_{\text{II}} \tag{C.10}$$

$$C^{\text{Myo}}_{ijpq}\xi_{pq}(\mathbf{a}^{\text{Myo}})n^{\text{III}}_j = C^{\text{IM}}_{ijpq}\xi_{pq}(\mathbf{a}^{\text{IM}})n^{\text{III}}_j \qquad \text{on} \quad \Gamma_{\text{III}} \tag{C.11}$$

$$a^{\text{Myo}}_i = a^{\text{IM}}_i \qquad \text{on} \quad \Gamma_{\text{III}} \tag{C.12}$$

$$C^{\text{IM}}_{ijpq}\xi_{pq}(\mathbf{a}^{\text{IM}})n^{\text{II}}_j + n^{\text{II}}_j = 0 \qquad \text{on} \quad \Gamma_{\text{II}} \tag{C.13}$$

The solutions to the problem (C.9)-(C.13), $\xi_{pq}(\mathbf{a}^{\text{Myo}})$ and $\xi_{pq}(\mathbf{a}^{\text{IM}})$, are found by solving the linear elastic problem with inhomogeneous Neumann conditions between the matrix and the fluid and continuity of auxiliary stresses between the two elastic phases.

These are the 3D cell problems and the ones used to compute the elastic parameters in Sec. 7.4. We must use the 3D problems when we have a variation in the z direction (i.e. in Sec. 7.4 we have cross-sections in the z direction that are disk and matrix or myocyte and matrix since this is different we must use the 3D problems). If the z cross-sections are all the same then it is possible to reduce these cell problems to 2D, which reduces the

computational complexity. It is the reduced cell problems that are used in Sec. 7.2 and Sec. 7.3. For the complete detailed reduction of these cell problems to 2D please see [73].

References

[1] I. Andreu, T. Luque, A. Sancho, B. Pelacho, O. Iglesias-García, E. Melo, R. Farré, F. Prósper, M.R. Elizalde, and D. Navajas. Heterogeneous micromechanical properties of the extracellular matrix in healthy and infarcted hearts. *Acta Biomaterialia*, 10(7):3235–3242, 2014.

[2] I. V. Andrianov, V. I. Bolshakov, V. V. Danishevs'kyy, and D. Weichert. Higher order asymptotic homogenization and wave propagation in periodic composite materials. *Proceedings of the Royal Society*, 464:1181–1201, 2008.

[3] P. Anversa, C. Beghi, Y. Kikkawa, and G. Olivetti. Myocardial response to infarction in the rat. morphometric measurement of infarct size and myocyte cellular hypertrophy. *American Journal of Pathology*, 118(3):484–492, 1985.

[4] J.-L. Auriault, C. Boutin, and C. Geindreau. *Homogenization of coupled phenomena in heterogenous media*, volume 149. John Wiley & Sons, 2010.

[5] L. C. Auton and C. W. MacMinn. From arteries to boreholes: steady-state response of a poroelastic cylinder to fluid injection. *Proceedings of the Royal Society A: Mathematical, Physical and Engineering Sciences*, 473, 2017.

[6] O. Babaniyi, B. Jadamba, A. A. Khan, M. Richards, M. Sama, and C. Tammer. Three optimization formulations for an inverse problem in saddle point problems with applications to elasticity imaging of locating tumor in incompressible medium. *J. Nonlinear Var. Anal.*, 4:301–318, 2020.

[7] N. Bakhvalov and G. Panasenko. *Homogenization: Averaging processes in Periodic Media*. Kluwer Academic Publishers, 1989.

[8] E. Bemer, M. Boutéca, O. Vincké, N. Hoteit, and O. Ozanam. Poromechanics: from linear to nonlinear poroelasticity and poroviscoelasticity. *Oil & Gas Science and Technology - Rev. IFP*, 56(6):531–544, 2001.

[9] L. Berger, D. Kay, K. Burrowes, V. Grau, S. Tavener, and R. Bordas. A poroelastic model of the lung. *arXiv preprint arXiv:1411.1491*, 2014.

[10] J. G. Berryman. Comparison of upscaling methods in poroelasticity and its generalizations. *Journal of Engineering Mechanics*, 131(9):928–936, 2005.

[11] J. G. Berryman and Thigpen L. Nonlinear and semilinear dynamic poroelasticity with microstructure. *Journal of Mechanical Physical Solids*, 33:97–116, 1985.

[12] M. A. Biot. Theory of elasticity and consolidation for a porous anisotropic solid. *Journal of applied physics*, 26(2):182–185, 1955.

[13] M. A. Biot. General solutions of the equations of elasticity and consolidation for a porous material. *J. appl. Mech*, 23(1):91–96, 1956.

[14] M. A. Biot. Theory of propagation of elastic waves in a fluid-saturated porous solid. ii. higher frequency range. *The Journal of the acoustical Society of america*, 28(2):179–191, 1956.

[15] M. A. Biot. Mechanics of deformation and acoustic propagation in porous media. *Journal of applied physics*, 33(4):1482–1498, 1962.

[16] A. Bottaro and T. Ansaldi. On the infusion of a therapeutic agent into a solid tumor modeled as a poroelastic medium. *Journal of Biomechanical engineering*, 134(8):084501, 2012.

[17] D. L. Brown, P. Popov, and Y. Efendiev. Effective equations for fluid-structure interaction with applications to poroelasticity. *Applicable Analysis: An International Journal*, 93(4):771–790, 2014.

[18] M. Bukac, I. Yotov, R. Zakerzadeh, and P. Zunino. *Effects of Poroelasticity on Fluid-Structure Interaction in Arteries: a Computational Sensitivity Study*, pages 197–220. Springer International Publishing, 2015.

[19] R. Burridge and J. B. Keller. Poroelasticity equations derived from microstructure. *The Journal of the Acoustical Society of America*, 70(4):1140–1146, 1981.

[20] P. Causin, G. Guidoboni, A. Harris, D. Prada, R. Sacco, and S. Terragni. A poroelastic model for the perfusion of the lamina cribrosa in the optic nerve head. *Mathematical biosciences*, 257:33–41, 2014.

[21] R. Chalasani, L. Poole-Warren, M. R. Conway, and B. Ben-Nissan. Porous orbital implants in enucleation: a systematic review. *Survey of ophthalmology*, 52(2):145–155, 2007.

[22] D. Chapelle, J. F. Gerbeau, J. Sainte-Marie, and I. E. Vignon-Clementel. A poroelastic model valid in large strains with applications to perfusion in cardiac modeling. *Computational Mechanics*, 46:91–101, 2010.

[23] D. Chapelle, J. F. Gerbeau, J. Sainte-Marie, and I. E. Vignon-Clementel. A poroelastic model valid in large strains with applications to perfusion in cardiac modeling. *Computational Mechanics*, 46(1):91–101, 2010.

[24] M. J. Chen, L. S. Kimpton, J. P. Whitley, M. Castilho, J. Malda, C. P. Please, S. L. Waters, and H. M. Byrne. Multiscale modelling and homogensation of fibre-reinforced hydrogels for tissue engineering. *European Journal of Applied Mathematics*, 31(1):143–171, 2018.

[25] A. H-D. Cheng. *Poroelasticity*, volume 27. Springer, 2016.

[26] K. K. Chiou, J. W. Rocks, C. Y. Chen, S. Cho, K. E. Merkus, A. Rajaratnam, P. Robison, M. Tewari, K. Vogel, S. F. Majkut, B. L. Prosser, D. E. Discher, and A. J. Liu. Mechanical signaling coordinates the embryonic heartbeat. *Proceedings of the National Academy of Sciences*, 113(32):8939–8944, 2016.

[27] D. Cioranescu and P. Donato. *An Introduction to Homogenization*, volume 17. Oxford University Press, 1999.

[28] J. Collis, D. L. Brown, M. Hubbard, and R. O'Dea. Effective equations governing an active poroelastic medium. *Proceedings of the Royal Society A: Mathematical, Physical and Engineering Sciences*, 2017.

[29] A. N. Cookson, J. Lee, C. Michler, R. Chabiniok, E. Hyde, D. A. Nordsletten, M. Sinclair, M. Siebes, and N. P. Smith. A novel porous mechanical framework for modelling the interaction between coronary perfusion and myocardial mechanics. *Journal of Biomechanics*, 45(5):850 – 855, 2012.

[30] S. C. Cowin. Bone poroelasticity. *Journal of biomechanics*, 32(3):217–238, 1999.

[31] O. L. Cruz-González, A. Ramírez-Torres, R. Rodríguez-Ramos, R. Penta, and F. Lebon. Hierarchical heterogeneous one-dimensional problem in linear viscoelastic media. *European Journal of Mechanics-A/Solids*, 95:104617, 2022.

[32] M. P. Dalwadi, I. M. Griffiths, and M. Bruna. Understanding how porosity gradients can make a better filter using homogenization theory. *Proceedings of the Royal Society A: Mathematical, Physical and Engineering Sciences*, 471(2182), 2015.

[33] Y. Davit, C. G. Bell, H. M. Byrne, L. A. Chapman, L. S. Kimpton, G. E. Lang, K. H. Leonard, J. M. Oliver, N. C. Pearson, and R. J. Shipley. Homogenization via formal multiscale asymptoticsand volume averaging:how do the two techniques compare? *Adv Water Resour*, 62:178–206, 2013.

[34] H. Dehghani, I. Noll, R. Penta, A. Menzel, and J. Merodio. The role of microscale solid matrix compressibility on the mechanical behaviour of poroelastic materials. *European Journal of Mechanics - A/Solids*, 83, 2020.

[35] H. Dehghani, R. Penta, and J. Merodio. The role of porosity and solid matrix compressibility on the mechanical behavior of poroelastic tissues. *Materials Research Express*, 6(3):035404, 2018.

[36] H. Dehghani and A. Zilian. Ann-aided incremental multiscale-remodelling-based finite strain poroelasticity. *Computational Mechanics*, pages 1–24, 2021.

[37] L. Dormieux, D. Kondo, and F.-J. Ulm. *Microporomechanics*. John Wiley and Sons, Ltd, 2006.

[38] G. Ertl and S. Frantz. Healing after myocardial infarction. *Cardiovascular Research*, 66(1):22–32, 2005.

[39] D. Fan, A. Takawale, J. Lee, and Z. Kassiri. Cardiac fibroblasts, fibrosis and extracellular matrix remodeling in heart disease. *Fibrogenesis and Tissue Repair*, 5(15), 2012.

[40] M. F. Flessner. The role of extracellular matrix in transperitoneal transport of water and solutes. *Peritoneal dialysis international*, 21(Suppl 3):S24–S29, 2001.

[41] M. Fraldi and A. R. Carotenuto. Cells competition in tumor growth poroelasticity. *Journal of the Mechanics and Physics of Solids*, 112:345–367, 2018.

[42] B. Gambin and E. Kröner. Higher-order terms in the homogenized stress-strain relation of periodic elastic media. *Phys. Stat. Solidi B*, 151:513–519, 1989.

[43] O. Gültekin, G. Sommer, and G. A. Holzapfel. An orthotropic viscoelastic model for the passive myocardium: continuum basis and numerical treatment. *Computer Methods in Biomechanics and Biomedical Engineering*, 19(15):1647–1664, 2016.

[44] A. Godier-Furnémont, Y. Arnold, R. Maidhof, and G. Vunjak-Novakovic. *Tissue Engineering Strategies for Cardiac Regeneration*, pages 443–475. 02 2011.

[45] D. Guan, F. Ahmad, P. Theobald, S. Soe, X. Luo, and H. Gao. On the aic-based model reduction for the general holzapfel-ogden myocardial constitutive law. *Biomech Model Mechanobiology*, 18(4):1213–1232, 2019.

[46] A. Guesmia, M. Kafini, and N. E. Tatar. General stability results for the translational problem of memory-type in porous thermoelasticity of type iii. *J. Nonlinear Funct. Anal. 2020*, 2020.

[47] R. Hambli and N. Hattab. *Application of Neural Network and Finite Element Method for Multiscale Prediction of Bone Fatigue Crack Growth in Cancellous Bone*. 11 2013.

[48] M. H. Holmes. *Introduction to perturbation methods*, volume 20. Springer Science & Business Media, 2012.

[49] G. Holzapfel and R. W. Ogden. Constitutive modelling of arteries. *Proceedings of The Royal Society A Mathematical Physical and Engineering Sciences*, 466:1551–1597, 04 2010.

[50] G. A. Holzapfel and R. W. Ogden. Constitutive modelling of passive myocardium: a structurally based framework for material characterization. *Phil. Trans. R. Soc. A.*, 367:3445–3475, 2009.

[51] M. Hori and S. Nemat-Nasser. On two micromechanics theories for determining micro-macro relations in heterogeneous solid. *Mechanics of Materials*, 31:667–682, 10 1999.

[52] Z. Hu, D. Metaxas, and L. Axel. In vivo strain and stress estimation of the heart left and right ventricles from mri images. *Medical Image Analysis*, 7(4):435–444, 2003.

[53] Z. Hu, D. Metaxas, and L. Axel. Left ventricle composite material model for stress-strain analysis. *Surgery Simulation and Soft Tissue Modeling*, 2673, 2003.

[54] C. Humeres and N. Frangogiannis. Fibroblasts in the infarcted, remodeling and failing heart. *JACC:Basic to translational science*, 4(3), 2019.

[55] J. T. Jacob, C. F. Burgoyne, S. J. McKinnon, T. M. Tanji, P. K. LaFleur, and E. Duzman. Biocompatibility response to modified baerveldt glaucoma drains. *Journal of biomedical materials research*, 43(2):99–107, 1998.

[56] G. Jayaraman. Water transport in the arterial wall—a theoretical study. *Journal of Biomechanics*, 16(10):833 – 840, 1983.

[57] V. Karageorgiou and D. Kaplan. Porosity of 3d biomaterial scaffolds and osteogenesis. *Biomaterials*, 26(27):5474–5491, 2005.

[58] M. Klanchar and J. M. Tarbell. Modeling water flow through arterial tissue. *Bulletin of Mathematical Biology*, 49(6):651–669, 1987.

[59] P. L. Kozlovskis, A. M. Gerdes, M. Smets, J. A. Moore, A. L. Bassett, and R. J. Myerburg. Regional increase in isolated myocyte volume in chronic myocardial infarction in cats. *Journal of Molecular and Cellular Cardiology*, 23(12):1459–1466, 1991.

[60] H-J. Kümpel. Poroelasticity: parameters reviewed. *Geophysical Journal International*, 105(3):783–799, 1991.

[61] P. Laurila and I. Leivo. Basement membrane and interstitial matrix components form separate matrices in heterokaryons of pys-2 cells and fibroblasts. *Journal of cell science*, 104(1):59–68, 1993.

[62] T. Lévy. Propagation of waves in a fluid-saturated porous elastic solid. *International Journal of Engineering Science*, 17(9):1005–1014, 1979.

[63] S. C. Lieber, N. Aubry, J. Pain, G. Diaz, S-J. Kim, and S. F. Vatner. Aging increases stiffness of cardiac myocytes measured by atomic force microscopy nanoindentation.

American Journal of Physiology-Heart and Circulatory Physiology, 287(2):H645–H651, 2004.

[64] P. Mascheroni and R. Penta. The role of the microvascular network structure on diffusion and consumption of anticancer drugs. *International journal for numerical methods in biomedical engineering*, 33(10):e2857, 2017.

[65] G. Mavko, T. Mukerji, and J. Dvorkin. *The rock physics handbook: Tools for seismic analysis of porous media*. Cambridge university press, 2009.

[66] K. May-Newman and A. D. McCulloch. Homogenization modeling for the mechanics of perfused myocardium. *Progress in Biophysics and Molecular Biology*, 69(2):463 – 481, 1998.

[67] M. L. McCain, H. Lee, Y. Aratyn-Schaus, A. G. Kléber, and K. K. Parker. Cooperative coupling of cell-matrix and cell-cell adhesions in cardiac muscle. *Proceedings of the National Academy of Sciences of the United States of America*, 109(25):9881–9886, 2012.

[68] C. C. Mei and B. Vernescu. *Homogenization methods for multiscale mechanics*. World scientific, 2010.

[69] L. Miller and R. Penta. Effective balance equations for poroelastic composites. *Continuum Mechanics and Thermodynamics*, 32(6):1533–1557, 2020.

[70] L. Miller and R. Penta. Double poroelasticity derived from the microstructure. *Acta Mechanica*, 232:3801–3823, 2021.

[71] L. Miller and R. Penta. Homogenized balance equations for nonlinear poroelastic composites. *Applied Sciences*, 11(14), 2021.

[72] L. Miller and R. Penta. Investigating the effects of microstructural changes induced by myocardial infarction on the elastic parameters of the heart. *Submitted to Biomechanics and Modelling in Mechanobiology*, 2022.

[73] L. Miller and R. Penta. Micromechanical analysis of the effective stiffness of poroelastic composites. *submitted to European Journal of Mechanics / A Solids*, 2022.

[74] E. Moeendarbary, L. Valon, M. Fritzsche, A. Harris, D. Moulding, A. Thrasher, E. Stride, L. Mahadevan, and G. Charras. The cytoplasm of living cells behaves as a poroelastic material. *Nature Materials*, 12, 2013.

[75] N. Moise, H. L. Struckman, C. Dagher, R. Veeraraghavan, and S.H. Weinberg. Intercalated disk nanoscale structure regulates cardiac conduction. *Journal of General Physiology*, 153(8), 2021.

[76] D. Nordsletten, A. Capilnasiu, W. Zhang, A. Wittgenstein, M. Hadjicharalambous, G. Sommer, R. Sinkus, and G. A. Holzapfel. A viscoelastic model for human myocardium. *Acta Biomaterialia*, 135:441–457, 2021.

[77] A. N. Norris and M. A. Grinfeld. Nonlinear poroelasticity for a layered medium. *The Journal of the Acoustical Society of America*, 98(1138), 1995.

[78] G. Olivetti, M. Melissari, T. Balbi, F. Quaini, E. Cigola, E. H. Sonnenblick, and P. Anversa. Myocyte cellular hypertrophy is responsible for ventricular remodelling in the hypertrophied heart of middle aged individuals in the absence of cardiac failure. *Cardiovasc Res*, 28(8):1199–1208, 1994.

[79] G. Olivetti, R. Ricci, C. Beghi, G. Guideri, and P. Anversa. Response of the border-zone myocardial infarction in rats. *The American journal of pathology*, 125:476–483, 1987.

[80] B. Owen, N. Bojdo, A. Jivkov, B. Keavney, and A. Revell. Structural modelling of the cardiovascular system. *Biomechanics and Modelling in Mechanobiology*, 17:1217–1242, 2018.

[81] W. J. Parnell and I. D. Abrahams. Dynamic homogenization in periodic fibre reinforcedmedia. quasi-static limit for sh waves. *Wave Motion*, 43:474–498, 2006.

[82] W. J. Parnell and I. D. Abrahams. Homogenization for wave propagation in periodic fibre-reinforced media with complex microstructure. i-theory. *Journal of the Mechanics and Physics of Solids*, 56:2521–2540, 2008.

[83] W. J. Parnell, M. B. Vu, Q. Grimal, and S. Naili. Analytical methods to determine the effective mesoscopic and macroscopic elastic properties of cortical bone. *Biomechanics and Modeling in Mechanobiology*, 11(6):883–901, 2012.

[84] M. Peirlinck, F. S. Costabal, J. Yao, J. M. Guccione, S. Tripathy, Y. Wang, D. Ozturk, P. Segars, T. M. Morrison, S. Levine, and E. Kuhl. Precision medicine in human heart modeling. *Biomechanics and Modelling in Mechanobiology*, 20:803–831, 2021.

[85] A. Pena, M. D. Bolton, and J. D. Pickard. Cellular poroelasticity: A theoretical model for soft tissue mechanics. In *Poromechanics*, pages 475–480, 1998.

[86] R. Penta, D. Ambrosi, and A. Quarteroni. Multiscale homogenization for fluid and drug transport in vascularized malignant tissues. *Mathematical Models and Methods in Applied Sciences*, 25(1):79–108, 2015.

[87] R. Penta, D. Ambrosi, and R. J. Shipley. Effective governing equations for poroelastic growing media. *The quarterly journal of mechanics and applied mathematics*, 67(1):69–91, 2014.

[88] R. Penta and A. Gerisch. Investigation of the potential of asymptotic homogenization for elastic composites via a three-dimensional computational study. *Computing and Visualization in Science*, 17(4):185–201, 2015.

[89] R. Penta and A. Gerisch. The asymptotic homogenization elasticity tensor properties for composites with material discontinuities. *Continuum Mechanics and Thermodynamics*, 29(1):187–206, 2017.

[90] R. Penta and A. Gerisch. An introduction to asymptotic homogenization. In *Multiscale Models in Mechano and Tumor Biology*, pages 1–26. Springer, 2017.

[91] R. Penta and J. Merodio. Homogenized modeling for vascularized poroelastic materials. *Meccanica*, 52(14):3321–3343, 2017.

[92] R. Penta, L. Miller, A. Grillo, A. Ramírez-Torres, P. Mascheroni, and R. Rodríguez-Ramos. Porosity and diffusion in biological tissues. recent advances and further perspectives. In *Constitutive modelling of solid continua*, pages 311–356. Springer, 2020.

[93] R. Penta, A. Ramírez-Torres, J. Merodio, and R. Rodríguez-Ramos. Effective governing equations for heterogenous porous media subject to inhomogeneous body forces. *Mathematics in Engineering*, 3(4):1–17, 2021.

[94] S. Pezzuto, D. Ambrosi, and A. Quarteroni. An orthotropic active–strain model for the myocardium mechanics and its numerical approximation. *European Journal of Mechanics - A/Solids*, 48:83–96, 2014.

[95] P. Ponte Castañeda. The effective mechanical properties of nonlinear isotropic composites. *Journal of the Mechanics and Physics of Solids*, 39(1):45–71, 1991.

[96] P. Ponte Castañeda and M. Zaidman. Constitutive models for porous materials with evolving microstructure. *Journal of the Mechanics and Physics of Solids*, 42(9):1459–1497, 1994.

[97] R. F. Potter and A. C. Groom. Capillary diameter and geometry in cardiac and skeletal muscle studied by means of corrosion casts. *Microvascular Research*, 25(1):68–84, 1983.

[98] P. P. Purslow. *The Extracellular Matrix of Skeletal and Cardiac Muscle*, pages 325–357. Springer US, 2008.

[99] A. Ramírez-Torres, S. Di Stefano, A. Grillo, R. Rodríguez-Ramos, J. Merodio, and R. Penta. An asymptotic homogenization approach to the microstructural evolution of heterogeneous media. *International Journal of Non-Linear Mechanics*, 106:245–257, 2018.

[100] A. Ramírez-Torres, R. Penta, R. Rodríguez-Ramos, and A. Grillo. Effective properties of hierarchical fiber-reinforced composites via a three-scale asymptotic homogenization approach. *Mathematics and Mechanics of Solids*, 2019.

[101] A. Ramírez-Torres, R. Penta, R. Rodríguez-Ramos, A. Grillo, L. Preziosi, J. Merodio, R. Guinovart-Díaz, and J. Bravo-Castillero. Homogenized out-of-plane shear response of three-scale fiber-reinforced composites. *Computing and Visualization in Science*, pages 1–9, 2018.

[102] A. Ramírez-Torres, S. Di Stefano, A. Grillo, R. Rodríguez-Ramos, J. Merodio, and R. Penta. An asymptotic homogenization approach to the microstructural evolution of heterogeneous media. *International Journal of Non-Linear Mechanics*, 106:245 – 257, 2018.

[103] A. Ramírez-Torres, R. Penta, R. Rodríguez-Ramos, J. Merodio, F.J. Sabina, J. Bravo-Castillero, R. Guinovart-Díaz, L. Preziosi, and A. Grillo. Three scales

asymptotic homogenization and its application to layered hierarchical hard tissues. *Int. J. Solids Struct.*, 130:190–198, 2018.

[104] E. Roan and C. M. Waters. What do we know about mechanical strain in lung alveoli? *American Journal of Physiology-Lung Cellular and Molecular Physiology*, 301(5):L625–L635, 2011.

[105] P. Royer, P. Recho, and C. Verdier. On the quasi-static effective behaviour of poroelastic media containing elastic inclusions. *Mechanics Research Communications*, 96:19–23, 2019.

[106] J. Scallan, V. H. Huxley, and R. J. Korthuis. Chapter 2: The interstitium. In *Capillary fluid exchange: regulation, functions, and pathology*, pages 21–26. Morgan & Claypool Publishers, 2010.

[107] M. Siklosi, O. E. Jensen, R. H. Tew, and A. Logg. Multiscale modeling of the acoustic properties of lung parenchyma. In *ESAIM: Proceedings*, volume 23, pages 78–97. EDP Sciences, 2008.

[108] N. P. Smith, D. P. Nickerson, E. J. Crampin, and P. J. Hunter. Multiscale computational modelling of the heart. *Acta Numerica*, 13:371–431, 2004.

[109] V. P. Smyshlyaev and K. D. Cherednichenko. On rigorous derivation of strain gradient effects in the overall behaviour of periodic heterogeneous media. *Journal of the mechanics and physics of solids*, 48:1325–1357, 2000.

[110] M. Taffetani, C. de Falco, R. Penta, D. Ambrosi, and P. Ciarletta. Biomechanical modelling in nanomedicine: multiscale approaches and future challenges. *Archive of Applied Mechanics*, 84(9-11):1627–1645, 2014.

[111] L. H. Tong, H. B. Ding, J. W. Yan, C. Xu, and Z. Lei. Strain gradient nonlocal biot poromechanics. *International Journal of Engineering Science*, 156, 2020.

[112] R. E. Tracy. Cardiac myocyte sizes in right compared with left ventricle during overweight and hypertension. *Journal of the American Society of Hypertension*, 8(7):457–463, 2014.

[113] H. Tzschätzsch, T. Elgeti, K. Rettig, C. Kargel, R. Klaua, M. Schultz, J. Braun, and I. Sack. In vivo time harmonic elastography of the human heart. *Ultrasound in Medicine & Biology*, 38(2):214–222, 2012.

[114] R. Vignjevic, J. C. Campbell, N. K. Bourne, and N. Djordjevic. Modelling shock waves in orthotropic elastic materials. *Journal of applied physics*, 104, 2008.

[115] H. F. Wang. *Theory of linear poroelasticity with applications to geomechanics and hydrogeology*. Princeton University Press, 2017.

[116] H. M. Wang, X.Y. Luo, H. Gao, R. W. Ogden, B. E. Griffith, C. Berry, and T. J. Wang. A modified holzapfel-ogden law for a residually stressed finite strain model of the human left ventricle in diastole. *Biomech Model Mechanobiology*, 13:99–113, 2014.

[117] S. Weiner and D. H. Wagner. The material bone: structure-mechanical function relations. *Annual review of materials science*, 28(1):271–298, 1998.

[118] A. J. Weinhaus and K. P. Roberts. *Anatomy of the Human Heart*, pages 51–79. Humana Press, 2005.

[119] P. N. Wells and H. D. Liang. Medical ultrasound: Imaging of soft tissue strain and elasticity. *J Royal Soc Interface*, 8:1521–1549, 2011.

[120] R. H. Whitaker. The normal heart: Anatomy of the heart. *Medicine*, 42(8):406–408, 2014.

[121] R. Zakerzadeh and P. Zunino. Fluid-structure interaction in arteries with a poroelastic wall model. In *2014 21th Iranian Conference on Biomedical Engineering (ICBME)*, pages 35–39, 2014.

[122] R. Zakerzadeh and P. Zunino. A computational framework for fluid–porous structure interaction with large structural deformation. *Meccanica*, 54:101–121, 2019.

[123] G. A Zampogna, U. Lācis, S. Bagheri, and A. Bottaro. Modeling waves in fluids flowing over and through poroelastic media. *International Journal of Multiphase Flow*, 110:148–164, 2019.

[124] Y. Zhang, V. H. Barocas, S. A. Berceli, C. E. Clancy, D. M. Eckmann, M. Garbey, G. S. Kassab, D. R. Lochner, A. D. McCulloch, R. Tran-Son-Tay, and N. A. Trayanova. Multi-scale modeling of the cardiovascular system: Disease development, progression, and clinical intervention. *Annals of biomedical engineering*, 44(9):2642–2660, 2016.